Durham University

Durham E-Theses

Development of surface replacement prostheses for the proximal interphalangeal and metacarpo phalangeal joints

Ash, Hayley

How to cite:

Ash, Hayley (1997) *Development of surface replacement prostheses for the proximal interphalangeal and metacarpo phalangeal joints*, Durham theses, Durham University. Available at Durham E-Theses Online: http://etheses.dur.ac.uk/5468/

Use policy

The full-text may be used and/or reproduced, and given to third parties in any format or medium, without prior permission or charge, for personal research or study, educational, or not-for-profit purposes provided that:

- a full bibliographic reference is made to the original source
- a link is made to the metadata record in Durham E-Theses
- the full-text is not changed in any way

The full-text must not be sold in any format or medium without the formal permission of the copyright holders.

Please consult the full Durham E-Theses policy for further details.

Academic Support Office, The Palatine Centre, Durham University, Stockton Road, Durham, DH1 3LE
e-mail: e-theses.admin@durham.ac.uk Tel: +44 0191 334 6107
http://etheses.dur.ac.uk

DEVELOPMENT OF SURFACE REPLACEMENT PROSTHESES FOR THE PROXIMAL INTERPHALANGEAL AND METACARPO-PHALANGEAL JOINTS

Hayley Ash B.Sc., M.Sc.

A thesis submitted for the degree of Doctor of Philosophy at the University of Durham

The copyright of this thesis rests with the author. No quotation from it should be published without the written consent of the author and information derived from it should be acknowledged.

Centre for Biomedical Engineering
School of Engineering
University of Durham
Science Laboratories
South Road
Durham
DH1 3LE

June 1997

19 FEB 1998

Abstract

There were two main aims of the project. A surface replacement prosthesis was previously designed at the University of Durham for the metacarpo-phalangeal joint (MCPJ). Tools were required to assess the joint prosthesis pre-operatively and post-operatively. The areas of assessment which the author was involved in were joint stiffness and a self-assessment questionnaire. The Durham arthrograph had previously been used for many clinical trials to assess joint stiffness objectively. However, the computer system was not portable. Hence a new computer system was developed, in LabVIEW, for a lap-top computer. Ten normal individuals were assessed to validate the system. A questionnaire was also developed for patients to self-assess the performance of their joints. The questionnaire assessed parameters such as range of movement, hand strength, stiffness and pain on visual analogue scales. The difficulty in performing activities of daily living were assessed on simple descriptive scales.

The second part of the project was to develop a surface replacement prosthesis for the proximal interphalangeal joint (PIPJ). Since there was inadequate information in the literature on the architecture of the PIPJ bearing surfaces and phalangeal bone shafts, a detailed study was performed on the bones from 83 PIPJs. Proximal and middle phalangeal bones were dissected, modelled in bone cement, sectioned and shadowgraphed. The shadowgraphs were measured and models of the proximal phalangeal heads were produced. These models were then used to design four PIPJ surface replacement prostheses over a range of sizes which covered 97.6% of the sample population of PIPJs.

It was proposed that the MCPJ and PIPJ prostheses would be made entirely from cross-linked polyethylene (XLPE). Hence wear tests on pin-on-plate apparatuses were carried out to investigate the wear characteristics of XLPE-on-XLPE compared with other biomaterial combinations. The wear of XLPE-on-XLPE was comparable with UHMWPE-on-stainless steel. XLPE-on-stainless steel wore 10 times faster than XLPE-on-XLPE, and UHMWPE-on-UHMWPE wore 100 times faster than XLPE-on-XLPE. Hence it was concluded that all XLPE joint prostheses were feasible as far as the wear considerations were concerned.

Acknowledgements

There are many people who have helped and encouraged me throughout this project, to whom I would like express my deepest gratitude:

To the Arthritis and Rheumatism Council for their continuous efforts in the fight against arthritis and for funding this project.

To Professor A Unsworth, my supervisor, for his continuous guidance and motivation throughout the project, and his expertise and advice.

To the experts in the mechanical and electrical workshops at the School of Engineering, University of Durham for the hours of work they invested into this project. I would also like to thank them for their friendship and tolerance.

To Patrick Jones and other members of the South Cleveland Hospital Medical Physics Department for their acceptance and advice, and for the use of their computing facilities.

To Charles Viva, Ian Haslock, and the staff and patients of the South Cleveland and Middlesbrough General Hospitals for the clinical experience gained through them.

To Newcastle University for the use of their shadowgraphing equipment, without which I may not have become so intimate with the proximal interphalangeal joints.

To DePuy International for their investment in this project, and for their industrial expertise and advice.

Finally I would like to thank my friends within the Engineering department who were invaluable in numerable ways. A big thank you must also go to those that consented to being my guinea pigs. I would also like to thank my parents and Alex for their endless support and encouragement, especially in the last couple of months.

Declaration

The work contained in this thesis has not been submitted elsewhere for any other degree or qualification and that, unless otherwise referenced, it is my own work.

Statement of copyright

The copyright of this thesis rests with the author. No quotation from it should be published without her prior written consent and any information derived from it should be acknowledged.

Contents

Chapter three

Dimensions of the proximal interphalangeal joint

Page

Chapter four

Design of a proximal interphalangeal joint surface replacement prosthesis

Chapter five

Wear characteristics of Cross-linked polyethylene

Page

Appendices

Appendices

List of Tables

Notation

α, $\alpha 1$, $\alpha 2$	Angle of inclination of the condyle to the transverse base-line
ϕ	Angle between the main dorsal surface and the longitudinal base-line
η	Angle between the joint prosthesis inter-condylar sulcus and the transverse base-line
θ	Angle of alignment of the head condyles
ρ	Angle between the medullary canal centre-line and the longitudinal base-line
σ	Angle between the head-line and the longitudinal base-line
ω	Arc of cartilage of the MP base
ψ	Angle of the joint prosthesis stem
a	Distance from the transverse head centre-line to the base of a condyle
A	Angle
ADL	Activities of daily living
Av	Voltage at angle A
b	Distance from the transverse head centre-line to the base of a condyle
c	Dorsal offset of the medullary canal centre-line to the PIPJ centre of rotation
Cal1	Potentiometer voltage output at 0°
Cal2	Potentiometer scaling factor
Cal3	Strain gauge scaling factor
CL	Centre-line
CMCJ	Carpal-metacarpal joint
COR	Centre of rotation
d	Distance from the PIPJ bearing surface to the change in angle of the dorsal surface of the phalangeal bone proximal to the PP head
D	Head diameter, sliding distance

Dmax	Maximum head condyle diameter
Dmin	Minimum head condyle diameter
Dbmax	Maximum base recess diameter
Dbmin	Minimum base recess diameter
DI	Dorsal interossei
DIPJ	Distal interphalangeal joint
DP	Distal phalangeal
EDC	Extensor digitorum communis
EP1	Flexion equilibrium position
EP2	Extension equilibrium position
EQP	Equilibrium position
ED	Energy dissipation
ES	Extension slope
F	Female, contact force
FDP	Flexor digitorum profundus
FDS	Flexor digitorum superficialis
FS	Flexion slope
H	Height
H1	Sectioned bone thickness
H2	Sectioned bone thickness
Hc	Medullary canal height
HDPE	High density polyethylene
Hf	Flange depth
Htp	Maximum head height
I	Index finger, interossei muscles
IPJ	Interphalangeal joint
ISat	Maximum inter-condylar sulcus depth (anterior face, transverse plane)
ISd	Joint prosthesis inter-condylar sulcus depth
ISf	Maximum inter-condylar sulcus depth (frontal plane)
L	Lumbricals, little finger, left hand, bone length
L1	Length from the joint prosthesis transverse centre-line to the maximum condyle diameter
L2	Width of the joint prosthesis maximum condyle diameter
Lbl	Longitudinal base-line
Lm	Distance from Tm to the PIPJ bearing surface
Lmw	Distance from Wm to the PIPJ bearing surface
Lp	Distance from Tp to the PIPJ bearing surface
Lpw	Distance from Wp to the PIPJ bearing surface

M	Middle finger, male
MC	Metacarpal
MCPJ	Metacarpo-phalangeal joint
MP	Middle phalangeal
MPS	Mid-position slope
NDS	Numerical descriptive scale
NRS	Numerical ratings scale
OA	Osteoarthritis
PI	Palmar interossei
PIPJ	Proximal interphalangeal joint
PMMA	Polymethymethacrylate (cement)
PP	Proximal phalangeal
PTPT	Peak-to-peak torque
q	Offset of the joint prosthesis stem to the PP head centre of rotation
r	Radius of curvature
R	Ring finger, right hand
RA	Rheumatoid arthritis
s	Joint prosthesis stem length
S.D.	Standard deviation
SDS	Simple descriptive scale
SS	Stainless steel
T	Tendon force, torque
TA	Torque at angle A
Tbl	Transverse base-line
Tm	MP minimum bone height
Tp	PP minimum bone height
UHMWPE	Ultra-high molecular weight polyethylene
v	Palmar offset of the MP stems to the MP base centre of rotation
V	Wear volume, voltage output
VAS	Visual analogue scale
W	Width, maximum head width
W1	Sectioned bone thickness
W2	Sectioned bone thickness
Wb	Maximum MP base width
Wc	Medullary canal width
Wm	Minimum MP width
Wp	Minimum PP width
Wtp	Maximum head width

XLPE	Cross-linked polyethylene
ZS	Zero strain reading

CHAPTER ONE

Introduction

Rheumatic disorders are a group of diseases that can affect the joints and some of the soft tissues of the body. There are over 200 different types[1,2]. The most well-known are back pain, tennis elbow, cervical spondylitis, osteoarthritis, rheumatoid arthritis, gout and ankylosing spondylitis. Rheumatic disorders are very common and nearly everyone who reaches the age of 75 years is likely to have, or to have had, some form of rheumatic complaint[3]. It is estimated that approximately 20 million people suffer from them in the UK, of which between seven and eight million are severely affected (approximately 14% of the population). Only 1 person in 50 will escape from being affected at some time during their life[2]. Mild cases may simply cause some aching and discomfort, however, the most severe cases can cause disability and agonising pain.

People of any age can be affected, although the prevalence increases with age[1,3,4]. For instance a sample of the population from 15-24 years found that 11% were affected by osteoarthritis. This increased to 51% for 15-84 years and 96% for people over 57 years. The prevalence of rheumatoid arthritis also increased with age to 4-5% amongst men and 15-16% amongst women after the age of 54 years[3]. In addition, as the number of elderly people in the community has dramatically increased in recent years, so the number of people affected by rheumatic disorders has also risen.

Patients suffering from rheumatic disorders can experience pain, stiffness, a lack of range of motion in their joints and a lack of strength. They can also feel tired, irritable, depressed and generally unwell[4]. They may be prevented from going to work and carrying out everyday activities such as toilet, cooking and washing. Rheumatic disorders are the single biggest cause of disability in the UK today and account for 88 million lost working days a year. They also cost the National Health Service approximately £500 million a year[2]. Hence it can be seen that rheumatic disorders cause emotional, functional and financial problems for individuals, their families and friends, and the state.

The rheumatic disorders of interest in this project were those encompassed by the general term arthritis, and in particular arthritis of the synovial joints. Arthritis is a disease which can cause painful, inflammation of joints and a breakdown in the joint structure. The two most common forms of arthritis are rheumatoid arthritis and osteoarthritis. The structure of a typical synovial joint is shown in Figure 1.1.

Figure 1.1 Synovial joint structure

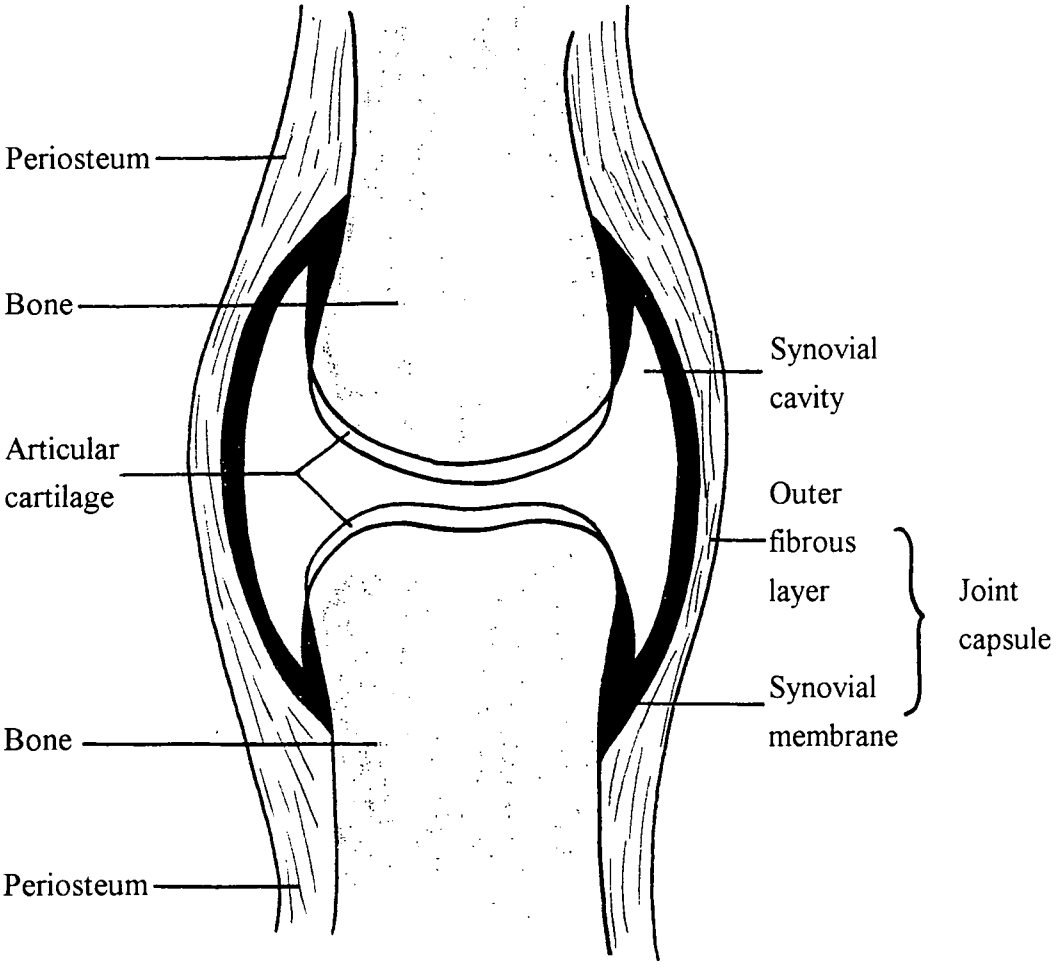

Articular cartilage covers the surfaces of the bones that articulate together. The joint is surrounded by a joint capsule that encloses the synovial cavity. The joint capsule consists of two prominent layers. The outer layer (fibrous capsule) consists of dense connective tissue and is attached to the periosteum of the bones. The fibrous capsule provides flexibility for movement, and strength to hold the bones together and resist dislocation.

The inner layer of the joint capsule is formed by the synovial membrane, which consists of loose connective tissue with elastic fibres and a variable amount of adipose tissue. It secretes synovial fluid which consists of hyaluronic acid and an interstitial fluid formed from blood plasma. The synovial fluid forms a thin film over the articulating surfaces which lubricates the joint. It provides nourishment for, and removes metabolic waste from, the articular cartilage which has no blood supply of its own in the adult. It also contains phagocytic cells that remove microbes and debris resulting from wear of the joint.

Rheumatoid arthritis (RA) can affect synovial joints, as well as other structures of the body such as the heart, lungs, eyes, nervous tissue and small arteries, hence it is sometimes referred to as 'rheumatoid disease'[3]. RA is a common disease in all parts of the world. It can occur in any sex, ethnic or racial group and at any age. Climate, geography and altitude do not affect the prevalence, although the effects of RA are increased in a wet or humid conditions[5].

In the UK RA affects 2-4% of the population[1,4], and although most may only have mild symptoms 1 in 200 women and 1 in 600 men are significantly affected[6]. The prevalence for women is greater than that of men[1,3,6], however, in older patients similar numbers of both sexes are affected[4]. The peak age of incidence is between 30-50 years (which coincides with the female menopause)[4].

RA is characterised by symmetrical, polyarthritis which mainly affects the smaller peripheral joints, although it can also affect the knees, hips and wrists. It has an unknown aetiology although it is thought that it may be an auto-immune response. The immune system of the body protects the body from outside invasion. To do this, the body has to distinguish between itself and the invader. It has been suggested that the distinction between body and invader fails in RA, hence the body starts to destroy itself[3]. Interestingly the disease can go into remission during pregnancy, and women taking the oral contraceptive pill are less likely to develop the disease[4].

RA can cause a breakdown in the structure of synovial joints (Figure 1.2). The lining of the joint capsule (synovium) becomes inflamed (synovitis) which causes swelling of the joint and pain. If the inflammation continues for several years then the articular cartilage and bone can be attacked by the diseased synovium and become eroded. The joint capsule and ligaments may also become weakened and stretched. In the most severe cases deformity of the joint can occur because the weakened joint capsule and ligaments can no longer resist the forces acting on the joint. The tendons can also become displaced and contractures may occur which add to the imbalance of forces on the joint. RA may also cause tendonitis, tendon rupture, subcutaneous nodules, and the skin can become thin and fragile and prone to infection or ulceration. Pins and needles may be felt as the swelling applies pressure to nerves.

The American Rheumatism Association listed several diagnostic criteria which would indicate RA[7]. These included morning stiffness, pain on motion or tenderness, swelling, involvement of the same joints on both sides of the body, subcutaneous nodules, X-ray changes, and changes in the synovial fluid and synovial membrane. Patients may also become anaemic, and 80% have a positive rheumatoid factor (proteins) in their blood, however, these are also found with other diseases[4].

RA can either start with mild symptoms and then gradually get worse, or the start can be much more acute in several joints at once. The joints may become painful, hot, red and swollen as the synovium becomes chronically inflamed. The joints may feel stiff particularly in the early morning (morning stiffness). The range of motion, hand strength and hand function may also be impaired. The symptoms depend on the severity and activity of the disease. The disease can flare-up or go into remission for several months. It is estimated that 10% of patients diagnosed with RA have a single attack and then recover completely, and 20% will experience only mild symptoms with long periods of remission. 65% will suffer from moderate to severe symptoms with flare-ups every few months and 10% will become severely disabled[4].

Osteoarthritis (OA) is a degenerative disease that only affects the joints. There are two main types of OA. Primary OA occurs without any obvious predisposition and may occur in one joint only, but usually involves many joints. Secondary OA results from injury or disease of a single joint which may have occurred many years earlier. The principal joints affected are the knees, hips, elbows, ankles, distal interphalangeal joints (DIPJs), thumb carpo-metacarpal joints, the big toes and the smaller joints of the

Figure 1.2 Effects of Rheumatoid arthritis on synovial joints

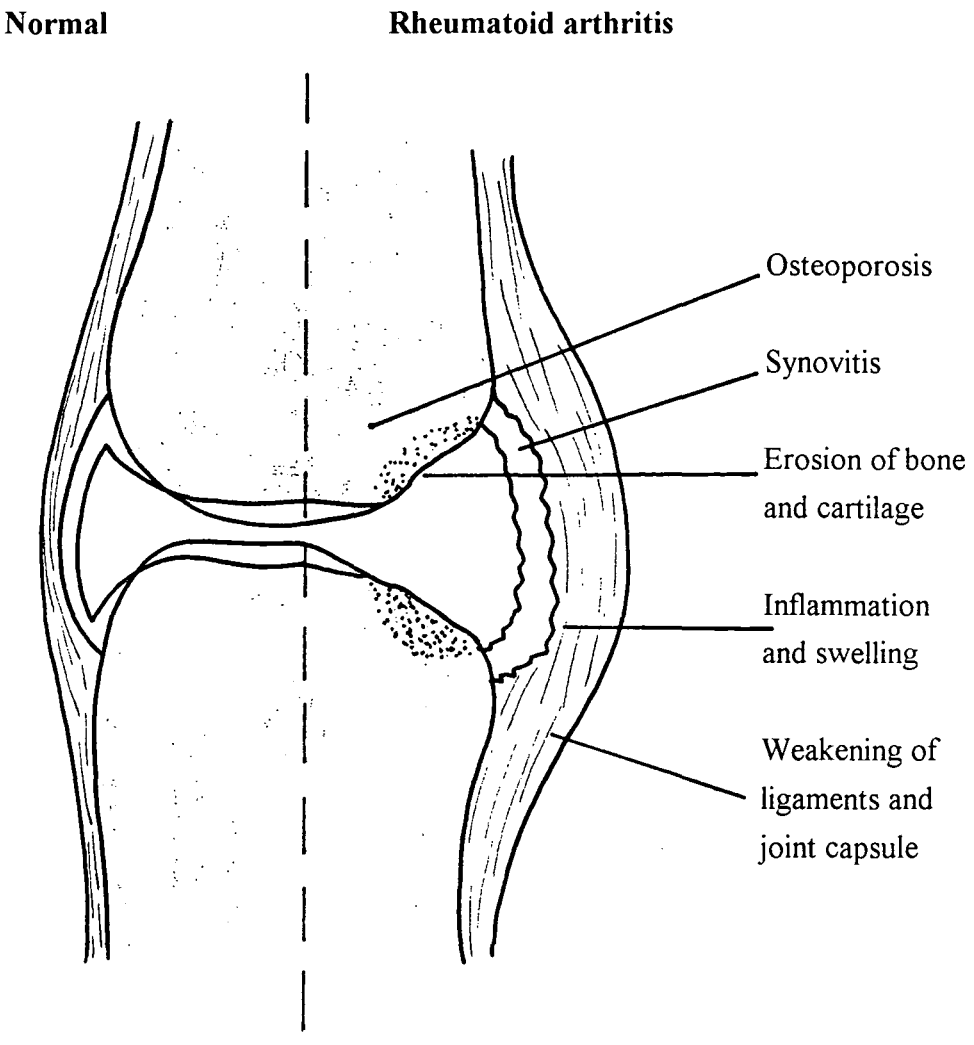

spine[4]. However, it can occur in any joint. The main symptoms are pain, limitation of motion, and stiffness particularly after lack of use of a joint.

Primary OA is much commoner in women than men, and is often associated with the menopause. It is strongly age related and usually occurs after the age of 40 years[1,3-5]. It has been estimated that less than 1% of the population are affected at 30 years, but over 80% are affected at 70 years, however, the majority of cases have only mild symptoms[4]. OA tends to run in families, but its prevalence varies between racial groups[5]. It is made worse with obesity[1,4] and diseases such as chronic depression and thyroid deficiency[4].

OA causes a break down of the articular cartilage (fibrillation). A hypertrophic reaction occurs in the underlying bone, causing it to become more dense (sclerotic) with cyst formations. The degraded cartilage wears away exposing the underlying bone, and causing narrowing of the joint. The two exposed bones then articulate against each other, causing crepitus of the joint, polishing of the bone ends and pain. Loose fragments of cartilage or bone cause synovitis resulting in inflamed, swollen joints. (This differs from RA where the diseased synovium causes erosion of the bone and articular cartilage). Osteophytes grow out from the periphery of the joint, and are composed of cartilage which then ossifies. An increased amount of synovial fluid may also be produced which is thinner than normal. The typical effects of OA on a synovial joint are shown in Figure 1.3.

The joints affected, severity, symptoms, disease progression and difficulties caused by arthritis vary between individuals. Gross deformity may not necessarily result in loss of function, reduction in strength and painful joints. Likewise joints with little articular surface and soft tissue destruction, and deformity may be painful and functionally useless. There are a range of treatments for arthritic joints which are used according to the severity and symptoms of the disease, and the response of the patient to the treatments.

During early stages of the disease several different drug treatments may be used. These include pain killers, anti-inflammatory drugs and steroids. They can relieve symptoms but do not necessarily prevent the disease from continuing to destroy the joint. The effects of these drugs are temporary and the effectiveness can decrease with repeated use. In addition, some of the drugs can produce side effects. However, for many patients drug treatments are satisfactory for their condition and their arthritis

Figure 1.3 Effects of Osteoarthritis on synovial joints

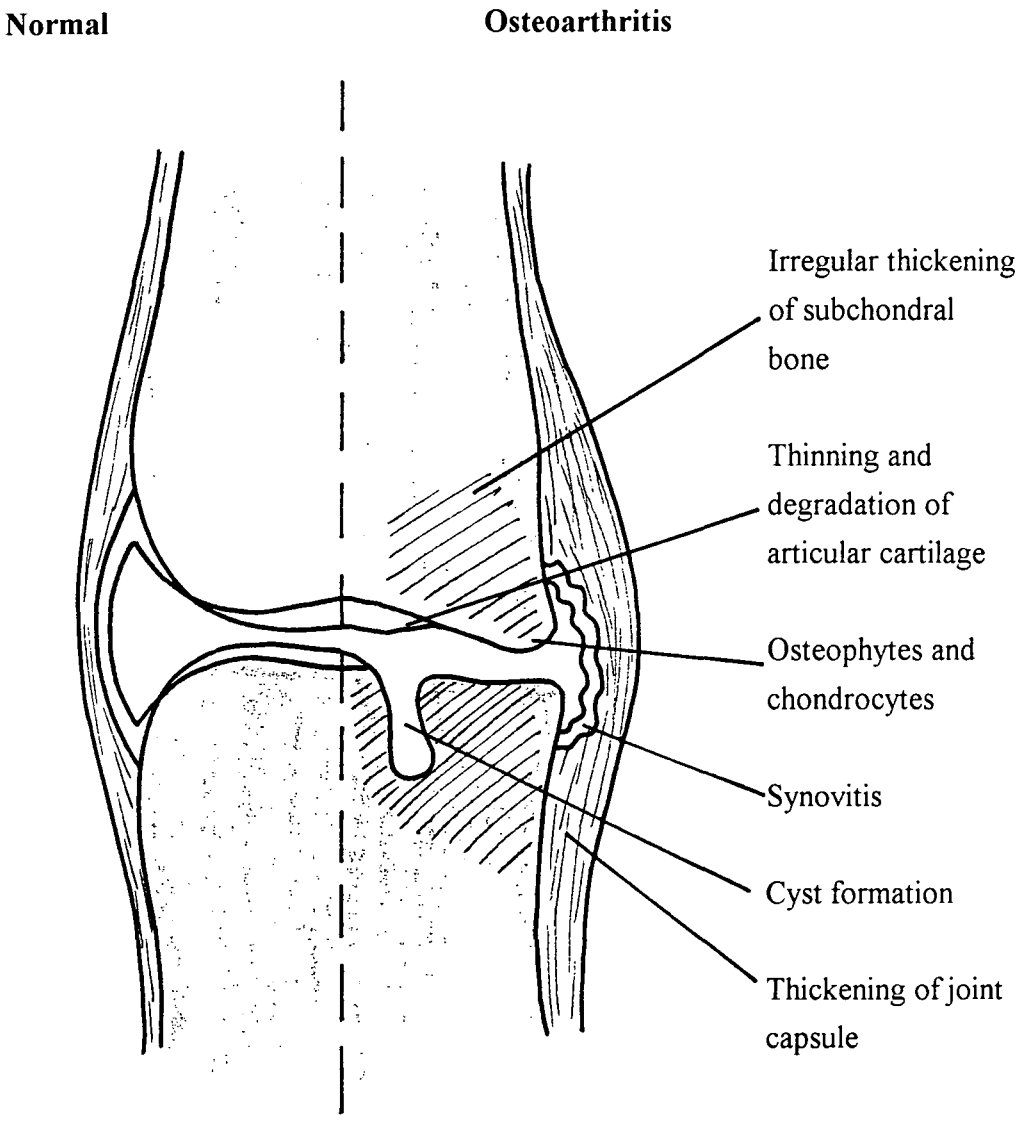

progresses no further. Physiotherapeutic techniques such as hot wax-baths and ultrasound may also be used to alleviate pain and stiffness, and increase joint function.

At a later stage of the disease minor surgery may be necessary, such as synovectomy or soft tissue reconstruction. During synovectomy the inflamed synovium is removed which can alleviate pain and reduce swelling. This in turn reduces the stress on the joint capsule, ligaments and tendons. It also prevents the diseased synovium from attacking the bone and articular cartilage. The synovium re-grows within 3-4 weeks. Synovectomy can delay the rheumatoid process, sometimes for several years, and preserve the joint structure. Reconstructive surgery may also be performed on the soft tissues surrounding the joints. The tendons can be rebalanced and stretched ligaments tightened. This increases the stability of the joints and can correct any joint deformity.

During the late stages of arthritis there may be no alternative than to perform arthrodesis or arthroplasty and total joint replacement. Arthrodesis fuses the bones of a joint together, preventing motion and alleviating pain. It is performed when a joint no longer responds to other forms of treatment and is unlikely to gain any advantage from being replaced by an artificial joint. Arthrodesis is commonly performed on the thumb if it becomes unstable, preventing grip tasks of the hand. By fusing the unstable joints, the thumb becomes a pillar against which the fingers can act, hence improving hand function. Arthrodesis is also performed on the DIPJs due to their size. They are fused in slight flexion to improve the remaining hand function. It is thought that fusing the joints does not impede hand function significantly due to the remaining movement in the other finger joints. Indeed hand function may be improved due to the alleviation of pain and instability in the joints. However, arthrodesis of most joints would be functionally limiting hence they are replaced with artificial joints.

Approximately 30,000 hip replacements and 5,000 knee replacements are performed each year, many due to OA[4]. No such figure has been reported for the finger joints, however, it is common for four joint prostheses to be implanted in one hand during a single operation. Hip and knee joint prostheses are generally successful and can produce good results for many years, however, finger joint prostheses have not shown such encouraging results especially long-term.

One of the first finger joint prostheses was designed in 1959 by Brannon and Klein[8] for the metacarpo-phalangeal joint (MCPJ). Since then there have been many designs (Section 2.4). The most commonly used joint prosthesis is still the Swanson[9] which consists of an integral silicone hinge. It can provide pain relief, correction of deformity

and an improved range of motion short-term, however, complications have occurred and the long-term performance has been shown to deteriorate[10-12]. It is debatable whether this is due to the design of the joint prosthesis or the progressive nature of the disease. Ultimately the progression of the disease may not be able to be halted. Hence preserving hand function for as long as possible must come from the joint prosthesis design itself. The impact of the joint prosthesis on the body, and vice versa, may be minimised by designing it as close to the original anatomy of the joints as possible. This is the concept of the latest generation of finger joint prostheses, namely surface replacement designs. There have been several designs of surface replacement joint prostheses for the MCPJ although no long-term clinical results have been reported.

Finger joint prostheses for the proximal interphalangeal joint (PIPJ) are not as well developed. In fact they tend to be smaller versions of the MCPJ prostheses, despite the differences in anatomy and biomechanics between the two joints. Hence there was a need for a surface replacement joint prosthesis designed specifically for the PIPJ. In addition, tools were required to assess the performance of a surface replacement joint prosthesis, designed at the University of Durham, for the MCPJ in clinical trials.

CHAPTER TWO

Anatomy, biomechanics and arthritis of the finger joints

2.1 Anatomy of the finger joints

2.1.1 The planes of the body

The anatomy of the body can be looked at as a whole or in different planes. These planes can be described as imaginary flat surfaces that pass through the body in a defined orientation. There are three main planes of the body which are shown in Figure 2.1. The planes have been used extensively in Chapters 3 and 4 to describe the anatomy of the bones of the proximal and middle phalanges. The sagittal plane is a vertical plane that divides the body into right and left sections. The sagittal plane can further be defined as mid-sagittal which passes through the mid-line of the body, or para-sagittal which is parallel to the mid-sagittal plane but does not pass through the mid-line of the body. However, in this thesis all of these planes have simply been described as the sagittal plane.

The frontal (or coronal) plane is also a vertical plane but lies at right angles to the sagittal plane and divides the body into anterior and posterior sections. It should be noted that the anatomical position of the body is with the palms showing anteriorly. Hence the dorsal surface of the bones can also be described as the posterior surface and the palmar or volar surface can be described as the anterior surface. The transverse, or horizontal, plane lies parallel to the ground and perpendicular to both the sagittal and frontal planes. Positions of the parts of the body can also be described as distal or proximal with respect to one another. For instance the tips of the fingers are distal to the wrist, and the palm of the hand is proximal to the fingers. Similarly parts of an individual bone can be described as proximal or distal.

The main movements associated with the planes of the body are flexion-extension, hyper-extension, abduction-adduction, rotation, pronation and supination. Flexion and extension are defined as movements that decrease and increase the angle between the surfaces of the articulating bones respectively, in the sagittal plane. Hyper-extension is extension of a joint beyond the anatomical position. Abduction and adduction are usually defined as movement of a bone away from and towards the mid-line of the body respectively. However, with the fingers they are defined as movement in relation to the mid-line of the middle finger. This movement takes place in the frontal plane.

Figure 2.1 The planes of the body

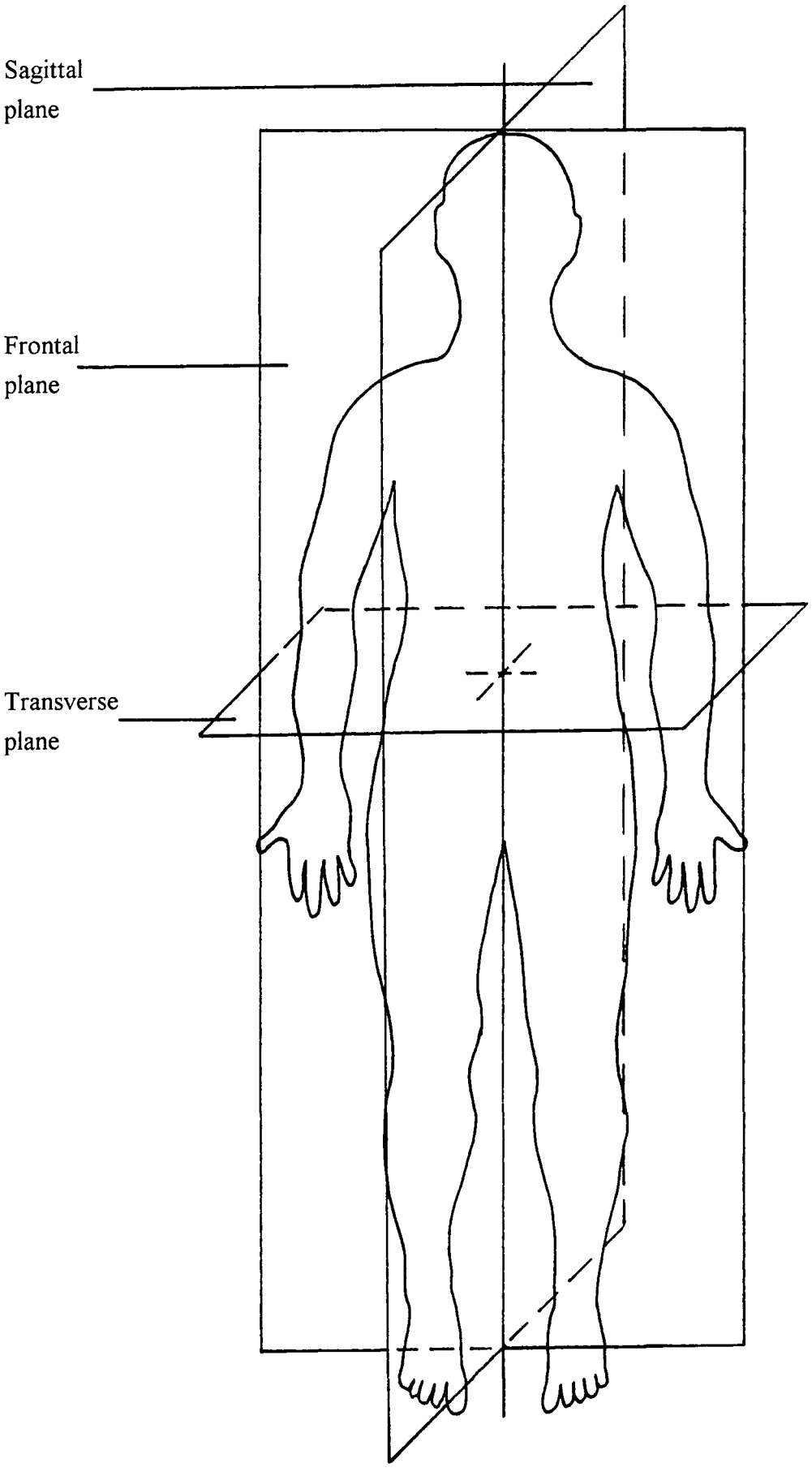

The medial and lateral sides of bones are defined as those nearest to and furthest away from the mid-line of the body respectively. However, with the bones of the hands and fingers it is clearer to describe the sides of the bones in terms of the radial and ulnar sides. This relates to positions of the radius and ulna in the forearm. Rotation is defined as movement of a bone about its longitudinal axis. Supination turns the palm of the hand anteriorly and pronation turns the palm of the hand posteriorly.

2.1.2 The bones of the hand

The bones of the hand consist of the carpals, metacarpals and phalanges (Figure 2.2). There are eight carpal bones arranged in two rows of four bones each. The bones of the proximal row (radial to ulnar) are the scaphoid, lunate, triquetral and pisiform. The bones of the distal row (radial to ulnar) are the trapezium, trapezoid, capitate and hamate. There are five metacarpal (MC) bones which make up the palm of the hand. There are fourteen phalangeal bones arranged in three rows (proximal, middle and distal). The fingers have three phalanges each but the thumb has only two as it has no middle phalanx. The metacarpals and phalanges consist of a proximal concave base, a shaft and a distal convex head. The convex phalangeal heads are bi-condylar and the two condyles are separated by an inter-condylar sulcus. The proximal phalangeal (PP) bases have part spherical facets, to articulate with the spherical MC heads. The middle phalangeal (MP) and distal phalangeal (DP) bases have two condylar shaped facets which are separated by an inter-condylar ridge. These articulate with the PP and MP heads respectively.

2.1.3 The metacarpo-phalangeal joint

The metacarpo-phalangeal joint (MCPJ) is a condylar joint between the convex MC head and the concave PP base. Active movement of flexion-extension and abduction-adduction is allowed, although abduction-adduction can not be performed when the fingers are flexed. Some passive rotation and gliding is also permitted. Flexion is greater than hyper-extension due to the tension in the flexor muscles during extension. Each joint has a palmar and two collateral ligaments. The collateral (metacarpo-phalangeal) ligaments originate from the sides of the MC head and run obliquely before they insert on the PP base. They are tight in flexion and loose in extension which gives the joints more stability when performing pinch and grip hand functions. The palmar (metacarpo-glenoidal) ligament lies between the collateral ligaments, which it is connected to. There is a structural and functional link between the four MCPJs.

Figure 2.2 The bones and joints of the hand

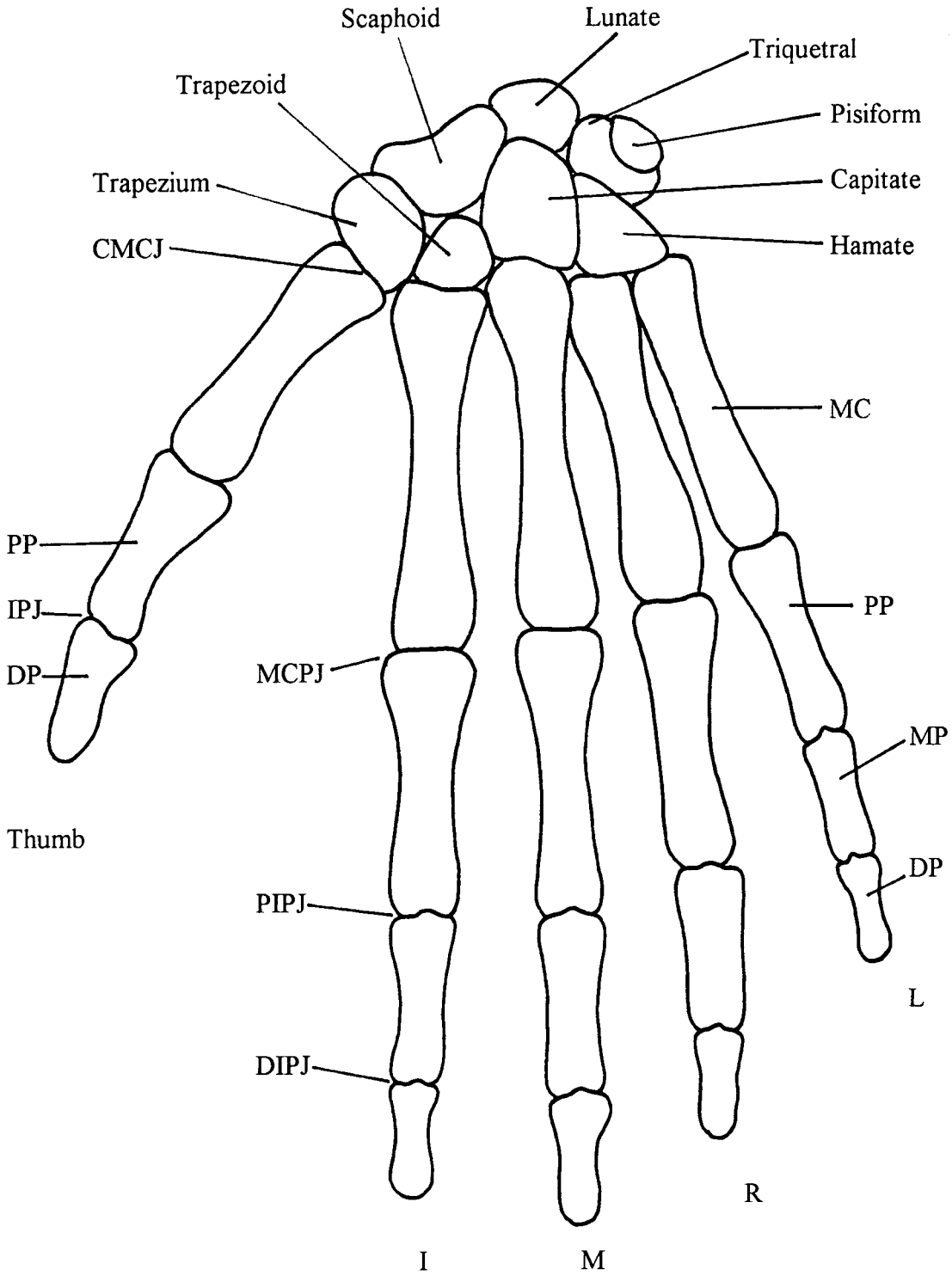

2.1.4 The interphalangeal joints

The interphalangeal joints (IPJs) consist of the proximal interphalangeal joints (PIPJs) and the distal interphalangeal joints (DIPJs). The PIPJ is between the convex PP head and the concave MP base. The DIPJ is between the convex MP head and the concave DP base. The DP head is non-articulating. The IPJs are bi-condylar and movement is primarily in flexion-extension. Some passive abduction-adduction, rotation and gliding are permitted allowing the fingers to adapt themselves to irregular shaped objects and accommodate external forces exerted on the joints. Hyper-extension is limited by the tension of the digital flexors and palmar ligaments. The IPJs have no muscular support in abduction-adduction hence they rely on the joint capsule and collateral ligaments to provide lateral joint stability.

2.1.5 Extrinsic and intrinsic muscles of the fingers

There are two main groups of muscles and associated tendons that act on the fingers. These are the extrinsic and the intrinsic muscles. The extrinsic muscles originate outside the hand (humerus, ulna and radius) and insert within the hand, whereas the intrinsic muscles originate and insert within the hand. The extrinsic muscles can be divided into two groups, anterior muscles (flexors) and posterior muscles (extensors). These two groups can also be divided into superficial and deep muscles depending on their anatomical position. The intrinsic muscles can be divided into three groups, thenar (act on the thumb), hypo-thenar (act on the little finger) and intermediate (act on all the digits except the thumb). The main muscles and tendons that act on the fingers can be seen in Figure 2.3.

2.1.5.1 Extrinsic finger muscles

There is one main extensor and two main flexors of the fingers. The Extensor digitorum communis (EDC) or Long extensor inserts on the distal phalanges via the terminal extensor, and on the middle phalanges via the medial band. It causes extension of the MCPJs and IPJs. The Flexor digitorum superficialis (FDS) inserts on the middle phalanx flexing the PIPJs and then the MCPJs. The Flexor digitorum profundus (FDP) inserts on the base of the distal phalanges flexing the DIPJ after the FDS has flexed the PIPJ, and is also a weak flexor of the PIPJs. The little and index fingers have an additional extensor each called the Extensor digiti minimi and Extensor indicis which extend the little and index fingers respectively by their insertion on the EDC tendons.

Figure 2.3 Muscles and tendons of the fingers

a) Sagittal plane

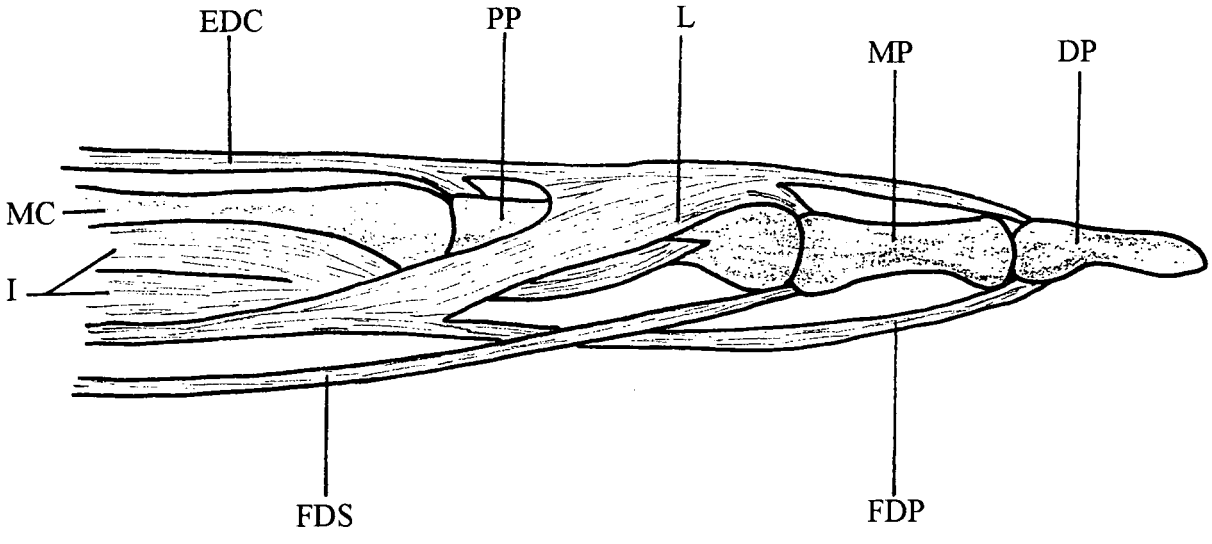

b) Frontal plane, posterior view

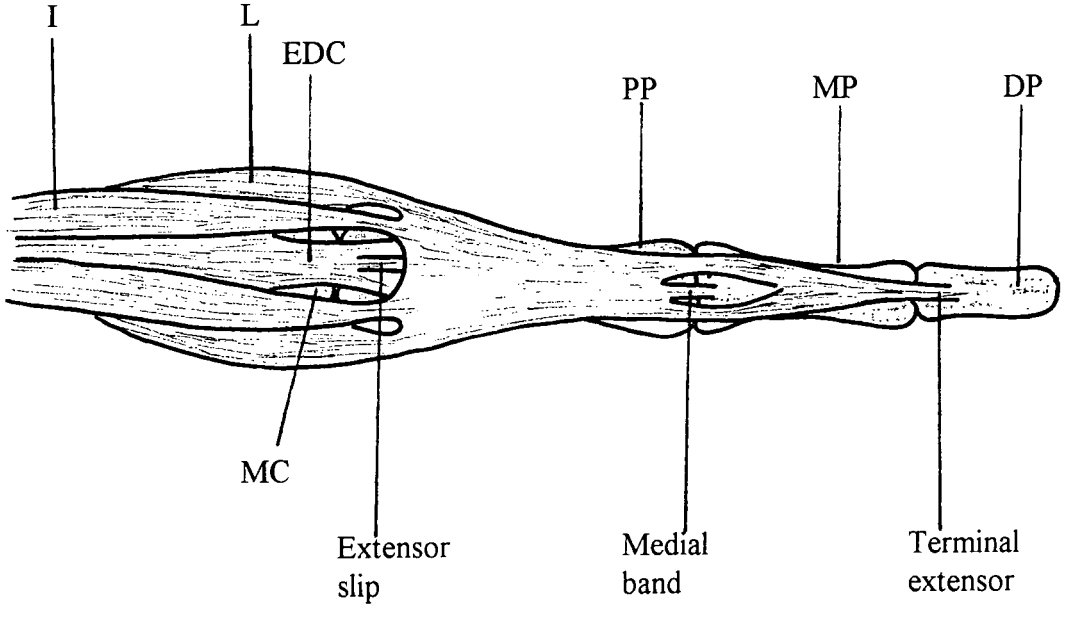

2.1.5.2 Intrinsic finger muscles

The Lumbrical muscles (L) consist of four muscles which originate from the FDP tendon and insert on the EDC tendon extending the IPJs. The Interossei muscles (I) consist of four dorsal muscles (DI) and three palmar muscles (PI). They originate from the sides of the metacarpals and insert on the proximal phalanges The dorsal muscles abduct and the palmar muscles adduct the fingers away from and towards the middle finger. The Lumbrical and Interossei muscles can also flex the MCPJs and extend the IPJs due to their origin on the metacarpals and partial insertion on the EDCs. They can also extend the middle and distal phalanges. The Abductor digiti minimi abducts the little finger away from the ring finger spreading the fingers and the Flexor digiti minimi brevis flexes the little finger at the MCPJ. The Opponens digiti minimi draws the little finger across the palm to meet the thumb which is known as opposition.

2.1.5.3 Muscle roles in hand function

There are four types of muscle roles during hand function. These are agonists, antagonists, synergists and fixators, although a muscle may have more than one role during a single hand function. Agonists, or prime movers, contract to cause the required hand action. Antagonists act in opposition to the prime mover producing counterbalancing moments and reducing subluxation forces. Synergists act to reduce unwanted movement and fixators stabilise the origin of the prime mover. They help the prime mover act more efficiently. Antagonists and synergists stiffen the joint for control purposes increasing the joint contact force and joint stability[13]. An example for the hand would be during flexion where the flexors act as prime movers, the extensors as antagonists and the interossei and lumbricals act as synergists.

Hand function requires strength and stability with the extrinsic and intrinsic tendon forces, constraining forces and joint contact forces balanced[14]. The constraining forces acting on the joint are exerted by the volar plate, collateral ligaments, palmar ligament and other soft tissues surrounding the joint. Extrinsic tendons transmit the large forces required for pinch and grip hand functions. Intrinsic muscles perform the fine positioning of the fingers and contribute less to the overall strength of the hand. The Interossei muscles position the pulps of the fingers. The Lumbrical muscles act as a feedback system between the flexor and extensor systems by modifying the relative tensions between them about the IPJs[15]. Any disturbance of the force bearing structures of a joint can cause a reduction in strength and stability, and result in reduced hand function.

2.2 Biomechanics of the finger joints

2.2.1 Range of motion

The MCPJs have two degrees of freedom allowing active motion in flexion-extension and abduction-adduction. A small amount of passive rotation about the transverse plane and gliding is also permitted. The range of motion is typically 0-100° of flexion, 0-45° of hyper-extension and 0-60° of abduction-adduction, although movement in abduction-adduction depends on the amount of flexion of the joint. It is at a maximum in extension and virtually zero in full flexion[16]. The IPJs have one degree of freedom allowing active motion in flexion-extension only accompanied by small amount of passive rotation and gliding. The range of movement is typically 0-90° and 0-100° of flexion for the DIPJ and PIPJ respectively.

2.2.2 Centre of rotation

The mechanical advantage of a joint is dependent on the position of the centre of rotation of the joint relative to the forces that act on the joint. There has been more work reported on the position of the MCPJ centre of rotation than the PIPJ, however, both have been open to debate. Some authors found that the centre of rotation of the MCPJ is constant[16-20] by successfully matching the path of motion or geometry of the PP head and MP base to the arc of a circle. However, others have reported that the MCPJ has a varying centre of rotation[21-24]. There has also been some debate over the conformity of the MCPJ which can influence whether the centre of rotation is constant or not. Some authors reported that the PP base had a greater radii than the MC head[20,56] whilst others did not find a significant difference in radii indicating that the MCPJ is conforming[19].

As far as the PIPJ is concerned Landsmeer[25] stated that the centre of rotation of the PIPJ moves volarly during flexion. However, it was reported by Kuczynski[26] that during flexion of the PIPJ from the fully extended position the collateral ligaments soon became tight as they passed over the apex of angulation of the side margin of the PP head. They remained tight as they moved over the more vertical plane of the side of the head with increased flexion. Most of the joints analysed did not exhibit a cam effect implying that the radius of curvature remains constant soon after the apex of angulation. Leibovic[27] also reported that the PIPJ centre of rotation does not change measurably over the range of motion of the joint.

The PIPJ has only been observed to be non-conforming, the PP base radii of curvature in the sagittal plane being greater than that of the MP base[27,28]. The non-congruous surfaces allow additional movements other than flexion-extension to take place such as abduction-adduction and rotation. This lack of conformity may indicate a varying centre of rotation of the joint, however, this will depend on the degree of non-conformity of the bearing surfaces and the forces acting on the joint.

2.2.3 Inter-relationships between the MCPJs, IPJs

The movement of the PIPJs and DIPJs is related due to the flexor and extensor systems which pass across both joints. This causes the joints to move synchronously in flexion-extension[29]. The DIPJ angle is dependent on the PIPJ angle[18]. Retinacular ligaments encourage the synchronous motion between the PIPJs and the DIPJs, with the amount of flexion supposedly in a ratio of 2:1 respectively[15]. The retinacular ligaments run from the flexor tendon sheaths on the proximal phalanx to the terminal tendon on the distal phalanx linking movement of the DIPJs and the PIPJs[30]. The range of movement of the MCPJs and PIPJs is also inter-related. With greater flexion of the MCPJs, the PIPJs range of movement increases. This relationship is influenced by the centres of rotation of the joints and the flexor and extensor systems that act across the two joints[18].

2.3 Arthritis of the finger joints

The hands are both strong and manipulative to perform both power and precision activities. They are used for communication not only between individuals, but also between an individual and the environment. In addition, they are on constant show. They are an essential part of everyday life. This is why arthritis of the finger joints can be so devastating. It can prevent a person from carrying out even simple everyday activities such as washing, grooming and toilet, which many of us take for granted. Functional aids can be used to make some tasks easier, however, in the most severe cases a person can lose their independence.

The main form of arthritis that affects the MCPJs and PIPJs is rheumatoid arthritis (RA), although these joints can also be affected by osteoarthritis (OA). As previously mentioned arthritis can cause painful, swollen joints, and the joint range of motion and hand strength may be significantly impaired. In severe cases the hands can also become cruelly deformed. There are inherent ulnar and volar forces acting on the MCPJs due

to the positioning and lines of action of the tendons. These are normally resisted by the joint capsule and ligaments surrounding the joint. The collateral ligaments are particularly important for maintaining alignment of the joints. However, when these structures are weakened or stretched, due to the effects of arthritis, deformity of the joints can occur. The tendons may also become displaced which further adds to the imbalance of forces on the joint. Volar or palmar subluxation and ulnar deviation can occur at the MCPJs, and Boutonniere or Swan-neck deformity can occur at the PIPJs (Figures 2.4 and 2.5).

2.4 Previous finger joint prosthesis designs

Several different methods have been described in Chapter 1 which are used in the treatment of arthritic joints. These included drug and physiotherapeutic treatments, synovectomy, soft-tissue reconstruction, arthroplasty, arthrodesis and total joint replacement. Due to the functional limitations of arthrodesis, total joint replacement is generally used for treating the MCPJs and PIPJs at the late stage of arthritis. Many attempts have been made in the past to produce an artificial finger joint that provides long-term correction of deformity, pain relief and some degree of restoration of hand function. There have been four main generations of MCPJ and PIPJ prostheses (Figure 2.6). This section briefly describes some of the designs, their achievements and the complications that were encountered especially long-term. These are then discussed further in Section 2.5.

2.4.1 First generation artificial finger joints

First generation artificial finger joints consisted of two-piece metallic hinges (for example the *Brannon and Klein*[8] and the *Flatt* joint prostheses[31]). The hinges were joined together with a screw, which formed the axis of rotation. They allowed movement in flexion-extension only, which was functionally limiting for the MCPJs. They achieved pain relief, joint stability, correction of deformities and an improvement in hand function and cosmetic appearance[8,32-36]. Increased hand strength was also reported for the *Flatt* joint prosthesis[33,34,37].

Fixation was achieved by the stems impinging on the medullary canal walls, however, this proved to be inadequate. The *Brannon and Klein* joint prosthesis had single, triangular-pronged stems which proved to be rotationally unstable[8,31,32,38], and stapling was later used to improve fixation[8]. The *Flatt* joint prosthesis had two-

Figure 2.4 Ulnar deviation and Volar subluxation of the MCPJs

a) Ulnar deviation

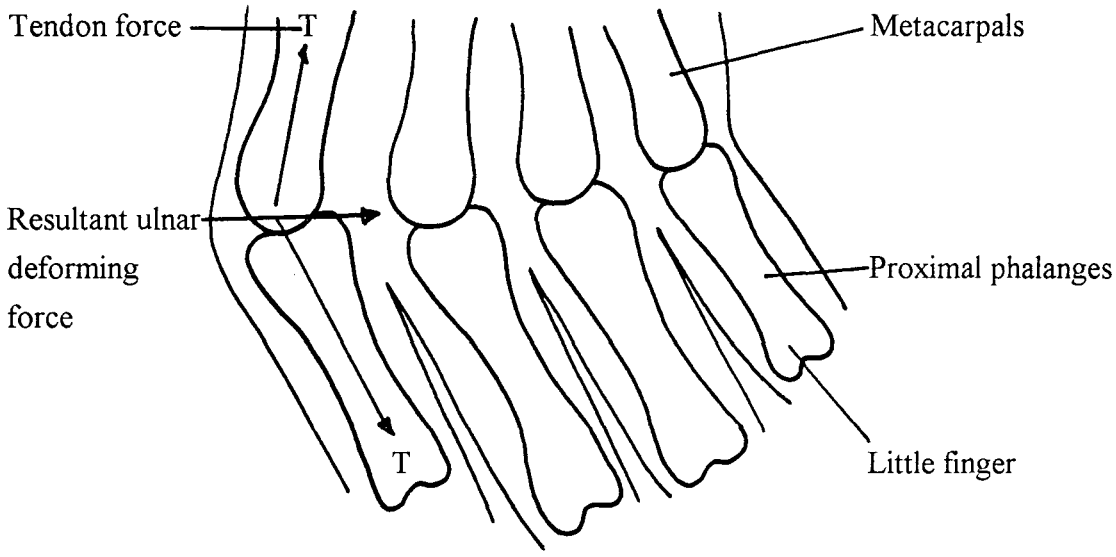

b) Palmar subluxation

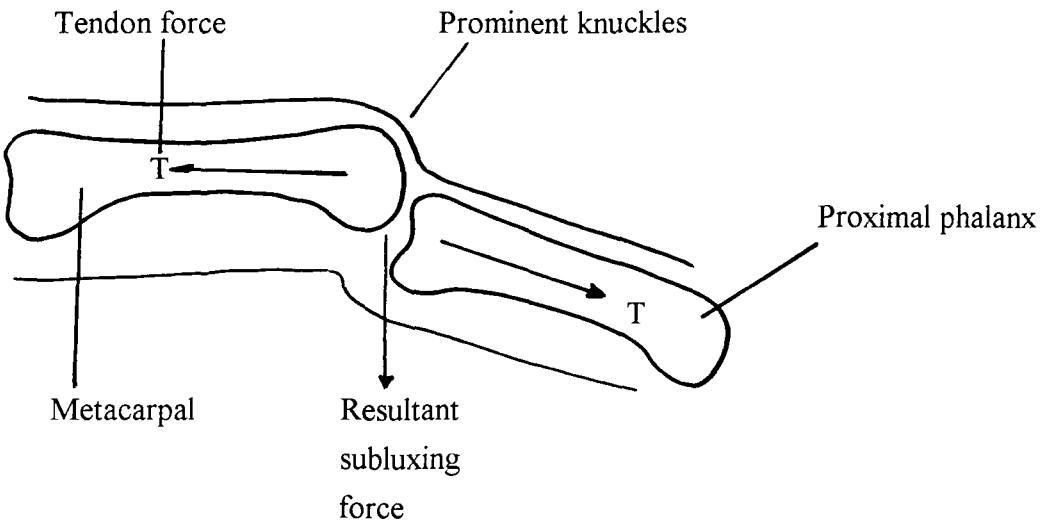

Figure 2.5 Boutonniere and Swan-neck deformities of the PIPJs

a) Boutonniere deformity

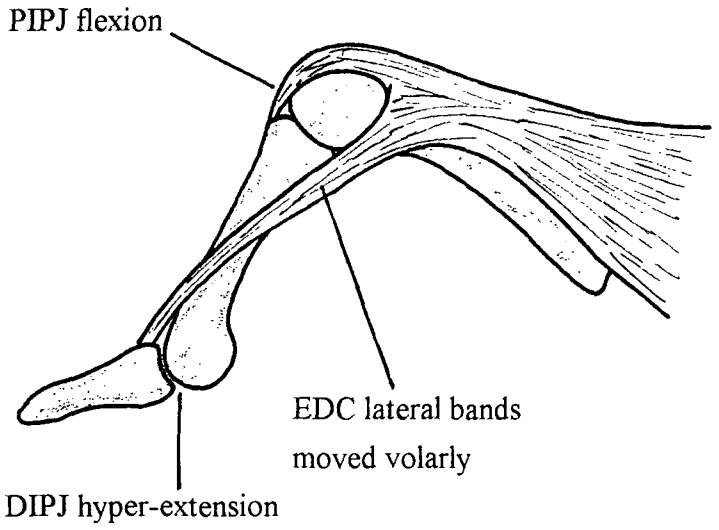

b) Swan neck deformity

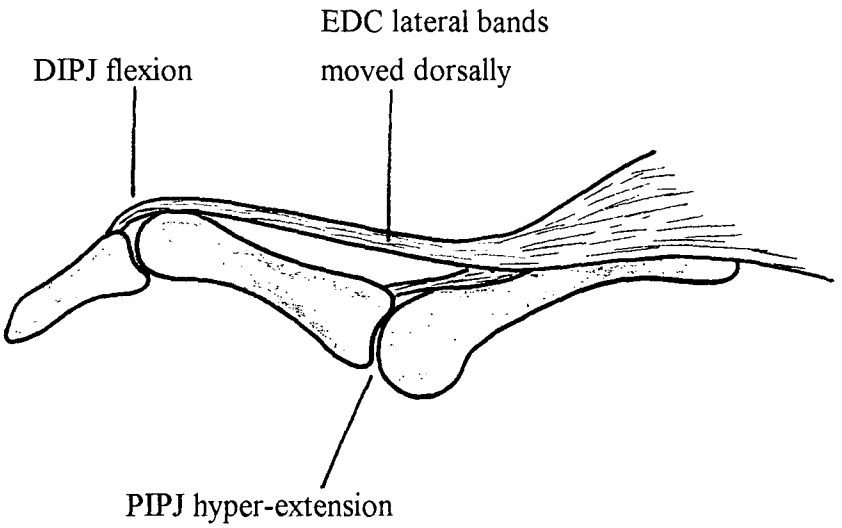

Figure 2.6 Previous finger joint prostheses designs

Brannon and Klein

Titanium two-piece hinge

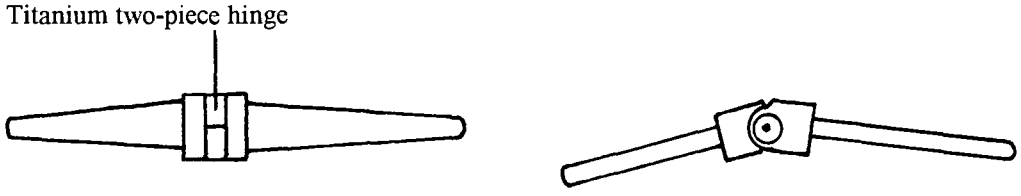

Flatt

Stainless steel two-piece hinge

Calnan and Reis

Polypropylene integral hinge

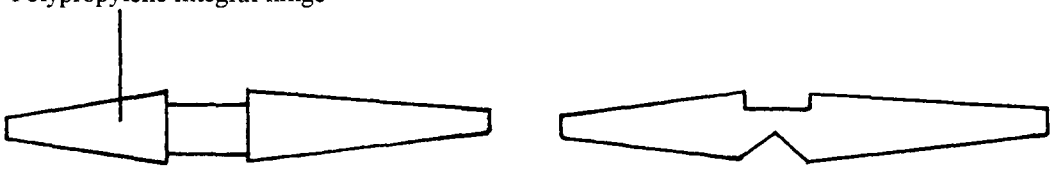

Nicolle and Calnan

Polypropylene integral hinge

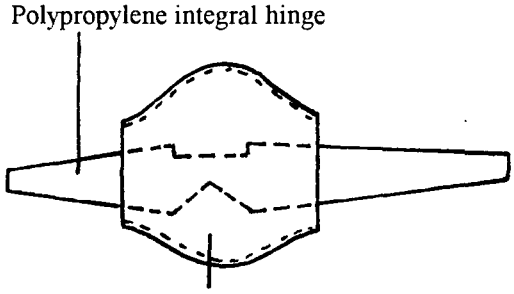

Silicone elastomer capsule

Swanson

Silastic integral hinge

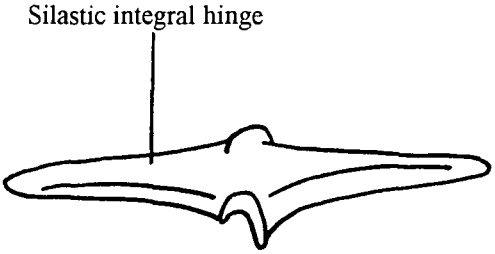

Griffiths and Nicolle

Hemi-spherical silicone rubber capsule

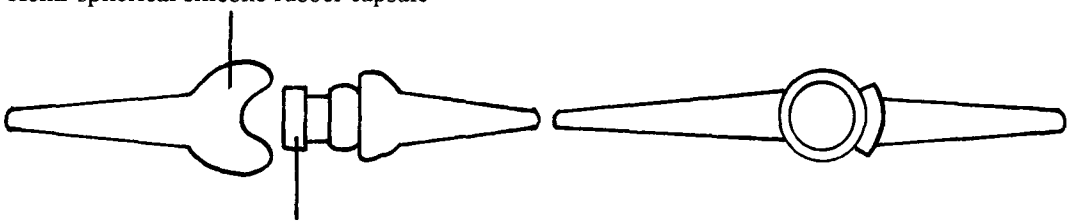

Convex stainless steel component

pronged stems, which were designed to allow the growth of bone and fibrous tissue between the prongs to improve fixation[31]. However, the joint prosthesis was still rotationally unstable[32,34,35,38].

Both the MCPJ and PIPJ ranges of motion decreased post-operatively, and further with time. However, the arc of motion was in a more extended arc, allowing the hands to open more and improving hand function[8,32-34]. In addition, after MCPJ replacement with the *Flatt* joint prosthesis, the PIPJs were able to move through a greater range of motion[18,34]. The centre of rotation of the joint prostheses was originally in line with stems which impeded extension of the joint. However, a redesign of the *Flatt* joint prosthesis with a volar centre of rotation improved active extension and reduced the pre-operative extensor lag of the joint[18,32,34].

The rigidity of the metallic stems and their relative hardness compared with the bone, however, caused complications. Bone resorption caused loosening of the joint prostheses, resulting in sinking and migration into the medullary canals[8,32-37] (although stapling of the Brannon and Klein prosthesis prevented this to some extent[8]). Penetration and fracture of the cortical bone of the shafts occurred where the prongs exerted large forces on the bone[32,37,39]. Screw and prong fracture also occurred due to high stresses exerted on the joint prostheses and resultant metal fatigue[18,32,34,37]. Joint alignment and hand function were improved post-operatively, however, they deteriorated with time, due to failure of the implants, lateral instability, and the progression of the disease causing a recurring imbalance in the tendons leading to recurrent deformities[8,32-36]. Additional complications included screw loosening, fibrosis around, and wear within the hinge mechanism, infection and sloughing off of the overlying skin[8,31,33,34,37].

2.4.2 Second generation artificial finger joints

The lack of range of movement (abduction-adduction and rotation) of the first generation of finger joint prostheses and the complications caused by inserting the rigid metallic hinges into the fingers prompted a second generation of artificial finger joints. These predominantly consisted of one-piece polymer hinges which acted as dynamic spacers. The integral hinges allowed movement in flexion-extension as well as some abduction-adduction and rotational movement. They provided flexibility of the joint whilst keeping the bone ends apart.

The *Swanson* silicone hinge is still the most widely used joint prosthesis today. The rectangular stems were free to piston in the medullary canals whilst still resisting rotation. Fixation of the stems was attempted but caused early breakage. Some bending occurred at the mid-section of the hinge but most occurred at the stems[9,40]. The first two *Calnan and Reis* joint prostheses were not integral hinges but were redesigned to increase lateral stability and make implantation of the joint prosthesis easier. The Mark III implant was a polypropylene integral hinge. It allowed movement in flexion-extension and a small amount of lateral and rotational movement. Discoid, and later rectangular cross-sectional shaped stems were used to achieve rotational stability of the implant. However, rigid fixation was not achieved by the shape of the stems alone, so they were notched and wedged into place by cement. The cement prevented movement which reduced pain and bone resorption, but made revision difficult[38,41,42].

The *Nicolle and Calnan* joint prosthesis was developed from the Calnan and Reis joint prosthesis. It consisted of a polypropylene hinge encapsulated in a ball of silicone elastomer, which prevented fibrosis around the hinge and maintained joint space. It also eliminated the need for cement fixation due to the support of the capsule against the bone ends[39]. The *Nicolle and Calnan* joint prosthesis was also redesigned though, by *Griffiths and Nicolle*, due to problems of instability, lack of resistance to compressive and torsional loads, tearing of the capsule and stem fracture[43-45]. The polypropylene hinge was replaced by a stainless steel cylindrical bearing in a polypropylene socket, and was surrounded by a more durable hemi-spherical silicone capsule.

The *Niebauer-Cutter* silicone integral hinge was reinforced with a core of Dacron-fibre mesh and the stems were also surrounded with Dacron-fibre mesh. Interference fixation was aided by growth of bone and fibrous tissue into the mesh. The two-block mid-section was connected by a thin hinge with a volar centre of rotation with respect to the stems. Lateral buttresses were also included to increase stability and to prevent migration of the implant into the medullary canals[46,47]. Additional second generation joint prostheses included the *Sutter* silicone hinge, and the *Kessler* silicone implant which was reinforced with Dacron-fibre and replaced just the MC head[48].

Second generation finger joint prostheses have generally been reported to achieve good results post-operatively with few complications, although some deterioration in the joint performance occurred long-term. They provided pain relief, correction of joint deformities and improved hand function and cosmetic appearance of the joints[10-

Figure 2.6 Previous finger joint prostheses designs (continued)

Niebauer-Cutter

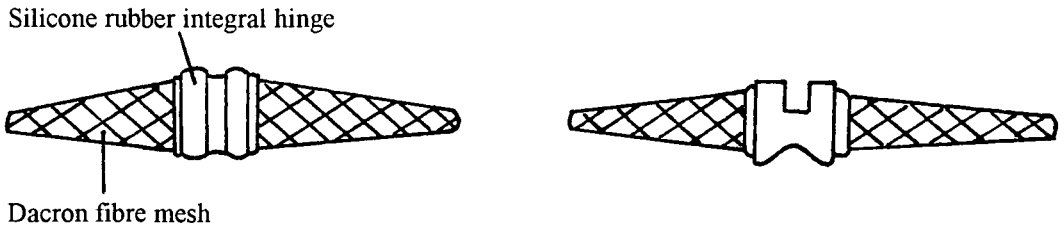

Steffee Mark III

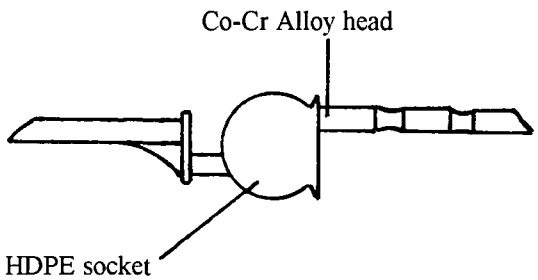

Schetrumpf

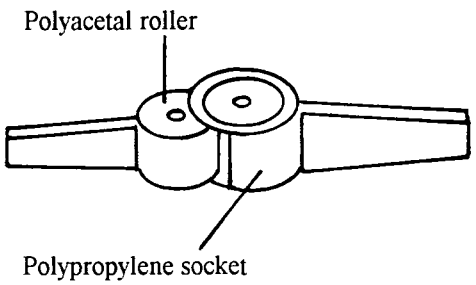

St Georg

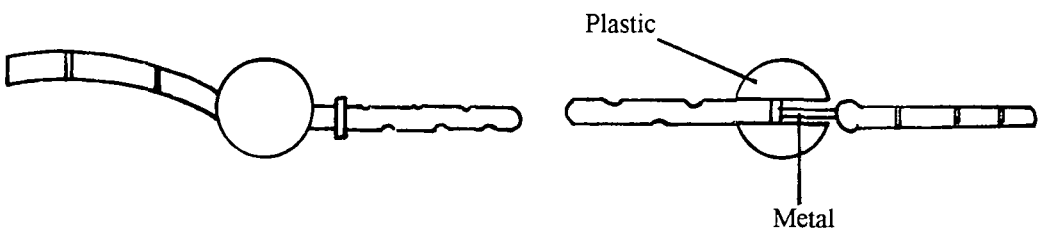

Link

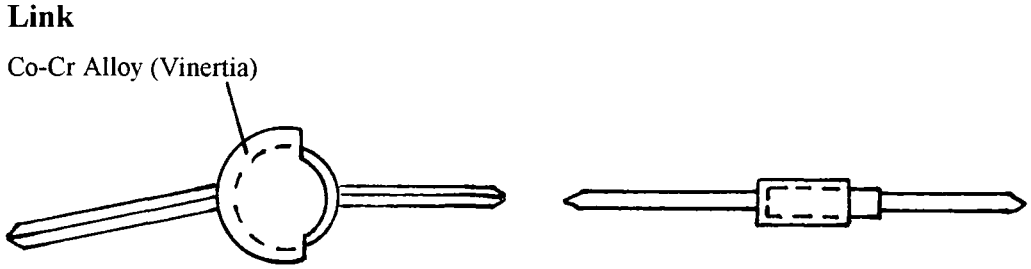

Alumina-ceramic

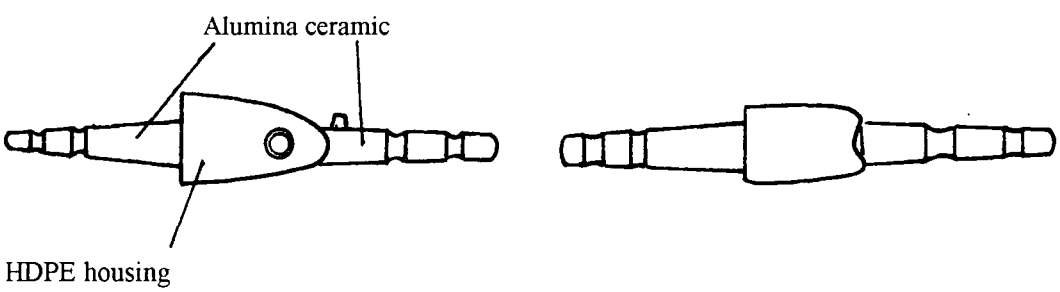

[12,39,40,45,46,48-57] (although some residual ulnar deviation occurred with the Niebauer-Cutter prosthesis[49,56]). They gave initial stability to the joints post-operatively[12,46,49,50,52,56], however, long-term stability was dependent on the support of the soft tissues surrounding the joint. A fibrous capsulo-ligamentous structure developed around the joint prostheses, however, the contribution that it had to stability was not agreed on. Some authors claimed that the capsule increased the stability of the joint long-term[9,38,41,42,57]. However, others claimed that the capsule gave little or insufficient stability to the joint[47,58].

Joint range of motion was reported to either remain constant or increase post-operatively, and in some cases it was in a more extended arc improving hand function[10-12,39,40,43,45,49,50-52,55-57]. However, joint mobility and hand function decreased with time[43,49,51,55,57]. This was attributed to fibrosis around the hinge mechanism for the Calnan and Reis design[55] which prompted the design of the *Nicolle and Calnan* encapsulated joint prosthesis[39]. The reported effect on strength varied between authors. Some found no increase in strength post-operatively[51,53], however, others found it to increase significantly[11,12,44,45,52]. It was hypothesised that the lack of strength was due to the alteration in the balance of the tendons, alignment of the joint and the crude joint substitute.

Complications included fracture of the joint prostheses either at the hinges or at the stems near the hinges caused by the large forces imposed on the implants[10-12,40,43,49,50,52,54,57,58]. However, fractured joint prostheses still acted as dynamic spacers. Bone resorption also caused implant loosening, instability, recurrence of deformities, buckling, dislocation and migration of the joint prostheses[10-12,39,40,43,47,49,50,57,58].

2.4.3 Third generation artificial finger joints

Although second generation prostheses were reported to produce good post-operative results, the problems of fracture and instability of the integral hinges prompted a third generation of artificial finger joints. These showed a move back to the two-part hinge concept of the first generation, however, the bearing surfaces were generally made from dissimilar materials such as a metal and polymer combination. In addition, many of the joint prostheses allowed movement in directions other than flexion-extension. Fixation was achieved by either by the use of cement (for example the *Steffee*, *St Georg*, *Link*, *Schultz* and the *Strickland* joint prostheses), or by interference of the stems with the

medullary canal walls (for example the *Mathy*, *Schetrumpf* and *Alumina ceramic* joint prostheses).

There were three *Steffee* joint prostheses. Mark I was designed with the centre of rotation in line with the stems, which resulted in an extensor lag and a poor range of motion. Mark II was designed with a volar centre of rotation compared with the line of the stems, but the joint prosthesis had problems of bone resorption, loosening, migration and perforation of the cortex by the distal stem. Hence Mark III was designed with a longer distal stem to improve fixation and disperse the force of the stem on the distal shaft bone. Thin collars were also used to locate the joint prosthesis against the bone ends, preventing migration of the implant and cement from welling out of the shafts of the bones. The joint prosthesis allowed movement of flexion-extension, abduction-adduction and rotation[29,59,60].

The *St Georg* joint prosthesis had a plastic MC component which consisted of a grooved stem attached to hollow sphere. A mid-line slot guided the metal ball end of the PP component. The two parts were connected with a transverse spindle. The centre of rotation was volar with respect to the line of the stems[59,61]. The *Mathy* joint prosthesis consisted of two plastic components and allowed movement in flexion-extension and some lateral and rotational movement. The *Link* joint prosthesis consisted of a two-piece vinertia® self-locking hinge. The PP component had a flat disc which fitted into a hollow flat cylindrical MC component[62]. The *Schetrumpf* joint prosthesis was similar to the *Link* joint prosthesis except that it was made from plastic. The MC socket had projections on the lateral walls which fitted into depressions in the PP roller. The centre of rotation was volar with respect to the line of the stems. Movement was restricted to flexion-extension only[63].

The *Alumina-ceramic* joint prosthesis consisted of a high density polyethylene (HDPE) bearing with alumina ceramic stems designed to reduce the risk of stem fracture. The joint prosthesis allowed flexion-extension and some abduction-adduction. However, the centre of rotation was in line with the stems which caused an extensor lag[64,65]. The *Strickland* joint prosthesis consisted of a metal on plastic hinge. It allowed flexion-extension and some abduction-adduction which decreased with increased flexion, simulating that of the natural joint[59]. Further third generation designs were described by *Schultz* (which consisted of a metal PP ball in a plastic MC socket)[59,65,66] *Weightman*[67] and *Walker*[61]. In addition, *Linscheid*[66] designed a two-piece, metal-on-plastic hinge specifically for the PIPJ.

Figure 2.6 Previous finger joint prostheses designs (continued)

Schultz

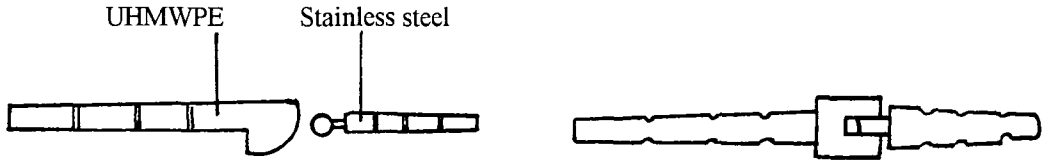

Strickland

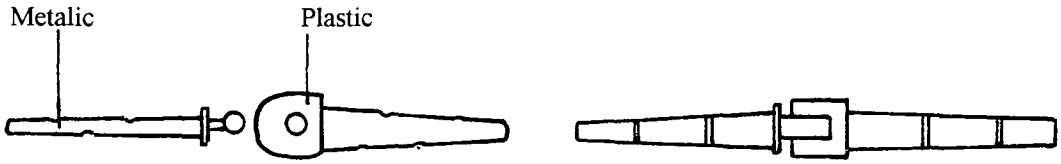

Linscheid

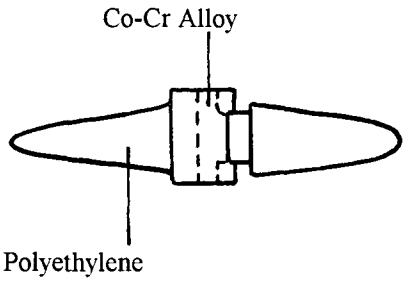

Welsh

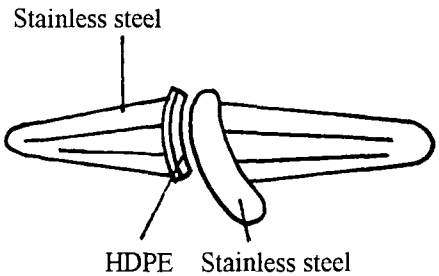

Beckenbaugh

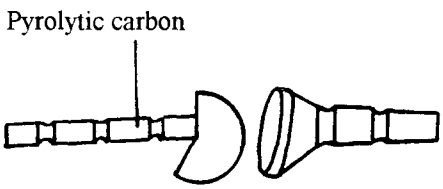

Hagert

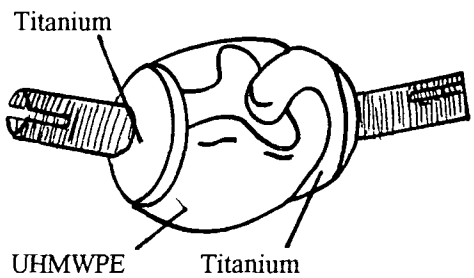

Varian (PIPJ)

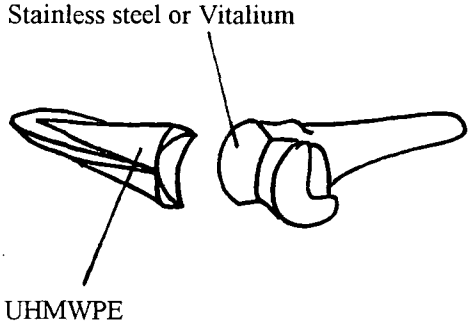

Durham (MCPJ)

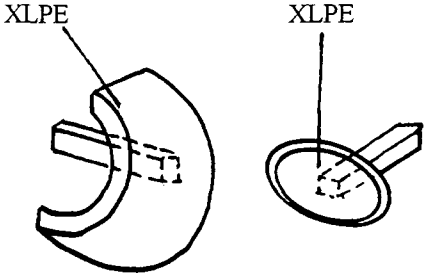

Third generation finger joint prostheses generally provided stable, pain free joints. Deformities were on the whole corrected which improved hand function and cosmetic appearance[60,62-65]. However, some residual ulnar drift at the MCPJ was reported for the *Steffee* joint prosthesis[60,61] and recurrence of deformities occurred for some of the joint prostheses in the long-term[60,65,66]. Range of motion remained constant or decreased, although it tended to be in a more extended arc post-operatively which improved hand function. It was also more controllable due to an increase in joint stability. However, it decreased in the long-term due to fibrosis around the hinges stimulated by moving parts of the joint prostheses being in close contact with surrounding tissue[60-62,65,66]. The effect on hand strength varied. An increase in hand strength was reported with the *Schetrumpf* joint prosthesis[63]. However, there was no measurable improvement in grip strength with the *Steffee* joint prosthesis[60,61] and there was a progressive decline in key pinch and grip strength with the *Schultz* joint prosthesis[65].

Complications with the use of cement included loosening at the bone-cement interface, causing pain, and removal problems for revision. In addition, a large amount of bone was resected for implantation of many of the joint prostheses making revision difficult. Implant fracture occurred and deformation of the plastic components was experienced[59,60,66,67], for example the Schultz metallic PP component exhibited neck fracture[65]. The *Schultz* joint prosthesis also caused extensor tendon re-dislocation which resulted in recurrence in deformities and the fingers returned to a more flexed position. Additional complications with the third generation designs included hinge dislocation and infection[60,62,64-66].

2.4.4 Fourth generation artificial finger joints

The first three generations of finger joint prostheses were rather clumsy in that they generally required the removal of most of the joint, which affected the attachment of the soft tissues surrounding the joints, and they were not anatomically correct. Hence the most recent fourth generation of artificial finger joints was developed to replace just the bearing surfaces with an anatomically correct joint prostheses. Minimal bone resection was required which preserved the attachment of the soft tissues surrounding the joint. It also allowed revision or the implantation of a more constrained device at a later date if necessary. The unconstrained/semi-unconstrained implants allowed natural joint movement and acted as spacers keeping the bone ends apart. They had virtually no intrinsic stability and relied on soft tissue support, hence soft tissue reconstruction

accompanied implantation. These prostheses were not suitable for grossly deformed joints or for cases where soft tissue reconstruction could not be achieved.

The *Welsh* MCPJ prosthesis consisted of stainless steel MC and PP components with a phalangeal HDPE button insert which articulated with the MC head. The MC head had a large volar protrusion to increase stability against volar subluxation. The two components were pressed into the bone ends without the need of cement for fixation[68]. The *Beckenbaugh* MCPJ prosthesis was made from pyrolytic carbon and had conforming spherical surfaces. However, it required the complete resection of the MC head which moved away from the ideal of minimal bone resection. It also had no intrinsic stability except a small amount of anterior-posterior support provided by the deep ball and socket joint[69].

The *Hagert* MCPJ prosthesis consisted of an ultra high molecular weight polyethylene (UHMWPE) MC head and a titanium PP socket, with two parallel levers each carrying a hemi-spherical wart. The joint prosthesis allowed flexion, lateral movement and simulated rotation from the warts being guided along the slots during flexion. The two components had hollow screw stems and fixation was achieved from interference of the screws with the medullary canals and bone in-growth around the screw[70]. The *Leeds* MCPJ prosthesis consisted of a MC convex spherical head and a PP concave base. The centre of rotation was volar with respect to the line of the stems. The MC component had a rectangular cross-sectional shaped stem to resist rotational movement of the joint prosthesis, whilst the PP component had a round cross-sectional shaped stem to ease manufacture. The stems were tapered to produce interference fixation with the medullary canal walls.

Varian designed a surface replacement prosthesis specifically for the PIPJ. It allowed movement in flexion-extension only. Fixation was achieved using cement. The metallic PP head had a concave V-shaped cross-section with a protrusion on the dorsal surface to prevent hyper-extension. The UHMWPE MP base had a convex V-shaped cross-section which conformed with the PP head. The axis of rotation was positioned volar to the line of the stems ensuring that the ligaments remained tight around the joint throughout the range of motion. This was necessary for stability of the joint[71].

The *Durham* MCPJ prosthesis was made entirely from cross-linked polyethylene (XLPE). It consisted of a hollow convex MC head and a conforming, concave PP base. The centre of rotation was volar with respect to the line of the stem. The MC component had a flat on the volar side to increase its rotational stability. The lateral

sides were also angled so that they did not impinge on the soft tissues surrounding the joint. The PP component was oval in the transverse plane to fit within the natural recess of the PP base and resist rotation. Fixation was achieved by the interference fit of square cross-sectional shaped stems with the medullary canal walls[72,73].

Few clinical trials have been completed on fourth generation finger joint prostheses hence their long-term performance is unknown. However, stable, pain free joints were achieved four years after surgery for the *Welsh* joint prosthesis[68]. The *Beckenbaugh* joint prosthesis achieved good biological fixation, mobility, and ulnar stability. However, recurrent deformity and dislocations were also reported[69]. Finally the *Hagert* joint prosthesis provided a satisfactory range of movement and grip function, with no signs of impaired function, although one case of implant fracture did occur[70].

2.5 Joint prosthesis design considerations

From the analysis of previous finger joint prosthesis designs and performances, much can be learnt and utilised in the development of new designs. The following section discusses some of the design considerations that need to be addressed, and how previous joint prostheses have failed or succeeded in satisfying them. The considerations can be divided into three main groups, namely joint prosthesis, surgical and patient considerations, as follows:

Joint prosthesis considerations

* Joint size and architecture
* Planes of motion
* Range of motion
* Mechanical advantage
* Stability
* Biomaterial
* Fixation
* Revision
* Lubrication
* Contact stress
* Manufacture

Surgical considerations

* Surgical technique
* Tooling
* Surgical time

	*	Surgical cost
	*	Sterilisation
Patient considerations	*	Pain relief
	*	Range of motion
	*	Hand strength
	*	Correction of deformity
	*	Cosmetic appearance

2.5.1 Anatomy

Human joints are designed to be as efficient as possible. This involves the shape of the articulating surfaces, and the presence and positioning of tendons and other soft tissues surrounding the joints. An implant should allow a joint to move throughout its natural planes of motion, and also allow the tendons and other soft tissues surrounding the joint to act naturally. The first, second and third generations of artificial joints generally did not satisfy these requirements, which may partly have been the reason why complications arose especially long-term. Fourth generation finger joint prostheses tended to be more anatomically correct and satisfied these requirements more fully.

Arthritis is such a destructive disease that its effects on the finger joints also have to be considered. Simply replacing the articulating surfaces and performing soft-tissue reconstruction may not improve hand function long-term. Fourth generation joint prostheses do allow the joints to function as naturally as possible, but they have little inherent stability and rely on the soft tissues surrounding the joint for joint stability. However, in many cases the ligaments are so badly damaged that they may contribute little to joint stability, and perhaps a more constrained design should be considered.

First to third generation joint prostheses were not anatomically correct and imposed unnatural biomechanics on the finger joints, but they did possess inherent stability. However, in the long-term they tended to fracture which generally led to recurring joint deformities and a reduction in hand function[12,49,52,54,57,60,66,67]. It could be concluded then, that an implant that imposes unnatural biomechanics on a joint will probably fail long-term. This implies that a more anatomically correct joint prosthesis should be used despite its lack of inherent stability. Such a joint prosthesis would require earlier joint replacement, so that the ligaments were still able to attain joint stability. A surface replacement joint prostheses would also be preferable to preserve the attachment of the ligaments surrounding the joint.

2.5.2 Range of motion

The majority of the first to third generation joint prostheses did not produce an increase in the joint range of motion post-operatively, although in many cases the range of motion moved to a more extended arc[10,55,65,66]. This allowed the hands to open more and increased their functional capacity. However, the range of motion decreased long-term due to fibrosis of the hinge mechanisms, fracture and migration of the joint prostheses and a general deterioration in the soft tissues surrounding the joints[43,49,51,55,57].

The lack of range of motion with previous joint prostheses may have been due to the poor condition of the soft tissues surrounding the joint which will not necessarily be improved post-operatively. However, these prostheses did not allow the joints to function in their natural planes of motion which may have impeded the function of the tendons. A more anatomically correct design may allow the tendons to function more efficiently and increase the joint range of motion long-term. (Little information is available on the joint range of motion of fourth generation finger joint prostheses to confirm this theory). Perhaps a long-term improvement in the joint range of motion is unrealistic for joints affected by such a destructive disease. However, by reducing the detrimental effects of the joint prosthesis on the range of motion it may be possible to restore and preserve joint motion for as long as possible.

2.5.3 Mechanical advantage

The mechanical advantage of a joint can be changed by altering the position of the centre of rotation of the joint and the lines of action of the tendons. However, the MCPJs and PIPJs have different mechanical advantages. Hence joint prostheses should be designed specifically for each joint otherwise the mechanical advantage of one or both joints would be compromised. Despite this, however, smaller versions of the MCPJ prostheses have been used in the past for PIPJ replacement. This may be one of the reasons why poorer results have been found for joint replacement of the PIPJs compared with the MCPJs[49].

Early MCPJ prostheses did not simulate the natural mechanical advantage of the joints due to the (incorrect) positioning of the centre of rotation in line with the stems[8,31]. This produced no improvement in the pre-operative extensor lag. Hence the centre of rotation was moved volarly, which increased the extensor tendon moment arm,

allowing the joints to be extended. More recent designs all tend to have a volar centre of rotation compared with the line of the stems.

The question of whether the centre of rotation of the MCPJs and PIPJs is constant or not also needs to be addressed. Some authors reported that the MCPJ centre of rotation moves volarly during flexion or that the surfaces are not conforming which suggests a varying centre of rotation[20-25]. Whereas others reported the opposite[16-20]. The first, third and fourth generations of finger joint prostheses generally assumed a constant centre of rotation. The centre of rotation of the second generation integral hinges may have varied throughout the range of motion, although the extent to which this happened is not clear. If the centre of rotation of the MCPJ does vary then the simplified motion of the previous joint prosthesis would have altered the mechanical advantage of the joint. The same debate should be considered for the design of a PIPJ prostheses.

2.5.4 Conformity

There has been some discussion on whether the MCPJs and PIPJs have conforming bearing surfaces or not. If they are non-conforming and are replaced by a conforming joint prosthesis then additional passive movements may be restricted although stability of the joint will be increased. If, however, they are conforming and are replaced by a non-conforming joint then stability of the joint will be decreased which may impede hand function. Two other factors to consider concerning the conformity of a joint are the contact stress and lubrication.

If the bearing surfaces are conforming then the joint contact force will be distributed over a greater area reducing the stress on the joint prosthesis. If, however, the concave radius of curvature is greater than the convex radius of curvature, the area of contact is reduced and the contact stress increased. Theoretically the contact area would be a point, although deformation of the bearing surface increases this. Nevertheless the contact stress for non-conforming bearing surfaces would be much greater than that for conforming bearing surfaces which may be detrimental to the prosthesis. However, conforming bearing surfaces may prevent lubricant from being entrained between the bearing surfaces producing dry operating conditions and an increase in wear rate. Wear debris trapped between the surfaces could also cause third body abrasive wear and not be able to escape. Non-conforming surfaces, however, would allow lubricant to become entrained between the surfaces and allow wear debris to escape which may reduce the wear rate.

It is obvious that a compromise must be made with respect to the conformity of the bearing surfaces of a joint prosthesis. Conforming surfaces may decrease the joint contact stress and increase stability slightly, however, non-conforming bearing surfaces will not impede additional passive movements of the joint and will allow lubricant to become entrained between the surfaces and allow wear debris to escape. Conforming bearing surfaces have been used in previous finger joint prosthesis designs (excluding the second generation integral hinges) although it is not clear what affect this has had on the performance of the joints.

2.5.5 Fixation

Fixation has been a common problem with previous joint prostheses. The methods of fixation that can be considered are cement, mechanical, interference, bone in-growth and adhesion, although adhesives have not been widely developed for use in the body. In comparison, no fixation was used as with the Swanson joint where the stems were free to piston in and out of the medullary canals[9]. Polymethylmethacrylate (PMMA) self curing cement can be used to lock the stems within the medullary canals (it does not form any adhesion with the stems of bone). The reamed bone cavities do not have to match the contours of the implant stems exactly. High stress concentrations and direct contact between the joint prosthesis and the bone are also avoided. However, as the cement cures its temperature can kill a layer of bone cells which can cause failure between the bone-cement interface and loosening. Cement and bone debris generated during surgery or from loosening can also damage the bearing surfaces increasing the wear rate through three-body abrasive wear. Cement fixation and the associated large amounts of bone resection also make revision difficult. Short-term fixation has been successful, but long-term loosening has occurred due to failure at the bone-cement interface[60,65-67].

Mechanical fixation can be achieved with the use of screws, bolts, pins or staples. Interference fixation is achieved from the stems impinging on the medullary canal walls. The stems may also have fins, barbs or expanding mechanisms to aid interference and resist rotation of the joint prosthesis. In addition, bone in-growth can occur in stems with an uneven surface finish or with porous materials which may improve fixation long-term[46,47]. An accurate hole and good bone stock is required to achieve adequate fixation. Short-term fixation has been successful, however, failure of the fixation has occurred long-term due to bone resorption[8,36,39,43,58].

2.5.6 Biomaterial

A biomaterial should be chosen by its mechanical, physical and chemical properties. It needs to be bio-compatible and able to be sterilised. The joint prosthesis should also produce minimal tissue reaction. Hence the wear of the bearing surfaces and the tissue reaction to the resulting wear debris are important. Other considerations include strength, ductility, hardness and manufacture. Bio-materials which have been used for finger joint replacements include metals (stainless steel, cobalt chrome alloy, titanium alloy), polymers (polyethylenes, silicone, polypropylene) and ceramics. The use of ceramics has been limited but is increasing particularly in hip joints. The choice of biomaterials is discussed further in Section 4.1.5.

First generation joint prostheses consisted of metallic hinges which were designed to correct deformity, impart stability to the joint and restore hand function. However, the hinges and stems tended to fracture due to their rigidity and the forces imposed on them. This was probably also partly due to their poor design. The hardness of metals compared with the bone also caused bone resorption resulting in implant loosening and migration. Perforation of the bone shafts also occurred[8,18,32-34,36,37].

Second generation joint prostheses consisted of one-piece polymer hinges. They aimed to provide a flexible implant whilst still imparting stability to the joint. However, the implants tended to fracture at the hinges or just outside the hinge mechanism due to fatigue and stress concentrations caused by the bone ends and the inherent subluxing forces of the joint. Some bone resorption was also reported despite the relative softness of polymers compared with bone[10-12,39,40,43,47,50,52,54,57,58]. Third generation joint prostheses generally used a combination of metals and polymers due to their low wear and friction characteristics. Implant fracture and deformation of the plastic components have been reported[59,60,66,67]. Fourth generation joint prostheses have also used metal and polymer combinations although few long-term results have been reported.

Previous joint prostheses have tended to fail partly due to the biomaterials used and probably also due to their design. Implant fracture occurred due to the large forces exerted on the joints, and significant bone resorption also occurred due to the high stresses exerted on the bone by the stems, (especially when made from metal). Cement can be used to isolate the bone from the stems, however, the quality and quantity of bone stock in rheumatoid PIPJs may prevent its use. Hence polymer-on-polymer combinations may provide the answer. These have been avoided in the past due to

their poor wear characteristics. However, they were considered in this project due to the development of XLPE, which has shown promising wear characteristics against itself.

2.5.7 Manufacture

Manufacturing costs depend on the material from which the joint prosthesis is made and the complexity of the manufacturing process. The manufacturing process depends on the biomaterial used, the properties required of the final joint prosthesis (strength, surface finish), the design of the joint prosthesis (size, shape, thickness, complexity of part), the required production rate, the cost of tooling and the overall cost of processing. The tooling and set-up costs can be reduced by simplifying the implant design and the number of different sizes of joint prostheses required. Hence as far as a manufacturing point of view is concerned designs should be simple and require a simple manufacturing process, and a minimum range of prostheses and tooling should be made. However, this may not be possible as other design requirements are taken into account. In addition, the range of joint prostheses should cover the whole population otherwise certain patients would be excluded from total replacement surgery.

2.5.8 Patient requirements

The main patient requirements are improvement in hand function, pain relief, correction of deformities and improved cosmetic appearance of the hands (range of motion has been discussed in Section 2.5.2). Previous joint prostheses have succeeded in achieving pain relief[8,32,40,46,60,63,64]. They act as spacers which keep the bone ends apart. In addition, swollen and painful synovium can be removed during the replacement arthroplasty. However, micro-motion between the joint prosthesis and the bone can cause discomfort for the patient. Hence adequate fixation is required to prevent movement or migration of the joint prosthesis.

Maintaining joint length and reducing hand deformities is not only important to the patients self esteem in replacement arthroplasty. It can also preserve soft tissue structures by reducing the stress on the supporting structures and preventing muscle contractures or dislocation of tendons. In the past good alignment and correction of deformity has been achieved with total joint replacement. However, recurrence in deformity seems to be inevitable[10-12,40,43,44,51-57]. This has been due to fracture and/or migration of the joint prosthesis due to the forces imposed on them and the natural progression of the disease. The progression of the disease may not be able to

be halted but soft tissue reconstruction and avoidance of implant failure may preserve the joints for as long as possible.

Hand strength has not always been improved post-operatively[51,53,60,65] and even if this has been achieved it has only been short-term. Again this may be due to the unnatural mechanical advantage imposed on the joints by "clumsy" joint prostheses, and the poor condition of the soft tissues surrounding the joint which were not improved simply by replacing the bearing surfaces of the joint. However, it may also have been due to the type of pinch function used to perform hand tasks pre-operatively and post-operatively. Patients may use key-pinch pre-operatively due to deformity of the hand. However, if the joints are realigned post-operatively then tip-pinch may be used to perform the same task. Tip-pinch is less powerful than key-pinch[75] hence the effective strength of the hand may appear not to improve even though manipulation and hand function may do so. The only influence that a joint prosthesis design may have on hand strength would be to allow the tendons to act in their most efficient plane and to disturb the soft tissues surrounding the joint as little as possible. Once again this implies that an anatomically correct, surface replacement joint prosthesis design may be the optimal design for the finger joints.

2.5.9 Surgical considerations

Ideally a joint prosthesis should be easy to implant and require minimal tooling. This would make the operational procedure as quick as possible which is particularly important as it is common for all of the MCPJs or PIPJs of one hand to be replaced in the same operation. The joint prostheses also needs to be sterilised without deforming the joint prosthesis or changing its mechanical characteristics. Probably one of the simplest finger joint replacement procedures is that for the Swanson integral hinge[9]. The bones are resected and the medullary canals reamed to take the stems of the joint prosthesis. Even though the joint prosthesis is a crude replacement for the MCPJs and PIPJs, and the clinical results are less than ideal, the simplicity of the surgical procedure should be noted.

2.5.10 Additional factors

There are additional factors which may affect the outcome of total joint replacement independent of the joint prosthesis itself. The pre-operative joint performance and condition and that of adjacent joints should be taken into account when assessing whether total joint replacement is suitable. Unstable joints may gain little benefit from

joint replacement and if the adjacent joints are in a poor condition then little may be gained from joint replacement apart from pain relief. The pre-operative condition should also be taken into account when assessing the post-operative joint performance. Comparing the post-operative joint performance of several individuals is not valid unless the pre-operative condition is known.

The surgical technique can also affect the post-operative joint performance. A joint prosthesis may not be aligned correctly between the bone ends which would increase the forces exerted on it by the body and may cause it to fail prematurely. In addition, if too much bone is resected then the joints may become unstable post-operatively. However, if too little bone is resection then joint function may be impeded. This also highlights the need for a range of joint prostheses to cover the variation in joint size of the population. Finally any drug treatments that the patients are receiving should be taken into consideration.

CHAPTER THREE

Dimensions of the proximal interphalangeal joints

3.0 Introduction

Information on the architecture of the PIPJ bones was required to design a joint prosthesis with anatomically shaped bearing surfaces and suitable stems for fixation. However, although the architecture of the MCPJ has been investigated on many occasions, little work has been completed on the PIPJ. Information did exist on the anatomy of the PIPJ bearing surfaces in general and on the soft tissues surrounding the joint. However, very few papers described the shape of the PIPJ bearing surfaces in detail and actual dimensions were very scarce indeed. Hence an in depth study was undertaken on the shapes and dimensions of the PIPJ bones.

3.1 Method

3.1.1 Proximal interphalangeal joint specimens

The PP and MP bones were dissected from 83 PIPJs leaving the articular cartilage intact. The 83 joints came from 21 hands of 11 cadavers (7 males and 4 females) whose average age was 68.27 years (range of 55-81 years). The joints had been preserved in formalin but it was thought that the dimensions of the cartilage and bones would not have been altered significantly by preservation. The ages and sexes of the cadavers are shown in Table 3.1. The left hand PIPJ bones from cadaver 1, all of the bones from cadaver 2 and the left hand, ring finger bones from cadaver 7 were missing. The right hand, little finger PP bone from cadaver 8 and the right hand, little finger MP bones from cadavers 8 and 9 were not used due to damage of the articular surfaces or bony growths around the articular surfaces which distorted the shape of the bone. This may have been caused by OA. Despite all of the PP and MP bones missing from cadaver 2, the cadaveric numbering system was kept the same to correspond with other work completed on the bones. It should be noted that the cadaveric numbering system used in Table 3.1 has been used throughout the thesis.

Table 3.1 Proximal interphalangeal joint specimen details

Cadaver	1	3	4	5	6	7	8	9	10	11	12
Sex	M	M	M	M	M	F	F	M	M	F	F
Age (Years)	55	59	59	65	78	65	80	81	55	79	75

3.1.2 Proximal interphalangeal joint shadowgraphing

The dimensions of the PP and MP bones were measured by shadowgraphing the bones and then measuring the required dimensions from the shadowgraphs. This method was used rather than methods such as magnetic resonance imaging or photography as it was inexpensive, accurate, and the equipment was readily available. Sectioning of the bones was required in the sagittal and transverse planes to produce information on the bearing surfaces across the width of the bone, and on the phalangeal shafts and medullary canals. Hence replicas of the bones were made to allow sectioning in both of these planes. Rubber moulds were made of the bones by covering them with layers of a silicone elastomer (Silcoset). The moulds were then left for 24 hours to cure fully. The silicone elastomer had a linear shrinkage of 0.1%.

Originally the moulds were cut to produce complete bone replicas (Figure 3.1a). Cutting the moulds in this way allowed the bones to be removed without the join of the moulds across the articular surfaces. However, it was not possible to fill the two halves of the mould and then realign them, hence half bone replicas had to be made. The moulds were cut in half (Figure 3.1b) and small lateral slits were made in the moulds to allow the bones to be removed. The slits did not impinge on the articular surfaces of the moulds. Once the bones were removed the slits were sealed, with more silicone elastomer, and the moulds were held vertically. They were then filled with layers of acrylic dental bone cement. This allowed any air entrapped in the replicas to escape and shrinkage of the cement was compensated for as far as possible. A similar method was used by Unsworth[76] in an investigation into the architecture of the MCPJs.

Shadowgraphs were taken of the original bones in the sagittal and frontal planes. The bones were shadowgraphed with the palmar side of the head and base in contact with the shadowgrapher, defined as the longitudinal base-line (Lbl), (Figure 3.2). Further sectioning, shadowgraphing, super-position and measurement of the shadowgraphs were completed with reference to the longitudinal base-line, where appropriate. The original bones were also rotated in the frontal plane from +45° to -45° to shadowgraph the profile of the articular cartilage around the bearing surface (Figure 3.3). It was not possible to shadowgraph the phalangeal heads over a larger range due to the protrusion

Figure 3.1 Silcoset rubber moulds for replica bone preparation

a) Bone mould for one-piece bone model

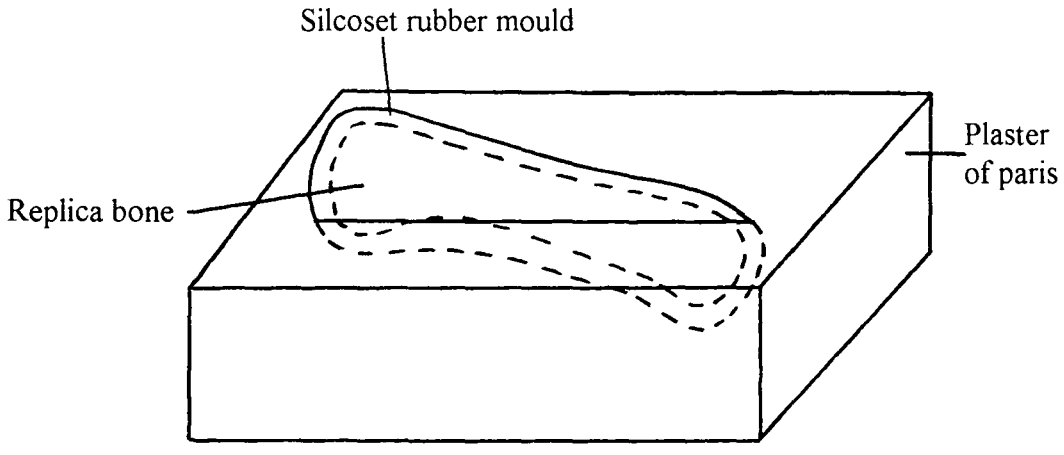

b) Bone moulds for two-piece bone model

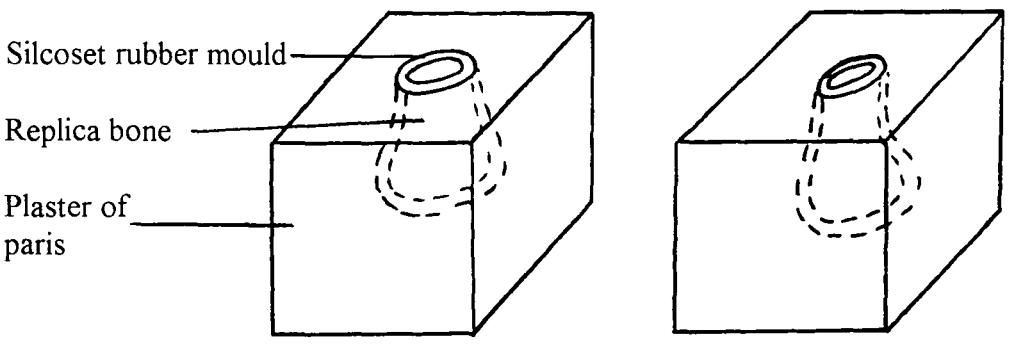

Figure 3.2 Frontal and sagittal plane phalangeal bone shadowgraphing

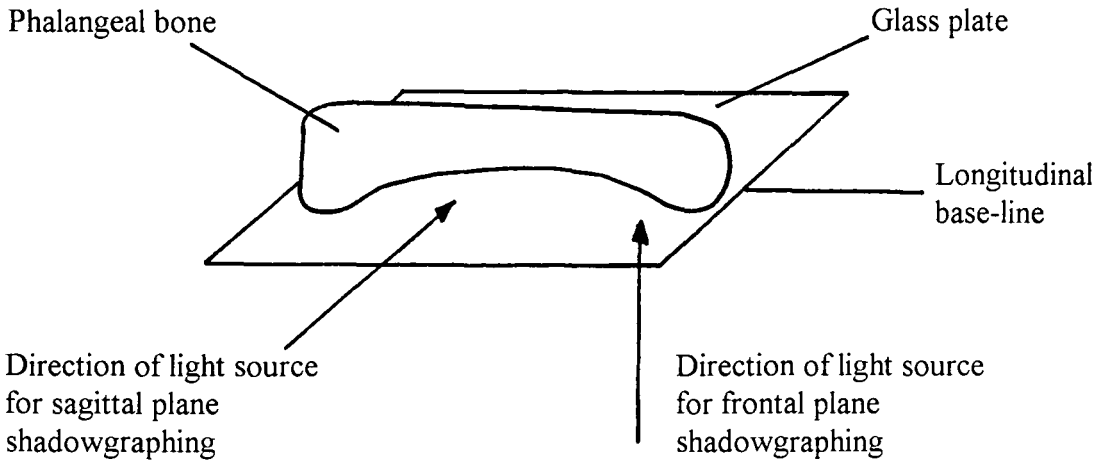

Figure 3.3 Rotation of bones about the frontal plane for shadowgraphing of the articular surfaces of the proximal phalangeal head

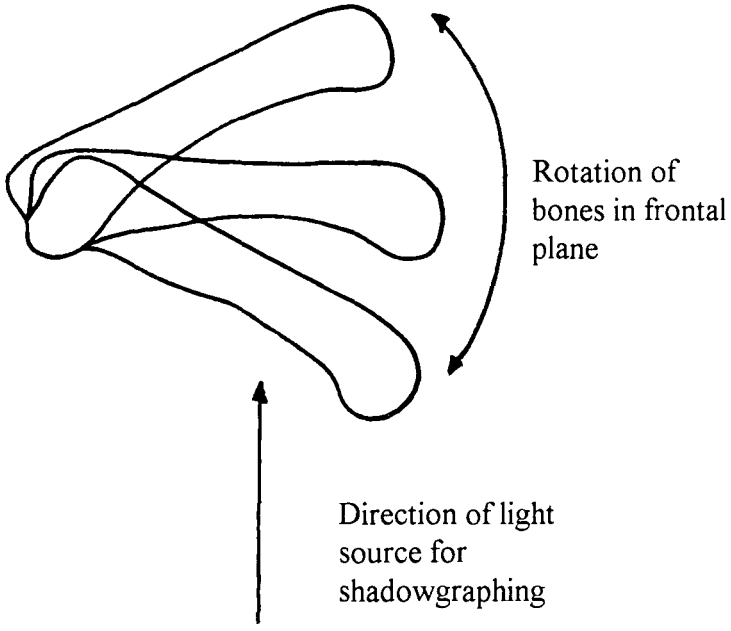

of the phalangeal shaft and base on the shadowgraphs at greater inclinations of the bones.

The original and replica bones were then set in clear plastic to hold the bones in the correct position for sectioning. It also allowed the shadowgraphs of the sections to be re-aligned. The replica bones were sectioned in the sagittal plane (parallel to the longitudinal axis of the bone) with an average section thickness of 0.95 mm. An average thickness of 0.99 mm of material was lost between sections. The original bones were sectioned in the transverse plane (perpendicular to the longitudinal base-line) leaving the PP and MP heads whole (Figure 3.4). The average section thickness was 1.68 mm and the average thickness of material lost between sections was 0.76 mm. The sections were then cleaned, shadowgraphed and the required dimensions measured.

3.1.3 Shadowgraph dimensions

The basic PP and MP dimensions measured from shadowgraphs of the intact bones in the frontal and sagittal planes are shown in Figure 3.5. The bone length (L) and the maximum head width (W) in the frontal plane were measured for the PP and MP bones. The maximum base width (Wb) in the frontal plane was measured for the MP bones. Circles were matched to the PP and MP head profiles in the sagittal plane, and the diameters of the best-fit circles were measured (defined as the head diameter, D). Circles were also matched to the PP and MP heads, and the MP bases of the sagittal sections of the bones. The maximum and minimum condyle head diameters were defined as Dmax and Dmin respectively, and the maximum and minimum base recess diameters were defined as Dbmax and Dbmin respectively. The circles matched to the shadowgraphs were in steps of 0.5 mm.

Ratios were found between the PP and MP lengths, maximum head widths and head diameters. This was to investigate any major differences between the individual fingers and to possibly produce a means of predicting the sizes of joint prostheses required for a patient before surgery commenced. The minimum heights and widths (Tp, Wp, Tm and Wm) and their distance from the PIPJ bearing surface (Lp, Lpw, Lm and Lmw) were also measured for the PP and MP bones respectively. This was undertaken to give an indication of the size of stem required for fixation of the PIPJ prosthesis within the medullary canal. However, transverse sectioning of the bones was also required to measure the actual dimensions of the canal and locate its position within the bone shaft.

Figure 3.4 Sectioning of the original and replica bones

a) Transverse plane sectioning of original bones

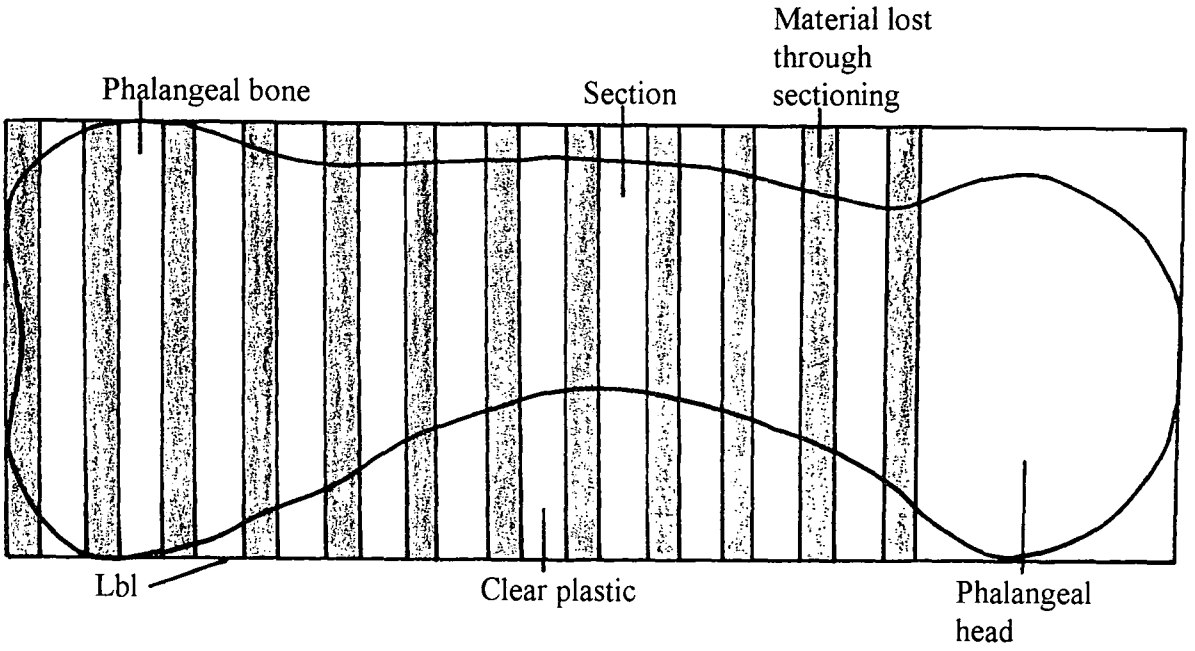

b) Sagittal plane sectioning of replica bones

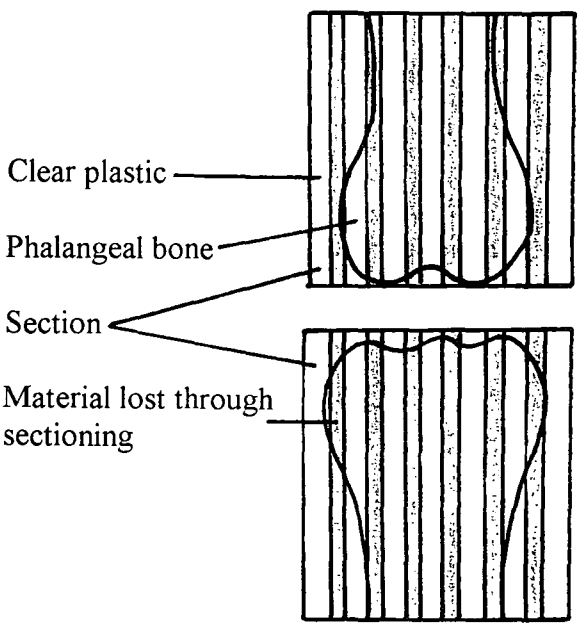

Figure 3.5 Basic phalangeal bone dimensions

A) Sagittal plane

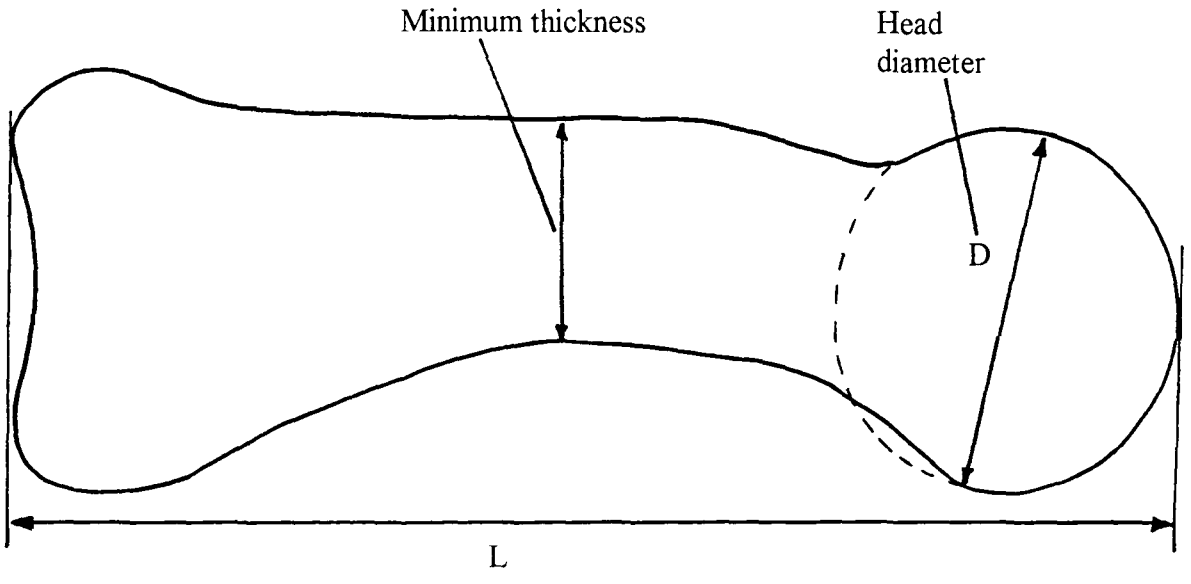

B) Frontal plane

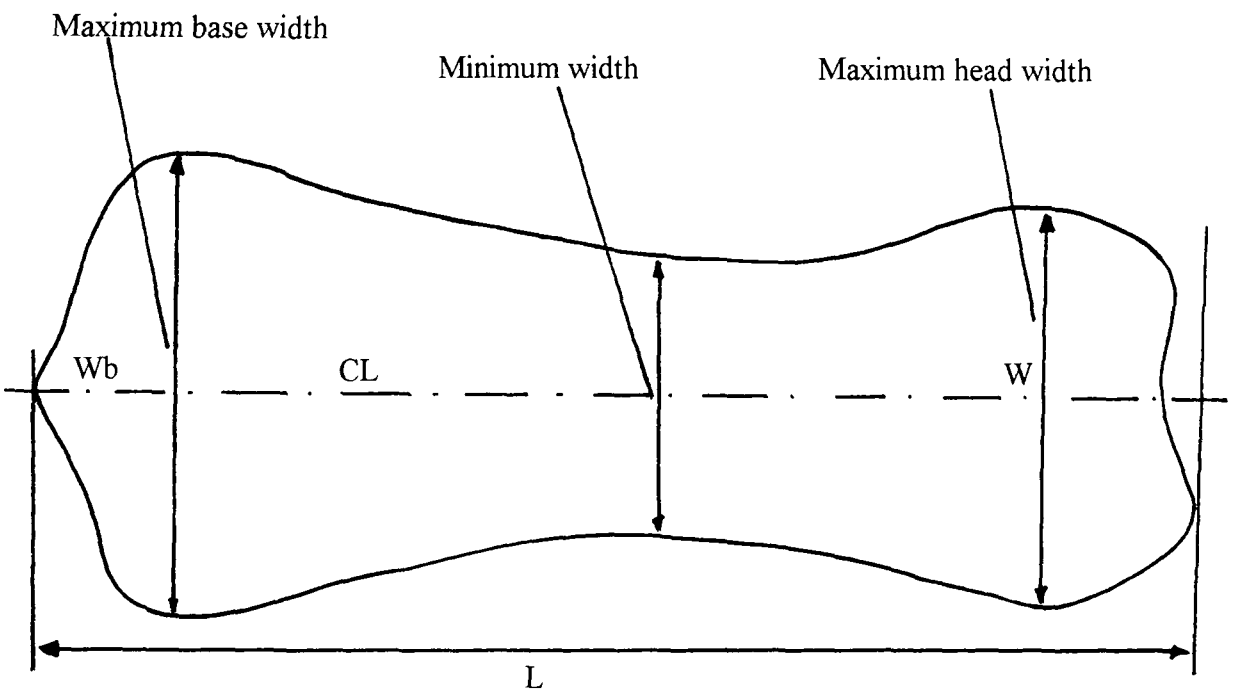

The alignment of the condyles in the frontal plane (θ) was also measured and 0° was taken as the perpendicular to the centre-line of the bone (Figure 3.6).

The dimensions measured from the transverse sections of the phalangeal shafts are shown in Figure 3.7. These dimensions were used to plot the medullary canals on sagittal and frontal plane shadowgraphs of the intact bones (Figures 3.8 and 3.9). The centre-lines of the medullary canal in the sagittal and frontal planes were marked on the shadowgraphs and then compared with the mid-lines of the bones. The longitudinal base-line, dorsal-line and head-line were also marked on the sagittal plane shadowgraphs. The longitudinal base-line was defined as the line between the most palmar aspects of the head and base of the bone (Lbl). The dorsal-line was defined as the line along the main dorsal surface of the phalanx (sagittal plane) and the head-line was defined as the line along the dorsal surface of the bone just proximal to the bone head (sagittal plane).

The angles between the longitudinal base-line, and the dorsal-line (ϕ), the head-line (σ) and the medullary canal centre-line just proximal to the PP head (ρ) were measured (Figure 3.10). Measurements of these angles were concentrated on the PP bones. The PIPJ centre of rotation was defined as the centre of the best-fit circle matched to the PP head on the shadowgraph of the intact bone in the sagittal plane. The centre-line of the medullary canal just proximal to the PP was projected into the PP head and the offset from the PIPJ centre of rotation (c) was measured (Figure 3.10). The distance from the change in angle of the dorsal surface of the PP bone and the PIPJ bearing surfaces (d) was also measured to indicate longest possible stem length for the PIPJ prosthesis.

The PP head was also studied in detail in the transverse plane to provide information on the bi-condylar shape of the articulating surfaces and to make sure that the PIPJ prosthesis would not impinge on the soft tissues surrounding the joint (Figure 3.11). A line was drawn joining the most palmar points of the two condyles and defined as the transverse base-line (Tbl). The PP head centre-line was drawn mid-way between the points of maximum width and was perpendicular to the base-line. Lines were also drawn along the radial and ulnar sides of the condyles between 2 mm from the anterior and posterior surfaces of the head. The angles between the radial and ulnar sides of the condyles and the transverse base-line ($\alpha 1$ and $\alpha 2$) were measured. The distances from the centre-line to the bases of the two condyles (a and b) were also measured as were the overall head height (Htp) and width (Wtp). The inter-condylar sulcus depth was measured in the transverse plane on the anterior face (ISat), and also in the frontal plane (ISf).

Figure 3.6 Alignment of proximal phalangeal head condyles, frontal plane

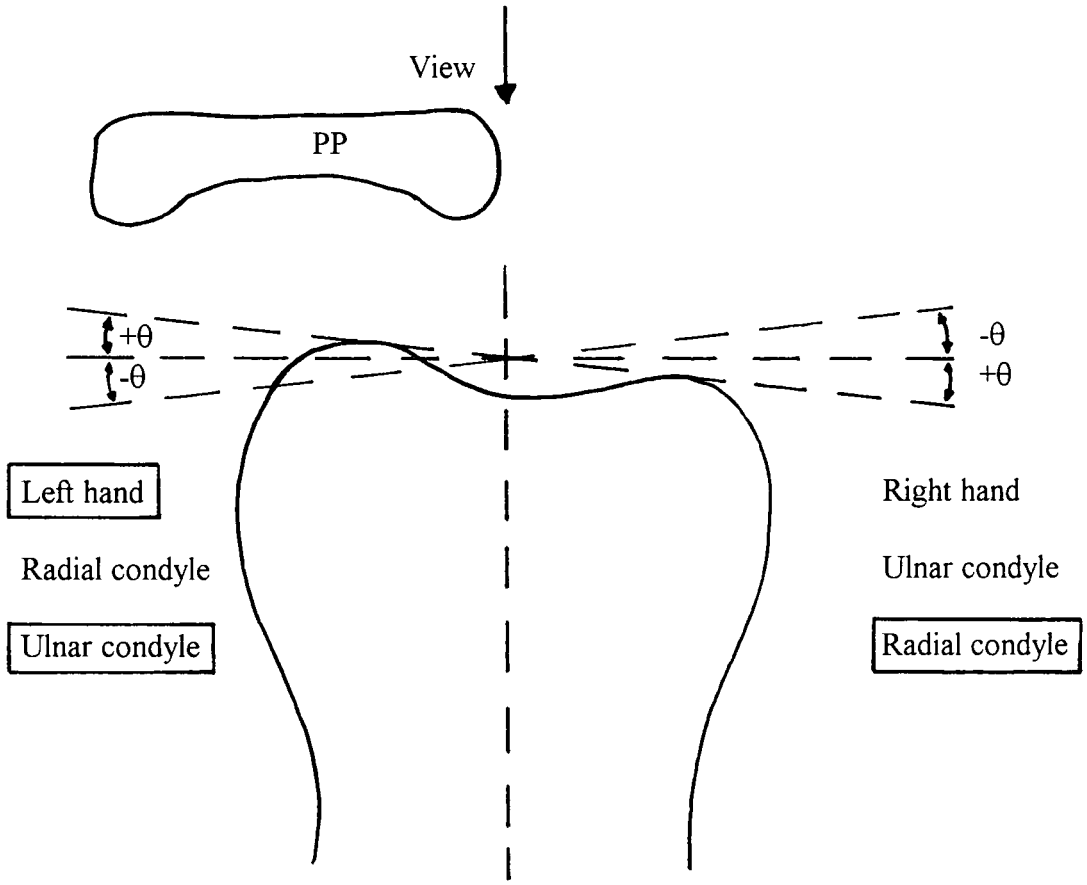

Figure 3.7 Phalangeal medullary canal dimensions, transverse plane

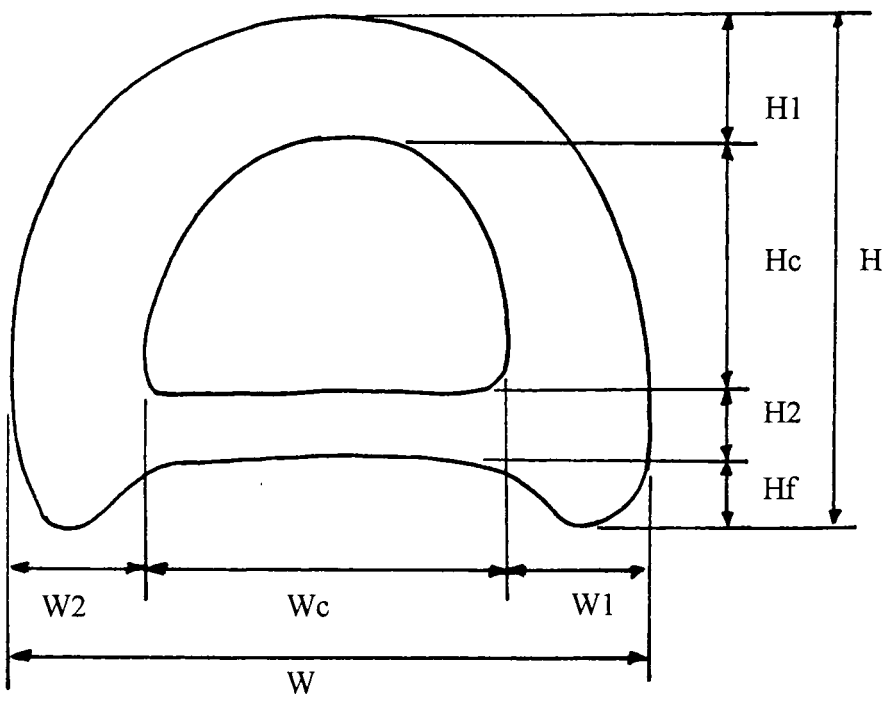

Figure 3.8 Phalangeal bone and medullary canal position, sagittal plane

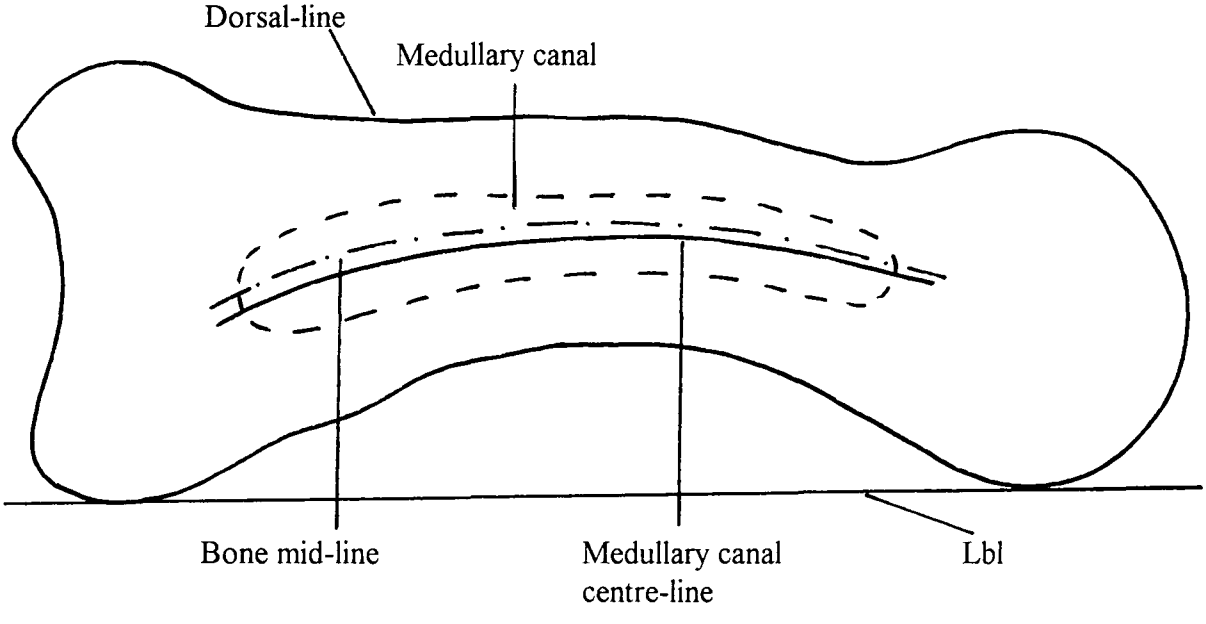

Figure 3.9 Phalangeal bone and medullary canal position, frontal plane

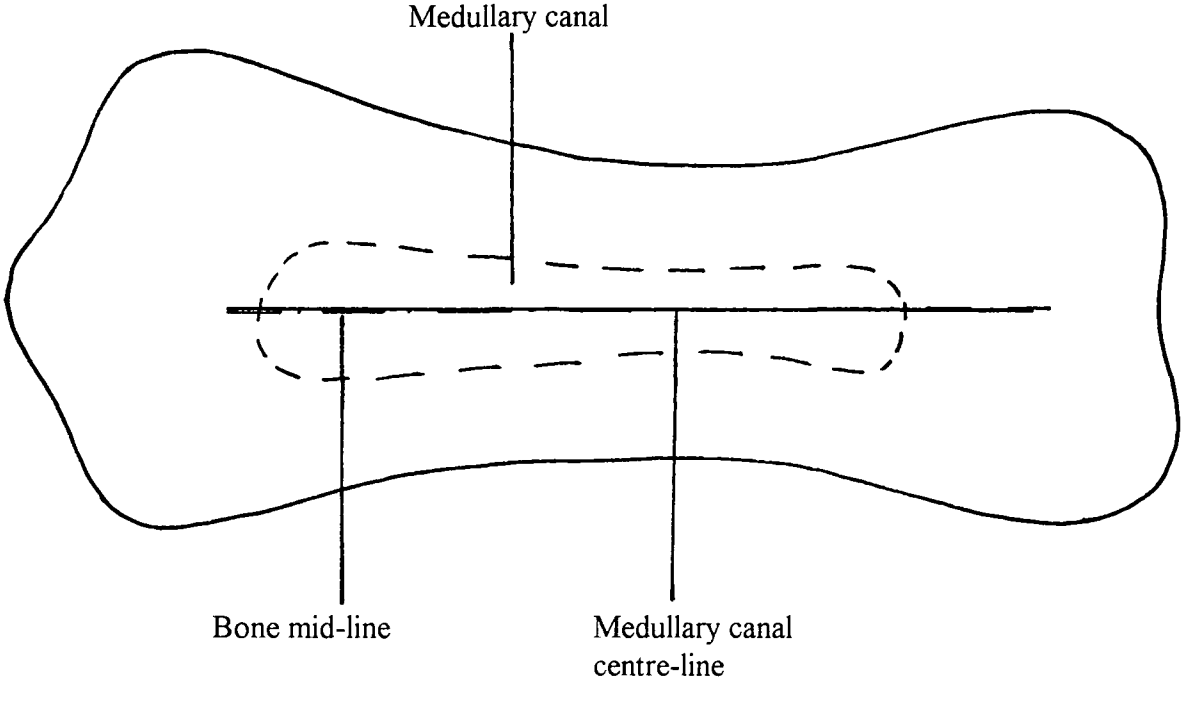

Figure 3.10 Proximal phalangeal head dimensions, sagittal plane

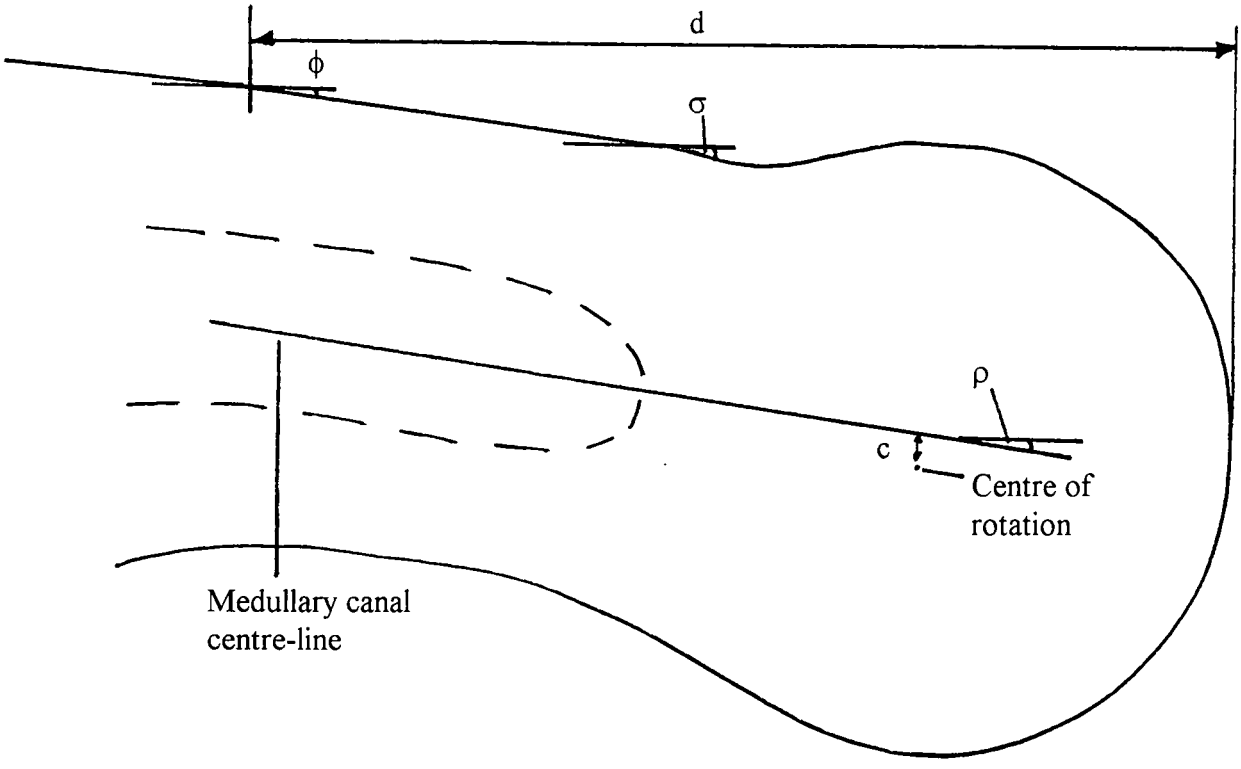

Figure 3.11 Proximal phalangeal head dimensions, transverse plane

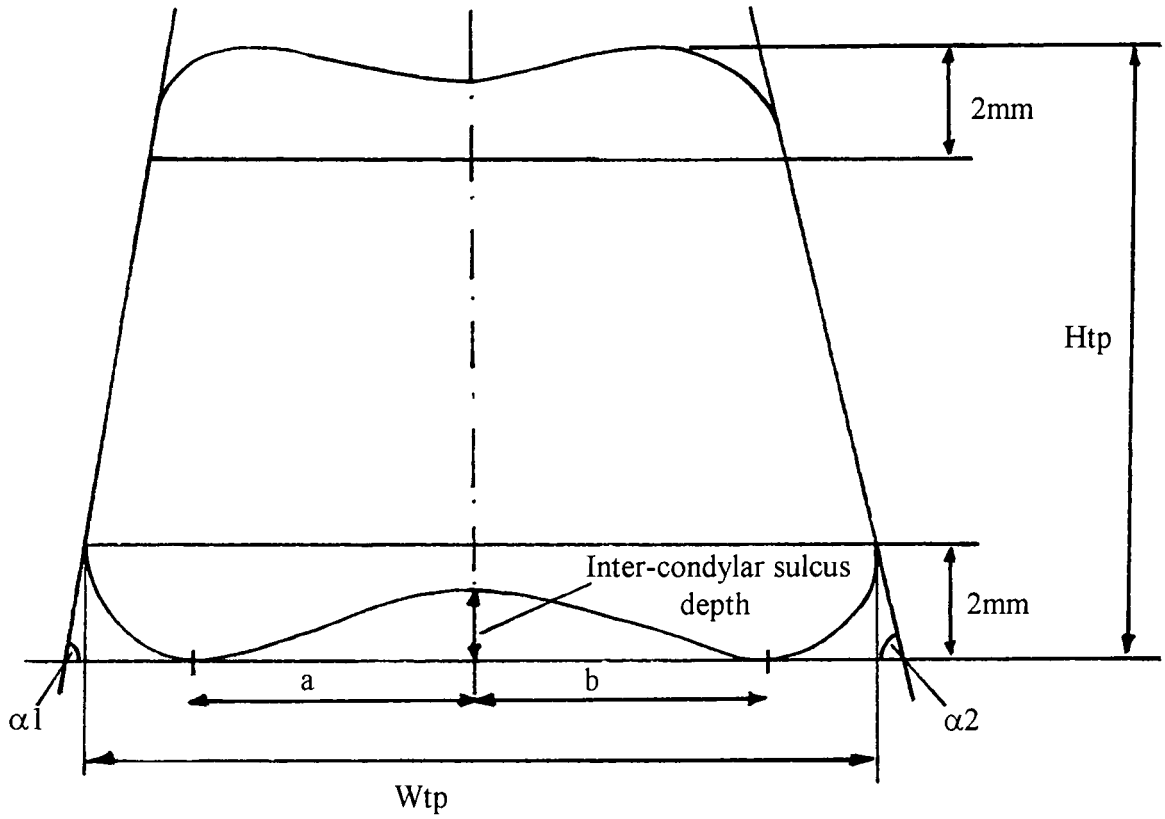

Three additional dimensions were also taken from the MP bases. These were the arc of cartilage of the MP base in the sagittal plane (ω), the offset of the MP stem from the PIPJ centre of rotation (v) and the length of a stem for the MP component stem. The later two are discussed further in Section 4.5.3 as they were more concerned with the design of the MP component rather than the actual dimensions of the MP base.

All of the dimensions measured with their notations are shown in Table 3.2. The dimensions were grouped by individual fingers (index, middle, ring and little) and the mean, standard deviation (S.D.) and percentage deviance (S.D./mean) were calculated for right/left hands, male/females and overall. This was done to show any significant differences between the hands, sexes or between the individual fingers which would have to be taken account of in the design of the PIPJ prosthesis.

3.2 Results

The results have been split into four main sections. These are the articulating surfaces, the phalangeal bones, and the medullary canal position and shape. The differences between males-females, right-left hands and the individual fingers are discussed along with the relationships between the bone lengths, head widths and head diameters. Summaries of the dimensions are given in tables throughout this section along with an overall mean which is the mean of the individual finger means. This mean has been given as it was thought that an overall mean of the individual measurements was mis-leading due to the slight differences in numbers of the individual fingers. The tables, where the individual dimensions are located in Appendix 1, are also given.

3.2.1 Articulating surfaces

The PP and MP heads were bicondylar and articulated against bicondylar recesses in the MP and DP bases respectively. The PP and MP heads and the MP base had a circular profile in the sagittal plane. The radius of curvature varied across the width of the bone producing the bi-condylar shaped articulating surfaces (Figure 3.12). The articulating surfaces were broader anteriorly than posteriorly and the condyles were not symmetrical or symmetrically aligned.

The head diameters ranged from 6-11 mm (mean 8.66 mm) for the PP head and 5-7.5 mm (mean 6.21 mm) for the MP head. The PP head heights (Htp) compared well with

Table 3.2 Summary of shadowgraph dimensions

Notation	Description
ϕ	Angle between the main dorsalsurface and the longitudinal base-line, sagittal plane
θ	Angle of alignment of the head condyles, frontal plane
$\alpha 1$	Angle of inclination of the condyle to the transverse base-line, transverse plane
$\alpha 2$	Angle of inclination of the condyle to the transverse base-line, transverse plane
a	Distance from the head centre-line to the base of a condyle, transverse plane
b	Distance from the head centre-line to the base of a condyle, transverse plane
c	Offset of medullary canal centre-line to the PIPJ centre of rotation
d	Distance from the PIPJ bearing surface to the end of the head-line
σ	Angle between the head line and the longitudinal base-line, sagittal plane
ρ	Angle between the medullary canal centre-line and the longitudinal base-line, sagittal plane
ω	Arc of cartilage of the MP base, sagittal plane
D	Head diameter, sagittal plane
Dmax	Maximum head condyle diameter, sagittal plane
Dmin	Minimum head condyle diameter, sagittal plane
Dbmax	Maximum base recess diameter, sagittal plane
Dbmin	Minimum base recess diameter, sagittal plane
H1	Sectioned bone thickness, transverse plane
H2	Sectioned bone thickness, transverse plane
Hc	Medullary canal height, transverse plane
Hf	Flange depth, transverse plane
Htp	Maximum head height, transverse plane
ISat	Maximum inter-condylar sulcus depth, anterior face, transverse plane
ISf	Maximum inter-condylar sulcus depth, frontal plane
L	Phalangeal length, sagittal plane
Lm	Distance from Tm to the PIPJ bearing surface, sagittal plane
Lmw	Distance from Wm to the PIPJ bearing surface, frontal plane
Lp	Distance from Tp to the PIPJ bearing surface, sagittal plane
Lpw	Distance from Wp to the PIPJ bearing surface, frontal plane
Tm	MP minimum bone height, sagittal plane
Tp	PP minimum bone height, sagittal plane
v	Palmar offset of the MP component stem to the centre of rotation of the PIPJ
W	Maximum bone head width, frontal plane
W1	Sectioned bone thickness, transverse plane
W2	Sectioned bone thickness, transverse plane
Wb	Maximum MP base width, frontal plane
Wc	Medullary canal width, transverse plane
Wm	Minimum MP width, frontal plane
Wp	Minimum bone width, frontal plane
Wtp	Maximum head width, transverse plane

Figure 3.12 Proximal phalangeal head shape in the sagittal, transverse and frontal planes

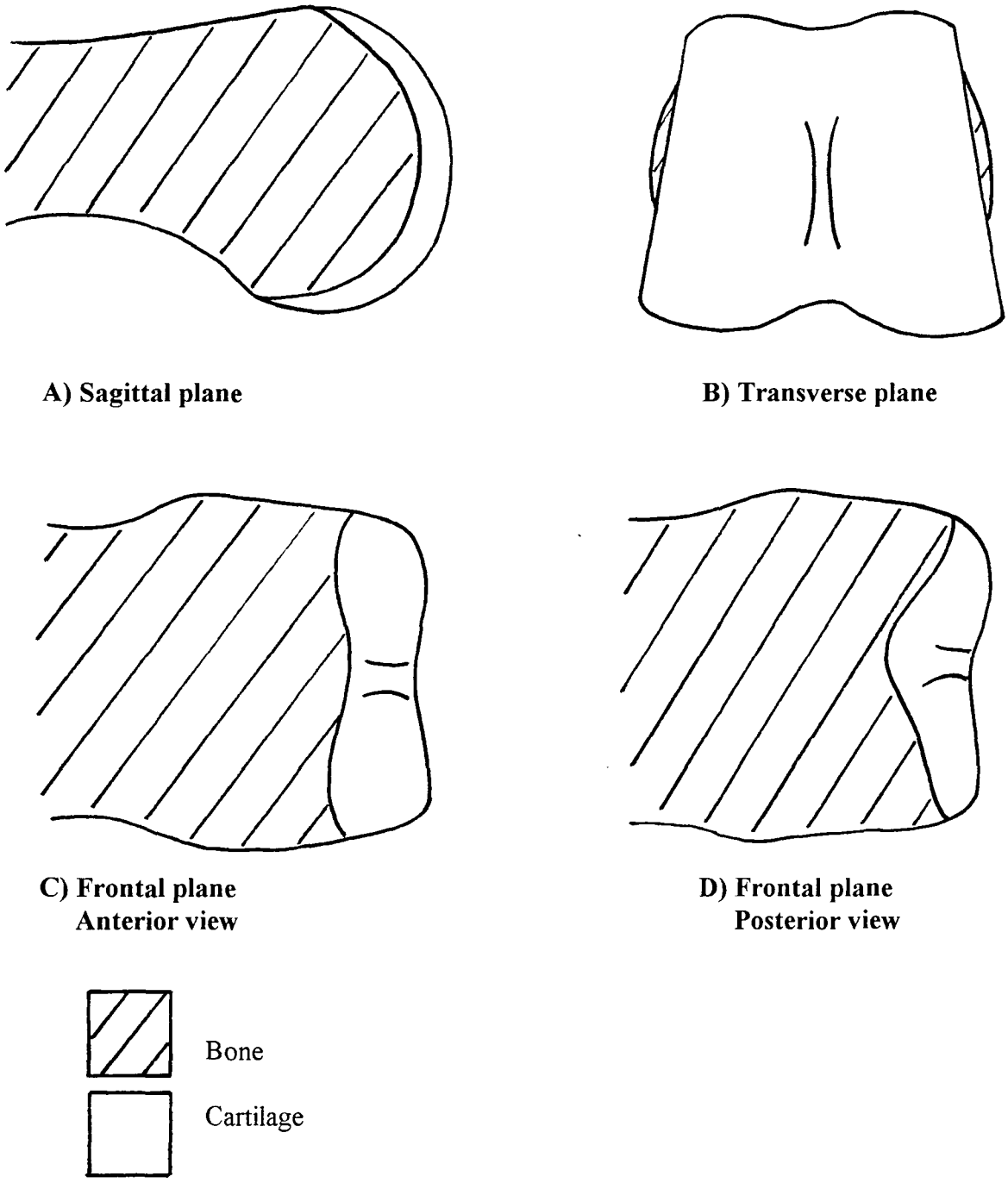

the head diameters (mean 8.58 mm). The maximum condyle diameters, measured from the PP head sagittal plane sections, were on average 0.45 mm less than the head diameters due to a slight mis-alignment of the condyles. The PP head minimum condyle diameters were on average 0.88 mm less than the maximum condyle diameters. The radius of curvature of the MP base was greater than that of the PP head showing that the PIPJs were not conforming joints. The MP base maximum recess diameters were on average 3.36 mm greater than the PP head maximum condyle diameters. The MP base maximum recess diameters were on average 1.06 mm greater than the minimum recess diameters. (Tables 3.3 and 3.4).

Table 3.3 Mean diameters and head height dimensions (mm)

Parameter	Bone	Index	Middle	Ring	Little	Mean	Table
D	PP	9.17	9.33	8.73	7.40	8.66	A1.1
D	MP	6.52	6.71	6.23	5.39	6.21	A1.2
Htp	PP	8.92	9.42	8.71	7.27	8.58	A1.3
Dmax	PP	8.57	8.81	8.33	7.13	8.21	A1.4
Dmin	PP	7.52	7.93	7.48	6.40	7.33	A1.5
Dbmax	MP	11.67	11.95	11.75	10.17	11.39	A1.6
Dbmin	MP	8.52	8.85	8.70	7.50	8.39	A1.7

Table 3.4 Mean differences between phalangeal diameter dimensions (mm)

Parameters	Index	Middle	Ring	Little	Mean
D (PP-MP)	2.65	2.62	2.50	2.01	2.45
Dmax - Dmin (MP)	3.15	3.10	3.05	2.67	2.99
D - Dmax (PP)	0.60	0.52	0.40	0.27	0.45
Dmax - Dmin (PP)	1.05	0.88	0.85	0.73	0.88
Dbmax - Dmax (MP-PP)	3.10	3.14	3.42	3.77	3.36
Dbmin - Dmin (MP - PP)	1.00	0.92	1.22	1.10	1.06

Shadowgraphs of the articular surfaces were taken by rotating the bones about the frontal plane from 45° to -45°. These shadowgraphs were then superimposed on one another and showed that the profile of the articular surface was approximately constant around the bearing surface, although it was broader at -45° (anteriorly) than at 45° (posteriorly), (Figure 3.13). Movement of the PIPJ has been reported to cover a range of approximately 0° extension to 100° flexion[29,67,77,78]. The radius of curvature of the PP head bearing surface profile was approximately constant over this range. The cartilage merged in with the bone shaft posteriorly and did not have the same radius of curvature as the rest of the articulating surface. However, this part of the cartilage would not articulate with the MP base. The average arcs of the MP bases, ω, (sagittal

Figure 3.13 Superimposed sagittal sections of the proximal phalangeal head in the frontal plane

Example 1

-45° → 45° 45° → -45°

Example 2

-45° → 45° 45° → -45°

plane) were found to be 78.8°, 79.0°, 77.0° and 74.53° for the index, middle, ring and little fingers respectively and 77.28° overall. This is discussed further in Section 4.5.3.

The maximum head widths (W) ranged from 8.5-15.5 mm (mean 12.13 mm) for the PP head and 8.5-12 mm (mean 10.40 mm) for the MP head. The maximum MP base widths ranged from 10.3-16.3 mm (mean 13.60 mm) and were on average 1.47 mm greater than the maximum PP head widths. The mean difference between the PP maximum head widths in the frontal plane and in the transverse plane (Wtp) was on average 0.22 mm (1.7% of W), (Table 3.5). This gave an idea of the discrepancies that the shadowgraphing technique introduced when measuring the phalangeal bone dimensions. The discrepancy may have been due to errors induced in tracing or measuring the shadowgraphs, or mis-alignment of the bones during shadowgraphing or sectioning.

Table 3.5 Mean head and base width dimensions (mm)

Parameter	Bone	Index	Middle	Ring	Little	Mean	Table
W	PP	12.57	13.28	12.27	10.41	12.13	A1.10
Wtp	PP	12.86	13.25	12.75	10.54	12.35	A1.11
W	MP	10.58	11.11	10.63	9.29	10.40	A1.12
Wb	MP	13.93	14.74	13.66	12.06	13.60	A1.13

The condyles of the PP heads were not in alignment in the frontal plane. The angle of alignment (θ) of the radial and ulnar condyles was measured, and positive and negative angles of alignment were defined as shown in Figure 3.6. The little finger PIPJs showed the greatest average mis-alignment of the condyles followed by the ring, index and then the middle finger (Table 3.6). The direction of mis-alignment was dependent on the individual fingers. The right hand was approximately a mirror image of the left. The little and ring PIPJs tended to have a more prominent radial condyle whilst the index and middle finger PIPJs had a more prominent ulnar condyle (Figure 3.14).

The angles of inclination of the radial and ulnar sides of the condyles to the transverse base-line ($\alpha 1$ and $\alpha 2$) were measured and it was found that both sides of the PP head inclined by similar amounts. The overall mean angles were 78.09° for $\alpha 1$ and 78.61° for $\alpha 2$. For $\alpha 1$ the left hand angles were larger than the right hand by a mean difference of 1.16°. However, for $\alpha 2$ the right hand angles were larger than the left hand by a mean difference of 0.75°. Hence the angles were also grouped according to whether the angle was on the radial or ulnar side. The overall average angle for the condyle on the ulnar side ($\alpha 1$ for the right hand and $\alpha 2$ for the left hand) was 78.12°

Figure 3.14 PP head condyle mis-alignment

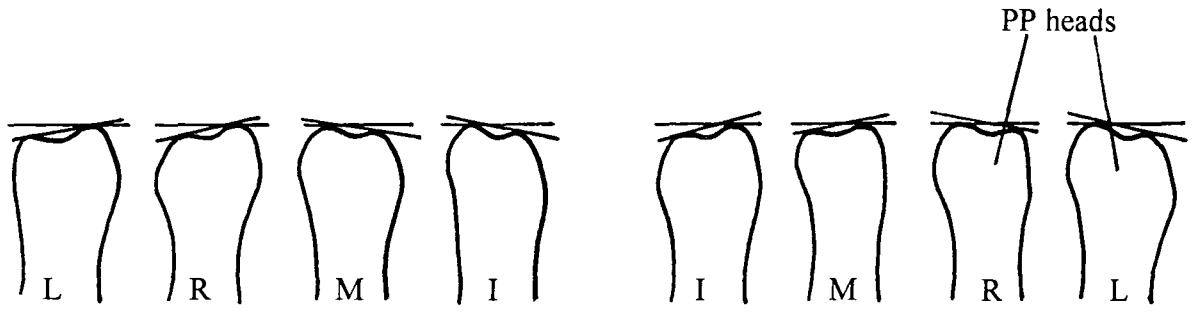

Left hand Right hand

	+θ	-θ
Left hand	Radial condyle	
		Ulnar condyle
Right hand		Radial condyle
	Ulnar condyle	

Figure 3.15 Centre of rotation of the PIPJ

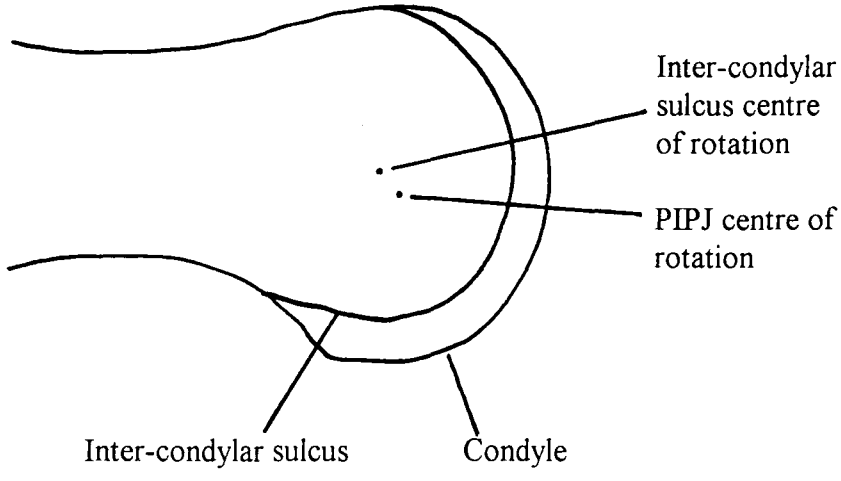

Table 3.6 Mean proximal phalangeal head condyle angles (°)

Parameter	Index	Middle	Ring	Little	Mean	Table
θ (right hand)	-0.41	-0.18	1.70	4.80		A1.14
θ (left hand)	1.55	1.15	-3.17	-6.00		
α1	76.00	76.18	76.91	80.67	77.44	A1.15
α1 (left hand)	79.89	79.67	78.57	79.80	79.48	
α1 (right hand)	77.75	77.75	77.56	80.21	78.32	
α2	79.64	79.09	77.45	81.33	79.38	A1.16
α2 (left hand)	74.44	75.67	80.57	81.00	77.92	
α2 (right hand)	77.30	77.55	78.67	81.16	78.67	

and the overall average angle for the radial side (α2 for the right hand and α1 for the left hand) was 79.08° (Table 3.6). Hence the radial side of the condyle of the PP heads was inclined slightly less than the ulnar side.

The distance from the base of each condyle to the centre-line of the PP head was measured to find the position of maximum condyle diameter. This could not necessarily be found from the sagittal sections of the replica bones due to the material removed during sectioning. The mean distance (a) was 4.56 mm and the mean distance (b) was 4.81 mm (Table 3.7). The maximum head width (W) was 12.14 mm, hence the maximum condyle diameters were positioned at a mean of approximately 77% of the width from the centre-line.

Table 3.7 Mean proximal phalangeal head transverse plane dimensions (mm)

Parameter	Index	Middle	Ring	Little	Mean	Table
a	4.93	5.01	4.60	3.68	4.56	A1.17
b	4.99	5.22	5.00	4.03	4.81	A1.18
ISat	0.90	0.92	0.74	0.61	0.79	A1.19
ISf	0.83	0.79	0.67	0.60	0.72	A1.20

The mean inter-condylar sulcus depth in the transverse plane, anterior face (ISat) was 0.79 mm. The mean inter-condylar sulcus depth in the frontal plane (ISf) was 0.72 mm. Hence the mean difference in depth was 0.05 mm (Table 3.7). However, the mean difference between the PP head maximum condyle diameter and minimum condyle diameter was 0.88 mm. Therefore it would have been expected to find the inter-condylar sulcus depth to be half of this (approximately 0.44 mm).

The sagittal plane sections were superimposed and the centres of rotation of the circles fitted to the sections were marked. Throughout the majority of the width of the bone the centres of rotation were approximately along one axis perpendicular to the sagittal plane. However, the centre of rotation of the circle fitted to the section with the minimum condyle diameter was displaced proximally and volarly to the other centres of rotation (Figure 3.15). This may have been for two reasons. Firstly the inter-condylar sulcus was less defined on the posterior surface of the phalangeal head as the condyles merged in with the shaft. Hence there may have been error in fitting a circle to this section. Secondly the inter-condylar sulcus may actually be displaced proximally and volarly to prevent the bearing surfaces from articulating between the PP inter-condylar sulcus and the MP inter-condylar ridge.

3.2.2 Phalangeal bones

The phalangeal lengths ranged from 29-52 mm (mean 43.24 mm) for the PP bones and from 16-35 mm (mean 27.35 mm) for the MP bones. Both the PP and MP bone shafts tapered longitudinally so that the cross-sectional area was smaller distally than proximally. Flanges were evident in the mid-section of the shaft on the radial and ulnar sides of the palmar surface for the attachment of the tendon sheaths and other soft tissues surrounding the joints. In the sagittal plane the dorsal surface of the bone was flat along the majority of the shaft with a slight inclination distally towards the longitudinal base-line of the bone at an angle defined as ϕ. This angle increased just proximal to the phalangeal head defined as σ. The mean angle between the main dorsal surface of the PP bone and the longitudinal base-line (ϕ) was 5.12°. The little finger had a much greater angle than the rest of the fingers which may have been due to the shorter length of the little finger bones. The mean angles between the head-line and the longitudinal base-line (σ) was 11.88° (Table 3.8). The mean ratio between σ and ϕ was 2.32.

Table 3.8 Mean phalangeal bone dimensions

Parameter	Bone	Units	Index	Middle	Ring	Little	Mean	Table
L	PP	mm	43.88	47.61	45.09	36.38	43.24	A1.21
L	MP	mm	26.30	31.45	29.89	21.76	27.35	A1.22
ϕ	PP	°	4.76	3.81	4.45	7.47	5.12	A1.23
σ	PP	°	10.71	11.19	12.60	13.00	11.88	A1.24
d	PP	mm	14.83	15.22	14.18	11.54	13.94	A1.25

The distance from the PIPJ bearing surface to the change in angle of the dorsal surface proximal to the PP head (sagittal plane) was defined as d. This was measured to indicate the maximum length of stem possible for the PP component. This is discussed further in Section 4.5.2. The mean distance was 13.94 mm.

The minimum bone thicknesses and widths in the sagittal and frontal planes are shown in Table 3.9 along with their distances from the PIPJ bearing surface. The shafts were wider in the frontal plane than in the sagittal plane. Hence the sagittal plane dimensions were more critical in the design of stems for fixation of the PIPJ prosthesis. The sagittal plane minimum thicknesses were also within the section of the bone where the stems of the PIPJ prosthesis would be fitted and would limit the size of stem allowed. The mean distance of the minimum shaft width in the frontal plane from the PIPJ bearing surface is mis-leading. In fact the minima occurred in two main regions of the bone, either just proximal to the phalangeal heads or within the main shaft of the bone. Hence the mean distances indicate an average of the two regions and not where the majority of the minima occurred.

Table 3.9 Mean minimum bone thicknesses and widths (sagittal and frontal planes) and their distances from the PIPJ bearing surface (mm)

Parameter	Plane	Bone	Index	Middle	Ring	Little	Mean	Table
Tp	Sagittal	PP	6.02	6.34	6.07	5.20	5.90	A1.26
Lp		PP	11.88	10.90	11.00	9.03	10.70	A1.27
Wp	Frontal	PP	9.99	10.11	9.52	8.33	9.49	A1.28
Lpw		PP	15.88	19.88	19.13	14.15	17.26	A1.29
Tm	Sagittal	MP	5.24	5.63	5.38	4.59	5.21	A1.30
Lm		MP	12.02	15.14	12.53	7.39	11.77	A1.31
Wm	Frontal	MP	8.04	8.46	7.97	7.25	7.93	A1.32
Wmw		MP	15.38	18.90	18.63	13.24	16.54	A1.33

3.2.3 Medullary canals

All of the proximal phalanges and most of the middle phalanges had medullary canals along the length of the bone shaft. However, with some of the smaller MP bones the medullary canals were not apparent throughout the length of the shaft. The bone surrounding the medullary canals was thicker on the radial and ulnar sides of the shaft, than dorsally and palmarly, and thicker dorsally than palmarly. The middle finger bones tended to have the thickest shaft bone and the little fingers had the thinnest. There was no significant difference between ring and index shaft bone thicknesses for the PP

although the ring fingers tended to have slightly thicker shaft bone than the index fingers for the MP (Table 3.10).

Table 3.10 Mean lateral, dorsal and palmar shaft thicknesses

Shaft	Bone	Index	Middle	Ring	Little	Mean	Table
Lateral	PP	2.31	2.34	2.27	2.10	2.26	A1.34
Dorsal	PP	2.15	2.21	2.15	1.88	2.10	A1.36
Palmar	PP	1.42	1.49	1.40	1.23	1.39	A1.38
Lateral	MP	1.97	2.24	2.18	1.99	2.10	A1.35
Dorsal	MP	1.58	1.73	1.73	1.66	1.68	A1.37
Palmar	MP	1.06	1.17	1.10	1.12	1.11	A1.39

The PP medullary canal centre-line coincided with the bone mid-line in the frontal plane due to approximately the same bone shaft thickness on the radial and ulnar sides of the canal. In the sagittal plane, however, the bone mid-line was found to be slightly dorsal to the medullary canal centre-line due to the thicker shaft bone dorsally than palmarly. The medullary canal centre-line was approximately a straight line in the frontal plane, however, in the sagittal plane it tended to arc along the length of the bone, (convex dorsally), following the palmar surface of the bone.

When marking the medullary canals on the sagittal plane shadowgraphs it was important also to mark the flanges and any concavity present on the palmar face of the bones, to create a true picture of the bone stock of the phalangeal shafts. Without consideration of the flanges or concavities of the palmar face of the phalangeal bones, the medullary canal centre-line seemed to coincide with the mid-line of the bone. However, taking them into consideration showed that the mid-line of the bone was dorsally offset from the medullary canal centre-line. This implies that a joint prosthesis stem designed to insert centrally in the shaft would not be located centrally within the medullary canal. Hence it was important to use the estimated positions of the medullary canals when designing the PIPJ prosthesis stems and not just the bone outline.

The angle between the PP medullary canal centre-line and the longitudinal base-line changed throughout the length of the shaft as the centre-line arced longitudinally, (convex dorsally) in the sagittal plane. It has already been reported earlier that the shaft just proximal to the PP head was at a steeper angle to the base-line than the rest of the phalangeal shaft. This was the region of the bone where a stem fixing the PP component of the PIPJ prosthesis would be located. Hence the angle between the

medullary canal centre-line and the longitudinal base-line in this part of the shaft was measured (ρ). The mean angle ρ was 10.64°. The mean angle of inclination of the medullary canal centre-line to the longitudinal base-line was 1.24° less than the mean angle between the head-line and the longitudinal base-line (σ). Hence it would be important to use estimated angle of the medullary canals when designing the PIPJ prosthesis stems and not just the bone outline (Section 4.5.2). The range of ρ for each of the fingers was similar (Table 3.11).

Table 3.11 Inclination and offset of the proximal phalangeal medullary canal centre-line

Parameter	Units	Index	Middle	Ring	Little	Mean	Table
ρ	°	9.76	10.48	11.65	10.68	10.64	A1.40
c	mm	0.83	0.83	0.80	0.57	0.76	A1.41

Unsworth and Alexander[17] found that the MC medullary canal centre-line was dorsal to the centre of rotation of the MCPJ. The mean offsets were 2.81 mm (S.D. 0.97), 2.67 mm (S.D. 0.74), 2.58 mm (S.D. 0.59) and 2.46 mm (S.D. 0.44) for the index, middle, ring and little fingers respectively. The palmar offset of the centre of rotation increased the moment arm of the weaker extensor tendons and decreased the moment arm of the stronger flexor tendons. The first Flatt metallic hinge joint prosthesis had the centre of rotation of the hinge in line with the stems which impoased unnatural biomechanics on the MCPJs and did not correct the pre-operative extensor lag. However, the importance of the dorsal offset of the stems compared with the centre of rotation of the joint was later acknowledged. A second joint prosthesis was designed with the centre of rotation moved palmarly, resulting in an improvement in active extension and hand function[18].

The alignment of the PP medullary canal centre-line and the centre of rotation of the PIPJ was measured (c). The centre-line was dorsally offset from the centre of rotation of the PIPJ. The mean offset was 0.76 mm. The centre-line offsets were similar for the index, middle and ring fingers, however, for the little finger they were much lower (Table 3.11). The dorsal offset between the medullary canal centre-line and the centre of rotation of the joint may not seem to be very large. However, compared with the size of the proposed PIPJ prostheses (7-10 mm maximum condyle diameter) it is suggested that this offset is significant, not only for restoring the natural mechanical advantage of the joint, but also in the design of the stem fixation.

3.2.4 Medullary canal shape

The positions of the phalangeal cross-sections in the transverse plane of particular interest are shown in Figure 3.16, and the typical cross-sections found at these positions are shown in Figure 3.17. The transverse cross-sections of the phalangeal bones varied along the length of the bone. The phalangeal bones tapered proximally to distally. As the phalangeal head merged into the shaft, the height and width of the cross-sections decreased slightly and then increased again throughout the rest of the shaft before merging with the phalangeal base proximally.

The dorsal surface of the transverse shaft sections was convex and the palmar side was either slightly concave or flat depending on the position of the cross-section. Flanges were apparent on the palmar side of the cross-sections throughout part of the shaft length for the attachment of tendon sheaths and other soft tissues surrounding the joint. The medullary canal was evident from just proximal to the phalangeal head to just distal to the phalangeal base, and increased in size proximally. Both the shaft and medullary canal cross-sectional shapes varied along the length of the shaft. The shaft walls were thicker laterally than dorsally and palmarly, and thicker dorsally than palmarly throughout the length of the medullary canal.

Just proximal to the bone head (2) the shaft width was much greater than the shaft height. The palmar side of the bone was convex and it could be seen where the shaft was merging into the bi-condylar phalangeal head. The cross-sectional area of the medullary canal was very small and the shaft walls were much thicker laterally than dorsally and palmarly. The shape of the medullary canal in this section was circular. At the thinnest part of the shaft (3) the palmar side of the bone was much flatter and despite the decrease in cross-sectional width, the medullary canal increased in size and was now more oval in shape rather than circular. The lateral walls decreased greatly in thickness but were still thicker than the dorsal or palmar walls (3).

At the mid-section of the shaft (4) flanges were evident on the palmar side of the cross-section and the palmar face was still fairly flat. The medullary canal was slightly greater than a semi-circle in shape and the shape of the canal followed the shape of the perimeter of the bone shaft . Just distal to the phalangeal base (5) the flanges were not evident but the palmar side of the bone was concave and the base merged into the shaft and the flanges. The medullary canal was still slightly greater than a semi-circle in shape. In the phalangeal base (6) the medullary canal was not evident.

Figure 3.16 Position of phalangeal transverse sections

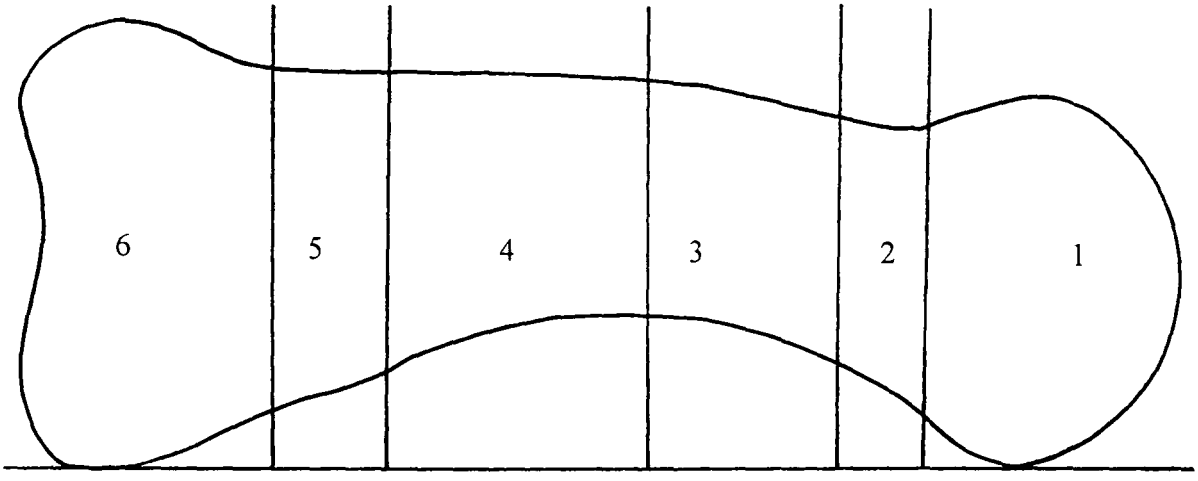

Section 1	:	Phalangeal head
Section 2	:	Shaft merging with head
Section 3	:	Shaft
Section 4	:	Shaft with flanges
Section 5	:	Shaft merging with base
Section 6	:	Phalangeal base

Figure 3.17 Transverse cross-sections of phalangeal bones

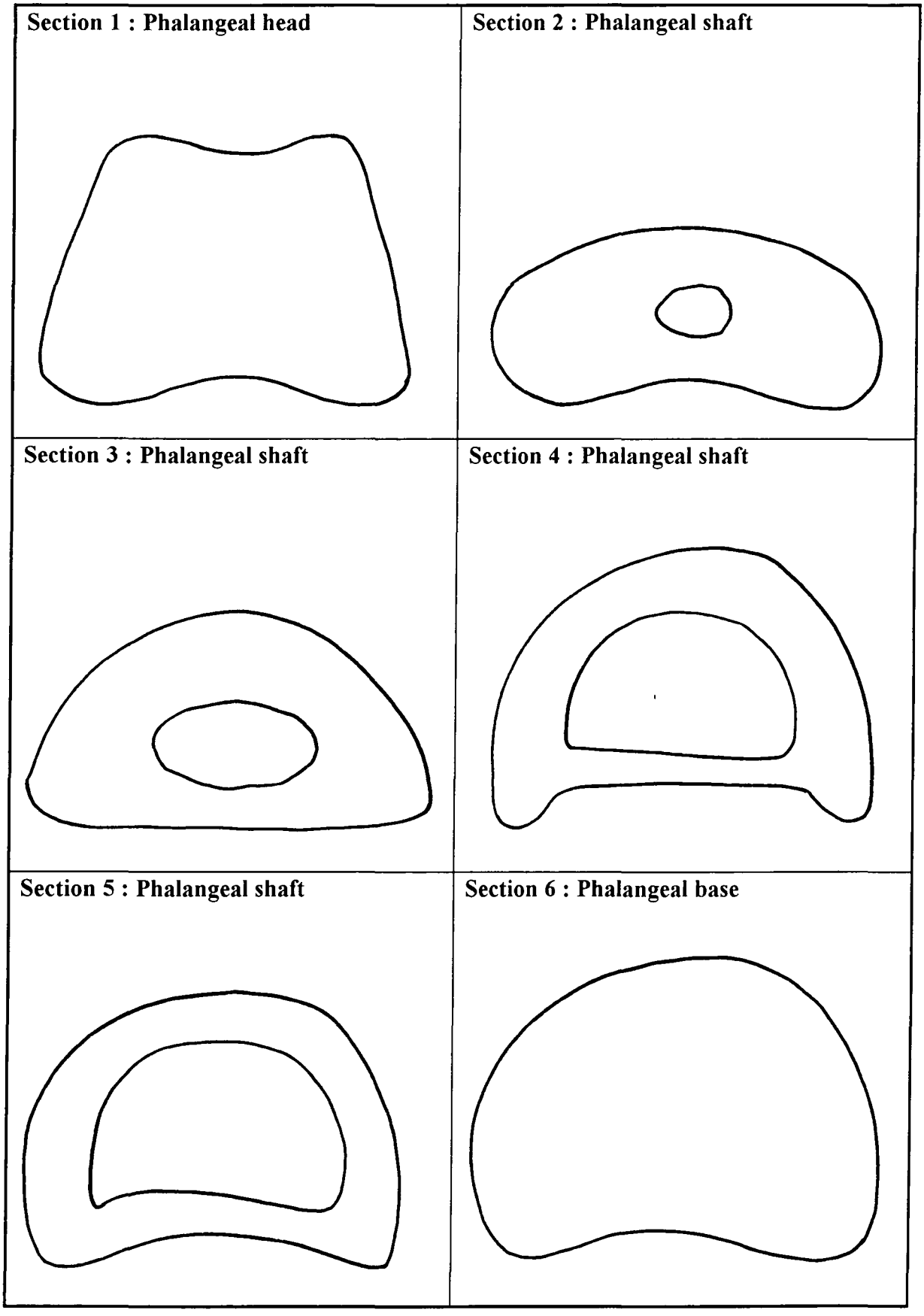

3.2.5 Dimension relationships

Relationships were found between the PP and MP bone lengths, maximum head widths and head diameters (Table 3.12). The mean PP ratios were L/W = 3.57 (W/L = 0.28), L/D = 5.00 (D/L = 0.20) and W/D = 1.41 (D/W = 0.71) and the mean MP ratios were L/W = 2.62 (W/L = 0.38), L/D = 4.35 (D/L = 0.23) and W/D = 1.66 (D/W = 0.60). However, the ratios varied according to the bone size. The smaller bones had slightly higher ratios than average and the larger bones had slightly lower ratios than average. Hence best-fit lines were also plotted each pair of data (Figures 3.18 - 3.23).

Table 3.12 Mean dimension ratios

Ratio	Bone	Index	Middle	Ring	Little	Mean	Table
L/W	PP	3.49	3.60	3.68	3.50	3.57	A1.42
L/D	PP	4.78	5.07	5.19	4.83	5.00	A1.44
W/D	PP	1.38	1.43	1.38	1.38	1.41	A1.46
L/W	MP	2.50	2.83	2.81	2.35	2.62	A1.43
L/D	MP	4.10	4.63	4.68	4.03	4.35	A1.45
W/D	MP	1.63	1.65	1.72	1.73	1.66	A1.47

The equations to the best-fit lines to the data are given in Table 3.13. The gradients of the best-fit lines were slightly lower than the ratios found between the dimensions. These equations could be used to predict the sizes of joint prosthesis required before surgery from X-rays. For example if a patient's maximum PP head widths were ascertained then the head diameters could be calculated and hence the sizes of joint prostheses known. R-Square values range between 0 and 1 for a best-fit line. An R-squared value near 0 indicates a poor fit, whereas a value near 1 indicates a good fit. The R-squared values for the PP were nearer 1 than those for the MP. Hence the relationships between bone length, head diameter and maximum head width for the PP were more meaningful than those for the MP. The low R-Squared values indicated the natural biological variations in the bone dimensions.

Table 3.13 Relationships between L, D and W (Trend-line equations to figures 2.19-2.24), and the corresponding R-Squared values

Proximal Phalanx		Middle Phalanx	
Relationship	**R-Squared Value**	**Relationship**	**R-Squared Value**
L = 3.93D + 9.14	0.60	L = 4.28D + 0.97	0.48
W = 0.24L + 1.88	0.73	W = 0.16L + 6.15	0.52
W = 1.22D + 1.53	0.75	W = 1.01 D + 4.20	0.57

Figure 3.18 : Relationship Between PP Bone Length and Head Diameter

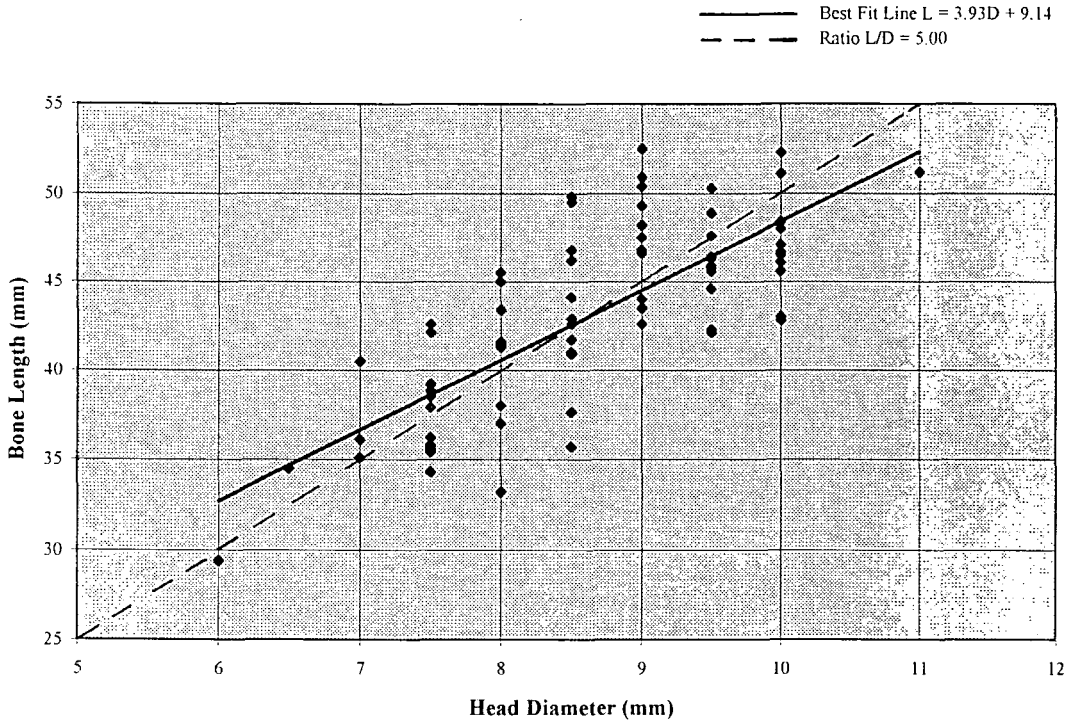

Figure 3.19 : Relationship Between MP Bone Length and Head Diameter

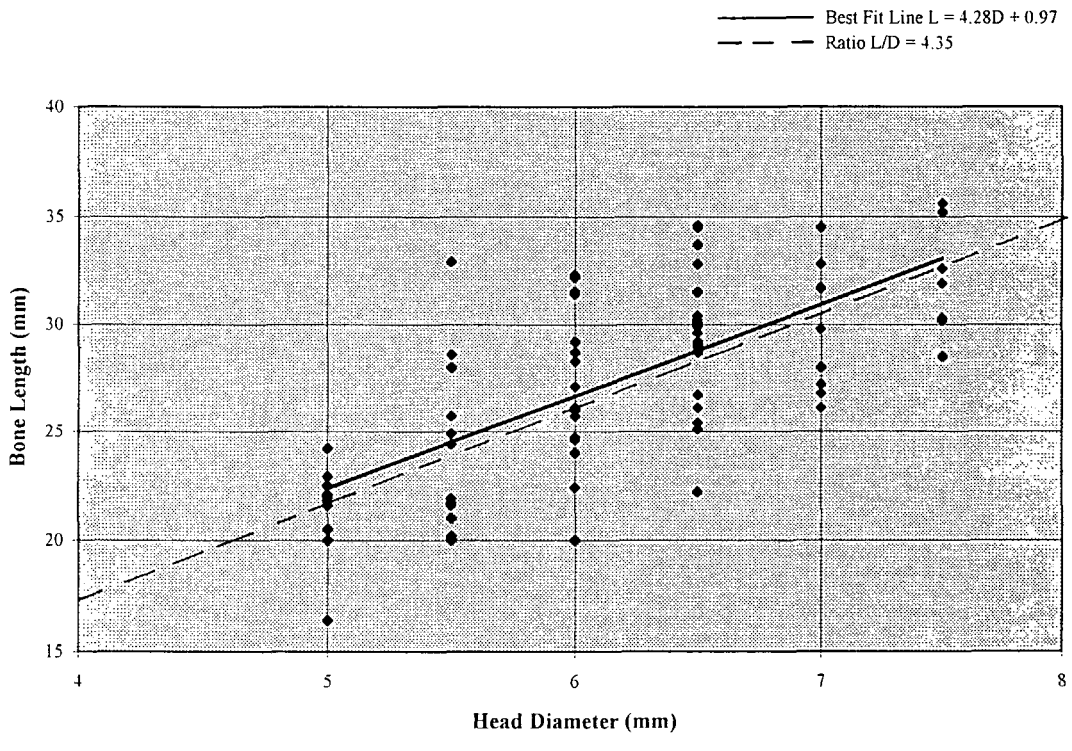

Figure 3.20 : Relationship Between PP Head Width and Head Diameter

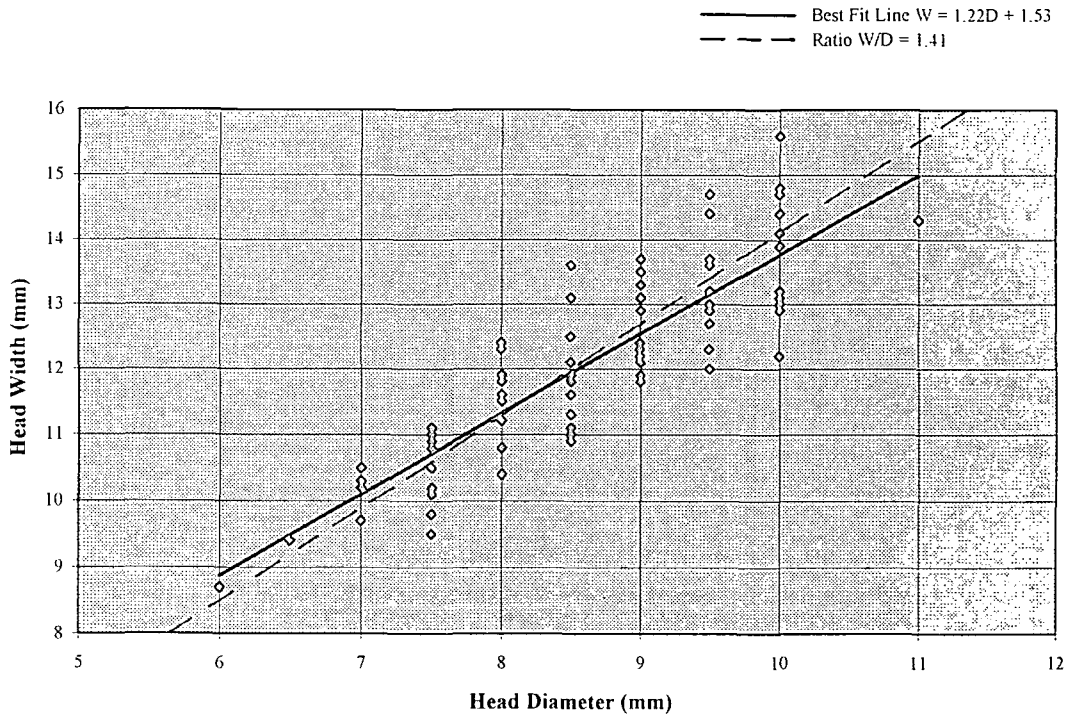

Figure 3.21 : Relationship Between MP Head Width and Head Diameter

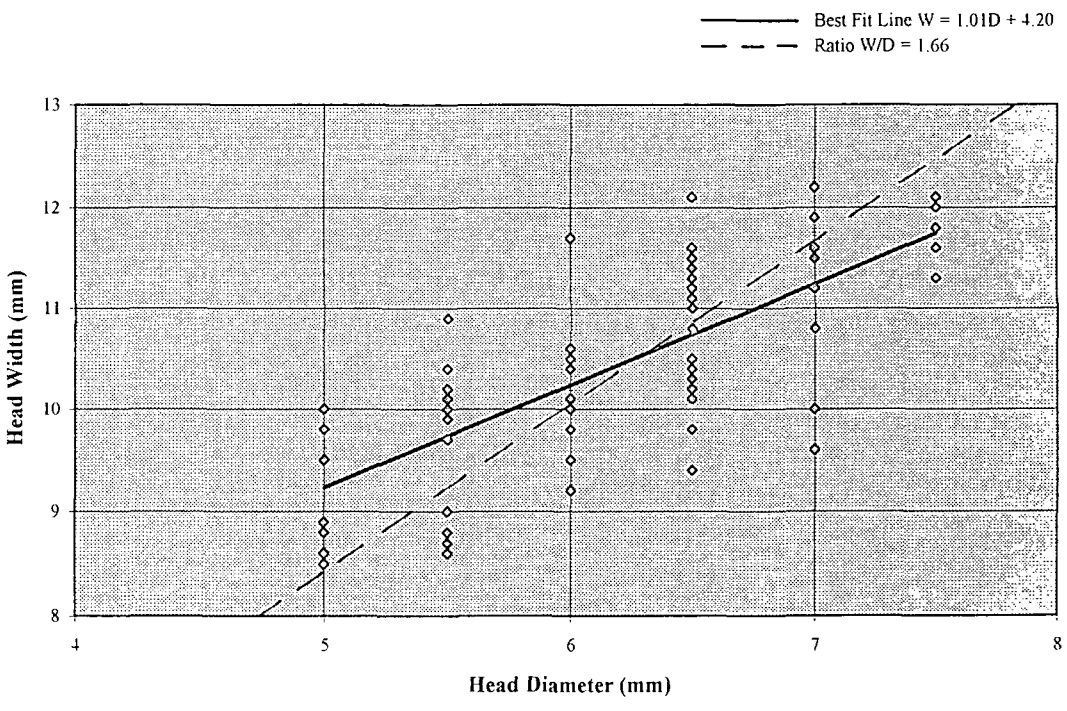

Figure 3.22 : Relationship Between PP Head Width and Bone Length

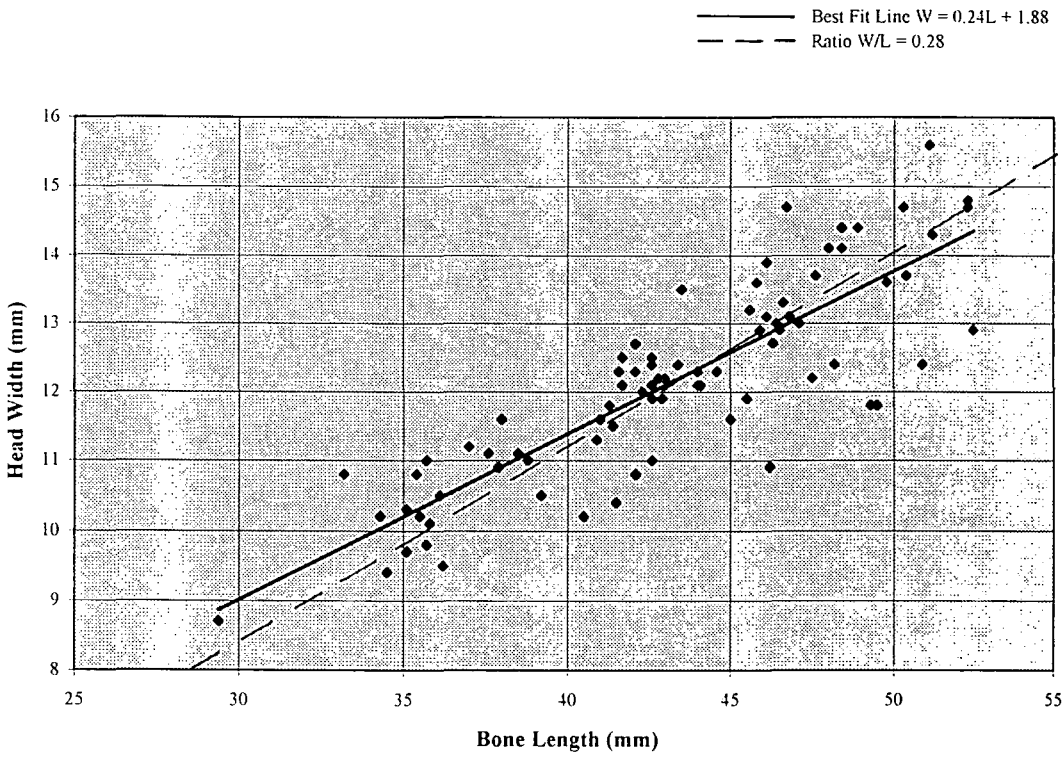

Figure 3.23 : Relationship Between MP Head Width and Bone Length

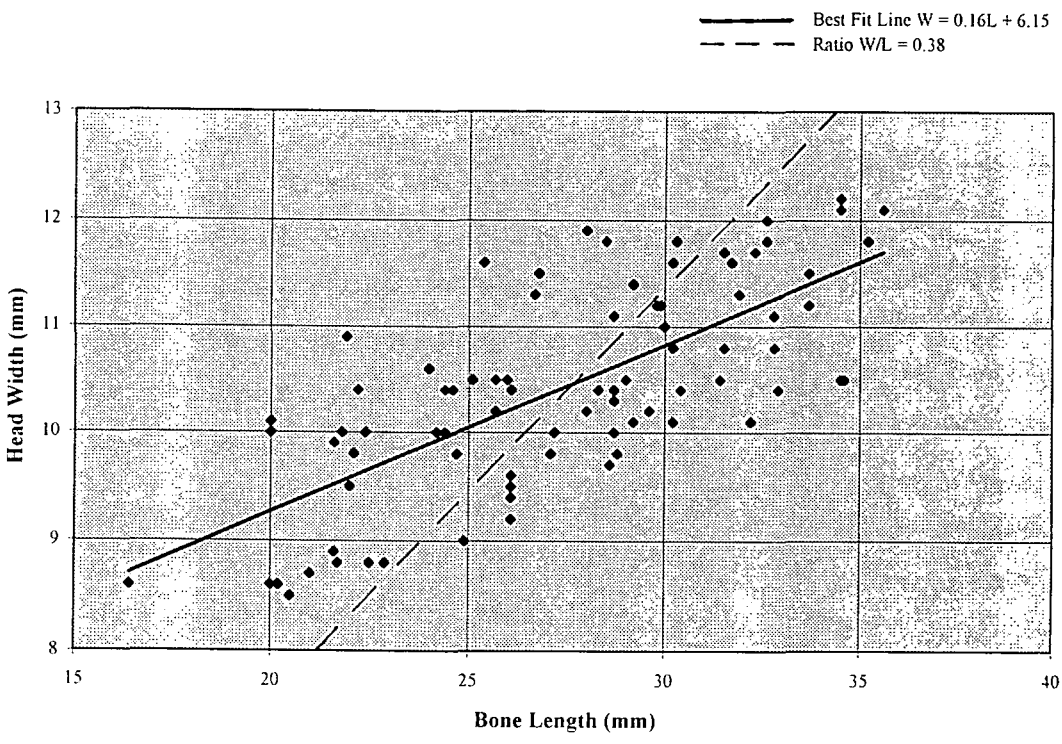

3.2.6 Individual finger differences

The dimensions were dependent on the individual fingers. The middle finger tended to have the largest bones and the little finger tended to have the smallest bones in terms of head diameter, head width, and length. The ring finger tended to be longer than the index finger, however, the index finger tended to be wider and have larger head diameters than the ring finger. The little finger tended to have the largest dorsal-line, head-line and medullary canal centre-line angles and also had larger angles of inclination of the radial and ulnar sides of the condyles. The middle, ring and index fingers had no set pattern as far as the angles were concerned but were overall significantly smaller than the little finger angles.

3.2.7 Right-left hand differences

For the majority of cases the right hand tended to have slightly larger dimensions than the left hand. The percentage difference was on average 2.5%, as a percentage of the left hand dimensions. Four cases had slightly larger left hand dimensions. These were the angles of inclination for the radial and ulnar sides of the condyles ($\alpha 1$ and $\alpha 2$) for the PP angle and the length and width for the MP. There was no information available on which hand was dominant for each of the cadavers.

3.2.8 Male-female differences

The male and female PP and MP bone dimensions, angles and relationships between some of the dimensions were compared. The percentage difference was calculated as a percentage of the female dimension. A positive percentage difference indicated that the male dimension was greater than the female and vice versa. It should be noted that the conclusions drawn were from a limited number of individuals and the size of bones of an individual was not necessarily be due to their sex.

Males tended to have larger PP and MP bones than females. The percentage differences are shown in Tables 3.14 and 3.15. Males also tended to have greater dorsal-line (ϕ), head-line (σ) and medullary canal centre-line (ρ) angles. However, females tended to have greater inter-condylar sulcus depths (ISat and ISf) and the radial and ulnar sides of the condyles were not as inclined as much as males ($\alpha 1$ and $\alpha 2$). Females also had a slightly greater offset of the centre of rotation from the medullary canal centre-line (c) and distance form the PIPJ bearing surface to the end of the head-line (d). However, the percentage difference between some of the dimensions was

dependent of the individual fingers (α2, ϕ, ρ, c d). Females tended to have larger L/W, L/D and W/D ratios for the PP and L/W for the MP, but slightly smaller L/D and W/D ratios for MP.

Table 3.14 Proximal phalangeal percentage differences between male and female dimensions

	D	Htp	Dmax	Dmin	W	Wtp	a	b	L
%	9.27	8.05	8.06	8.46	10.35	9.15	5.91	3.17	3.26

	α1	α2	ISat	ISf	ϕ	σ	ρ	c	d
%	-2.87	-2.02	-6.98	-4.05	15.12	18.06	6.67	-3.85	-3.14

	L/W	L/D	W/D
%	-6.20	-6.56	-1.44

Table 3.15 Middle phalangeal percentage differences between male and female dimensions

	D	Dbmax	Dbmin	W	Wb	L	L/W	L/D	W/D
%	6.17	5.91	8.13	6.56	9.15	9.39	-2.99	0.45	1.81

3.3 Discussion

It is widely accepted that the PIPJ is a hinge joint with the main plane of motion in the sagittal plane (flexion-extension). A small amount of passive abduction and adduction and rotation are permitted due to the non-congruity of the joint, the shape of the articulating surfaces and the tension in the soft tissues surrounding the joint. This accommodates external forces applied to the joint and allows large irregular objects to be gripped as well as fine precision tasks to be performed. The majority of previous studies on the PIPJ bearing surfaces have concentrated on the conformity of the joint and the contributions of the bearing surfaces to the deviation of the fingers from the longitudinal and transverse planes.

3.3.1 Conformity

There has been some debate in the past over the conformity of the MCPJ. Some authors reported that the PP base had a greater radius of curvature than the MC head[20,56] whilst others did not find a significant difference in radii indicating that the MCPJ was more conforming[19]. However, the PIPJ has only been observed to be non-

conforming, (the MP base radius of curvature in the sagittal plane was greater than that of the PP head[27,79]) although no dimensions were reported. In this study it was also found that the PIPJ was not congruous. The maximum and minimum diameters were on average 11.39 mm and 8.39 mm for the MP base recesses and 8.21 mm and 7.33 mm for the PP head. The MP base recesses were on average 3.18 mm and 1.06 mm greater than the PP head condyles for the maximum and minimum diameters respectively.

3.3.2 Deviation

The contributions of the geometric bearing surfaces to the deviation of the digits at the PIPJ can be divided into three components. Coronal deviation occurs when the two condyles of the bicondylar PP head (or the MP base) are out of alignment in the frontal plane or when one condyle is slightly larger than the other in this plane. Torsion or tilt occurs when the two condyles are out of alignment in the transverse plane or again if one condyle is slightly larger than the other. Rotation may also occur if the inter-condylar sulcus or ridge is not vertical in the transverse plane (Figure 3.24). The resultant deviation is a sum of the individual coronal, torsion and rotational deviation components which may not necessarily all be in the same direction.

Deviation of the more distal phalanges was observed by Holcomb[28] who found that they did not lie parallel with the proximal phalanges in full flexion. This was most apparent in the index and little fingers. The contribution to coronal deviation and tilt at the PIPJ was measured with immobilisation of the metacarpals and the MCPJs. In general the index and ring fingers moved towards the ulnar side compared with the middle finger during flexion, and the little finger moved towards the radial side. Tilt was small and fell within the error of the measuring technique and the type of apparatus used. The main factor contributing to the divergence was coronal deviation, although on average the coronal deviation of the middle and ring fingers was very small.

The two condyles of the PP head did not project by the same amount resulting in coronal deviation of the distal phalanges. The PP head was also not symmetrical due to the slight difference in the radii of curvature of the two condyles. The most prominent condyle was on the ulnar side for the index finger and on the radial side for the other fingers producing coronal deviation towards the ulnar side for the index finger and towards the radial side for the other fingers during flexion (towards the second web space).

Figure 3.24 Coronal deviation, torsion (tilt) and rotation of the proximal phalangeal head

a) Coronal deviation (frontal plane)

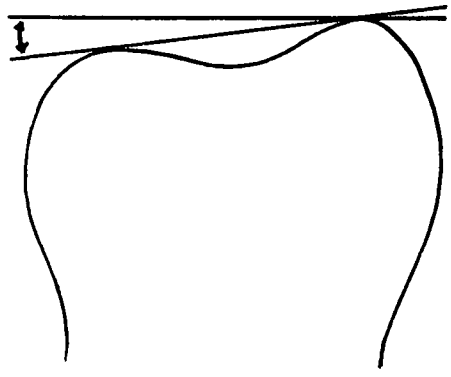

b) Torsion or tilt (transverse plane)

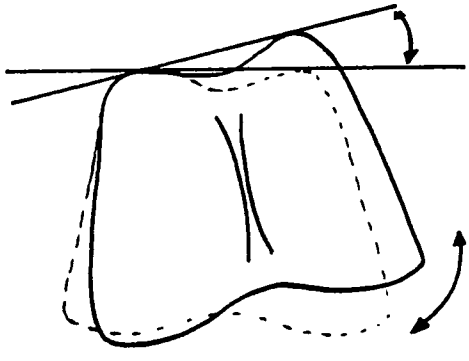

c) Rotation (transverse plane)

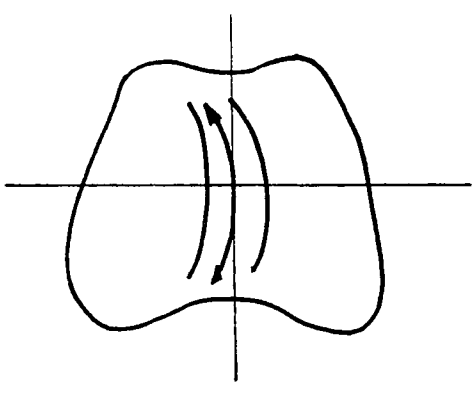

Torsion (or tilt) of the PP heads was reported for the index and middle fingers and opposed movement produced in these joints by deviation and rotation. The index, middle and little fingers were tilted slightly towards the ring finger in the transverse plane. The resultant of a combination of these deviations produced supination for index finger and pronation for the ring and little fingers so that tips of the fingers converged towards each other as the fingers were flexed. Similarly the metacarpals were orientated in the palm of the hand such that the alignment of the heads produces splaying of the fingers during extension allowing increased movement of the hand. Hence deviation at each of the joints in the hand can increase hand function by giving the hand a greater range of mobility.

Tilt and rotation of the PP head were not measured in this study due to limitations in the shadowgraphing technique used and the method of sectioning chosen. However, the condyles of the PP head were not symmetrical and one condyle was slightly larger than the other. This would result in coronal deviation and tilt of the middle phalanx about the proximal phalanx during flexion. The degree to which the condyles were not in alignment was measured in the frontal plane. The condyles on the radial side were more prominent for the little and ring fingers, and the condyles on the ulnar side were more prominent for the index and middle fingers. Hence the middle finger had a different prominent condyle to those reported in the literature[28]. However, the condyles of the middle finger were on average out of alignment by only 0.18° for the right hand and 1.15° for the left hand. This was similar to the index finger. The little and ring fingers had the greatest difference in alignment in the frontal plane. The coronal deviation produced by these alignments would be slightly towards the ulnar side for the index and middle fingers and towards the radial side for the ring and little fingers.

3.3.3 Centre of rotation

The centre of rotation of a joint is dependent not only on the geometry of the bearing surfaces but also on the influence of the soft tissues surrounding the joint. As mentioned before, there has been some debate on whether the centre of rotation of the MCPJ varies or not. Some authors reported that it was constant[16-20] by successfully matching the path of motion or geometry of the MC head and PP base to the arc of a circle. However, others reported that it varied because the MCPJ was cam shaped and not concentrically circular[21-24]. They reported that the radius of curvature was least in extension and maximum in flexion. This provided two advantages during pinch and grip functions. Firstly the mechanical advantage of the flexor tendons was increased

during flexion, and secondly the collateral ligaments became taut in flexion which increased the stability of the joint. Simultaneous sliding and rolling of the surfaces of the MCPJ were also reported when the hand was flexed or extended.

Landsmeer[25] stated that the PIPJ centre of rotation moved volarly during flexion. However, Kuczynski[26] reported that during flexion of the PIPJ from the fully extended position the collateral ligaments soon became tight as they passed over the apex of angulation of the side margin of the PP head. They remained tight as they moved over the more vertical plane of the side of the head with increased flexion. Most of the joints analysed did not exhibit a cam effect like the MCPJ implying that the radius of curvature remained constant soon after the apex of angulation. Leibovic[25] also reported that the PIPJ centre of rotation did not change measurably over the range of motion.

In this study the PP head and MP base were circular in the sagittal plane. However, the bearing surfaces were not conforming implying that the centre of rotation of the PIPJ may vary throughout its range of motion. However, the amount that it may vary is unclear without further investigation.

3.3.4 Trapezoidal shape

Leibovic et al[27] reported that the bicondylar PP head was roughly trapezoidal with the volar margin roughly twice the dorsal margin. It was found in this study that the profile of the PP head in the transverse plane was indeed roughly trapezoidal. However, by modelling the profile to a quadrilateral shape, with parallel dorsal and volar surfaces and angled lateral sides, the ratio of the volar margin to the dorsal margin was nearer 1.4 than 2.

3.3.5 Arc of cartilage

The MP base has been reported to encompass an arc of 110°[27] in the sagittal plane with the PP head arc of cartilage of 210°[27]. This compares well with the joint prosthesis proposed by Varian[72] which had a bearing surface of arc of 210° for the PP head although only a mid-portion of was part-circular (195°). The MP base had an arc of 110° in the sagittal plane. However, from this study it was found that the MP base encompassed a maximum arc of 90° in the sagittal plane. The mean was approximately 77° which was much lower values than previously published values. The PP head had an arc of approximately 200° although the dorsal aspect of the cartilage was not of a

circular profile in the sagittal plane as the bone and cartilage merged into the shaft. However, this area of the cartilage is not used in articulation as hyperextension of the PIPJ is prevented by the soft tissues surrounding the joint.

3.3.6 Bicondylar V-Shape

The joint prosthesis proposed by Varian[72] consisted of a V-shaped articulating surface. The angle of the V was between 120°-140° depending on size of the joint prosthesis. It is true that the mid-portion of the PP head articulating surface can be approximated to a V-shape but the average angle was approximately 152° when the profiles of right and left hand bones in the transverse plane were superimposed. This is discussed further in Section 4.3.

3.3.7 Medullary canals

Marsden and Nicol[80] scaled radiographs of MC and PP bones in the sagittal and frontal planes such that the MC bones were 70 mm long and the PP bones were 45 mm long. They found that the MC canal started just proximal to the MC head and distal to this point cancellous bone was present. The medullary canals were tapered and long stems created alignment problems. They concluded that joint prosthesis stems must be short to fit all bones (20 mm for MC bones of 70 mm length and 15 mm for PP bones of 45 mm length).

Similarly, in this study it was found that the dorsal shaft of the PP bones changed in angle proximal to the PIPJ. Hence any stem used for fixation of the PP component of the PIPJ prosthesis would have to be secured in the region of the shaft before the change in angle so that problems in alignment of the stem within the shaft could be avoided. The distances from the PIPJ bearing surface to the change in angle were 14.83, 15.22, 14.18 and 11.54 mm for the index, middle, ring and little fingers respectively and 13.94 mm overall. (The average length of the PP bones was 43.24 mm).

Walker and Erkman[24] found that the medullary canals were trumpet shaped, converging to a minimum size at the mid-shaft where after they diverged again in the MC bones and remained parallel in the PP bones. The medullary outline was not smooth but displayed ripples and waves up to 1/2 mm in depth. Sectional views show the MC medullary canals to resemble an isosceles triangle, apex volarly while the PP medullary canals were approximately semi-circular with the base downwards. In this

study the PP and MP shafts were also found to be semi-circular throughout the parts of the shaft with the base downwards. The shape of the medullary canals varied throughout the shaft from circular to oval and then semi-circular. The centre-line of the PP medullary canals was offset dorsally to the centre of rotation of the PIPJ. This has previously been found with the MC and PP medullary canals with respect to the MCPJ centre of rotation[17].

3.3.8 Radius of curvature, head width and bone lengths

The mean phalangeal head widths and bone lengths from this study, and those of Unsworth and Alexander[17] are shown in Table 3.16, along with the ratios between the MC and PP bone dimensions and the actual MC and MP bone dimensions. The PP and MP head widths were largest for the middle, index, ring and then the little fingers. However, for the MC bones the index fingers appeared to have larger head widths than the middle fingers, and the ring and little fingers were similar. For all of the bones the middle fingers had the longest bones followed by the ring, index and little fingers. The ratios varied for the different fingers.

Table 3.16 Phalangeal head widths and bone lengths

	Index	Middle	Ring	Little	Mean
MC head width[17]	17.27	16.80	14.50	14.38	15.74
PP head width	12.85	13.31	12.66	10.45	12.32
MP head width	10.58	11.11	10.63	9.29	10.40
Ratio of MC[17]: PP bone width	1.34	1.21	1.15	1.38	1.27
Ratio of MC[17] : MP bone width	1.63	1.51	1.36	1.55	1.51
MC bone length[17]	69.6	68.8	57.6	54.9	62.73
PP bone length[17]	43.2	47.0	43.7	35.0	42.23
PP bone length	43.88	47.61	45.09	36.38	43.24
MP bone length	26.30	31.45	29.89	21.76	27.35
Ratio of MC[17]: PP bone length	1.59	1.45	1.28	1.51	1.46
Ratio of MC[17] : MP bone length	2.65	2.19	1.93	2.52	2.32

Linear relationships occurred between the MCPJ size and MC bone length. The index, middle and ring fingers had similar ratios (0.35) but the little finger showed a greater joint radius per unit bone length (0.60)[17]. Relationships between the lengths, head widths and head diameters were found in this study for the proximal and middle phalanges. The ratios W/D were similar for all fingers for the PP and MP bones, however, the ratios L/W and L/D were smaller for the index and little fingers than the

middle and ring fingers. Hence the difference in lengths of the different fingers had greater impact on the ratios than the head widths or diameters.

3.4 Summary

The bones from 83 PIPJs were dissected, modelled, sectioned and shadowgraphed. The dimensions of the bones and articulating surfaces and the shape and position of the medullary canal were investigated. The PIPJ is a bicondylar joint consisting of the concave base of the MP and the convex head of the PP. The articulating surfaces were broader anteriorly than posteriorly, and circular in the sagittal plane. The profile of the bearing surface was approximately constant around the articulating surface. The condyles blended into the shaft of the bone posteriorly which changed the radius of curvature of the PP head in this region. The MP base had a greater radius of curvature than the PP head resulting in a non-conforming joint.

The shafts of the PP and MP bones tapered distally. In the sagittal plane the dorsal surface of the bone was flat along the majority of the shaft with a slight inclination distally towards the longitudinal base-line of the bone. This angle increased just proximal to the phalangeal heads. The dorsal surface of the bone was convex transversely. The palmar surface of the shaft was slightly arced longitudinally and either flat or slightly convex transversely. The medullary canal was central in the bone in the frontal plane and slightly volar in the bone in the sagittal plane. The centre-line of the canal was dorsally offset from the centre of rotation of the joint. The medullary canal varied in shape and size throughout the length of the shaft. The shaft bone thickness was thicker laterally than dorsally and palmarly, and thicker dorsally than palmarly. Flanges were apparent on the palmar surface of the shaft for the attachment of the tendon sheaths and other soft tissues surrounding the joint.

Relationships were found between the bone lengths, head widths and head diameters. Right hand bones tended to be slightly larger than left hand bones and males tended to have larger bones than females. The middle fingers tended to have the largest bones and the little fingers tended to have the smallest bones. The ring fingers tended to have longer bones than the index fingers, however, the index finger tended to have wider bones than the ring fingers with larger head diameters.

CHAPTER FOUR

Design of a proximal interphalangeal joint surface replacement prosthesis

4.1 Design criteria

The design considerations for a surface replacement joint prosthesis included the anatomy and conformity of the bearing surfaces, range of motion, mechanical advantage, biomaterials and fixation, as well as surgical and patient considerations (Section 3.3). An ideal joint prosthesis would theoretically satisfy all of these considerations, however, in practice this was not possible and a compromise had to be reached. The following section discusses the design criteria developed from the previous list of design considerations.

4.1.1 Anatomy

Some compromises on the natural joint anatomy were required to reduce the number of joint prostheses required. Despite the differences between the joints of different fingers and different hands (dimensions, angles, alignment of the condyles, ratios between different dimensions) it was not practical from a surgical or financial point of view to have individual prostheses for each joint, as well as having the range of sizes required for the population. Hence one design was produced over a range of sizes for all of the fingers, using the average dimensions taken from all of the PIPJs. The main concern was that a single surface replacement design would require symmetrical condyles. This compromised the natural mis-alignment of the condyles which were different for the right and left hand PIPJs. This in turn could impede the rotational or lateral movement of the PIPJs, although it would not necessarily significantly impede hand function due to the contributions of the MCPJs and the DIPJs.

4.1.2 Range of movement

The bearing surfaces of the PP and MP components were designed to be circular in the sagittal plane, to conform with the natural anatomy of the PIPJs. The MP base was required to encompass a maximum arc of 90° (average 77.28°) and the PP head a minimum arc from -45° to 100° (to allow for the overlap of the MP base at maximum extension). This not only allowed a natural range of movement in flexion-extension,

but also restored any contribution of the bearing surfaces to the natural stability of the joint.

4.1.3 Conformity of the bearing surfaces

When designing the PIPJ surface replacement prosthesis the hardest criteria to address was the conformity of the bearing surfaces. The bearing surfaces of the PIPJ were found to be non-conforming. The radii of curvature of the MP base were significantly greater than those of the PP head. This implied a varying centre of rotation during flexion-extension and point contact between the bearing surfaces, although in reality the cartilaginous bearing surfaces deform to produce a larger contact area. Non-conforming surfaces can also allow lubricant to become entrained betweeen the surfaces and allow wear debris to escape. However, the three main targets of joint replacement are to achieve pain relief, a reasonable range of motion and stability. If the soft tissues surrounding the joint are in a poor condition then there may be a problem with joint stability, and any contribution to stability from the bearing surfaces must be welcomed. Hence the bearing surfaces were designed to be conforming despite the fact that this may alter the mechanical advantage, movement and lubrication of the joint. Conforming surfaces would also result in a lower joint contact stress.

4.1.4 Mechanical advantage

The PP head had a constant centre of curvature, but the bearing surfaces were not conforming possibly resulting in a change in the centre of rotation of the PIPJ throughout its range of motion. However, as discussed in Section 4.1.3 the bearing surfaces of the joint prosthesis were designed to be conforming. Hence the main design criteria with reference to the mechanical advantage of the joint was the positioning of the centre of rotation with respect to the stems of the components. This was found to be palmarly for the PP heads (Section 3.2.3) and slightly dorsally for the MP bases (Section 4.5.4).

4.1.5 Biomaterial choice

Third generation joint prostheses had articulating bearing surfaces and commonly used the bearing combination of metal-on-polymer, which has been shown to produce low friction and wear. However, the size of the PIPJ advocates the use of cementless, one-piece components. Hence if a metal-on-polymer bearing surface combination were used, one of the components would require a metallic stem which would be in direct

contact with the bone. This has been shown to cause bone resorption due to the hardness of the metal compared with the bone, and high contact stresses at the metal-bone interface[32,34,35]. Hence metals were not a preferred choice of material for the PIPJ prosthesis.

Polymer-on-polymer bearing surfaces have been avoided in the past because they produce high wear rates. However, the wear of XLPE sliding against itself has been encouraging and has comparable wear rates with metal-on-polymer combinations[73]. Further investigations were carried out on the wear characteristics of XLPE sliding against itself compared with other biomaterial combinations and the results were found to support those of the initial wear tests (Chapter 5).

XLPE also has the ability to be injection moulded, unlike UHMWPE. This would simplify the manufacture of the joint prostheses and reduce production costs. The XLPE may also promote less reaction with the bone than metals (due to its lower hardness compared with metals), resulting in less bone resorption, which can cause loosening. Hence the PIPJ surface replacement prosthesis was made entirely from XLPE. This allowed the design of complex PP and MP components.

4.1.6 Fixation to bone

When a joint prosthesis is implanted into a bone the normal stress pattern in the bone is changed, which can result in bone resorption and may eventually cause loosening of the joint prosthesis. Loosening can cause wear debris from the bone-joint prosthesis interface which can become trapped between the bearing surfaces causing third body wear. It can also be deposited in the surrounding soft tissues causing inflammation and pain. Secure fixation is therefore required. The availiable methods of fixation are mechanical, cement, bone in-growth or interference fit (Section 2.5.8). The main consideration when selecting the type of fixation for the PIPJ surface replacement prosthesis was the bone stock available in the proximal and middle phalanges. In addition, the bone stock may be in poor condition due to the effects of arthritis. These made the use of cement or mechanical fixation impractical. Hence the only feasible method of fixation was by interference fit.

4.1.7 Surgical considerations

The three main surgical considerations were the surgical technique, the tooling and the time required to perform the surgery, which are all inter-related. Ideally the surgical

time should be as short as possible for patient welfare and cost. The surgical technique should be as simple as possible to reduce the risk of error and to reduce the surgical time. The latter is particularly important as more than one joint may be replaced at a time. The tooling should also be as simple as possible and the amount of tooling required should be minimal. A set of tools would be required for each size of joint prosthesis, of which a maximum of four different sizes may be implanted during one operation. Hence the design should require minimal and uncomplicated tooling which will simplify the surgical technique and reduce the cost of the tooling. In addition, the number of sizes of joint prosthesis should be minimal to minimise the tooling costs.

4.1.8 Summary of the design criteria

From the previous considerations the following design criteria were produced:

* One design over a range of sizes to cover all of the joints
* Symmetrical condyles
* Circular PP head bearing surface profile in the sagittal plane (-45° to 100° min.)
* Circular MP base bearing surface profile in the sagittal plane (90° arc max.)
* Offset of the PP and MP stems to the PIPJ centre of rotation
* Conforming bearing surfaces
* Manufactured from cross-linked polyethylene (XLPE)
* Interference fixation
* Simple surgical technique (minimal and uncomplicated tooling)

4.2 Distribution of proximal interphalangeal joint sizes

The sizes of the PIPJs were defined by the PP head diameter (D), which ranged from 6-11 mm (to the nearest 0.5 mm). The surface replacement joint prosthesis sizes were based on this parameter. To identify the range of sizes of joint prostheses required to cover the natural anatomical range of PIPJs, the joints were distributed in diameter size steps of 1 mm. Both sets of circles, of integer diameters (6-11 mm) and half sizes (6.5-10.5 mm), were fitted to the PP heads. Figure 4.1 shows the distribution of PIPJs in both integer sizes and half sizes of the PP head diameters.

From Figure 4.1 it can be seen that the three half sizes of 7.5, 8.5 and 9.5 mm, or the four integer sizes of 7, 8, 9 and 10 mm cover the majority of the population. However, although the three half sizes covered 91.5% of the population, this range neglected the

Figure 4.1: Distribution of the Proximal Phalangeal Joint Sizes (by Proximal Phalangeal Head Diameter) in Integer and Half Sizes

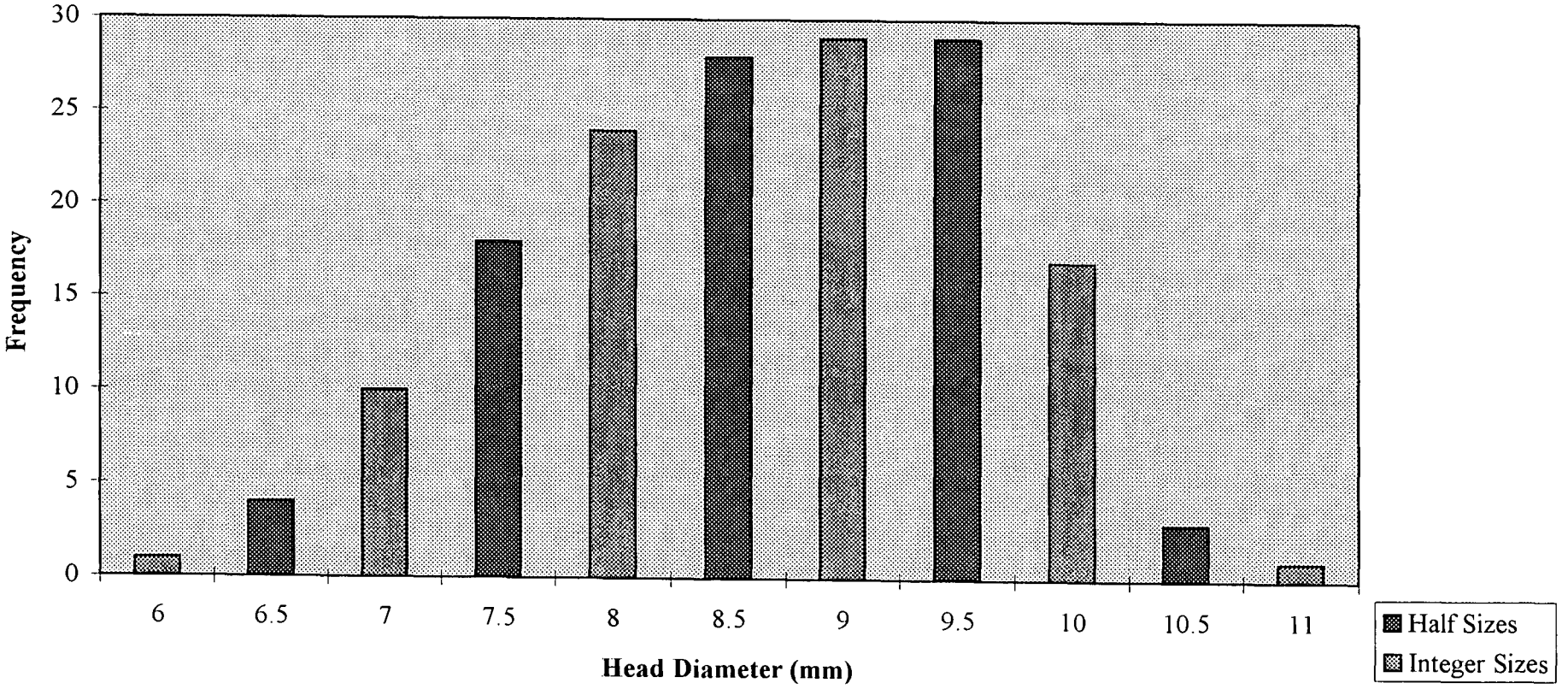

6.5 sizes which tended to be those of the little finger. In fact 20% of the little finger joints were not included in the three half size range. The range also neglected the 10.5 size, although this was distributed between both middle and index finger joints. The four integer sizes covered 97.6% of the population and only two joints were neglected from this range. These were one middle finger joint and one little finger joint. The range of four integer sizes also covered a slightly greater proportion of the population than a range of four half sizes. Hence a range of four integer sizes of joint prostheses of 7, 8, 9 and 10 mm were developed for the surface replacement of the PIPJs.

Admittedly some joints will ultimately fall outside this range of joint prostheses. But as a new design it is unlikely that a full range of sizes would be developed until promising results were found from extensive clinical trials. The four joint prosthesis are thought to be the mimimum range that would cover an acceptable proportion of the popultation for clinical trials. Any individuals with joints outside this range would either recieve the nearest size of joint prosthesis to their joints or be excluded until a wider range of prostheses was developed.

The PIPJ dimensions were re-distributed by PIPJ prosthesis size as opposed to individual fingers. The distribution of the finger joints by joint size and the re-distributed PIPJ dimensions are shown in Appendix 2. A summary of the average dimensions required for the design of the PIPJ surface replacement prostheses is shown in Table 4.1.

4.3 Proximal interphalangeal joint models

Models were developed for the PP heads rather than the MP bases for two reasons. Firstly it was possible to acquire more information on the PP heads due to the fact that they were convex. Secondly the surface replacement joint prosthesis had conforming bearing surfaces which compromised the natural shape, and any model of, the MP base. Four models of the PP heads were produced in the transverse plane (7, 8, 9 and 10 mm head diameter).

The horizontal base-line and centre-line were marked on the shadowgraphs of the PP heads in the transverse plane. The shadowgraphs were then super-imposed and a tracing of the estimated average PP head shape for each PIPJ size was produced (Figures 4.2). The horizontal base-line and centre-line were marked on the four tracings. In addition, lines were drawn joining the two condyles on the posterior face

Table 4.1 Summary of dimensions distributed into prosthetic sizes (by PP head diameter) of 7, 8, 9 and 10mm

Parameter	Units	Size			
		7 mm	**8 mm**	**9 mm**	**10 mm**
σ	°	12.80	12.39	11.24	11.53
ϕ	°	6.90	5.35	4.69	4.18
$\alpha 1$	°	79.80	78.50	77.79	76.94
$\alpha 2$	°	81.30	80.50	77.38	76.12
c	mm	0.67	0.70	0.79	0.86
ρ	°	10.50	11.09	10.69	9.94
θ	°	-0.10	-0.08	0.12	0.21
a	mm	3.54	4.30	4.77	5.21
b	mm	3.97	4.58	5.04	5.30
ISat	mm	0.60	0.76	0.90	0.91
ISf	mm	0.59	0.64	0.79	0.81
Wtp	mm	10.27	11.65	12.83	13.36
Htp	mm	7.24	8.05	9.00	9.74
d	mm	11.71	13.22	14.61	15.33
ω	°	78.8	79.0	77.0	74.53
v	mm	0.0	0.10	0.15	0.29

(i), along the lateral sides of the condyles (ii), and along the inter-condylar sulcus on the anterior face (iii). The tracings of the bearing surfaces were then used to develop models of the bearing surfaces using the following criteria :

* The models were symmetrical about the centre-line
* The height of the models was taken as the joint size (7, 8, 9, 10 mm)
* The radii of curvature were constant about the bearing surface (apart from the inter-condylar sulcus which decreased in depth on the posterior aspect to merge with the bone shaft)
* Where possible changes in the radii of curvature of the bearing surface across the width of the bone were made linear

The resultant models of the PP heads in the transverse plane can be seen in Figure 4.3.

The maximum widths of the models were found to be 10.2, 11.6, 12.8 and 13.4 mm for the 7, 8, 9, and 10 mm sizes respectively. These compared well with the average measured PP head widths in the transverse plane of 10.27, 11.65, 12.83 and 13.36 mm respectively. The maximum widths were set at 1.5 mm from the horizontal base-line for the 7, 8 and 9 mm models and 2 mm for the 10 mm model. The angles between the

Figure 4.2 **Tracings of the estimated proximal phalangeal head shape, transverse plane (x 10 magnification)**

a) 7 mm head diameter

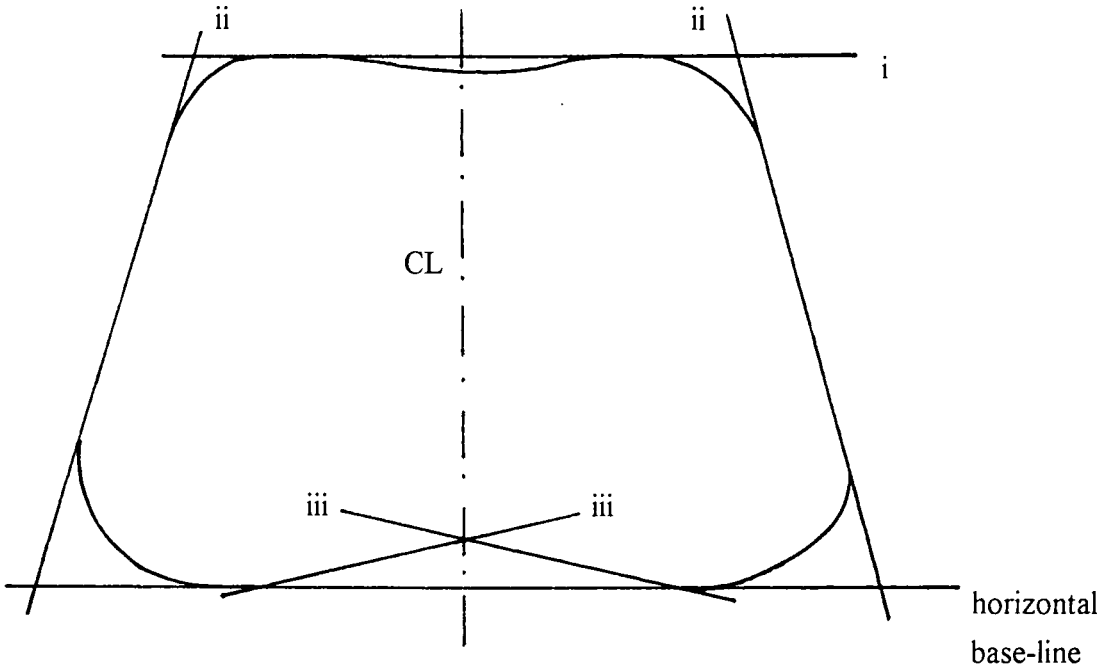

b) 8 mm head diameter

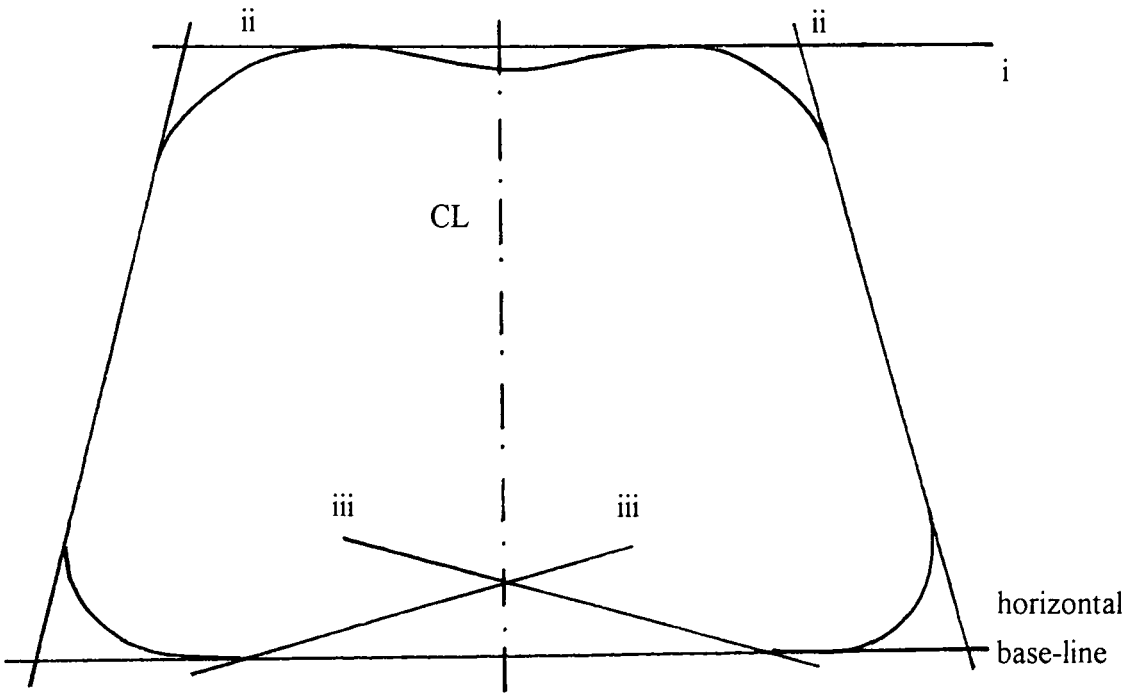

c) 9 mm head diameter

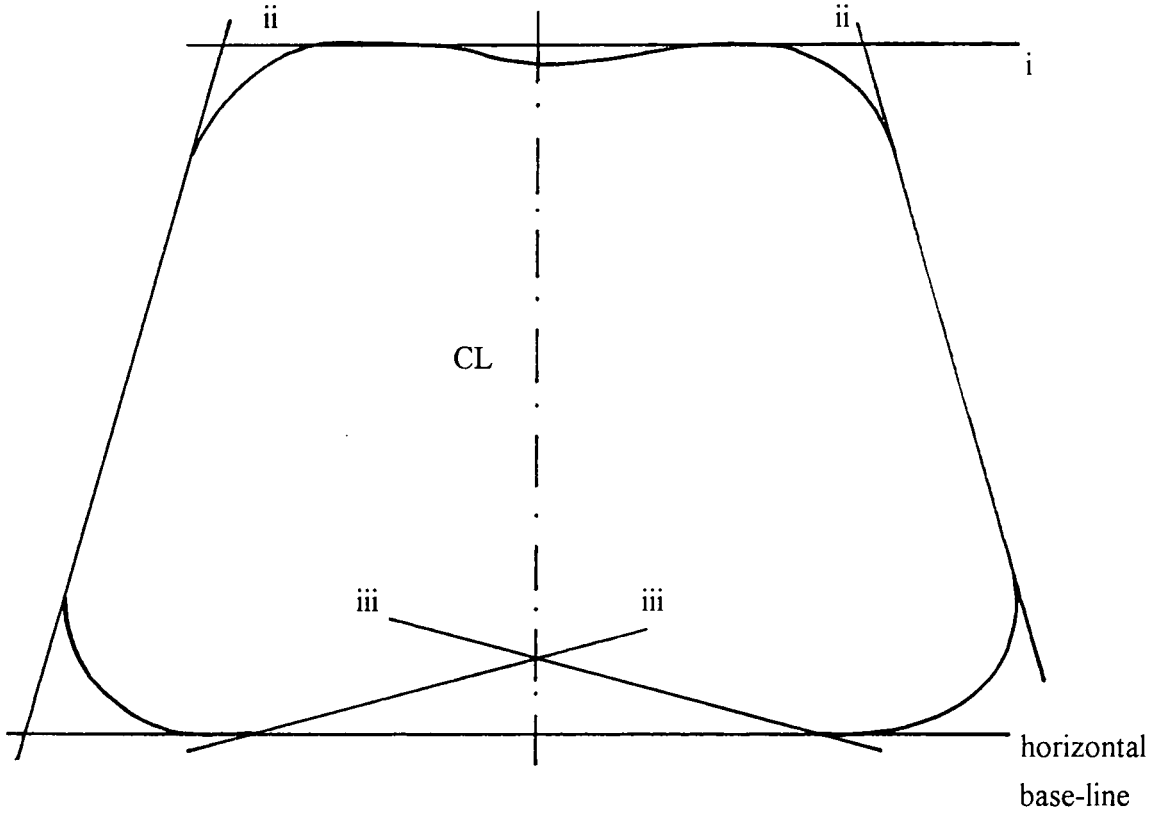

d) 10 mm head diameter

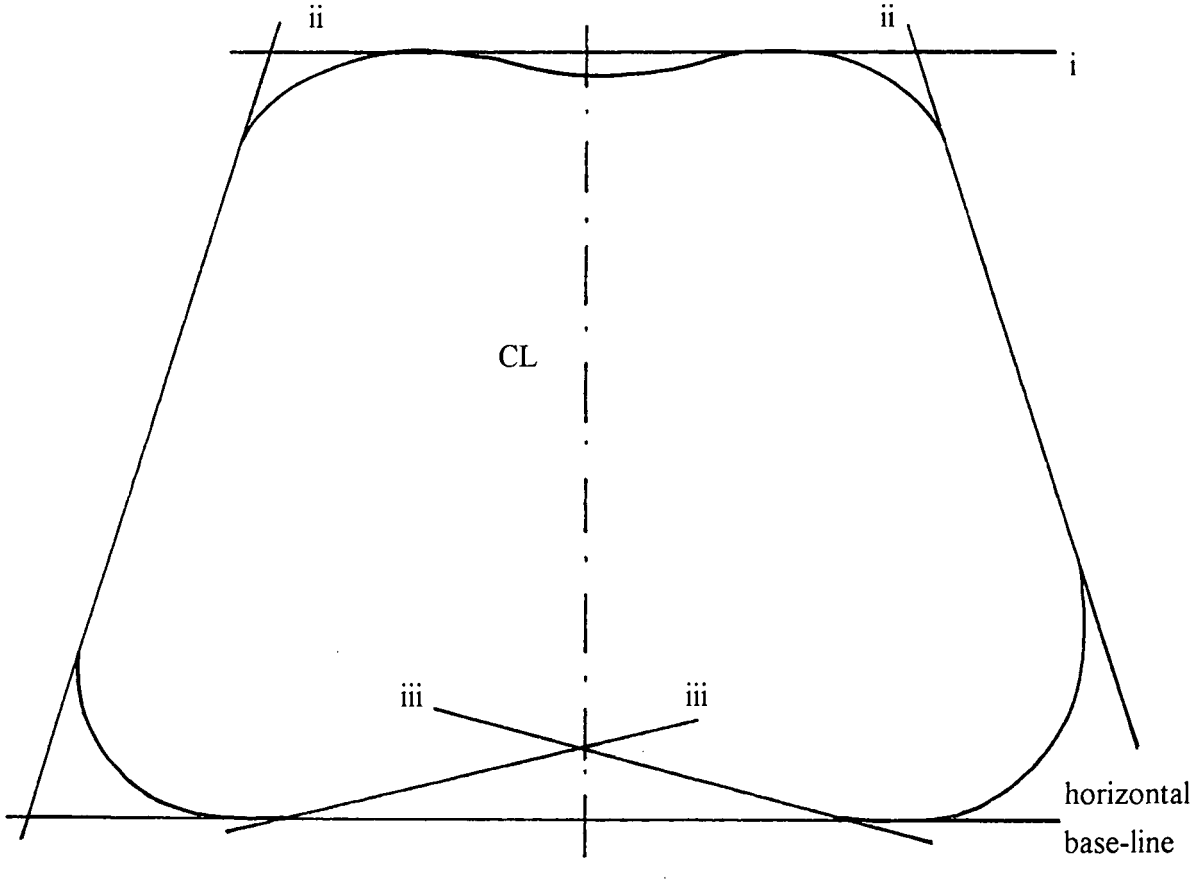

Figure 4.3 Models of the proximal phalangeal head bearing surface, transverse plane (x 10 magnification, dimensions in mm unless otherwise stated)

a) 7 mm head diameter

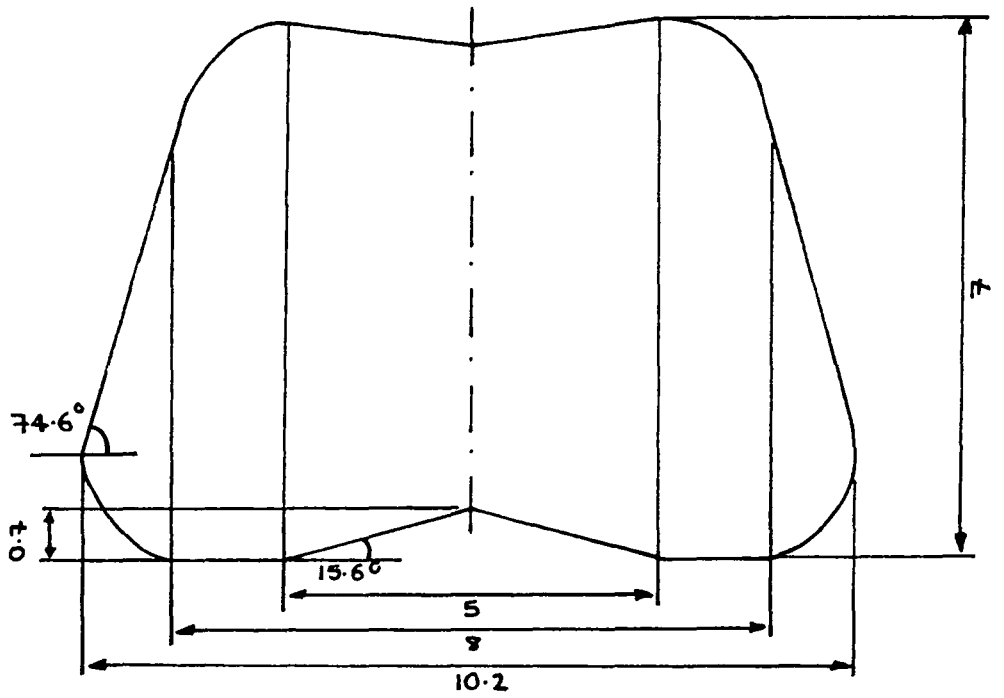

b) 8 mm head diameter

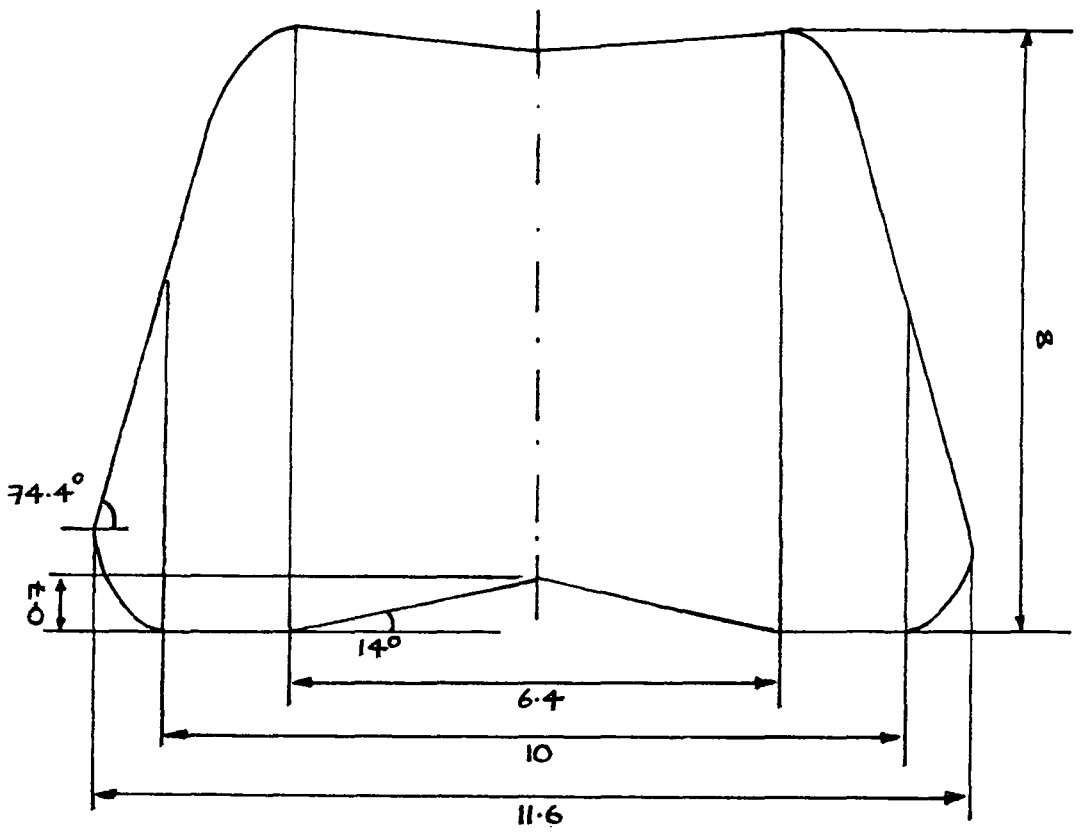

c) 9 mm head diameter

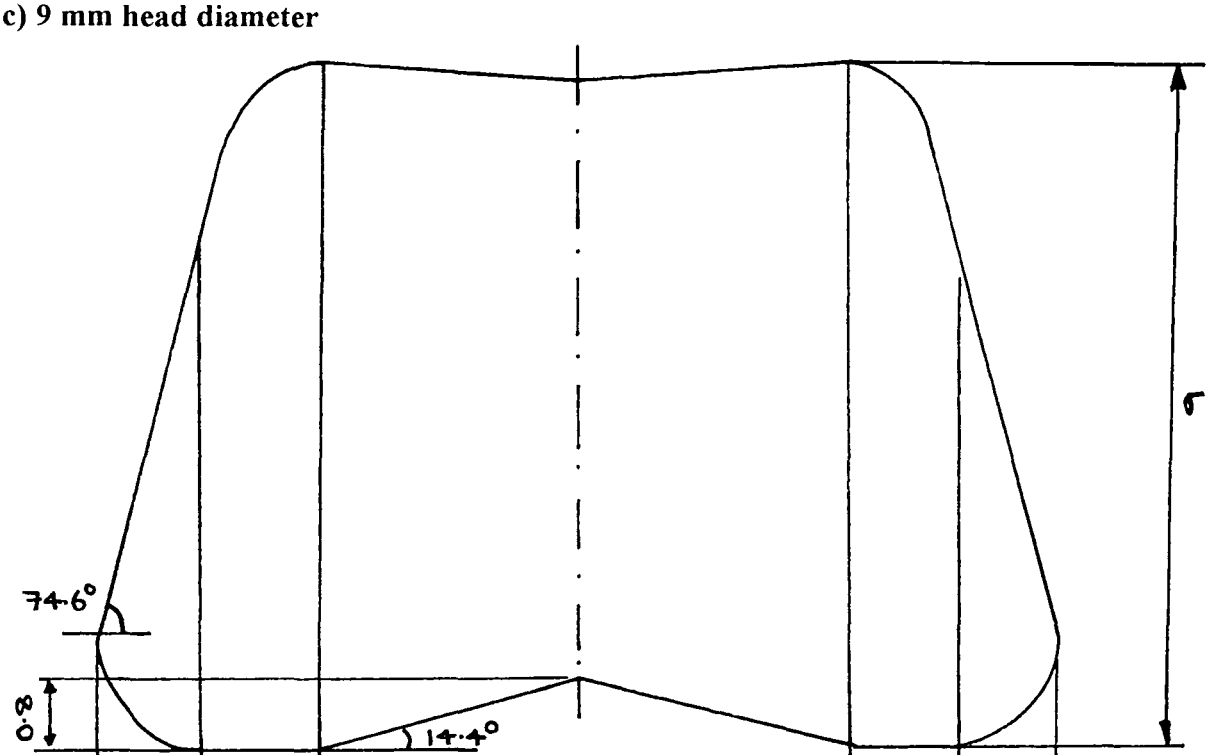

d) 10 mm head diameter

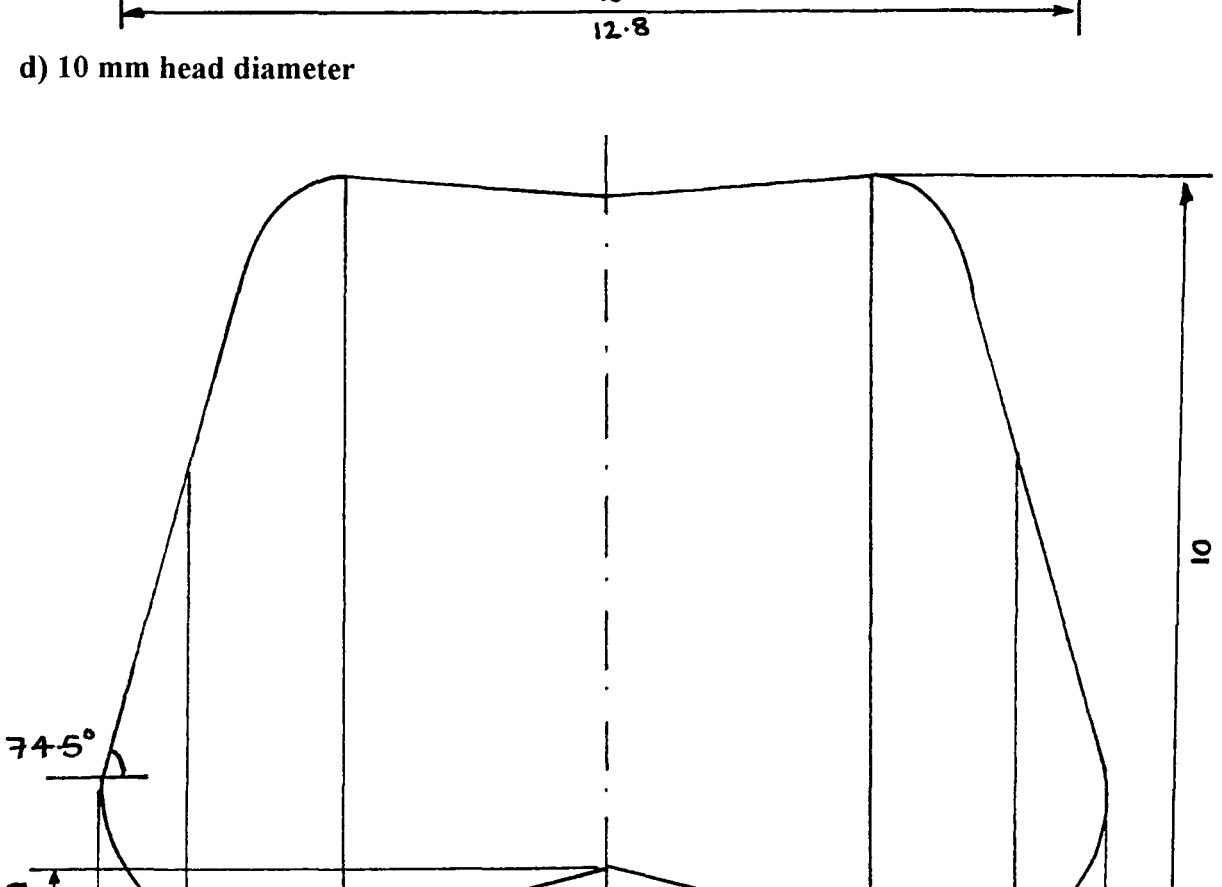

lateral sides of the condyles and the horizontal base-line were set at approximately 75°. This was slightly lower than the average measured angles $\alpha 1$ and $\alpha 2$. However, it reduced the possibility of the joint prostheses overlapping the end of the bones, and impinging on the soft tissues surrounding the joint. The sides of the condyles were also rounded off 1.5 mm from the top and bottom of the condyles for this reason (1 mm from the top for the 7 mm model and 2 mm from the bottom of the condyles for the 10 mm model).

The minimum condyle diameter occurred at the centre-line. The inter-condylar sulcus depths were 0.7, 0.8, 0.9, and 0.9 mm for the 7, 8, 9 and 10 mm models respectively. These compared well with the measured inter-condylar sulcus depth values, ISat, of 0.61, 0.74, 0.92 and 0.90 respectively. The condyles increased linearly in diameter from the centre-line at an angle of approximately 14° until the maximum condyle width was achieved. The condyles then remained at the maximum condyle diameter for a width of 1.5, 1.8, 1.5 and 2 mm for the 7, 8, 9 and 10 mm models respectively. The models imply corners at the changes of diameter of the condyles. However, in practice the bearing surfaces could be rounded in these regions if required.

4.4 Feasibility of a PIPJ surface replacement prosthesis

Ideally a surface replacement joint prostheses replaces just the damaged articular surfaces with minimal bone resection. This not only leaves sufficient bone stock for revision, but also leaves the ligaments surrounding the joint intact. The PIPJ has no muscular support laterally, hence it is important that the collateral ligaments are preserved to maintain lateral stability of the joint. This is especially important with surface replacement joint prostheses as the unconstrained joint prostheses, themselves, provide little stability to the joints. The main problems with a surface replacement joint prosthesis occurred with the PP component due to the shape of its bearing surfaces.

The feasibility of a surface replacement joint prosthesis for the PP head was assessed by super-imposing a hollow cylinder on the sagittal shadowgraphs of the PP heads. A 1 mm thick cylinder and a 2 mm stem were marked on PP heads of sizes ranging from 6-11 mm (Figure 4.4). These were thought to be the minimum thicknesses that could be considered. The hollow cylinder left little bone stock within the joint prosthesis itself, regardless of the size of the joint. Even with the 10 mm size, a maximum of only 1.5 mm of bone remained posterior to the stem. In addition, a bicondylar shaped bearing surface would reduce the bone stock within the joint prosthesis further. Hence a

Figure 4.4 **Proximal phalangeal head with a hollow cylinder, surface replacement joint prosthesis marked**

a) 7 mm head diameter

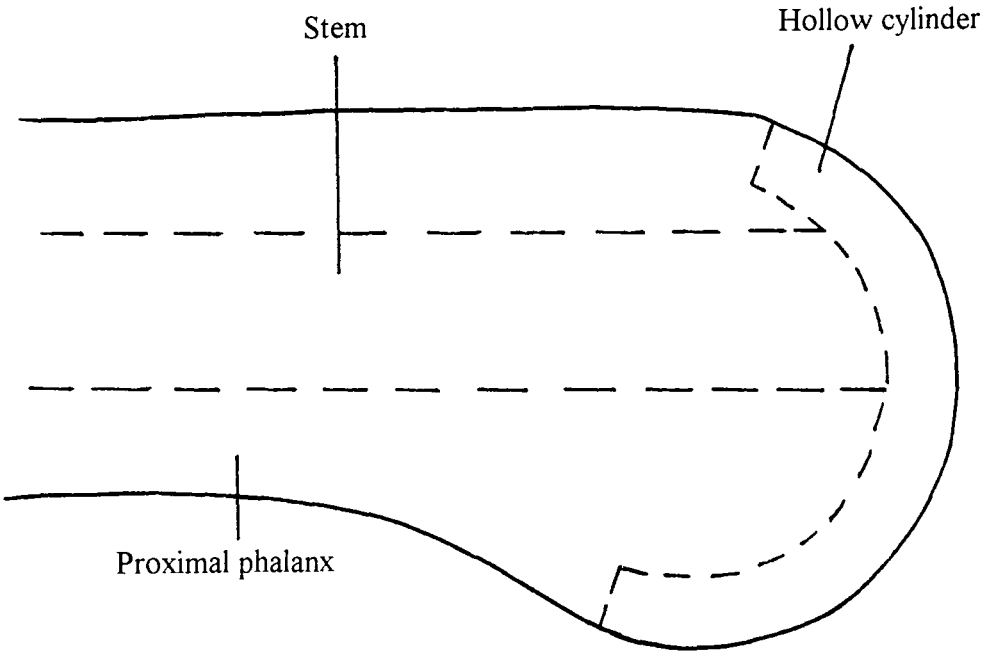

b) 8 mm head diameter

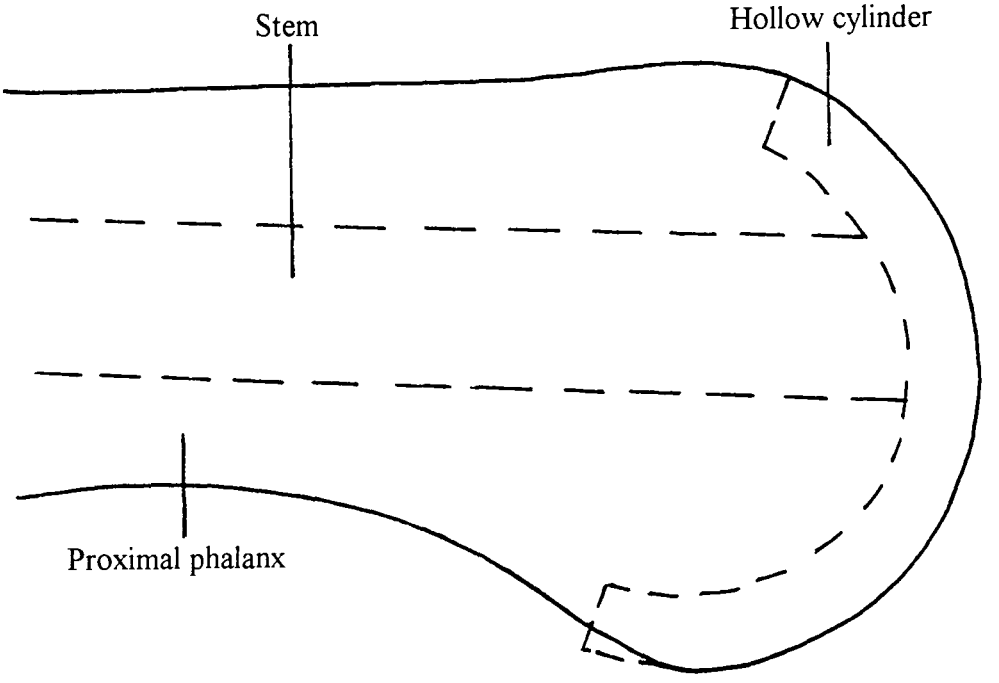

c) 9 mm head diameter

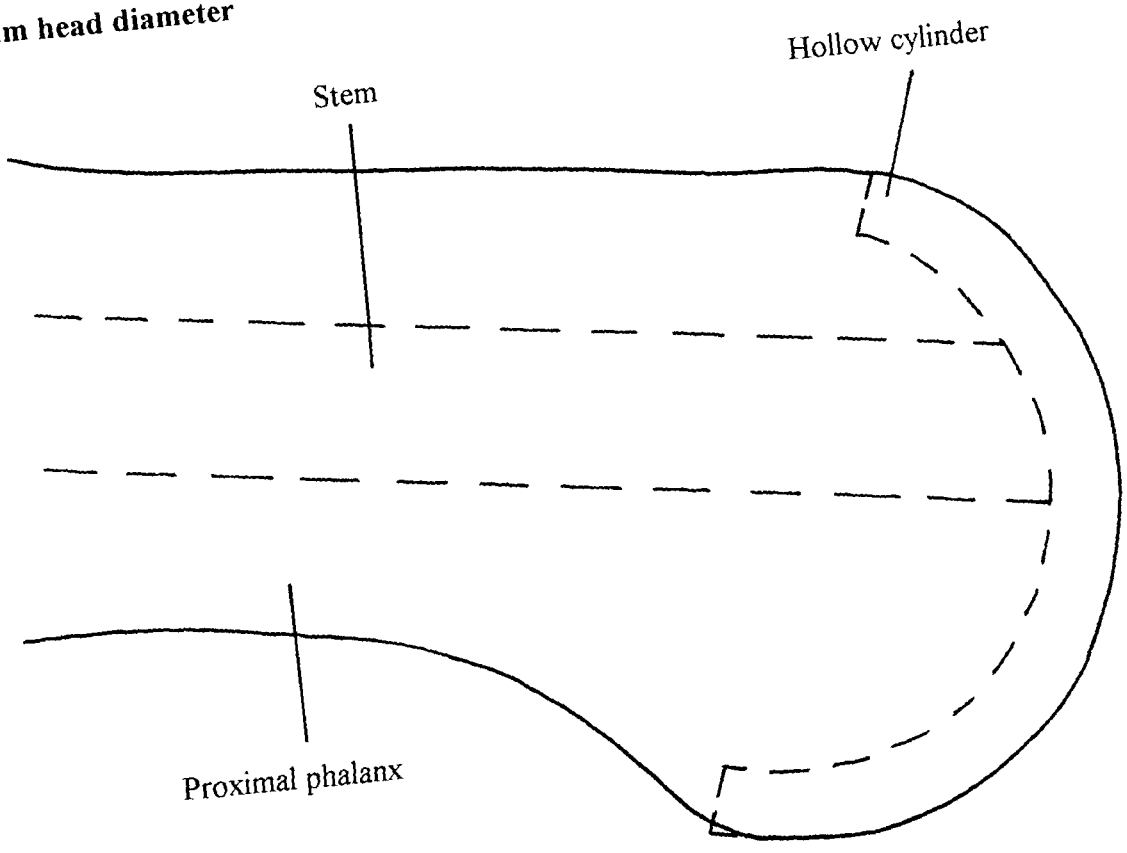

d) 10 mm head diameter

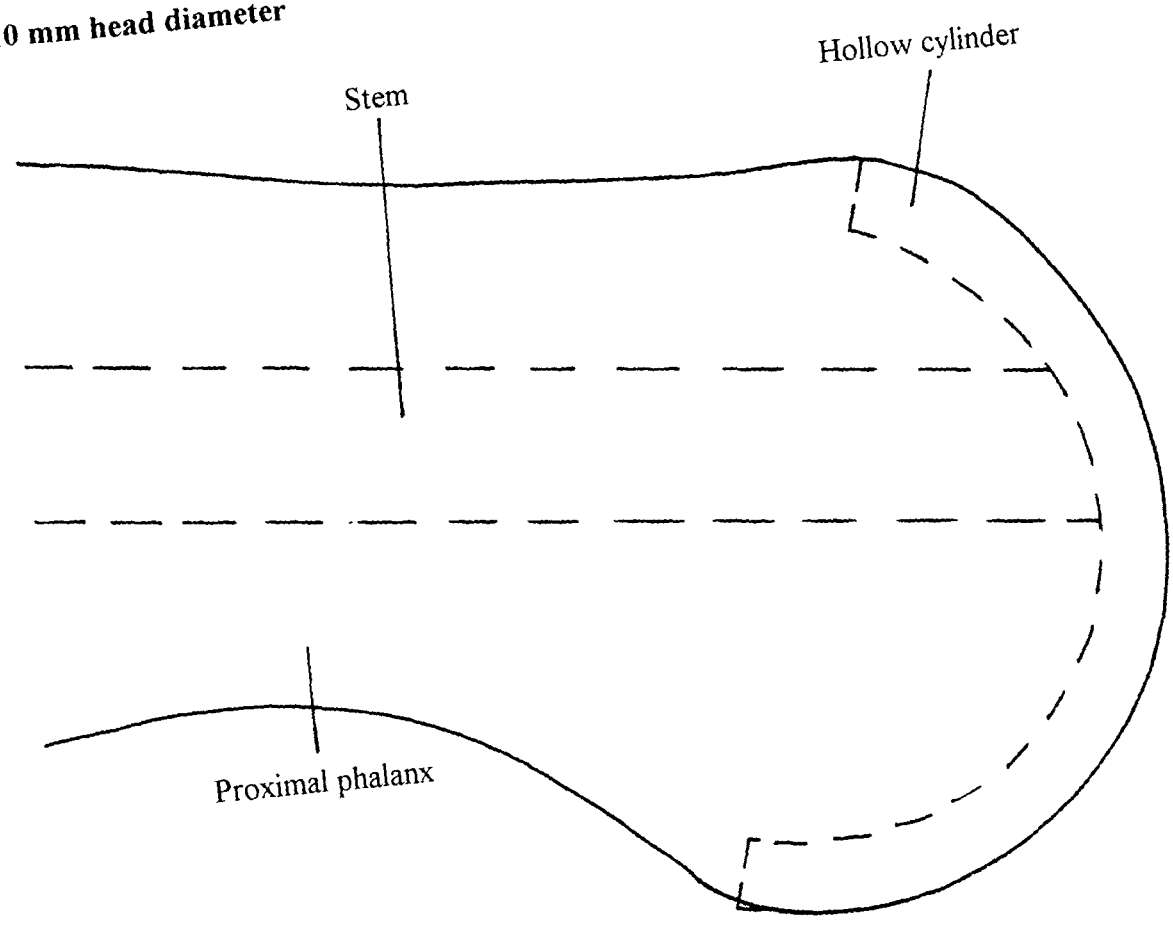

hollow surface replacement joint prosthesis was not feasible for the PIPJs due to the small joint sizes involved, hence any design required a solid head.

The main concern of a solid joint prosthesis was the positioning of the collateral ligaments on the PP head. The larger amounts of bone removal necessary for a solid joint prosthesis may have interfered with the attachment of the collateral ligaments. However, by comparing the origins of the soft tissues surrounding the PIPJs with the position of a solid half cylindrical joint prosthesis it was thought that such a joint prosthesis would not require the complete resection of the collateral ligaments or their reattachment at a remote site. The design would also simplify the preparation of the PP head for the joint prosthesis.

The problems encountered with the amount of bone stock left between the PP component bearing surfaces and the stem did not occur with the MP component due to the convex shape of the component at the bone-bearing surface interface. In addition, the component was designed to fit within the natural recess which would only require the removal of the MP base cartilage and little bone. Hence the collateral ligament attachments were not affected by implantation of the MP component.

The feasibility study also highlighted possible problems of the design of stems for interference fixation of the joint prosthesis with the phalangeal bones due to the small sizes of the phalangeal bone shafts. The three main considerations for interference fixation were the shape, size and offset of the stems from the centre of rotation of the joint. (The cross-sectional shape and size of the stems is discussed in Section 4.5.2). It was also noted that to get an even interference fixation the angle of inclination of the stems was important. In addition, the PP shaft angle changed just proximal to the head. Hence the stems lengths were limited by the distance from the bearing surface to the change in angle of the PP shaft. However, despite these problems the design of stems suitable for interference fixation of the PP and MP components was feasible. Hence a two-piece surface replacement joint prosthesis with a solid PP head, and stems for interference fixation was designed.

4.5 Development of a proximal interphalangeal joint prosthesis

The design of each of the two components was divided into two sections. Firstly the design of the bearing surfaces and secondly the design of the stems to achieve secure fixation. From the design considertions discussed in Section 4.1, the PP head models

and the feasibility study of a surface replacement joint prosthesis, the following summary of the required design criteria for a PIPJ surface replacement prosthesis was produced :

* Four joint prostheses of similar design over a range of sizes (7, 8, 9, 10 mm by head diameter)
* Bi-condylar bearing surfaces with symmetrical condyles
* Conforming bearing surfaces
* Circular PP head sagittal plane profile covering a minimum arc of -45° to 100° flexion
* Circular MP base sagittal plane profile covering a maximum arc of 90°
* Solid PP head
* Stems for interference fixation with full consideration to the cross-sectional shape, size, length and angle of inclination
* Simple surgical technique (minimal and uncomplicated tooling)

4.5.1 Proximal phalangeal component bearing surface

To simplify the preparation of the PP head, a single cut to remove the diseased cartilage was preferred. Further cuts would lengthen the surgical procedure, be complicated due to the small amount of bone stock available and move away from the ideal of minimal bone resection. Assuming the single cut to coincide with the centre of rotation of the PP head, an arc of 180° in the sagittal plane was required. It was observed that the natural PP head cut away from the circular profile at approximately 100° flexion. This was possibly to allow room for the soft tissues during full flexion of the joint. In addition, the circular profile was required up to a position of 45° hyper-extension for full extension of the joint. Hence the PP head component bearing surface consisted of a 180° arc from 100° flexion to 80° of hyper-extension in the sagittal plane (Figure 4.5a).

In the transverse plane the PP component was designed as close to the four models as possible (Figures 4.3 a-d). It may be noted that the transverse plane shape of the PP head was taken with respect to the longitudinal base-line. However, the PP component was designed with the bone-joint prosthesis interface vertical. Hence the shape of the PP head in the transverse plane and with the bone-joint prosthesis interface vertical were not identical. However, the variation between the two shapes was within 0.2 mm. Hence the models of the PP head in the transverse plane were taken as the basis for the design of the PP component (end view) to simplify the design process (Figure 4.5b).

Figure 4.5 Proximal phalangeal component

a) Side view

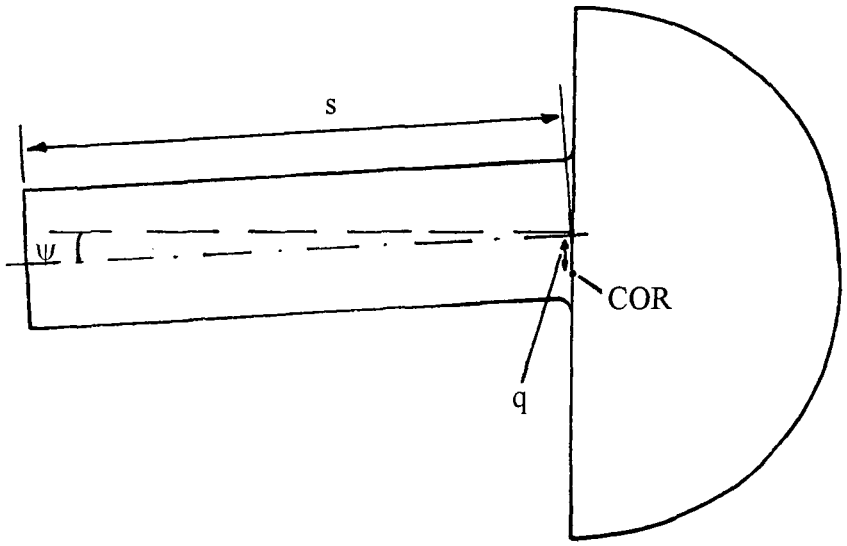

b) PP head end view

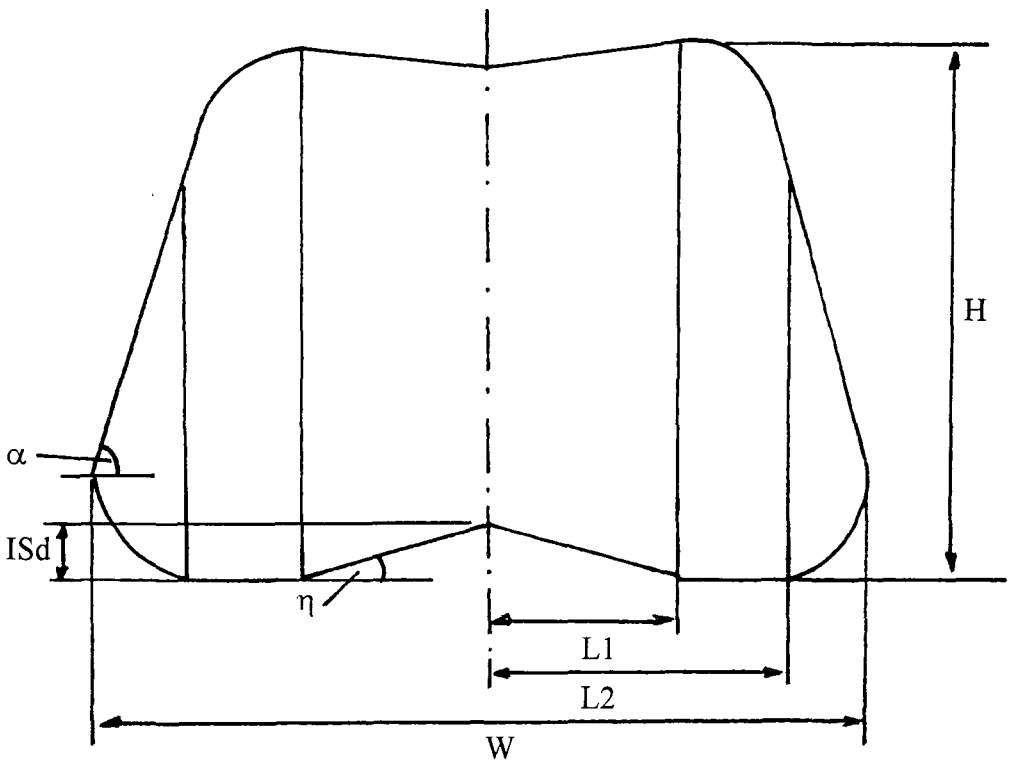

The inter-condylar sulcus depths of the models were slightly greater than those measured for the 7 and 8 mm sizes, however, the depths of the models were used to increase the stability of the joint slightly. The depth of the inter-condylar sulcus on the posterior face of the models (transverse plane) was 3 mm for each of the four sizes. Hence the inter-condylar sulcus was decreased linearly at a tangent to the minimum condyle diameter to a depth of 3 mm on the dorsal aspect. This still left a circular profile in the sagittal plane over the range of motion of the joint.

Table 4.2 shows a summary of the major dimensions of the models in the transverse plane where W : width. H : height. α : angle of tilt of the condyles in the transverse plane. ISd : inter-condylar sulcus depth. L1 : distance from the centre-line to the maximum condyle diameter. L2 : the width of maximum condyle diameter. η : angle of the line from the maximum condyle diameter to the minimum condyle diameter, (Figure 4.5b). The rest of the PP head was rounded off so that it would not protrude from the ends of the bone and impinge on the soft tissues surrounding the joint.

Table 4.2 Summary of proximal phalangeal head model dimensions

Parameter	Units	7 mm	8 mm	9 mm	10 mm
W	mm	10.2	11.6	12.8	13.4
H	mm	7	8	9	10
α	°	74.6	74.4	74.6	74.5
ISd	mm	0.7	0.8	0.9	0.9
L1	mm	2.5	3.2	3.5	3.5
L2	mm	1.5	1.8	1.5	2.0
η	°	15.6	14.0	14.4	14.4

4.5.2 Proximal phalangeal component fixation

The only viable method of fixation for the PP and MP components was interference fixation (press fit) of the stems with the phalangeal bones. The five considerations for designing such stems were the offset of the stem from the centre of rotation of the PIPJ, the angle of the stems, the stem length, and the cross-sectional shape and size.

The average offsets of the centre-line of the PP medullary canal to the centre of rotation of the PIPJ were 0.67, 0.70, 0.79 and 0.86 mm for the 7, 8, 9 and 10 mm sizes respectively. However, these were measured perpendicular to the longitudinal base-line. Using trigonometry it was calculated that the dorsal offset of the centre-line of the PP medullary canal to the centre of rotation of the PP component along the bone-joint

prosthesis interface (q) were slightly less at 0.66, 0.69, 0.78 and 0.85 mm respectively (Figure 4.5).

All of the angles in the sagittal plane were also measured with respect to the longitudinal base-line. However, during surgery the dorsal surfaces of the phalanges would be used as the reference for any surgical tooling. In addition, when the PIPJ was in the neutral position (0° flexion), the dorsal surfaces of the PP and MP bones were in alignment and not the longitudinal base-lines. When describing the arc of the PP head in the sagittal plane (80° hyper-extension to 100° flexion) it was important to note that this was with reference to the dorsal surface of the PP. Therefore the required inclination of the stems with respect to the dorsal surface of the PP was (ρ - ϕ). The angle between the stem and the perpendicular to the bone-joint prosthesis interface (ψ) was therefore [10° - (ρ - ϕ)]. The average angles ψ for the four joint prosthesis sizes are shown in Table 4.3 (Figure 4.5a).

Table 4.3 Associated proximal phalangeal stem angles (°)

Parameter	7 mm	8 mm	9 mm	10 mm
ρ	10.50	11.09	10.69	9.94
ϕ	6.90	5.35	4.69	4.18
ρ-ϕ	3.60	5.74	6.00	5.76
ψ	6.40	4.26	4.00	4.24

The distance from the PIPJ bearing surface to the change in angle of the dorsal surface of the PP (d) was measured to indicate any limitations of the length of stem of the PP component. However, again this was measured parallel to the longitudinal base-line. The limitation of the stem length (s) due to d was calculated by taking the dorsal surface of the PP as reference and taking the radius of the PP head into account (Figure 4.6). The calculated values of the limitation of the stem length (s) were 8.14, 9.21, 10.12 and 10.34 mm for the 7, 8, 9 and 10 mm sizes respectively. Hence stem lengths of 8, 9, 10 and 10 mm respectively were used to account for the width and offset of the stems.

A range of cross-sectional shapes were fitted to the shadowgraphs of the transverse sections of the PP. The different cross-sectional shapes of stem considered are shown in Figure 4.7. The shapes were assessed on how well they fitted the medullary canals, the amount of overlap of the bone they produced, the thickness of bone stock left, rotational stability and the ease of manufacture (Figure 4.8). The results are shown in Table 4.4.

Figure 4.6 Limitation of the length of the proximal phalangeal component stem

a) With reference to the longitudinal base-line

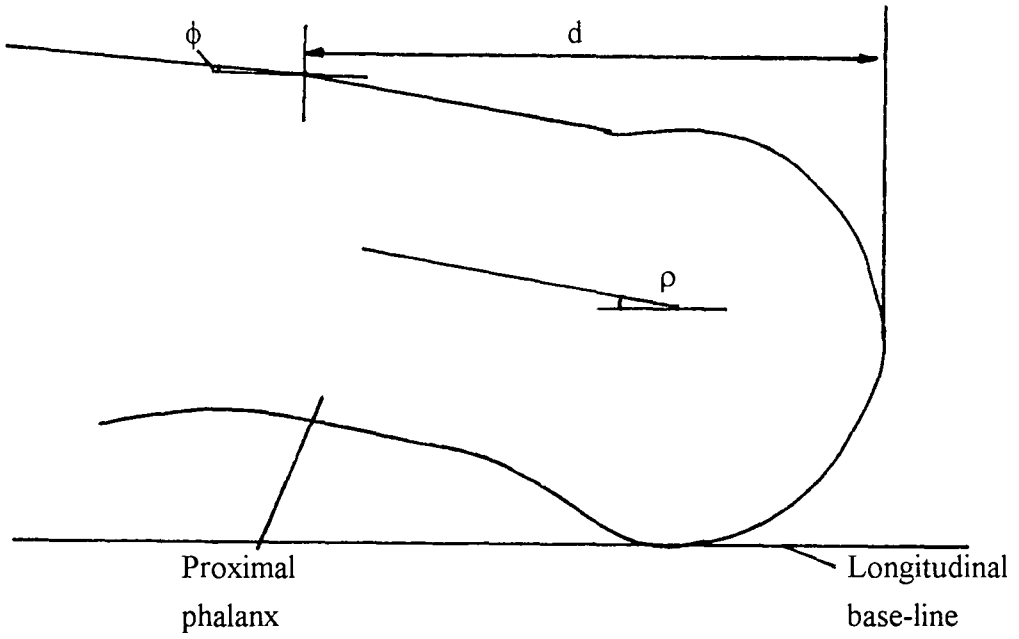

b) With reference to the dorsal surface of the proximal phalanx

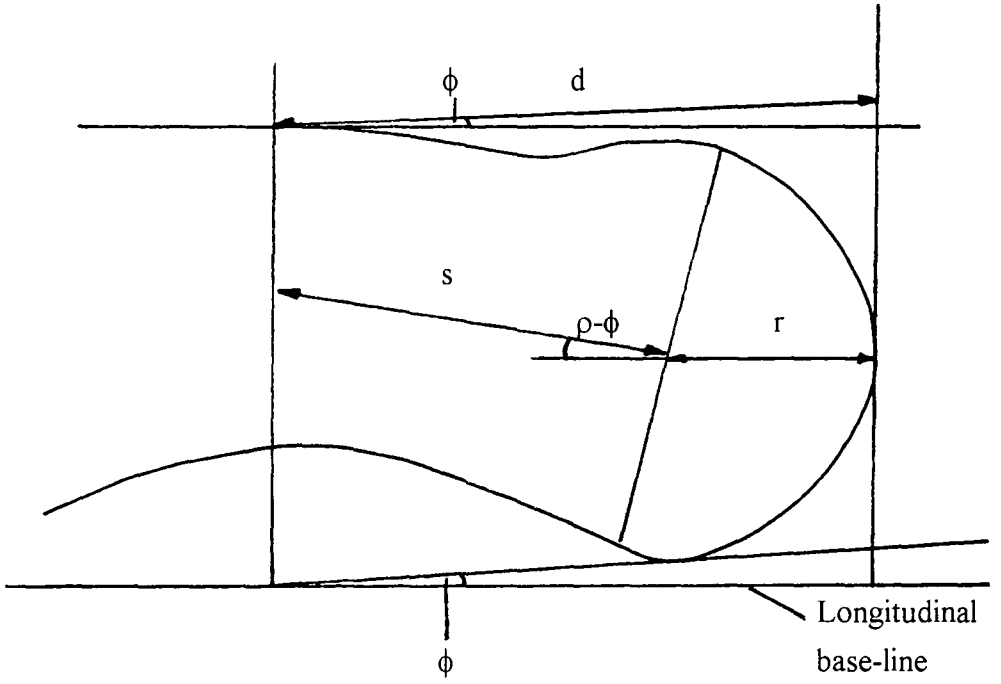

Figure 4.7 Stem cross-sectional shapes

Ellipse	Semi-circle
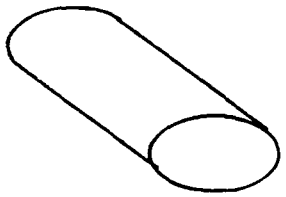	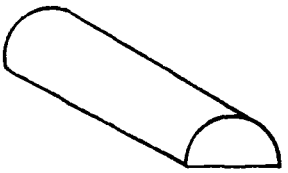
> Semi-circle	< Semi-circle
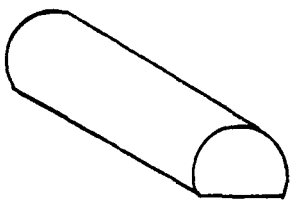	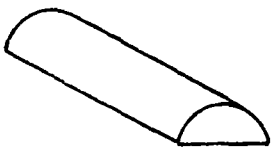
Fins	Triangle
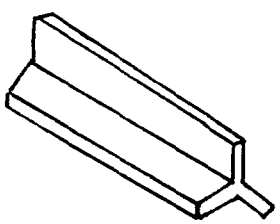	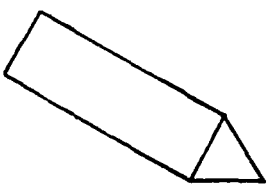
Triangle with corners cut away	Indented triangle
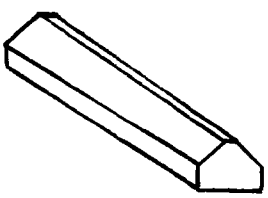	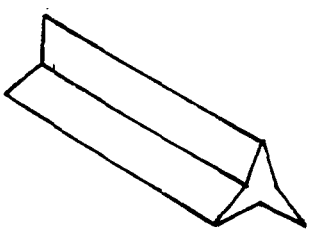
Circle	Square
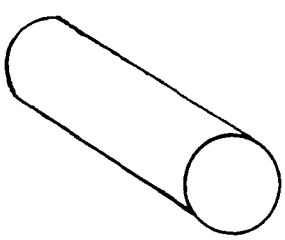	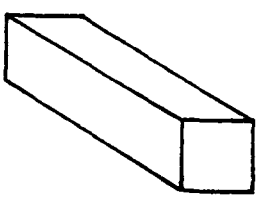

Figure 4.8 **Fit of cross-sectional shapes to the transverse sections of the proximal and middle phalangeal bones**

a) Ellipse

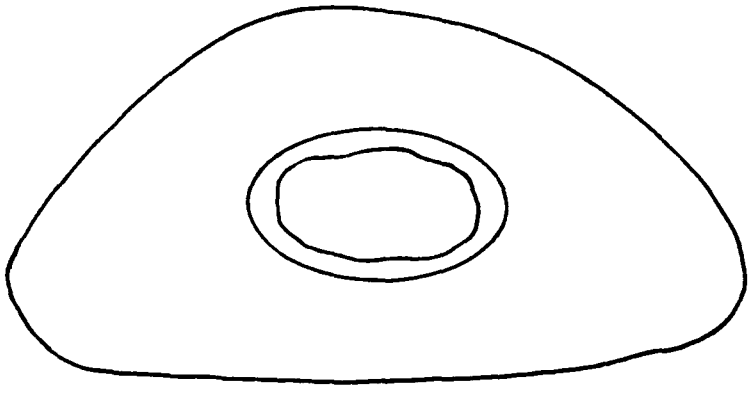

b) Semi-circle

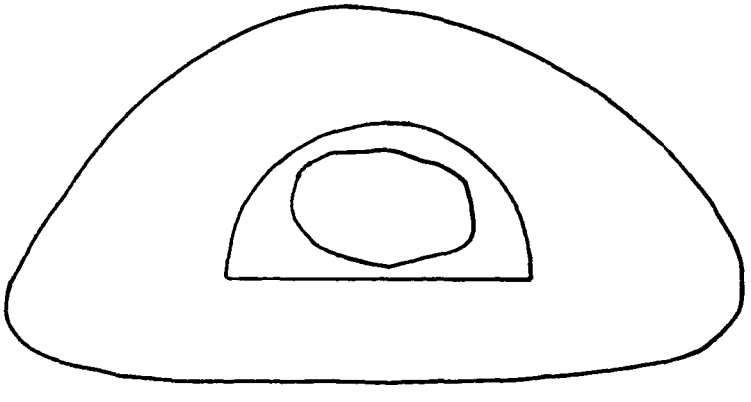

c) Triangle

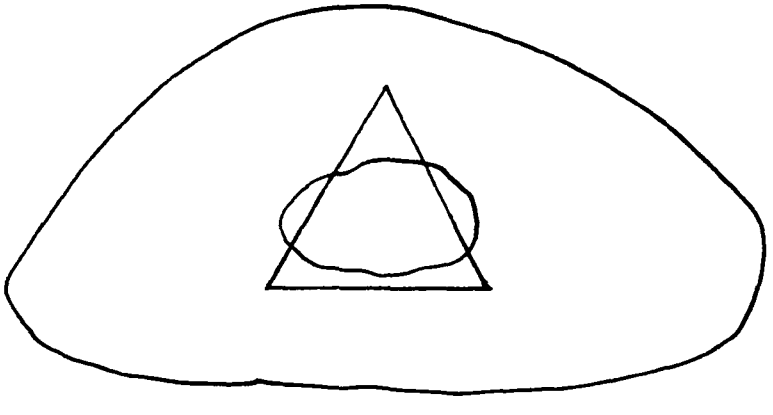

Table 4.4 Evaluation of different stem cross-sectional shapes

Stem cross-sectional shape	Fit	Description of fit	Manufacture	Rotational stability
Ellipse	Excellent	Fits all canal equally	Difficult	Unknown
Semi-circle	Good	Overlap laterally-palmarly	Easy	Good
> semi-circle	Poor	Overlap laterally-palmarly	Easy	Good
< semi-circle	Poor	Overlap laterally-palmarly	Easy	Good
Fins	Good	Variable overlap	Fair	Unknown
Triangle	Poor	Overlap on all corners	Easy	Good
Triangle with corners cut away	Good	Overlap laterally-palmarly	Fair	Good
Indented triangle	Poor	Overlap on corners and undercut on sides	Fair	Good
Circle	Poor	Undercut laterally	Easy	Poor
Square	Poor	Overlap on corners	Easy	Good

The best fit cross-sectional shape for the PP was an ellipse. However, there were concerns over the rotational stability of the shape. A semi-circular shape had a good fit and rotational stability. It overlapped the bone slightly palmarly on the lateral aspects, but not to such a degree that the amount of remaining bone stock was of concern. In addition, it was felt that a stem of semi-circular cross-section would be easier to manufacture than one with an elliptical cross-section. Hence the semi-circular cross-section was chosen for the PP component stems.

Different sized semi-circles (increasing in radius by 0.25 mm steps) were then fitted to the shadowgraphs of the PP in the transverse plane. The best size of semi-circular cross-section for each joint prosthesis size was 2, 2.5, 2.5 and 2.75 mm for the 7, 8, 9 and 10 mm PP components respectively.

4.5.3 Middle phalangeal component bearing surface

The bearing surfaces of the PIPJ surface replacement prosthesis were designed to be conforming. The MP component base was designed to conform with the PP component head. The only alteration to the bearing surface shape was to the inter-condylar sulcus ridge which was lowered to prevent increased wear at this point. The MP component was also designed to fit within the natural recess of the MP base. Hence the other considerations to the MP base bearing surfaces were the arc in the sagittal plane (or height), width and thickness.

To measure the required arc of the MP component in the sagittal plane, circles of the appropriate PP head size were matched to the shadowgraphs of the MP bases. The best-fit arc of this circle to the MP base was then measured. Ideally the MP component would not protrude from the original line of the bone and cartilage, however, it was easier to align the circles with the sagittal plane profile rather than sunk into the bone. This did not alter the arc of the circle that fitted the MP base. The average arcs of the MP bases , ω, (sagittal plane) were found to be 78.8, 79.0, 77.0 and 74.53° for the 7, 8, 9 and 10 mm sizes respectively and 77.28° overall.

The average dimensions were used to design the PP and MP components to produce a joint prosthesis which was overall as close to the original anatomy as possible. However, the stability of the PIPJs was a major factor when designing the joint prosthesis. This was the main reason why the bearing surfaces were designed to be conforming. Hence instead of using the average arc of the bases for the design of the MP component, the maximum arc of 90° was used to maximise the stability that the joint prosthesis could bring to the PIPJs. It was thought that this would not significantly restrict the range of motion of the joint. This would only be a problem at the limits of the range of motion of the joint which probably would not be achieved with badly affected rheumatoid joints. In addition, such a joint prosthesis still fitted within the MP bones without reducing the bone stock or overlapping the bones detrimentally.

The width of the MP component was chosen partly due to the shape of the PP head and partly due to the width of the MP base. It was not possible to measure the arc of cartilage in the frontal plane due to the shape of the bone. So the width of the MP component was evaluated by superimposing outlines of the PP component bearing surface on the shadowgraphs of the MP bones in the frontal plane. The widths were 8, 10, 10, and 11 mm for the 7, 8, 9 and 10 mm sizes respectively. The MP base bearing surfaces were elliptically shaped in the transverse plane using the previously evaluated width and height (calculated from the arc in the sagittal plane) as the major axes. These were then super-imposed on the transverse plane shadowgraphs of the MP bones to cross-check their suitability.

The thickness of the bearing surface was kept to a minimum to minimise the amount of bone removal necessary. It was thought that the minimum thickness that could be considered would be 1.5 mm. However, it should be stressed that this would need to be tested in the future on a joint simulator or with finite element analysis methods to assess whether it was adequate or not.

4.5.4 Middle phalangeal component fixation

A similar method for designing the stems of the PP components was used for the MP components. However, the MP bones did not have a medullary canal in the part of the bone where the stem would be located. Hence the cross-sectional shape of the stem had to be evaluated with respect to overall shape of the bone in the transverse plane. Similarly to the PP component, the most suitable cross-sectional shape was the semi-circle when rotational stability was considered as well as the fit and manufacture. The best size of semi-circular cross-section for each joint prosthesis size was 1.5, 2, 2 and 2.5 mm (by radius to the nearest 0.25 mm) for the 7, 8, 9 and 10 mm sizes respectively.

Unlike the PP components the stems were kept parallel to the centre-line of the MP bearing surface (sagittal plane) because it was felt that an angled stem may complicate the surgical procedure unnecessarily. Interestingly it was found that the stems were offset slightly palmarly from the centre of rotation of the joint, when located centrally within the bone. The palmar offsets of the stems, v, were on average 0, 0.1, 0.15 and 0.3 mm for the 7, 8, 9 and 10 mm sizes respectively. The lengths of stem were also evaluated and found to be on average 5.5, 5.5, 6 and 6.5 mm respectively (to the nearest 0.5 mm). The overall MP component shape is shown in Figure 4.9.

4.6 Surgical tooling design

The PIPJ surface replacement prosthesis was designed such that the surgical procedure and tooling was as simple as possible. However, the main difficulty with the design of such tooling was the alignment of the tools relative to the bones, due to the small sizes and irregular shapes of the phalanges, and also the alignment of the middle phalanx with the proximal phalanx. The surgical procedure would consist of four main stages. These are evaluation of the joint size, removal of the required amount of bone and cartilage from the PP head and MP base, reaming holes for the stems and press fitting the two components. The tooling requirements for these stages are as follows:

Evaluation of the joint size could be performed by two methods. Firstly the PP maximum head width could be ascertained from X-rays. Using the relationships

Figure 4.9 Middle phalangeal component

a) Side view

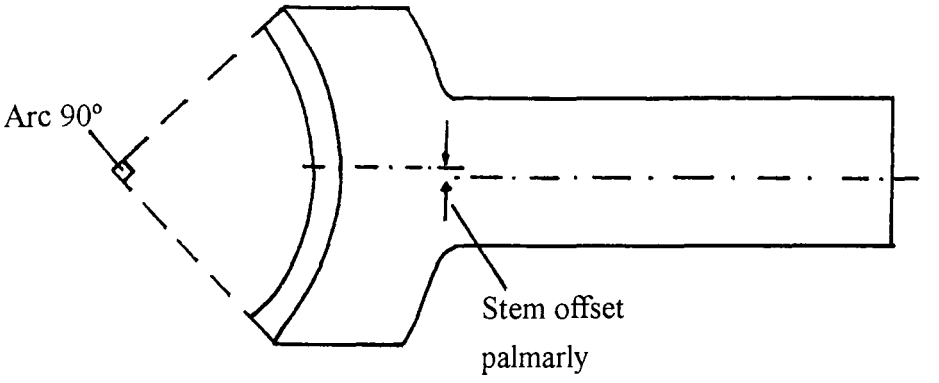

b) Plan

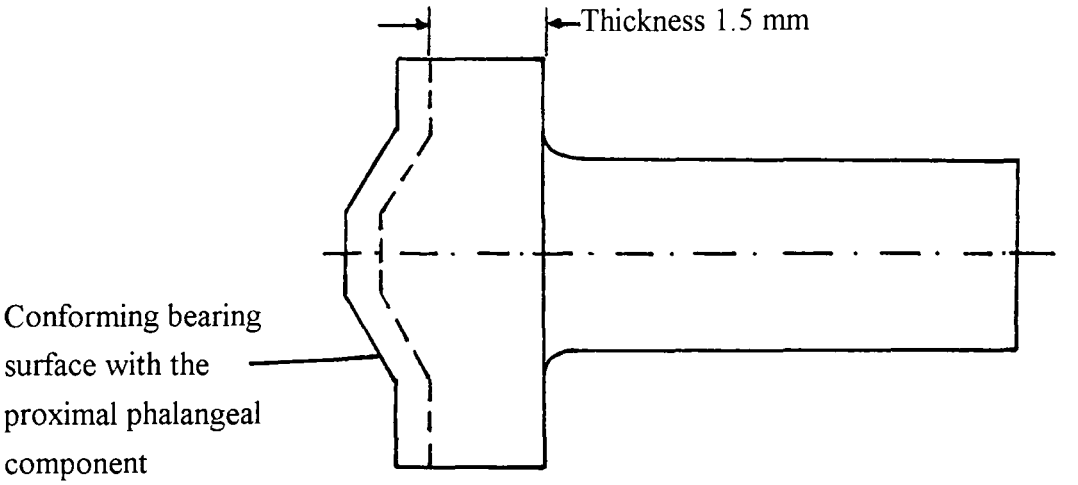

c) End view

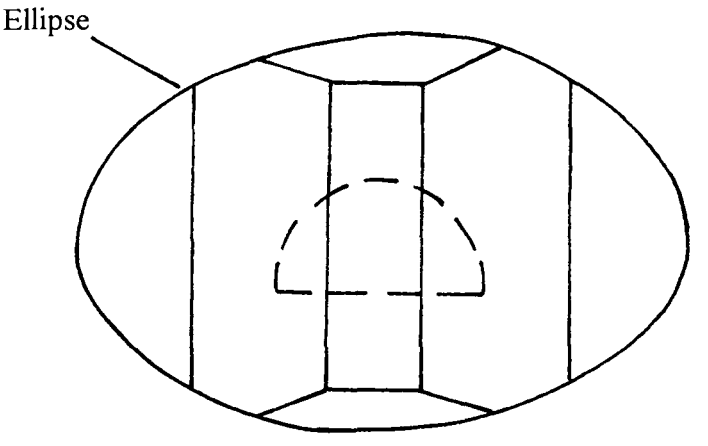

developed in Section 3.2.5 the head diameters of the joints could be estimated. However, the accuracy of this method would depend on the alignment of the hand during X-ray and the magnification of the X-rays. In addition, there was some overlap between the maximum head width and the head diameter, hence this would only give an estimate of the head diameter. Alternatively the joint size could be ascertained during surgery using a tool (Figure 4.10a).

The removal of the bone and cartilage from the PP head was simplified by using a single cut. Using the dorsal surface of the PP as a reference a cut at 80° to this reference would be performed using a guide (Figure 4.10b). The main problem with this tool is the alignment with the end of the PP head so that the cut coincides with the centre of rotation of the PP head. If the incorrect amount of bone was removed then the joint prosthesis may overlap the bone end and impinge on the soft tissues surrounding the joint, and the mechanical advantage and laxity of the joint would be altered.

Once the required amount of bone and cartilage was removed it may be possible to simply press fit the PP stem into the medullary canal, although reaming may be necessary which would require a guide (Figure 4.10c). However, difficulty may occur in the alignment of the reamer guide with the PP bone. A gap between the guide and the bone on the dorsal surface could result in the hole and hence the PP component being positioned incorrectly. However, the gap may be unavoidable due to the change in angle of the dorsal surface of the PP. Hence it may be more accurate to simply press fit the joint prosthesis by eye without reaming a hole for the stem.

It is also not clear how much tooling will be required for the MP component. Some of the damaged cartilage and bone may need to be removed and a hole for the stem reamed. However, it may be possible to just simply press fit the component into the MP base. This would depend on the quality of the cartilage and the bone of the MP base. If cartilage and bone removal is necessary then cutting and reaming guides may also be required (Figure 4.10d). However, if guides are required then alignment of the guides with the MP bone and alignment of the MP bone with reference to the PP bone would need to be considered and could be complicated.

Figure 4.10 Surgical tooling for the PIPJ surface replacement prosthesis

a) Joint sizer

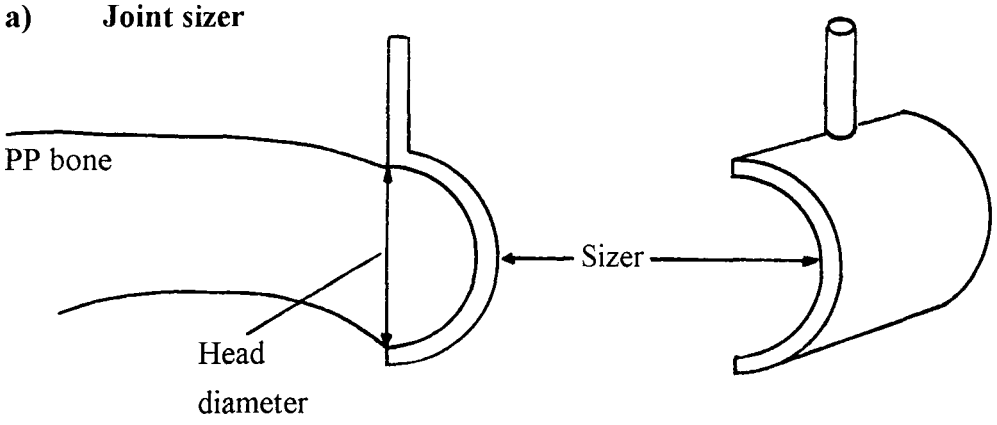

b) Proximal phalangeal head cutter guide

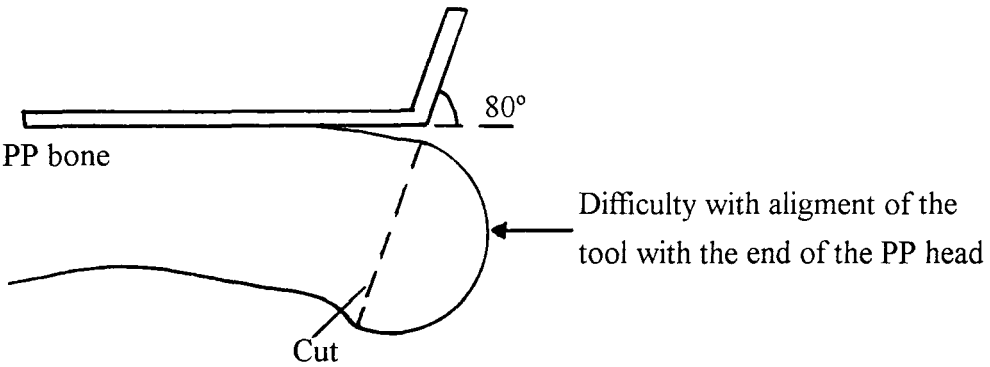

c) Proximal phalangeal head reamer guide

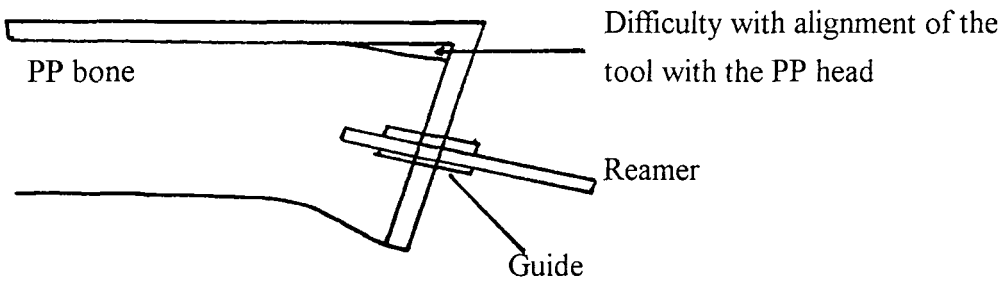

d) Middle phalangeal base cutter and reamer guides

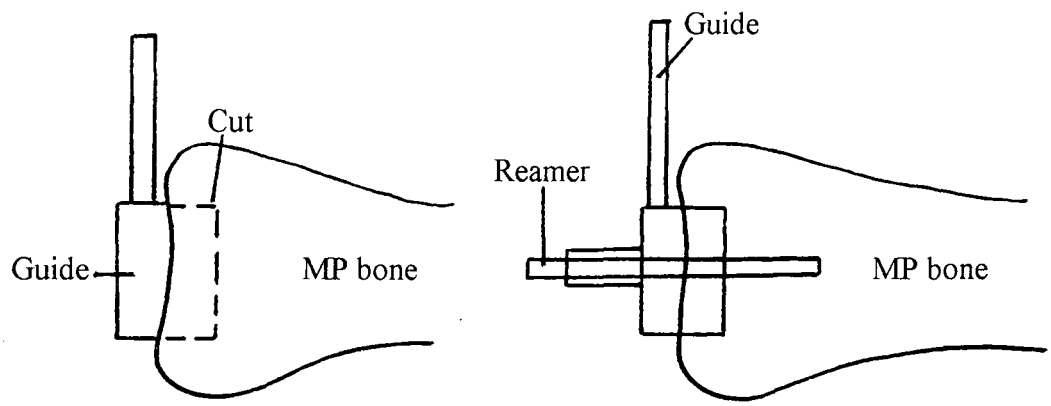

4.7 Forces exerted on the PIPJ prosthesis

It is possible to measure the forces exerted by the fingers during hand functions, such as grip and pinch, using strain gauged devices or sphygmomanometers. However, the forces exerted across the finger joints themselves can not be measured directly. To estimate the finger joint contact forces, theoretical models have been developed. Due to the complexity of the hand functions and the number of tendons and other soft tissue structures involved, certain assumptions were made to simplify the models and produce statically determinate solutions. These assumptions included frictionless tendon sheaths, relationships between the tendons, active or passive extensor tendon action, a single line of action of the tendons, the maximum force that each tendon could produce (which was related to its physiological cross-sectional area), two or three dimensional hand functions and constant moment arms of the tendons[175,176,177].

The fingers were modelled during both pinch (tip, pulp, radial and ulnar) and grip hand functions. However, differences occurred between the models in addition to the those assumptions listed above. These included the joint angles, the application of the forces exerted on the fingers, the moment arms and the method of solution of the models. Consequently there was some variation in the predicted joint contact forces produced by the models. Three models have been considered to estimate the forces that the PIPJ prostheses are likely to encounter in the body, these being those reported by Chao et al[175], Chao and An[176] and Weightman and Amis[177]. These models were chosen because they gave full information on the position of the hands and the direction of the joint contact forces.

Both the Chao and An[176] and Chao et al[175] models were three-dimensional models of pinch and grip hand functions. Solutions with compressive tendon forces, tensile joint contact forces, or excessive joint contact forces or extensor forces were eliminated and the final results were an average of the remaining solutions. It should be noted that the results for pinch from the Chao et al[175] model were an average of tip, pulp, radial and lateral pinches, hence this may account for the slight differences in the joint contact forces compared with those for just tip pinch[176]. In particular increased

lateral forces may be expected during radial and ulnar pinch, however, this does not appear to be so for the PIPJ.

Weightman and Amis[177] produced a model for pinch hand functions. They hypothesised that the differences between the solutions of previous models was partly due to the different hand positions adopted for each of the models. Hence they calculated joint contact forces for a range of pinch functions from pulp to tip. The joint contact forces reduced from pulp to tip pinch, but the shear forces increased. The model produced lower joint forces than both the Chao et al[175] and Chao and An[176] models (Table 4.5) which may have been due to the fact that the model was over-simplified. For example, the model was in two dimensions only, they assumed that the role of the extensor tendon was passive and the flexor tendons were modelled as one force.

Table 4.5 Finger joint angles and PIPJ contact force in terms of the unit forces applied (P)

Reference	Hand function	Finger or position	DIPJ angle (°)	PIPJ angle (°)	MCPJ angle (°)	PIPJ contact force
Chao et al[175]	**Pinch**	Index	25	50	48	5.99 P
		Middle				7.31 P
		Little				6.46 P
	Grip	Index	23	48	62	4.35 P
		Middle				7.11 P
		Little				6.02 P
Chao and An[176]	**Pinch**	Middle	20	20	10	8.29 P
	Grip	Middle	23	48	62	7.13 P
Weightman and	**Pinch**	1	0	0	20	5.9 P
Amis[177]		2	19	35	52	4.8 P
		3	42	51	34	4.2 P
		4	53	55	29	3.8 P
		5	60	65	15	3.5 P

For each of the models single unit forces were applied to the appropriate phalangeal bones and the joint contact forces were calculated per unit applied force(s), P, (Figure 4.11). The details of the finger joint angles and the joint contact forces are shown in Table 4.5. The joint contact forces for the PIPJ ranged from 3.2P - 8.29P, and within

Figure 4.11 Forces on the finger bones during pinch and grip hand functions

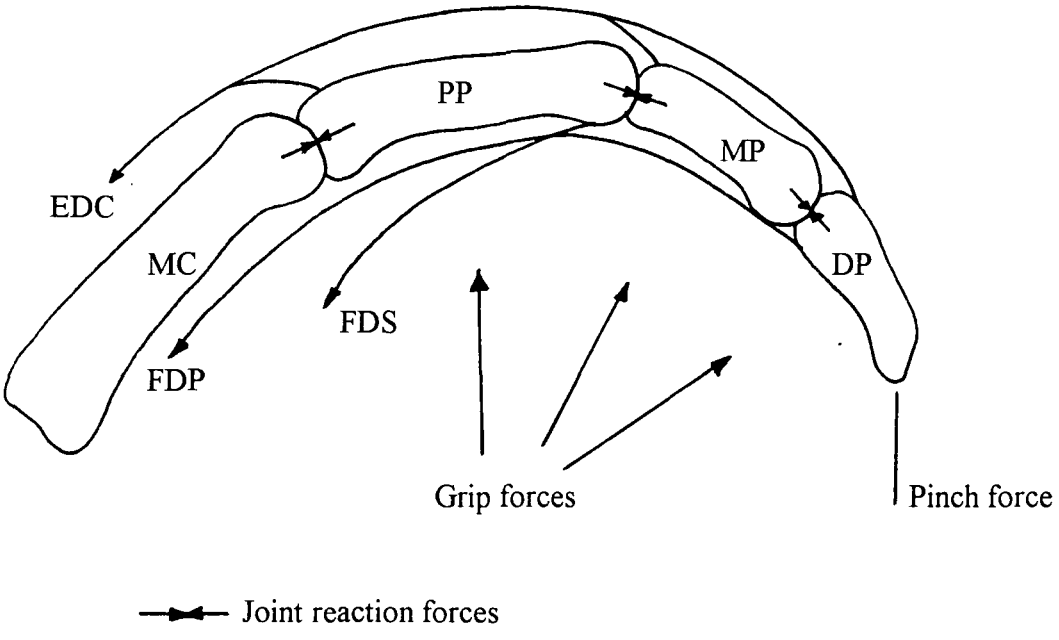

Figure 4.12 Definition of the joint contact force components acting on the PIPJ prosthesis

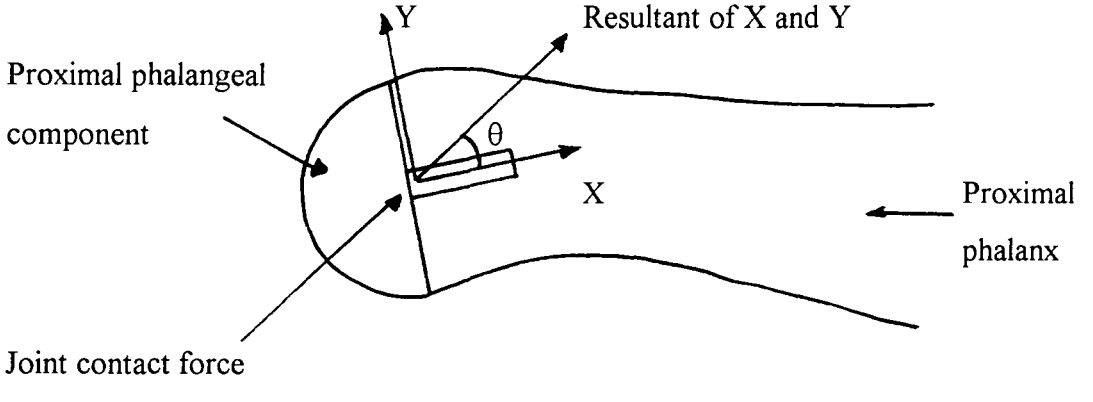

each model, the joint contact forces [per unit of force(s) applied] were greater for pinch than for grip hand functions. However, the direction of the joint contact force is also important, as this defines the size of axial and shear forces that the PIPJ prostheses may be subjected to. In particular the MP component lies within the end of the base of the bone and hence will receive some support from the bone surrounding it. However, this is not the case with the PP component, hence the interface alone between the PP head and stem will have to withstand the shear forces. Therefore the joint contact forces were resolved perpendicular and parallel to the back face of the PP component (Figure 4.12), and the axial and shear force values are given in Table 4.6.

Table 4.6 Axial and shear forces on the PIPJ prostheses

Reference	Hand function	Finger or position	X	Y	Z	θ
Chao et al[175]	**Pinch**	Index	5.99	0.21	0.26	2.00
		Middle	6.66	3.01	-0.36	24.35
		Little	6.38	1.03	0	9.19
	Grip	Index	4.34	-0.27	-0.28	-3.55
		Middle	6.83	1.97	-0.28	16.09
		Little	6.00	0.51	0	4.86
Chao and An[176]	**Pinch**	Middle	8.15	1.54	0.05	10.69
	Grip	Middle	6.68	2.48	0.05	20.38
Weightman and	**Pinch**	1	5.88	-0.51	-	-5
Amis[177]		2	4.57	1.48	-	18
		3	3.64	2.10	-	30
		4	3.19	2.07	-	33
		5	2.64	2.30	-	41

The axial forces (X) ranged from 2.64P to 8.15P, and the shear forces (Y and Z) ranged from -0.36P to 3.01P depending on the model and hand function. By replacing P with 65N (tip and pulp pinch measured by An et al[178]) and dividing by the cross-sectional area of the PP heads or stems, where appropriate, the maximum axial and shear stresses were calculated for each of the joint prostheses (Table 4.7). Sixty five newtons was used because the individual forces exerted during pinch were greater than those for grip, and this study found larger forces compared with other pinch strength studies[179,180].

The maximum axial and shear stresses occurred with the 7 mm prosthesis and were 9.460 MPa and 31.130 MPa respectively (Table 4.7). The shear stresses were much greater than the axial stresses for each of the joint prostheses. Hence the yield shear stress of XLPE was measured on a Hounsfield 25K universal testing machine (2mm diameter cylindrical samples at an extension rate of 5mm/min) and was found to be 31.7 MPa. This was only slightly greater than the maximum shear stress calculated for the 7 mm prosthesis and hence would leave no factor of safety in the 7 mm design. However, it should be noted that there are several factors that may reduce the maximum shear stress that may be exerted on the 7 mm prosthesis.

Table 4.7 Maximum axial and shear stresses on the PIPJ prostheses

Prosthesis (mm)	Stem radii (mm)	Stem CSA ($x10^{-6}$ mm^2)	Head back CSA ($x10^{-6}$ mm^2)	Max. axial stress MPa	Max. shear stress MPa
7	2	6.285	56	9.460	31.130
8	2.5	9.817	80	6.622	19.930
9	2.5	9.817	90	5.886	19.930
10	2.75	11.879	110	4.816	16.470

Firstly the 65N was measured for the index and middle fingers of healthy males. Whereas the 7 mm prosthesis is more likely to be inserted into the little or ring fingers which produce lower pinch and grip forces[180]. Secondly the joint prostheses will be inserted into rheumatoid patients who invariably have much lower (approximately one third[181]) pinch and grip strengths compared with normal individuals. In addition the patients may be female; females generally have lower pinch and grip strengths compared with males[178]. Therefore the forces exerted on the joint prostheses (especially the 7 mm prosthesis) may not be as great as those produced from 65N of external force.

If problems with lack of shear strength were found with the 7 mm PIPJ prosthesis the stem cross-sections could be increased to increase the shear strength, however, this may compromise the amount of bone stock left after reaming and press-fit of the prosthesis. Alternatively a flat could be added to the palmar side of the PP

component, as with the Durham MCPJ prosthesis, to take some of the shear force. This may also increase the rotational stability of the prosthesis

In summary, the shear forces to which the joint prostheses may be subjected in the body were calculated from theoretical models and pinch and grip strength data. The maximum shear stresses were much greater than the axial stresses and hence the yield shear stress of XLPE was measured. All of the shear stresses were less than the yield stress of XLPE, although only just for the 7 mm prosthesis. However, the forces exerted on the 7 mm prosthesis may be lower than those used for calculating the maximum shear stress. Hence it is postulated that all four of the joint prostheses are theoretically are strong enough to withstand the forces exerted on them in the body.

4.8 Chapter summary

A surface replacement joint prosthesis was designed for the PIPJs. Four different sizes were designed with maximum condyle diameter (sagittal plane) of 7, 8, 9 and 10 mm. The joint prosthesis consisted of two parts, a convex PP head and a concave MP base. Due to the small sizes of the joint, the PP component was required to have a solid head. However, it was thought that this would not affect significantly the attachment of the collateral ligaments. In addition, the solid head simplified the surgical technique. Fixation of the two components was achieved through interference fit between the component stems and the phalangeal bones.

The PP head bearing surfaces were circular in the sagittal plane but with varying diameter across the width of the bone producing the bicondylar shape. The sides of the condyles were inclined in the transverse plane such that the bearing surfaces were broader anteriorly than posteriorly. This prevented the joint prosthesis from overlapping the end of the bone and impinging on the soft tissues surrounding the joint. The bearing surface covered the range of motion from 100° flexion to 80° hyper-extension. The inter-condylar sulcus was 'filled in' dorsally to merge with the bone shaft. The stems were semi-circular in cross-section. They were offset dorsally from the centre of rotation of the joint and angled such that they coincided with the centre-line of the medullary canal. The length of stem was limited by the change in angle of the bone shaft just proximal the PP head.

The MP bearing surfaces were designed to conform with the PP heads to increase the stability of the joint. The bearing surfaces covered an arc of 90° in the sagittal plane and were elliptical in the transverse plane. The stems located within the MP base where there was no medullary canal and were semi-circular in cross-section. They were parallel to the centre line of the joint prosthesis in the sagittal and frontal planes, to simplify the surgical technique. They were offset slightly palmarly in the sagittal plane.

The surgical tools needed to implant the two components were also considered. The surgical tools for the PP component included a joint sizer, a cutting guide, a flat oscillating cutter, a reamer guide and possibly a reamer. The surgical tools for the MP component included a cutting guide, a rotating cutter, a reamer guide and a reamer. However, difficulties may occur in the design of such tooling due to alignment of the tools with the phalangeal bones, and the alignment of the MP bone with the PP bone.

CHAPTER FIVE

Wear characteristics of Cross-linked polyethylene

5.0 Introduction

The main concern with the wear of finger joint prostheses is the body's reaction to the wear debris produced at the bone-stem interface and the bearing surfaces. Wear debris can stimulate cellular activity which consists of an inflammatory and a foreign body reaction. This involves macrophage (inflammatory cells) and foreign giant cell activity. The activated macrophages can stimulate osteoclasts which cause bone resorption. This in turn can cause loosening and failure of the joint prosthesis, and pain for the patient. The cellular reactions are dependent on the morphology and volume of the wear debris[81]. Biomaterials may be tolerated in bulk, however, small wear debris particles may produce adverse reactions[82]. The nature of the wear mechanisms of the bearing surfaces can determine the morphology and volume of wear debris produced.

Plastic-on-plastic bearing surfaces have been avoided in the past due to high friction and wear rates compared with other material combinations. However, encouraging results have been found with XLPE[73,83,84]. It has been reported that the wear rates and friction of XLPE-on-XLPE are in a similar range to those of UHMWPE-on-stainless steel[73]. The improved wear resistance compared with other polyethylenes may be due to the additional strength of the cross-links. Cross-linking of the XLPE is achieved through a silane-grafting process. Silane is added to the polyethylene and the mixture is then autoclaved during which cross-links form between the polyethylene chains. The length of time that the polyethylene is heated for determines the amount of cross-links that are formed.

In addition, wear is proportional to load, and the loads encountered in the finger joints are small compared with other joints in the body[23]. The loads are also likely to be less than those encountered in normal individuals due to the loss in hand strength associated with patients with arthritis[85]. Hence an all XLPE joint prosthesis could realistically be considered for the finger joints. However, little work has been completed on the wear characteristics of XLPE-on-XLPE. Hence further wear tests were required to justify the manufacture of the Durham MCPJ and PIPJ surface replacement prostheses entirely from XLPE from a wear point view.

5.1 Types of wear

There are three main types of wear mechanisms found in artificial joints. These are adhesive, abrasive and fatigue wear. More than one mechanism can be present at any one time, and the contribution of the individual wear mechanisms to the overall wear of the bearing surfaces may change with sliding distance. The different wear mechanisms produce different types, sizes and numbers of wear particles[86]. *Adhesive wear* is the transfer of material from one surface to the other due to the forces of adhesion between the two bearing surfaces. If the forces of adhesion between two asperities are greater than the yield stress of one of the asperities then the asperity will shear off and transfer to the opposite bearing surface. In similar bearing surface materials wear can take place from both surfaces, whereas with dissimilar materials wear tends to occur from the softer material and adhere to the harder material. The amount of adhesive wear depends on the load, lubricant, sliding speed and nature of the material[87]. Polymer transfer films were found to form on metallic counterfaces when tests were run in distilled water or saline solution[86,88-90].

Abrasive wear is the removal of material from one bearing surface by harder asperities on the counterface. The hard asperities gouge out, or cut, material from the softer bearing surface producing scratches or grooves in the direction of sliding. Hard particles between the bearing surfaces can also cause wear of both surfaces, which is called *three-body abrasive wear*. The amount of abrasive wear is dependent on the energy required to detach particles from the bearing surfaces[87]. *Fatigue wear* is the removal of material as a result of cyclic stress. Fatigue cracks can form and propagate with the subsequent formation of wear debris. The amount of fatigue wear is dependent on a material's ability to deform elastically and on the morphology of the counterface[87]. Fatigue cracks may form below the surface where the shear stress, caused by the contact stress, is greatest. They then propagate towards the surface forming wear particles.

The amount of wear between two bearing surfaces is dependent on the lubrication present between the bearing surfaces. Lubrication is the separation or partial separation of two bearing surfaces by a film of, for example, synovial fluid in human joints. In previous wear tests distilled water, saline solution, bovine synovial fluid and bovine serum have all been commonly used as lubricants. If the bearing surfaces are completely separated then no wear will occur (full film lubrication). Products in the lubricants may also produce boundary lubrication. For example, proteins in synovial fluid or serum can form a protective coating of the bearing surfaces.

5.2 Wear coefficient

The wear of different materials tested under the same operating conditions can be compared by calculating the corresponding wear coefficients. The wear coefficient can be calculated from Archard's wear equation and is proportional to the wear volume, and inversely proportional to the contact force and the sliding distance:

$$\textit{Wear coefficient (k)} = \frac{\textit{Wear volume (V)}}{\textit{Contact force (F) x Sliding distance (D)}}$$

Although the original work by Archard[91] was developed to model adhesive wear, the wear equation has been applied to many wear tests where other wear mechanisms are also present. This is valid if the loading conditions of the bearing surfaces are not too severe, that is the contact force or sliding speed are not too great[92]. The units of the wear coefficient are generally mm^3/Nm.

The wear volume can be found by measuring the change in dimensions of the bearing surfaces, however, this does not account for creep[90]. Alternatively the weight loss can be measured, and the wear volume can be found by dividing the weight loss by the material density. For this method, uniform density is assumed. With both methods, control pins and plates should be included in the tests to compensate for absorption of the lubricant by the bearing surfaces.

5.3 Wear test apparatus

The three most common types of wear tests have been carried out on pin-on-disc, pin-on-plate and joint simulator apparatuses. The wear characteristics investigated have included the wear mechanisms involved and the amount and size of wear debris created. Ideally the tests should subject materials to the same conditions that a joint prosthesis would encounter in the human body. The extent to which each of these three types of apparatus simulates *in-vivo* conditions varies. Test parameters such as temperature, lubricant, joint force and surface roughness can be varied. However, the type of motion between the bearing surfaces is inherent to the type of apparatus used (although the magnitude speed and stroke length can also be varied).

The geometry of the bearing surfaces of pin-on-disc and pin-on-plate tests differs significantly from finger joint prostheses. Pin-on-disc wear tests consist of a stationary

pin which articulates against a rotating disc. Tri-pin-on-plate tests have also been carried out[82,93]. The relative movement between the two surfaces is continuous, unidirectional and at a constant speed. Pin-on-plate tests consist of a stationary pin articulating against reciprocating plates. The relative movement between the two surfaces changes direction every half a cycle and the speed is generally approximately sinusoidal.

The reciprocating movement of pin-on-plate tests may be seen to be closer to that of *in-vivo* conditions compared with pin-on-disc tests. Other advantages are that there may be less tendency for hydrodynamic lubrication (which is not seen in natural or artificial joints) to function and wear debris may be allowed to escape from between the bearing surfaces. In addition, the ratio of specimen excursion to contact area is similar to joint prostheses and directional changes of the machine may produce different wear characteristics compared with pin-on-disc apparatuses[90]. It has generally been reported that the wear of unidirectional tests is greater than that of reciprocating wear tests[87,89,94], although Fisher[86] found that reciprocating wear tests produced slightly greater wear rates. Brown et al[94] found that the wear mechanisms of UHMWPE against stainless steel seemed to be the same for both pin-on-plate and pin-on-disc tests, however, Kumar et al[89] reported that different wear debris was produced from the two tests.

Pin-on-plate and pin-on-disc tests can provide information on the wear characteristics of different material combinations and the effect of different operating conditions. Estimation of the wear and life expectancy of joint prostheses, however, is not necessarily valid due to the different dynamics of the tests compared with natural joints. To achieve this, joint simulator tests should be used. Joint simulators load and articulate joint prostheses as close to the natural joint as possible. Not only do they provide information on the wear of different joint prostheses and biomaterial combinations but they also highlight any inadequacies of the joint prostheses, such as fracture or increased wear in certain regions.

Despite careful choice of wear machines and test parameters there are significant differences between *in-vitro* wear tests and *in-vivo* conditions. *In-vitro* tests are continuous tests with simplified joint motion. The loading in pin-on-flat tests is often static and the geometry of the bearing surfaces do not resemble those of a joint prosthesis. These differences may be reflected in the higher wear rates of hip joint prostheses *in-vivo* compared with those predicted *in-vitro*, by as much as one or two orders of magnitude[86]. (The higher wear rates may also be due to bone and bone

cement particles *in-vivo* which is discussed in Section 5.4.4). Hence it should be remembered that *in-vitro* tests can give an indication of the wear characteristics of material combinations compared with one another, but not necessarily the actual wear expected in the body. However, *in-vitro* wear tests are the only means of providing information on material and joint prosthesis wear characteristics before they are used in the body.

5.4 Wear test parameters

The ASTM produced a standard for reciprocating pin-on-flat wear tests[95]. The parameters were developed with reference to the hip joint. However, some can also be applied to wear tests for finger joints as well. The standardised parameters were motion, contact area, counterface roughness, frequency, average speed, axial load, contact stress, lubricant, pin diameter and temperature. These parameters are discussed more fully in the following section.

5.4.1 Lubrication

The most common lubricants which have been used in previous wear tests are distilled water, saline solution, bovine serum and synovial fluid. Alternatively, some tests have been run with no lubricant at all[96]. Ideally human synovial fluid should be used to simulate *in-vivo* conditions but this is not practical. However, the wear mechanisms and wear rates have been shown to vary when testing polyethylene-on-metal with different lubricants. Significant differences have occurred between distilled water or saline solution and serum or synovial fluid.

A transfer film of polyethylene formed on the metallic counterface during tests in distilled water or saline solution. However, no transfer films occurred when the tests were run in bovine serum or synovial fluid[86,88-90]. Transfer films have also not been found on explanted metal-on-plastic joint prostheses. It has been hypothesised that the proteins in serum and synovial fluid may contribute to boundary lubrication of the bearing surfaces, changing the wear mechanisms involved and preventing adhesion of the polyethylene to the metallic counterface[88,90,96]. Lower wear and frictional properties have also been found in biological lubricants than in water and saline solution[89,90] (although this has not been found by all authors[82,96]). McKellop[90] found that four times as much wear was produced in water than in serum, and saline solution showed eight times as much wear.

Finally, a constant wear rate of polyethylene-on-metals has been found in bovine serum. However, the wear rate was stepped when a similar test was run in distilled water[81,93]. The periods of different wear rates were attributed to different wear processes. It was thought that the low wear rates were caused by microscopic asperity wear, and the higher wear rates were caused by macroscopic asperity wear due to fatigue failure from large sub-surface stress concentrations in the polymer surface[81,88,93]. Presumably the different lubricating properties of bovine serum prevented this stepping from occurring although it was not stated how.

No differences in wear mechanisms or wear rates were found when testing polyethylene-on-ceramics in serum, saline solution or distilled water. No polyethylene transfer films were found when testing in any of the lubricants. This was attributed to the corrosive resistance of the ceramics which prevented the polyethylene from adhering to the ceramic counterface[89]. No such results have been reported for polymer-on-polymer combinations.

In summary, it has generally been reported that bovine serum and synovial fluid seem to reproduce the wear mechanisms found in the body closer than non-biological lubricants. The ASTM recommended that bovine serum should be used as a lubricant for pin-on-flat wear tests. However, bovine serum characteristics may change during exposure to the environment and denaturing of the proteins can occur due to the forces imposed on them. Hence frequent renewal of the lubricant is essential[82]. However, renewal has lead to transient increases in wear and friction of polyethylene against metal for several hours. This was associated with changes in the properties of the synovial fluid, which may have been related to the rate of heat generation at the bearing surfaces[90]. Distilled water and saline solution, on the other hand, are readily available, reproducible, and inexpensive. However, the polyethylene transfer films found on metallic counterfaces indicate a difference in wear mechanisms compared with *in-vivo* conditions. Tests run under dry conditions show increased wear compared with those run with lubricants[96].

5.4.2 Temperature

The effect of temperature on the wear of materials in the ranges seen in biomaterial wear tests is not clear. The majority of previous wear tests have been run with a lubricant which not only lubricates the bearing surfaces but can also maintain the materials at the required temperature and disperse the high temperatures developed at the bearing surfaces. Previous wear tests have generally been run at 37°C (body temperature), which was also recommended by the ASTM. Three tests were run at

lower temperatures (18°C[97], 20°C[98] and 24-26°C[89]) but the reported wear coefficients show no significant difference compared with other reported values.

5.4.3 Speed

The effects of the differences in motion between the different types of wear test apparatuses have been discussed in Section 5.3. The ASTM recommended oscillating motion to simulate *in-vivo* conditions. This implies that pin-on-plate or joint simulator apparatuses should be used rather than pin-on-disc. In addition to the type of motion, the speed can also affect the wear rate by affecting the bearing surface temperature due to frictional heating and the viscoelastic response of the materials. Hence by increasing the speed, the wear rate may increase[86,98,99]. It is unclear at what speed this would happen significantly, however, little change in the wear rate was found between speeds of 0.03-0.24 m/s[99]. To simulate *in-vivo* conditions it has been estimated that an average speed between 0.02 and 0.05 m/s should be used[96]. The recommended average sliding speed by the ASTM was 0.05 m/s to simulate the hip joint during walking.

The cyclic frequency has most commonly been taken between 1-1.5 Hz[82,83,89,100] to simulate *in-vivo* conditions[96]. The stroke length or path length used partly depends on the type of apparatus used. Pin-on-disc apparatuses tend to have longer path lengths compared with pin-on-plate apparatuses and also tend to run at higher speeds. Ideally the path length should be equivalent to that of a joint prosthesis. This would ensure a similar ratio of specimen excursion to contact area compared with a joint prostheses, and with the correct frequency it would achieve a comparable sliding speed[90].

5.4.4 Surface roughness

The plate roughness has been seen to alter wear rates significantly, especially of polyethylene when sliding against metal counterfaces[88,89,93,98,100]. Typical values of surface roughness in previous wear tests are shown in Table 5.1. The surface finish was between 0.0016-0.02 μm[82,100] for ceramics, 0.01-0.055 μm[81,88,94] for metals, and between 0.15-1.5 μm[100,103] for UHMWPE and XLPE. The ASTM recommended a surface roughness of 0.025-0.05 μm for metal counterfaces when tested against polyethylene[95].

The surface roughness of the metals in previous wear tests compare well with the metallic components of hip joint prostheses, which are between 0.025-0.05 μm[81,95].

Table 5.1 Surface roughness of previous wear test materials

Ref.	Pin		Flat	
	Material	**Roughness (μm)**	**Material**	**Roughness (μm)**
97	UHMWPE	0.7	UHMWPE	0.65-0.8
98	UHMWPE		Stainless steel	0.05-0.4
100	UHMWPE	0.15	Ceramic	0.02
94	UHMWPE	0.37	Stainless steel	0.01
81	UHMWPE		Stainless steel	0.01-0.02
88	UHMWPE		Stainless steel	0.01-0.055
95	UHMWPE		Metals	0.05
82	UHMWPE		Ceramic	0.0016
83	UHMWPE, XLPE	0.6-0.8	UHMWPE, XLPE	0.6-0.8
74	UHMWPE	0.696	UHMWPE	0.656-0.782
101	UHMWPE		Stainless steel	0.025
102	UHMWPE		Stainless steel, Al_2O	0.015-0.1
103	XLPE		XLPE	1.1-1.5

However, significantly higher wear rates have been found from explanted joint prostheses compared with those predicted *in-vitro*[86]. One reason for this may be the deterioration of the surface finish of the femoral head from scratching by bone and bone cement particles[86,96,104,105].

5.4.5 Contact force

The wear rate is theoretically proportional to the joint contact force (Section 5.2). However, deviations can occur at higher loads due to creep, frictional heating and softening of the polymer. Wear may also increase due to a reduction in support of the hydrodynamic film[106]. However, the limit where this occurs is unclear. Previous wear tests have indeed shown that the wear rate is dependent on the joint contact force but not proportionally[73,83,84]. However, Brown et al[94] found that the wear rate was independent of the joint contact force from 25-145 N and Wright et al[99] reported only a slight increase of wear with higher loads.

The natural joint contact force will depend on the activity, joint and individual. It has been estimated that the contact force across the MCPJ is approximately 10-15 N[23] during normal unloaded motion, with a maximum of 200 N during grip pinch, (although the forces exerted on the joints in patients with arthritis may be less than these due to damage to the soft tissues surrounding the joint and a reduction in hand strength). However, during grip pinch the joints are usually stationary and hence no wear will take place, although the intermittent higher loads may cause some deterioration in the

bearing surfaces. Further, the articulating surface of the PP base is in contact with the MC head at all times at the MCPJ. However, the MC head is cyclically loaded which increases the likelihood of fatigue wear. The same is true for the MP base and PP head at the PIPJ. Likewise pins are continuously loaded during *in-vitro* wear tests whereas the plates or discs are cyclically loaded.

5.4.6 Geometry

Although the joint contact area does not theoretically affect the wear coefficient of a material, the geometry of the bearing surfaces may affect the lubrication mechanisms present. For instance, curved surfaces may aid hydrodynamic lubrication[82] and the congruity and extent of the bearing surfaces may determine whether lubricant can get between the surfaces or not. This may be especially critical with patients with arthritis of the finger joints where a lack of range of motion may prevent exposure of parts of the bearing surfaces of the MC or PP heads to lubricant. Further, small misalignments of the pins can cause wedge effects which could give rise to lubrication where aligned pins would not. Finally with pin-on-flat apparatus edge effects from flat-ended pins may be reduced by cutting chamfers around the bearing surface[96]. However, wear of the pin may subsequently produce a flat surface across the entire pin once more. The ASTM recommended flat pin bearing surfaces for pin-on-flat wear tests.

5.4.7 Test length

The wear test length should duplicate the required joint prosthesis life as the wear mechanisms may be dependent on the sliding distance. For instance, a wear curve may consist of a wearing in period followed by a steady state period of wear. At longer distances, however, the wear rate may increase due to an additional fatigue wear mechanism[98]. *In-vitro* pin-on-flat tests may exhibit different lubricating and wear properties compared with *in-vivo* conditions, however, they are necessary to complete tests equivalent to a joint prosthesis life of, for example, 10 years in a few months. However, it should also be noted that material ageing may not be experienced during *in-vitro* tests.

Wear rates can be found per million cycles or per unit sliding distance. However, converting this to wear per year to estimate the life expectancy of a joint prosthesis is difficult. The number of cycles or distance that a joint covers per year is not known. Estimates of 1.5[93],1.8[73] and 2[96] million cycles per year for the hip joint, and 1 million cycles per year[73] for the MCPJ have been made.

5.4.8 Material considerations

The method of manufacture of the materials for wear tests can affect the wear characteristics of the material. For example, it has been reported that the orientation of the molecules in polymers can affect the wear rates[94]. Orientation perpendicular to the wearing surface reduced the ductility of the polymer resulting in rougher surfaces during wear, due to shearing of the material, and subsequently higher wear rates. Whereas orientation parallel to the wear surface improved the wear rates slightly. Finally sterilisation processes can affect the wear characteristics of materials. Hence materials should undergo the same sterilisation processes as joint prostheses before they are tested.

5.5 Pin-on-plate wear tests of XLPE and UHMWPE

5.5.1 Apparatus

To simply compare the wear characteristics of XLPE-on-XLPE with other material combinations, pin-on-flat wear tests were carried out rather than using joint simulator apparatus. Pin-on-plate apparatus was chosen rather than pin-on-disc due to its more realistic motion compared with *in-vivo* conditions. Pin-on-plate wear tests were performed on XLPE-on-XLPE, UHMWPE-on-UHMWPE, and XLPE and UHMWPE on stainless steel.

The reciprocating pin-on-plate apparatus used is shown in Figure 5.1. The plates were held securely in a lubricant bath, which had the capacity for four plates. The bath was attached, via a connecting rod, to variable throw crank shaft. The crank shaft was driven by a 125 W d.c. shunt motor, which produced the reciprocating motion between the plates and the stationary pins. The required stroke length was achieved by adjusting the eccentricity of the connecting rod on the crank shaft.

The pins were located in pin holders which were held vertically in cantilever arms attached to the main rig. The pin holders were free to move vertically in the cantilever arms which allowed them to move downwards when wear of the pins took place. Lever arms rested on the pin holders to apply force on the pins. Weights were added at positions along the lever arm to exert the required forces on the pins. A screw mechanism allowed adjustment of the lever arms so that they were horizontal and the point of contact was in the centre of the pin holder. Calibration of the forces exerted

Figure 5.1 Reciprocating pin-on-plate apparatus

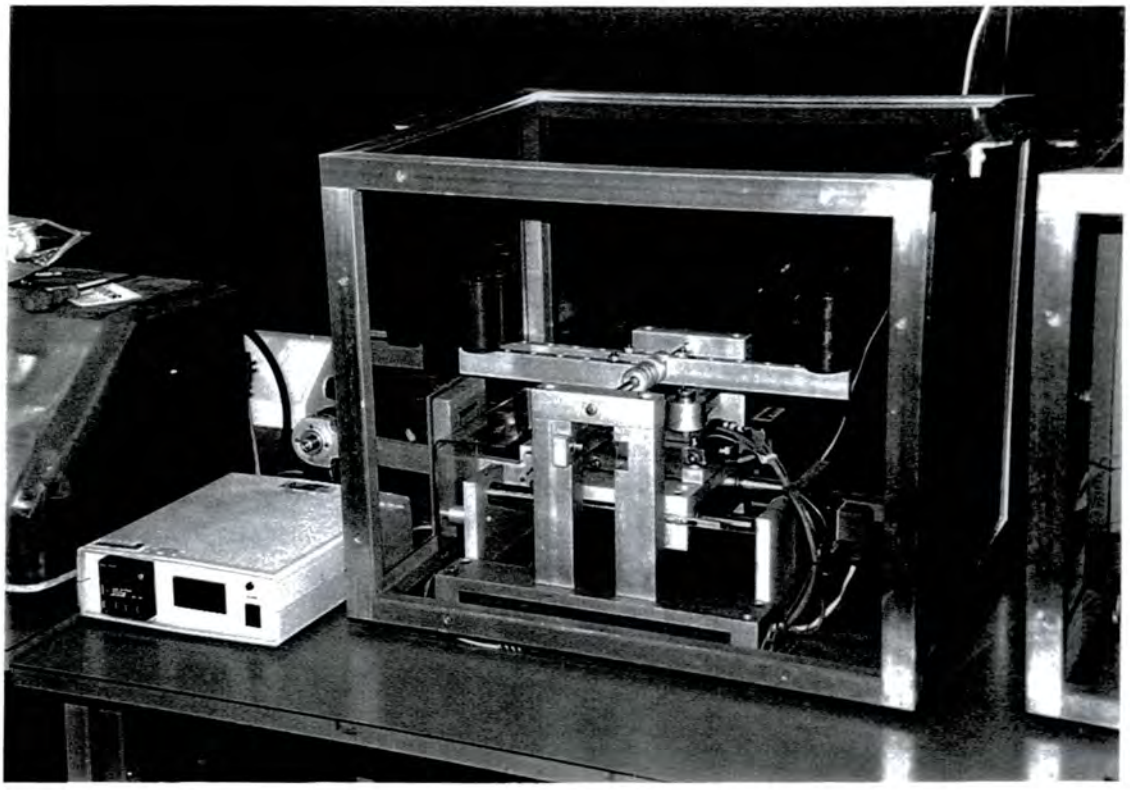

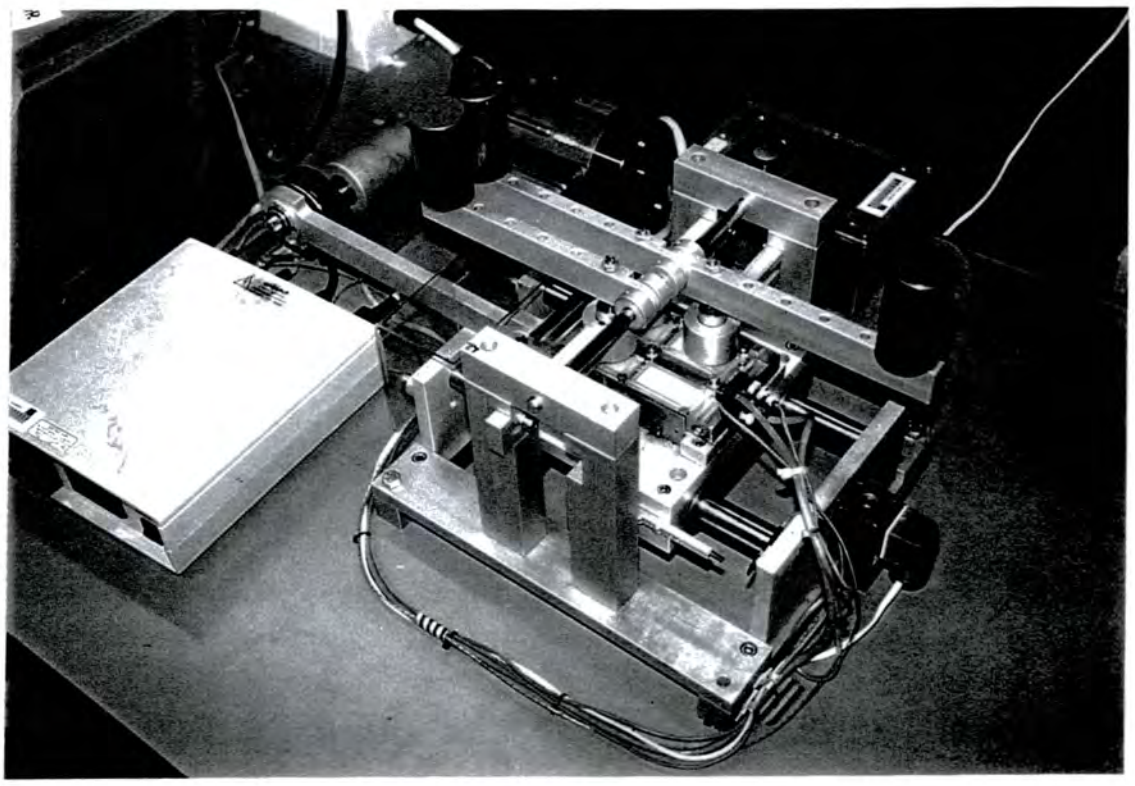

on the pins using the lever arm and weights was carried out and is shown in Appendix 4.

The temperature of the bath was controlled by a thermocouple feedback system. This varied the temperature of a heating pad below the bath until the desired bath temperature was achieved. If the thermocouple was resting on the bath base then water higher up in the bath was up to 2°C lower (at 37°C) due to heat losses to the environment. Hence the thermocouple was positioned at the same height as the plate bearing surface to bring the bearing surfaces to body temperature. The level of lubricant in the bath was electronically controlled, and lubricant was fed into the bath from an elevated reservoir when required. The system also contained a cut out to prevent the bath from running dry. This stopped the motor, turned off the heating pad and prevented lubricant from being fed into the bath. An electronic counter was used to measure the number of cycles covered during the wear tests, from which the total sliding distance could be calculated. A perspex case covered each machine to prevent contamination of the bath and plates from the environment.

5.5.2 Operating conditions

Forces of 10 N or 40 N were applied to the pins. Ten N corresponded to the estimated joint contact force of the MCPJ during normal, unloaded movement[23]. Forty N was also used to investigate the effect of elevated contact forces on the wear characteristics of the materials, and to allow for larger than expected joint forces in the MCPJ. The change in weight of the pins and plates was measured on a Mettler AE 200 balance with an accuracy of ±0.1 mg. Control pins and plates were also included in the tests to compensate for an increase in weight due to absorption of the lubricant. In some cases they could also indicate contamination of the baths. For example, polyethylene can absorb oil which, if it should contaminate the water bath from the rest of the rig, would show as an increase in the weight of the control pin.

The tests were run at 37°C (body temperature). The stroke length was set at 19 mm, (38 mm path length). This was the previously estimated path length of the MCPJ throughout 90° movement of flexion-extension[83]. Although with an average radius of curvature of the MC head of 7.5 mm the stroke length of the MCPJ is nearer 13.5 mm. However, for comparison with previous work[73,83,84,94,97] the stroke length was kept at 19 mm. Previous pin-on-plate tests have most commonly been run at average speeds of 0.02-0.04 m/s (frequency 1-1.5 Hz). As the length of these tests was planned to be several hundred kilometres, a speed of 0.04 m/s was chosen. This was equivalent to 63

rpm for a 19 mm stroke, with a test running time of several months. A faster speed was not used to prevent unnecessary damage to the motor, elevated wear rates and stress to the pins, which may have caused them to shear.

There has been much discussion in the past over the lubricant that should be used in wear tests. Elevated wear rates have been found in water and saline compared with bovine serum or synovial fluid. In addition, polyethylene transfer films have occurred on metallic counterfaces when tested in water or saline. These have not occurred in serum or synovial fluid, and have not been seen on explanted metal-on-polymer joint prostheses. Hence it seems that serum and synovial fluid reproduce *in-vivo* conditions closer than distilled water or saline solution. However, the effect of degradation of the serum and synovial fluid is not known. Frequent replacement of the lubricants is required throughout the wear tests and increases in wear rate have occurred for a few hours after a change of lubricant[90]. In comparison distilled water is reproducible and does not degrade, hence tests can be run almost continuously.

It is also important to consider that *in-vitro* wear tests give a ranking of the amount of wear from different material combinations rather than an estimation of the amount of wear that may be experienced *in-vivo*. The ranking of the wear from different materials in the past has not been dependent on the lubricant. In addition, the scatter of results for a particular biomaterial combination (for example polyethylene-on-stainless steel), is such that wear coefficients for water and saline tests overlap those for serum and synovial fluid (Tables A5.41-4, Appendix 5). Hence when comparing the wear characteristics of different material combinations there seems to be no advantage to using serum or synovial fluid than distilled water. In addition, distilled water is simple to use, represents no biological hazard, is inexpensive and readily available. Further, very few wear tests have been carried out using XLPE and those that have, have been carried out in distilled water. Hence distilled water was used for the pin-on-plate lubricant to simplify the tests, achieve reproducible conditions and to be able to compare the results with previous XLPE wear tests.

In summary, all of the wear tests were conducted on pin-on-plate reciprocating wear machines. The tests were carried out at a temperature of 37°C, in distilled water, at an average speed of 0.04 m/s with a stroke length of 19 mm. The gel content for the XLPE used in Test 1 was 77% and for all of the other tests it was 78%. A summary of the test materials, applied force and total sliding distance is shown in Table 5.2. In addition, the surface roughnesses of the plates were measured before the wear tests on a Taylor Hobson Talysurf Mark IV (Table 5.3).

Table 5.2 Pin-on-plate test parameters

	Force (N)	Distance (km)	Pin material	Plate material
Test 1	10	212.93	XLPE	XLPE
Test 2	10	605.70	XLPE	XLPE
Test 3	40	499.38	XLPE	XLPE
Test 4	10	557.26	XLPE	XLPE
Test 5	40	683.63	XLPE	XLPE
Test 6	10/40	224.23	UHMWPE	UHMWPE
Test 7	10	161.87	UHMWPE	UHMWPE
Test 8	10/40	170.52	UHMWPE	UHMWPE
Test 9	10	222.71	UHMWPE	Stainless steel
Test 10	40	224.56	UHMWPE	Stainless steel
Test 11	10	167.13	XLPE	Stainless steel
Test 12	40	168.28	XLPE	Stainless steel

Table 5.3 Plate surface roughness before testing

	Pin material	Plate material	Longitudinal roughness (μm)	Transverse roughness (μm)
Test 1	XLPE	XLPE	1.509	1.438
Test 2	XLPE	XLPE	1.283	1.229
Test 3	XLPE	XLPE	1.356	1.247
Test 4	XLPE	XLPE	1.225	1.103
Test 5	XLPE	XLPE	1.200	1.058
Test 6	UHMWPE	UHMWPE	1.467	0.502
Test 7	UHMWPE	UHMWPE	1.500	0.533
Test 8	UHMWPE	UHMWPE	1.522	0.478
Test 9	UHMWPE	Stainless steel	0.032	0.035
Test 10	UHMWPE	Stainless steel	0.030	0.035
Test 11	XLPE	Stainless steel	0.033	0.031
Test 12	XLPE	Stainless steel	0.034	0.030

5.5.3 Pin-on-plate test procedure

The stroke length was set to 19 mm. The bath, pin and plate holders, and pins and plates were cleaned with acetone. A mark was put on the corner of the plates so that they could be replaced in the correct orientation after each weighing session. The pins and plates were then weighed three times each and the average weights calculated. The pins and plates were positioned in the rig and weights were applied to the lever arms to apply either 10 N or 40 N of force to the pins. The lever arms were positioned so that they acted through the centre of the pins holder and were horizontal. The lubricant level was set so that distilled water covered the plates, and the lubricant bath was left to

equilibrate at 37°C for two hours before the test was started. The motor was switched on and the speed increased to 0.04 m/s (equivalent to approximately 63 rpm).

Initially the pins and plates were weighed every two days, however, after the wearing in period of each test they were weighed each week (equivalent to approximately 25 km). The motor was stopped and the pins and plates removed from their holders. They were washed in acetone, dried and weighed three times each and the average weights were calculated. They were then replaced in the rig and the water bath was left to equilibrate for two hours before the test was restarted. The wear volumes were calculated from the change in weight of the pins and plates, taking into account any water absorption. The densities used to calculate the wear volumes were 0.949×10^{-6} and 0.953×10^{-6} kg mm^{-3} for XLPE and UHMWPE respectively. Graphs of wear volume (mm^3) against sliding distance (km) were plotted and the wear coefficients calculated using the slopes of these graphs.

5.6 Results

The wear of the pins and plates was looked at in terms of the corresponding wear coefficients and the wear mechanisms present. Initially only the pins were weighed in line with previous pin-on-plate tests. It was thought, wrongly, that because the pins were in contact with the plates continuously that they would wear far more than the plates, which were only cyclically loaded. However, early on in Test 1 (XLPE-on-XLPE, 10 N) it was observed that wear tracks were forming on the plates. Hence from 40 km the plates were weighed as well as the pins. The graphs of wear volume against sliding distance are shown in Figures 5.2-5.13.

5.6.1 XLPE pins against XLPE plates

Test 1 (10 N). Deep wear tracks were formed on the XLPE plates with shallow score marks in the direction of sliding indicating an abrasive wear mechanism. The injection moulded plate surface was worn away within the first couple of kilometres, changing the surface characteristics. The machining marks of the pins were also worn away (within 25 km) and shallow score marks were formed in the direction of sliding. No material transfer or tearing of the polymer surfaces was seen which would indicate adhesive wear. The wear curves were linear throughout the test indicating that a fatigue component was probably not introduced in the pin and plate wear. The large

Figure 5.2 : Pin-on-Plate Wear Test of XLPE Pins against XLPE Plates Under 10N Loading (Test 1)

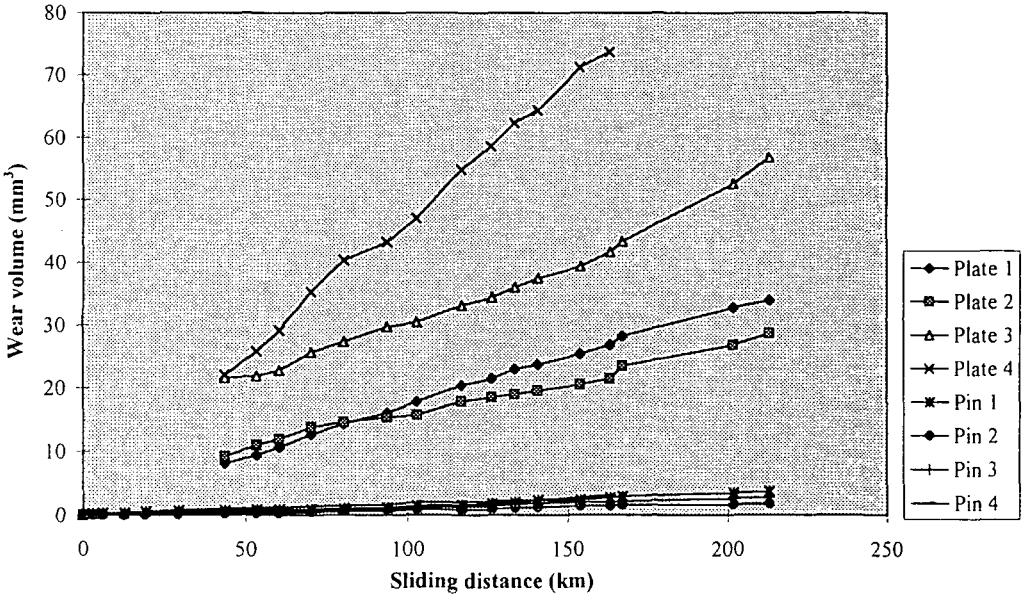

Figure 5.3 : Pin-on-plate wear test of XLPE pins against XLPE plates under 10N loading (Test 2)

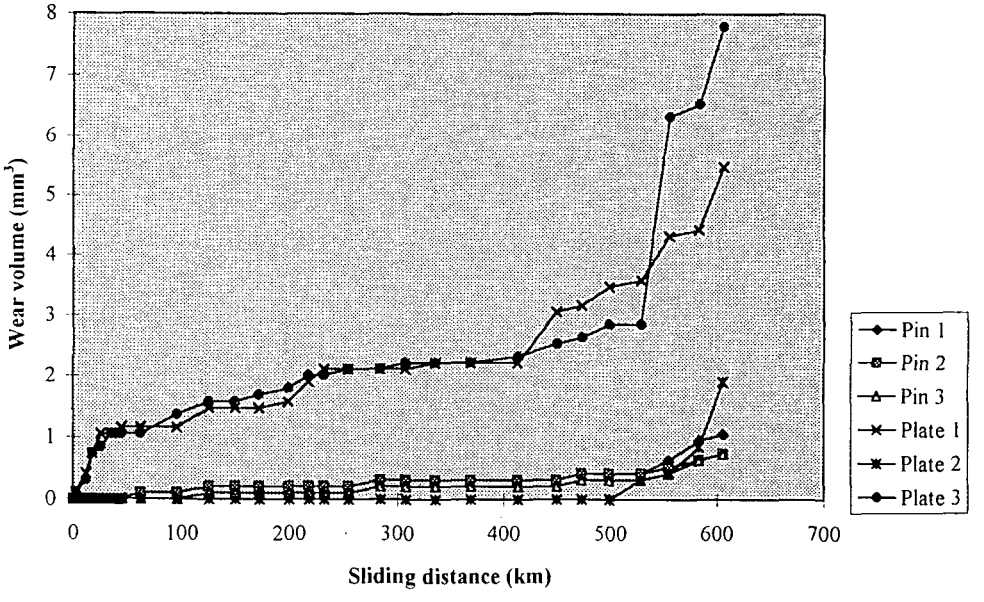

Figure 5.4 : Pin-on-plate test of XLPE pins against XLPE plates under 40N loading (Test 3)

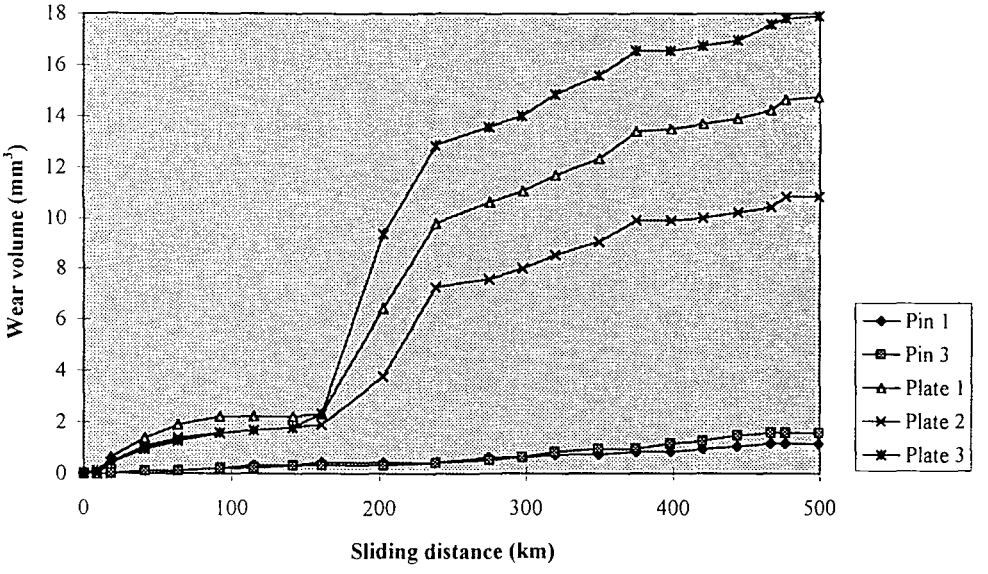

Figure 5.5 : Pin-on-plate test of XLPE pins against XLPE plates under 10N loading (Test 4)

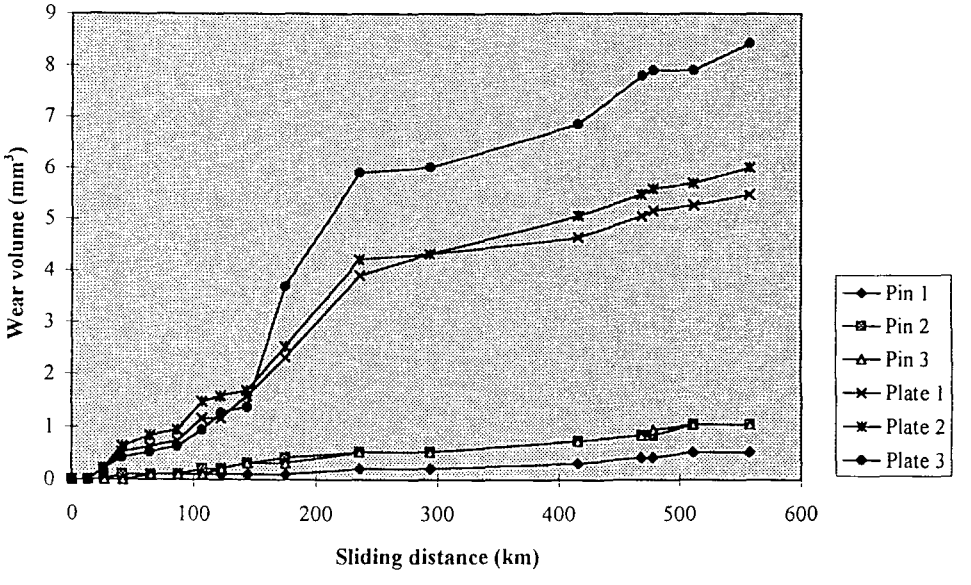

Figure 5.6 : Pin-on-plate test of XLPE pins against XLPE plates under 40N loading (Test 5)

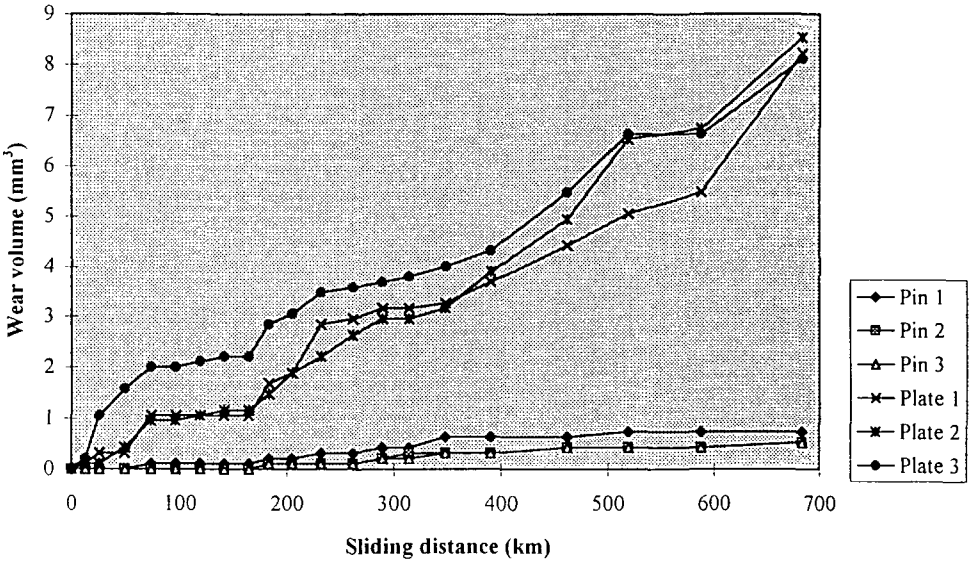

Figure 5.7 : Pin-on-plate test of UHMWPE pins against UHMWPE plates under 10 N and 40 N loading (Test 6)

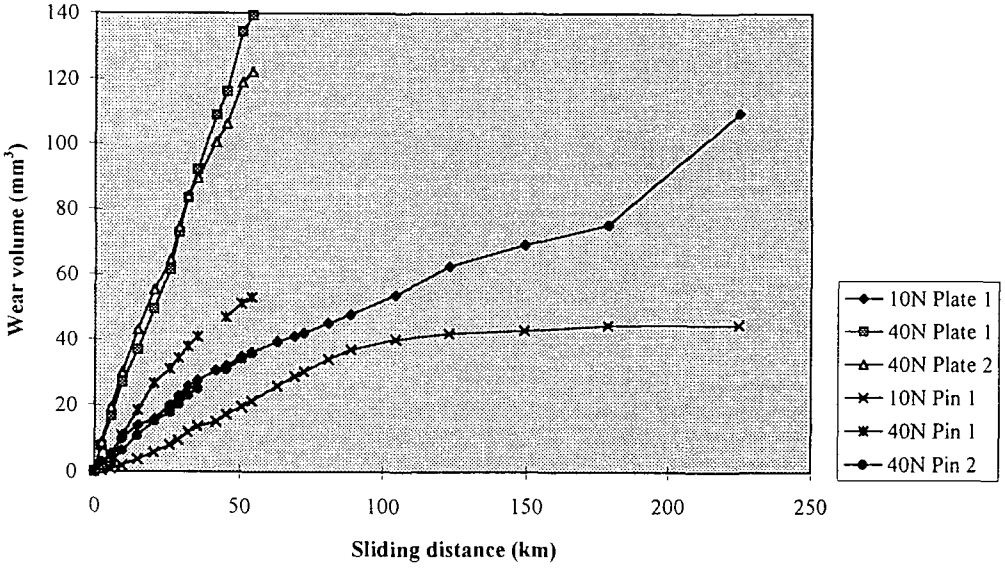

Figure 5.8 : Pin-on-plate wear test of UHMWPE pins against UHMWPE plates under 10N loading (Test 7)

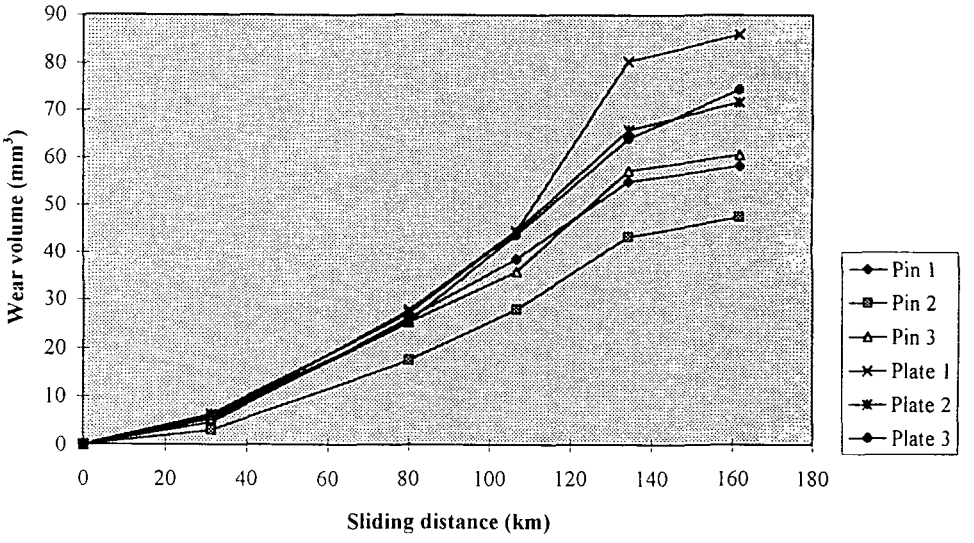

Figure 5.9 : Pin-on-plate test of UHMWPE pins against UHMWPE plates under 10N and 40N loading (Test 8)

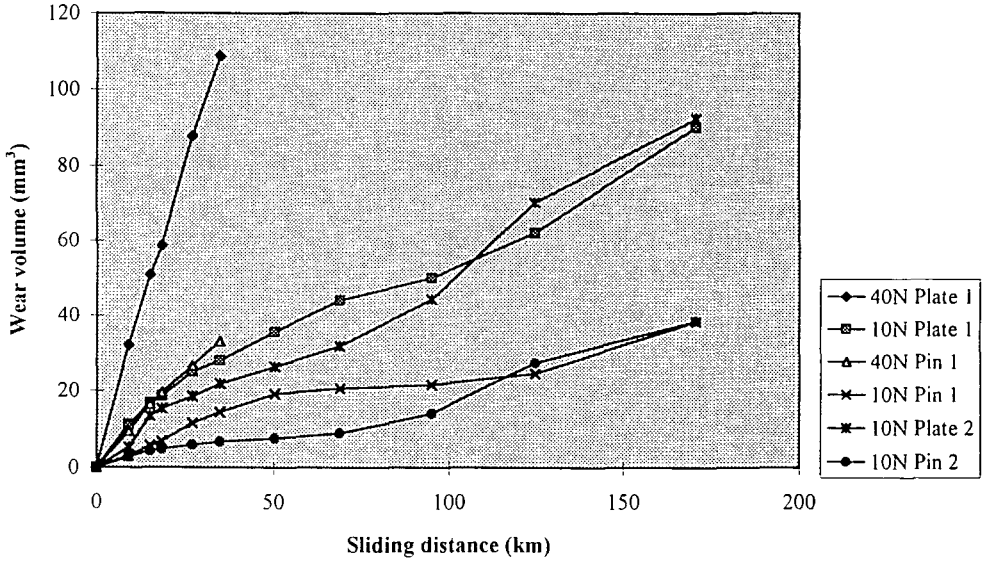

Figure 5.10 : Pin-on-plate wear test of UHMWPE pins against stainless steel plates under 10N loading (Test 9)

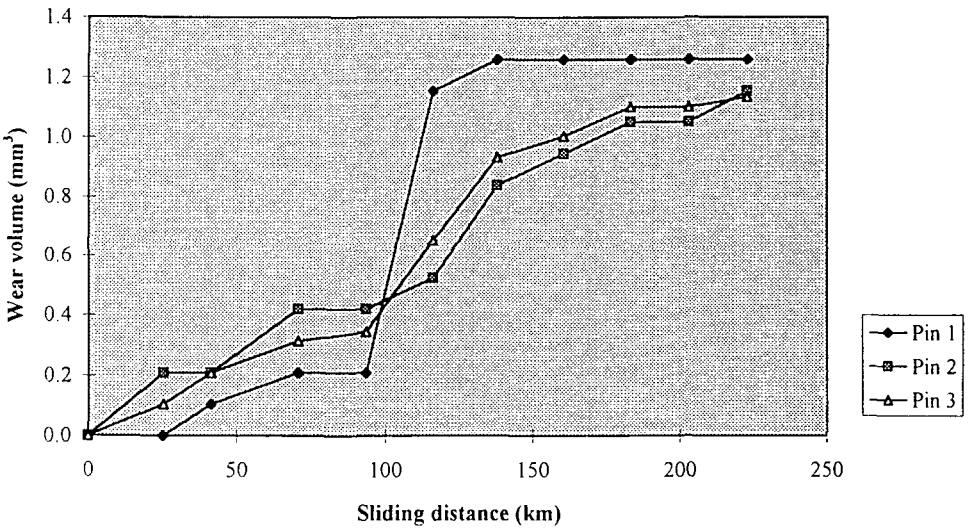

Figure 5.11 : Pin-on-plate wear test of UHMWPE pins against stainless steel plates under 40N loading (Test 10)

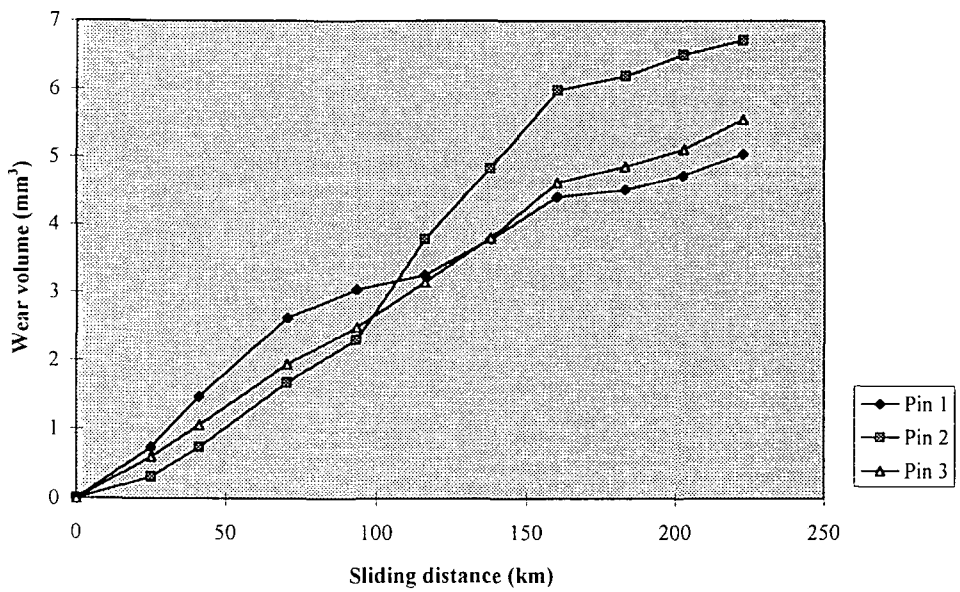

Figure 5.12 : Pin-on-plate wear test of XLPE pins against stainless steel plates under 10 N loading (Test 11)

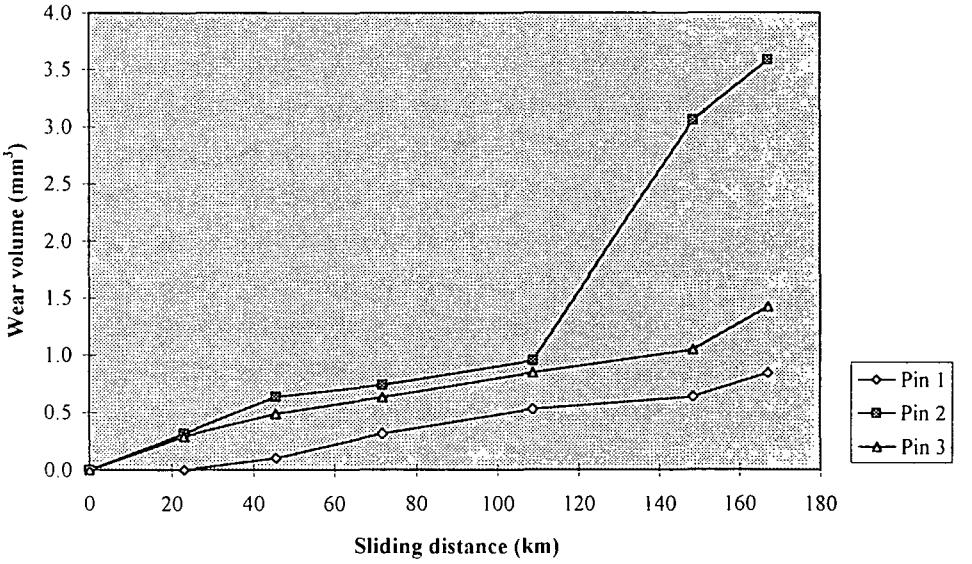

Figure 5.13 : Pin-on-plate wear test of XLPE pins against stainless steel plates under 40 N loading (Test 12)

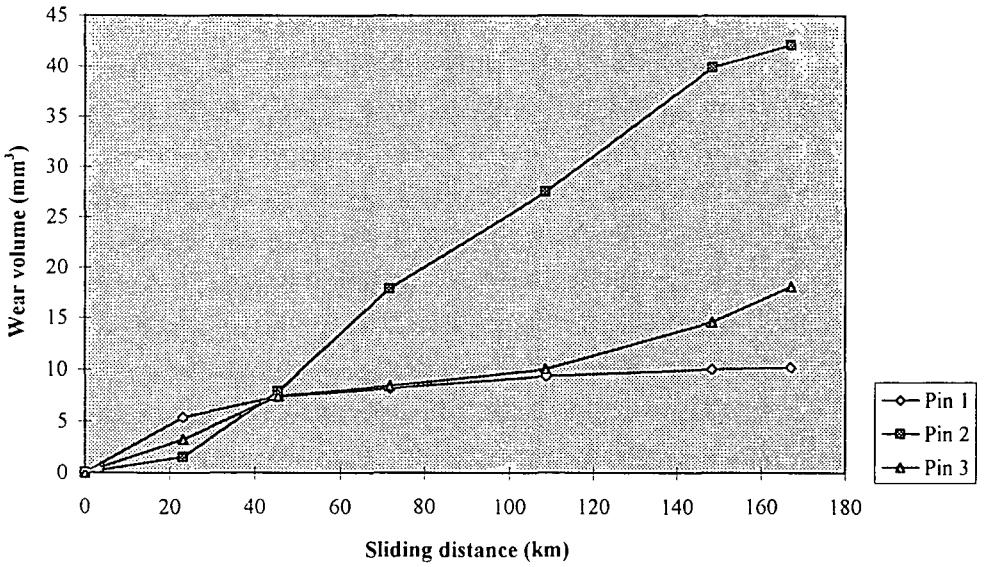

amount of wear may have resulted in the surface material being worn away too quickly for fatigue wear to occur.

The wear of the pins and plates in Test 1 was much greater than expected and turned out to be much greater than the other XLPE-on-XLPE tests in this study. Hence the results were not used in the calculation of the average XLPE wear coefficients. The XLPE used for Test 1 was from a different batch than all of the other XLPE tests, which may account for the elevated wear rates (this is discussed further in Section 5.7.1). However, the significance of Test 1 should not be under-estimated. The large amount of wear debris formed brought attention to the fact that the plates were wearing at a considerable rate as well as the pins.

Tests 2 to 5 showed periods of different wear rates. Within each period the wear rate was linear although occasional steps in the wear rate occurred. A wearing in period was seen with most of the plates, but not with the pins. The plates wore significantly more than the pins in both the 10 N and 40 N tests.

10 N tests (Tests 2 and 4, Figures 5.3 and 5.5). Due to the higher than expected wear experienced in Test 1 two further tests were run at 10 N. Shallow wear tracks were formed on the surfaces of the XLPE plates. Shallow grooves and ridges were observed in the direction of sliding, across the width of the wear track, indicating an abrasive wear mechanism (Figure 5.14b). Some surface polishing was also observed. Little pin wear occurred. Scratches were evident in the direction of sliding on the pins, which removed some of the machining marks. However, the machining marks were still visible in parts at the end of the tests, up to 600 km (Figure 5.15b). No evidence of adhesive or fatigue wear were found. However, periods of increased wear rate were observed indicating the presence of an additional wear mechanism, possibly fatigue. Uncharacteristically in Test 2, Plate 2 showed no wear until 500 km where it started to wear at a similar rate to the other two plates.

40 N tests (Tests 3 and 5, Figures 5.4 and 5.6). Shallow wear tracks were formed on the plate surfaces, however, these were more defined than the plates tested at 10 N. Some scratches in the direction of sliding were observed indicating an abrasive wear mechanism, however, there were large areas of surface polishing without scratches along the length of the wear track. The machining marks of the pins were worn away and some rounding of the pins at the sides of the wear tracks was observed. Score marks in the direction of sliding were formed. No evidence of adhesive or fatigue wear was found, however, like the tests run at 10 N, the wear rates increased for certain

Figure 5.14 XLPE plate before and after a wear test against a XLPE pin

a) Before

b) After

Figure 5.15 A XLPE pin before and after a wear test against a XLPE plate

a) Before

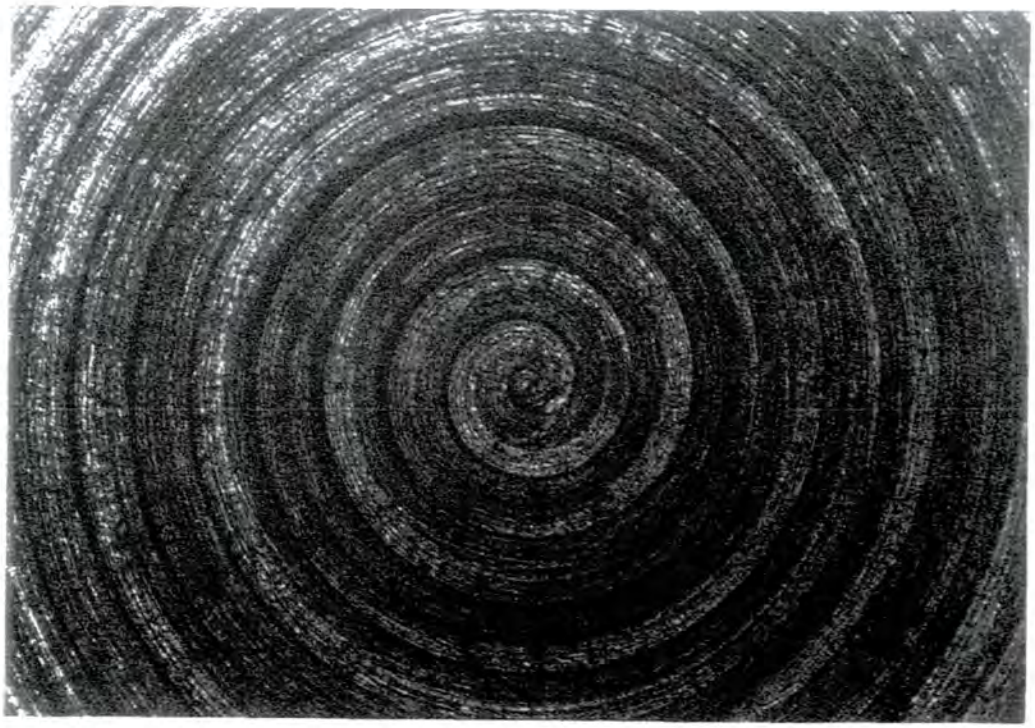

b) After

periods indicating the presence of an additional wear mechanism, possibly fatigue. Uncharacteristically in Test 3, Pin 2 showed no wear at all throughout the whole of the test (500 km).

5.6.2 UHMWPE pins against UHMWPE plates

The UHMWPE pins and plates showed very high levels of wear of both surfaces compared with the other material combinations tested. Wear debris could be seen floating on the top of the water bath. The 40 N tests were limited in distance due to shearing of the pins between 35 and 55 km. The plates wore significantly more than the pins and the lowest wear from the 40 N pins was comparable to the highest wear of the 10 N plates (Figures 5.7 and 5.9). The wear rates of the 40 N pins and plates were linear, however, they varied slightly throughout the 10 N tests. The pins and plates showed no significant wearing in period, although this may have been masked by the large amount of that occurred.

Initially transfer of material between the pins and plates was observed with tearing or pitting in the plate surface, indicating adhesive wear (Figure 5.16b). However after approximately 90 km (10 N tests) no transfer of material or tearing (pitting) was observed. Deep wear tracks formed in the plates and the machining marks of the pins were removed within the first couple of kilometres. Some score marks were also seen in the direction of sliding on both the pin and plate surfaces (Figures 5.16b and 5.17b). This indicated abrasive wear and possibly three-body wear from the large amounts of wear debris generated. Polishing of the plate wear tracks and of the pins was observed and a large amount of rounding of the pins at the sides of the wear tracks occurred. No evidence of fatigue wear was observed. Similarly to Test 1, the large amount of wear may have resulted in the surface material being worn away too quickly for fatigue wear to occur.

5.6.3 UHMWPE and XLPE pins against stainless steel plates

No wear of the stainless steel plates was observed at all. Transfer films of UHMWPE and XLPE were observed on the plates along the length of the wear track indicating an adhesive wear mechanism. This was more distinct in the central portion of the wear track (where the relative sliding speed was greatest) rather than at the ends, and was also more distinct with the 40 N tests. The machining marks were worn away from the pins and shallow score marks were formed in the direction of sliding indicating an

Figure 5.16 An UHMWPE plate before and after a wear test against an UHMWPE pin

a) Before

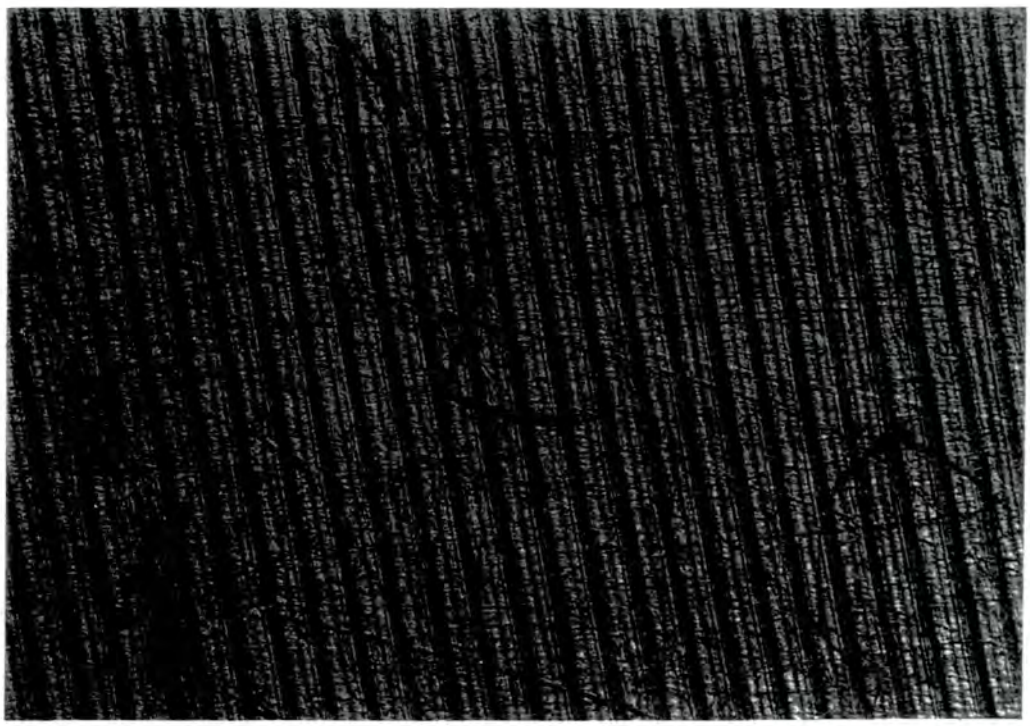

b) After

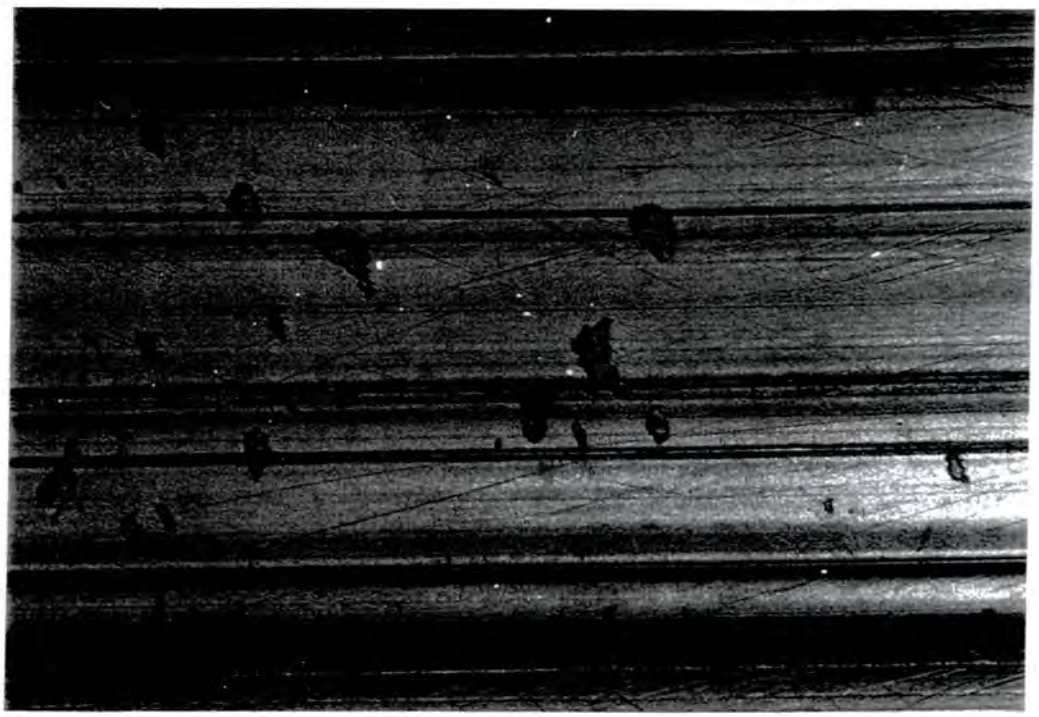

Figure 5.17 **An UHMWPE pin before and after a wear test against an UHMWPE plate**

a) Before

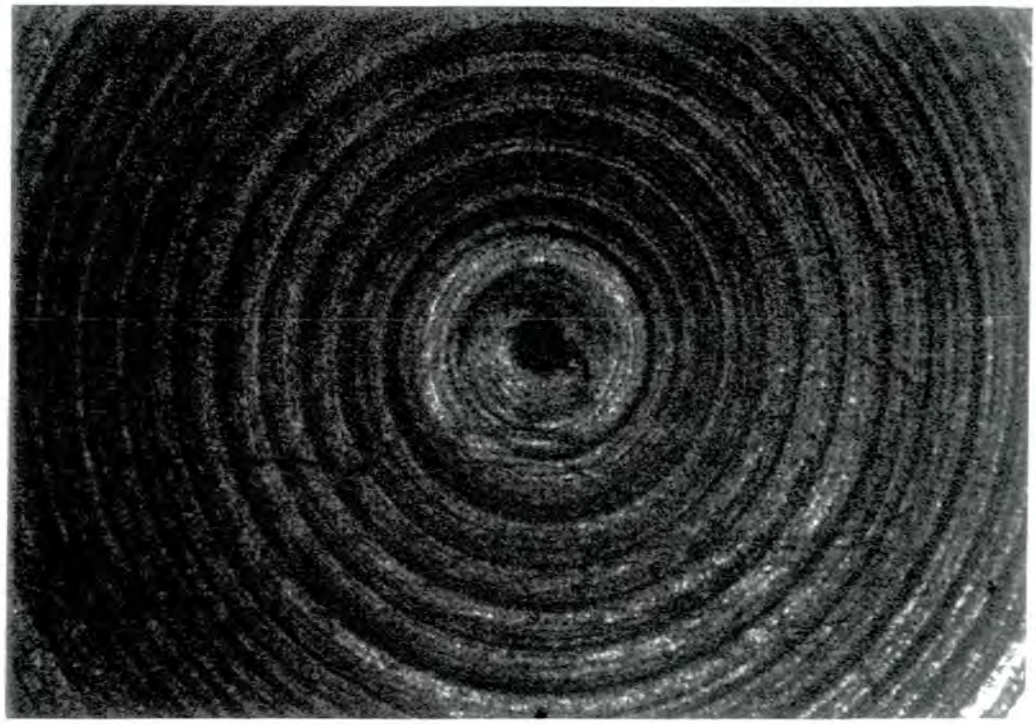

b) After

abrasive wear mechanism. The pins remained flat throughout the length of the tests. The XLPE pins wore more than the UHMWPE pins against the stainless steel plates.

The UHMWPE pins showed no wearing in period. The 10 N pins showed a significant increase in wear rate from approximately 100 km to 140 km after which the wear rate decreased again (especially Pin 1, Figure 5.10). The 40 N pins showed steady wear throughout the test, although Pin 2 did have a period of increased wear rate between 100 km and 160 km (Figure 5.11). The XLPE pins generally showed no significant wearing in period and wore fairly constantly throughout the tests. One 10 N pin had a significant increase in wear rate at approximately 110 km (Pin 2).

5.6.4 Wear volume/sliding distance ratios and wear coefficients

Trend-lines were fitted to the wear volume/sliding distance graphs shown in Figures 5.2-513. They were fitted to the individual wear periods and to the whole wear curves. The slopes of the trend-lines (mm^3/km) were then used to calculate the corresponding wear coefficients (mm^3/Nm). The wear coefficients were found for individual stages of the wear curves as well as for the whole curves to enable a fair comparison of the wear between the different material combinations and previous results. The average pin and plate wear coefficients are shown in Tables 5.4 and 5.5. The wear volumes, equations of the trend-lines, volume/sliding distance ratios and wear coefficients are shown in Appendix 5.

Table 5.4 Average and range of pin wear coefficients (k)

Materials	Force (N)	Average wear distance (km)	k range x 10^{-6} (mm^3/Nm)	k Ave. x 10^{-6} (mm^3/Nm)
XLPE	10	187.59	0.080 - 0.170	0.123
XLPE	40	204.13	0.008 - 0.058	0.0285
XLPE	10	581.51	0.07 - 0.190	0.125
XLPE	40	609.93	0.018 - 0.073	0.0395
UHMWPE	10	175.15	20.270 - 37.260	29.275
UHMWPE	40	447.73	17.070 - 26.750	22.876
XLPE/SS	10	222.71	0.460 - 1.790	1.017
XLPE/SS	40	224.56	1.893 - 6.345	3.619
UHMWPE/SS	10	167.13	0.540 - 0.660	0.587
UHMWPE/SS	40	168.28	0.638 - 0.805	0.700

Table 5.5 Average and range of plate wear coefficients (k)

Materials	Force (N)	Average wear distance (km)	k range x 10^{-6} (mm^3/Nm)	k Ave. x 10^{-6} (mm^3/Nm)	k plate k pin
XLPE	10	185.15	1.03 - 1.31	1.176	9.56
XLPE	40	203.92	0.215 - 0.653	0.410	14.39
XLPE	10	581.51	0.740 - 1.640	1.060	8.48
XLPE	40	591.51	0.255 - 1.000	0.540	13.67
UHMWPE	10	175.15	43.600 - 55.200	49.567	1.69
UHMWPE	40	47.73	60.420 - 80.29	68.367	1.52

5.6.4.1 Pin wear coefficients

The UHMWPE-on-UHMWPE pins wore most, followed by the XLPE-on-stainless steel pins, UHMWPE-on-stainless steel pins and then the XLPE-on-XLPE pins . The average wear coefficients were in the order of 10^{-5}, 10^{-6}, 10^{-7}, and 10^{-7} respectively. Theoretically the wear rate is proportional to load, hence the pins tested at 40 N were expected to wear approximately four times as much as the pins tested at 10 N. However, the wear coefficients at 40 N compared with 10 N were much lower for XLPE-on-XLPE pins and UHMWPE-on-UHMWPE pins. In fact over the first ≈200 km the XLPE pins tested at 40 N wore at a lower rate than those at 10 N. On average over the whole tests (≈600 km) the wear rates of the XLPE and UHMWPE pins tested at 40 N were approximately three times greater than those of the 10 N pins.

In contrast, for both the XLPE and UHMWPE pins wearing against stainless steel plates, the average wear coefficients of the pins tested at 40 N were greater than four times those at 10 N. The UHMWPE pins tested at 40 N wore nearly five times as much as the pins at 10 N, and for XLPE the ratio was approximately fourteen times. Even when neglecting the wear rate of the highest wearing 40 N pin the ratio was approximately seven times.

5.6.4.2 Plate wear coefficients

For polyethylene-on-polyethylene combinations the plates wore significantly more than the pins. The wear coefficients of the XLPE plates (10 N and 40 N) were approximately 9-14 times that of the XLPE pins. The wear coefficients of the UHMWPE plates (10 N and 40 N) were approximately 1.5-1.7 times that of the UHMWPE pins. The UHMWPE plates wore significantly more than the XLPE plates. The average wear coefficients were in the order of 10^{-5} and 10^{-6} respectively. No stainless steel plate wear was found against either UHMWPE or XLPE. The average

wear coefficients of the XLPE plates tested at 40 N were less than at 10 N. In fact the 40 N plates only wore twice as much as the 10 N plates. However, unlike the UHMWPE-on-UHMWPE pins, the average wear coefficients for UHMWPE plates at 40 N were greater than those at 10 N, and wore by approximately 5.5 times more.

5.7 Discussion

Difficulty arises in the comparison of wear results in the literature due to the different operating conditions used such as force, lubrication, temperature, speed, sliding distance, motion and type of apparatus. There has also been considerable scatter in the previously reported wear coefficients over several orders of magnitude, even with similar experimental conditions. In addition, the presentation of wear results has varied and it is not always possible to convert the results into a format that can be compared with other results. For example contact pressure may be quoted without the contact area, hence the contact force can not be calculated. Hence wear tests with different material combinations were performed in this study to directly compare the wear of XLPE-on-XLPE with other material combinations when tested under the same operating conditions and on the same rigs. In addition, the results were then compared with those from previous tests where appropriate.

5.7.1 Gel content of cross-linked polyethylene

Only the wear coefficients from Test 1 compare with those found from the majority of previous wear tests of XLPE-on-XLPE on pin-on-plate or finger function simulator apparatuses, and even these are at the lower range[73,83,84]. The other XLPE-on-XLPE tests found significantly lower wear rates which compare better with more recent work carried out, although Joyce et al[103] found slightly lower wear rates overall. The reasons for the differences in results between Tests 2-5, and Test 1 and the majority of previous results may be due to the degree of cross-linking of the polyethylene. The percentage gel content is equivalent to the percentage of cross-linking of the polyethylene. Hence XLPE with a lower gel content would be expected to wear more.

It is not known what the gel content of the XLPE used in the majority of previous tests was, how old it was or where the material was kept prior to the tests. Ageing of the material can cause a breakdown in the cross-linking decreasing the wear resistance of the XLPE. Hence if the gel content was originally lower than that used for Tests 2-5, or the material had been kept for some time (particularly in daylight) then a lower gel

content may have been responsible for the higher wear rates. The material used for Test 1 was from a different batch than the other XLPE tests. The gel content of the XLPE used in Test 1 was 77% compared with 78% for all other tests, and this small difference would not be expected to give such a large difference in wear. However, the age of the material was not known, hence the true gel content may have been lower than 77% which may have produced the uncharacteristically high wear rates. In addition, the gel content of the XLPE tested by Joyce et al[103] was 87% which may account for the slightly lower wear rates compared with Tests 2-5.

5.7.2 Pin and plate wear

In previous tests the change in wear of the plates in polymer-on-polymer wear tests was not measured. These tests have shown that polymer plates wore significantly more than pins (the stainless steel plates showed no wear). The XLPE plates wore between 9-14 times that of the pins and the UHMWPE plates wore between 1.5-1.7 times that of the pins. This may have been due to the different loading conditions of the pins and plates. The pins were loaded continuously throughout the tests, whereas the plates were subjected to cyclic loading along the length of the wear track. Cyclic loading increases the possibility of fatigue wear which may have caused the higher plate wear.

Short[83] did measure the plate wear of UHMWPE-on-UHMWPE but only right at the end of the test. Wear coefficients of 349 x 10^{-6} mm^3/Nm (10 N) and 196 x 10^{-6} mm^3/Nm (40 N) were found. These were both approximately three times that of the average pin wear.

5.7.3 Wear mechanisms

Abrasive wear has been found to be the predominant wear mechanism in previous wear tests of XLPE-on-XLPE with grooves and scratches in the direction of sliding. Some adhesive wear was also found with a material transfer between the pins and plates[73,83,84]. Adhesive wear was the predominant wear mechanism in previous tests of UHMWPE-on-UHMWPE, with surface polishing, film transfer and some two and three-body abrasive wear. A distinct change to a higher wear regime was attributed to the onset of a fatigue wear mechanism with cracks forming in the wear surface[74].

Adhesive, abrasive and fatigue wear have all been found in previous wear tests of UHMWPE against stainless steel. Initially adhesive wear was the dominant wear mechanism with a little abrasive wear. The adhesive wear resulted in the formation of

transfer films on the metal counterfaces when tested in distilled water or saline solution but not with biological lubricants due to the effect of the proteins in the lubricants. As the tests progressed abrasive wear took over as the dominant wear mechanism with an additional fatigue component as well. Ridges in the polyethylene surface parallel to the sliding direction indicated abrasive wear[81].

Grooves and scratches in the direction of sliding were found in all of the tests performed for this study. Abrasive wear is associated with the removal of material from a softer bearing surface by a cutting action of asperities from the harder bearing surface. However, with similar materials abrasive wear is not necessarily expected, but some degree of abrasive wear was found on the pins and plates in tests of XLPE and UHMWPE against themselves. This may have been caused by regions of harder material on one surface removing material from softer regions on the opposite bearing surface, or from three body abrasive wear from wear debris or contamination trapped between the bearing surfaces.

The predominant wear mechanism associated with polymer-on-polymer combinations is adhesive wear. However, no evidence of adhesive wear was found in the XLPE-on-XLPE tests and tearing (pitting) and transfer of the material was only seen in the UHMWPE-on-UHMWPE tests up to approximately 90 km. This is not to say that adhesive wear did not occur throughout the length of both tests. The tears associated with adhesive wear may have been filled with transferred material, and transferred material may have been removed through abrasive wear to form wear debris or may not have been clearly visible. Adhesive wear may have been present but on a microscopic level.

No evidence of fatigue wear was seen in any of the polymer-on-polymer tests, however, changes to higher wear rates in the XLPE-on-XLPE tests indicated that an additional wear mechanism was present, possibly fatigue. Again, although no cracks were seen in the wear surfaces (typical of fatigue wear), they may have been present on a microscopic level and hence not detected.

Abrasive wear of the UHMWPE and XLPE pins when sliding against stainless steel plates was found. This was indicated by grooves and scratches on the pin surfaces in the direction of sliding. Transfer films of UHMWPE and XLPE formed on the stainless steel plates within the first 25 km of the tests through adhesive wear. This was expected as the tests were run in distilled water. It has been suggested that the cross-linking of polyethylene inhibits the orientation and movement of the polymer molecules

necessary to form the transfer film[107]. However, transfer films were found on the stainless steel counterfaces when sliding against XLPE pins.

Stepping in the wear rate of UHMWPE against stainless steel was found when testing in distilled water[81]. This was associated with the removal of material from peaks or ridges on the polymer surface[93]. Thin section polarised light microscopy showed high residual shear strains under these peaks in the polymer surface prior to the loss of material. The strains were higher in the plane parallel to the direction of sliding[93]. Stepping was not seen in the polymer-on-metal tests, nor the UHMWPE-on-UHMWPE tests, but it was observed in the tests of XLPE-on-XLPE. However, the pins and plates were only weighed once a week. Hence smaller steps in the wear rates of the other materials may not have been detected.

5.7.4 Wear coefficients

During polymer-on-metal wear tests the polymer pins wear significantly more than the metallic plates. In addition, the plate wear of polymer-on-polymer combinations was not measured in previous wear tests. Hence a comparison between the wear rates of different material combinations tested in this study and previous wear results can only be made by looking at the wear of the pins. However, the significantly higher wear rates of the plates compared with the pins in polymer-on-polymer combinations should not be neglected.

The XLPE-on-XLPE pins showed the lowest pin wear coefficients from all of the material combinations tested in this study. These were 0.123×10^{-6} and 0.0285×10^{-6} mm^3/Nm for 10 N and 40 N respectively (up to 200 km). Previous tests have found much higher wear coefficients, between 1.1×10^{-6} and 13.15×10^{-6} mm^3/Nm[73,83,84], although the length of these tests ranged from 27 to 300 km (Table A5.42, Appendix 5). The previous results compare more favourable with the wear coefficients from Test 1 which were between 0.83×10^{-6} and 2.15×10^{-6} mm^3/Nm for the pins. The higher wear rates may have been due to a lower gel content of the XLPE used or ageing of the material (Section 5.7.1).

The UHMWPE-on-stainless steel pins showed slightly higher wear than the XLPE-on-XLPE pins, although the average wear coefficients were of the same order. The average UHMWPE wear coefficients were 0.587×10^{-6} and 0.700×10^{-6} mm^3/Nm for 10 N and 40 N respectively. They may have been higher due to the hard asperities on the metallic counterface producing larger amounts of abrasive wear compared with the

XLPE-on-XLPE combination. Previous tests have found an enormous range of wear coefficients for UHMWPE-on-stainless steel from (0.0035×10^{-6})[93] to (9.05×10^{-6})[89] mm^3/Nm (Table A5.41, Appendix 5). Admittedly the wear coefficients found in this study were at the upper range of those found from previous tests. This may have been due to the apparatus, the testing procedure or the materials tested. Hence it was important to perform tests of UHMPWE-on-stainless steel on the same rigs as the XLPE-on-XLPE tests for a direct comparison of results.

XLPE-on-stainless steel pins showed higher wear than XLPE-on-XLPE and UHMWPE-on-stainless steel pins. The average wear coefficients were 1.017×10^{-6} and 3.619×10^{-6} mm^3/Nm for 10 N and 40 N respectively. Fisher et al[108] found an increase in the wear rate of irradiated polyethylene on unidirectional tri-pin-on-disc wear tests. Irradiation can produce cross-linking of polymers, hence the reasons for higher wear of irradiated polyethylene in unidirectional testing may be relevant to the testing of XLPE.

During repetitive sliding in a particular direction alignment of the polymer chains on the bearing surface can occur. This can result in an increase in the strength of the polymer in the direction of alignment but decrease its strength perpendicular to this direction. However, cross-links in a polymer can prevent this alignment from happening. Hence this may explain why the UHMWPE showed superior wear characteristics compared with XLPE when sliding against stainless steel in the reciprocating pin-on-plate tests.

However, in applications where the relative movement between the bearing surfaces is not simply in a straight line (for example in some artificial joints) the UHMWPE may not become aligned and the XLPE may wear less than UHMWPE due to the strength of its cross-links. Indeed Wang et al[109] found a lower wear rate with irradiated polyethylene when tested on a bi-axial hip joint simulator compared with that of unirradiated polyethylene.

UHMWPE-on-UHMWPE pins showed much higher wear coefficients than any of the other material combinations tested. The average wear coefficients were 29.275×10^{-6} and 22.876×10^{-6} mm^3/Nm for 10 N and 40 N respectively. In previous wear tests wear coefficients from 5.6 - 101.34×10^{-6} mm^3/Nm have been found for contact forces from 5 to 40 N (Table A5.43, Appendix 5). The large wear rates may be attributed to the poor resistance of UHMWPE-on-UHMPWE to adhesive and abrasive wear, and the wear debris may also produce additional large amounts of three-body abrasive wear.

The UHMWPE and XLPE plates wore by 1.5-1.7 and 9-14 times that of the UHMWPE and XLPE pins respectively. The higher plate wear rates may have been due to the cyclic loading conditions of the plates compared with the continuous loading of the pins. This may have caused an additional fatigue wear mechanism to act on the plates. The increased XLPE plate wear rate is an important consideration when deciding whether the material is suitable for an all XLPE joint prosthesis. In a MCPJ prosthesis the PP component would be loaded all of the time, but the MC would be cyclically loaded (similarly the MP base and PP head in the PIPJ). Hence the higher XLPE plate wear rate can not simply be ignored. In a UHMWPE-on-stainless steel joint prosthesis virtually no wear of the cyclically loaded stainless steel plate would occur.

The average XLPE-on-XLPE plate wear rate was much greater than that of the pins. However, at 40 N the average XLPE-on-XLPE plate wear rate was less than the UHMWPE-on-stainless steel pin wear rate, although at 10 N it was slightly larger. The total wear of the bearing surface combinations is the total pin and plate wear. At 10 N the total XLPE-on-XLPE wear rate was 0.123 + 1.176 = 1.299 compared with 0.587 for UHMWPE-on-stainless steel, and at 40 N it was 0.0285 + 0.410 = 0.4385 compared with 0.700 for UHMWPE-on-stainless steel. Hence the total wear rate of XLPE-on-XLPE was about twice that of UHMPWE-on-stainless steel at 10 N but only about 0.6 times at 40 N.

5.7.5 Test repeatability

The shapes of the wear curves of the pins or plates within each test showed a remarkable similarity (despite some scatter in the amount of wear produced). The different wear periods started and finished simultaneously and a change in wear rate in the plates was matched with a corresponding change (although smaller) in the pins. However, when comparing different tests run in an identical manner the same similarities were not found. Tests 2 and 4 were conducted under the same operating conditions and on the same rig, however, the shapes of the wear curves differed significantly, even though the overall wear rates were similar. Similarly Tests 3 and 5 were conducted under the same operating conditions and on the same rig. The wear curves differed significantly and the overall wear of Test 5 was less than half that of Test 3. The reason for the similarity in shape of the wear curves within the same tests, but not between tests, is not clear. However, it indicates that some dominant feature to the method of testing must be present.

The possibility that there was an inherent fault with the pin-on-plate rigs was considered. However, simultaneous changes in wear rates can be observed in previous wear tests on different apparatuses, although it has never been commented on[73,74,84,93,103]. In addition, although a couple of tests showed a higher wear rate for Pin 2, this was not the case throughout all of the tests, and the order of wear of the pins and plates varied between tests.

The materials used for each test were from the same batches (apart from Test 1) and the pins and plates were chosen randomly for each test. The possibility of ageing of the material is not convincing since although the shapes of the wear curves from Tests 3 and 4 are similar, Test 2 showed a greater similarity with Test 5. All of the tests were run on the same two rigs, under the same operating conditions (apart from contact force), and using the same procedure for measuring the change in weight of the pins and plates. The pins and plates were carefully relocated in the same orientation and position after each weighing session and allowed to equilibrate at 37°C for two hours before the tests were restarted. Control pins and plates were included in all of the tests to compensate for water absorption and any variations in the readings introduced by the weighing balance. The same weighing balance was used throughout the tests and was recalibrated before each set of readings was taken.

Two possibilities which can not be accounted for are changes in the environment and the fact that a common bath was used for each test. Firstly there is a possibility that changes in the environment may somehow have influenced the wear rates of the pins and plates. This was considered since the only obvious difference between the tests was when they took place. Further, Tests 3 and 4 ran at approximately the same time and the shapes of the graphs are similar. However, they differ from the shapes of the graphs produced from Tests 2 and 5 which were run at different times. Changes in the environment may have occurred within the water bath itself or in the laboratory where the tests were run. Changes in the temperature or humidity of the lab may have affected the apparatus. For instance they may have affected the contact between the pin holders and the cantilever arms which held the pin holders vertically. This in turn may have altered the forces exerted on the pins and hence the pin and plate wear rates. To test this theory, tests should be run simultaneously in a controlled environment and using an identical source of lubricant to standardise the bath environment.

Secondly all four pins and plates were tested in a common bath. Hence wear debris from one bearing surface was free to interact with the other bearing surfaces. In addition, any contamination of the baths (such as dust) may have affected the wear

rates of the pins and plates. Tests in individual baths would be required to investigate this theory further.

5.7.6 Contact force

Wear is theoretically proportional to force, as the real area of contact of the articulating surfaces is proportional to the force across the surfaces. However, the polymer-on-polymer wear coefficients decreased with force. The XLPE and UHMWPE pins at 40 N wore approximately three times as much as than those of the 10 N pins when articulating against XLPE and UHMPWE plates respectively. This agreed with the findings of Short[83] who tested UHMWPE-on-UHMWPE and XLPE-on-XLPE at 10 N and 40 N and found the 40 N pins to wear 2.57 and 3.23 times as much as the 10 N pins respectively.

Other polymer-on-polymer tests have found an increase in wear coefficient with force. Sibly[73] found that XLPE-on-XLPE pins at 40 N wore 9.09 times as much as those tested at 10 N, however, the reported wear coefficients were much greater than those found in this study. Atkinson[97] found the wear coefficient of UHMWPE-on-UHMWPE pins to increase with contact force from 6-32 N and Stokoe[74] reported a similar result with forces between 5-19 N. In contrast to the polymer-on-polymer results in this study, polymer-on-metal wear coefficients also increased with force. UHMWPE and XLPE pins tested at 40 N wore nearly five and seven times as much as the pins at 10 N respectively, when wearing against stainless steel. There have been few results to compare directly with these for UHMWPE pins against stainless steel plates although Brown[87] interestingly found that the wear rates were independent of the force in the range of 25-145 N. It has generally been found that wear rates increase with force but not proportionally. Hence the wear coefficients do not remain constant with a change in force. This shows that other factors affect wear in addition to the force across the articulating surfaces.

5.8 Application to artificial finger joints

There are two main advantages of an all XLPE finger joint prosthesis over the use of a a metal and polymer combination. Firstly XLPE is softer than metal and may therefore produce less reaction with the bone, prolonging the life of a finger joint prosthesis. Secondly XLPE can be injection moulded which may simplify manufacture of the joint prosthesis, especially with the complex shapes encountered in the PIPJ. However, at

the beginning of this project it was not clear whether the wear characteristics of XLPE-on-XLPE would be acceptable when compared with that of UHMWPE against stainless steel. This study showed that the wear of XLPE-on-XLPE pins was of the same order of UHMWPE-on-stainless steel pins. However, the XLPE plates wore significantly more than the XLPE pins, whereas the stainless steel plates did not appear to wear at all. The wear from both XLPE bearing surfaces was twice that of the UHMWPE-on-stainless steel combination. However, this may be acceptable especially when combined with the advantages of XLPE over metal.

CHAPTER SIX

Development of a portable computer system for the Durham arthrograph

6.0 Introduction

There are many different ways in which the performance of a joint can be assessed. Objective assessment methods include grip and pinch strength, range of movement, stiffness and hand tasks. Individually, none of these give an overall picture of the joint performance. Therefore as many as possible should be used to produce a comprehensive assessment of the joint. A MCPJ surface replacement prosthesis was designed at the University of Durham for patients whose natural joints had been destroyed by arthritis. During future pilot studies of the joint prosthesis, objective assessment of hand strength, joint range of movement, and joint stiffness would be performed, as well as assessing the joints using a subjective questionnaire. The joints would be assessed pre-operatively and post-operatively over several months to determine the short-term and long-term performance of the joint prosthesis. The author was involved in the development of the objective joint stiffness assessment and the subjective questionnaire (Chapter 7).

Joint stiffness has been defined as the resistance to passive motion of a joint throughout the normal range of motion in the usual functional plane[110]. Stiffness, and the intensity and duration of morning stiffness are three of the many recognised symptoms of RA[111-114]. Indeed, morning stiffness is one of the diagnostic criteria for RA set out by the American Rheumatism Association[7]. Joint stiffness can be assessed either objectively or subjectively.

Objective stiffness assessment generally measures the resistance of a joint to motion imposed on it. This is done using a piece of equipment called an arthrograph. Both knee and MCPJ arthrographs have previously been used[113-116]. The results are definitive and a valid comparison can be made between results of one patient taken at different times, or between different individuals. The Durham MCPJ arthrograph has been used in several previous clinical trials[112,114,117,118]. The arthrograph imposed motion on the MCPJ and the resistance to the motion was recorded. A computer collected the resistive torque-angular displacement data and calculated the required stiffness parameters. The original computer system consisted of an Apple computer

and a program written in Apple-Basic. However, the computer system was not portable and so a new computer system was required for a lap-top computer.

6.1 Stiffness components

All of the soft tissues that surround a joint (joint capsule, ligaments, tendons, muscles, skin etc.) contribute to the overall stiffness of the joint, as well as the bearing surfaces themselves. In 1960 Wright and Johns built an arthrograph to measure the passive resistance of the MCPJ to sinusoidal motion imposed on it[113]. This was the first time that joint stiffness was able to be quantified. The resistive torque was measured as a function of angular displacement, velocity and acceleration. The individual components of stiffness were defined as elasticity, viscosity, inertia, friction (coulomb) and plasticity.

Plasticity was measured as the reduction in torque when a finger was held at particular position over a length of time (otherwise known as stress-relaxation due to the viscoelastic properties of the soft tissues). Elasticity was measured as the torque remaining after stress-relaxation, and was a function of angular displacement. Elasticity and plasticity were the major components of MCPJ stiffness in normal individuals and patients with arthritis, and were approximately equal[113]. Viscosity contributed to less than 10% of the overall stiffness and was a function of velocity. Friction contributed to less than 1% of the overall stiffness, even in badly damaged joints, and was independent of displacement or velocity. Finally inertia was negligible at physiological accelerations.

If a joint is subjected to sinusoidal motion and the resistive torque is plotted against angular displacement for one cycle then a hysteresis loop is formed (Figure 6.1). The hysteresis is partly due to the viscous and frictional stiffness components but mainly due to the viscoelastic properties of the soft tissues surrounding the joint[113]. When the joint is moved into flexion, during the first half of the cycle, the extensors are strained. The resistive torque produced by the tendons and other soft tissues surrounding the joint reduces with time (stress-relaxation). Therefore, when the joint is then moved into extension the resistive torque is lower than when the joint was moving into flexion. By moving further into extension, in the second half of the cycle, the flexors behave in the same way as the extensors did in the first half of the cycle. Hence a hysteresis loop is formed from which several parameters can be measured to give an overall picture of the stiffness of the joint.

Figure 6.1 Joint stiffness hysteresis loop

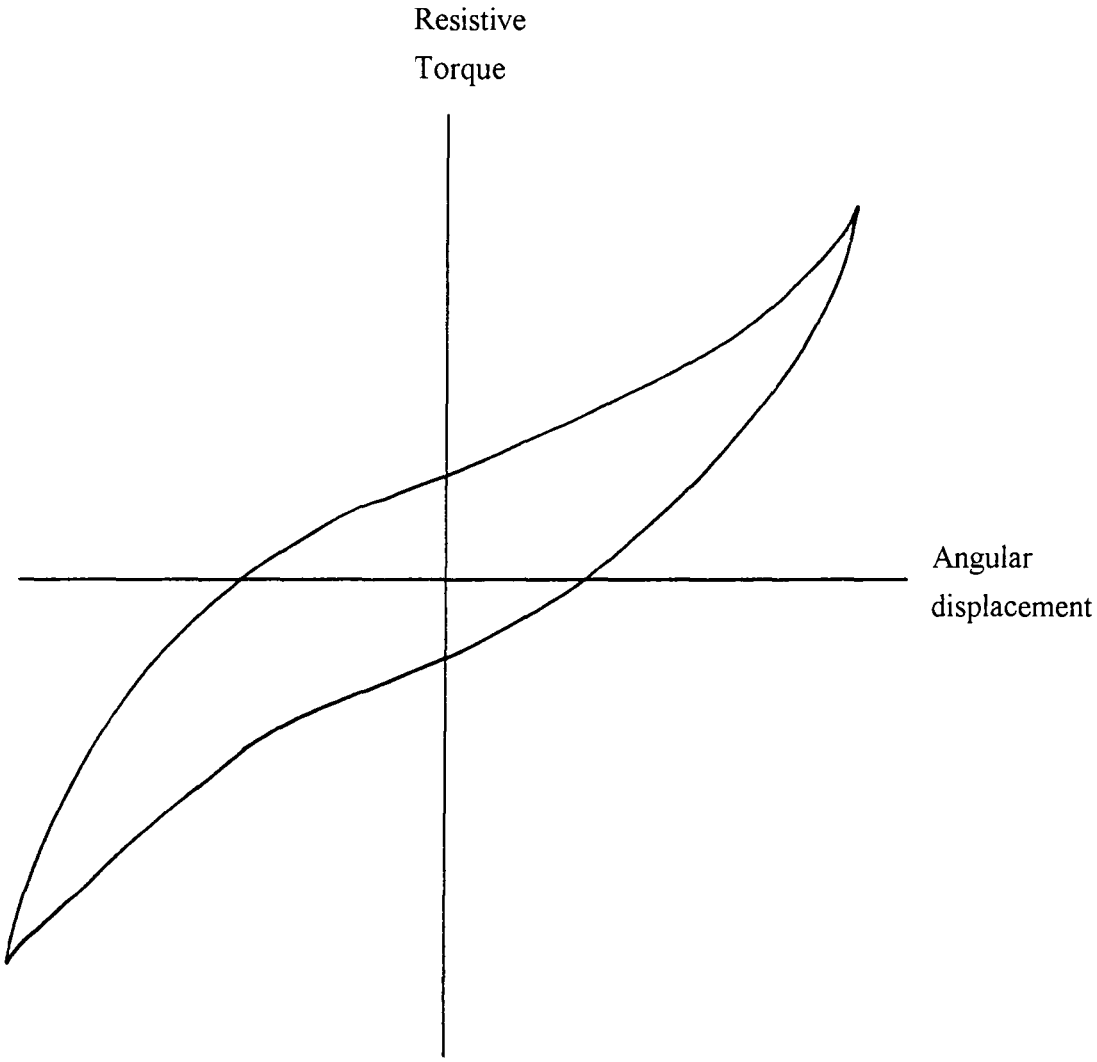

6.2 Previous joint stiffness assessment apparatus

The following section reviews the previous methods of measuring joint stiffness. It concentrates on the apparatus and methods used rather than human and environmental factors which were found to affect joint stiffness. These are discussed in Section 6.5.

As previously mentioned the first arthrograph was built by Wright and Johns to measure MCPJ stiffness[113]. The arthrograph imposed sinusoidal motion on the MCPJ. It was thought that sinusoidal motion would reduce the likelihood of active muscle involvement during motion of the joint. (The torques produced by active muscle involvement are much larger than those resulting from passive motion of the joint and can easily be distinguished). Movement was in flexion-extension which would probably be considered as the usual functional plane of the MCPJs. Originally the sinusoidal motion was derived from a pendulum, however, to produce a wider range of frequencies the apparatus was motorised. Different hysteresis loops were formed by varying the frequency and amplitude of oscillation due their affect on the velocity dependent stiffness components. This emphasised the importance of careful consideration of these two parameters when performing joint stiffness assessment and when comparing different results.

Backlund and Tiselius[119] used a vertical (flexion-extension) MCPJ arthrograph to measure the stiffness of normal individuals compared with patients with RA. The apparatus was a simplified version of Wright and Johns'[113] apparatus. Such et al[120] also used a vertical (flexion-extension) arthrograph to measure the passive resistance to sinusoidal motion of the knee joint. The effect of the weight of the limb was eliminated by a counterbalance. However, Thompson et al[110] stated that the effects of limb mass and elastic resistance could not be separated. They proposed therefore that horizontal arthrographs should be used to minimise the effects of the limb mass, eliminate the need for a counterbalance system and allow absolute the measurements of joint stiffness. Hence they developed a horizontal (flexion-extension) knee arthrograph.

In 1981 Unsworth et al[121] developed a horizontal (flexion-extension) arthrograph for the MCPJ. However, since the arthrograph was un-motorised only elasticity and coulomb friction could be measured. The velocity dependent stiffness components such as plasticity and viscous friction could not be measured. Therefore only approximately half of the overall stiffness of the joint was measured according to Wright and Johns'[113] estimation of the proportion of the individual stiffness components. In addition, joint stiffness is defined as the 'resistance to passive motion' of a joint hence the static tests

contradicted this definition. In 1982 a motorised arthrograph was developed to allow dynamic stiffness studies to be undertaken[114].

Finally Howe et al[122] developed a horizontal arthrograph to measure the stiffness of the MCPJs of the index, middle and ring fingers of both hands in abduction-adduction. Movement in the horizontal plane eliminated the torque arising from the weight of the finger, however, it could be argued that this is not the 'usual' functional plane of the MCPJs. Movement in flexion-extension may be more appropriate for joint stiffness assessment of the MCPJs.

Several attempts have also been made to estimate joint stiffness by the measurement of displacement of a joint due to a known force rather than measuring the resistance of a joint due to a known displacement. Scott[115] attempted to estimate joint stiffness from the elevation of a relaxed finger from the neutral position by an extension spring. Joint stiffness was expressed as the elevation distance. The torque exerted on the joint was dependent on the length of the individual's finger hence comparison between individuals was not valid. However, the study did highlight the importance of the rotational history of the joint. The height resulting from the application of the extension spring increased with the amount of times the joint had been tested. This indicated a decrease in joint stiffness which was probably due to alignment of the tissues in the direction of rotation.

Sundararaj and Mani[123] measured stiffness as the distance between the pulp of the finger and the palm during maximal passive finger flexion with the MCPJs held at 90° flexion. However, similarly to Scott's method of testing[115] the results were dependent not only on the stiffness of the joints but also on the length of the fingers. Hence comparison between individuals was not valid. Finally Flowers and Pheasant[124] applied a torque to the PIPJs and the resulting joint angles were measured.

Each of the previous three methods were simple and easy to perform, however, there were several disadvantages of the apparatus used. The methods of testing were static, hence velocity dependent stiffness components could not be measured. In addition, the static tests contradicted the stiffness definition of the 'resistance to passive motion of a joint'. The usefulness of the format of the results of the tests are questionable as they are not comparable with those from other testing methods. The sensitivity of the apparatus to change is also questionable. Finally it is difficult to see how active muscle involvement was distinguishable from passive resistance.

From analysing previous apparatuses and testing methods it is apparent that many did not actually measure the previously defined joint stiffness. In addition, in some cases the parameters measured are not particularly useful as they were not comparable with the results from other authors. Hence the validity of the results may be questionable. In summary joint stiffness assessment should satisfy the following requirements:

(i) Dynamic tests should be carried out to measure the overall joint stiffness (including the velocity dependent components). This also conforms with the stiffness definition of the resistance to passive motion of the joint.

(ii) Motion should be sinusoidal to reduce the likelihood of active muscle involvement.

(iii) The plane of motion of the joint during testing should be the 'usual' functional plane. For MCPJs this should be flexion-extension.

(iv) Horizontal arthrographs should be used to minimise the effect of the limb (finger) and eliminate the need for a counterbalance.

(v) The amplitude and frequency of the motion of the joint should be defined and they should not affect the inertial joint stiffness component which is negligible at physiological accelerations[113].

(vi) The history of rotation of the joint should be standardised, as far as possible, to eliminate the effect of repeated rotation of a joint on the joint stiffness.

(vii) Standard, defined stiffness parameters should be measured to enable a direct comparison with other work.

(viii) A standard testing procedure should be followed (Section 6.8).

6.3 The Durham arthrograph

The Durham arthrograph was first described by Unsworth et al[114]. Since then it has been used for many clinical trials[112,117,125]. The arthrograph was designed to measure the joint stiffness of the right hand, index finger, MCPJ. It imposed sinusoidal, flexion-

extension motion on the MCPJ in the horizontal plane, and the resistance to this motion was measured (requirements i-iv, Section 6.2).

Originally the amplitude of motion was 4° and several hysteresis loops were produced at various positions of joint flexion to provide the joint stiffness information throughout the range of motion of the joint[112,114,125]. It was observed that at two angular positions, during the range of motion of the joint, the net torque on the joint was zero. The position where this occurred during flexion of the joint differed to that during extension. This was attributed to the viscoelastic properties of the soft tissues surrounding the joint.

Unsworth et al[121] suggested that joints tested with the centre position of the cycle remote to the equilibrium position would appear stiffer than when centred about the equilibrium position (due to the imbalance of the soft tissues surrounding the joint). Hence two individuals with the same joint stiffness, but tested at a specified joint angle, may appear to have different joint stiffnesses if their equilibrium positions differed. Therefore Bromley[85] modified the testing procedure so that joint stiffness was measured from a single hysteresis loop which was centred about the equilibrium position of the joint. Since the flexion and extension equilibrium positions differed, the average of these two positions was used as the datum and defined as the mean equilibrium position.

The amplitude and frequency can affect joint stiffness due to the velocity dependent stiffness components[113]. In addition, Bromley[85] highlighted the fact that larger values of amplitude and frequency could give rise to significant inertial torques from the finger. Hence a graph was produced showing the acceptable combination of amplitude and frequency as far as inertia was concerned, from which a combination of 20° amplitude and 0.1 Hz were selected (requirement v, Section 6.3). The arthrograph was modified accordingly and this apparatus was used for this study.

The arthrograph consisted of a main frame, an arm rest, a drive mechanism and a computer interface to collect, store and analyse the data (Figure 6.2). The arm rest consisted of a wooden board with a finger grip and thumb support mounted on it. The arm rest supported the patient's right arm with the wrist in the neutral position, the middle, ring and little fingers curled around a cylinder grip, and the thumb in the thumb support. The index finger was strapped in the finger carriage which supported the finger whilst holding it in the correct position for testing. The index finger was free to move in flexion-extension without impinging on the cylinder. The whole arm rest could

Figure 6.2 The Durham Arthrograph

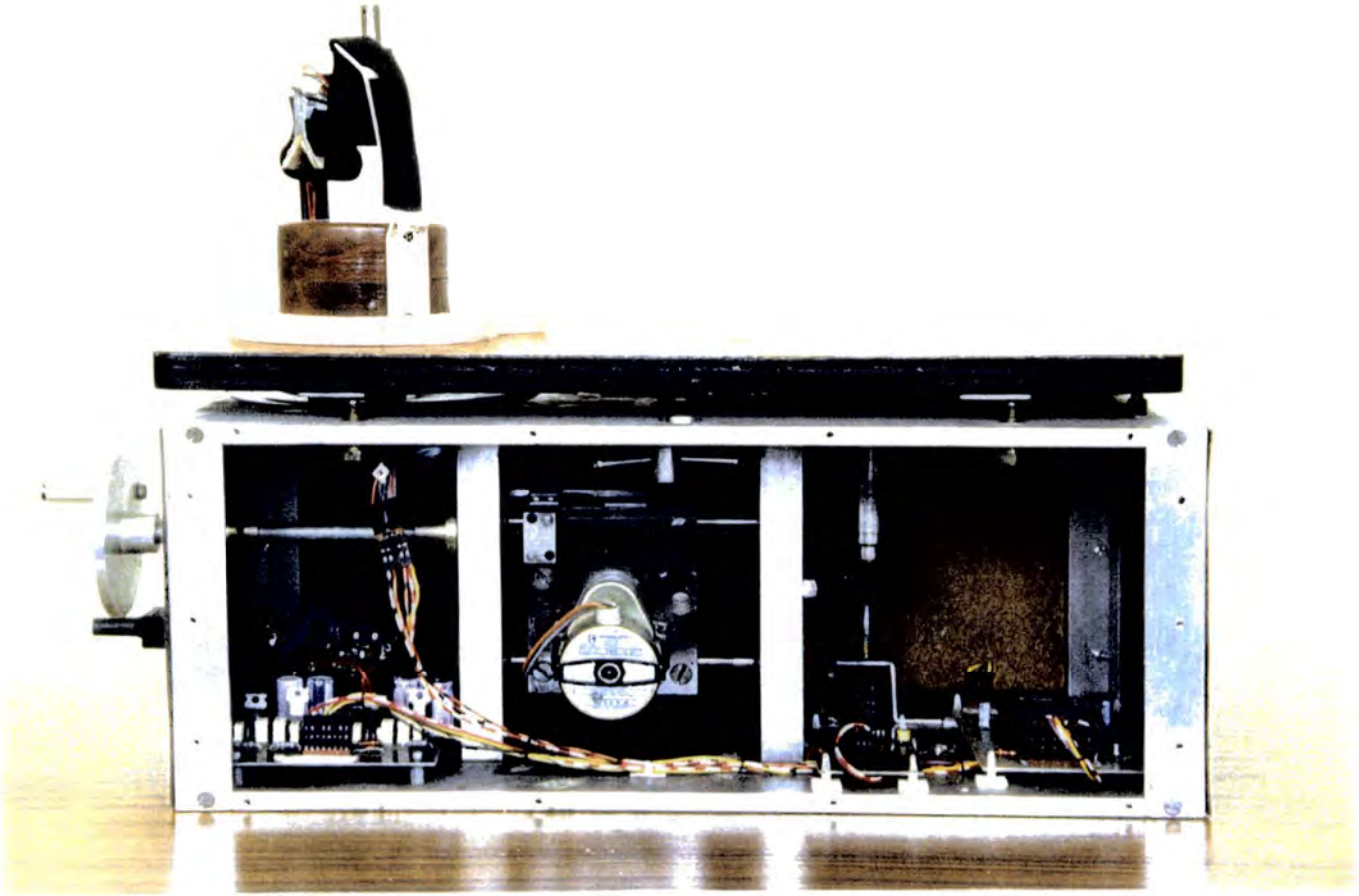

be moved in any direction within the horizontal plane over the main frame to enable alignment of the centre of rotation of the finger with the centre of rotation of the arthrograph. Once alignment was achieved the board was locked into position by three levers mounted below the main frame.

The drive mechanism has been described extensively by Unsworth et al[114]. A scotch yoke mechanism produced sinusoidal motion of the index finger carriage. The angle of flexion of the carriage could also be varied manually by approximately 60°. The index finger carriage consisted of a V-block screwed to the end of a stainless steel cantilever which had strain gauges mounted on it (Figure 6.3). The cantilever was attached to the pivot of the arthrograph. The height of the finger carriage was adjustable for small hands, and foam pads could also be added to raise to arm. A potentiometer measured the angular position of the carriage and hence the MCPJ.

6.4 Joint stiffness parameters

Comparison between different studies should be exercised with caution not only because different apparatuses and testing procedures may have been used but also because of differences in the definition of the parameters measured. For instance Unsworth et al[114] produced a series of smaller hysteresis loops for each joint over the range of motion of the joint. The total area of the loops was calculated and defined as the dissipative energy of the joint. However, other authors have found the area of a single loop (over a different amplitude of oscillation), also defined as the dissipated energy of the joint[85,120,122]. Hence a direct comparison between the two dissipated energies would not be valid. The area of the hysteresis loop has also been measured as a percentage of the triangle subtended by the loop[122].

Elastic stiffness of a joint has generally been measured as the slope of the hysteresis loop. But the methods of measuring these slopes has also varied between authors. Unsworth et al[114] found the slope of the line joining the centroids of the individual hysteresis loops over the range of motion of the joint. It was pointed out that this was less than the mean slopes of the individual loops. Howe et al[122] measured the mean slope of a single loop, excluding the peripheries, whereas Bromley[85] measured the slope of different parts of a single loop. Hence again, comparison between elastic stiffness from each of these studies would not be valid.

Figure 6.3 The Durham arthrograph strain gauge finger carriage

A standard apparatus, testing procedure and definition of the stiffness parameters measured for all joint stiffness assessments would be ideal, however, this does not exist. Hence a detailed description of the apparatus, testing procedure and definition of parameters measured are required for all joint stiffness assessments. These should be taken into account when analysing the stiffness results and comparing them with other work. The apparatus used for this study has been described in Section 6.3. The testing procedure was standardised and is given in Section 6.8. The stiffness parameters measured were identical to those defined by Bromley[85]. Figure 6.4 shows the parameters measured from the hysteresis loop and they are defined as follows :

Angular displacement was defined as positive when in flexion from the datum and negative when in extension from the datum. The *centre position of the cycle* (datum) was defined as the mean of the maximum and minimum angles, and coincided with the mean equilibrium position of the joint. The *torque range* or *peak to peak torque* was defined as the difference between the maximum and minimum torques. The *energy dissipation* was defined as the area of the hysteresis loop.

The *flexion equilibrium position (EP1)* was defined as the angular displacement, during joint flexion, where the resistive torque of the joint was zero. The *extension equilibrium position (EP2)* was defined as the angular displacement, during joint extension, where the resistive torque of the joint was zero. The *mean equilibrium position (EQP)* was defined as the mean of EP1 and EP2, and was taken as the datum. The *flexion slope* was defined as the slope of the best fit straight line (fitted by the least squares method) through the last quarter of the cycle in flexion (10°). The *extension slope* was defined as the slope of the best fit straight line through the last quarter of the cycle in extension (10°). Finally the *mid-position slope* was defined as the slope of the best fit straight line though the middle half of the cycle (20°).

6.5 Factors affecting joint stiffness

The factors that may affect objective joint stiffness can be grouped into four categories. These are human, time, joint diseases and medical treatment. Human factors include sex, age, hand (right or left) and individual variation. Time factors include day-to-day and circadian variation. There are many diseases that may affect joint stiffness, however, for this study the effects of RA have been focused on. Finally medical treatments for RA or other complaints may include physiotherapeutic methods or

Figure 6.4 Joint stiffness parameters

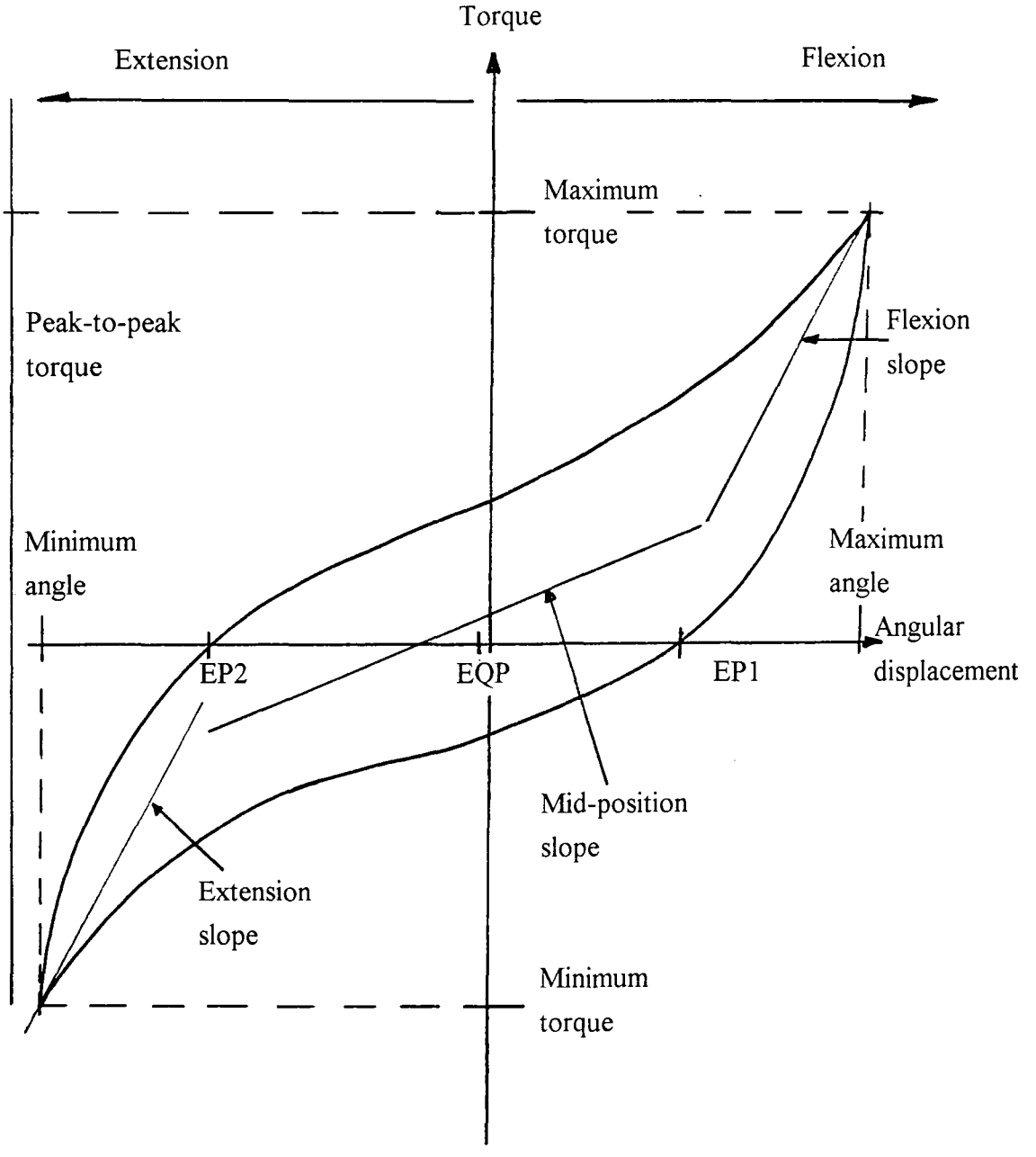

Energy dissipation = Area of hysteresis loop

drugs. The effects of these factors on objective stiffness are discussed in the following section.

6.5.1 Human variation

Females are generally less stiff than males[110,113,119,120-122,125-127]. Unsworth et al[121] reported that males were generally larger than females, and females may also have different sized muscles than males of the same subject mass. Hence the difference in stiffness may not be only to do with sex. However, Such et al[120] observed that males were still stiffer than females when age and joint size were taken into account. It is difficult to compare the results from different investigations due to the different parameters measured and the different methods of measurement used. However, female stiffness parameters (dissipative energy, peak-to-peak torque etc.) have been found to be between 60% and 86% that of males[110,119,120,125]. The effect of sex on the equilibrium position is not clear. Some authors found the equilibrium position of females to be in greater flexion than males[110,112,121], however, the opposite has also been found[125].

Joint stiffness has generally been found to increase with age[111,113,120,122,126], (this included both dissipative energy[120] and elastic stiffness[113,122]) However, some authors found no increase in elastic stiffness[120], dissipative energy[122] or overall joint stiffness[110]. Again it is difficult to compare the results of different authors due to the different parameters measured and the different measurement techniques used. There are several factors that may produce a change in joint stiffness with age. These are changes in the collagen structure, muscle size, laxity of the ligaments, articular cartilage roughness and synovial fluid viscosity[113,120,122].

An increase in elastic stiffness may occur with age due to cross-linking of the proteins in the collagen of the soft tissues surrounding the joint, making them become more rigid[113]. In addition, an increase in muscles size increases the elastic stiffness of the muscle as well as the viscous losses when moving. Hence an increase in muscle size with age would also increase the joint stiffness. Joint size has also been found to increase with age due to hypertrophy which may increase joint stiffness[122]. Finally an increase in the surface roughness of the articular cartilage or a reduction in the synovial fluid viscosity and cartilage elasticity age may increase the dissipative energy slightly. However, frictional forces have been found to be <1% in normal MCPJs[113] hence changes in friction may not significantly change the overall joint stiffness.

MCPJ stiffness has been found to correlate with finger joint circumference[111,122] and body mass[121], but not with wrist circumference[121]. It has also been reported that knee stiffness increased with thigh muscle size and knee circumference[120]. Finally a wide scatter in joint stiffness parameters naturally occurs between individuals[110-112,115] and differences have been found between the MCPJ stiffnesses of each hand[122,128].

6.5.2 Time variation

Investigations into the effects of circadian variation on joint stiffness have shown that it increases significantly in the early hours of the morning and is at its lowest during the afternoon[112,118,119,127,129]. Many patients with RA complain of morning stiffness (measured subjectively as severity or duration) and it is a recognised symptom of the disease[7]. However, both patients with RA and normal individuals exhibit circadian variation of joint stiffness even though the normal individuals did not notice morning stiffness[111,115,118,126-128]. Hence although stiffness shows circadian variation, morning stiffness may be related to other symptoms such as pain, lack of grip strength and reduced range of motion rather than joint stiffness.

Pain, grip strength and joint size also show circadian variation in patients with RA[129]. It is interesting to note though that Wright[128] found that patients with RA complained of morning stiffness but normal individuals did not, even though some of the normal individuals were weaker than the patients with RA. Pain and joint size were highest in the early morning when grip strength was at its lowest[111,115,119,126,128,130].

It has been suggested that circadian variation in joint stiffness is not the result of nocturnal inactivity[128,130]. It may be related to circadian variations in the immune and inflammatory responses which are dependent on the concentrations of circulating steroids in the body[115,129,130]. A decrease in the circadian variation of joint stiffness and grip strength have been found with corticosteroid treatment of patients with RA and normal individuals which supports this theory[115,126,128]. In addition, a correlation has been found between urinary 17-ketosteroid excretion and grip strength. It has also been suggested that tissue swelling may be one cause of morning stiffness in patients with RA, as decreases in finger joint size and stiffness were found with anti-inflammatory drugs[131].

There is limited documentation on the day-to-day variation in joint stiffness, however, little variation has been reported for subjective stiffness[131] or objective stiffness[115]. Such et al[120] found day-to-day variations of 2.6-7.2% for dissipative stiffness of the

knee and 2.4-7.2% for elastic stiffness. Finally it should be noted that the viscoelastic properties of the soft tissues surrounding the joint will affect joint stiffness measurements especially with stationary measuring methods. Unsworth et al[121] found stress relaxation to result in a steady state torque of 66% that of the initial torque.

6.5.3 Rheumatoid arthritis

The reported effect of RA on joint stiffness has varied between authors. Some reported an increase in joint stiffness of patients with RA compared with normal individuals[113,119]. This was particularly prominent in patients with active RA[113]. However, others authors reported no increase or a slight decrease compared with normal individuals[111,122,125,127], despite the patients complaining of stiffness. Helliwell et al[111] pointed out that although the earlier studies had shown an increase in joint stiffness of patients with arthritis compared with normal individuals, they did not use the equilibrium position as the datum. Later studies had used the equilibrium position as the datum and had found no increase in stiffness which may account for the differences.

However, an important study by Bromley[85] showed that patients with active RA showed a significant increase in joint stiffness compared with normal individuals, particularly in the early stages of the disease. Further, patients who had been suffering from the disease for a long period of time were no stiffer or in some cases less stiff than normal individuals. Hence the contradicting results of the joint stiffness of patients with RA and normal individuals from different authors may be due to differences in the stage and activity of RA of the patients tested.

Changes in the joint structure may occur due to RA which will affect joint stiffness. Some may increase joint stiffness such as swelling of the soft tissues and roughening of the bearing surfaces. However, other factors may decrease joint stiffness such as stretching and weakening of the ligaments surrounding the joint. In active, early stage RA the joints are swollen but little damage to the soft tissues may have occurred. However, soft tissue damage may occur long-term. Hence this would explain why active, early stage RA joints would have an increased stiffness compared with normals individuals. However, non-active or long-term RA joints would be expected to show little change, or even a decrease, in joint stiffness.

The effect of circadian variation has been discussed in Section 6.4.2. It is interesting to note that in general both normal individuals and patients with arthritis have shown

circadian variation in joint stiffness[126], however, only the patients complained of morning stiffness[115,126]. Hence it seems that what patients with RA experience as morning stiffness is in fact a misinterpretation of pain, limited motion and reduced joint strength[125]. Grip strength has been indicative of duration of morning stiffness[132] as has swelling of the hands[115]. However, normal individuals have also been found to have a similar circadian variation to patients with arthritis in grip strength and joint size.

6.5.4 Medical treatments

The temperature of the underlying tissues surrounding a joint can affect joint stiffness. Increasing the temperature of the tissues decreases their elastic modulus, resulting in a decrease in joint stiffness. However, joint stiffness is dependent on the depth of heating of the tissues, and increasing skin surface temperature without heating the deeper soft tissues may not significantly decrease joint stiffness. It has been reported that increasing the temperature of a joint in water baths has decreased the joint stiffness (and vice versa with decreasing the joint temperature)[113,119,126]. However, it has been generally reported that increasing or decreasing the *temperature* of the skin above the finger joints does not significantly change joint stiffness because the change in temperature does not reach the deep underlying tissues[85,113,119,125].

Physiotherapeutic methods have been used to heat the deep tissues to decrease joint stiffness. The most common physiotherapeutic treatments used on patients with RA are short-wave-diathermy, ultrasound, hot-wax-baths and exercise. The effects of several physiotherapeutic treatments on joint stiffness have been investigated short-term and long-term. Short-term assessment investigated the effect of single treatments, whereas long-term assessment investigated the effect of many treatments over several weeks.

Short-wave-diathermy aims to heat the deep underlying tissues by setting up an alternating electric field in the joint causing the ions in the joint to oscillate (capacitance method). Some of the kinetic energy of the ions is dissipated as heat when they collide with the tissue molecules heating the deeper structures of the joints[85]. The heat produced at any one point is determined by the resistance of the tissues at that point. An increase in fluid content of the tissues makes them more rigid giving more resistance and increasing the heating effect.

When *ultrasound* passes through the soft tissues surrounding a joint, the tissue oscillates at a rapid rate and the periodic tension and compression is thought to have a

similar effect to massage. This may increase the permeability of cell membranes which in turn reduces oedema. A reduction in oedema in and around the MCPJ may reduce the viscous resistance of the tissues, lowering dissipated energy. The velocity of ultrasound depends on the elasticity, density and temperature of the substance, and hence its penetration. Hence differences in the tissues of diseased and normal joints may alter the effectiveness of ultrasound treatment[85].

Hot-wax-baths aim to transfer the energy released from the latent energy of solidification of the wax to the underlying tissues of the hand. However, the depth of penetration of heat applied at the skin's surface is limited by the rate at which circulation is able to disperse the energy[85]. *Active and passive exercise* consists of gripping soft rubber objects, precision handling and gentle but frequent flexion-extension of the patients joints by a physiotherapist.

None of the physiotherapeutic treatments had any long-term effect on joint stiffness. Short-wave-diathermy decreased joint stiffness short-term[85,125,127] and a shift in the equilibrium position also occurred in patients with RA[125,127]. It has been reported that ultrasound has produced a decrease in joint stiffness[125,127]. However, other authors found ultrasound to have no significant effect on joint stiffness[85,117]. Nor did hot-wax-bath therapy or exercise[117,125,133]. However, in combination hot-wax-bath and ultrasound treatments have been effective in decreasing joint stiffness parameters short-term. The absorption rate of ultrasound depends on the temperature of the body, and increases with increasing temperature. Hence a hot-wax-bath treatment followed by pulsed ultrasound effectively increases the temperature of some of the underlying tissues. This consequently increases the absorption rate of the subsequent ultrasound therapy. More heat can then be dissipated to the underlying tissues decreasing joint stiffness[85,117,125].

The changes in stiffness are thought to be due to changes in the viscoelastic properties of the joint capsule and the tissues surrounding the joint. A reduction in stiffness levels was more significant in patients with a high, initial joint stiffness[85]. In addition, physiotherapeutic treatments that were effective on patients with RA did not decrease stiffness in normal individuals[117,125]. Ultrasound or short-wave-diathermy are said to act locally to reduce the effects of inflammation hence normal individuals are unlikely to be affected. Interestingly pain relief from wax bath treatment followed by active hand exercise and wax bath alone was achieved but not exercise alone, and subjective stiffness was reduced in all treatments[4].

Anti-inflammatory drugs and corticosteroids can improve the condition of joints affected by RA. The main improvements reported have been of subjective stiffness or grip strength. However, Wright and Plunkett[126] also reported a decrease in objective joint stiffness and Scott[115] described an increased finger displacement for a known torque with corticosteroid treatment. A reduction in circadian variation of grip strength and stiffness was also found[115,128,126]. Additional effects of drugs on joints have been a decrease in the duration of morning stiffness[126,134,135], decrease in subjective stiffness[115], decrease in hand volume (swelling)[115], and an increase in grip strength[115,128,134,135]. No significant differences have been found in normal individuals subjected to the same drugs treatments.

Finally synovectomy and cast immobilisation can affect joint stiffness. Joint stiffness was found to decrease after synovectomy in a patient with RA. This was thought to be due to the swollen tissues being removed[119]. A slight increase in stiffness was found from cast immobilisation of healthy joints but this shortly returned to normal after the casts were removed[124].

6.5.5 Summary of the factors affecting joint stiffness

The reported effect of several factors on joint stiffness has varied between authors. However, in general the following conclusions can be made:

* Males are stiffer than females
* Joint stiffness increases with age
* There is considerable variation between individuals
* Joint stiffness increases with body mass and joint size
* There is some difference between hands

* There is little day-to-day variation
* Circadian variation occurs with a significant increase in the early hours of the morning in patients with RA as well as normal individuals, despite only patients with RA complaining of morning stiffness.

* There is no significant difference between the joint stiffness of non-acute patients with RA and normal individuals
* Physiotherapeutic treatments have no long-term affect on joint stiffness. However, short-wave-diathermy or hot-wax-baths followed by ultrasound may reduce joint stiffness short-term.

* Corticosteroids can reduce circadian variation of joint stiffness and anti-inflammatory drugs can reduce joint stiffness of patients with arthritis.

6.6 Development of a portable system for the Durham arthrograph

The original data acquisition program for the Durham arthrograph was written in Apple-Basic, the latest version of which was written by Bromley[85]. However, the computer system was not portable hence a new system was developed for a lap-top computer. The Apple-Basic program was not compatible with the lap-top, nor with the lap-top data acquisition card hence the program was rewritten in LabVIEW (for windows version 3.3.1 from National Instruments).

LabVIEW is a graphical programming package which uses icons to build programs rather than lines of source code. The programs are called virtual instruments (VIs). Each program (or VI) consists of a front panel and a block diagram. The front panel acts as the user interface during the running of the program. It can simply display information for the user or it can contain interactive functions for the user to control the running of the program or insert information. The block diagram is effectively the program source code. A VI can contain a series of block diagrams which are initiated in sequence. Within the block diagrams subVIs may be called upon which act in a similar manner to subroutines found in other programming languages. Each subVI also consists of a front panel and block diagram.

A block diagram of the arthrograph and computer system is shown in Figure 6.5. The computer system consisted of a Slimnote 5100C RM lap-top computer and a DAQCard-1200 data-acquisition card (National Instruments). The driver software used to interface between the data-acquisition card and LabVIEW was NI-DAQ version 4.9.0 (National Instruments). The details of the data-acquisition card (DAQCard-1200) and the NI-DAQ driver software are shown in Appendix 6.

The author was unable to find a hard copy of the Apple-Basic program in the literature so a copy was included in Appendix 6. Additional bold typing indicates the main sections of the program and a summary of the notation used and the calculation of the stiffness parameters is included. Figure 6.6 shows a flow diagram of the main stages of

Figure 6.5 Flow diagram for the arthrograph and computer system

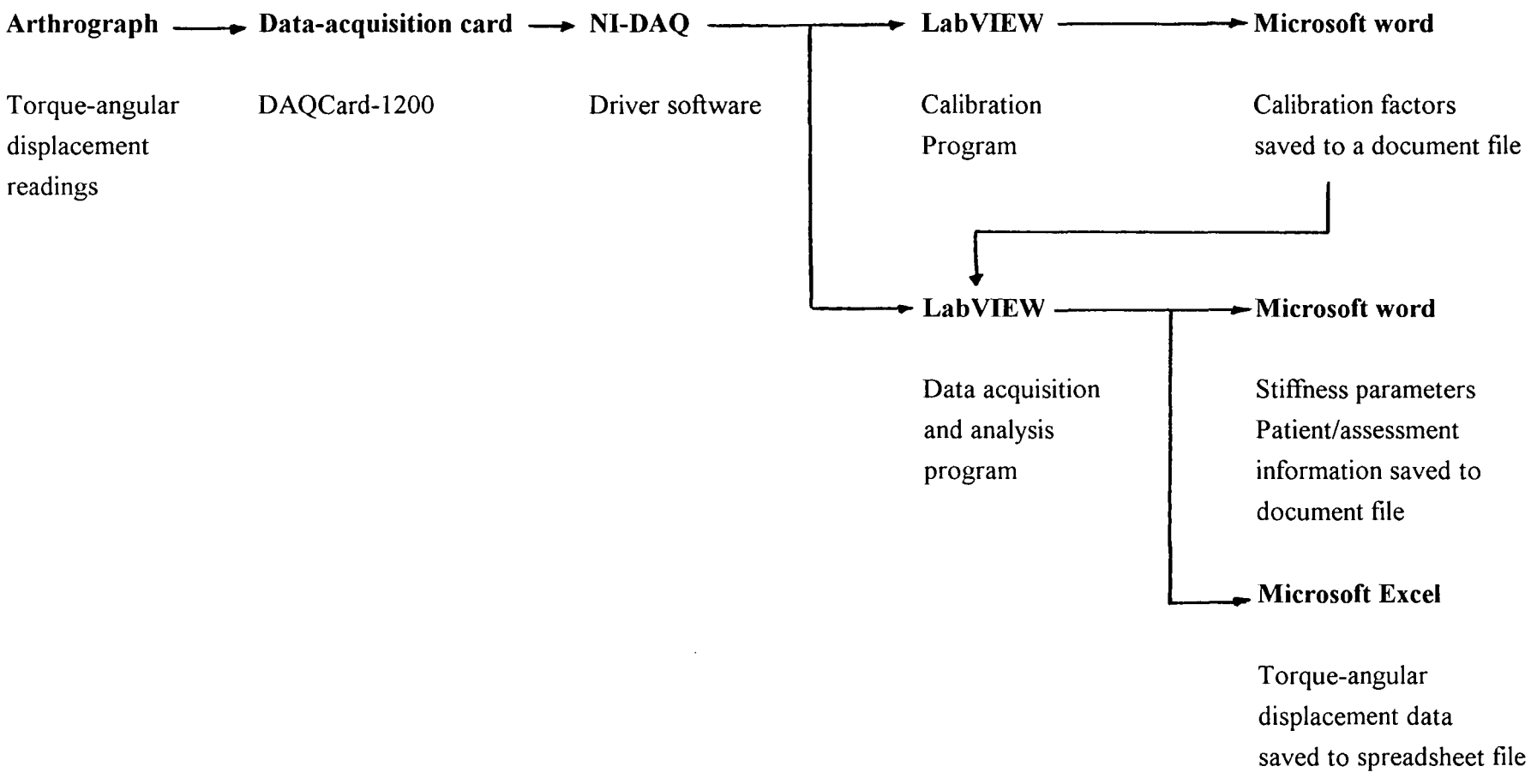

Figure 6.6 **Flow diagram of Apple-Basic arthrograph data acquisition and analysis program**

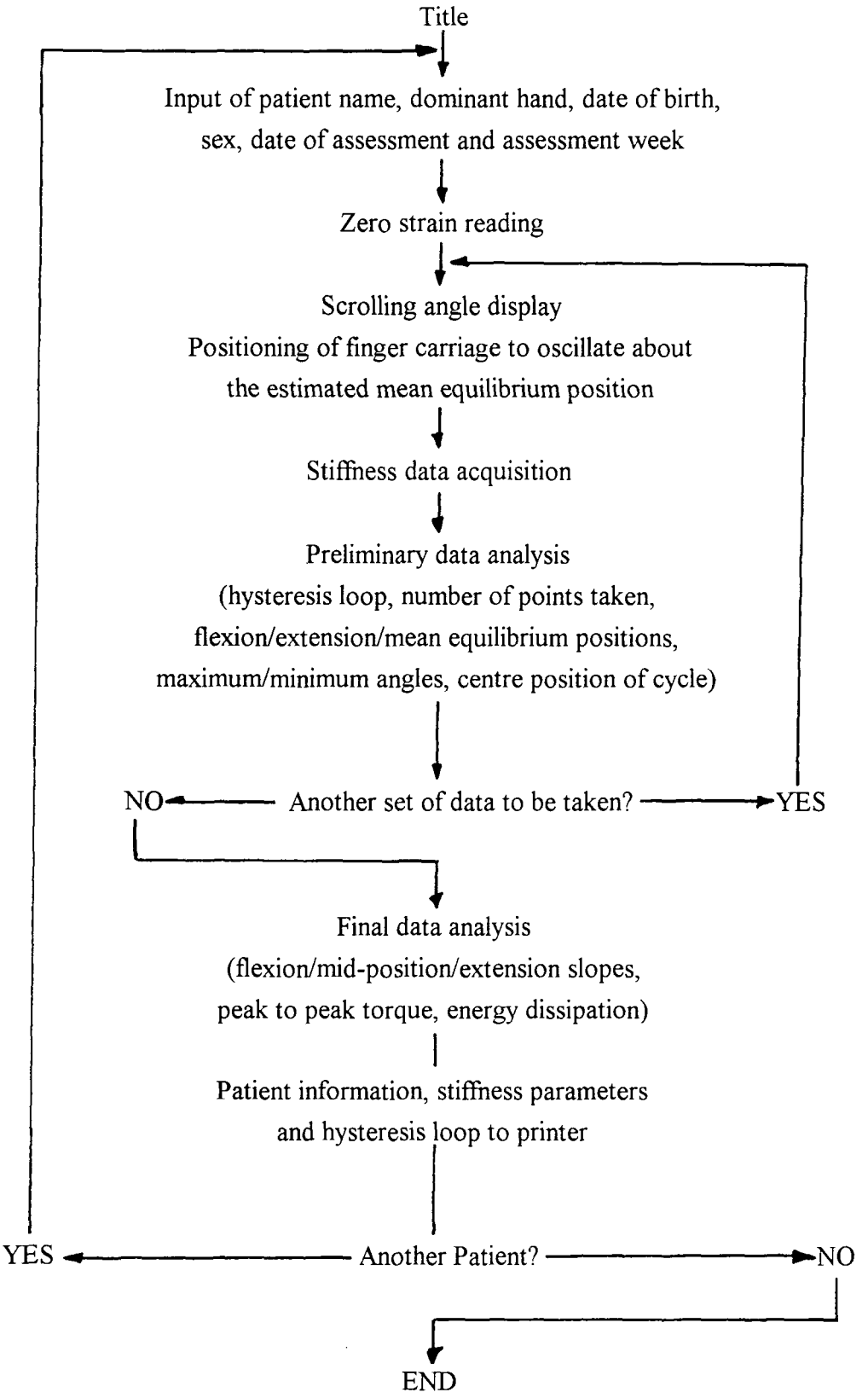

the data acquisition program. The program consisted of four main sections. These were input of patient and assessment information, joint stiffness data acquisition, calculation of stiffness parameters, and the print out of the assessment information, stiffness parameters and hysteresis loop. The stiffness parameters calculated were maximum, minimum and peak-to-peak torques, maximum and minimum angles, centre position of the cycle, flexion, extension and mean equilibrium positions, energy dissipation, flexion, mid-position and extension slopes.

Two programs were written to replace the Apple-Basic data acquisition and analysis program. A calibration program was written to calculate the corresponding calibration values for the arthrograph and save them in a specified document file. A joint stiffness data acquisition and analysis program then read the calibration values from the specified document file, acquired joint stiffness data from the arthrograph, calculated the required joint stiffness parameters from this data and stored the parameters and data to document and spreadsheet files when prompted. Patient and assessment information could also be entered and stored to the document file.

6.6.1 LabVIEW arthrograph calibration program

It was not clear how the calibration factors were calculated for the Apple-Basic program, nor why two values for the calibration factor C2 were included in the program. A separate calibration program was written from the data acquisition and analysis program so that the arthrograph could be recalibrated without having to reprogram either of the LabVIEW programs. This eliminated the risk of reprogramming incorrectly and also allowed users not familiar with LabVIEW to recalibrate the arthrograph whenever necessary. The calibration program is shown in Appendix 7, along with a description of the program structure and components, and the operating instructions.

The arthrograph contained a rotary potentiometer to measure the angular displacement of the joint, and a strain gauge system to measure the resistive torque of the joint to the sinusoidal motion imposed on it by the arthrograph drive system. The potentiometer and strain gauge system were calibrated manually and both were shown to be linear (Section 6.7). Hence the calibration of each device simply required a zero reading and a scaling factor.

The Apple-Basic program took a zero strain reading from the strain gauge system within the main program. This method was also adopted for the LabVIEW programs.

It allowed the user to observe whether the computer system and arthrograph were working correctly before taking joint stiffness readings. In addition, if the normal zero strain reading was known then it could be used as a reference value to judge whether the arthrograph needed recalibrating. (The strain gauge system was mounted externally to the main frame of the arthrograph and was most likely device to be knocked).

Hence the calibration program calculated the calibration factors Cal1 and Cal2 for the potentiometer, and Cal3 for the strain gauge system. Cal1, Cal2 and Cal3 are defined as follows :

Potentiometer calibration

MCPJ angular displacement angle (A°) = (Av - Cal1) / Cal2

Where Av = Potentiometer voltage output at angle A (V)
Cal1 = Potentiometer voltage output at angle 0° (V)
Cal2 = Scaling factor (slope of the angle against voltage graph) (V/°)

Strain gauge calibration

MCPJ resistive torque T (Nm) = (TA - ZS) x Cal3

Where TA = Strain gauge system voltage output at angle A (V)
ZS = Strain gauge system voltage output with no load applied to the strain gauges defined as the zero strain reading (V)
Cal3 = Scaling factor (slope of the torque against voltage graph) (Nm/V)

The potentiometer scaling factor was simply calculated from the difference between full extension 0° carriage angle voltage and the full flexion angle from this position, divided by the range of motion of the carriage. This was simpler than moving the carriage manually throughout its entire range and was valid as the potentiometer was linear over its operational range. The strain gauge scaling factor was calculated by applying known weights to the arthrograph. The potentiometer and strain gauge calibration factors were then stored in a document file which could be accessed by the joint stiffness data acquisition and analysis program. A flow diagram of the LabVIEW arthrograph calibration program is shown in Figure 6.7.

Figure 6.7 Flow diagram of the LabVIEW arthrograph calibration program

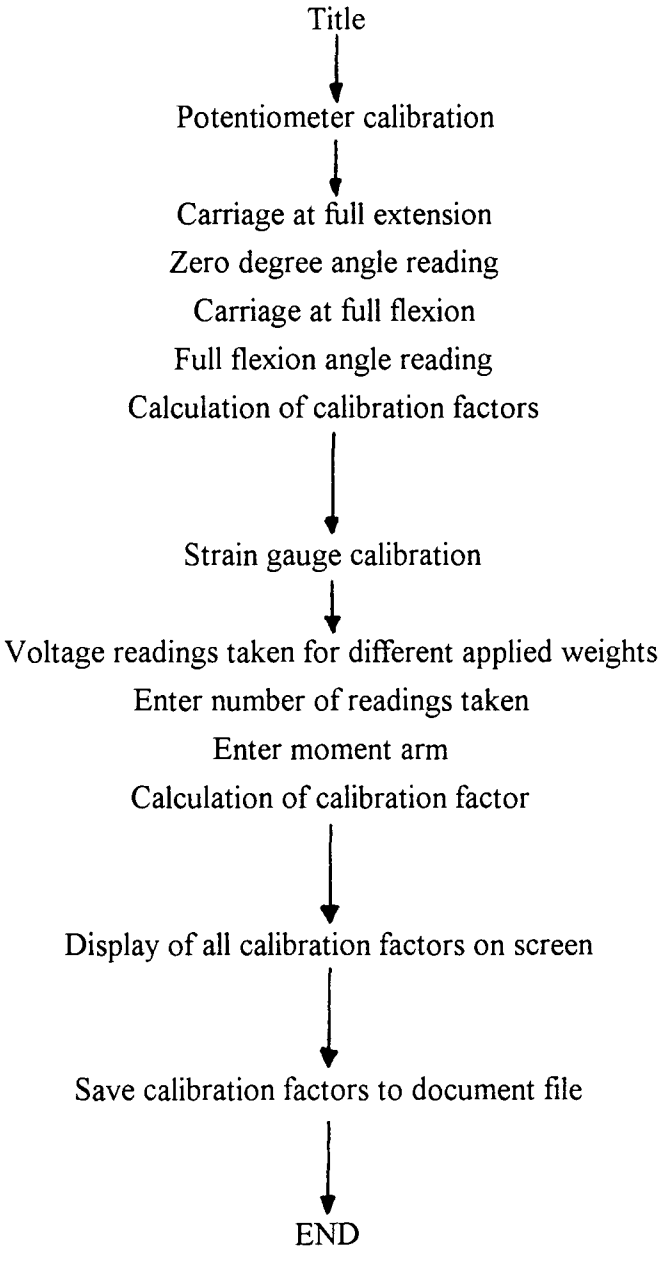

6.6.2 LabVIEW data acquisition and analysis program

A flow diagram of the LabVIEW data acquisition and analysis program is shown in Figure 6.8. The arthrograph calibration values were read in at the beginning of the program from the specified document file. The program then prompted the user to input patient and assessment details (name, assessment time, date, week). Other patient details such as sex, age and dominant hand were covered in the subjective questionnaire which was designed to accompany the joint stiffness assessment and from the patient medical records (with consent).

The importance of the position of the datum of the hysteresis loop has already been discussed in Section 6.3. It has been found that the mean equilibrium position of the MCPJ is on average approximately 20° flexion[117]. Hence the program prompted the user to position the finger carriage such that the full extension position was 0° (centre position of the cycle 20° flexion). A cycle of data was then taken and the flexion, extension and mean equilibrium positions, the maximum and minimum angles and the centre position of the cycle were calculated. These were shown on the screen along with the resultant hysteresis loop. The carriage was then manually moved to attempt to coincide the centre position of the cycle with the estimated mean equilibrium position. Another set of data was then taken and a new estimate of the mean equilibrium position taken. This process was continued until the centre position of the cycle approximately coincided with the mean equilibrium position.

The additional stiffness parameters of maximum, minimum and peak-to-peak torques, flexion, mid-position and extension slopes and energy dissipation were then calculated. The program then prompted the user to save the patient and assessment information, and the calculated stiffness parameters to a document file. The torque-angular displacement data were then saved to a spreadsheet file. The program is shown in Appendix 8, along with a description of the program structure and components, and the operating instructions. The joint assessment procedure is given in Section 6.8.

6.7 Calibration of the Durham arthrograph

The arthrograph was calibrated manually *and* by using the calibration program. The manual potentiometer calibration was performed using a protractor mounted on the arthrograph base frame, with a pointer mounted on the finger carriage. The finger carriage was moved in steps of 10° from -10-70° and the voltage reading taken at each

Figure 6.8 Flow diagram of the LabVIEW joint stiffness data acquisition and analysis program

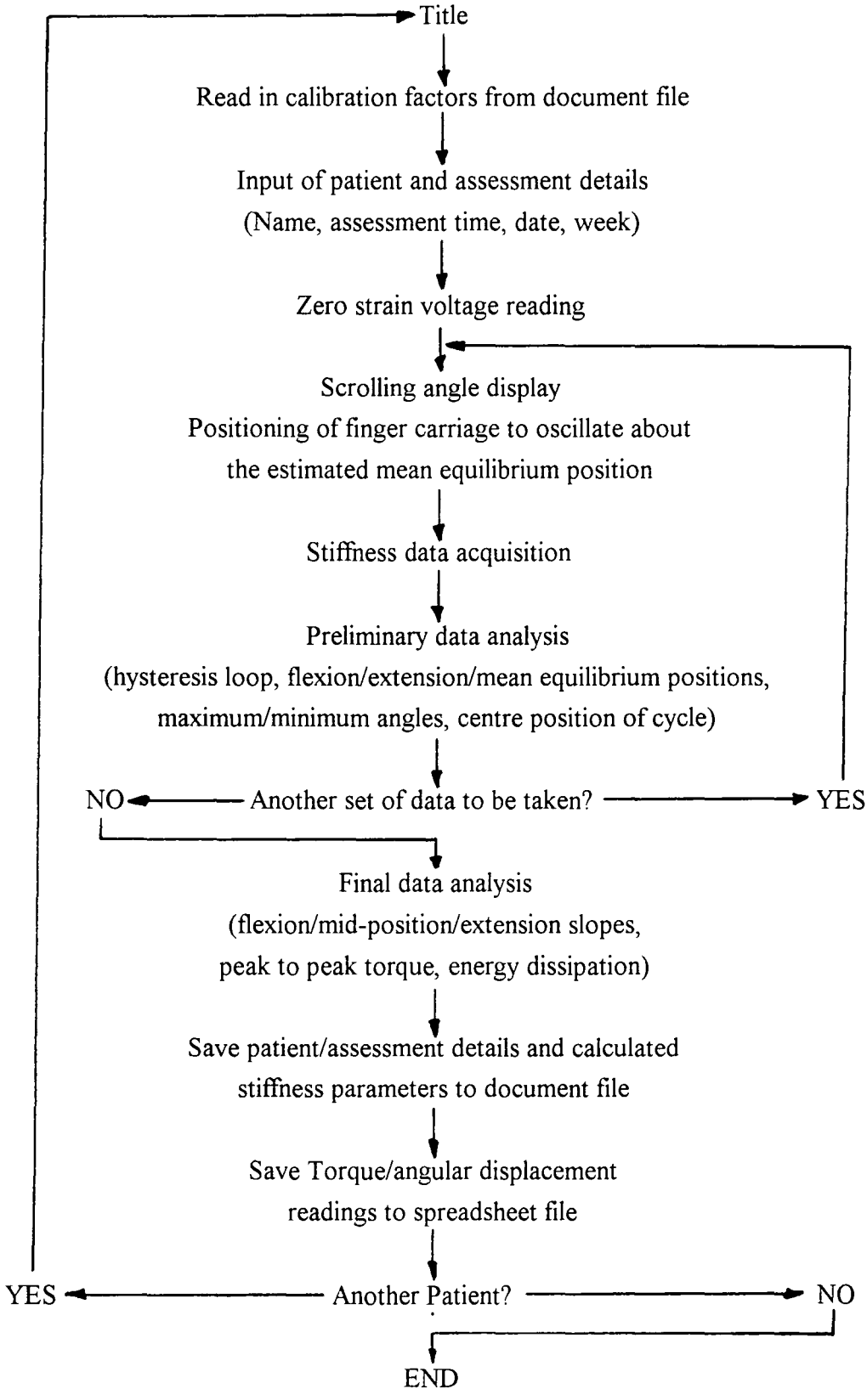

step. The calibration graph is shown in Figure 6.9. The potentiometer was linear throughout the operational range. A trend-line was fitted to the graph using the Microsoft excel package and the equation of the graph was V = 0.0407A + 1.1258 [where V was the potentiometer voltage and A is the finger carriage angle(°)]. The potentiometer calibration equation has already been given as A° = (Av - Cal1) / Cal2 (where A° is the MCPJ angular displacement and Av is the potentiometer voltage at angle A). Hence from the manual calibration the potentiometer calibration values were Cal1 = 1.1258 and Cal2 = 0.0407.

The calibration program was designed to calibrate the potentiometer from two readings. The first was at 0° with the finger carriage at full extension. The second was with the carriage at full flexion (with full extension still at 0°). The range of the sinusoidal motion was fixed at 38°. Hence Cal1 was taken as the 0° reading and Cal2 was the difference between the full extension and full flexion readings divided by 38. This method was simpler than manually moving the carriage throughout its range of motion, and valid as the potentiometer had already been found to be linear over the operational range. The calibration values calculated by the calibration program were Cal1 = 1.1258 and Cal2 = 0.0397.

The strain gauge system was calibrated by applying weights to the finger carriage at a known distance from the pivot (moment arm). The moment arm was 42 mm. Weights were applied in a positive (increased the strain gauge voltage) and negative (decreased the strain gauge voltage) direction. The calibration graph can be seen in Figure 6.10. The equation of the trend-line fitted to this data was V = 6.215T + 0.4201 [where V was the strain gauge voltage for an applied torque T (Nm)]. The calibration equation has already been defined as T = (TA - ZS) x Cal3 (where TA is the strain gauge voltage at angle A and ZS is the zero strain voltage). Hence Cal3 = 0.1609. The weights were then applied again using the calibration program. The zero strain value = 0.42 and Cal3 = 0.1628.

The calibration values calculated from the calibration program were saved in file C:\LabVIEW\hayley\test.doc. They were very close to the calibration values calculated manually.

Figure 6.9 Arthrograph potentiometer calibration graph

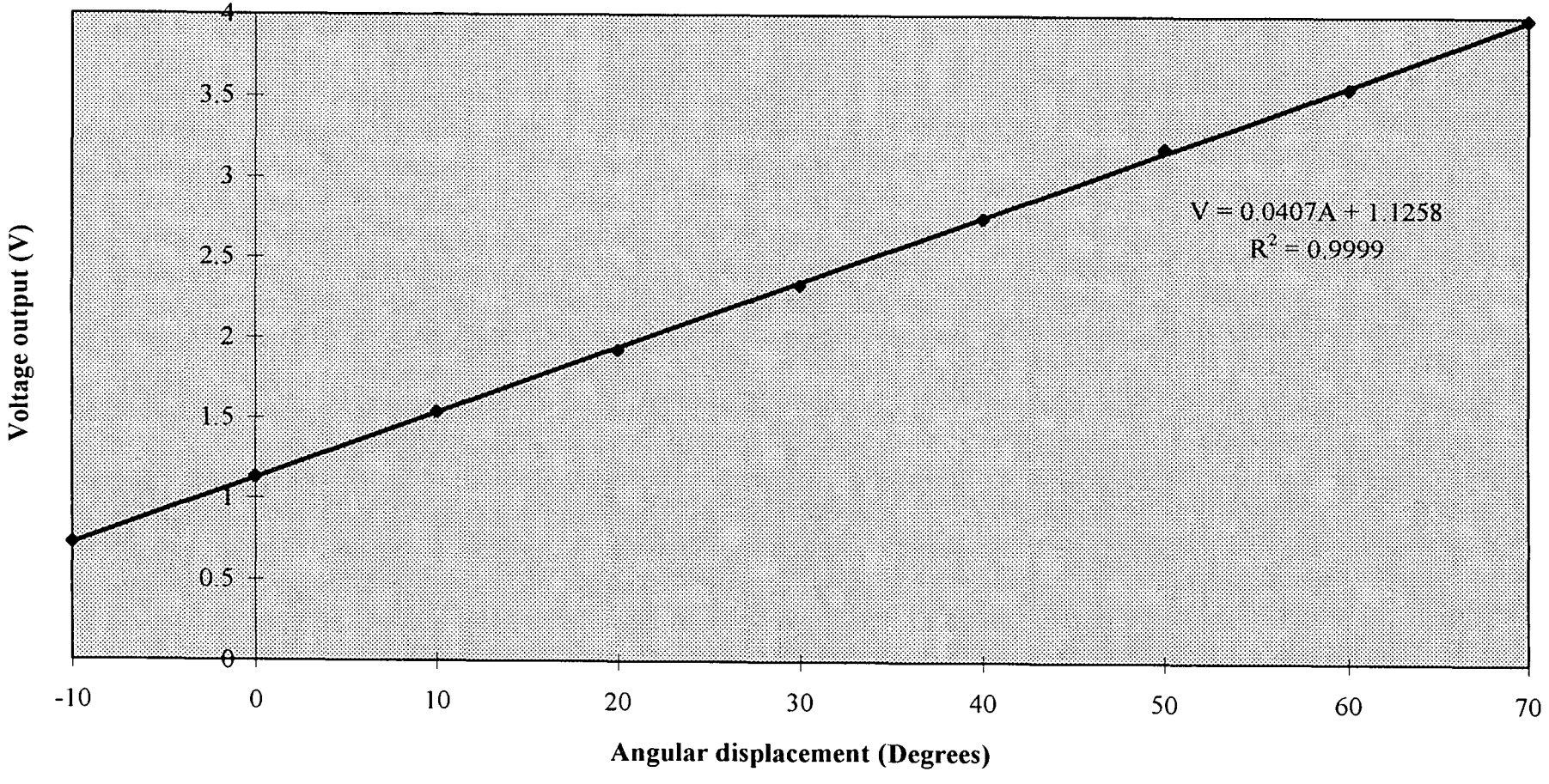

Figure 6.10 Arthrograph strain gauge calibration graph

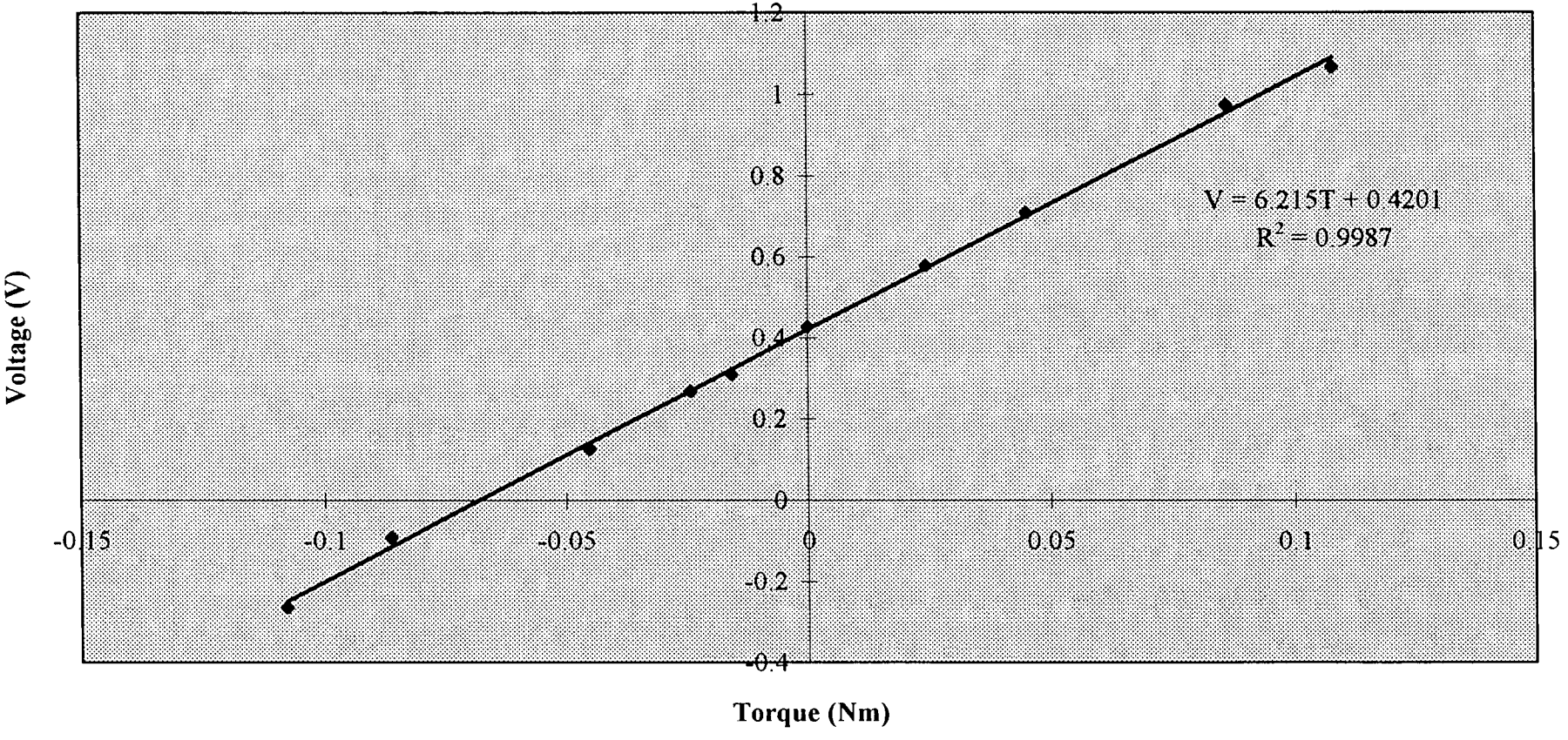

6.8 Joint stiffness assessment method

Ten normal subjects were tested to validate the portable computer system. These consisted of 3 females and 7 males. The average ages were 23.67 years (range of 22-26 years) for the females, 26.14 years (range 23-31 years) for the males and 25.40 years overall. The individual details can be seen in Table 6.1.

Table 6.1 Joint stiffness assessment individual details

Individual	1	2	3	4	5	6	7	8	9	10
Sex	M	M	F	F	F	M	M	M	M	M
Age	31	25	22	26	23	31	24	25	24	23

The individuals were tested three times each. Between each test the individual was removed from the arthrograph and then relocated. This method was used as it highlights the variation that can be expected between different tests of the same individual. Knowledge of this variation is required for valid analysis of joint stiffness data. For example, a patient may experienced a 5% decrease in joint stiffness post-operatively. However, if the natural variation of a normal individual between different tests was 10% then it would be mis-leading to draw conclusions from the change in stiffness post-operatively.

The following standard testing procedure was followed to reduce the intra-rater variability, (and inter-rater variability for testing in the future). The testing procedure was a modified version of that developed by Bromley[85].

(1) The range of movement of the individual's right index finger was checked to ensure that the oscillation performed to measure joint stiffness was not uncomfortable. If it was then no stiffness assessment was undertaken. (In practice none of the normal individuals tested had any problems with the range of movement of their fingers. However, a reduced range of movement and pain may well prevent patients with RA from completing this assessment).

(2) The LabVIEW joint stiffness data acquisition program was run following the instructions on the screen. The individual and assessment information was entered into the computer.

(3) The arthrograph motor was switched on and the carriage was allowed to rotate until it was at full extension. The motor was then turned off and a zero strain

reading was taken. Originally the carriage was positioned at full flexion (corresponding to Bromley's work[85]) but this was changed as it was easier to align to hand with the carriage in full extension.

(4) The individual's right hand index finger was located in the finger carriage with the strap around the proximal phalanx. The individual's forearm was positioned on the arm rest, with the wrist joint and MCPJ in the neutral position and the elbow joint at 90°. The middle, ring and little fingers were curled around the cylinder for support and the thumb was held in the support sling. The centre of rotation of the MPCJ was aligned with the centre of rotation of the carriage by altering the position of the arm rest above the main frame of the arthrograph. When this was achieved the arm rest was locked in place.

(5) The carriage was manually positioned to approximately 0°, such that the centre position of the cycle would be approximately 20° flexion, a rough estimate of the MCPJ equilibrium position. (This position may vary for patients with rheumatoid arthritis if the range of movement from 0-40° was not comfortable).

(6) The individual was asked to relax and not to resist the movement of the carriage. The motor was switched on and after one cycle a set of torque-angular displacement readings were taken. One cycle was allowed before the readings were taken to let the individual become accustomed to the movement of the carriage and relax. The hysteresis loop of readings taken without the one loop delay were distorted due to active involvement of the muscles of the finger. In several tests it took more than one cycle for the individuals to relax. Once the readings were taken the motor was switched off at full extension.

(7) The computer produced a plot of the resultant hysteresis loop and calculated the mean equilibrium position of the loop and the centre position of the cycle. The carriage was then moved, if necessary, so that the mean equilibrium position and the centre position of the cycle approximately coincided. The procedure was then repeated from (6).

(8) When a set of readings was taken and the calculated mean equilibrium coincided with the centre position of the cycle the hand was removed from the arthrograph.

(9) The computer was prompted for further analysis of the collected data and the maximum, minimum and peak-to-peak torques, flexion, mid-position and

extensions slopes and the energy dissipation were calculated. (A typical screen at this stage is shown in Figure 6.11). The assessment information and the calculated stiffness parameters were then saved to a document file and the torque-angular displacement data was saved to a spreadsheet file.

6.9 Normal individual results and comparison with previous joint stiffness data

The average female, male and overall joint stiffness parameters from the ten normal individuals tested are shown in Table 6.2. The average percentage variances of the individuals are also given (standard deviation divided by the parameter mean). Two typical hysteresis loops (one male and one female) can be seen in Figure 6.12. The mean equilibrium position of the MCPJs was 21.75° flexion which corresponded well with the original estimated mean equilibrium position and with other work performed on the MCPJs with the Durham arthrograph[85,112,117,125]. The average difference between the centre position of the cycle and the mean equilibrium position was 0.54°.

Table 6.2 Average stiffness parameters and percentage variance (%) of the overall, female and male means

Parameter	Overall	%	Female	%	Male	%
Equilibrium position (°)	21.748	4.270	23.000	3.923	21.202	4.419
EP1 (°)	30.159	4.640	31.580	2.825	29.549	5.418
EP2 (°)	13.322	8.838	14.416	7.403	12.853	9.453
Peak-to-peak torque (Nm)	0.0797	7.075	0.0744	9.260	0.0819	6.139
Maximum torque (Nm)	0.0411	8.747	0.0375	9.091	0.0431	8.600
Minimum torque (Nm)	-0.0383	8.486	-0.0369	10.32	-0.0388	7.414
Flexion slope (Nm/° x10^{-3})	3.071	9.975	2.956	9.593	3.120	10.139
Mid-position slope (Nm/° x10^{-3})	1.106	13.329	0.985	12.265	1.158	13.780
Extension slope (Nm/° x10^{-3})	2.252	10.299	1.895	12.345	2.405	9.422
Energy dissipation (J x10^{-3})	12.872	9.540	11.729	10.213	12.872	9.253

The flexion, mid-position and extension slopes were checked by recalculating them using Excel 5.0 and the energy dissipation was checked by manually calculating the area of the hysteresis loops. The maximum torque was slightly greater in magnitude than the minimum torque, and the flexion slope was greater than the extension slope. The flexion and extension slopes were much greater than the mid-position slope. Overall males had slightly greater stiffness values than females, however, there was

Figure 6.11 Main screen for the LabVIEW joint stiffness data acquisition and analysis program

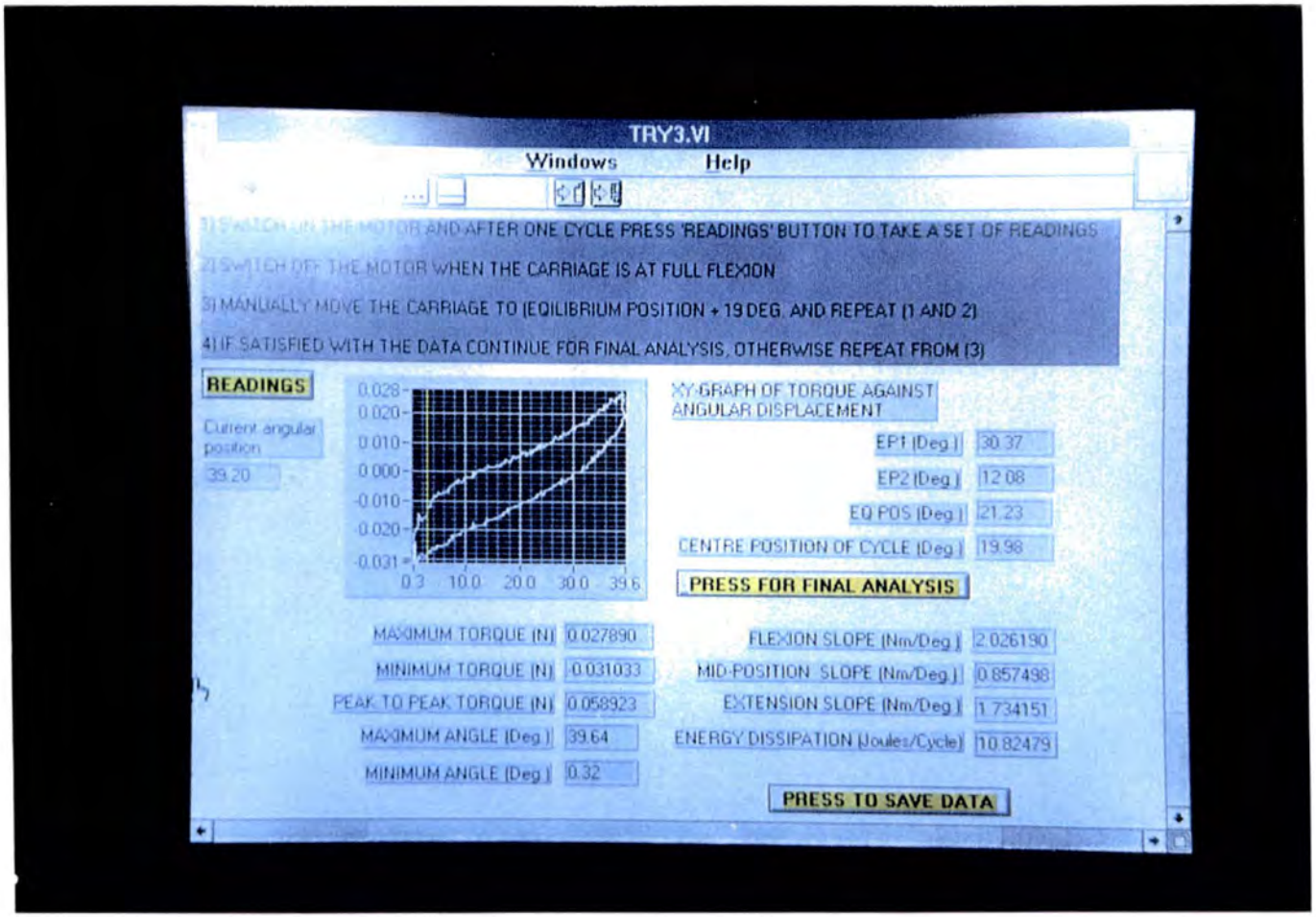

Figure 6.12 Typical stiffness hysteresis loops for the MCPJs of normal individuals a) Male MCPJ stiffness hysteresis loop

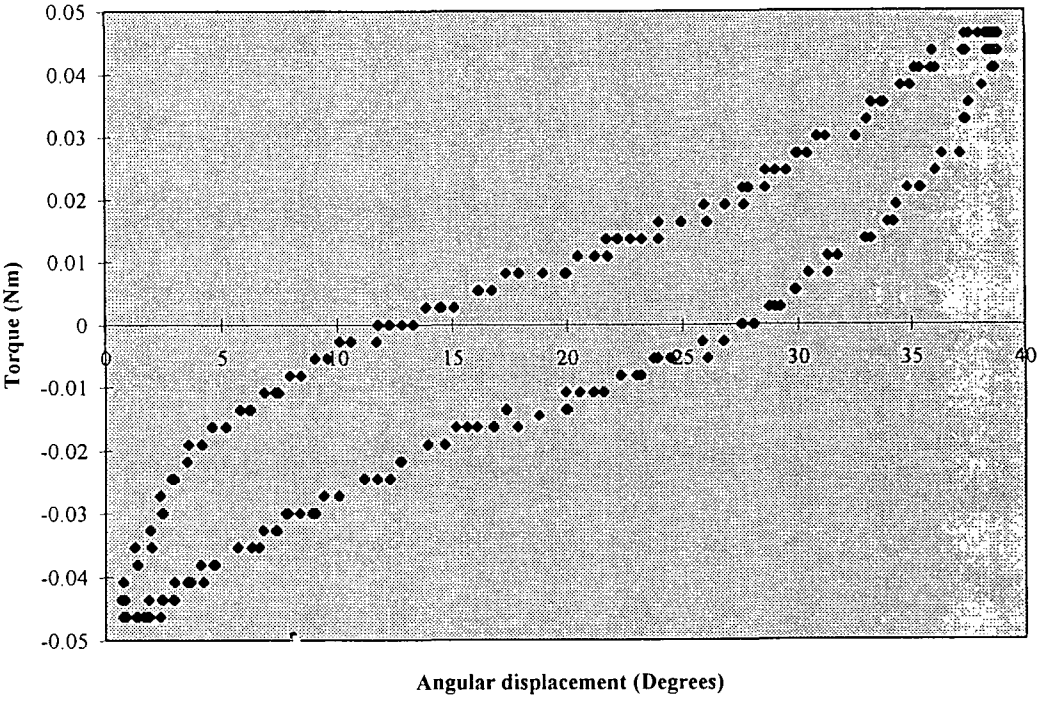

b) Female MCPJ stiffness hysteresis loop

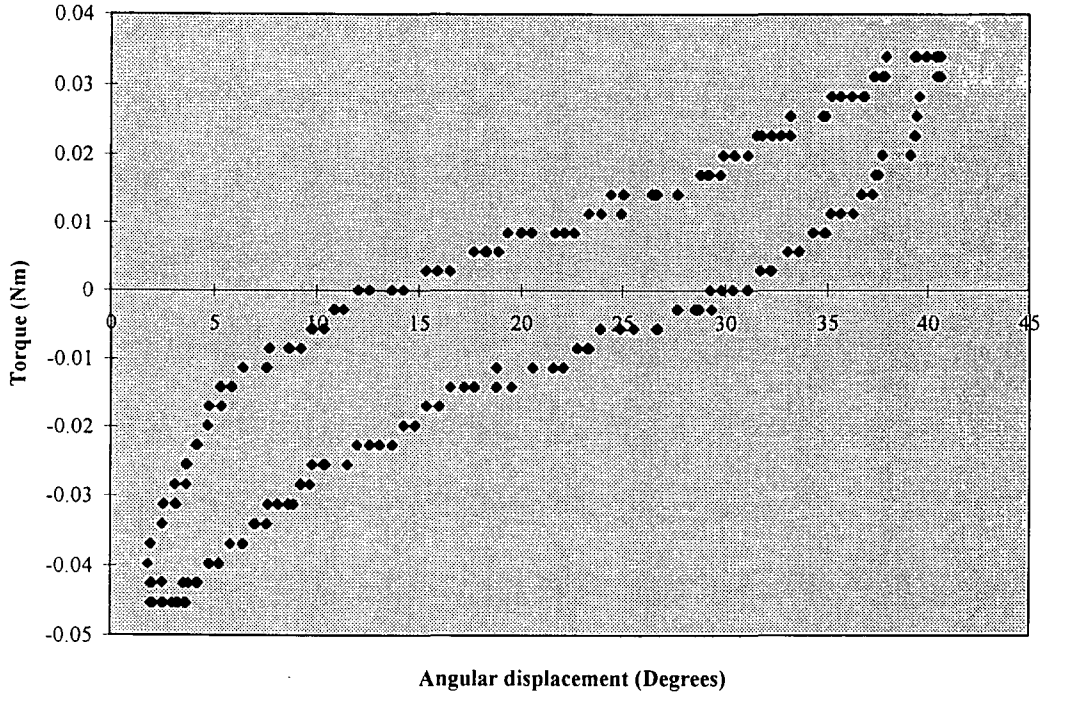

some overlap between the two groups. Other authors have also found males to be stiffer than females[110,113,119,120-122,125-127]. The stiffness parameters found in this study were also compared with the work of Bromley[85]. This was the only previous study which used the Durham arthrograph and calculated stiffness parameters from a single hysteresis loop (20° amplitude), centred about the mean equilibrium position. Repeatability tests were performed on five normal individuals (1-3 with the joint being removed between tests and 4-5 with the joint in place for the duration of the tests). The range and average peak-to-peak torque, flexion, extension and mid-position slopes, and the energy dissipation for each of the individuals and percentage variance of the parameters can be seen in Table 6.3. The mean values and percentage variances from this study compared well with those reported by Bromley[85].

Table 6.3 Joint stiffness parameters (Bromley[85])

		PTPT (Nm)	FS (Nm/° x10^{-3})	MPS (Nm/° x10^{-3})	ES (Nm/° x10^{-3})	ED (J x10^{-3})
Average	**Mean**	0.0886	3.69	1.36	2.54	12.53
	%	7.3	13.97	5.26	13.64	6.02
Range	**Mean**	0.053-0.118	1.63-5.15	0.87-1.88	1.69-3.93	9.48-15.9
	%	5.0-10.0	7.5-22.9	1.5-10.9	8.3-21.88	2.7-12.2

6.10 Summary

The Durham arthrograph was designed to assess joint stiffness of the MCPJ objectively. The original computer system read resistive torque and angular displacement values from the arthrograph during sinusoidal motion imposed on the MCPJ, and calculated the required stiffness parameters. However, the original computer system was not portable and so a new system was developed for a lap-top computer. The computer system consisted of a DAQCard-1200, NI-DAQ driver software and LabVIEW programming package. A calibration program was written for the arthrograph potentiometer and strain gauge system. The calculated calibration factors were Cal1 = 1.1258, Cal2 = 0.0397 and Cal3 = 0.1628. The zero strain value was 0.42. A joint stiffness data acquisition and analysis program was also written and validated using ten normal individuals.

CHAPTER SEVEN

Development of subjective questionnaires for the assessment of metacarpo-phalangeal joint replacement

7.0 Introduction

When evaluating the performance of joint prostheses it is necessary to consider the patient's perspective, as well as taking objective measurements. A patient should have an improved quality of life post-operatively, regardless of the results of objective measurements. In effect overall hand function is more important than individual parameters such as strength, range of movement or stiffness. Subjective questionnaires can be used to provide information on a patient's view of the effect of replacement surgery on the condition and performance of their joints. Background information can also be acquired such as if any other of the patient's joints are affected by arthritis, the symptoms of their arthritis and their ability to perform normal daily activities.

Due to individual interpretation of ratings scales, the actual scores have no quantitative meaning. However, they can be used to assess a patient over a period of time, although direct comparison between individuals is not valid. The validity of the scales is also open to debate when assessing certain parameters. For example differences have occurred between the results from the subjective and objective stiffness assessment of patients. It is thought that subjective stiffness is related to pain, strength and range of movement rather than the actual stiffness of the joints[127].

Despite the limitations of ratings scales it was important to include subjective questionnaires in the assessment of the Durham MCPJ prosthesis due to the invaluable information that they can provide. In addition, by the time patients have finger joint replacements, their hands are usually deformed, painful and weak, and have a severe lack of range of movement. Hence some patients may be unable to complete the objective forms of assessment. In these cases subjective assessment may be the only possible method of assessing the performance of the joints.

Nearly fifty questionnaires were analysed, however, they tended to assess either general health or just one aspect of the condition of a patient's hands, such as pain, stiffness or hand function. None were individually suitable for this project. Therefore two new subjective questionnaires were developed, one for pre-operative assessment and one for post-operative assessment.

7.1 Subjective ratings scale assessment terms

The general requirements of ratings scales are that they are valid, reliable, sensitive to the magnitude of change that can reasonably be expected with the treatments under study, and they produce results that can be statistically analysed[136]. They should be relevant to the disease process and a patient's problems, concise, coherent and easy to use.

Validity is whether a question is assessing the required parameter or not. Due to individual interpretation of the scales and a patient's understanding of the description of their condition, there is difficulty in precisely defining assessed parameters such as stiffness or weakness. For example both patients with RA and normal subjects exhibited circadian variation in objectively measured stiffness. However, only patients with RA experienced the subjective feeling of morning stiffness[127]. Validity of a new scale is assessed by comparing it with existing measures of the same parameters. For example a new scale could be compared with previously validated scales or objectively measured results. In addition, the patient's perception of the parameter assessed can be investigated. However, not all parameters can be measured objectively (such as pain), and a correlation between scales does not necessarily mean that the new scale is valid.

Reliability is whether a scale measures a parameter in a reproducible way. It is an index of the extent to which measurements of an individual on different occasions, or by different observers are reproducible. Every scale may produce a different score from every other scale. Stating that a scale is accurate to within a certain number of units gives no indication of its value in assessing individuals, unless the likely overall range of the scores is known. Therefore reliability is quoted as the ratio of the variability between individuals to the total variability in the scores. It is the proportion of the variability in scores which was due to true differences between individuals. It is expressed as a number between 0 and 1, where 0 indicates no reliability and 1 indicates perfect reliability[137].

The degree of agreement between raters is defined as the inter-rater reliability. The degree of agreement between observations made by the same rater on different occasions is defined as the intra-rater reliability. The agreement between observations of the same patient on different occasions, separated by a set time interval, is defined as the test-retest reliability. Inter-rater, intra-rater and test-retest reliability should all be greater than 0.5 for a reliable scale, although greater values may be required[137].

7.2 Ratings scales

The ratings scales used in previous subjective assessments can be placed into three main categories, visual analogue scales (VAS), numerical ratings scales (NRS) and simple descriptive scales (SDS). There are also a few other types of scales which will be described later. VAS, NRS and SDS correlate well[138], however, there are advantages and disadvantages for each scale which are discussed in the following section. The scales can be used to assess a patient by an external examiner or for self-assessment.

7.2.1 Visual analogue scales

Visual analogue scales (VAS) generally consist of a 100 mm line with 10 mm lines crossing the main line at right angles at the two extremities. The scales also contain *end limits* such as 'very severe pain' and 'no pain' labelling the two extremities (Figure 7.1). Intermediate markers and descriptions have been used (such as mild, moderate and severe[139,140]) but are generally avoided as they tend to influence where a patient marks the scale[141]. A cross or perpendicular line is marked on the scale corresponding to the perceived patient condition.

Figure 7.1 Horizontal visual analogue scale for assessing pain

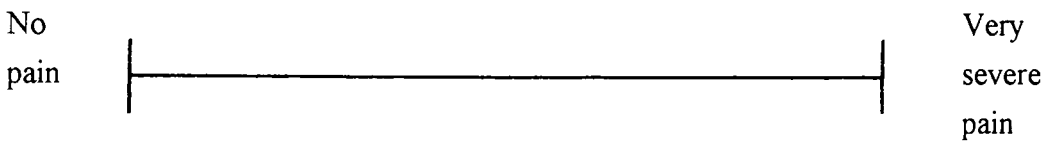

VAS have been used to assess pain[138,139,140,142-148], stiffness[142,133], functional capacity[145,149] and grip strength[150]. Dellhag and Burckhardt[142] assessed self-estimated hand function before performing any grip strength or hand function tests. End limits of no hand function and full hand function were used, where hand function was defined as the ability to use the hand to perform some activity. Taal et al[151] assessed the effect of arthritis on overall well-being.

Both vertical and horizontal VAS have been used, however, horizontal VAS were more accurate and resulted in less confusion in the interpretation of the scales by the patient. Dixon and Bird[141] investigated the reproducibility of a 10 cm vertical VAS by asking a subject to mark the same place on a scale more than once. Subjects tended to estimate

too high and the reproducibility varied depending on where the original mark was on the scale. Errors in perspective also occurred with vertical VAS.

VAS have also been used to rate the perceived degree of improvement over time[152,153]. This has been achieved by using a scale with end limits of much worse and much better, with a marker in the centre of the line indicating the perceived condition before treatment. Alternatively a comparison can be made before and after treatment by showing a patient where they had marked the scale before treatment and then asking them to indicate with a second line their post-treatment condition.

Vertical and horizontal VAS correlate well, although horizontal VAS generally produce slightly lower scores[154]. VAS are reliable and valid and correlate well with other scales[138,142,147]. They have also been described as the most sensitive scales for the estimation of pain[145,150].

7.2.2 Numerical ratings scales

The most commonly used numerical ratings scales (NRS) are 11-point (0-10) or 5-point (0-4) scales. These rate an assessment parameter from, for example, 0-10, where 0 and 10 have descriptions defining the end limits of the scale. For example 0 may correspond to no pain and 10 may correspond to very severe pain (Figure 7.2). NRS have been used to assess stiffness[130,131] pain[130,131,133,138,142,146,], a patient's ability to perform tasks[133], and patient self-efficacy (how certain the patient was of being able to complete a task)[147]. Finally the Dutch-AIMS scale of health status rated mobility, physical activity, dexterity, household activities, social activities, activities of daily living (ADL), pain, depression and anxiety on 11-point NRS. 0 corresponded to good health status and 10 corresponded to bad health status[151].

Figure 7.2 Numerical ratings scale for assessing pain

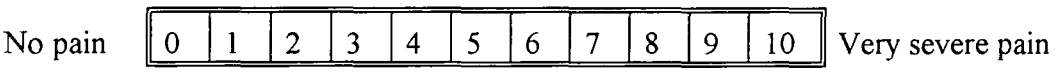

NRS have been described as a compromise between VAS and SDS[138]. They offer a greater degree of freedom than SDS, but a more limited choice than VAS. However, the meaning of the numbers is not known and the difference between say 1 and 2 may not be the same as that between 7 and 8. Downie et al[138] plotted numerical scores from NRS against the descriptions from SDS used to assess pain. They found an

overlap of the numerical scores for the descriptions, indicating differences in the interpretation of the two scales by different patients. However, NRS were the most reliable scales compared with VAS and SDS. In addition, NRS eliminate the need to measure the scales to produce a score unlike VAS, and may therefore reduce error in the readings. NRS are reliable and valid[138,151,155].

7.2.3 Simple descriptive scales

Simple descriptive scales (SDS) rate an assessment parameter by matching a patient/raters perception of a patient's condition to one of a list of worsening descriptions. There are two main types of SDS. The first describes an assessment parameter using adjectives of severity (Figure 7.3). The scales contain little specific description of the patient's condition, hence there is a certain amount of individual interpretation of the descriptive stages. These are the most commonly used SDS.

Figure 7.3 Simple descriptive scale for assessing pain

None	Mild	Moderate	Severe

The second type of SDS contain more detail in its stages of description, and are specific to a particular parameter. In 1949 Steinbrocker et al[116] defined the stages of RA using a four stage SDS. The descriptive stages were early, moderate, severe and terminal, and contained descriptions of the damage that could be experienced by RA at each stage. They also used a four stage SDS for the classification of functional impairment. The end stages contained descriptions of complete functional capacity with the ability to carry on all usual duties without handicaps, and largely or wholly incapacitated with a patient bedridden or confined to a wheelchair, permitting little or no self-care.

A high reliability has been found with SDS[156], however, this may be due to the limited number of choices available to the patient. There are generally large differences between the descriptive stages which result in a lack of sensitivity in the scales. Indeed Downie et al[138] commented on the lack of sensitivity of SDS for detecting relatively small changes. A variety of parameters have been assessed using SDS including pain[138,157], functional capacity[116,145,150,154,156,158,159], health[157], feelings[157], the effects of RA[116,159] and pain interference at work[157].

The most common use of SDS was to assess the ability to perform ADL. The descriptive stages used varied slightly between authors as did the ADL assessed. However, the stages generally assessed whether a patient could perform an ADL or not, and how much difficulty the patient had in performing the ADL[139,140,144,145,149,157, 159,160]. (For example without any difficulty, with some difficulty, with much difficulty, unable to do were used[144]). The categories of ADL assessed were dressing and grooming, rising, eating, walking, hygiene, and reach or grip activities[144]. In addition, reasons for the difficulty in performing the ADL were investigated by some authors[139,160]. These included weakness, pain, synovitis, joints, thumb problems, IPJ problems, MCPJ problems, sensory problems, tendon problems, wrist problems, other joints involved, other reasons[139,160].

A variation on SDS are numerical descriptive scales (NDS), which appear to be a mixture of NRS and SDS (Figure 7.4). However, on closer inspection it can be seen that the parameter (in this case pain) is assessed by the description, and a number is then assigned to the corresponding description. The score has no meaning other than the description that it is assigned to, and is therefore not particularly useful. However, NDS have been extensively used in the past to rate parameters such as pain[136,152,153,159,161], tenderness[140,162], functional capacity[136,140,143,152,161,163-165], personal mobility[152,161], joint range of motion[159], degree of dependence[136], feelings[161] and drug toxicity[164]. They have also been used to show the trend of an assessment parameter, for example better = 1, same = 2, worse = 3[164]. Similarly to the SDS, NDS are reliable and valid[136,143,163-165].

Figure 7.4 Numerical descriptive scale for assessing pain

1	No pain
2	Mild pain
3	Moderate pain
4	Severe pain
5	Unbearable pain

The scores from several assessed parameters have also been added together to produce an overall score. Fries et al[164] assessed the severity of pain and its general trend using NDS and the two scores were added together and defined as the Discomfort Index. Similarly Jette[136] assessed the degree of dependence, the degree of difficulty and the

amount of pain experienced in performing specific ADL. The individual scores were added together and defined as the Functional Status Index.

Summing individual scores, however, to produce one index is not particularly useful and can cause confusion in the overall index. For an individual NDS the score directly corresponds to a description of the assessed parameter. However, when many scores are added together the overall index has no meaning. In addition, one score can dominate and hide smaller, but significant, changes in the other scores. In effect the sensitivity of the scales are reduced. Lee et al[165] assessed the difficulty in performing 17 movements and added the scores together to give an index of functional impairment. The method was too crude to detect minor changes.

7.2.4 Additional methods of subjective assessment

Jette[136] compared three self-report methods for assessing dependence, the difficulty in performing activities and pain. These were a NDS, a ladder scale and index cards. The ladder scale can be seen as a cross between a NRS and a VAS. The scale consisted of 12 rungs with the top rung labelled 'unable to do this activity, extreme difficulty and severe pain' and the bottom rung labelled 'used no help, extreme ease and no pain'. Patients were asked to rate each activity as a rung on the ladders. In a similar way seven index cards were used to rate the same activities. Cards one and seven carried the same labels as the end rungs of the ladders. Patients were asked to rate each activity by choosing a card from 1 to 7. This method corresponded to a NRS as the intermediate cards were numbered 2-6.

Subjective assessment can also take the form of a simple yes/no answer. For example Carthum et al[166] assessed the presence or absence of pain, tenderness, heat and crepitus in the individual joints of the hand. Finally morning stiffness is one of the diagnostic criteria for RA. This has generally been assessed subjectively as the duration of morning stiffness in minutes[146,152,153,159].

7.3 Durham subjective assessment parameters

A self-assessment subjective questionnaire was required to assess the effect of replacing MCPJs affected with arthritis with artificial finger joints. The performance of the joints could be assessed with parameters such as pain, stiffness, range of movement, grip strength and hand function. However, these parameters are not necessarily dependent

of the condition of the MCPJs alone. For example, grip strength may be dependent on the stability of the thumb and the strength of the muscles acting on the MCPJs, as well as MCPJ pain and deformity. Simply replacing the MCPJs will not change the condition of the thumb or the muscles, hence grip strength may not necessarily change post-operatively. Therefore to make a full assessment of a patient, before and after surgery, background information on the patient was also required as well as the performance of the joints.

The following list of the required assessment parameters was compiled using previous questionnaires and taking into account the objective methods of assessment to be used (namely stiffness, range of motion and pinch/grip strength). It was hoped that the additional background information would give a wider appreciation of the performance of the joints both subjectively and objectively.

Patients and assessment details	*	Name, age, sex
	*	Dominant hand
	*	Occupation and hobbies
	*	Date and time of assessment
Condition of the joints	*	Duration of arthritis
	*	Joints affected by arthritis
	*	Symptoms of arthritis
	*	Duration of morning stiffness
Joint performance	*	Pain during resisted motion
	*	Pain during non-resisted motion
	*	Stiffness
	*	Range of movement
	*	Appearance
	*	Hand strength
	*	Overall hand function
	*	Activities of daily living

Nearly fifty questionnaires were analysed, all of them to do with either arthritis or hand assessment. However, none of them covered all of the required assessment parameters for this study. Hence two new questionnaires were compiled from previous questionnaires, one for pre-operative assessment and one for post-operative assessment. Only ratings scales from questionnaires that were valid, reliable and

sensitive to change were used. It should be noted that this did not necessarily mean that the new questionnaires were valid, reliable and sensitive to change. The different ratings scales used to assess the required parameters for this study are discussed as follows :

Pain has been assessed on various VAS[139,140,143-148,154], NRS[133,146,130,131], SDS and NDS[152,153,157,159,164] of the general forms shown in Figures 7.1-7.4. In addition, Dellhag et al[133,142] rated pain on resisted motion on a 10-point NRS and pain on non-resisted motion on a vertical VAS. Carthum et al[166] simply noted the presence or absence of pain in the joints of the hand. The trend of joint pain over time has also been investigated using NDS, with the descriptive stages of better (1), same (2), and worse (3)[164].

Ritchie et al[162] reported that the main problem in the assessment of pain was the difficulty in recognising and grading the response to pain. They proposed that tenderness was probably the most reliable parameter of joint inflammation in patients with RA. *Tenderness* was rated using a NDS with descriptive stages of the patient had no tenderness (0), the patient complained of pain (1), the patient complained of pain and winced (2), and the patient complained of pain, winced and withdrew (3)[140,162]. Tenderness has also been rated simply on its presence or absence in joints of the hand[166], and as a count of the affected joints[146].

Joint stiffness has been rated on a vertical VAS[133] with end limits of no stiffness and maximal stiffness. It has also been rated on an 11-point NRS with end limits of 0 (none) to 10 (most severe)[130,131]. *Range of motion* has previously been rated using NDS[159]. The NDS was a 5-point scale rating restriction of movement with descriptive stages of nil (0), mild (1), moderate (2), severe (3), and completely crippled (4). *Grip strength* was subjectively assessed by Downie et al[150] using a vertical VAS and a SDS. The SDS was a 4-point scale with descriptive stages of very weak, weak, normal and strong. However, grip strength measured on a sphygmomanometer correlated poorly with subjective grip strength with arthritic patients, although a better correlation was found with normals[150]. This implied that arthritic patients may have confused grip strength with other factors such as pain or stiffness.

Functional ability has been assessed either by the time that it took a patient to complete set tasks[166-170], or the difficulty that they had in performing tasks or ADL[9133,142]. The latter was rated using either SDS or NDS. Functional hand tests consist of tasks which are meant to represent the hand functions needed for ADL.

There are several recognised hand function tests. These include the Arthritis hand function test (AHFT)[167,168], the Jebsen hand function test (JHFT)[167,169], the Smith hand function test[170] and the Sollerman hand function test[133,142]. The advantage of functional hand tests is that patients all perform the same tasks, under the same conditions. The disadvantages are that the tasks are only representative of the activities that the patients may perform each day and do not assess what the patients actually achieve. In addition, many of the tests only rate whether a patient can or can not perform a task and the time taken to perform the task, rather than the degree to which the task was performed regardless of time. In some of the tasks patients with RA rarely approached the norm and lesser degrees of improvement were obscured by these hand function tests[158].

In many ways the assessment of ADL is more valid and relevant to the patients. The most widely used questionnaire to assess the difficulty that patients have in performing ADL is the Health assessment questionnaire (HAQ)[142-144,171,172]. The activities covered were divided into categories of dressing and grooming, arising, eating, walking, hygiene, reach, grip, and other heavy or precision activities. The activities were rated on a NDS with descriptive stages of without any difficulty (0), with some difficulty (1), with much difficulty (2) and unable to do (3).

The Adenbrooke and Odstock hospital hand assessments used similar categories rated on a SDS with descriptive stages of easy, fair, difficult and impossible[139,160]. They also investigated the reasons for the any difficulty which were chosen from a list of weakness, pain, synovitis, joints, thumb problems, IPJ problems, MCPJ problems, sensory problems, tendon problems, wrist problems, other joints involved, other reasons[139,160]. The Leeds hand assessment used a SDS with descriptive stages of no difficulty, slight, moderate, severe and impossible[140]. Other variations on these SDS and NDS have also been reported[136,163-165,173]. Difficulty in performing ADL has also been assessed on a VAS[149,174].

Two more complicated NDS scales are NUDS[155] (North-Western University Disability Scales) and AIMS[142,151,161,167,171] (Arthritis Impact Measurement Scales). These assessed functional ability under categories of walking, dressing, hygiene, eating and feeding, speech, activity, ADL, pain and depression. Each category contained a number of activities of increasing difficulty. The patient was scored on the most difficult activity in each category that they can perform. Finally the degree of dependence was rated on a NDS with descriptive stages of used no help (1), used equipment (2), used human assistance (3), used equipment and human assistance (4),

and unable or unsafe to do this activity (5), and formed part of a Functional Status Index[136].

7.4 Durham pre-operative patient assessment questionnaire discussion

The two main aims of the pre-operative questionnaire were to assess the patient's self-perceived condition and performance of their joints and to gather background information about the patient. Section 1 included the date and time of assessment and the surname/initials and dominant hand of the patient. (Age, sex and previous medical history would be acquired from the patient's medical records with their consent). Dominant hand and occupation/hobbies were also included as it was thought that they may influence the type of activities performed by a patient in their ADL, and the amount of activity that the hands were subjected to. The date and time of assessment were included to account for circadian and day-to-day fluctuations in the condition of the joints.

The initial condition of a patient's MCPJs and their adjacent joints can be influential on the post-operative performance of any finger joint prosthesis. It is also important to have information about the condition of a patient's joints when comparing the results from different individuals. Hence Section 2 assessed how long a patient had suffered from arthritis, which joints were affected and their symptoms (unstable, swollen, weak, tender to touch, stiff, painful, reduced range of movement). Self-perceived pain (with resisted and non-resisted motion) and joint stiffness were also assessed on horizontal VAS. The time period 'over the past week' was used to eliminate differences due to fluctuations in the arthritis and circadian and day-to-day variations.

Horizontal VAS were used to assess pain and stiffness rather than NDS or SDS as they were the most commonly used scales in previous questionnaires for these categories. The scales were valid and reliable[133,142,144,147,148]. Horizontal scales were used rather than vertical scales to eliminate as far as possible any confusion or influential factors when using VAS. The scales were 10 cm long with end markers of no pain and very severe pain or no stiffness and maximal stiffness. No intermediate markers or dialogue were used to minimise the possibility of influencing where a patient marked the scale[141]. Range of motion, strength and appearance were not assessed in the pre-operative questionnaire as it was important to limit the length of the questionnaire.

Overall functional capacity was assessed in Section 3 in the form of the difficulty encountered when performing ADL and the reasons for these difficulties. The categories from the HAQ[144] were assessed on a SDS as opposed to a NDS as no obvious advantages could be gained from using NDS. A five stage SDS was used, rather than a four stage SDS, to increase the sensitivity of the scale. The stages of difficulty were no difficulty in performing this activity, slight difficulty in performing this activity, moderate difficulty in performing this activity, severe difficulty in performing this activity, impossible to do this activity.

The ADL assessed were dressing, hygiene, eating and cooking, housework and others (heavy and precision activities). The activities and scales have been used in previous questionnaires and were valid and reliable[144,159,159,164]. Reasons for the difficulty in performing the activities were also assessed to give a better understanding of the problems that arthritic patients with ADL. These were weakness (1), pain (2), lack of range of movement (3), sensory problems (4), other reasons (5). The pre-operative questionnaire is shown in Appendix 9.

7.5 Durham post-operative patient assessment questionnaire discussion

The main aim of the post-operative patient assessment questionnaire was to compare the performance of the joints post-operatively and pre-operatively. This was achieved in two ways. Firstly some of the questions included in the pre-operative questionnaire were also included in the post-operative questionnaire. Secondly the patients were asked to compare directly the post-operative and pre-operative condition of their joints.

Section 1 rated joint pain and stiffness on horizontal VAS. The scales were identical to those used in section 2 of the pre-operative questionnaire. Pain with resisted and non-resisted motion were rated on scales with end markers of no pain and very severe pain, whilst joint stiffness was rated on a scale with end markers of no stiffness and maximal stiffness. Section 2 rated pain, stiffness, range of movement, overall hand function, appearance and strength as a direct comparison of the pre-operative and post-operative condition of the joints. The categories were rated on horizontal VAS indicating whether a patient felt that his/her joints were much better, much worse or the same. These horizontal VAS were used in previous clinical trials and were valid and reliable[133,142,144,147,148]. Section 3 was identical to Section 3 on the pre-operative assessment questionnaire. It assessed the difficulty in performing ADL and the reasons for this difficulty on SDS. The post-operative questionnaire is shown in Appendix 9.

In summary, nearly fifty questionnaires were analysed to find a suitable questionnaire to assess subjectively the performance of the MCPJ surface replacement from the patient's point of view. However, none of them covered all the required areas of assessment. Hence two new questionnaires were compiled from previous questionnaires. Only ratings scales from questionnaires that were valid, reliable and sensitive to change were used. It should be noted that this did not necessarily mean that the new questionnaires were valid and reliable. The questionnaires were developed with the help of rheumatologists from South Cleveland and Middlebrough General Hospitals, to ensure that all of the relevant areas of assessment were covered and that the questions were in a suitable format for the patients. In addition, it was suggested that it may be useful for an occupational therapist to be present during the assessment both from a patient and medical assessment point of view. As yet, the two new questionnaires have not been used on patients.

CHAPTER EIGHT

Summary and further work

8.1 Summary

8.1.1 Proximal interphalangeal joint surface replacement design

A surface replacement joint prosthesis was designed specifically for the PIPJ. It was designed to be anatomically correct, simulate the natural biomechanics of the joint and preserve the attachments of the ligaments surrounding the joint. To develop such a joint prosthesis, detailed information on the architecture of the bearing surfaces and medullary canals was required. There was little information in the literature and few dimensions given. Therefore an extensive study on the architecture and dimensions of the proximal and middle phalangeal bones was undertaken.

The bones from 83 PIPJs were dissected, replicated in plastic, sectioned and shadowgraphed in the sagittal, frontal and transverse planes. Dimensions of the bearing surfaces, medullary canals and the overall bone sizes were then measured from the shadowgraphs. The feasibility of a PIPJ surface replacement prosthesis was assessed. Such a design was feasible, however, the PP head was required to be solid. Models of the PP heads were developed, from which four PIPJ prostheses were designed. The joint prostheses consisted of two parts, a convex PP head and a concave MP base. The PP heads were designed from the models and the MP bases were designed to conform with the PP heads. The components were bi-condylar to replicate the natural PIPJ bearing surfaces. Semi-circular cross-sectioned stems were designed to produce interference fixation within the phalangeal bones. The stems were offset from the centre of rotation of the joint so that they were aligned correctly within the bones. The four joint prostheses covered 97.6% of the population of joints examined.

8.1.2 Wear characteristics of XLPE against itself

Wear tests of XLPE against itself, XLPE and UHMWPE against stainless steel, and UHMWPE against itself were carried out on pin-on-plate reciprocating apparatuses. The tests were run at 37°C, 63rpm, under 10 N and 40 N loading and in distilled water. The plates wore significantly more than the pins for polymer-on-polymer combinations, possibly due to fatigue wear. No wear of the stainless steel plates was

found. The main wear mechanism of XLPE against XLPE was abrasive wear. For UHMWPE and XLPE against stainless steel, and UHMWPE against itself the main wear mechanisms were adhesive and abrasive wear. The XLPE-on-XLPE pins wore the least followed by UHMWPE-on-stainless steel, XLPE-on-stainless steel and then UHMWPE-on-UHMWPE. The orders of magnitude of the corresponding pin wear coefficients were 10^{-7}, 10^{-7}, 10^{-6}, 10^{-5} respectively. The UHMWPE-on-UHMWPE plates also wore significantly more than the XLPE-on-XLPE plates. The orders of magnitude of the corresponding plate wear coefficients were 10^{-6}, 10^{-5} respectively. The wear rates of the polymer pins and plates were dependent on load but not proportionally.

The comparable wear rates of XLPE against itself and UHMWPE against stainless steel, combined with the fact that the forces found in the finger joints are much smaller than those in the rest of the body, suggested that it was feasible to make an all XLPE finger joint prosthesis as far as the wear considerations were concerned. XLPE also has the advantage that it can be injection moulded, which would simplify the manufacture of the complex shapes associated with the bearing surfaces of the PIPJs.

8.1.3 Objective joint stiffness assessment

A portable computer system was developed for the Durham arthrograph. The arthrograph measured the joint stiffness of the MCPJ and was to be used for the pre-operative and post-operative assessment of the Durham MCPJ prosthesis. A calibration program and a data collection and analysis program were written in LabVIEW, to run on a lap-top computer. The computer system also included a DAQCard-1200 and NI-DAQ driver software (all made by National Instruments). The portability of the new computer system would make transportation of the apparatus for clinical trials easier, and the user friendly interface would allow assessors with limited computing experience to perform joint stiffness assessment.

The arthrograph measured the resistive torque of the MCPJ to sinusoidal motion imposed on it (20° amplitude, 0.1 Hz). The stiffness parameters measured were the equilibrium position, centre position of the cycle, maximum, minimum and peak-to-peak torques, flexion, mid-position and extension slopes, and the energy dissipation per cycle. Data was only used for final analysis when the equilibrium position of the joint coincided with the centre position of the cycle. The new computer system was

validated by testing ten normal individuals and comparing these results with results obtained from previous studies using the original Apple-Basic program[85].

8.1.4 Subjective self-assessment patient questionnaire

Pre-operative and post-operative subjective questionnaires were designed for patients to self-assess the performance their joints during clinical trials of the Durham MCPJ prosthesis. The questionnaires were designed to obtain a patient's perspective on the condition and overall performance of their joints. Parameters such as pain, joint stiffness, range of motion and overall hand function were assessed on visual analogue scales. The difficulty in performing activities of daily living were assessed on simple descriptive scales, along with the reasons for any difficulties. The questionnaires also covered areas such as the joints affected by arthritis and the symptoms encountered.

8.2 Further work

8.2.1 Proximal interphalangeal joint surface replacement design

A range of surface replacement joint prostheses specifically for the PIPJs have been developed from an initial concept through to technical drawings. The designs were developed with careful consideration to the anatomy and biomechanics of the PIPJs. Manufacturing and surgical considerations were also taken into account, as far as possible, although the designs should be approved by a manufacturer and surgeon and modified if necessary.

Finite element analysis (FEA) models of the joints should be developed to investigate any significant weaknesses within the designs. The small cross-sections of the phalangeal bones allowed only very thin stems to be designed for interference fixation of the PP and MP components. Hence it would be important to assess whether the stems could withstand the forces that they would be subjected to in the body, particularly at the interfaces with the PP head and MP base. Stress concentrations in these areas may cause the stems to shear. Therefore the stems may need to be enlarged or re-designed taking into account the bone stock available. The FEA models could also predict possible regions of high wear.

The joint prostheses should then be tested on a finger function simulator (FFS). The design of the FFS should reproduce the *in-vivo* conditions of the PIPJ as close as

possible. Areas for consideration would be the forces exerted on the PIPJ when moving and during static hand functions, the planes, range and frequency of motion, the temperature and the lubricant. These would give a more realistic estimate of the wear that may be experienced in the body than pin-on-plate wear tests, and could also highlight any structural defects in the PIPJ prosthesis design. For instance when the Durham MCPJ prosthesis was tested in a FFS increased wear was found on the dorsal aspect of the PP base due to the subluxing forces exerted on the joint prosthesis[73]. In addition, Swanson joint prostheses were found to fracture at a similar time span to that experienced in the body[73]. As far as the PIPJ design is concerned three main areas of interest would be the strength of the stems, wear between the inter-condylar ridge and inter-condylar sulcus, and the decision to make the bearing surfaces conforming.

The surgical tools required to implant the prostheses need to be developed further in collaboration with a surgeon and manufacturer. The surgical technique and tools could then be tested by implanting the joint prostheses in cadavers. Once ethical approval and approval from the Medical Devices Agency were obtained clinical trials could take place.

8.2.2 Wear characteristics of XLPE against itself

The pin-on-plate tests in this study were carried out in distilled water. However, there has been much debate over which lubricant should be used for wear tests. Distilled water was used because it was reproducible, inexpensive and simple to use. In addition, the few previous tests that have been carried out on UHMWPE and XLPE against themselves have also been run in distilled water, hence it was easier to compare results. However, serum or synovial fluid are thought to reproduce *in-vivo* conditions better than distilled water or saline solution. Hence identical tests should be run on the same rigs but in either synovial fluid or serum. This will enable a direct comparison with the results from this study and highlight any differences in the wear characteristics of polymer-on-polymer combinations introduced by biological lubricants.

This study concentrated on the wear rate of XLPE against itself compared with other biomaterial combinations. Little work was completed on the wear mechanisms and wear debris produced. However, cellular reactions are dependent on the morphology or the wear debris as well as the wear volume[81]. Smaller wear debris may produce a more adverse cellular reaction than larger wear debris. The morphology and volume

of wear debris are determined by the material combination, test conditions and the wear mechanisms present. Hence these should also be investigated, when testing in a biological lubricant, and compared with other biomaterial combinations (particularly UHMWPE-on-stainless steel).

Finally, it was observed that the pins or plates within each test underwent changes to higher or lower wear regimes simultaneously. However, these wear periods did not compare well with identical tests run on the same rigs. It was hypothesised that two possible causes for this may be variations in the environment and the fact that a common bath was used for all of the pins and plates in one test. To run the tests in a controlled environment may be too expensive, however, the second theory could be investigated by carrying out tests in distilled water but with individual chambers in the lubricant bath. This would not allow debris from one pin and plate combination to come in contact with the other pins and plates.

8.2.3 Durham MCPJ prosthesis assessment

The Durham arthrograph with the new portable computer system and the self-assessment patient questionnaires will be used in the clinical trials of the Durham MCPJ prosthesis. They could also be used to assess the performance of other MCPJ prostheses such as the Swanson joint prosthesis, or be adapted for assessment of the Durham PIPJ prosthesis.

Finally the pre-operative and post-operative questionnaires were compiled from many different questionnaires since no one questionnaire could be found that covered all of the required areas of assessment. All of these questionnaires were validated, reliable (intra and inter-rater) and sensitive to change. However, it could be argued that this does not necessarily mean that the compiled questionnaires would be valid, reliable or sensitive to the amount of change expected after MCPJ replacement. Hence testing of the questionnaires could be undertaken to investigate their suitability for assessing the performance of the Durham MCPJ prosthesis.

References

1 **Symmons D and Bankhead C (1994).** Health Care Needs Assessment for Musculo-skeletal Diseases. The First Step - Estimating the Number of Incident and Prevalent Cases. The Arthritis and Rheumatism Council for Research.

2 **Annual Summary (1992).** The Arthritis and Rheumatism Council for Research.

3 **Wright V and Haslock I with Champey B (1977).** Rheumatism for Nurses and Remedial Therapists. William Heinemann Medical Books Ltd. Great Britain.

4 **Lever R (1990).** A Guide to Common Illness. Penguin Books Ltd.

5 **Kippel JH and Dieppe PA (1994).** Rheumatology. St Louis, London, Mosby.

6 **Rheumatoid Arthritis.** A Handbook for Patients. The Arthritis and Rheumatism Council for Research.

7 **Ropes MW, Bennett GA, Cobb S, Jacox R and Jessar RA (1959).** 1958 Revision of Diagnostic Criteria for Rheumatoid Arthritis. Arthritis and Rheumatism, 2, 16-20.

8 **Brannon EW and Klein G (1959).** Experiences with a Finger Joint Prosthesis. Journal of Bone and Joint Surgery, 41A, 1, 87-102.

9 **Swanson AB (1969).** Finger Joint Replacement by Silicone Rubber Implants and the Concept of Implant Fixation by Encapsulation. Annals of the Rheumatic Diseases, 28, Supplement 47-55.

10 **Nalebuff EA (1984).** The Rheumatoid Hand. Reflections on Metacarpo-Phalangeal Arthroplasty. Clinical Orthopaedics and Related Research, 182, 150-159.

11 **Lynch A and Colville J (1987).** Metacarpo-Phalangeal Joint Arthroplasty of the Rheumatoid Hand. Irish Medical Journal, 80, 2, 58-60.

12 **Fleming SG and Hay EL (1984).** Metacarpo-Phalangeal Joint Arthroplasty Eleven Year Follow Up Study. Journal of Hand Surgery, 9-B, 3, 300-302.

13 **Purves W K, Berme N and Paul J P (1979).** Finger Joint Biomechanics. Disability - Proceedings Seminar Rehabilitation (Eds RM Kenedi, JP Paul and J Hughes), Macmillan, London, 318-332.

14 **An KN, Chao EYS, Cooney WP and Linscheid RL (1985).** Forces in the Normal and Abnormal Hand. Journal of Orthopaedic Research 3, 2, 202-211.

15 **Linscheid RL and Chao EYS (1973).** Biomechanical Assessment of Finger Function in Prosthetic Joint Design. Orthopaedic Clinics of North America, 4, 2, 317-330.

16 **Youm Y, Gillespie TE, Flatt AE and Sprague BL (1978).** Kinematic Investigation of Normal Metacarpo-Phalangeal Joint. Journal of Biomechanics, 11, 109-118.

17 **Unsworth A and Alexander WJ (1979).** Dimension of the Metacarpo-Phalangeal Joint with Particular Reference to Joint Prostheses. Engineering in Medicine, 8, 2, 75-80.

18 **Flatt AE and Fischer GW (1969).** Biomechanical Factors in the Replacement of Rheumatoid Finger Joints. Annals of the Rheumatic Diseases, 28, Supplement 36-41.

19 **Unsworth A, Dowson D and Wright V (1971).** Cracking Joints. A Bioengineering Study of Cavitation in the Metacarpo-Phalangeal Joint. Annals of the Rheumatic Diseases, 30, 348-357.

20 **Bartel DL, Fischer GW and Flatt AE (1968).** An Investigation of Human Finger Joint Motion Using the Method of Over-Determined Collocation. 21st Conference on Engineering in Medicine and Biology.

21 **Aleksandrowicz R, Pagowski S and Seyfreid A (1974).** Anatomic-Geometric and Kinematic Analysis of the Metacarpo-Phalangeal Articulation of the III Digit of the Human Hand. Folia Morphologica, 4, 353-361.

22 **Pagowski S and Piekarski K (1977).** Biomechanics of Metacarpo-Phalangeal Joint. Journal of Biomechanics, 10, 205-209.

23 **Tamai K, An KN, Linscheid RL, Cooney WP and Chao EYS (1988).** Three-Dimensional Geometric Analysis of the Metacarpo -Phalangeal Joint. Journal of Hand Surgery, 13-A, 4, 521-529.

24 **Walker PS and Erkman MJ (1975).** Laboratory Evaluation of a Metal-Plastic Type of Metacarpo-Phalangeal Joint Prosthesis. Clinical Orthopaedics and Related Research, 112, 349-355.

25 **Landsmeer JMF (1955).** Anatomical and Functional Investigations on the Articulation of the Human Fingers. Acta Anatomica, 25, Supplement 24, 1-69.

26 **Kuczynski K (1968).** The Proximal Interphalangeal Joint. Journal of Bone and Joint Surgery, 50-B, 3, 656-663.

27 **Leibovic SJ and Bowers WH (1994).** Anatomy of the Proximal Interphalangeal Joint. Hand Clinics, 10, 2, May, 169-178.

28 **Holcomb GR, Irving TE and Smith RD (1958).** Coronal Deviation and Tilt in the Proximal Interphalangeal Joints of Man. American Journal of Physical Anthropology, 16, 429-440.

29 **Linscheid RL and Dobyns JH (1979).** Total Joint Arthroplasty. The Hand. Mayo Clin Proc, 54, 516-526.

30 **Stack HG (1962).** Muscle Function in the Fingers. Journal of Bone and Joint Surgery, 44-B, 4, 899-909.

31 **Flatt AE (1960).** The Prosthetic Replacement of Rheumatoid Finger Joints. Rheumatism, 16, 90-97.

32 **Blair WF, Shurr DG and Blackwater JA (1984).** Metacarpo-Phalangeal Joint Arthroplasty with a Metallic Hinged Prosthesis. Clinical Orthopaedics and Related Research, 184, 56-163.

33 **Flatt AE (1967).** Prosthetic Substitution for Rheumatoid Finger Joints. Plastic and Reconstructive Surgery, 40, 6, 565-570.

34 **Flatt AE and Ellison MR (1972).** Follow-Up Notes on Articles Previously Published in Journal. III. Restoration of Rheumatoid Finger Joint Function. Journal of Bone and Joint Surgery, 54-A, 6, 1317-1322.

35 **Girzadas DV and Clayton ML (1969).** Limitations of Use of Metallic Prostheses in the Rheumatoid Hand. Clinical Orthopaedics and Related Research, 67, 127-132.

36 **Zachariae L (1967).** Experience of Flatt Finger Joint Prostheses. Acta Orthopaedica Scandinavica, 38, 329-340.

37 **Flatt AE (1961).** Restoration of Rheumatoid Finger Joint Function. Journal of Bone and Joint Surgery, 43-A, 5, 753-773.

38 **Calnan JS and Reis ND (1968).** The Development and Use of an Artificial Finger Joint. Biomedical Engineering, 314-319.

39 **Nicolle FV and Calnan JS (1972).** A New Design of Finger Joint Prosthesis for the Rheumatoid Hand. The Hand, 4, 2, 135-146.

40 **Swanson AB, Maupin BK, Gajjar NV and de Groot Swanson G (1985).** Flexible Implant Arthroplasty in the Proximal Interphalangeal Joint of the Hand. Journal of Hand Surgery (American Volume), 10A, 6, 1, 796-805.

41 **Reis ND and Calnan JS (1969).** Integral Hinge Joint. Annals of the Rheumatic Diseases, 28, Supplement, 59-62.

42 **Calnan JS and Reis (1968).** Artificial Finger Joints in Rheumatoid Arthritis. I Development and Experimental Assessment. Annals of the Rheumatic Diseases, 27, 207-218.

43 **Griffiths RW and Nicolle FV (1975).** Three Years' Experience of Metacarpo-Phalangeal Joint Replacement in the Rheumatoid Hand. The Hand, 7, 3, 275-283.

44 **Nicolle FV (1977).** Modified Design of Encapsulated Metacarpo-Phalangeal Joint Prosthesis for the Rheumatoid Hand. IMechE, 133-135.

45 **Nicolle FV and Gilbert S (1979).** Assessment of Past Results and Current Practice in the Treatment of Rheumatoid Metacarpo-Phalangeal Joints. Five Year Review. The Hand, 11, 2, 151-156.

46 **Niebauer JJ, Shaw JL and Doren WW (1969).** Silicone-Dacron Hinge Prosthesis. Design, Evaluation and Application. Annals of the Rheumatic Diseases, 28, Supplement 56-58.

47 **Niebauer JJ and Landry RM (1971).** Dacron-Silicone Prosthesis for the Metacarpo-Phalangeal and Interphalangeal Joints. The Hand, 3, 1, 55-61.

48 **Kessler I (1974).** A New Silicone Implant for Replacement of Destroyed Metacarpal Heads. The Hand, 6, 3, 308-310.

49 **Goldner JL and Urbaniak JR (1973).** The Clinical Experience with Silicone-Dacron Metacarpo-Phalangeal Joint and Interphalangeal Joint Prostheses. Journal of Biomedical Materials Research Symposium, 4, 137-163.

50 **Urbaniak JR (1974).** Prosthetic Arthroplasty of the Hand. Clinical Orthopaedics and Related Research, 104, October, 9-22.

51 **Bieber EJ, Weiland AJ and Volenec-Dowling S (1986).** Silicone-Rubber Implant Arthroplasty of the Metacarpo-Phalangeal Joints for Rheumatoid Arthritis. Journal of Bone and Joint Surgery, 68-A, 2, 206-209.

52 **Braun RM and Chandler J (1972).** Quantitative Results Following Implant Arthroplasty of the Proximal Finger Joints in the Arthritic Hand. Clinical Orthopaedics and Related Research, 83, 135-143.

53 **Mannerfelt L and Andersson K (1975).** Silastic Arthroplasty of the Rheumatoid Hand. Irish Medical Journal, 80, 2, 58-60.

54 **Beckenbaugh RD, Dobyns JH, Linscheid RL and Bryan RS (1976).** Review and Analysis of Silicone-Rubber Metacarpo-Phalangeal Implants. Journal of Bone and Joint Surgery, 58-A, 4, 483-487.

55 **Derkash RS, Niebauer JJ and Lane CS (1986).** Long-Term Follow-Up of Metacarpal-Phalangeal Arthroplasty with Silicone Dacron Prostheses. Journal of Hand Surgery, 11-A, 4, 553-558.

56 **Urbaniak JR, McCollum DE and Goldner JL (1970).** Metacarpo-Phalangeal and Interphalangeal Joint Reconstruction. Southern Medical Journal, 63, 11, 1281-1290.

57 **Wilson YG, Sykes PJ and Niranjan NS (1993).** Long-Term Follow-Up of Swanson Silastic Arthroplasty of the Metacarpo-Phalangeal Joints in Rheumatoid Arthritis. Journal of Hand Surgery (British and European Vol), 18-B, 81-91.

58 **Hagert CG (1975).** Metacarpo-Phalangeal Joint Implants. Scandinavian Journal of Plastic and Reconstructive Surgery, 9, 216-226.

59 **Gillespie TE, Flatt AE, Youm Y and Sprague BL (1979).** Biomechanical Evaluation of Metacarpo-Phalangeal Joint Prosthesis Designs. Journal of Hand Surgery, 4, 6, 508-521.

60 **Steffee AD, Beckenbaugh RD, Linscheid RL and Dobyns JH (1981).** The Development, Technique and Early Clinical Results of Total Joint Replacement for the Metacarpo-Phalangeal Joint of the Fingers. Orthopaedics, 4, 2, 175-180.

61 **Walker PS, Straub IR, Davidson W and Moneim MS (1977).** Development and Evaluation of a Mechanical Finger Prosthesis. IMechE, 127-129.

62 **Deavas M and Shah V (1975).** Link Arthroplasty of the Metacarpo-Phalangeal Joints. Journal of Bone and Joint Surgery, 57-B, 1, 72-77.

63 **Schetrumpf J (1975).** A New Metacarpo-Phalangeal Joint Prosthesis. The Hand, 7, 1, 75-77.

64 **Doi K, Kuwata N and Kawai S (1984).** Alumina Ceramic Finger Implants : A Preliminary Biomaterial and Clinical Evaluation. Journal of Hand Surgery, 9-A, 5, 740-749.

65 **Minami M, Yamazaki J, Kato S and Ishii S (1988).** Alumina Ceramic Prosthesis Arthroplasty of the Metacarpo-Phalangeal Joint in the Rheumatoid Hand. Journal of Arthroplasty, 3, 2, 157-166.

66 **Adams BD, Blair WF and Shurr DG (1990).** Schultz Metacarpo-Phalangeal Arthroplasty: A Long-Term Follow-Up Study. Journal of Hand Surgery, 15-A, 4, 641-645.

67 **Linscheid RL, Dobyns JH, Beckenbaugh RD and Cooney WP (1979).** Proximal Interphalangeal Joint Arthroplasty with a Total Joint Design. Mayo Clinic. Proceedings, 54, 227-240.

68 **Weightman B, Evans DM and Light D (1983).** The Laboratory Development of a New Metacarpo-Phalangeal Prosthesis. The Hand, 15, 1, 57-68.

69 **Welsh RP, Hastings DE and White R (1982).** Resurfacing Arthroplasty for the Metacarpo-Phalangeal Joint. Acta Orthopaedica Belgica, 48, 6, 924-927.

70 **Beckenbaugh RD (1983).** Preliminary Experience With a Non-Cemented Non-Constrained Total Joint Arthroplasty for the Metacarpo-Phalangeal Joints. Orthopaedics, 6, 8, 962-965.

71 **Hagert CG, Branemark PI, Albretsson T, Strid KG and Irstam L (1986).** Metacarpo-Phalangeal Joint Replacement with Osseointegrated Endoprostheses. Scandinavian Journal of Plastic and Reconstructive Surgery, 20, 207-218.

72 **UK Patent Application GB 2 126 097 A** (Application No 8318105)

73 **Sibly TF and Unsworth A (1991).** Wear of XLPE against Itself: A Material Suitable for Surface Replacement of the Finger Joint. Journal of Biomedical Engineering, 13, May, 217-220.

74 **Stokoe SM (1990).** A Finger Function Simulator . PhD Thesis, University of Durham.

75 **Swanson AB, Matev IB, De Groot G (1974).** The Strength of the Hand. New York University Medical School Interclinical Information Bulletin, 13, 1, 1-8.

76 **Unsworth A (1971).** A Study of Some Physical and Tribological Characteristics of Human Joints. PhD Thesis, University of Leeds.

77 **Solonen KA and Hoyer P (1967).** Positioning of the Pulley Mechanism when Reconstructing Deep Flexor Tendons of Fingers. Acta Orthopaedica Scandinavica, 38, 3, 321-328.

78 **The Committee on Joint Motion, American Academy of orthopaedic Surgeons**. As quoted in Joint Motion : Methods of Measuring and Recording. American Acta of Orthopaedic Surgery 1965.

79 **Kuczynski K (1975)**. Less-Known Aspects of the Proximal Interphalangeal Joints of the Human Hand. The Hand, 7, 1, 31-33.

80 **Marsden DC and Nicol AC (1994).** Geometric Modelling for Metacarpo-Phalangeal Joint Prosthesis Stems. 7th Meeting of the European Society of Biomechanics, July 8-11, Aarhus, Denmark.

81 **Cooper JR, Dowson D and Fisher J (1992).** Mechanisms of the Generation of Wear Particles of UHMWPE. Wear Particles, D. Dowson et al (Eds). Elsevier Science Publishers BV, 29-39.

82 **Saikko V (1993).** Wear and Friction Properties of Prosthetic Joint Materials Evaluated on a Reciprocating Pin-on-Flat Apparatus. Wear, 166, 169-178.

83 **Short C (1993).** Wear Testing on Polyethylene for Finger Joint Replacement. Third Year Report, University of Durham.

84 **Walker DA (1990).** An Investigation into the Wear of a XLPE Finger Prosthesis. Third Year Report. University of Durham.

85 **Bromley J (1989).** The Design and Application of Microprocessor Based Systems for Clinical Measurement of Joint Stiffness and Grip Strength. PhD Thesis, University of Durham.

86 **Fisher J.** Wear of UHMWPE in Total Artificial Joints. Current Orthopaedics, 164-169.

87 **Brown KJ, Atkinson JR, Dowson D and Wright V (1976).** The Wear of UHMWPE and a Preliminary Study of its Relation to the In-Vivo Behaviour of Replacement Hip Joints. Wear, 40, 255-264.

88 **Cooper JR, Dowson D and Fisher J (1993).** The Effect of Transfer Film and Surface Roughness on the Wear of Lubricated UHMWPE. Clinical Materials, 14, 295-302.

89 **Kumar P, Oka M, Ikeuchi K, Shimizu K, Yamamuro T, Okumura H and Kotoura Y (1991).** Low Wear Rate of UHMWPE against Zirconia Ceramic in Comparison to Alumina Ceramic and SUS 316L Alloy. Journal of Biomechanical Materials Research, 25, 813-828.

90 **McKellop H (1981).** Wear of Artificial Joint Materials II. Twelve-Channel Wear-Screening Device: Correlation of Experimental and Clinical Results. Engineering in Medicine, 10, 3, 123-136.

91 **Archard JF (1953).** Contact and Rubbing of Flat Surfaces. Journal of Applied Physics, 24, 8, 981-989.

92 **Williams JA (1994).** Engineering Tribology. Oxford: Oxford University Press. Oxford Science Productions.

93 **Cooper JR, Dowson D and Fisher J (1993).** Macroscopic and Microscopic Wear Mechanisms in UHMWPE. Wear, 162-164, 378-384.

94 **Brown KJ, Atkinson JR and Dowson D (1982).** The Wear of UHMWPE. Part II: The Effects of Reciprocating Motion, Orientation in the Polyethylene, and a Preliminary Study of the Wear of Polyethylene Against Itself. Journal of Lubrication Technology, 104, January 17-22.

95 Standard practise for reciprocating pin-on-flat evaluation of friction and wear properties of polymeric materials for use in total joint prostheses. ASTM Designation: F 732 - 82 (Reapproved 1991). ASTM Committee F-4 on Medical and Surgical Materials and Devices. ASTM standards.

96 **Dumbleton JH (1978).** Wear and its Measurement for Joint Prosthesis Material. Wear, 49, 297-326.

97 **Atkinson JR (1976).** An Investigation into the Wear of UHMWPE when a Polyethylene Wear Pin is Loaded Against a Reciprocating Polyethylene Counterface Lubricated by Bovine Synovial Fluid at Ambient Temperature (18°C). Leeds University.

98 **Bellow DG and Viswanath NS (1993).** An Analysis of the Wear of Polymers. Wear, 162-164, 1048-1053.

99 **Wright KWJ, Dobbs HS and Scales JT (1982).** Wear Studies on Prosthetic Materials Using Pin-on-Disc Machine. Biomaterials, 3, January, 41-48.

100 **Ben Abdallah A and Treheux D (1991).** Friction and Wear of UHMWPE Against New Ceramics. Wear, 142, 43-56.

101 **Weightman B and Light D (1985).** A Comparison of RCH 1000 and Hi-Fax 1900 UHMWPEs. Biomaterials, 6, May, 177-183.

102 **Weightman B and Light D (1986).** The Effect of the Surface Finish of Alumina and Stainless Steel on the Wear Rate of UHMWPE. Biomaterials, 7, January, 20-24.

103 **Joyce TJ, Ash HE and Unsworth A (1996).** The Wear of Cross-Linked Polyethylene against Itself. Part H: Journal of Engineering in Medicine, 210, 11-16.

104 **Caravia L, Dowson D, Fisher J and Jobbins B (1990).** The Influence of Bone and Bone Cement Debris on Counterface Roughness in Sliding Wear Tests of UHMWPE on Stainless Steel. Part H: Journal of Engineering in Medicine, 204, 65-70.

105 **Dowson D, Taheri S and Wallbridge NC (1987).** The Role of Counterface Imperfections in the Wear of Polyethylene. Wear, 119, 277-293.

106 **Tweedale PJ.** Factors Affecting the Wear of Prostheses Materials. National Centre of Tribology. AEA Technology.

107 **Shen C and Dumbleton JH (1974).** The Friction and Wear Behaviour of Irradiated Very High Molecular Weight Polyethylene. Wear, 30, 349-364.

108 **Fisher J, Chan KL, Hailey JL, Shaw D and Stone M (1995).** Preliminary Study of the Effect of Ageing Following Irradiation on the Wear of UHMWPE. Journal of Arthroplasty, 10, 5, 689-692.

109 **Wang A, Sun DC, Stark C and Dumbleton JH (1996).** Effects of Sterilisation Methods on the Wear of UHMWPE Acetabular Cups. Fifth World Biomaterials Congress. May 29 - June 2, Toronto, Canada.

110 **Thompson DT, Wright V and Dowson D (1978).** A New Form of Knee Arthrograph for the Study of Stiffness. Engineering in Medicine, 7, 2, 84-92.

111 **Helliwell PS, Howe A and Wright V (1987).** The Measurement of Stiffness in the Rheumatoid Hand. Engineering in Medicine, 16, 4, 203-207.

112 **Yung P, Unsworth A and Haslock I (1984).** Measurement of Stiffness in the Metacarpo-Phalangeal Joint: Circadian Variation. Clin. Phys. Physiol. Meas. 5, 2, 57-65.

113 **Wright V and Johns RJ (1960).** Observations on the Measurement of Joint Stiffness. Arthritis and Rheumatism, 3, 328-340.

114 **Unsworth A, Yung P and Haslock I (1982).** Measurement of Stiffness in the Metacarpo-Phalangeal Joint: The Arthrograph. Clin. Phys. Physiol. Meas. 3, 4, 273-281.

115 **Scott JT (1960).** Morning Stiffness in Rheumatoid Arthritis. Annals of the Rheumatic Diseases, 19, 361-368.

116 **Steinbrocker O, Traeger CH and Batterman RC (1949).** Therapeutic Criteria in Rheumatoid Arthritis. Journal of the American Medical Association, 140, 8, 659-662.

117 **Bromley J, Unsworth A and Haslock I (1994).** Changes in Stiffness Following Short and Long-Term Application of Standard Physiotherapeutic Techniques. British Journal of Rheumatology, 33, 1-6.

118 **Rhind VM (1988).** The Validity and Inter-relationship of Subjective and Objective Measurements of Stiffness in Human Joints. MSc Thesis, University of Durham.

119 **Backlund L and Tiselius P (1967).** Objective Measurement of Joint Stiffness in Rheumatoid Arthritis. Acta Rheumatologica Scandinavica, 13, 275-288.

120 **Such CH, Unsworth A, Wright V and Dowson D (1975).** Quantitative Study of Stiffness in the Knee Joint. Annals of the Rheumatic Diseases, 34, 286-291.

121 **Unsworth A, Bey PMA and Haslock I (1981).** Stiffness in the Metacarpo-Phalangeal Joints of Young Adults. Clin. Phys. Physiol. Meas. 2, 2, 123-133.

122 **Howe A, Thompson D and Wright V (1985).** Reference Values for Metacarpo-Phalangeal Joint Stiffness in Normals. Annals of the Rheumatic Diseases, 44, 469-476.

123 **Sundararaj and Mani (1984).** Interphalangeal Joint Stiffness Following Claw Hand Reconstruction. Journal of Hand Surgery, 9B, 1, February, 79-82.

124 **Flowers KR and Pheasant SD (1988).** The Use of Torque Angle Curves in the Assessment of Digital Joint Stiffness. Journal of Hand Therapy, January-March, 69-74.

125 **Yung P, Unsworth A and Haslock I (1986).** Measurement of Stiffness in the Metacarpo-Phalangeal Joint: The Effects of Physiotherapy. Clin Phys Physiol Meas, 7, 2, 147-156.

126 **Wright V and Plunkett TG (1966).** Scientific Assessment of the Results of Physical Treatment - Measurement of Stiffness. Annals of Physical Medicine, 8, 280-291.

127 **Yung P (1981).** The Human Metacarpo-Phalangeal Joint: Quantification of Stiffness and the Effects of treatment. MSc Thesis, University of Durham.

128 **Wright V (1959).** Some Observation on Diurnal Variation of Grip. Clinical Science, 18, 17-23.

129 **Harkness JAL, Richter MB, Panayi GS, Van de Pette K, Unger A, Pownall R and Geddawi M (1982).** Circadian Variation in Disease Activity in Rheumatoid Arthritis. British Medical Journal, 284, 20, February, 551-554.

130 **Kowanko IC, Pownall R, Knapp MS, Swannell AJ and Mahoney PGC (1981).** Circadian Variations in the Signs and Symptoms of Rheumatoid Arthritis and in the Therapeutic Effectiveness of Flurbiprofen at Different Times of Day. Journal of Clinical Pharmacology, 11, 477-484.

131 **Kowanko IC, Knapp MS, Pownall R and Swannell AJ (1982).** Domicilary Self-Measurement in Rheumatoid Arthritis and the Demonstration of Circadian Rhymicity. Annals of the Rheumatic Diseases, 41, 453-455.

132 **Myers DB, Grennan DM and Palmer DG (1980).** Hand Grip Function in Patients with Rheumatoid Arthritis. Archives of Physical Medicine and Rehabilitation, 61, 369-373.

133 **Dellhag B, Wollersjo I and Bjelle A (1992).** Effect of Active Hand Exercise and Wax Bath Treatment in Rheumatoid Arthritic Patients. Arthritis Care and Research, 5, 2, June, 87-92.

134 **Myers DB, Wilson K and Palmer DG (1979).** Relative Changes in Maximum Grip Strength, Work and Power Output During Hand Grip Assessment of Rheumatoid Patients in a Drug Trial. Proceedings. University of Otago Medical School, 57, 3, 64-65.

135 **Myers DB, Wilson K and Palmer DG (1981).** An Objective Measurement of Change in Morning Stiffness. Rheumatology, 135-137.

136 **Jette AM (1980).** Functional Status Index: Reliability of a Chronic Disease Evaluation Instrument. Archives of Physical Medicine and Rehabilitation, 61, 395-401.

137 **Streiner DL and Norman GR (1989).** Health Measurement Scales. A Practical Guide to their Development and Use. Oxford University Press, New York.

138 **Downie WW, Leatham PA, Rhind VM, Wright V, Branco JA and Anderson JA (1978).** Studies with Pain Ratings Scales. Annals of the Rheumatic Diseases, 37, 378-381.

139 **Adenbrooke's Hospital.** Occupational Therapy Department, Unilateral-Bilateral Hand Function Test Score Sheet.

140 **Leeds Hand Assessment.**

141 **Dixon JS and Bird HA (1981).** Reproducibility along a 10 cm Vertical Visual Analogue Scale. Annals of the Rheumatic Diseases, 40, 87-89.

142 **Dellhag B and Burckhardt CS (1995).** Predictors of Hand Function in Patients with Rheumatoid Arthritis. Arthritis Care and Research, 8, 1, 16-20.

143 **Ekdahl C, Eberhardt K, Andersson SI and Svensson B (1988).** Assessing Disability in Patients with Rheumatoid Arthritis. Scandinavian Journal of Rheumatology, 17, 263-271.

144 **Health Assessment Questionnaire (HAQ).**

145 **Huskisson EC, Jones J and Scott PJ (1976).** Application of Visual-Analogue Scales to the Measurement of Functional Capacity. Rheumatism and Rehabilitation, 15, 185-187.

146 **Huskisson EC, Sturrock RD and Tugwell P (1983).** Measurement of Patient Outcome. British Journal of Rheumatology, 22, Supplement 86-89.

147 **Lorig K, Chastin RL, Ung E, Shoor S and Holman HR (1989).** Development and Evaluation of a Scale to Measure Perceived Self-Efficacy in People with Arthritis. Arthritis and Rheumatism, 32, 1, 37-44.

148 **Scott J and Huskisson EC (1979).** Accuracy of Subjective Measurement Made With or Without Previous Scores: An Important Source of Error in Serial measurement of Subjective States. Annals of the Rheumatic Diseases, 38, 558-559.

149 **Tugwell P, Bombardier T, Buchanan WW, Goldsmith CH, Grace E and Hanna B (1987).** The MACTAR Patient Preference Disability Questionnaire - An Individualised Functional Priority Approach for Assessing Improvement in Physical Disability in Clinical Trials in Rheumatoid Arthritis. Journal of Rheumatology, 14, 3, 446-451.

150 **Downie WW, Leatham PA, Rhind VM, Pickup ME and Wright V (1978).** The Visual Analogue Scale in the Assessment of Grip Strength. Annals of the Rheumatic Diseases, 37, 382-384.

151 **Taal E, Rasker JJ, Seydel ER and Wiegman O (1993).** Health Status, Adherence with Health Recommendations, Self-Efficacy and Social Support in Patients with Rheumatoid Arthritis. Patient Education and Counselling, 20, 63-76.

152 **Dixon JS, Pickup ME, Lowe JR, Hallett C, Lee MR and Wright V (1980).** Discriminatory Indices of Response of Patients with Rheumatoid Arthritis Treated with D-Penicillamine. Annals of the Rheumatic Diseases, 39, 301-311.

153 **Rhind VM, Bird HA and Wright V (1980).** A Comparison of Clinical Assessments of Disease Activity in Rheumatoid Arthritis. Annals of the Rheumatic Diseases, 39, 135-137.

154 **Scott J and Huskisson EC (1979).** Vertical or Horizontal Visual Analogue Scales. Annals of the Rheumatic Diseases, 38, 560.

155 **Canter GJ, De La Torre R and Mier M (1961).** A Method for Evaluating Disability in Patients with Parkinson's Disease. Journal of Nervous and Mental Disease, 133, 143-147.

156 **Recht L, Lithman T, Rasmussen JO and Mathiesen FK (1988).** A Test to Detect Hand Dysfunction. The Practitioner, 232, 1236-1239.

157 **Nottingham City Hospital and University.** Arthritis in the Community Questionnaire.

158 **MacBain KP and Reg OT (1970).** Assessment of Function in the Rheumatoid Hand. CJOT, 37, 3, 95-102.

159 **McGuire RJ and Wright V (1971).** Statistical Approach to Indices of Disease Activity in Rheumatoid Arthritis, with Reference to a Trial of Indomenthacin. Annals of the Rheumatic Diseases, 30, 574-580.

160 **Odstock Hospital, Rehabilitation Unit.** Hand Assessment.

161 **Meenan RF, Gertman PM and Mason JH (1980).** Measuring Health Status in Arthritis. Arthritis and Rheumatism, 23, 2, 146-152.

162 **Ritchie DM, Boyle JA, McInnes JM, Jasani MK, Dalakos TG, Grieveson P and Buchanan WW (1968).** Clinical Studies with an Articular Index for the Assessment of Joint Tenderness in Patients with Rheumatoid Arthritis. Quarterly Journal of Medicine, 37, 147, 393-406.

163 **Convery FR, Minteer MA, Amiel D and Connett KL (1977).** Polyarticular Disability: A Functional Assessment. Archives of Physical and Medical Rehabilitation, 58, 494-499.

164 **Fries JF, Spitz P, Kraines RG and Holman HR (1980).** Measurement of Patient Outcome in Arthritis. Arthritis and Rheumatism, 23, 2, 137-145.

165 **Lee P, Jasani MK, Dick WC and Buchanan WW (1973).** Evaluation of a Functional Index in Rheumatoid Arthritis. Scandinavian Journal of Rheumatology, 2, 71-77.

166 **Carthum CJ, Clawson DK and Decker JL (1969).** Functional Assessment of the Rheumatoid Hand. American Journal of Occupational Therapy, 23, 122-125.

167 **Backman C, Mackie H and Harris J (1991).** Arthritis Hand Function Test: Development of a Standardised Assessment Tool. The Occupational Therapy Journal of Research, 11, 4, 244-256.

168 **Backman C and Mackie H (1995).** Arthritis Hand Function Test: Inter-Rater Reliability Among Self-Trained Raters. Arthritis Care and Research, 8, 1, 10-15.

169 **Jebsen RH, Taylor Nm Trieschmann RB, Trotter MJ and Howard LA (1969).** An Objective and Standardised Test of Hand Function. Archives of Physical and Medical Rehabilitation, 50, 311-319.

170 **Smith HB (1973).** Smith Hand Function Evaluation. American Journal of Occupational Therapy, 27, 5, 244-251.

171 **Archenholtz B and Bjelle A (1991).** Reliability and Validity of a Swedish Version of the Arthritis Impact Measuring Scales. Scandinavian Journal of Rheumatology, 20, 219.

172 **Yelin E, Lubeck D, Holman H and Epstein W (1987).** The Impact of Rheumatoid Arthritis and Osteoarthritis: The Activities of Patients with Rheumatoid Arthritis and Osteoarthritis Compared with Controls. Journal of Rheumatology, 14, 4, 710-717.

173 **Katz S, Downs TD, Cash HR and Grotz RC (1970).** Progress in Development of the Index of ADL. The Gerontologist, 1, 20-30.

174 **MACTAR Assessment Questionnaire.**

175 **Chao EY, Opgrande JD and Axmear FE (1976).** Three-Dimensional Force Analysis of Finger Joints in Selected Isometric Hand Functions. J Biomechanics, 9, 387-396.

176 **Chao EY and An KN (1978).** Determination of Internal Forces in the Human Hand. Journal of the Engineering Mechanics Division, 255-272.

177 **Weightman B and Amis AA (1982).** Finger Joint Force Predictions Related to Design of Joint Replacements. J Biomed Eng, 4, 197-205.

178 **An KN, Cooney WP, Chao EY and Linscheid RL (1978).** Functional Strength Measurement of Normal Fingers. Orthopaedic Biomechanics Laboratory, Mayo Clinic.

179 **Swanson AB, Matez IB and De Groot G (1974).** The Strength of the Hand. NY University Medical School Interclinical Information Bulletin, 13, 1, 1-8.

180 **Cantrell T (1976).** Measurement of Weakness and Dysfunction in the Rheumatoid Hand. Rheumatol Rehabil, 15, 182-184.

181 **Pearson R, MacKinnon MJ, Meek AP, Myers DB and Palmer DG (1982).** Diurnal and Sequential Grip Function in Normal Subjects and Effect of Temperature Change and Exercise of the Forearm on Grip Function in Patients with Rheumatoid Arthritis and in Normal Controls. Scand J Rheumatology, 11, 113-118.

APPENDICES

APPENDIX ONE

PIPJ dimensions grouped by individual fingers (index, middle, ring and little)

Table A1.1 PP head diameter (D), sagittal plane (mm)

	Right				Left			
	Index	Middle	Ring	Little	Index	Middle	Ring	Little
1	9	9.5	8.5	7.5				
3	9.5	10	9	8.5	9	10	9	8
4	10	11	10	8	9	10	9.5	7.5
5	10	10	9.5	7.5	9.5	9.5	9	7.5
6	10	10	9.5	7.5	10	9.5	9	7.5
7	8.5	9.5	8.5	7.5	9.5	9.5	/	7
8	8.5	8	7.5	/	8.5	8.5	7.5	6
9	10	10	9	8	10	10	8.5	8
10	8.5	8	8.5	7	8	9	8.5	7
11	7.5	8	8.5	7.5	9.5	8	7.5	6.5
12	9	9	9	7	9	9	8.5	8
Mean	**9.14**	**9.36**	**8.86**	**7.60**	**9.20**	**9.30**	**8.56**	**7.20**
S.D.	**0.80**	**0.96**	**0.64**	**0.44**	**0.60**	**0.64**	**0.64**	**0.60**
Overall mean	**9.17**	**9.33**	**8.73**	**7.40**				
S.D.	**0.71**	**0.82**	**0.66**	**0.56**				
Male mean	**9.42**	**9.73**	**9.04**	**7.58**				
S.D.	**0.65**	**0.67**	**0.46**	**0.43**				
Female mean	**8.75**	**8.69**	**8.14**	**7.07**				
S.D.	**0.61**	**0.61**	**0.58**	**0.62**				
Difference (%)	**7.66**	**11.97**	**11.06**	**7.21**				

Table A1.2 MP head diameter (D), sagittal plane (mm)

	Right				Left			
	Index	Middle	Ring	Little	Index	Middle	Ring	Little
1	6.0	6.5	6.0	5.5				
3	6.5	7.5	6.5	5.5	6.0	7.5	6.0	6.0
4	7.5	7.0	7.5	6.0	7.0	7.5	7.0	5.5
5	6.5	7.0	6.0	5.0	6.5	6.5	6.0	5.0
6	7.0	7.0	6.5	5.0	6.0	6.5	6.0	5.0
7	6.5	6.5	6.0	5.0	6.5	6.5		5.0
8	7.0	6.0	5.5		5.5	5.5	5.0	5.0
9	6.5	7.5	6.5		7.0	7.5	6.5	6.0
10	6.5	5.5	6.5	5.0	6.5	7.0	7.0	5.5
11	6.0	6.5	7.0	5.5	6.0	6.5	5.5	5.5
12	7.5	6.5	6.0	5.5	6.5	6.5	5.5	6.0
Mean	**6.68**	**6.68**	**6.36**	**5.33**	**6.35**	**6.75**	**6.06**	**5.45**
S.D.	**0.49**	**0.57**	**0.53**	**0.33**	**0.45**	**0.60**	**0.64**	**0.42**
Overall mean	**6.52**	**6.71**	**6.23**	**5.39**				
S.D.	**0.50**	**0.59**	**0.60**	**0.38**				
Male mean	**6.58**	**6.96**	**6.46**	**5.42**				
S.D.	**0.43**	**0.57**	**0.46**	**0.40**				
Female mean	**6.44**	**6.31**	**5.79**	**5.36**				
S.D.	**0.58**	**0.35**	**0.59**	**0.35**				
Difference (%)	**2.17**	**10.30**	**11.57**	**1.12**				

Table A1.3 PP maximum head height (Htp), transverse plane (mm)

	Right				Left			
	Index	Middle	Ring	Little	Index	Middle	Ring	Little
1	8.7	8.8	9.1	7.2				
3	9.2	11.4	8.5	7.7	9.1	9.5	8.6	8.1
4	9.2	9.5	9.2	7.6	9.0	9.4	8.9	7.4
5	9.5	10.6	9.4	7.7	9.1	10.7	9.5	7.4
6	8.7	9.2	9.1	7.3	8.9	9.6	8.3	7.2
7	8.7	9.4	8.2	7.6	9.3	9.6		7.7
8	8.4	8.8	7.8		8.1	8.4	7.8	4.9
9	10.2	10.5	9.7	7.9	10.0	10.3	9.7	8.0
10	8.8	8.0	8.6	7.3	8.6	8.9	8.9	6.9
11	7.7	8.0	8.2	6.3	8.2	8.1	7.8	6.4
12	8.8	9.6	9.2	7.8	8.8	9.8	8.8	7.7
Mean	**8.90**	**9.44**	**8.82**	**7.44**	**8.91**	**9.43**	**8.70**	**7.17**
S.D.	**0.61**	**1.02**	**0.57**	**0.44**	**0.52**	**0.75**	**0.63**	**0.90**
Overall mean	**8.81**	**9.43**	**8.77**	**7.31**				
S.D.	**0.59**	**0.90**	**0.60**	**0.72**				
Male mean	**9.15**	**9.72**	**9.04**	**7.52**				
S.D.	**0.47**	**0.90**	**0.44**	**0.34**				
Female mean	**8.50**	**8.96**	**8.26**	**6.91**				
S.D.	**0.47**	**0.68**	**0.51**	**1.01**				
Difference (%)	**7.65**	**8.48**	**9.44**	**8.83**				

Table A1.4 PP head maximum condyle diameter (Dmax), sagittal plane (mm)

	Right				Left			
	Index	Middle	Ring	Little	Index	Middle	Ring	Little
1	8.5	9	8.5	7				
3	9	10	8	8	8.5	9.5	8.5	7
4	9.5	9.5	9	7.5	8.5	9	9	7.5
5	9.5	9.5	9	7.5	9	9.5	8.5	7.5
6	8.5	9	8.5	7	9	9	8.5	7.5
7	8	9	8.5	7	8	9		7
8	7.5	7.5	7.5		8	7.5	7	6
9	9.5	9.5	8.5	7.5	9	9	8.5	8
10	8.5	7.5	8.5	6.5	8	8.5	8	6.5
11	7	8	8.5	7	9.5	8	7.5	6.5
12	8.5	8.5	8	7	8.5	9	8.5	7
Mean	**8.55**	**8.82**	**8.41**	**7.20**	**8.60**	**8.80**	**8.22**	**7.05**
S.D.	**0.78**	**0.81**	**0.42**	**0.40**	**0.49**	**0.60**	**0.58**	**0.57**
Overall mean	**8.57**	**8.81**	**8.33**	**7.13**				
S.D.	**0.66**	**0.72**	**0.51**	**0.50**				
Male mean	**8.85**	**9.12**	**8.54**	**7.29**				
S.D.	**0.46**	**0.59**	**0.31**	**0.45**				
Female mean	**8.07**	**8.31**	**7.93**	**6.79**				
S.D.	**0.73**	**0.61**	**0.56**	**0.36**				
Difference (%)	**9.67**	**9.75**	**7.66**	**7.36**				

Table A1.5 PP head minimum condyle diameter (Dmin), sagittal plane (mm)

	Right				Left			
	Index	Middle	Ring	Little	Index	Middle	Ring	Little
1	8	8.5	8	6.5				
3	7.5	8.5	7.5	7	7	8	7.5	6.5
4	8	8.5	8	7	7.5	8	8	6.5
5	8.5	8.5	8	6.5	8	8.5	7.5	6.5
6	8	8.5	8	6.5	8	8.5	8	6.5
7	7.5	8.5	7.5	6	7.5	8		6
8	7.5	7	6.5		6.5	7.5	6.5	5.5
9	8	8.5	8	6.5	8	8	8	7.5
10	7.5	6.5	7.5	6	6.5	7.5	7	6
11	6.5	7	7	6	6.5	6.5	6	6
12	7.5	8	7.5	6.5	8	8	7.5	6.5
Mean	**7.68**	**8.00**	**7.59**	**6.45**	**7.35**	**7.85**	**7.33**	**6.35**
S.D.	**0.49**	**0.74**	**0.47**	**0.35**	**0.63**	**0.55**	**0.67**	**0.50**
Overall mean	**7.52**	**7.93**	**7.48**	**6.40**				
S.D.	**0.59**	**0.66**	**0.58**	**0.44**				
Male mean	**7.73**	**8.15**	**7.77**	**6.58**				
S.D.	**0.50**	**0.56**	**0.32**	**0.38**				
Female mean	**7.19**	**7.56**	**6.93**	**6.07**				
S.D.	**0.56**	**0.63**	**0.56**	**0.32**				
Difference (%)	**7.51**	**7.80**	**12.12**	**8.40**				

Table A1.6 MP base maximum condyle diameter (Dbmax), sagittal plane (mm)

	Right				Left			
	Index	Middle	Ring	Little	Index	Middle	Ring	Little
1	13	13	11	9				
3	12	11	12	11	11	12	12	10
4	13	13	13	9	13	12	12	10
5	13	13	12	10	11	13	10	10
6	12	13	13	13	13	13	11	12
7	13	13	13	11	11	13		10
8	10	10	9		11	11	13	8
9	12	13	12		12	12	13	11
10	12	12	11	8	11	11	11	9
11	10	11	11		9	9	10	9
12	13		13	12	10	11	13	11
Mean	**12.09**	**12.20**	**11.82**	**10.38**	**11.20**	**11.70**	**11.67**	**10.00**
S.D.	**1.08**	**1.08**	**1.19**	**1.58**	**1.17**	**1.19**	**1.15**	**1.10**
Overall mean	**11.67**	**11.95**	**11.75**	**10.17**				
S.D.	**1.21**	**1.16**	**1.18**	**1.34**				
Male mean	**12.15**	**12.38**	**11.77**	**10.17**				
S.D.	**0.77**	**0.74**	**0.89**	**1.34**				
Female mean	**10.88**	**11.14**	**11.71**	**10.17**				
S.D	**1.36**	**1.36**	**1.58**	**1.34**				
Difference (%)	**11.70**	**11.13**	**0.51**	**0.00**				

Table A1.7 MP base minimum condyle diameter (Dbmin), sagittal plane (mm)

	Right				Left			
	Index	Middle	Ring	Little	Index	Middle	Ring	Little
1	9	9	9	7				
3	10	9	9	8	10	9	9	8
4	10	11	9	8	9	9	9	7
5	9	7	9	7	8	9	9	7
6	9	9	10	9	8	10	8	9
7	11	11	9	8	6	10		6
8	9	9	7		8	7	8	7
9	8	9	8		8	9	11	8
10	9	9	10	7	8	7	8	7
11	8	8	9		7	7	6	7
12	8		9	8	7	9	8	7
Mean	**9.09**	**9.10**	**8.91**	**7.75**	**7.90**	**8.60**	**8.44**	**7.30**
S.D.	**0.90**	**1.14**	**0.79**	**0.66**	**1.04**	**1.11**	**1.26**	**0.78**
Overall mean	**8.52**	**8.85**	**8.70**	**7.50**				
S.D.	**1.14**	**1.15**	**1.05**	**0.76**				
Male mean	**8.84**	**8.92**	**9.08**	**7.67**				
S.D.	**0.77**	**1.00**	**0.83**	**0.75**				
Female mean	**8.00**	**8.75**	**8.00**	**7.17**				
S.D.	**1.41**	**1.30**	**1.07**	**0.69**				
Difference (%)	**10.50**	**1.94**	**13.50**	**6.97**				

Table A1.8 PP head condyle diameters across the bone width, sagittal plane (mm)

	Whole	1	2	3	4	5	6	7	8
1RI	9	/	8.5	8.5	8	8.5	8		
1RM	9.5	/	8.5	9	8.5	8.5	9	7.5	
1RR	8.5	/	8	8	8.5	8	/		
1RL	7.5	/	7	7	6.5	6.5			
3RI	9.5	8	8.5	7.5	8.5	9	8.5		
3RM	10	/	9	9	8.5	10	11	10.5	
3RR	9	7	8.5	7.5	8	8.5	/		
3RL	8.5	8	8	7.5	7	7			
3LI	9	8.5	8.5	7	8.5	8.5	/		
3LM	10	/	9	9	8	9	9	9.5	/
3LR	9	/	8.5	8	7.5	8			
3LL	8	/	7	6.5	6.5	7			
4RI	10	/	8.5	9.5	8.5	8.5	8	9	8
4RM	11	/	9	9.5	9	8.5	9.5	9.5	/
4RR	10	/	8	8.5	8	8.5	9	8.5	/
4RL	8	/	7.5	7.5	7	7.5	7	/	
4LI	9	/	8.5	8.5	7.5	7.5	8.5	8	/
4LM	10	/	8.5	8.5	8.5	8	9	9	/
4LR	9.5	/	8.5	8.5	8.5	8	9	8.5	/
4LL	7.5	/	7	7	6.5	7.5	6.5		
5RI	10	/	8.5	9.5	8.5	8.5	9	/	
5RM	10	/	9	9.5	8.5	8.5	9.5	8.5	/
5RR	9.5	/	8	9	8	9	9	8.5	6.5
5RL	7.5	/	7	6.5	7	7.5	/		
5LI	9.5	/	9	9	8	9	8.5	/	
5LM	9.5	/	9	9.5	9	8.5	9	9	/
5LR	9	/	8.5	8.5	7.5	8.5	8		
5LL	7.5	/	7.5	7	6.5	7	/		
6RI	10	/	8.5	8.5	8	8.5	8.5	/	
6RM	10	/	8.5	9	8.5	9	9	/	
6RR	9.5	/	8.5	8.5	8	8.5	8.5		
6RL	7.5	/	6.5	7	6.5	7	7		
6LI	10	/	9	8.5	8	8.5	9	/	
6LM	9.5	/	8	9	9	8.5	9	8.5	/
6LR	9	/	7	8	8	8	8.5	7.5	
6LL	7.5	/	7.5	7	6.5	7	/		
7RI	8.5	/	8	8	7.5	8	8		
7RM	9.5	/	8.5	9	8.5	9	9		
7RR	8.5	/	8.5	7.5	8.5	8.5	8	/	
7RL	7.5	6.5	7	6	7	6	/		
7LI	9.5	/	8	7.5	7.5	8	/		
7LM	9.5	/	8.5	9	8	8.5	9	/	
7LL	7	/	7	6.5	6	6.5	/	/	

8RI	8.5	/	7.5	7.5	7.5	7.5	/		
8RM	8	/	7.5	7	7	7.5	/		
8RR	7.5	6	7	6.5	7.5	7			
8LI	8.5	/	8	6.5	7.5	7			
8LM	8.5	/	7.5	7.5	7.5	7.5	/		
8LR	7.5	/	7	6.5	6.5	6.5	/		
8LL	6	6	5.5	5.5	/				

9RI	10	8.5	9.5	8.5	8	8.5	9	8.5	/
9RM	10	8.5	9	9.5	8.5	8.5	9	9	/
9RR	9	/	8.5	8.5	8.5	8	8.5	8.5	/
9RL	8	/	7.5	7.5	6.5	7	7	/	
9LI	10	/	8.5	9	8.5	8	9	8.5	/
9LM	10	/	8.5	8.5	9	8	8.5	9	
9LR	8.5	/	7.5	8.5	8.5	8	8.5	8.5	8
9LL	8	/	7.5	8	7.5	8	8	/	

10RI	8.5	/	8	8	7.5	8.5			
10RM	8	6.5	6.5	7.5	7.5	7			
10RR	8.5	/	7.5	7.5	8	8.5	/		
10RL	7	6	6.5	6	6.5				
10LI	8	/	8	6.5	7.5	7.5	/		
10LM	9	/	8	8	7.5	8.5	/		
10LR	8.5	/	8	7.5	7	8	/	/	
10LL	7	6	6.5	6	6				

11RI	7.5	/	7	7	6.5	7	7		
11RM	8	/	7.5	7.5	7	8	8	/	
11RR	8.5	/	8.5	8	7	8.5	9	/	
11RL	7.5	/	6.5	6.5	6	7	7		
11LI	9.5	/	8.5	8	6.5	8.5	9.5	/	
11LM	8	/	8	8	6.5	7.5	8	/	
11LR	7.5	/	7.5	7	6	7	7	/	
11LL	6.5	/	6	6	6	6.5			

12RI	9	/	8.5	8	7.5	7.5	8	8	
12RM	9	/	8.5	8.5	8	8	8.5	8	/
12RR	9	7	8	7.5	7.5	8	8	/	
12RL	7	/	7	6.5	6.5	7	/		
12LI	9	/	8.5	8.5	8	8	8.5	/	
12LM	9	/	8.5	8.5	8	8	9	8.5	
12LR	8.5	/	8	8	7.5	8	8.5	7.5	
12LL	8	/	6.5	6.5	6.5	7.5	7		

Table A1.9 MP base recess diameters across the bone width, sagittal plane (mm)

	1	2	3	4	5	6	7	8	9
1RI	/	13	9	10	12	/			
1RM	/	13	12	10	9	10	11		
1RR	11	9	9	9	10	/			
1RL	/	9	9	7	7	/			
3RI	/	11	11	10	12	12	/		
3RM	/	10	10	9	11	/	/		
3RR	/	12	9	9	11	/			
3RL	/	/	8	9	9	11			
3LI	/	10	11	10	10	/	/		
3LM	/	11	9	9	11	12	/	/	
3LR	/	12	11	11	9	11	/		
3LL	/	10	9	8	9	15			
4RI	/	11	10	10	17	13	16	16	/
4RM	/	17	17	13	13	12	11	/	
4RR	/	/	12	11	9	10	11	13	
4RL	/	9	8	8	9	17	/		
4LI	/	/	15	14	9	9	13	/	
4LM	/	15	12	10	9	9	9	15	/
4LR	/	16	10	9	9	11	12	/	
4LL	/	10	8	8	7	10	/		
5RI	/	14	10	9	9	11	10	/	
5RM	/	/	14	10	9	7	10	12	/
5RR	/	10	9	9	10	12	/		
5RL	/	10	8	7	8	9	/		
5LI	/	11	9	8	11	18	/		
5LM	/	13	12	9	9	10	11	/	
5LR	/	9	9	9	10	10			
5LL	/	9	7	7	8	10			
6RI	/	12	16	10	9	10	/		
6RM	/	17	13	10	9	11	/		
6RR	/	15	12	10	12	13	/		
6RL	/	13	9	9	9	13	/		
6LI	/	/	/	14	15	12	8	9	13
6LM	/	/	15	13	11	11	11	10	/
6LR	/	/	11	10	8	9	10		
6LL	/	/	12	9	9	9	/		
7RI	/	13	12	11	14	11	/		
7RM	/	18	11	11	12	13	/		
7RR	/	13	12	10	11	9	/		
7RL	/	10	8	9	11				
7LI	/	11	9	6	8	6			
7LM	/	14	13	12	10	11			
7LL	/	10	6	6	/				

8RI	/	9	9	10	10	/			
8RM	/	15	10	9	9	10			
8RR	/	9	8	7	8				
8LI	/	8	8	11	/				
8LM	/	/	11	7	9	/			
8LR	/	14	8	8	8	/			
8LL	/	8	8	7					

9RI	/	/	8	9	12	12	/	12	
9RM	/	13	11	10	9	10	10	/	/
9RR		12	10	9	8	9	10	/	
9RL	/								
9LI	/	14	14	14	8	11	12	/	/
9LM	/	/	17	12	10	9	10	12	/
9LR	/	12	13	11	11	11	12	15	
9LL	/	11	11	9	8	11	8	/	

10RI	12	12	10	9	9	/			
10RM	14	11	9	12	15	9			
10RR	/	/	10	11	11	11			
10RL	/	8	7	7	/				
10LI	/	8	8	8	11	/			
10LM	/	7	9	10	11	14	/		
10LR	/	11	8	9	10	/			
10LL	/	9	7	9	/				

11RI	/	/	9	8	8	8	10		
11RM	/	9	11	9	8	8	11		
11RR	/	10	11	11	9	11			
11RL		9							
11LI	/	9	9	7	7	8	9		
11LM	/	/	8	8	7	9			
11LR	/	7	6	7	9	10			
11LL	/	7	8	9	9				

12RI	/	/	10	8	10	10	13	12	
12RM									
12RR	/	13	12	9	9	13	/		
12RL	/	/	12	12	8	10	/		
12LI	/	10	10	7	8	9	9	/	
12LM	/	/	11	12	9	10	11	/	
12LR	/	9	10	9	8	11	13	/	
12LL	/	/	10	8	7	11	/		

Table A1.10 PP maximum head width (W), frontal plane (mm)

	Right				Left			
	Index	Middle	Ring	Little	Index	Middle	Ring	Little
1	12.3	14.4	10.9	9.5				
3	12.7	14.7	12.1	11.0	12.4	12.9	11.9	10.8
4	13.9	14.3	13.1	11.2	13.5	14.1	13.2	10.8
5	13.2	15.6	13.7	10.9	13.6	14.7	13.3	11.1
6	12.2	13.0	12.3	10.2	12.2	12.7	12.1	10.1
7	12.1	12.9	13.1	9.8	12.0	13.0		9.7
8	11.6	11.5	10.5		11.1	11.3	11.0	8.7
9	14.4	14.8	13.7	11.6	14.1	14.7	13.6	11.8
10	12.5	12.4	11.9	10.5	12.3	13.0	12.1	10.3
11	11.0	11.9	12.5	10.2	12.3	11.6	10.8	9.4
12	12.2	12.4	11.8	10.2	12.4	12.9	11.8	10.4
Mean	**12.55**	**13.45**	**12.33**	**10.51**	**12.59**	**13.09**	**12.20**	**10.31**
S.D.	**0.93**	**1.30**	**0.99**	**0.62**	**0.84**	**1.09**	**0.93**	**0.85**
Overall mean	**12.57**	**13.28**	**12.27**	**10.41**				
S.D.	**0.89**	**1.22**	**0.97**	**0.75**				
Male mean	**13.02**	**13.95**	**12.61**	**10.75**				
S.D.	**0.76**	**0.97**	**0.84**	**0.61**				
Female mean	**11.84**	**12.19**	**10.74**	**9.77**				
S.D.	**0.51**	**0.65**	**1.46**	**0.54**				
Difference (%)	**9.97**	**14.44**	**17.19**	**10.03**				

Table A1.11 PP maximum head width (Wtp), transverse plane (mm)

	Right				Left			
	Index	Middle	Ring	Little	Index	Middle	Ring	Little
1	12.5	12.1	13.9	9.8				
3	13.0	14.0	12.0	10.7	12.5	13.8	12.2	11.5
4	13.2	13.8	14.0	11.0	13.0	14.0	13.1	10.8
5	13.9	15.3	14.3	10.6	13.9	14.6	13.7	11.0
6	12.8	13.5	12.5	10.8	12.6	13.3	12.8	10.0
7	11.8	12.7	12.6	10.6	12.5	13.8		9.6
8	12.1	12.1	11.2		11.9	11.8	11.7	8.7
9	14.5	15.0	13.7	12.2	14.4	14.7	14.0	11.6
10	13.2	11.3	13.1	10.6	12.6	13.2	12.3	10.4
11	11.8	12.2	12.5	10.0	12.2	12.1	10.9	9.7
12	12.8	12.4	12.1	10.3	12.8	12.6	12.3	10.8
Mean	**12.84**	**13.17**	**12.90**	**10.66**	**12.84**	**13.39**	**12.66**	**10.41**
S.D.	**0.81**	**1.21**	**0.93**	**0.62**	**0.72**	**0.94**	**0.91**	**0.87**
Overall mean	**12.86**	**13.25**	**12.75**	**10.54**				
S.D.	**0.76**	**1.11**	**0.94**	**0.76**				
Male mean	**13.24**	**13.74**	**13.20**	**10.85**				
S.D.	**0.68**	**1.07**	**0.75**	**0.62**				
Female mean	**12.24**	**12.46**	**11.90**	**9.96**				
S.D.	**0.39**	**0.57**	**0.61**	**0.66**				
Difference (%)	**8.17**	**10.27**	**10.92**	**8.94**				

Table A1.12 MP maximum head width (W), frontal plane (mm)

	Right				Left			
	Index	Middle	Ring	Little	Index	Middle	Ring	Little
1	9.8	10.8	10.1	8.6				
3	10.5	11.6	11.1	10.1	10.4	11.8	10.4	10.0
4	11.9	11.8	11.3	10.0	11.5	12.0	11.6	9.9
5	11.6	12.2	11.7	10.0	11.3	12.1	11.7	9.8
6	10.0	10.8	10.8	8.8	9.8	11.1	10.5	8.8
7	10.4	10.4	10.4	8.5	9.4	11.0		8.6
8	10.4	10.5	10.0		10.9	10.2	10.0	8.6
9	11.2	12.1	11.5		11.2	11.8	11.2	10.5
10	10.6	10.5	10.2	9.5	10.4	11.4	10.3	8.9
11	10.0	10.1	9.6	8.7	9.2	10.2	9.7	8.8
12	11.8	10.5	10.1	9.0	9.8	10.5	10.4	9.5
Mean	**10.75**	**11.03**	**10.62**	**9.24**	**10.39**	**11.21**	**10.64**	**9.34**
S.D.	**0.72**	**0.72**	**0.66**	**0.62**	**0.78**	**0.69**	**0.66**	**0.65**
Overall mean	**10.58**	**11.11**	**10.63**	**9.29**				
S.D.	**0.77**	**0.71**	**0.66**	**0.64**				
Male mean	**10.78**	**11.54**	**10.95**	**9.58**				
S.D.	**0.68**	**0.55**	**0.57**	**0.61**				
Female mean	**10.24**	**10.43**	**10.03**	**8.81**				
S.D.	**0.79**	**0.26**	**0.29**	**0.32**				
Difference (%)	**5.27**	**10.64**	**9.17**	**8.74**				

Table A1.13 MP maximum base width (Wb), frontal plane (mm)

	Right				Left			
	Index	Middle	Ring	Little	Index	Middle	Ring	Little
1	13.2	14.3	12.4	10.9				
3	13.9	15.5	14.2	12.2	13.8	14.6	13.2	11.9
4	15.0	15.6	14.7	13.0	14.5	15.4	14.7	12.4
5	15.0	16.2	14.9	13.7	15.4	16.2	15.0	13.2
6	13.6	14.8	13.8	11.8	14.0	14.8	13.8	11.6
7	13.5	14.2	13.1	11.1	13.4	14.3		11.1
8	13.6	13.4	11.5		13.1	13.4	12.4	10.3
9	15.8	16.3	14.9	13.2	15.2	16.3	14.9	13.5
10	13.6	14.7	13.3	14.0	13.2	14.2	13.5	11.6
11	12.9	13.3	12.7	10.7	12.6	12.9	12.3	10.7
12	13.9	14.4	13.8	12.8	14.0	14.7	14.1	12.7
Mean	**14.00**	**14.79**	**13.57**	**12.24**	**13.92**	**14.68**	**13.77**	**11.90**
S.D.	**0.84**	**0.97**	**1.05**	**1.14**	**0.86**	**1.03**	**0.95**	**1.00**
Overall mean	**13.93**	**14.74**	**13.66**	**12.06**				
S.D.	**0.85**	**1.00**	**1.01**	**1.00**				
Male mean	**14.32**	**15.30**	**14.10**	**12.54**				
S.D.	**0.84**	**0.75**	**0.80**	**0.92**				
Female mean	**13.38**	**13.82**	**12.84**	**11.34**				
S.D.	**0.45**	**0.61**	**0.83**	**0.93**				
Difference (%)	**7.03**	**10.71**	**9.81**	**10.58**				

Table A1.14 Alignment of PP head condyles (θ), frontal plane (°)

	Right				Left			
	Index	Middle	Ring	Little	Index	Middle	Ring	Little
1	-1.0	1.5	1.5	6.5				
3	0	4.0	1.5	6.5	0	-1.5	-3.0	-8.5
4	1.0	-1.0	3.0	5.5	0	2.0	-3.5	-7.0
5	-1.0	-2.0	3.5	5.0	1.5	0.5	-4.0	-7.5
6	-6.0	-2.5	6.5	7.0	6.0	4.0	-6.0	-8.0
7	-2.5	0	-1.0	5.0	2.5	2.0		-4.0
8	6.0	-1.0	1.0		1.5	-1.5	-2.5	-3.0
9	-2.5	-0.5	0	-3.5	0.5	1.0	-1.0	-5.0
10	-1.5	1.5	6.0	5.0	1.5	1.5	-1.0	-5.0
11	5.0	0	-4.5	8.0	0.5	0.5	-5.5	-7.0
12	-2.0	-2.0	1.5	3.0	1.5	3.0	-2.0	-5.0
Mean	**-0.41**	**-0.18**	**1.70**	**4.80**	**1.55**	**1.15**	**-3.17**	**-6.00**
S.D.	**3.26**	**1.82**	**2.95**	**3.06**	**1.59**	**1.67**	**1.68**	**1.67**
Overall mean	**0.69**	**0.45**	**-0.48**	**-0.86**				
S.D.	**2.75**	**1.87**	**3.46**	**5.92**				
Male mean	**-0.12**	**0.65**	**0.27**	**-0.69**				
S.D.	**2.60**	**2.00**	**3.70**	**6.27**				
Female mean	**1.56**	**0.13**	**-1.86**	**-0.43**				
S.D.	**2.80**	**1.60**	**2.42**	**5.29**				

Table A1.15 Angle of the lateral condyle inclination (α1), transverse plane (°)

	Right				Left			
	Index	Middle	Ring	Little	Index	Middle	Ring	Little
1	81	76	72	76				
3	79	88	85	82	80	86	85	71
4	73	75	73	84	79	77	75	77
5	70	71	76	79	70	80	85	81
6	90	71	77	82	80	79	77	81
7	74	73	70	72	75	72		77
8	79	79	83		85	83	72	83
9	70	71	75	72	84	75	69	85
10	66	75	76	80	69	77	74	76
11	76	76	77	82	84	88	82	87
12	78	83	82	89	82	88	75	80
Mean	76.00	76.18	76.91	79.80	78.80	80.50	77.11	79.80
S.D.	6.24	5.11	4.48	5.04	5.42	5.28	5.36	4.47
Overall mean	77.33	78.24	77.00	79.80				
S.D.	6.03	5.62	4.90	4.76				
Male mean	76.23	77.00	76.85	78.92				
S.D.	6.80	5.08	4.93	4.14				
Female mean	79.13	80.25	77.29	81.42				
S.D.	3.89	5.87	4.83	5.37				
Difference (%)	-3.66	-4.05	-0.57	-3.07				

Table A1.16 Angle of the lateral condyle inclination (α2), transverse plane (°)

	Right				Left			
	Index	Middle	Ring	Little	Index	Middle	Ring	Little
1	85	80	74	83				
3	83	70	83	75	72	81	82	69
4	77	80	72	81	74	76	75	89
5	76	74	75	88	74	72	82	84
6	72	80	75	78	85	71	77	89
7	76	78	81	78	79	70		72
8	77	85	86		74	84	81	83
9	81	75	77	84	68	78	73	81
10	84	80	68	90	81	71	78	75
11	79	81	79	82	70	78	81	86
12	86	87	82	77	74	78	83	82
Mean	79.64	79.09	77.45	81.60	75.10	75.90	79.11	81.00
S.D.	4.27	4.58	5.07	4.59	4.89	4.50	3.31	6.54
Overall mean	77.48	77.57	78.20	81.30				
S.D.	5.10	4.82	4.45	5.66				
Male mean	77.85	76.00	76.23	82.00				
S.D.	5.45	3.92	4.14	6.15				
Female mean	76.88	80.13	81.86	80.00				
S.D.	4.43	5.04	2.03	4.31				
Difference (%)	1.26	-5.15	-6.88	2.50				

Table A1.17 Distance from the PP head centre-line to base of condyle (a), transverse plane (mm)

	Right				Left			
	Index	Middle	Ring	Little	Index	Middle	Ring	Little
1	4.7	4.9	5.9	3.2				
3	5.5	6.3	5.3	4.2	5.6	5.7	4.9	4.4
4	5.2	5.3	4.8	4.0	4.9	4.7	4.4	2.8
5	5.8	5.0	5.2	3.7	5.0	6.6	5.1	3.6
6	5.0	4.2	3.6	4.2	4.0	4.8	4.1	3.4
7	4.9	5.0	4.8	3.8	5.2	5.2		3.8
8	4.6	4.5	3.4		4.1	4.5	4.0	3.6
9	4.8	5.0	4.9	5.2	5.4	5.5	4.4	3.6
10	4.1	4.2	4.9	3.5	4.1	4.9	4.3	3.6
11	4.9	4.3	4.7	3.4	4.3	5.1	4.0	3.7
12	5.2	4.5	3.7	3.6	5.3	4.8	5.2	3.9
Mean	**4.97**	**4.84**	**4.65**	**3.88**	**4.79**	**5.18**	**4.49**	**3.64**
S.D.	**0.44**	**0.59**	**0.74**	**0.54**	**0.58**	**0.59**	**0.44**	**0.38**
Overall mean	**4.89**	**5.00**	**4.58**	**3.76**				
S.D.	**0.52**	**0.62**	**0.63**	**0.48**				
Male mean	**4.93**	**5.16**	**4.75**	**3.80**				
S.D.	**0.56**	**0.69**	**0.57**	**0.58**				
Female mean	**4.81**	**4.74**	**4.26**	**3.69**				
S.D.	**0.41**	**0.31**	**060**	**0.16**				
Difference (%)	**2.49**	**8.86**	**11.50**	**2.98**				

Table A1.18 Distance from the PP head centre-line to base of condyle (b), transverse plane (mm)

	Right				Left			
	Index	Middle	Ring	Little	Index	Middle	Ring	Little
1	4.8	5.0	5.2	4.0				
3	6.2	6.0	5.4	4.7	5.6	6.5	5.4	4.4
4	5.3	5.4	5.3	3.9	4.8	4.9	5.6	3.7
5	5.7	5.2	5.3	3.8	4.6	5.1	5.0	4.0
6	4.4	5.2	4.9	4.3	4.9	4.4	5.2	4.1
7	4.3	5.2	5.3	3.8	4.7	5.4	4.9	3.6
8	4.3	5.6	4.1		4.3	4.8	4.8	3.8
9	5.8	5.6	4.7	4.4	4.7	4.7		3.7
10	5.2	4.3	5.0	3.8	4.9	5.3	4.7	3.7
11	4.7	5.5	5.4	4.5	4.6	5.2	4.8	4.1
12	5.4	5.1	4.4	3.7	5.4	4.7	5.1	5.0
Mean	**5.10**	**5.28**	**5.00**	**4.09**	**4.85**	**5.10**	**5.06**	**4.01**
S.D.	**0.62**	**0.41**	**0.42**	**0.34**	**0.37**	**0.55**	**0.28**	**0.43**
Overall mean	**4.98**	**5.20**	**5.03**	**4.05**				
S.D.	**0.53**	**0.49**	**0.36**	**0.37**				
Male mean	**5.15**	**5.20**	**5.14**	**4.04**				
S.D.	**0.52**	**0.58**	**0.27**	**0.31**				
Female mean	**4.71**	**5.19**	**4.85**	**4.07**				
S.D.	**0.43**	**0.30**	**0.41**	**0.47**				
Difference (%)	**9.34**	**0.19**	**5.98**	**-0.74**				

Table A1.19 Maximum depth of inter-condylar sulcus of PP head (Isat), transverse plane, anterior face (mm)

	Right				Left			
	Index	Middle	Ring	Little	Index	Middle	Ring	Little
1	0.7	1.0	0.7	0.5				
3	0.8	1.2	1.0	0.8	1.1	1.0	1.1	0.8
4	1.0	1.0	1.0	0.6	0.9	0.9	0.9	0.5
5	1.0	1.1	0.6	0.5	0.9	1.0	0.8	0.5
6	0.6	0.7	0.7	0.5	0.6	0.9	0.7	0.6
7	1.0	1.1	0.9	0.7	1.2	1.1		0.7
8	0.7	0.8	0.8		0.8	0.7	0.7	0.5
9	1.1	1.0	0.8	0.6	0.8	0.8	0.6	0.6
10	0.9	0.6	0.9	0.5	0.9	0.8	0.9	0.5
11	1.1	1.1	1.0	0.6	1.2	0.9	0.8	0.6
12	0.9	0.7	0.9	0.6	0.6	1.0	1.1	0.9
Mean	**0.89**	**0.94**	**0.85**	**0.59**	**0.90**	**0.91**	**0.84**	**0.62**
S.D.	**0.16**	**0.19**	**0.13**	**0.09**	**0.20**	**0.11**	**0.16**	**0.13**
Overall mean	**0.90**	**0.92**	**0.85**	**0.61**				
S.D.	**0.18**	**0.16**	**0.15**	**0.12**				
Male mean	**0.87**	**0.92**	**0.82**	**0.58**				
S.D.	**0.16**	**0.16**	**0.15**	**0.10**				
Female mean	**0.94**	**0.93**	**0.89**	**0.66**				
S.D.	**0.21**	**0.16**	**0.12**	**0.12**				
Difference (%)	**-7.45**	**-1.08**	**-7.87**	**-12.12**				

Table A1.20 Maximum depth of inter-condylar sulcus of PP head (Isf), frontal plane (mm)

	Right				Left			
	Index	Middle	Ring	Little	Index	Middle	Ring	Little
1	0.9	0.8	0.6	0.5				
3	1.2	1.0	0.9	0.7	0.9	1.3	1.0	0.8
4	1.0	0.8	0.6	0.7	1.2	0.9	0.8	0.5
5	0.9	0.8	0.5	0.6	0.8	0.7	0.6	0.7
6	0.6	0.6	0.5	0.4	0.6	0.6	0.5	0.5
7	0.8	0.9	0.6	0.5	0.9	0.9		0.7
8	0.5	0.7	0.6		0.8	0.7	0.5	0.6
9	0.7	0.7	0.8	0.8	0.7	0.7	0.5	0.4
10	0.8	0.5	0.5	0.6	0.7	0.7	0.5	0.4
11	0.7	0.8	1.2	0.6	1.1	0.8	0.7	0.8
12	0.8	0.8	0.7	0.6	0.8	0.8	0.7	0.6
Mean	**0.81**	**0.76**	**0.68**	**0.60**	**0.85**	**0.81**	**0.64**	**0.60**
S.D.	**0.18**	**0.13**	**0.20**	**0.11**	**0.17**	**0.19**	**0.16**	**0.14**
Overall mean	**0.83**	**0.79**	**0.67**	**0.60**				
S.D.	**0.18**	**0.16**	**0.19**	**0.13**				
Male mean	**0.85**	**0.78**	**0.64**	**0.58**				
S.D.	**0.19**	**0.20**	**0.18**	**0.14**				
Female mean	**0.81**	**0.80**	**0.71**	**0.63**				
S.D.	**0.16**	**0.07**	**0.21**	**0.09**				
Difference (%)	**4.94**	**-2.50**	**-9.86**	**-7.94**				

Table A1.21 PP length (L), (mm)

	Right				Left			
	Index	Middle	Ring	Little	Index	Middle	Ring	Little
1	44.0	48.9	46.2	36.2				
3	42.1	46.7	42.6	35.7	42.6	46.5	42.6	33.2
4	46.1	51.2	46.1	37.0	43.5	48.4	45.6	35.4
5	45.6	51.1	47.6	37.9	45.8	50.3	46.6	38.5
6	42.8	47.1	44.6	35.5	43.3	46.3	44.0	35.8
7	41.7	45.9	46.8	35.7	42.3	46.4		35.1
8	41.0	41.4	39.2		37.6	40.9	38.8	29.4
9	48.4	52.3	50.4	38.0	48.0	52.3	49.8	41.3
10	41.7	43.4	42.9	36.1	41.6	46.8	44.4	35.1
11	42.6	45.5	42.6	35.1	42.1	45.0	42.1	34.5
12	47.5	50.9	49.3	40.5	48.2	52.5	49.5	41.5
Mean	**43.95**	**47.67**	**45.30**	**36.77**	**43.50**	**47.54**	**44.82**	**35.98**
S.D.	**2.43**	**3.36**	**3.15**	**1.56**	**3.00**	**3.33**	**3.33**	**3.47**
Overall mean	**43.88**	**47.61**	**45.09**	**36.38**				
S.D.	**2.73**	**3.35**	**3.24**	**2.72**				
Male mean	**44.26**	**48.56**	**45.65**	**36.59**				
S.D.	**2.21**	**2.62**	**2.43**	**1.92**				
Female mean	**42.88**	**46.06**	**44.04**	**35.97**				
S.D.	**3.23**	**3.79**	**4.17**	**3.74**				
Difference (%)	**3.22**	**5.43**	**3.66**	**1.72**				

Table A1.22 MP length (L), (mm)

	Right				Left			
	Index	Middle	Ring	Little	Index	Middle	Ring	Little
1	24.7	30.2	29.2	20.2				
3	25.1	30.2	28.7	20.0	24.6	30.3	28.3	20.0
4	28.0	32.6	31.9	22.4	26.8	32.6	31.7	21.6
5	25.4	34.5	31.5	21.8	26.7	34.5	32.3	22.1
6	27.2	32.8	31.5	22.5	27.1	32.8	31.4	22.9
7	26.1	30.4	28.7	20.5	26.1	30.0		20.0
8	22.2	26.0	24.4		21.9	25.7	24.2	16.4
9	29.9	35.6	33.7		29.8	35.2	33.7	25.7
10	24.0	29.0	28.0	22.0	24.4	29.2	28.7	21.6
11	28.7	30.2	26.1	21.0	26.4	29.6	28.6	21.7
12	28.5	34.6	32.2	24.9	28.8	34.5	32.9	26.1
Mean	**26.36**	**31.46**	**29.63**	**21.70**	**26.26**	**31.44**	**30.20**	**21.81**
S.D.	**2.22**	**2.72**	**2.69**	**1.44**	**21.13**	**2.84**	**2.83**	**2.66**
Overall mean	**26.30**	**31.45**	**29.89**	**21.76**				
S.D.	**2.18**	**2.78**	**2.77**	**2.17**				
Male mean	**26.44**	**32.28**	**30.82**	**21.90**				
S.D.	**1.89**	**2.19**	**1.92**	**1.48**				
Female mean	**26.09**	**30.13**	**28.16**	**21.51**				
S.D.	**2.57**	**3.08**	**3.24**	**2.98**				
Difference (%)	**1.34**	**7.14**	**1.09**	**1.81**				

Table A1.23 Angle between PP dorsal surface and base-line (ϕ), sagittal plane (°)

	Right				Left			
	Index	Middle	Ring	Little	Index	Middle	Ring	Little
1	5	6	5	6				
3	3	2	2	7	4	2	9	
4	5	3	3	7	3	4	5	8
5	6	4	4	7	6	4	5	8
6	5	5	3	7	4	5	5	8
7	6	3	4	8	4	4		4
8	6	2	4		5	3	5	9
9	5	5	5	9	4	4	5	5
10	7	4	8	9	7	7	5	8
11	3	2	4	7	4	3	2	8
12	4	4	3	9	4	4	3	8
Mean	**5.00**	**3.64**	**4.09**	**7.60**	**4.50**	**4.00**	**4.89**	**7.33**
S.D.	**1.21**	**1.30**	**1.50**	**1.02**	**1.12**	**1.26**	**1.79**	**1.56**
Overall mean	**4.76**	**3.81**	**4.45**	**7.47**				
S.D.	**1.19**	**1.30**	**1.69**	**1.31**				
Male mean	**4.92**	**4.23**	**4.92**	**7.42**				
S.D.	**1.27**	**1.37**	**1.82**	**1.11**				
Female mean	**4.50**	**3.13**	**3.57**	**7.57**				
S.D.	**1.00**	**0.78**	**0.90**	**1.59**				
Difference (%)	**9.33**	**35.14**	**37.82**	**-1.98**				

Table A1.24 Angle between PP head-line and base-line (σ), sagittal plane (°)

	Right				Left			
	Index	Middle	Ring	Little	Index	Middle	Ring	Little
1	12	9	14	11				
3	21	12	14	16	13	13	18	
4	13	11	12	12	11	13	12	13
5	7	11	11	10	8	10	11	13
6	6	11	11	15	9	11	13	14
7	11	9	12	13	9	11		10
8	12	10	11		10	11	13	13
9	12	13	12	18	12	13	14	12
10	12	14	15	17	14	14	14	13
11	12	15	15	15	8	8	12	15
12	9	8	9	9	4	8	9	8
Mean	**11.55**	**11.18**	**12.36**	**13.60**	**9.80**	**11.20**	**12.89**	**12.33**
S.D.	**3.70**	**2.08**	**1.82**	**2.91**	**2.75**	**1.99**	**2.33**	**2.00**
Overall mean	**10.71**	**11.19**	**12.60**	**13.00**				
S.D.	**3.40**	**2.04**	**2.08**	**2.60**				
Male mean	**11.54**	**11.92**	**13.15**	**13.75**				
S.D.	**3.63**	**1.49**	**1.92**	**2.31**				
Female mean	**9.38**	**10.75**	**11.57**	**11.86**				
S.D.	**2.45**	**2.44**	**1.99**	**2.64**				
Difference (%)	**23.03**	**10.88**	**13.66**	**15.94**				

Table A1.25 Distance from the PIPJ bearing surface to end of the head-line (d), sagittal plane (mm)

	Right				Left			
	Index	Middle	Ring	Little	Index	Middle	Ring	Little
1	15.0	14.7	12.2	14.1				
3	13.5	15.2	12.3	10.9	13.8	14.6	12.5	
4	18.7	18.6	14.4	13.7	15.9	16.5	14.8	13.4
5	11.2	13.9	13.9	11.4	13.2	14.7	13.2	10.6
6		13.2	14.9	11.4	15.4	14.6	12.1	11.8
7	12.1	14.5	14.9	11.9	12.2	11.6		10.0
8	14.8	18.0	13.4		12.9	14.3	12.4	10.4
9	18.7	18.2	18.1	10.0	18.8	15.0	14.3	14.3
10	13.5	12.2	11.2	9.5	11.1	14.1	13.4	11.8
11	14.3	11.8	13.2	9.7	19.9	17.5	13.7	11.3
12	12.4	17.3	18.4		19.2	19.1	20.3	
Mean	**14.42**	**15.24**	**14.26**	**11.40**	**15.24**	**15.20**	**14.08**	**11.70**
S.D.	**2.42**	**2.33**	**2.18**	**1.55**	**2.98**	**1.95**	**2.35**	**1.40**
Overall mean	**14.83**	**15.22**	**14.18**	**11.54**				
S.D.	**2.74**	**2.16**	**2.26**	**1.49**				
Male mean	**14.90**	**15.04**	**13.64**	**11.91**				
S.D.	**2.61**	**1.73**	**1.70**	**1.55**				
Female mean	**14.73**	**15.51**	**15.19**	**10.66**				
S.D.	**2.94**	**2.68**	**2.77**	**0.82**				
Difference (%)	**1.15**	**-3.03**	**-10.20**	**11.73**				

Table A1.26 PP minimum shaft thickness (Tp), sagittal plane (mm)

	Right				Left			
	Index	Middle	Ring	Little	Index	Middle	Ring	Little
1	6	6.8	5.9	5.4				
3	6.8	6.5	6	5.5	5.9	6.4	6	5.7
4	6.7	7.5	6.8	5.7	6.1	6.5	6.8	5.3
5	6.4	6.9	6.7	5.5	6.5	7.1	6.5	6.1
6	6.4	6.6	6.6	5	6.3	6.6	6.4	5
7	5.8	6.4	6.3	4.7	6.1	6.6		4.9
8	5.6	6	5.4		6.3	6	5.4	4.5
9	6.2	6.9	6.7	6.1	6.4	7.2	6.3	6.1
10	5.8	5.7	6	4.9	5.7	6.1	6	4.7
11	5.3	4.3	5.2	4.5	5.2	5.4	5	4.2
12	5.6	5.8	5.8	5	5.4	5.8	5.6	5.1
Mean	**6.05**	**6.31**	**6.13**	**5.23**	**5.99**	**6.37**	**6.00**	**5.16**
S.D.	**0.48**	**0.85**	**0.54**	**0.49**	**0.44**	**0.57**	**0.58**	**0.64**
Overall mean	**6.02**	**6.34**	**6.07**	**5.20**				
S.D.	**0.45**	**0.71**	**0.55**	**0.56**				

Table A1.27 Distance (Lp) from the minimum shaft thickness (Tp) to the PIPJ bearing surface, sagittal plane (mm)

	Right				Left			
	Index	Middle	Ring	Little	Index	Midde	Ring	Little
1	10	10	9	8				
3	9	9.5	11	9	9.5	11	10	7.5
4	14	14	9	10	10	10	10	8
5	10.5	11	11	7.5	11	11	11	12
6	15	11	14	9	15	10	12	9
7	11	12	10	8.5	15	11		9
8	11	11	12		12	10	8	7
9	11	13	13	10	13	11	11	10
10	9.5	10	12	9	10	10.5	10	9.5
11	12	11	10	8.5	16	10.5	12	9
12	12	12	14	11	13	9.5	11	9
Mean	**11.36**	**11.32**	**11.36**	**9.05**	**12.45**	**10.45**	**10.56**	**9.00**
S.D.	**1.82**	**1.35**	**1.80**	**1.04**	**2.34**	**0.55**	**1.24**	**1.39**
Overall mean	**11.88**	**10.90**	**11.00**	**9.03**				
S.D.	**2.10**	**1.11**	**1.59**	**1.20**				

Table A1.28 PP minimum shaft width (Wp), sagittal plane (mm)

	Right				Left			
	Index	Middle	Ring	Little	Index	Middle	Ring	Little
1	9.3	9.7	9	7.9				
3	10.5	11	10.1	8	10.2	10.7	9.8	8.2
4	11.2	11.5	10.8	9.6	11	11.4	10.8	9.1
5	10.8	11	9.6	8.8	10.2	10.8	10	8.8
6	9.9	10.6	10.2	8.1	10.5	10.6	10	8.1
7	8.9	9.3	10	7.1	8.4	9.8		7
8	9.2	8.7	7.4		9.5	8.4	7.6	7.2
9	11.2	11.2	10.8	9	10.8	11.2	10.7	9.5
10	10.4	9.3	9.1	9.1	10.4	10	9.1	8.5
11	8.7	9.3	9.7	7.9	9.6	9.4	8.4	7.7
12	9.6	9.4	8.8	8.5	9.4	9	8.4	8.4
Mean	**9.97**	**10.09**	**9.59**	**8.40**	**10.00**	**10.13**	**9.42**	**8.25**
S.D.	**0.90**	**0.98**	**0.99**	**0.74**	**0.78**	**0.98**	**1.11**	**0.79**
Overall mean	**9.99**	**10.11**	**9.52**	**8.33**				
S.D.	**0.82**	**0.96**	**1.02**	**0.75**				

Table A1.29 Distance (Lpw) from the minimum shaft width (Wp) to the PIPJ bearing surface, sagittal plane (mm)

	Right				Left			
	Index	Middle	Ring	Little	Index	Middle	Ring	Little
1	18	23	23	11				
3	10	11	10	9	10.5	11	11	9.5
4	12	12	11	9	11	11	11	10.5
5	13	27	27	19	26	29.5	26	20
6	11	12	11	9.5	12	10.5	11	11
7	24.5	27	26	21	25	12		20.5
8	12	23	20		12	23	21	17
9	11.5	13	12	20	13	12	24	13
10	11	26	11.5	11.5	11.5	26	24	18
11	14	26	24.5	10	23.5	25	23.5	10
12	26	27	27	10.5	26	30.5	28	23
Mean	**14.82**	**20.64**	**18.45**	**13.05**	**17.05**	**19.05**	**19.94**	**15.25**
S.D.	**5.59**	**7.00**	**7.32**	**4.88**	**7.01**	**8.44**	**6.97**	**5.02**
Overall mean	**15.88**	**19.88**	**19.13**	**14.15**				
S.D.	**6.25**	**7.57**	**7.01**	**4.95**				

Table A1.30 MP minimum shaft thickness (Tm), sagittal plane (mm)

	Right				Left			
	Index	Middle	Ring	Little	Index	Middle	Ring	Little
1	4.9	5.9	5.7	4.1				
3	5.6	5.9	5.3	4.9	5.6	6.3	5.6	5.2
4	5.8	6.8	6.5	5.1	5.8	6.3	6.2	4.8
5	5.2	6	5.7	4.6	5.5	6.1	5.6	4.4
6	4.9	5.6	5.5	4.7	5.4	5.9	6	4.8
7	4.8	5.2	4.8	3.8	4.9	5.2		3.9
8	5.1	5	4.3		5.3	4.9	4.6	4.6
9	6	6.5	6.1		6	6.5	6	5.2
10	5.4	4.9	5.2	5.4	5	5.1	5	4.4
11	4.3	4.2	4.9	3.7	4.6	5.3	4.4	4
12	5.2	5	5.3	4.6	4.8	5.6	4.8	5
Mean	**5.20**	**5.55**	**5.39**	**4.54**	**5.29**	**5.72**	**5.36**	**4.63**
S.D.	**0.49**	**0.77**	**0.61**	**0.58**	**0.46**	**0.58**	**0.67**	**0.46**
Overall mean	**5.24**	**5.63**	**5.38**	**4.59**				
S.D.	**0.46**	**0.67**	**0.62**	**0.50**				

Table A1.31 Distance (Lm) from the MP minimum shaft thickness (Tm) to the PIPJ bearing surface, sagittal plane (mm)

	Right				Left			
	Index	Middle	Ring	Little	Index	Middle	Ring	Little
1	12.5	16	14	6				
3	13	19	14	8	13.5	17	13.5	9
4	17.5	18	17	12	15.5	19	18	10
5	14.5	20	15	8	14	19.5	16	8
6	12.5	16	14	6	13	15.5	16	6
7	6.5	14	7	4.5	6	10		4.5
8	9.5	9	6.5		10	10	6	3.5
9	16	18	16.5		15.5	18	16	11.5
10	14.5	11	8	7	7	12.5	10	6.5
11	10.5	7.5	7	4	7	14	5	3.5
12	11.5	17	14	12.5	12.5	17	17	10
Mean	**15.59**	**15.05**	**12.09**	**7.56**	**11.40**	**15.25**	**13.06**	**7.25**
S.D.	**3.09**	**4.17**	**4.08**	**2.99**	**3.63**	**3.50**	**4.88**	**2.88**
Overall mean	**12.02**	**15.14**	**12.53**	**7.39**				
S.D.	**3.33**	**3.77**	**4.36**	**2.86**				

Table A1.32 MP minimum shaft width (Wm), frontal plane (mm)

	Right				Left			
	Index	Middle	Ring	Little	Index	Middle	Ring	Little
1	7.6	8.2	8	7.3				
3	8.7	8.8	8.2	8.3	9	9	8	8.5
4	8.1	9.8	9.6	8.4	9.5	10.4	9.2	9.3
5	8.6	8.6	8	7.2	8.3	9.1	8.1	7
6	8	8.3	8.1	6.7	8.1	8.8	8.4	6.7
7	7.4	8	7.4	6.2	7.3	8.2		6.3
8	7.7	7.7	7		7.8	7.8		6.7
9	8.4	9.1	8.6		8.6	9.1	8.4	7.7
10	8	8.3	7.7	7.1	8.4	8.6	7.7	6.9
11	7.5	7.6	7.5	7	7.2	7.5	7.7	7
12	7.5	7.3	6.8	6.5	7.2	7.7	7	6.9
Mean	**7.95**	**8.34**	**7.90**	**7.19**	**8.14**	**8.59**	**8.06**	**7.30**
S.D.	**0.46**	**0.72**	**0.77**	**0.75**	**0.78**	**0.87**	**0.65**	**0.93**
Overall mean	**8.04**	**8.46**	**7.97**	**7.25**				
S.D.	**0.62**	**0.79**	**0.71**	**0.83**				

Table A1.33 Distance (Lmw) from the minimum shaft width (Wm) to the PIPJ bearing surface, frontal plane (mm)

	Right				Left			
	Index	Middle	Ring	Little	Index	Middle	Ring	Little
1	14	19	19	12				
3	15.5	19	18	13	14	20	18	12.5
4	17	19	21	14	16	17	19	14
5	12.5	21	20	12.5	14	20	20	13
6	18	11	20	15	17	21	20	15
7	15.5	19	17	12.5	15	19		12
8	12.5	15	14		13	15.5		9.5
9	18	22	20.5		18	23	22	16
10	14	19.5	19	13.5	13.5	18.5	18.5	13.5
11	19	19.5	14	14	15	18	15	11
12	15.5	21	19	14	16	20	20	15
Mean	**15.59**	**18.64**	**18.32**	**13.39**	**15.15**	**19.20**	**19.06**	**13.10**
S.D.	**2.22**	**3.10**	**2.41**	**0.96**	**1.60**	**2.11**	**2.04**	**2.01**
Overall mean	**15.38**	**18.90**	**18.63**	**13.24**				
S.D.	**1.92**	**2.62**	**2.24**	**1.57**				

Table A1.34 PP mean lateral shaft thickness

	Right				Left			
	Index	Middle	Ring	Little	Index	Middle	Ring	Little
1	2.15	2.35	2.63	2.19				
3	2.40	2.70	2.50	2.30	2.44	2.69	2.70	2.64
4	2.85	2.79	2.70	2.51	2.87	2.72	2.64	2.51
5	2.63	2.10	2.15	2.13	2.78	2.43	2.47	2.36
6	2.42	2.31	2.32	1.98	2.21	2.19	2.16	1.85
7	2.41	2.42	2.41	2.12	2.45	2.27		2.04
8	1.90	2.07	1.63		2.05	2.29	1.77	1.72
9	2.07	2.41	2.13	2.28	2.22	2.67	2.17	2.33
10	2.16	1.92	1.99	1.88	2.41	2.00	2.18	1.96
11	1.82	2.15	2.31	1.74	1.86	2.22	2.15	1.70
12	2.20	2.21	2.11	1.85	2.15	2.19	2.09	1.98
Mean	**2.27**	**2.31**	**2.28**	**2.10**	**2.34**	**2.37**	**2.26**	**2.11**
S.D.	**0.31**	**0.26**	**0.27**	**0.24**	**0.31**	**0.25**	**0.29**	**0.33**
Finger mean	**2.31**	**2.34**	**2.27**	**2.10**				
S.D.	**0.30**	**0.25**	**0.27**	**0.28**				

Table A1.35 MP mean lateral shaft thickness

	Right				Left			
	Index	Middle	Ring	Little	Index	Middle	Ring	Little
1	2.58	2.73	2.89	2.68				
3	1.68	2.25	2.01	1.64	1.77	1.93	1.89	1.63
4	2.67	2.79	2.71	2.70	2.59	2.74	2.77	2.69
5	2.30	2.41	2.35	2.43	2.39	2.52	2.66	2.48
6	2.43	2.64	2.61	2.49	2.45	2.61	2.62	2.54
7	1.65	1.98	1.79	1.50	1.61	2.30		1.55
8	1.80	2.27	1.86	1.61	1.68	1.88	1.84	1.52
9	1.76	2.06	1.93	1.74	1.63	2.05	1.80	1.53
10	1.63	1.83	1.79	1.67	1.79	1.89	1.83	1.70
11	1.84	2.00	1.76	1.92	2.04	2.14	1.94	2.29
12	1.76	2.07	1.96	1.77	1.72	2.03	2.50	1.63
Mean	**2.01**	**2.28**	**2.14**	**2.01**	**1.97**	**2.21**	**2.21**	**1.96**
S.D.	**0.40**	**0.33**	**0.42**	**0.46**	**0.37**	**0.32**	**0.42**	**0.48**
Finger mean	**1.97**	**2.24**	**2.18**	**1.99**				
S.D.	**0.38**	**0.32**	**0.41**	**0.46**				

Table A1.36 PP mean dorsal shaft thickness

	Right				Left			
	Index	Middle	Ring	Little	Index	Middle	Ring	Little
1	2.09	2.1	2.72	1.99				
3	2.26	2.62	2.46	2.19	2.38	2.72	2.79	2.67
4	2.75	2.67	2.64	2.35	2.35	2.93	2.62	2.24
5	2.56	1.97	2.12	1.77	2.39	2.38	2.17	2.21
6	2.29	2.15	2.27	1.71	2.01	2.05	2.08	1.44
7	2.25	2.1	2.38	2.18	2.11	2.23		1.83
8	1.76	1.73	1.08		2.03	2.1	1.68	1.56
9	1.96	2.2	2.09	1.98	2.09	2.59	2.01	2.13
10	2.1	1.88	1.95	1.52	2.4	1.95	1.96	1.63
11	1.67	2.03	2.08	1.43	1.84	2.03	2.03	1.31
12	2	2.11	1.88	1.68	1.79	1.91	1.99	1.82
Mean	**2.15**	**2.14**	**2.15**	**1.88**	**2.14**	**2.29**	**2.15**	**1.88**
S.D.	**0.32**	**0.28**	**0.45**	**0.31**	**0.23**	**0.35**	**0.35**	**0.42**
Finger mean	**2.15**	**2.21**	**2.15**	**1.88**				
S.D.	**0.27**	**0.32**	**0.39**	**0.36**				

Table A1.37 MP mean dorsal shaft thickness

	Right				Left			
	Index	Middle	Ring	Little	Index	Middle	Ring	Little
1	1.7	2.14	2.08	1.25				
3	1.28	1.76	1.7	1.55	1.82	1.24	1.68	1.55
4	2.27	2.11	1.87	1.83	1.84	2.2	2.32	1.13
5	1.5	1.97	1.72	1.15	1.53	2.24	2.12	1.27
6	1.53	1.65	1.97	1.58	1.7	2	1.79	1.54
7	1.5	1.95	1.73	1.8	1.77	2.03		1.9
8	1.75	1.45	1.25		1.53	1.47	1.33	1
9	1.6	1.73	1.7		1.68	1.68	1.8	1.93
10	1.65	1.65	1.53	1.37	1.5	1.4	1.5	1.37
11	1.8	1.45	1.6	1.1	1.73	1.78	1.52	1.35
12	1.53	1.62	1.52	1.58	1.67	1.65	2.56	1.48
Mean	**1.65**	**1.77**	**1.70**	**1.47**	**1.68**	**1.77**	**1.85**	**1.45**
S.D.	**0.25**	**0.24**	**0.23**	**0.27**	**0.12**	**0.34**	**0.41**	**0.30**
Finger mean	**1.58**	**1.73**	**1.73**	**1.66**				
S.D.	**0.26**	**0.20**	**0.28**	**0.39**				

Table A1.38 PP mean palmar shaft thickness

	Right				Left			
	Index	Middle	Ring	Little	Index	Middle	Ring	Little
1	1.48	1.75	1.85	1.66				
3	1.23	1.58	1.55	1.2	1.49	1.63	1.34	1.59
4	1.38	1.76	1.42	1	1.49	1.72	1.48	1.26
5	1.67	1.66	1.52	1.37	1.52	1.92	1.71	1.57
6	1.46	1.46	1.43	1.07	1.52	1.33	1.29	1.04
7	1.61	1.68	1.66	1.38	1.63	1.45		1.45
8	1.24	1.06	1.25		1.18	1.21	1.06	0.89
9	1.63	1.67	1.27	1.13	1.35	1.62	1.36	1.21
10	1.24	1.32	1.43	1.16	1.54	1.32	1.3	1.02
11	1.12	1.14	1.18	0.99	1.35	1.19	1.23	1.08
12	1.42	1.49	1.35	1.33	1.31	1.31	1.23	1.15
Mean	**1.41**	**1.51**	**1.45**	**1.23**	**1.44**	**1.47**	**1.33**	**1.23**
S.D.	**0.18**	**0.24**	**0.19**	**0.21**	**0.14**	**0.24**	**0.18**	**0.24**
Finger mean	**1.42**	**1.49**	**1.40**	**1.23**				
S.D.	**0.16**	**0.24**	**0.19**	**0.22**				

Table A1.39 MP mean palmar shaft thickness

	Right				Left			
1	Index	Middle	Right	Little	Index	Middle	Ring	Little
2	1.3	1.32	1.62	1.2				
3	0.83	1.2	0.88	1.58	1.02	0.84	0.98	1.13
4	0.89	1.26	1.03	1.13	0.88	1.12	1.37	1.07
5	0.95	1.32	1.06	1.35	1.03	1.46	1.3	0.93
6	1.13	1.35	1.13	0.88	1.03	1.18	0.97	1.04
7	1.33	1.5	1.17	1.4	1.2	1.25		0.9
8	0.85	1.13	1.08		1.43	0.93	0.93	0.55
9	1.03	1.25	1.16		1.08	1.28	1.17	1.17
10	1.03	1.44	1.08	0.93	0.9	1.13	0.87	0.87
11	0.94	0.85	0.7	0.7	1.38	1	0.84	1
12	0.83	1.08	1.02	1.13	1.02	1.02	1.44	1
Mean	**1.01**	**1.25**	**1.08**	**1.14**	**1.10**	**1.12**	**1.10**	**0.97**
S.D.	**0.18**	**0.18**	**0.22**	**0.28**	**0.19**	**0.18**	**0.23**	**0.17**
Finger mean	**1.06**	**1.17**	**1.10**	**1.12**				
S.D.	**0.24**	**0.19**	**0.20**	**0.25**				

Table A1.40 Angle between the PP medullary canal centre-line and the base-line (ρ), sagittal plane (°)

	Right				Left			
	Index	Middle	Ring	Little	Index	Middle	Ring	Little
1	8	9	12	11				
3	13	9	12	11	13	13	13	
4	6	11	13	12	10	7	11	5
5	4	11	8	6	9	8	9	10
6	8	11	12	14	9	11	14	12
7	10	10	12	12	10	12		10
8	12	6	10		9	11	14	11
9	15	9	12	12	11	13	14	12
10	9	14	15	17	11	14	14	8
11	12	15	10	13	8	10	10	11
12	10	8	10	8	8	8	8	8
Mean	**9.73**	**10.27**	**11.45**	**11.60**	**9.80**	**10.70**	**11.89**	**9.67**
S.D.	**3.05**	**2.45**	**1.78**	**2.87**	**1.47**	**2.28**	**2.28**	**2.16**
Overall mean	**9.76**	**10.48**	**11.65**	**10.68**				
S.D.	**2.43**	**2.38**	**2.03**	**2.73**				
Male mean	**9.69**	**10.77**	**12.23**	**10.83**				
S.D.	**2.87**	**2.19**	**1.93**	**3.16**				
Female mean	**9.88**	**10.00**	**10.57**	**10.43**				
S.D.	**1.45**	**2.60**	**1.76**	**1.76**				
Difference (%)	**-1.92**	**7.70**	**15.70**	**3.84**				

Table A1.41 Dorsal offset of the PP medullary canal centre-line to the centre of rotation, sagittal plane (mm)

	Right				Left			
	Index	Middle	Ring	Little	Index	Middle	Ring	Little
1	0.8	1.0	0.8	0.7				
3	0.8	0.9	0.8	0.2	0.7	0.7	0.7	/
4	1.0	0.8	0.6	0.5	0.8	1.1	0.8	0.9
5	1.1	0.8	1.0	0.7	0.7	0.8	0.8	0.3
6	1.0	0.6	0.8	0.7	0.7	0.8	0.9	0.5
7	0.7	0.9	0.8	0.2	0.8	0.7		0.7
8	0.5	1.5	0.9		1.0	0.9	0.7	0.5
9	0.9	1.2	0.6	0.5	1.0	0.7	0.6	0.6
10	0.9	0.6	0.7	0.4	0.8	0.6	0.7	0.9
11	0.6	0.7	0.9	0.6	1.0	0.7	1.0	0.4
12	0.7	0.6	0.8	0.9	0.9	0.9	1.0	0.7
Mean	**0.82**	**0.86**	**0.79**	**0.54**	**0.84**	**0.80**	**0.80**	**0.61**
S.D.	**0.18**	**0.26**	**0.12**	**0.22**	**0.12**	**0.14**	**0.13**	**0.20**
Overall mean	**0.83**	**0.83**	**0.80**	**0.57**				
S.D.	**0.15**	**0.22**	**0.12**	**0.21**				
Male mean	**0.86**	**0.82**	**0.75**	**0.58**				
S.D.	**0.13**	**0.18**	**0.12**	**0.21**				
Female mean	**0.78**	**0.87**	**0.87**	**0.57**				
S.D.	**0.17**	**0.26**	**0.10**	**0.21**				
Difference (%)	**10.25**	**-5.75**	**-13.79**	**1.75**				

Table A1.42 Ratio between PP length and maximum head width (L/W)

	Right				Left			
	Index	Middle	Ring	Little	Index	Middle	Ring	Little
1	3.58	3.40	4.24	3.81				
3	3.31	3.18	3.52	3.25	3.44	3.60	3.58	3.07
4	3.32	3.58	3.52	3.30	3.22	3.43	3.45	3.28
5	3.45	3.28	3.47	3.48	3.37	3.42	3.50	3.47
6	3.51	3.62	3.63	3.48	3.55	3.65	3.64	3.54
7	3.45	3.56	3.57	3.64	3.53	3.57		3.62
8	3.53	3.60	3.73		3.39	3.62	3.53	3.38
9	3.36	3.53	3.68	3.28	3.40	3.56	3.66	3.50
10	3.34	3.50	3.61	3.44	3.38	3.60	3.67	3.41
11	3.87	3.82	3.41	3.44	3.42	3.88	3.90	3.67
12	3.89	4.10	4.18	3.97	3.89	4.07	4.19	3.99
Mean	**3.51**	**3.56**	**3.69**	**3.51**	**3.46**	**3.64**	**3.68**	**3.49**
S.D.	**0.19**	**0.24**	**0.26**	**0.22**	**0.17**	**0.19**	**0.22**	**0.23**
Overall mean	**3.49**	**3.60**	**3.68**	**3.50**				
S.D.	**0.18**	**0.22**	**0.24**	**0.23**				
Male mean	**3.40**	**3.49**	**3.63**	**3.41**				
S.D.	**0.10**	**0.14**	**0.19**	**0.17**				
Female mean	**3.62**	**3.78**	**3.79**	**3.67**				
S.D.	**0.21**	**0.21**	**0.29**	**0.22**				
Difference (%)	**-6.08**	**-7.67**	**-4.22**	**-7.08**				

Table A1.43 Ratio between MP length and maximum head width (L/W)

	Right				Left			
	Index	Middle	Ring	Little	Index	Middle	Ring	Little
1	2.52	2.80	2.89	2.35				
3	2.39	2.60	2.59	1.98	2.37	2.57	2.72	2.00
4	2.35	2.76	2.82	2.24	2.33	2.72	2.73	2.18
5	2.19	2.83	2.69	2.18	2.36	2.85	2.76	2.26
6	2.72	3.04	2.92	2.56	2.77	2.95	2.99	2.60
7	2.51	2.92	2.76	2.41	2.78	2.73		2.33
8	2.13	2.48	2.44		2.01	2.52	2.42	1.91
9	2.67	2.94	2.93		2.66	2.98	3.01	2.45
10	2.26	2.76	2.75	2.32	2.35	2.56	2.79	2.43
11	2.87	2.99	2.72	2.41	2.87	2.90	2.95	2.47
12	2.42	3.30	3.19	2.77	2.94	3.29	3.16	2.75
Mean	**2.46**	**2.86**	**2.79**	**2.36**	**2.54**	**2.81**	**2.84**	**2.34**
S.D.	**0.22**	**0.21**	**0.19**	**0.21**	**0.29**	**0.23**	**0.20**	**0.25**
Overall Mean	**2.50**	**2.83**	**2.81**	**2.35**				
S.D.	**0.26**	**0.22**	**0.20**	**0.23**				
Male mean	**2.46**	**2.80**	**2.81**	**2.30**				
S.D.	**0.18**	**0.15**	**0.12**	**019**				
Female mean	**2.57**	**2.89**	**2.81**	**2.44**				
S.D.	**0.33**	**0.29**	**0.29**	**0.27**				
Difference (%)	**-4.28**	**-3.11**	**0**	**-5.74**				

Table A1.44 Ratio between PP length and head diameter (L/D)

	Right				Left			
	Index	Middle	Ring	Little	Index	Middle	Ring	Little
1	4.89	5.14	5.44	4.83				
3	4.43	4.67	4.73	4.20	4.73	4.65	4.73	4.15
4	4.61	4.65	4.61	4.63	4.83	4.84	4.80	4.72
5	4.28	5.11	5.01	5.05	4.82	4.29	5.18	5.13
6	4.28	4.71	4.69	4.73	4.33	4.87	4.89	4.77
7	4.91	4.83	5.51	4.76	4.45	4.88		5.01
8	4.82	5.18	5.23		4.42	4.81	5.17	4.90
9	4.84	5.23	5.60	4.75	4.80	5.23	5.86	4.90
10	4.91	5.43	5.05	5.16	5.20	5.20	5.22	4.01
11	5.68	5.69	5.01	4.68	4.43	5.63	5.61	5.31
12	5.28	5.66	5.48	5.79	5.36	5.83	5.82	5.19
Mean	**4.81**	**5.12**	**5.12**	**4.86**	**4.74**	**5.02**	**5.25**	**4.81**
S.D.	**0.40**	**0.36**	**0.34**	**0.39**	**0.33**	**0.44**	**0.40**	**0.40**
Overall mean	**4.78**	**5.07**	**5.19**	**4.83**				
S.D.	**0.37**	**0.40**	**0.37**	**0.41**				
Male mean	**4.69**	**4.92**	**5.06**	**4.76**				
S.D.	**0.27**	**0.31**	**0.37**	**0.29**				
Female mean	**4.92**	**5.31**	**5.40**	**5.09**				
S.D.	**0.45**	**0.41**	**0.26**	**0.35**				
Difference (%)	**-4.67**	**-7.34**	**-6.30**	**-6.48**				

Table A1.45 Ratio between MP length and head diameter (L/D)

	Right				Left			
	Index	Middle	Ring	Little	Index	Middle	Ring	Little
1	4.12	4.65	4.87	3.67				
3	3.86	4.03	4.42	3.64	4.10	4.04	4.72	3.33
4	4.00	4.35	4.25	3.73	3.83	4.35	4.53	3.93
5	3.91	4.93	5.25	4.36	4.11	5.31	5.38	4.42
6	3.89	4.69	4.85	7.10	4.52	5.05	5.23	4.58
7	4.02	4.68	4.78	4.10	4.02	4.62		4.00
8	3.42	4.33	4.44		3.98	4.67	4.84	3.28
9	4.60	4.75	5.18		4.26	4.69	5.18	4.28
10	4.69	5.27	4.31	4.40	3.75	4.17	4.10	3.93
11	4.78	4.65	3.73	3.82	4.35	4.55	5.20	3.95
12	3.80	5.32	5.37	4.53	4.43	5.31	5.98	4.35
Mean	**4.10**	**4.63**	**4.68**	**4.03**	**4.14**	**4.68**	**5.02**	**4.01**
S.D.	**0.40**	**0.32**	**0.47**	**0.30**	**0.24**	**0.42**	**0.51**	**0.41**
Overall mean	**4.12**	**4.65**	**4.83**	**4.02**				
S.D.	**0.33**	**0.37**	**0.52**	**0.36**				
Male mean	**4.13**	**4.64**	**4.79**	**4.03**				
S.D.	**0.30**	**0.41**	**0.42**	**0.37**				
Female mean	**4.10**	**4.77**	**4.91**	**4.00**				
S.D.	**0.39**	**0.33**	**0.66**	**0.37**				
Difference (%)	**0.73**	**-2.73**	**-2.44**	**0.75**				

Table A1.46 Ratio between PP maximum head width and head diameter (W/D)

	Right				Left			
	Index	Middle	Ring	Little	Index	Middle	Ring	Little
1	1.37	1.52	1.21	1.27				
3	1.34	1.47	1.34	1.29	1.38	1.29	1.32	1.35
4	1.39	1.30	1.31	1.40	1.50	1.41	1.39	1.44
5	1.32	1.56	1.44	1.45	1.43	1.55	1.48	1.48
6	1.22	1.30	1.29	1.36	1.22	1.34	1.34	1.35
7	1.42	1.36	1.54	1.31	1.26	1.37		1.39
8	1.36	1.44	1.40		1.31	1.33	1.47	1.45
9	1.44	1.48	1.52	1.45	1.41	1.47	1.60	1.69
10	1.47	1.55	1.40	1.50	1.54	1.44	1.42	1.47
11	1.47	1.49	1.47	1.36	1.29	1.45	1.44	1.45
12	1.36	1.38	1.31	1.45	1.38	1.43	1.39	1.30
Mean	**1.38**	**1.44**	**1.38**	**1.38**	**1.37**	**1.41**	**1.43**	**1.44**
S.D.	**0.07**	**0.09**	**0.10**	**0.07**	**0.10**	**0.07**	**0.08**	**0.10**
Overall mean	**1.38**	**1.43**	**1.40**	**1.41**				
S.D.	**0.08**	**0.08**	**0.09**	**0.09**				
Male mean	**1.39**	**1.44**	**1.37**	**1.42**				
S.D.	**0.09**	**0.10**	**0.10**	**0.10**				
Female mean	**1.36**	**1.42**	**1.43**	**1.39**				
S.D.	**0.06**	**0.04**	**0.07**	**0.06**				
Difference (%)	**2.21**	**1.41**	**-2.80**	**2.16**				

Table A1.47 Ratio between MP maximum head width and head diameter (W/D)

	Right				Left			
	Index	Middle	Ring	Little	Index	Middle	Ring	Little
1	1.63	1.66	1.68	1.56				
3	1.62	1.54	1.71	1.84	1.73	1.37	1.73	1.67
4	1.50	1.57	1.51	1.67	1.64	1.60	1.66	1.80
5	1.78	1.74	1.95	2.00	1.74	1.86	1.95	1.96
6	1.43	1.54	1.66	1.76	1.63	1.71	1.75	1.76
7	1.60	1.60	1.73	1.70	1.45	1.69		1.72
8	1.60	1.75	1.82		1.98	1.85	2.00	1.72
9	1.72	1.61	1.77		1.60	1.57	1.72	1.75
10	1.63	1.91	1.57	1.90	1.60	1.63	1.47	1.62
11	1.64	1.55	1.37	1.58	1.53	1.57	1.76	1.60
12	1.57	1.62	1.68	1.64	1.51	1.62	1.89	1.58
Mean	**1.61**	**1.64**	**1.67**	**1.74**	**1.64**	**1.65**	**1.77**	**1.72**
S.D.	**0.09**	**0.11**	**0.15**	**0.14**	**0.14**	**0.14**	**0.15**	**0.11**
Overall mean	**1.63**	**1.65**	**1.72**	**1.73**				
S.D.	**0.12**	**0.12**	**0.16**	**0.12**				
Male mean	**1.63**	**1.68**	**1.70**	**1.77**				
S.D.	**0.09**	**0.14**	**0.14**	**0.13**				
Female mean	**1.61**	**1.66**	**1.75**	**1.65**				
S.D.	**0.15**	**0.09**	**0.18**	**0.06**				
Difference (%)	**1.24**	**1.20**	**-2.86**	**7.27**				

APPENDIX TWO

PIPJ dimensions grouped by joint prosthesis sizes (by PP head diameter) of 7, 8, 9, and 10 mm

Table A2.1 Distribution of PIPJs by joint size (PP head diameter) (mm)

No.	Size									
	6	6.5	7	7.5	8	8.5	9	9.5	10	11
1	8LL	11LL	7LL	1RL	3LL	1RR	1RI	1RM	3RM	4RM
2			10RL	4LL	4RL	3RL	3RR	3RI	3LM	
3			10LL	5RL	8RM	7RI	3LI	4LR	4RI	
4			12RL	5LL	9RL	7RR	3LR	5RR	4RR	
5				6RL	9LL	8RI	4LI	5LI	4LM	
6				6LL	10RM	8LI	5LR	5LM	5RI	
7				7RL	10LI	8LM	6LR	6RR	5RM	
8				8RR	11RM	9LR	9RR	6LM	6RI	
9				8LR	11LM	10RI	10LM	7RM	6RM	
10				11RI	12LL	10RR	12RI	7LI	6LI	
11				11RL		10LR	12RM	7LM	9RI	
12				11LR		11RR	12RR	11LI	9RM	
13						12LR	12LI		9LI	
14							12LM		9LM	

Table A2.2 Distribution of PIPJs by integer joint sizes (PP head diameter) of 7, 8, 9 and 10 mm

No.	Size				No.	Size			
	7	8	9	10		7	8	9	10
1	1RL	1RR	1RI	3RI	16		9LL	7LI	9LI
2	4LL	3RL	1RM	3RM	17		10RM	7LM	9LM
3	7RL	3LL	3RR	3LM	18		10LI	9RR	
4	7LL	4RL	3LI	4RI	19		10LR	9LR	
5	10RL	5RL	3LR	4RR	20		11RI	10RI	
6	10LL	5LL	4LI	4LM	21		11RM	10RR	
7	11RL	6RL	4LR	5RI	22		11LM	10LM	
8	11LR	6LL	5RR	5RM	23		12LR	11RR	
9	11LL	8RI	5LR	5LI	24		12LL	11LI	
10	12RL	8RM	6RR	5LM	25			12RI	
11		8RR	6LR	6RI	26			12RM	
12		8LI	6LM	6RM	27			12RR	
13		8LM	7RI	6LI	28			12LI	
14		8LR	7RM	9RI	29			12LM	
15		9RL	7RR	9RM					

N.B. 8LL (integer size 6 mm) and 4RM (integer size 11 mm) are excluded from these sizes.

Table A2.3 Finger distribution of the PIPJ sizes (PP head diameter) of 7, 8, 9 and 10 mm

Joint size (mm)	Finger Distribution			
	Index	Middle	Ring	Little
7	0	0	1	10
8	3	5	5	11
9	9	7	13	0
10	8	9	1	0

Table A2.4 Angle between the PP head-line and the longitudinal base-line, σ, sagittal plane (°)

7mm		8mm		9mm		10mm	
Joint	Angle	Joint	Angle	Joint	Angle	Joint	Angle
IRL	11	1RR	14	1RI	12	3RI	21
4LL	13	3RL	16	1RM	9	3RM	12
7RL	13	3LL		3RR	14	3LM	13
7LL	10	4RL	12	3LI	13	4RI	13
10RL	17	5RL	10	3LR	18	4RR	12
10LL	13	5LL	13	4LI	11	4LM	13
11RL	15	6RL	15	4LR	12	5RI	7
11LR	12	6LL	14	5RR	11	5RM	11
11LL	15	8RI	12	5LR	11	5LI	8
12RL	9	8RM	10	6RR	11	5LM	10
		8RR	11	6LM	11	6RI	6
		8LI	10	6LR	13	6RM	11
		8LM	11	7RI	11	6LI	9
		8LR	13	7RM	9	9RI	12
		9RL	18	7RR	12	9RM	13
		9LL	12	7LI	9	9LI	12
		10RM	14	7LM	11	9LM	13
		10LI	14	9RR	12		
		10LR	14	9LR	14		
		11RI	12	10RI	12		
		11RM	15	10RR	15		
		11LM	8	10LM	14		
		12LR	9	11RR	15		
		12LL	8	11LI	8		
				12RI	9		
				12RM	8		
				12RR	9		
				12LI	4		
				12LM	8		
Average	12.80	Average	12.39	Average	11.24	Average	11.53
S.D.	2.32	S.D.	2.80	S.D.	2.72	S.D.	3.20

Table A2.5 Angle between the PP main dorsal surface and the longitudinal base-line, ϕ, sagittal plane (°)

7mm		8mm		9mm		10mm	
Joint	**Angle**	**Joint**	**Angle**	**Joint**	**Angle**	**Joint**	**Angle**
IRL	6	1RR	5	1RI	5	3RI	3
4LL	8	3RL	7	1RM	6	3RM	2
7RL	8	3LL		3RR	2	3LM	2
7LL	4	4RL	7	3LI	4	4RI	5
10RL	9	5RL	7	3LR	9	4RR	3
10LL	8	5LL	8	4LI	3	4LM	4
11RL	7	6RL	7	4LR	5	5RI	6
11LR	2	6LL	8	5RR	4	5RM	4
11LL	8	8RI	6	5LR	5	5LI	6
12RL	9	8RM	2	6RR	3	5LM	4
		8RR	4	6LM	5	6RI	5
		8LI	5	6LR	5	6RM	5
		8LM	3	7RI	6	6LI	4
		8LR	5	7RM	3	9RI	5
		9RL	9	7RR	4	9RM	5
		9LL	5	7LI	4	9LI	4
		10RM	4	7LM	4	9LM	4
		10LI	7	9RR	5		
		10LR	5	9LR	5		
		11RI	3	10RI	7		
		11RM	2	10RR	8		
		11LM	3	10LM	7		
		12LR	3	11RR	4		
		12LL	8	11LI	4		
				12RI	4		
				12RM	4		
				12RR	3		
				12LI	4		
				12LM	4		
Average	**6.90**	**Average**	**5.35**	**Average**	**4.69**	**Average**	**4.18**
S.D.	**2.17**	**S.D.**	**2.06**	**S.D.**	**1.53**	**S.D.**	**1.15**

Table A2.6 Angle of the lateral condyle inclination, α1, transverse plane (°)

7mm		8mm		9mm		10mm	
Joint	**Angle**	**Joint**	**Angle**	**Joint**	**Angle**	**Joint**	**Angle**
IRL	76	1RR	72	1RI	81	3RI	79
4LL	77	3RL	82	1RM	76	3RM	88
7RL	72	3LL	71	3RR	85	3LM	86
7LL	77	4RL	84	3LI	80	4RI	73
10RL	80	5RL	79	3LR	85	4RR	73
10LL	76	5LL	81	4LI	79	4LM	77
11RL	82	6RL	82	4LR	75	5RI	70
11LR	82	6LL	81	5RR	76	5RM	71
11LL	87	8RI	79	5LR	85	5LI	70
12RL	89	8RM	79	6RR	77	5LM	80
		8RR	83	6LM	79	6RI	90
		8LI	85	6LR	77	6RM	71
		8LM	83	7RI	74	6LI	80
		8LR	72	7RM	73	9RI	70
		9RL	72	7RR	70	9RM	71
		9LL	85	7LI	75	9LI	84
		10RM	75	7LM	72	9LM	75
		10LI	69	9RR	75		
		10LR	74	9LR	69		
		11RI	76	10RI	66		
		11RM	76	10RR	76		
		11LM	88	10LM	77		
		12LR	75	11RR	77		
		12LL	80	11LI	84		
				12RI	78		
				12RM	83		
				12RR	82		
				12LI	82		
				12LM	88		
Average	**79.80**	**Average**	**78.50**	**Average**	**77.79**	**Average**	**76.94**
S.D.	**5.02**	**S.D.**	**5.07**	**S.D.**	**5.13**	**S.D.**	**6.57**

Table A2.7 Angle of the lateral condyle inclination, α2, transverse plane (°)

7mm		8mm		9mm		10mm	
Joint	**Angle**	**Joint**	**Angle**	**Joint**	**Angle**	**Joint**	**Angle**
IRL	83	1RR	74	1RI	85	3RI	83
4LL	89	3RL	75	1RM	80	3RM	70
7RL	78	3LL	69	3RR	83	3LM	81
7LL	72	4RL	81	3LI	72	4RI	77
10RL	90	5RL	88	3LR	82	4RR	72
10LL	75	5LL	84	4LI	74	4LM	76
11RL	82	6RL	78	4LR	75	5RI	76
11LR	81	6LL	89	5RR	75	5RM	74
11LL	86	8RI	77	5LR	82	5LI	74
12RL	77	8RM	85	6RR	75	5LM	72
		8RR	86	6LM	71	6RI	72
		8LI	74	6LR	77	6RM	80
		8LM	84	7RI	76	6LI	85
		8LR	81	7RM	78	9RI	81
		9RL	84	7RR	81	9RM	75
		9LL	81	7LI	79	9LI	68
		10RM	80	7LM	70	9LM	78
		10LI	81	9RR	77		
		10LR	78	9LR	73		
		11RI	79	10RI	84		
		11RM	81	10RR	68		
		11LM	78	10LM	71		
		12LR	83	11RR	79		
		12LL	82	11LI	70		
				12RI	96		
				12RM	87		
				12RR	82		
				12LI	74		
				12LM	78		
Average	**81.30**	**Average**	**80.50**	**Average**	**77.38**	**Average**	**76.12**
S.D.	**5.62**	**S.D.**	**4.59**	**S.D.**	**5.12**	**S.D.**	**4.59**

Table A2.8 Dorsal offset of the PP medullary canal centre-line to the PIPJ centre of rotation, sagittal plane (mm)

7mm		8mm		9mm		10mm	
Joint	**Offset**	**Joint**	**Offset**	**Joint**	**Offset**	**Joint**	**Offset**
IRL	0.7	1RR	0.8	1RI	0.8	3RI	0.8
4LL	0.9	3RL	0.2	1RM	1.0	3RM	0.9
7RL	0.2	3LL		3RR	0.8	3LM	0.7
7LL	0.7	4RL	0.5	3LI	0.7	4RI	1.0
10RL	0.4	5RL	0.7	3LR	0.7	4RR	0.6
10LL	0.9	5LL	0.3	4LI	0.8	4LM	1.1
11RL	0.6	6RL	0.7	4LR	0.8	5RI	1.1
11LR	1.0	6LL	0.5	5RR	1.0	5RM	0.8
11LL	0.4	8RI	0.5	5LR	0.8	5LI	0.7
12RL	0.9	8RM	1.5	6RR	0.8	5LM	0.8
		8RR	0.9	6LM	0.8	6RI	1.0
		8LI	1.0	6LR	0.9	6RM	0.6
		8LM	0.9	7RI	0.7	6LI	0.7
		8LR	0.7	7RM	0.9	9RI	0.9
		9RL	0.5	7RR	0.8	9RM	1.2
		9LL	0.6	7LI	0.8	9LI	1.0
		10RM	0.6	7LM	0.7	9LM	0.7
		10LI	0.8	9RR	0.6		
		10LR	0.7	9LR	0.6		
		11RI	0.6	10RI	0.9		
		11RM	0.7	10RR	0.7		
		11LM	0.7	10LM	0.6		
		12LR	1.0	11RR	0.9		
		12LL	0.7	11LI	1.0		
				12RI	0.7		
				12RM	0.6		
				12RR	0.8		
				12LI	0.9		
				12LM	0.9		
Average	**0.67**	**Average**	**0.70**	**Average**	**0.79**	**Average**	**0.86**
S.D.	**0.25**	**S.D.**	**0.26**	**S.D.**	**0.12**	**S.D.**	**0.18**

Table A2.9 Angle between the PP medullary canal centre-line and the longitudinal base-line, ρ, sagittal plane (°)

7mm		8mm		9mm		10mm	
Joint	**Angle**	**Joint**	**Angle**	**Joint**	**Angle**	**Joint**	**Angle**
IRL	11	1RR	12	1RI	8	3RI	13
4LL	5	3RL	11	1RM	9	3RM	9
7RL	12	3LL		3RR	12	3LM	13
7LL	10	4RL	12	3LI	13	4RI	6
10RL	17	5RL	6	3LR	13	4RR	13
10LL	8	5LL	10	4LI	10	4LM	7
11RL	13	6RL	14	4LR	11	5RI	4
11LR	10	6LL	12	5RR	8	5RM	11
11LL	11	8RI	12	5LR	9	5LI	9
12RL	8	8RM	6	6RR	12	5LM	8
		8RR	10	6LM	11	6RI	8
		8LI	9	6LR	14	6RM	11
		8LM	11	7RI	10	6LI	9
		8LR	14	7RM	10	9RI	15
		9RL	12	7RR	12	9RM	9
		9LL	12	7LI	10	9LI	11
		10RM	14	7LM	12	9LM	13
		10LI	11	9RR	12		
		10LR	14	9LR	14		
		11RI	12	10RI	9		
		11RM	15	10RR	15		
		11LM	10	10LM	14		
		12LR	8	11RR	10		
		12LL	8	11LI	8		
				12RI	10		
				12RM	8		
				12RR	10		
				12LI	8		
				12LM	8		
Average	**10.50**	**Average**	**11.09**	**Average**	**10.69**	**Average**	**9.94**
S.D.	**3.07**	**S.D.**	**2.41**	**S.D.**	**2.09**	**S.D.**	**2.84**

Table A2.10 Alignment of PP head condyles, θ, frontal plane (°)

7mm		8mm		9mm		10mm	
Joint	**Angle**	**Joint**	**Angle**	**Joint**	**Angle**	**Joint**	**Angle**
IRL	6.5	1RR	1.5	1RI	-1.0	3RI	0
4LL	-7.0	3RL	6.5	1RM	1.5	3RM	4.0
7RL	5.0	3LL	-8.5	3RR	1.5	3LM	-1.5
7LL	-4.0	4RL	5.5	3LI	0	4RI	1.0
10RL	5.0	5RL	5.0	3LR	-3.0	4RR	3.0
10LL	-5.0	5LL	-7.5	4LI	0	4LM	2.0
11RL	8.0	6RL	7.0	4LR	-3.5	5RI	-1.0
11LR	-5.5	6LL	-8.0	5RR	3.5	5RM	-2.0
11LL	-7.0	8RI	6.0	5LR	-4.0	5LI	1.5
12RL	3.0	8RM	-1.0	6RR	6.5	5LM	0.5
		8RR	1.0	6LM	4.0	6RI	-6.0
		8LI	1.5	6LR	-6.0	6RM	-2.5
		8LM	-1.5	7RI	-2.5	6LI	6.0
		8LR	-2.5	7RM	0	9RI	-2.5
		9RL	-3.5	7RR	-1.0	9RM	-0.5
		9LL	-5.0	7LI	2.5	9LI	0.5
		10RM	1.5	7LM	2.0	9LM	1.0
		10LI	1.5	9RR	0		
		10LR	-1.0	9LR	-1.0		
		11RI	5.0	10RI	-1.5		
		11RM	0	10RR	6.0		
		11LM	0.5	10LM	1.5		
		12LR	-2.0	11RR	-4.5		
		12LL	-5.0	11LI	0.5		
				12RI	-2.0		
				12RM	-2.0		
				12RR	1.5		
				12LI	1.5		
				12LM	3.0		
Average	**-0.10**	**Average**	**-0.08**	**Average**	**0.12**	**Average**	**0.21**
S.D.	**5.78**	**S.D.**	**4.51**	**S.D.**	**2.94**	**S.D.**	**2.7**

Table A2.11 Distance from the PP head centre-line to the base of the condyle, a, transverse plane (mm)

7mm		8mm		9mm		10mm	
Joint	**Distance**	**Joint**	**Distance**	**Joint**	**Distance**	**Joint**	**Distance**
IRL	3.2	1RR	5.9	1RI	4.7	3RI	5.5
4LL	2.8	3RL	4.2	1RM	4.9	3RM	6.3
7RL	3.8	3LL	4.4	3RR	5.3	3LM	5.7
7LL	3.8	4RL	4.0	3LI	5.6	4RI	5.2
10RL	3.5	5RL	3.7	3LR	4.9	4RR	4.8
10LL	3.6	5LL	3.6	4LI	4.9	4LM	4.7
11RL	3.4	6RL	4.2	4LR	4.4	5RI	5.8
11LR	4.0	6LL	3.4	5RR	5.2	5RM	5.0
11LL	3.7	8RI	4.6	5LR	5.1	5LI	5.0
12RL	3.6	8RM	4.5	6RR	3.6	5LM	6.6
		8RR	3.4	6LM	4.8	6RI	5.0
		8LI	4.1	6LR	4.1	6RM	4.2
		8LM	4.5	7RI	4.9	6LI	4.0
		8LR	4.0	7RM	5.0	9RI	4.8
		9RL	5.2	7RR	4.8	9RM	5.0
		9LL	3.6	7LI	5.2	9LI	5.4
		10RM	4.2	7LM	5.2	9LM	5.5
		10LI	4.1	9RR	4.9		
		10LR	4.3	9LR	4.4		
		11RI	4.9	10RI	4.1		
		11RM	4.3	10RR	4.9		
		11LM	5.1	10LM	4.9		
		12LR	5.2	11RR	4.7		
		12LL	3.9	11LI	4.3		
				12RI	5.2		
				12RM	4.5		
				12RR	3.7		
				12LI	5.3		
				12LM	4.8		
Average	**3.54**	**Average**	**4.30**	**Average**	**4.77**	**Average**	**5.21**
S.D.	**0.33**	**S.D.**	**0.60**	**S.D.**	**0.46**	**S.D.**	**0.65**

Table A2.12 Distance from the PP head centre-line to the base of the condyle, b, transverse plane (mm)

7mm		8mm		9mm		10mm	
Joint	**Distance**	**Joint**	**Distance**	**Joint**	**Distance**	**Joint**	**Distance**
IRL	4.0	1RR	5.2	1RI	4.8	3RI	6.2
4LL	3.7	3RL	4.7	1RM	5.0	3RM	6.0
7RL	3.8	3LL	4.4	3RR	5.4	3LM	6.5
7LL	3.6	4RL	3.9	3LI	5.6	4RI	5.3
10RL	3.8	5RL	3.8	3LR	5.4	4RR	5.3
10LL	3.7	5LL	4.0	4LI	4.8	4LM	4.9
11RL	4.5	6RL	4.3	4LR	5.6	5RI	5.7
11LR	4.8	6LL	4.1	5RR	5.3	5RM	5.2
11LL	4.1	8RI	4.3	5LR	5.0	5LI	4.6
12RL	3.7	8RM	5.6	6RR	4.9	5LM	5.1
		8RR	4.1	6LM	4.4	6RI	4.4
		8LI	4.3	6LR	5.2	6RM	5.2
		8LM	4.8	7RI	4.3	6LI	4.9
		8LR	4.9	7RM	5.2	9RI	5.8
		9RL	4.4	7RR	5.3	9RM	5.6
		9LL	3.7	7LI	4.7	9LI	4.7
		10RM	4.3	7LM	5.4	9LM	4.7
		10LI	4.9	9RR	4.7		
		10LR	4.7	9LR	4.8		
		11RI	4.7	10RI	5.2		
		11RM	5.5	10RR	5.0		
		11LM	5.2	10LM	5.3		
		12LR	5.1	11RR	5.4		
		12LL	5.0	11LI	4.6		
				12RI	5.4		
				12RM	5.1		
				12RR	4.4		
				12LI	5.4		
				12LM	4.7		
Average	**3.97**	**Average**	**4.58**	**Average**	**5.04**	**Average**	**5.30**
S.D.	**0.37**	**S.D.**	**0.52**	**S.D.**	**0.36**	**S.D.**	**0.58**

Table A2.13 Maximum depth of the inter-condylar sulcus of the PP head, ISat, transverse plane, anterior face (mm)

7mm		8mm		9mm		10mm	
Joint	**Depth**	**Joint**	**Depth**	**Joint**	**Depth**	**Joint**	**Depth**
IRL	0.5	1RR	0.7	1RI	0.7	3RI	0.8
4LL	0.5	3RL	0.8	1RM	1.0	3RM	1.2
7RL	0.7	3LL	0.8	3RR	1.0	3LM	1.0
7LL	0.7	4RL	0.6	3LI	1.1	4RI	1.0
10RL	0.5	5RL	0.5	3LR	1.1	4RR	1.0
10LL	0.5	5LL	0.5	4LI	0.9	4LM	0.9
11RL	0.6	6RL	0.5	4LR	0.9	5RI	1.0
11LR	0.8	6LL	0.6	5RR	0.6	5RM	1.1
11LL	0.6	8RI	0.7	5LR	0.8	5LI	0.9
12RL	0.6	8RM	0.8	6RR	0.7	5LM	1.0
		8RR	0.8	6LM	0.9	6RI	0.6
		8LI	0.8	6LR	0.7	6RM	0.7
		8LM	0.7	7RI	1.0	6LI	0.6
		8LR	0.7	7RM	1.1	9RI	1.1
		9RL	0.6	7RR	0.9	9RM	1.0
		9LL	0.6	7LI	1.2	9LI	0.8
		10RM	0.6	7LM	1.1	9LM	0.8
		10LI	0.9	9RR	0.8		
		10LR	0.9	9LR	0.6		
		11RI	1.1	10RI	0.9		
		11RM	1.1	10RR	0.9		
		11LM	0.9	10LM	0.8		
		12LR	1.1	11RR	1.0		
		12LL	0.9	11LI	1.2		
				12RI	0.9		
				12RM	0.7		
				12RR	0.9		
				12LI	0.6		
				12LM	1.0		
Average	**0.60**	**Average**	**0.76**	**Average**	**0.90**	**Average**	**0.91**
S.D.	**0.10**	**S.D.**	**0.18**	**S.D.**	**0.17**	**S.D.**	**0.17**

Table A2.14 Maximum depth of the inter-condylar sulcus of the PP head, ISf, frontal plane (mm)

7mm		8mm		9mm		10mm	
Joint	**Depth**	**Joint**	**Depth**	**Joint**	**Depth**	**Joint**	**Depth**
IRL	0.5	1RR	0.6	1RI	0.9	3RI	1.2
4LL	0.5	3RL	0.7	1RM	0.8	3RM	1.0
7RL	0.5	3LL	0.8	3RR	0.9	3LM	1.3
7LL	0.7	4RL	0.7	3LI	0.9	4RI	1.0
10RL	0.6	5RL	0.6	3LR	1.0	4RR	0.6
10LL	0.4	5LL	0.7	4LI	1.2	4LM	0.9
11RL	0.6	6RL	0.4	4LR	0.8	5RI	0.9
11LR	0.7	6LL	0.5	5RR	0.5	5RM	0.8
11LL	0.8	8RI	0.5	5LR	0.6	5LI	0.8
12RL	0.6	8RM	0.7	6RR	0.5	5LM	0.7
		8RR	0.6	6LM	0.6	6RI	0.6
		8LI	0.8	6LR	0.5	6RM	0.6
		8LM	0.7	7RI	0.8	6LI	0.6
		8LR	0.5	7RM	0.9	9RI	0.7
		9RL	0.8	7RR	0.6	9RM	0.7
		9LL	0.4	7LI	0.9	9LI	0.7
		10RM	0.5	7LM	0.9	9LM	0.7
		10LI	0.7	9RR	0.8		
		10LR	0.5	9LR	0.5		
		11RI	0.7	10RI	0.8		
		11RM	0.8	10RR	0.5		
		11LM	0.8	10LM	0.7		
		12LR	0.7	11RR	1.2		
		12LL	0.6	11LI	1.1		
				12RI	0.8		
				12RM	0.8		
				12RR	0.7		
				12LI	0.8		
				12LM	0.8		
Average	**0.59**	**Average**	**0.64**	**Average**	**0.79**	**Average**	**0.81**
S.D.	**0.11**	**S.D.**	**0.13**	**S.D.**	**0.19**	**S.D.**	**0.21**

Table A2.15 PP maximum head width (Wtp), transverse plane (mm)

7mm		8mm		9mm		10mm	
Joint	**Width**	**Joint**	**Width**	**Joint**	**Width**	**Joint**	**Width**
IRL	9.8	1RR	13.9	1RI	12.5	3RI	13.0
4LL	10.8	3RL	10.7	1RM	12.1	3RM	14.0
7RL	10.6	3LL	11.5	3RR	12.0	3LM	13.8
7LL	9.6	4RL	11.0	3LI	12.5	4RI	13.2
10RL	10.6	5RL	10.6	3LR	12.2	4RR	14.0
10LL	10.4	5LL	11.0	4LI	13.0	4LM	14.0
11RL	10.0	6RL	10.8	4LR	13.1	5RI	13.9
11LR	10.9	6LL	10.0	5RR	14.3	5RM	15.3
11LL	9.7	8RI	12.1	5LR	13.7	5LI	13.9
12RL	10.3	8RM	12.1	6RR	12.5	5LM	14.6
		8RR	11.2	6LM	13.3	6RI	12.8
		8LI	11.9	6LR	12.8	6RM	13.5
		8LM	11.8	7RI	11.8	6LI	12.6
		8LR	11.7	7RM	12.7	9RI	14.5
		9RL	12.2	7RR	12.6	9RM	15.0
		9LL	11.6	7LI	12.5	9LI	14.4
		10RM	11.3	7LM	13.8	9LM	14.7
		10LI	12.6	9RR	13.7		
		10LR	12.3	9LR	14.0		
		11RI	11.8	10RI	13.2		
		11RM	12.2	10RR	13.1		
		11LM	12.1	10LM	13.2		
		12LR	12.3	11RR	12.5		
		12LL	10.8	11LI	12.2		
				12RI	12.8		
				12RM	12.4		
				12RR	12.1		
				12LI	12.8		
				12LM	12.6		
Average	**10.27**	**Average**	**11.65**	**Average**	**12.83**	**Average**	**13.36**
S.D.	**0.45**	**S.D.**	**0.80**	**S.D.**	**0.62**	**S.D.**	**2.33**

Table A2.16 PP maximum head height (Htp), transverse plane (mm)

7mm		8mm		9mm		10mm	
Joint	**Height**	**Joint**	**Height**	**Joint**	**Height**	**Joint**	**Height**
IRL	7.2	1RR	9.1	1RI	8.7	3RI	9.2
4LL	7.4	3RL	7.7	1RM	8.8	3RM	11.4
7RL	7.6	3LL	8.1	3RR	8.5	3LM	9.5
7LL	7.7	4RL	7.6	3LI	9.1	4RI	9.2
10RL	7.3	5RL	7.7	3LR	8.6	4RR	9.2
10LL	6.9	5LL	7.4	4LI	9.0	4LM	9.4
11RL	6.3	6RL	7.3	4LR	8.9	5RI	9.5
11LR	7.8	6LL	7.2	5RR	9.4	5RM	10.6
11LL	6.4	8RI	8.4	5LR	9.5	5LI	9.1
12RL	7.8	8RM	8.8	6RR	9.1	5LM	10.7
		8RR	7.8	6LM	9.6	6RI	8.7
		8LI	8.1	6LR	8.3	6RM	9.2
		8LM	8.4	7RI	8.7	6LI	8.9
		8LR	7.8	7RM	9.4	9RI	10.2
		9RL	7.9	7RR	8.2	9RM	10.5
		9LL	8.0	7LI	9.3	9LI	10.0
		10RM	8.0	7LM	9.6	9LM	10.3
		10LI	8.6	9RR	9.7		
		10LR	8.9	9LR	9.7		
		11RI	7.7	10RI	8.8		
		11RM	8.0	10RR	8.6		
		11LM	8.1	10LM	8.9		
		12LR	8.8	11RR	8.2		
		12LL	7.7	11LI	8.2		
				12RI	8.8		
				12RM	9.6		
				12RR	9.2		
				12LI	8.8		
				12LM	9.8		
Average	**7.24**	**Average**	**8.05**	**Average**	**9.00**	**Average**	**9.74**
S.D.	**0.52**	**S.D.**	**0.50**	**S.D.**	**0.48**	**S.D.**	**0.73**

A2.17 Distance from the PIPJ bearing surface to the change in angle of the PP dorsal surface (d), sagittal plane (mm)

7mm		8mm		9mm		10mm	
Joint	**Distance**	**Joint**	**Distance**	**Joint**	**Distance**	**Joint**	**Distance**
IRL	14.1	1RR	12.2	1RI	15.0	3RI	13.5
4LL	13.4	3RL	10.9	1RM	14.7	3RM	15.2
7RL	11.9	3LL		3RR	12.3	3LM	14.6
7LL	10.0	4RL	13.7	3LI	13.8	4RI	18.7
10RL	9.5	5RL	11.4	3LR	12.5	4RR	14.4
10LL	11.8	5LL	10.6	4LI	15.9	4LM	16.5
11RL	9.7	6RL	11.4	4LR	14.8	5RI	11.2
11LR	13.7	6LL	11.8	5RR	13.9	5RM	13.9
11LL	11.3	8RI	14.8	5LR	13.2	5LI	13.2
12RL		8RM	18.0	6RR	14.9	5LM	14.7
		8RR	13.4	6LM	14.6	6RI	
		8LI	12.9	6LR	12.1	6RM	13.2
		8LM	14.3	7RI	12.1	6LI	15.4
		8LR	12.4	7RM	14.5	9RI	18.7
		9RL	10.0	7RR	14.9	9RM	18.2
		9LL	14.3	7LI	12.2	9LI	18.8
		10RM	12.2	7LM	11.6	9LM	15.0
		10LI	11.1	9RR	18.1		
		10LR	13.4	9LR	14.3		
		11RI	14.3	10RI	13.5		
		11RM	11.8	10RR	11.2		
		11LM	17.5	10LM	14.1		
		12LR	18.4	11RR	13.2		
		12LL		11LI	19.9		
				12RI	12.4		
				12RM	17.3		
				12RR	18.4		
				12LI	19.2		
				12LM	19.1		
Average	**11.71**	**Average**	**13.22**	**Average**	**14.61**	**Average**	**15.33**
S.D.	**1.65**	**S.D.**	**2.29**	**S.D.**	**2.39**	**S.D.**	**2.21**

A2.18 Arc of the middle phalangeal base, sagittal plane (°)

7mm		8mm		9mm		10mm	
Joint	**Arc**	**Joint**	**Arc**	**Joint**	**Arc**	**Joint**	**Arc**
IRL	80	1RR	90	1RI	73	3RI	74
4LL	90	3RL	74	1RM	82	3RM	83
7RL	76	3LL	74	3RR	78	3LM	77
7LL	76	4RL	85	3LI	82	4RI	71
10RL	78	5RL	84	3LR	80	4RR	73
10LL	78	5LL	90	4LI	78	4LM	70
11RL	80	6RL	75	4LR	87	5RI	72
11LR	76	6LL	90	5RR	81	5RM	81
11LL	72	8RI	76	5LR	88	5LI	71
12RL	82	8RM	72	6RR	82	5LM	82
		8RR	69	6LM	84	6RI	66
		8LI	69	6LR	90	6RM	76
		8LM	71	7RI	68	6LI	70
		8LR	74	7RM	70	9RI	70
		9RL		7RR	69	9RM	78
		9LL	84	7LI	62	9LI	74
		10RM	87	7LM	66	9LM	79
		10LI	74	9RR	83		
		10LR	90	9LR	84		
		11RI	72	10RI	75		
		11RM	74	10RR	80		
		11LM	86	10LM	79		
		12LR	82	11RR	63		
		12LL	75	11LI	65		
				12RI	72		
				12RM	87		
				12RR	72		
				12LI	74		
				12LM	79		
Average	**78.8**	**Average**	**79.0**	**Average**	**77.0**	**Average**	**74.53**
S.D.	**4.83**	**S.D.**	**7.45**	**S.D.**	**7.80**	**S.D.**	**4.86**

A2.19 Offset of the MP stem from the PIPJ centre of rotation

7mm		8mm		9mm		10mm	
Joint	**Offset**	**Joint**	**Offset**	**Joint**	**Offset**	**Joint**	**Offset**
IRL	0	1RR	-0.2	1RI	0.2	3RI	0
4LL	0	3RL	0	1RM	0.3	3RM	-0.4
7RL	-0.1	3LL	0	3RR	-0.3	3LM	0.3
7LL	0.1	4RL	0	3LI	0.3	4RI	0.7
10RL	0	5RL	0.3	3LR	0	4RR	0.3
10LL	0	5LL	0.3	4LI	0.5	4LM	0
11RL	-0.2	6RL	0	4LR	0	5RI	0.8
11LR	0.2	6LL	-0.3	5RR	0.2	5RM	0.5
11LL	0	8RI	0.6	5LR	0	5LI	0.5
12RL	0	8RM	-0.1	6RR	-0.3	5LM	0.8
		8RR	0	6LM	0.1	6RI	0.5
		8LI	0.7	6LR	-0.3	6RM	0.5
		8LM	0.1	7RI	0.3	6LI	0
		8LR	-0.3	7RM	0.3	9RI	0.6
		9RL		7RR	0.2	9RM	0
		9LL	0	7LI	0.2	9LI	-0.2
		10RM	0	7LM	0.6	9LM	0
		10LI	-0.5	9RR	0.5		
		10LR	0.3	9LR	0.1		
		11RI	0.6	10RI	0.2		
		11RM	0.3	10RR	-0.4		
		11LM	-0.5	10LM	0.2		
		12LR	0.4	11RR	0.3		
		12LL	0.5	11LI	-0.6		
				12RI	0.3		
				12RM	0.3		
				12RR	0.2		
				12LI	0.7		
				12LM	0.5		
Average	**0.0**	**Average**	**0.10**	**Average**	**0.15**	**Average**	**0.29**
S.D.	**0.11**	**S.D.**	**0.34**	**S.D.**	**0.30**	**S.D.**	**0.36**

All dimensions in mm unless otherwise stated.

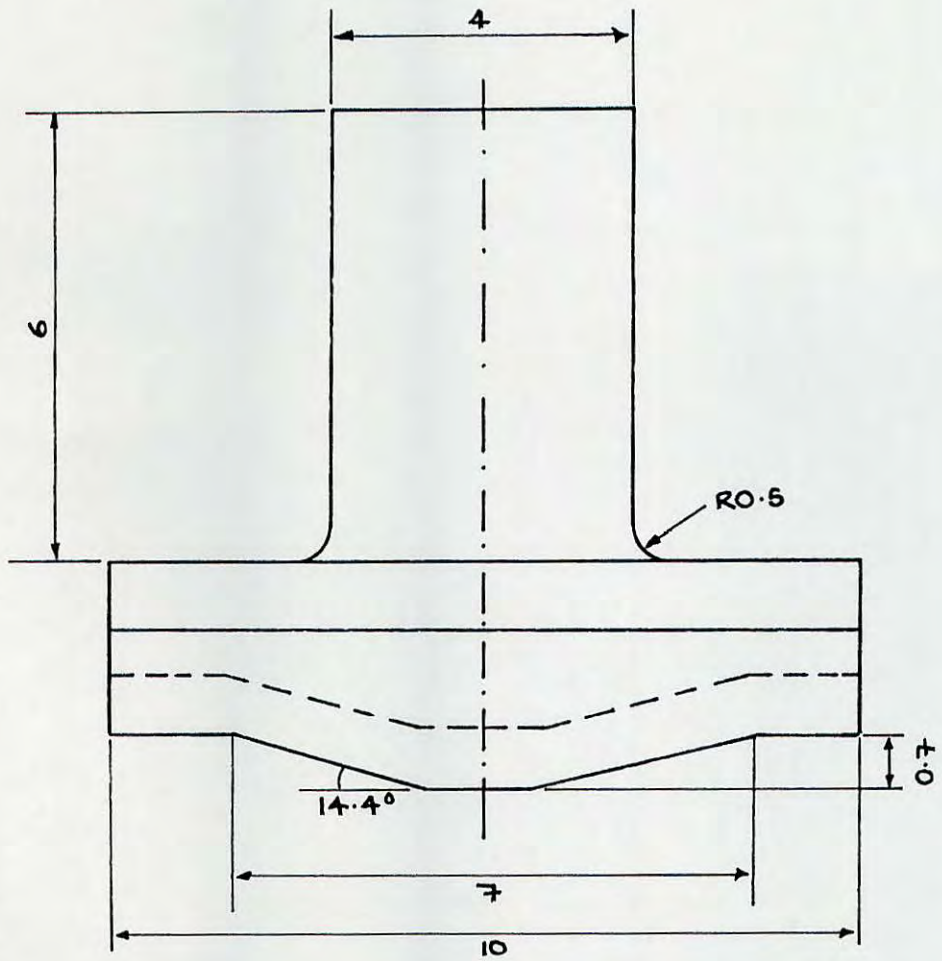

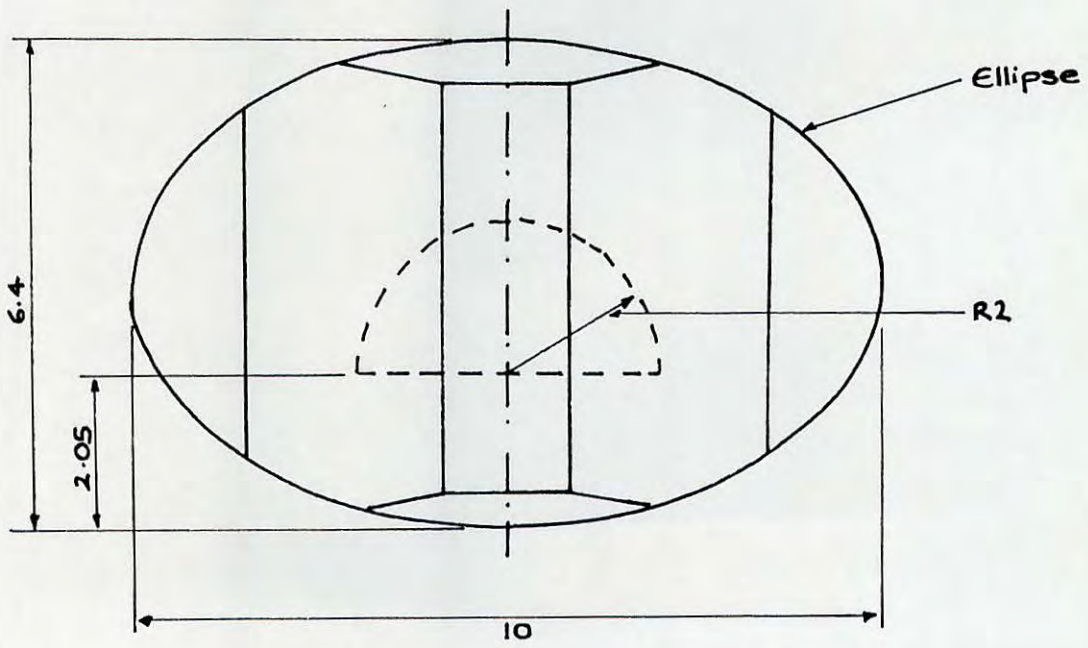

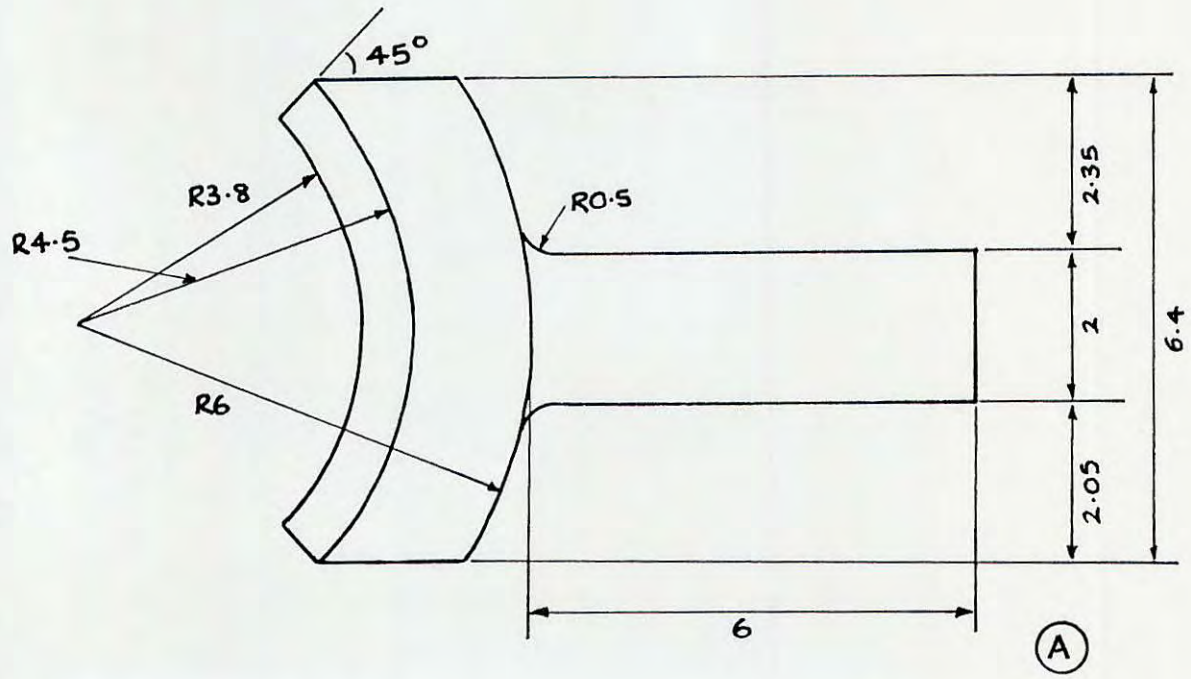

Notes: 0·15mm palmar offset of stem with respect to the centre of rotation of the middle phalangeal base. (A)

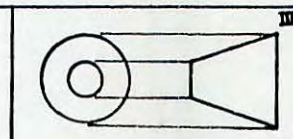

Scale 10:1

Feb 1997

9mm PIPJ surface replacement prosthesis. Middle phalangeal base.

Hayley Ash.

Figure A3.7

All dimensions in mm unless otherwise stated.

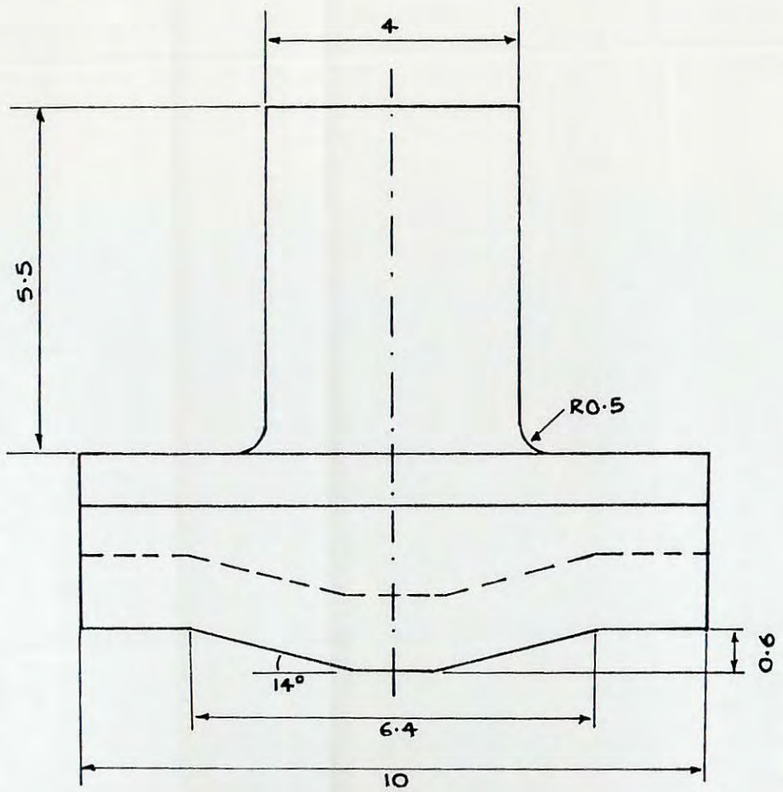

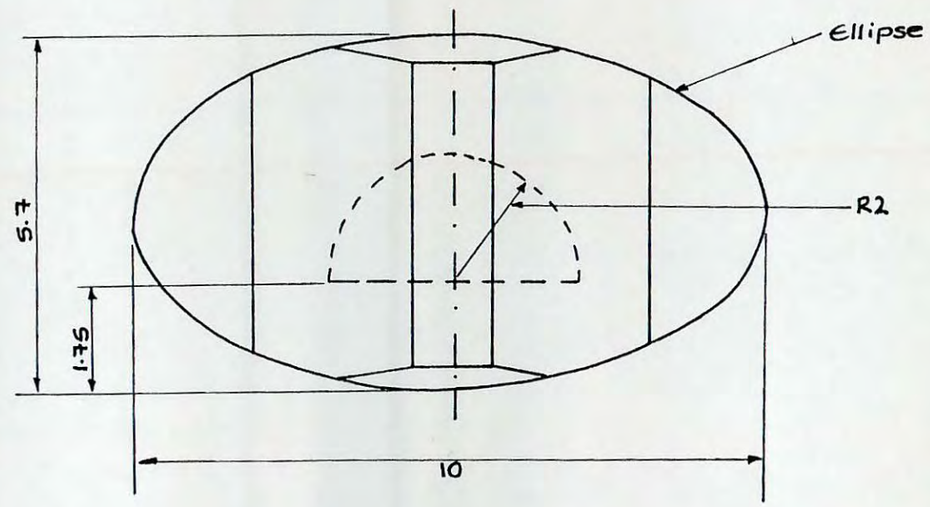

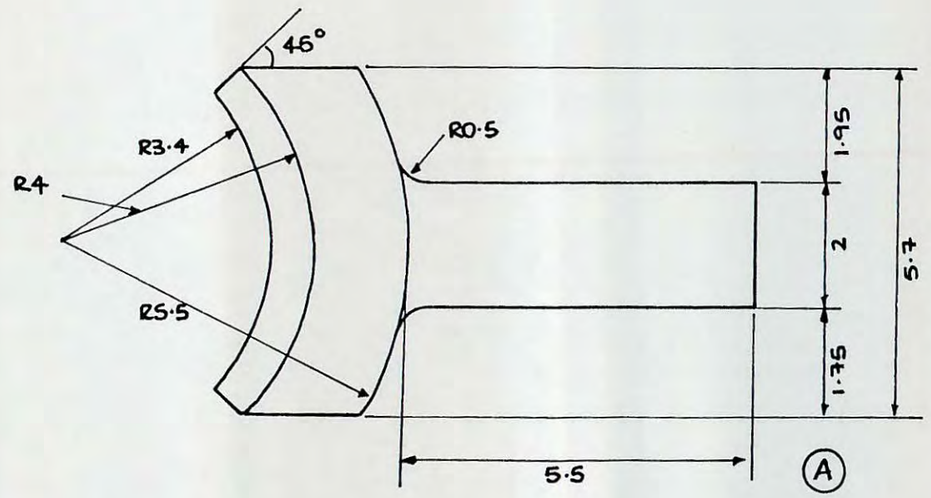

Notes: 0·1mm palmar offset of stem with respect to the centre of rotation of the middle phalangeal base. (A)

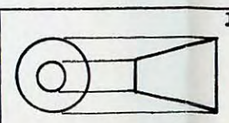

Scale 10:1	8mm PIPJ surface replacement prosthesis. Middle phalangeal base.
Feb. 1997	Hayley Ash.
	Figure A3·6

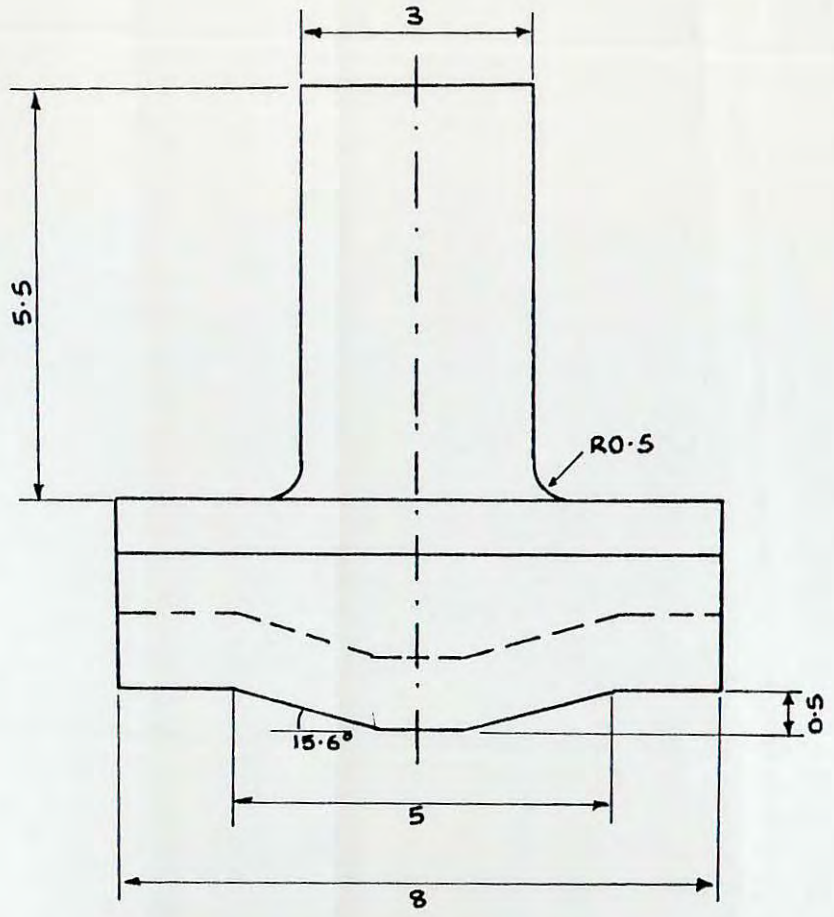

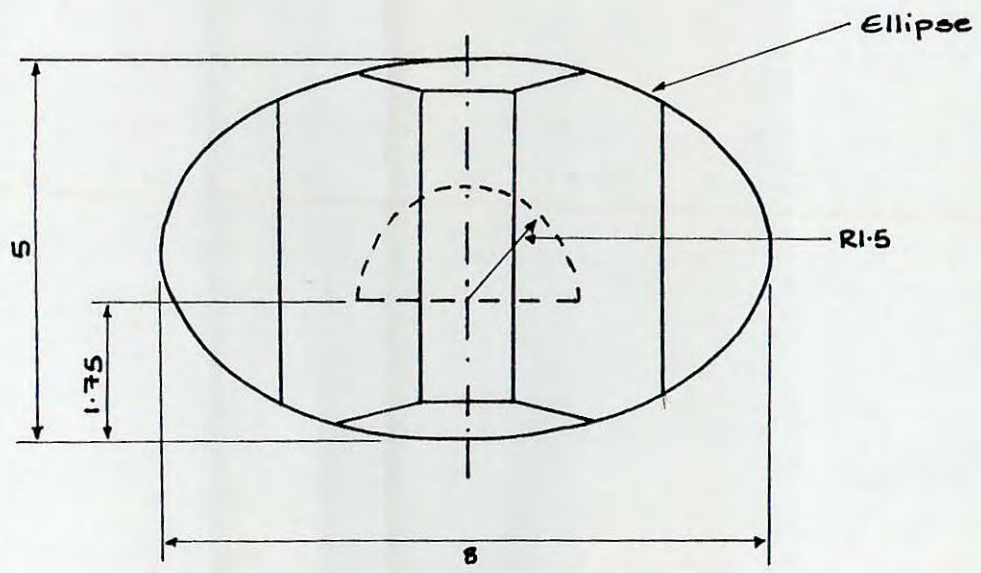

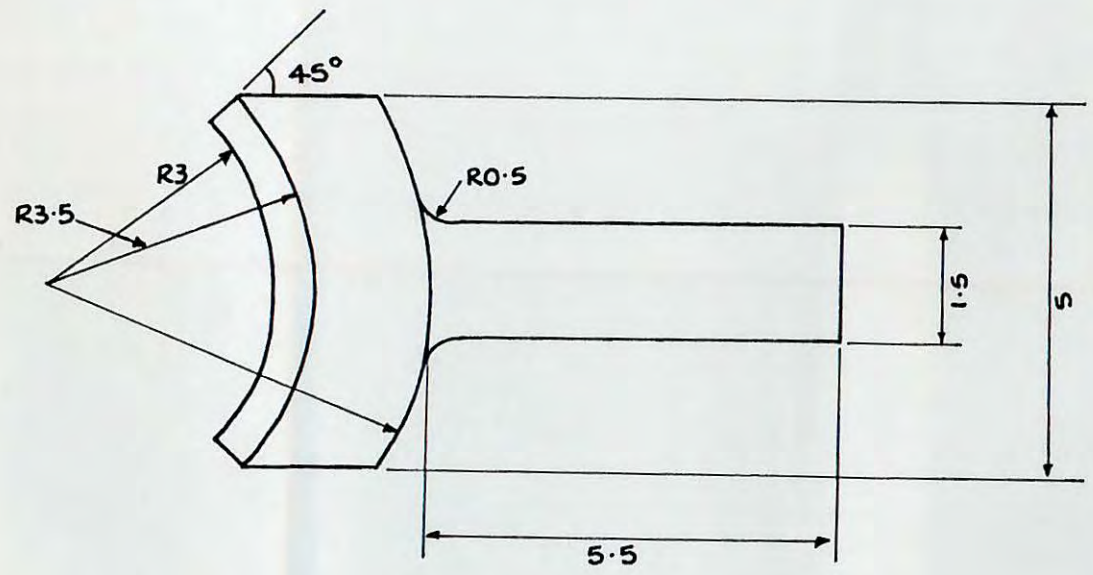

Notes: No offset of stem with respect to the centre of rotation of the middle phalangeal base. All dimensions in mm unless otherwise stated.

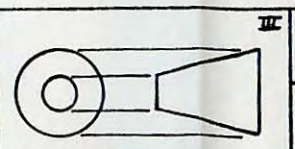

Scale 10:1	7mm PIPJ surface replacement prosthesis. Middle phalangeal base.
Feb. 1997	Hayley Ash.
	Figure A 3·5

All dimensions in mm unless otherwise stated

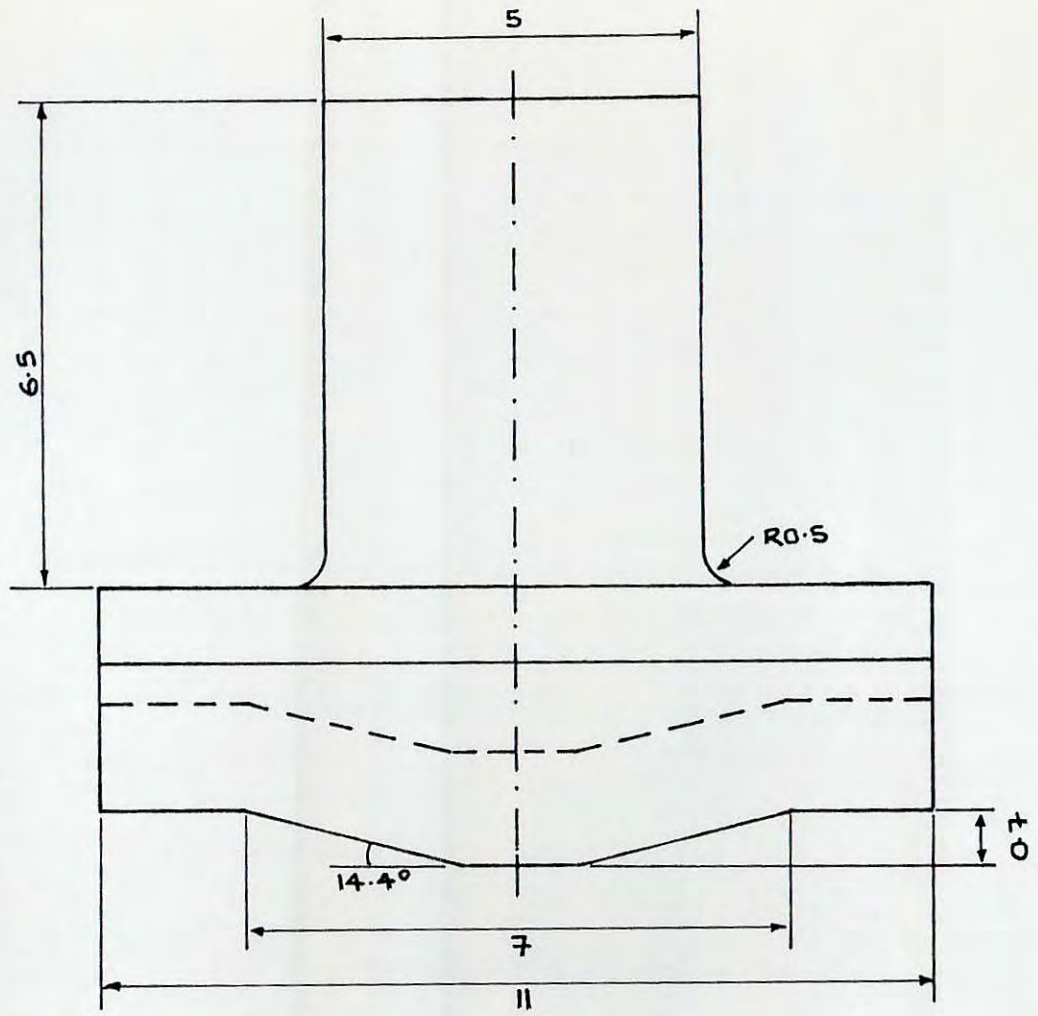

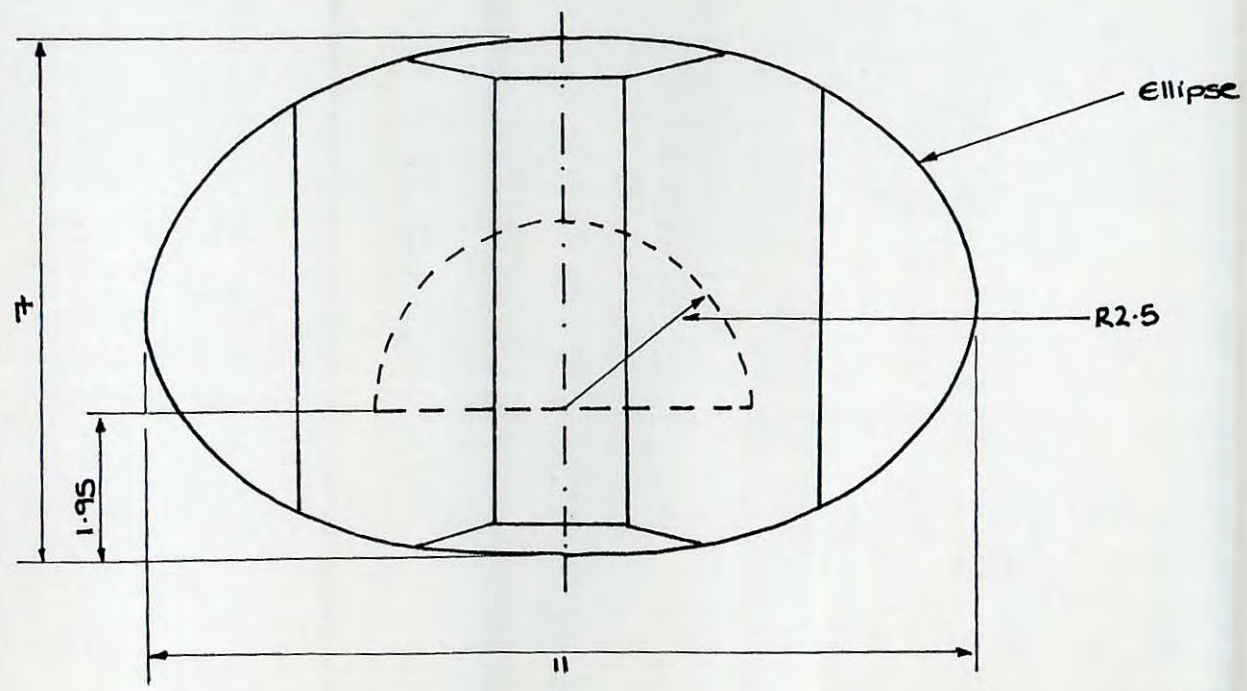

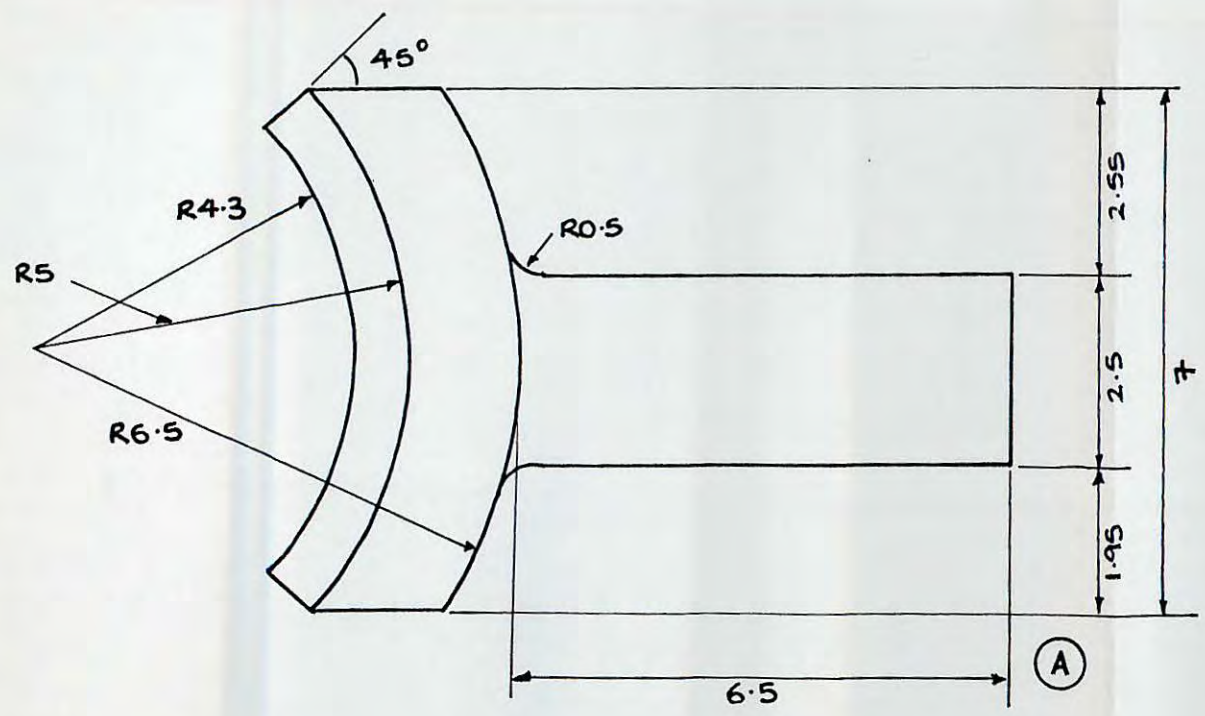

Notes: 0·3mm palmar offset of stem with respect to the centre of rotation of the middle phalangeal base. (A)

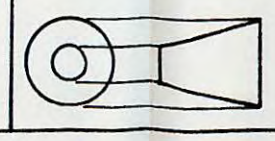

Scale 10:1

Feb. 1997

10mm PIPJ surface replacement prosthesis. Middle phalangeal base.

Hayley Ash.

Figure A3·8

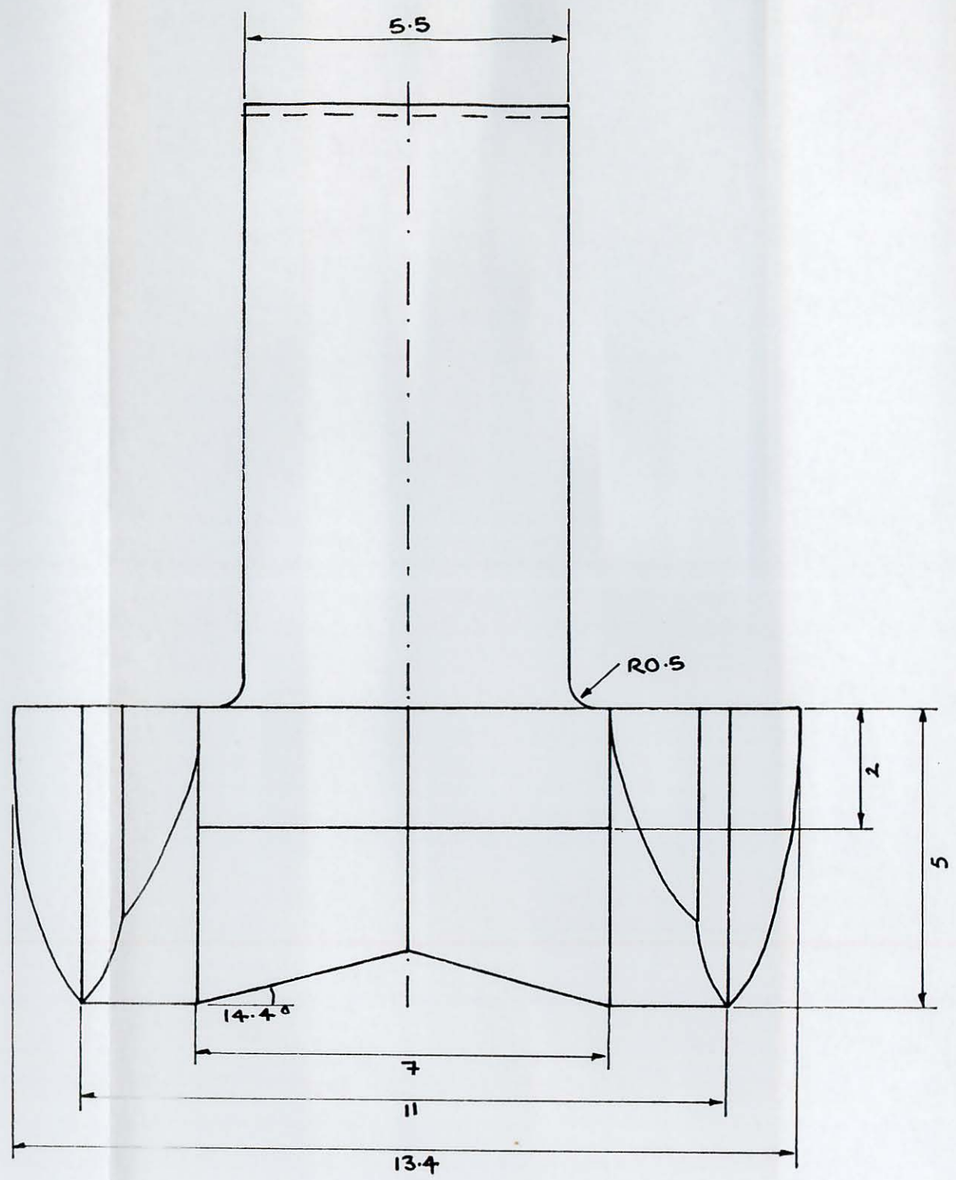

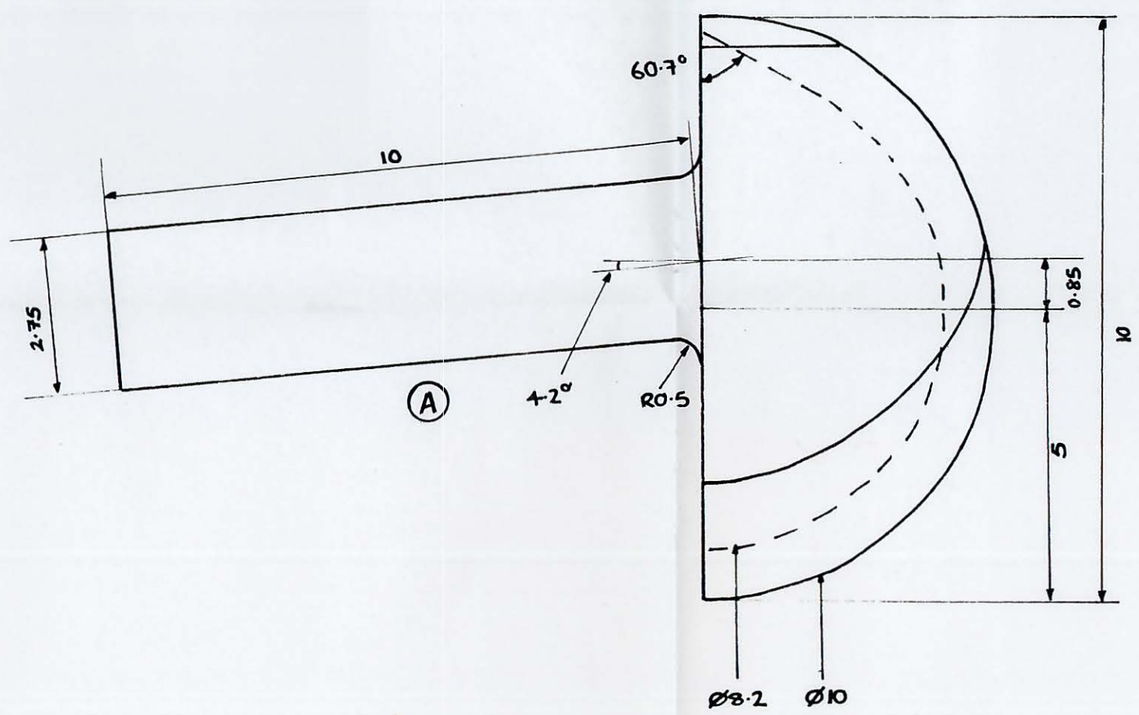

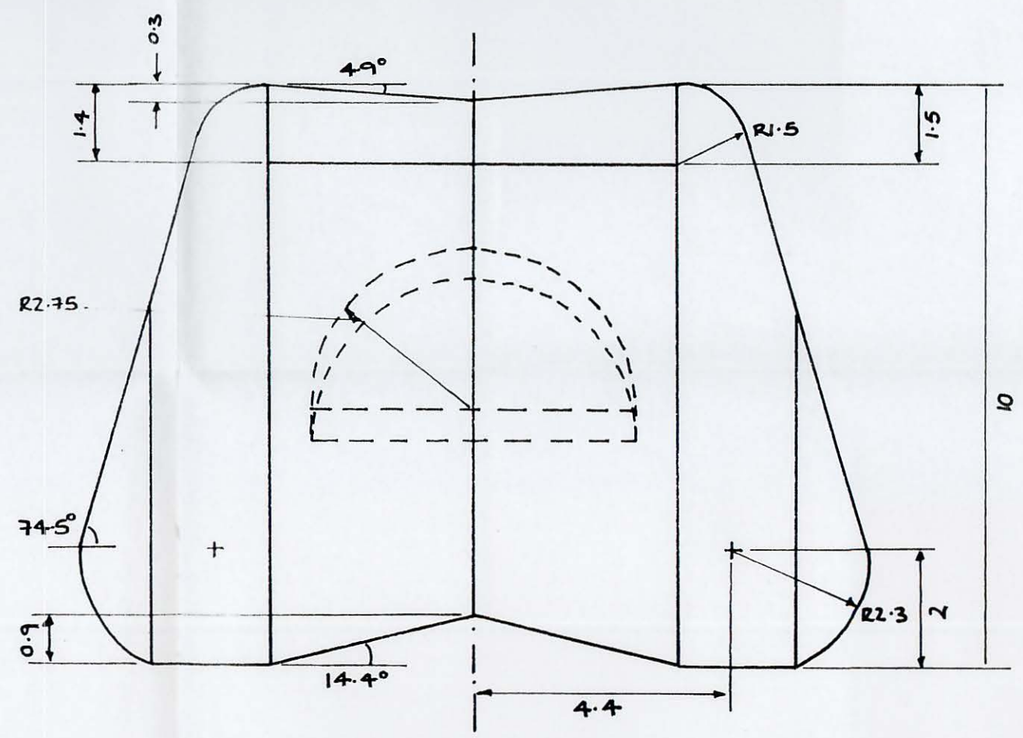

All dimensions in mm unless otherwise stated.	Notes : 0·85mm dorsal offset of the stem from the centre of rotation of the proximal phalangeal head, and 4·2° inclination to the perpendicular to the bone head interface (A)		Scale 10:1	10mm PIPJ surface replacement prosthesis. Proximal phalangeal head.	Hayley Ash.
			Feb 1997		Figure A3·4

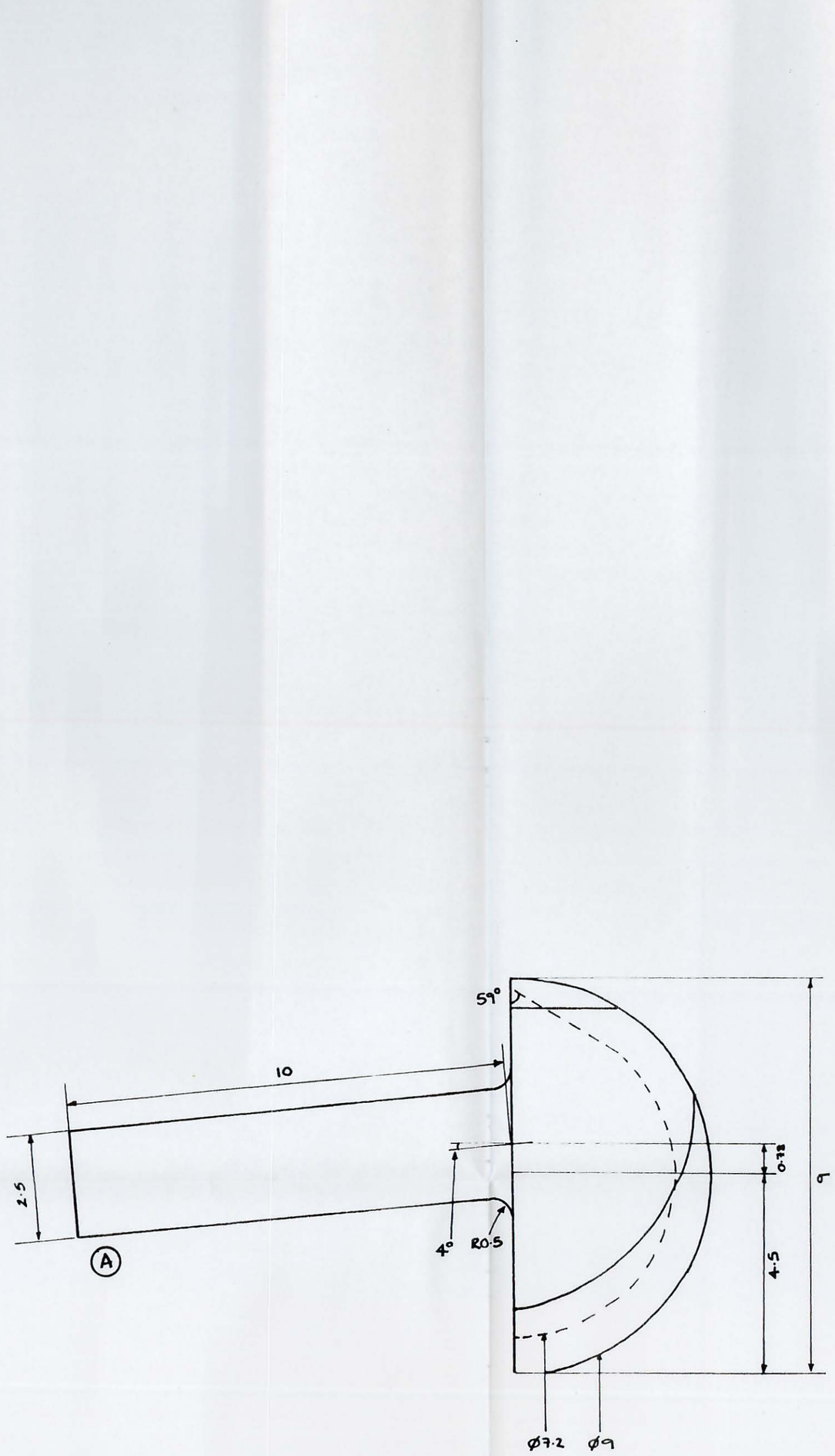

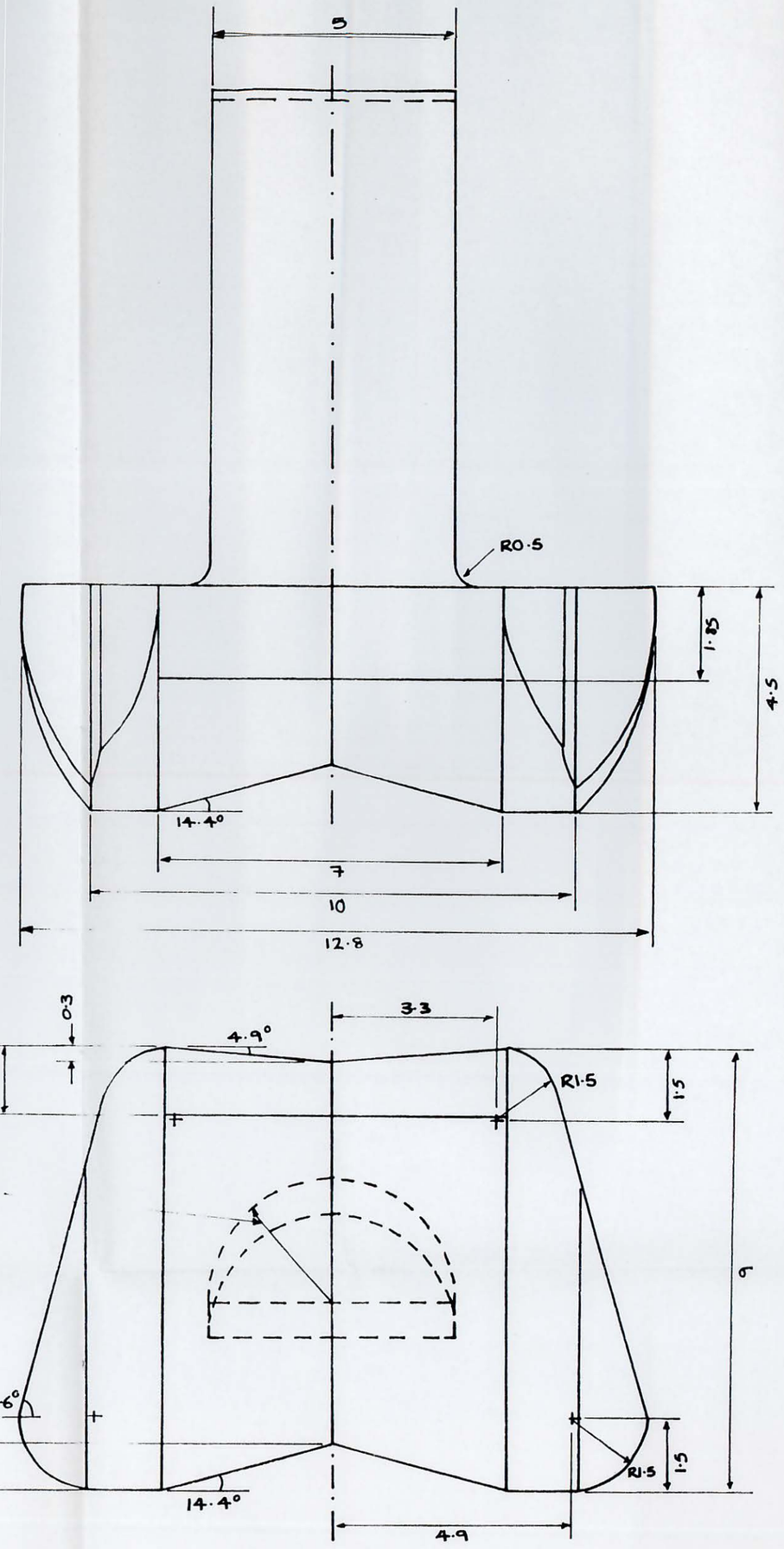

All dimensions in mm unless otherwise stated.	Notes: 0·78mm dorsal offset of the stem from the centre of rotation of the proximal phalangeal head, and 4° inclination to the perpendicular to the bone-head interface (A)	II	Scale 10:1 Feb 1997	9mm PIPJ surface replacement prosthesis. Proximal phalangeal head	Hayley Ash Figure A3·3

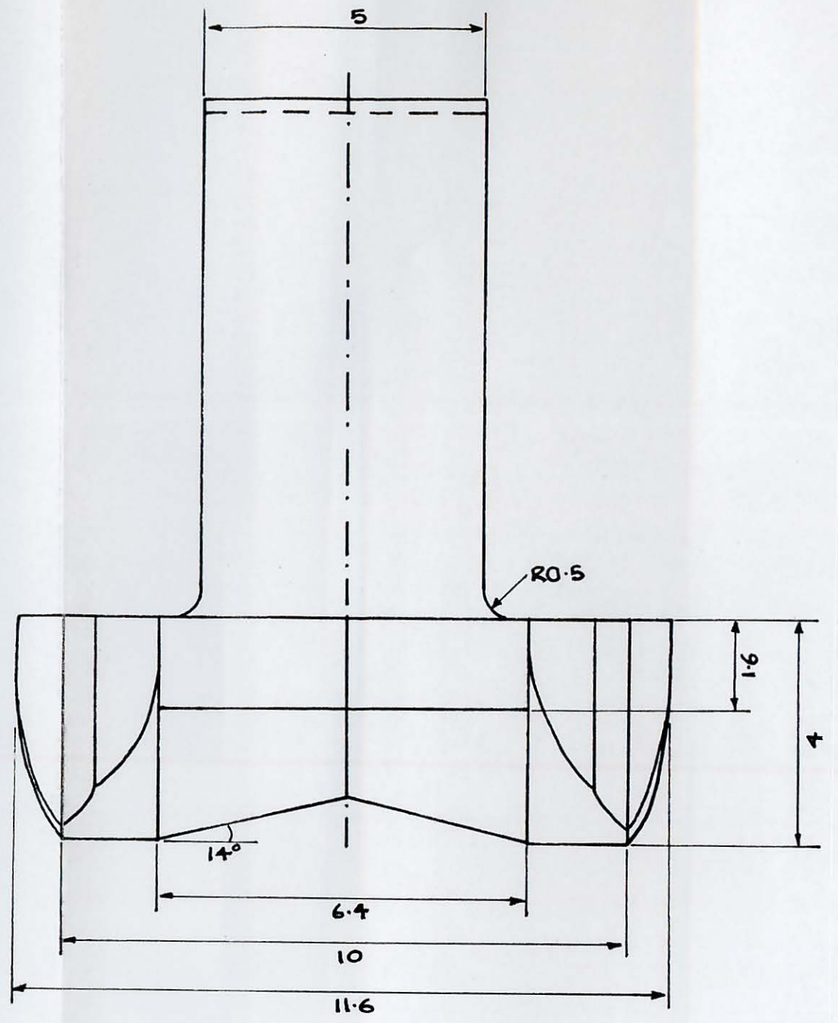

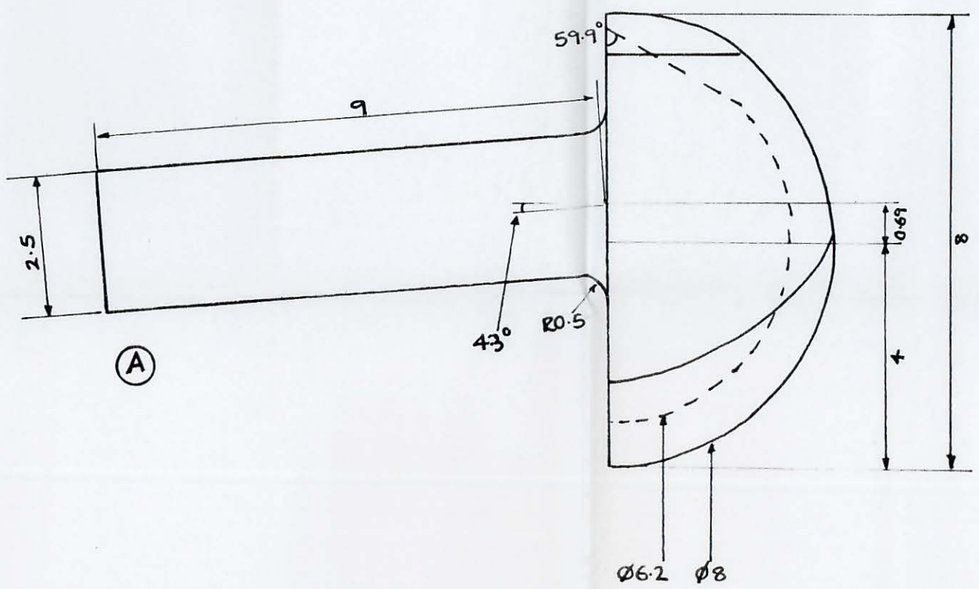

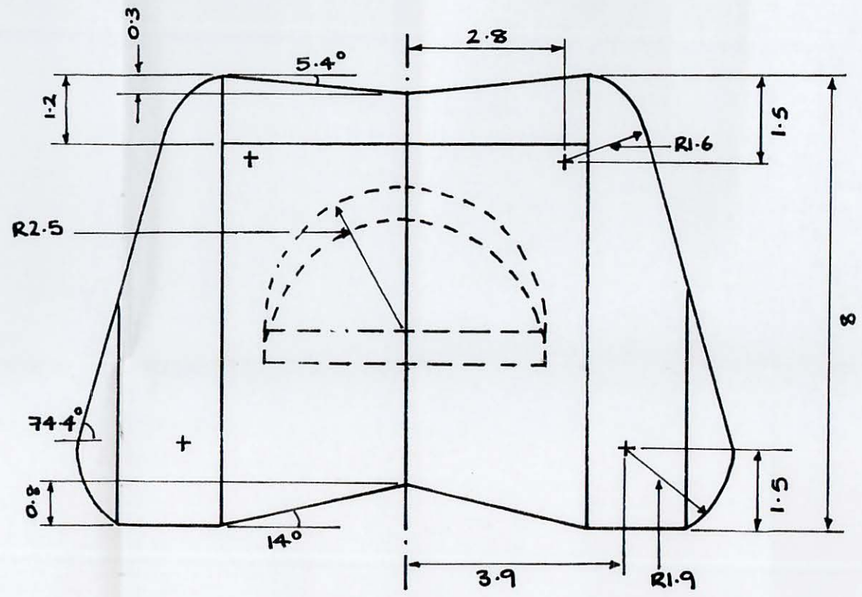

All dimensions in mm unless otherwise stated	Notes: 0·69mm dorsal offset of the stem from the centre of rotation of the proximal phalange—I head, and 4·3° inclination to the perpendicular to the bore - head interface (A)	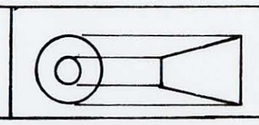	Scale 10:1 Feb. 1997	8mm PIPJ surface replacement prosthesis. Proximal phalangeal head.	Hayley A. Figure A3·2

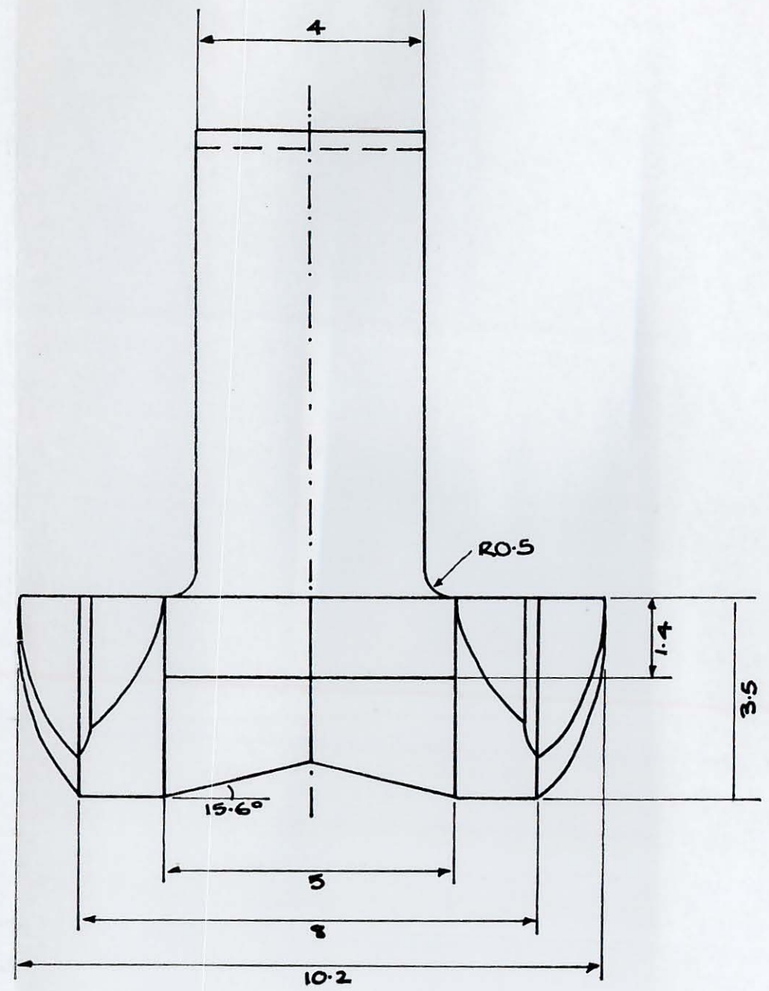

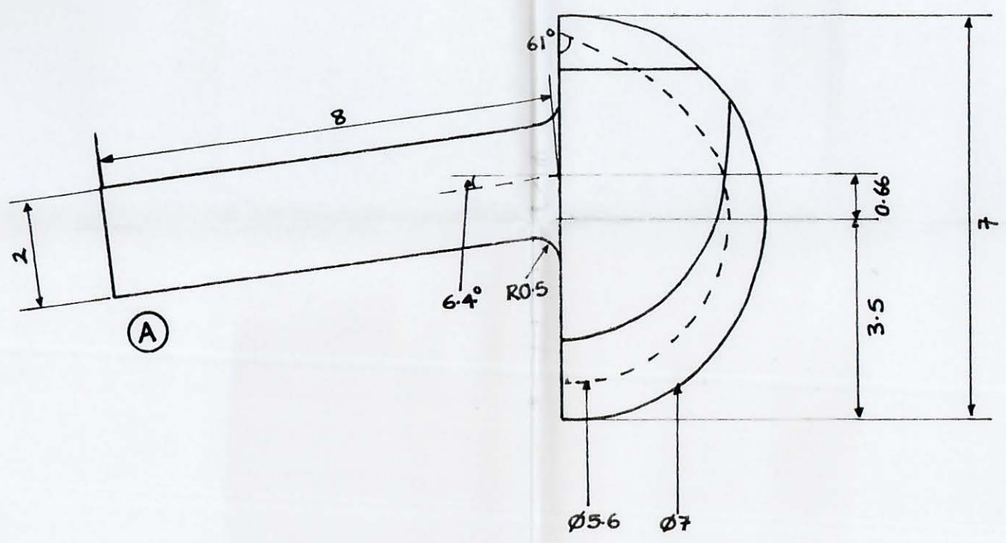

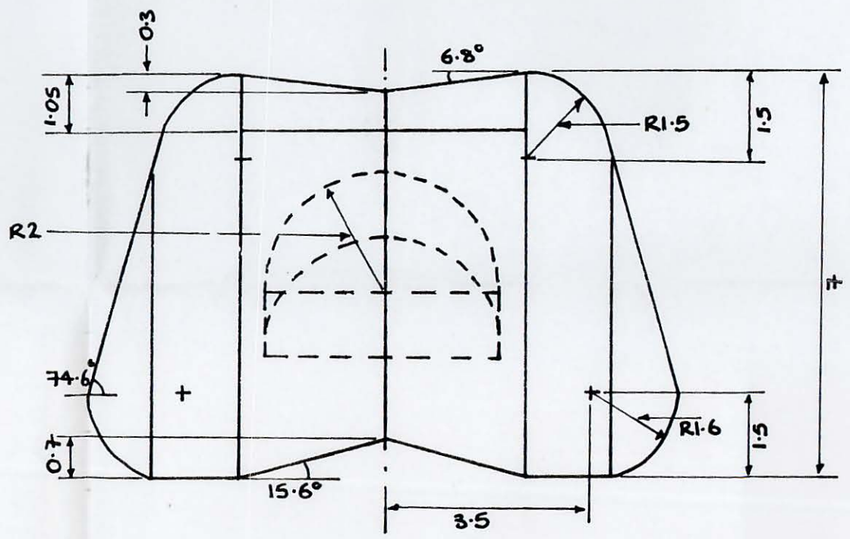

All dimensions in mm unless otherwise stated	Notes : 0·66mm dorsal offset of the stem from the centre of rotation of the proximal phalangeal head, and 6·4° inclination to the perpendicular to the bone-head interface (A)	III	Scale 10 : 1 Feb. 1997	7mm PIPJ surface replacement prosthesis. Proximal phalangeal head.	Hayley Ash. Figure A3·1

APPENDIX FOUR

Calibration of the pin-on-plate wear test rigs

Appendix 4 describes the theoretical and experimental methods used in order to calculate the forces exerted on the pins by the lever arms and additional weights. The additional weights required to exert forces of 10 N and 40 N were then calculated. The experimental results are also compared with theoretical calculations.

A4.1 Theoretical calculation of pin forces

The apparatus used to exert the required forces on the pins include the lever arm (150g), pin holder (78g), a screw and nut to adjust the level of the lever arm (9g), additional weights and a peg to locate the additional weights at one of five different positions on the lever arm (14g), (Figures A4.1 and A4.2). The additional weights required to exert forces of 10 N and 40 N on the pins when applied to the lever arm system were calculated by taking moments about the pivot of the lever arm.

The lever arm was measured and weighed and theoretically split into five components in order to calculate its centre of gravity. The measurements are shown in Figure A4.3 and the five lever arm components are shown in Figure A4.4. The volume, mass and distance of the centre of gravity from the pivot end of the lever arm for each component was calculated. The density of the aluminium lever arms was taken as 2695 kgm^{-3}. The centre of gravity of the lever arm was then calculated from the centres of gravity of the individual components.

A4.1.1 Calculation of the lever arm component volumes (I - V)

I) Pin holes (6 mm diameter, 18.5 mm depth)

Volume $= \pi(3\times10^{-3})^2\times18.5\times10^{-3}$

$= 2.615\times10^{-6}\ m^3$

II) Screw hole (5 mm inner diameter, 5.75 mm outer diameter, 25.3 mm depth)

Volume $= \pi[(5+5.75)/2\times10^{-3}]^2\times25.3\times10^{-3}$

$= 0.574\times10^{-6}\ m^3$

Figure A4.1 Lever arm system

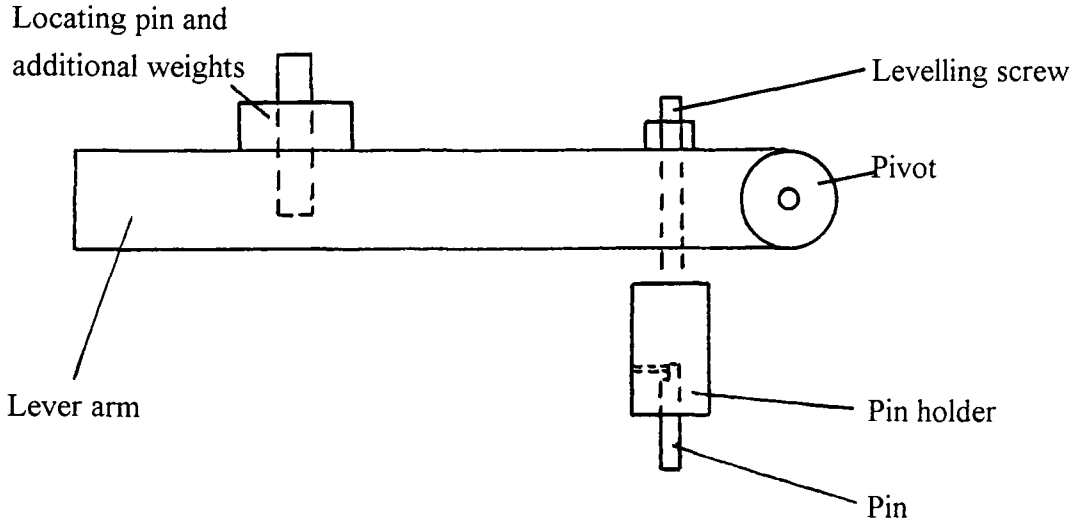

Figure A4.2 Force diagram of the lever arm system

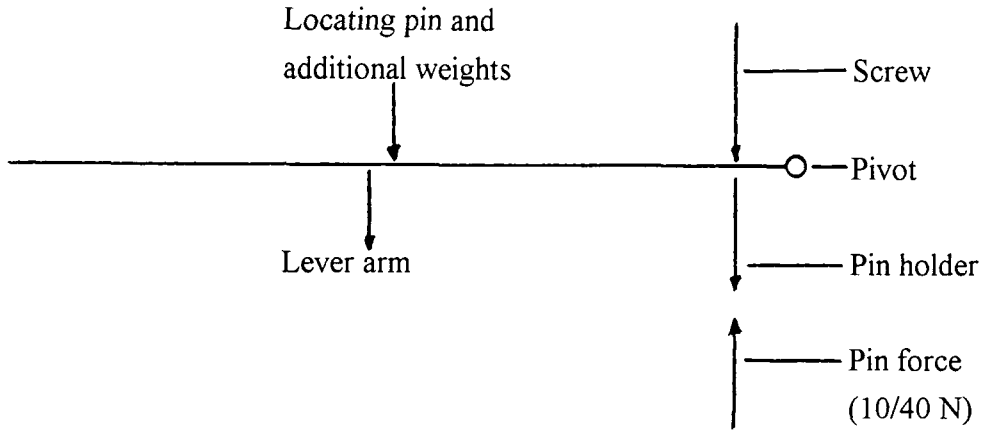

Figure A4.3 Lever arm dimensions (mm)

A) Side view

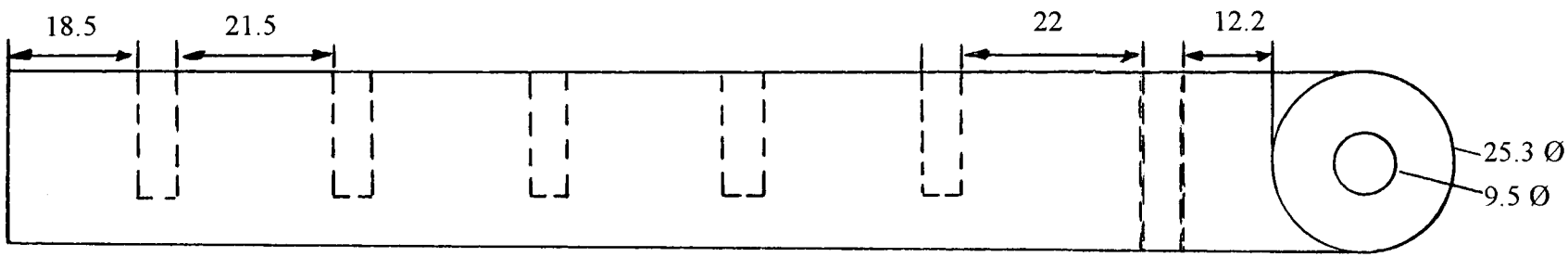

B) Plan

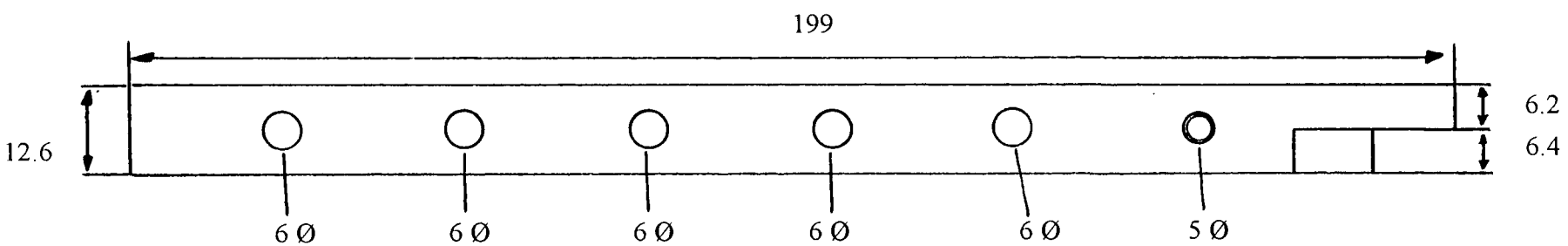

Figure A4.4 Lever arm components (I-V)

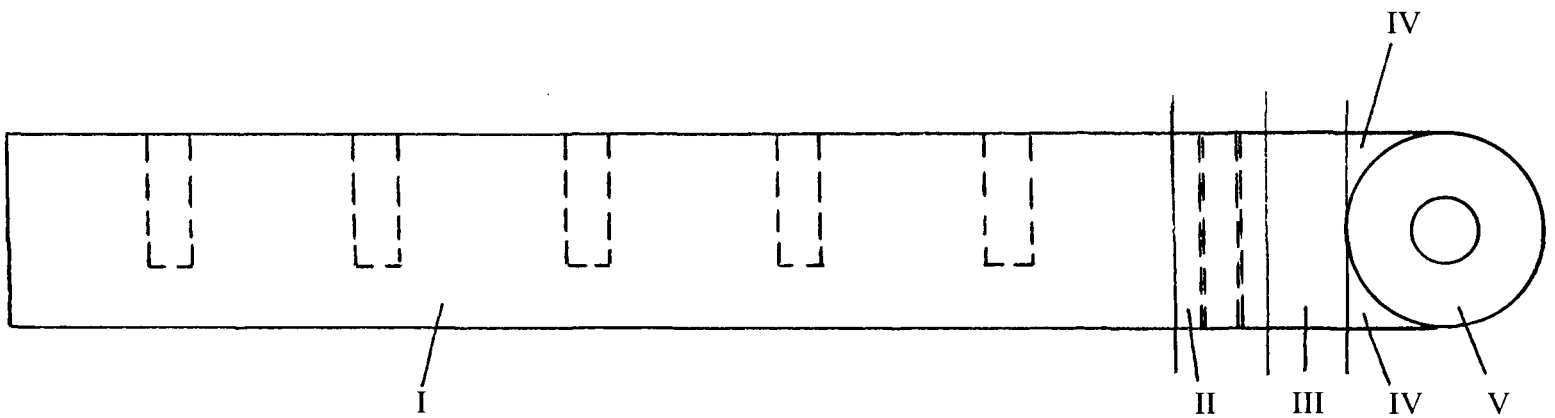

III) Circular triangular parts (25.3 mm circle diameter)

Square volume = $(25.3x10^{-3})^2x12.6x10^{-3}$

= $8.065x10^{-6}$ m^3

Circle volume = $\pi(25.3x10^{-3}/2)^2x12.6x10^{-3}$

= $6.334x10^{-6}$ m^3

Volume = $[(12.6+6.2)/(4x12.6)]x(8.065-6.334)x10^{-6}$

= $0.646x10^{-6}$ m^3

IV) Circle (25.3 mm diameter, 6.4 mm depth)

Volume = $\pi(25.3x10^{-3}/2)^2x6.4x10^{-3}$

= $3.217x10^{-6}$ m^3

V) Circle (9.5 mm diameter, 6.2 mm depth)

Volume = $\pi(9.5x10^{-3}/2)^2x6.2x10^{-3}$

= $0.439x10^{-6}$ m^3

A4.1.2 Calculation of the lever arm component (I-V) mass and distance from the centre of gravity to the pivot end of the arm (COG)

I) Volume = $[(153x25.3x12.6)x10^{-6}]-[2.615x10^{-6}]$

= $46.158x10^{-6}$ m^3

Mass = 124.406 g

COG = 122.5 mm

II) Volume = $[(3.5+5+3.5)x(25.3x12.6)x10^{-9}]-[0.574x10^{-6}]$

= $3.251x10^{-6}$ m^3

Mass = 7.475 g

COG = 40.0 mm

III) Volume = $(912.2-3.5)x(25.3x12.6)x10^{-9}$

= $2.773x10^{-6}$ m^3

Mass = 7.475 g

COG = 29.7 mm

IV)	Volume	=	0.646×10^{-6} m^3
	Depth	=	(12.6+6.2)
		=	18.8 mm
	Area	=	34.4×10^{-3} m^2
	Length of triangle	=	8.287 mm
	Mass	=	1.740 g
	COG	=	22.538 mm
V)	Volume	=	$\pi[(25.3 \times 10^{-3}/2) \times 2 - (9.5 \times 10^{-3}/2) \times 2] \times 6.2 \times 10^{-3}$
		=	2.677×10^{-6} m^3
	Mass	=	7.216 g
	COG	=	12.65 mm

A4.1.3 Calculation of the lever arm mass and distance from the centre of gravity to the pivot end of the arm (COG)

Lever arm mass	=	Sum of individual component masses
	=	149.600 g
Lever arm mass x COG	=	Sum of individual component mass x COG
	=	15942.342 gmm
Lever arm COG	=	Total mass x COG Total mass
	=	106.567 m

The theoretical total mass of a lever arm was 149.6 g compared to the actual weight of 150 g (± 1 g). The distance of the centre of gravity of the lever arm from the pivot end of the arm was 106.567 mm. The distance from the centre of the pivot the pivot end of the lever arm was 12.65 mm, hence the distance from the lever arm centre of gravity to the centre of the pivot was 93.917 mm.

A4.1.4 Calculation of additional weights required to exert 10 N and 40 N on the pins by the lever arms

From Figure A4.2 an equation to calculate the pin force (F), for a weight (P) applied to the lever arm at a distance (d) from the pivot can be derived as below. Table A4.1 shows the theoretical additional weights required to exert 10 N and 40 N on the pins when placed at different positions (holes) along the lever arms. The theoretical pin forces were also calculated when weights of 80 g, 274 g and 595 g were added to different positions along the lever arms for comparison with experimental forces (Table A4.2).

$$(149.6x93.917) + Pd + 14d + (87x27.35) = 27.35F$$

Table A4.1 Theoretical additional weights (g) required to exert 10 N and 40 N on the pins by the lever arms

Hole	d (mm)	Additional weight required for pin force of 10 N (g)	Additional weight required for pin force of 40 N (g)
1	54.85	194.76	1719.63
2	82.35	125.04	1140.70
3	109.85	90.24	851.63
4	137.35	69.37	678.31
5	164.85	54.46	562.82

Table A4.2 Theoretical pin forces (N) with additional weights added to the lever arm

Hole	Pin force (N) with 80 g added	Pin force (N) with 274 g added	Pin force (N) with 595 g added
1	7.753	11.569	17.885
2	8.682	14.412	23.894
3	9.115	17.256	29.904
4	10.541	20.099	35.913
5	11.471	22.942	41.922

A4.2 Experimental method of evaluating the pin forces

A spring balance, weighing balance, button load transducer and a piezo-electric load transducer were all used to evaluate the forces exerted on the pins by the lever arms and additional weights. The piezo-electric load transducer proved to be the most sensitive and reproducible method. The piezo-electric transducer was calibrated at 10X and 100X magnification. Figures A4.5 and A4.6 show the calibration graphs for the two magnitudes of amplification of the piezo-electric load transducer.

Weights of 80g, 274g and 595g were applied to the lever arm at each of the five positions. The average forces exerted on the pins are shown in Table A4.3. The theoretical and experimental pin forces from Tables A4.2 and A4.3 are shown in Figure A4.7. It was found that the experimental pin forces were less than the theoretical pin forces for the same additional weights, but not by a consistent amount. The differences can be attributed to friction within the system and errors in the theoretical calculations. However, the experimental pin force graphs were linear and were used to calculate the weights required to exert 10 N and 40 N on the pins, (Figure A4.8, Table A4.4).

Table A4.3 Experimental pin forces (N) with additional weights added to the lever arm

Hole	Pin force (N) with 80 g added	Pin force (N) with 274 g added	Pin force (N) with 595 g added
1	7.534	11.45/8	17.614
2	8.319	13.837	23.500
3	9.282	16.903	29.263
4	10.281	19.552	34.732
5	11.146	22.826	40.839

Figure A4.5 Calibration graph for the 10x amplifier

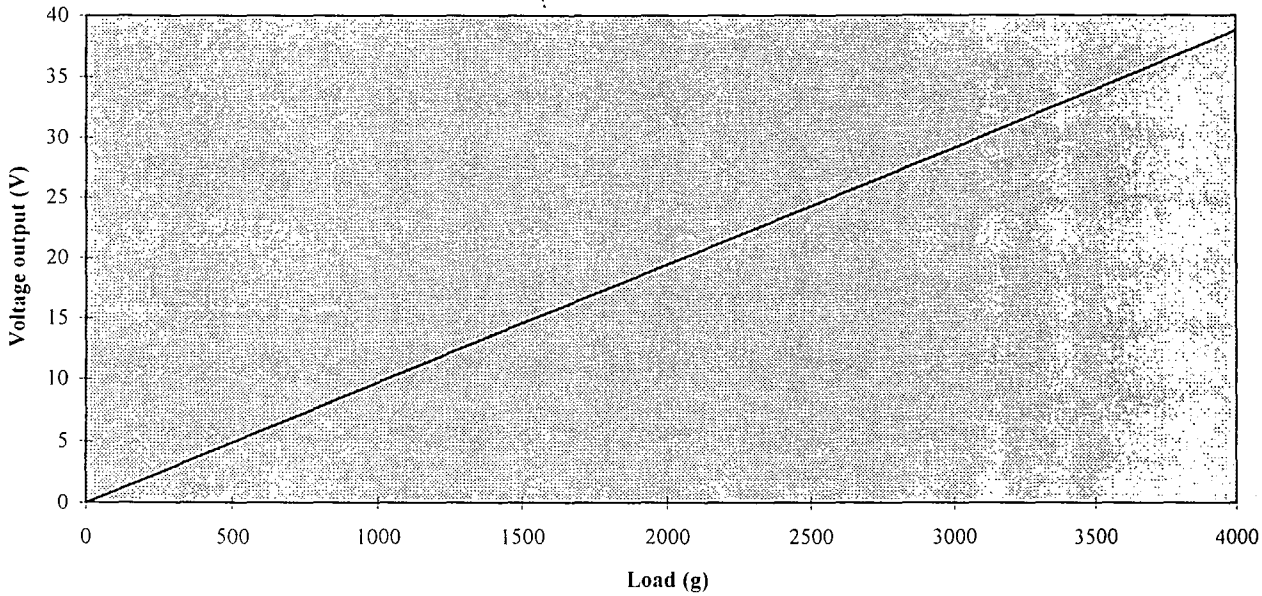

Figure A4.6 Calibration graph for the 100x amplifier

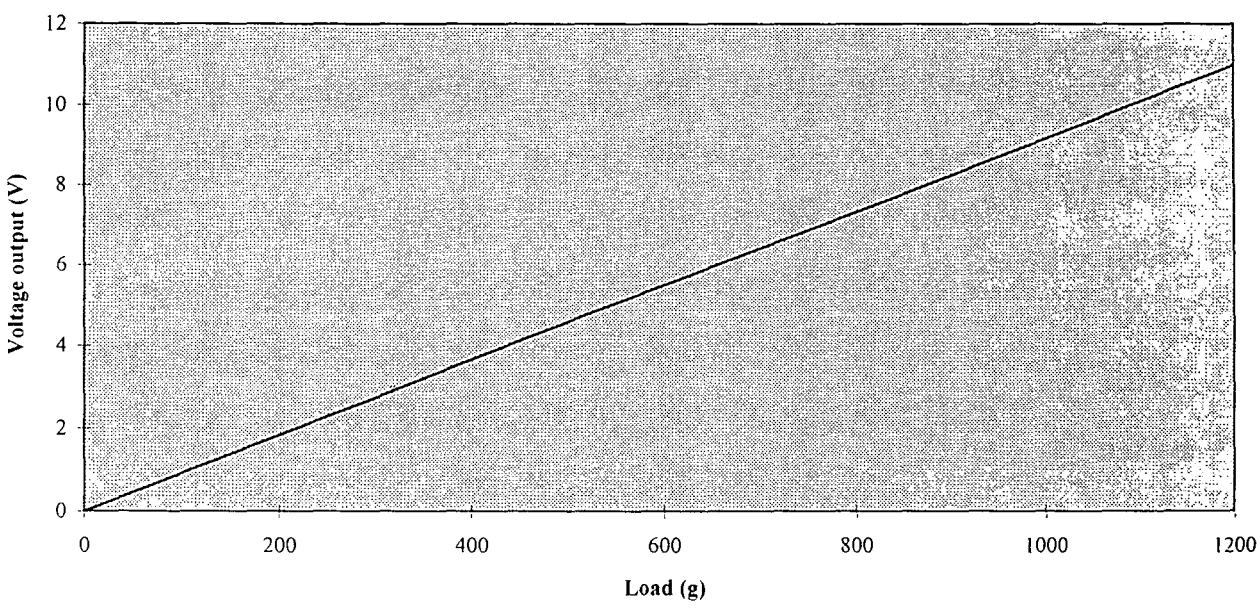

Figure A4.7 Experimental and theoretical pin forces

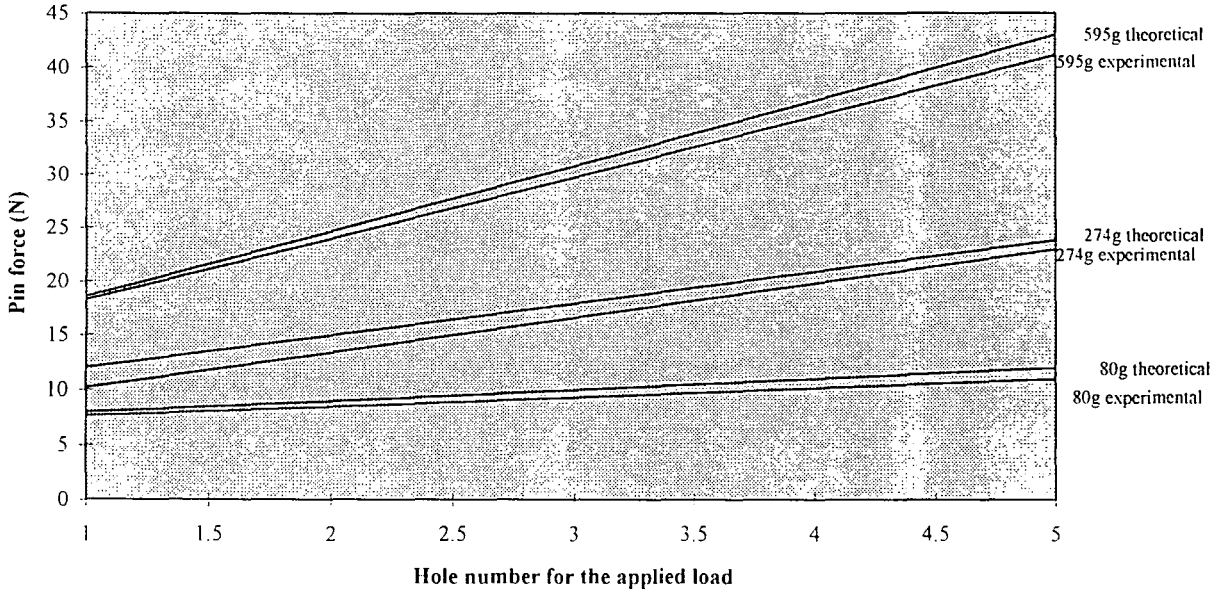

Figure A4.8 Experimental pin forces

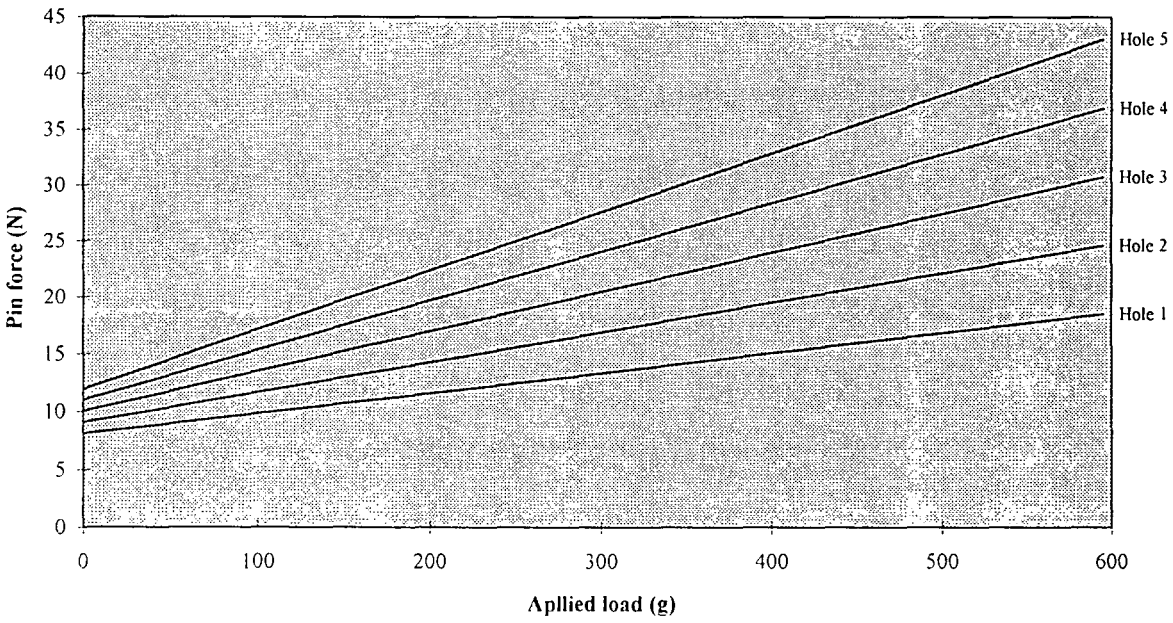

Table A4.4 Experimental additional weights (g) required to exert 10 N and 40 N on the pins by the lever arms

Hole number	Pin force			
	10N	**20N**	**30N**	**40N**
1	205g			
2	140g	480g		
3	100g	355g		
4	75g	285g	495g	
5	60g	230g	405g	575g

A4.3 Summary

The theoretical and experimental forces exerted on the pins by the lever arms and additional weights have been found. Experimental forces were always lower than the corresponding theoretical forces, showing that experimental calibration is required for accurate loading of the pins. Friction between the pin holders and the cantilever arms, and margins of errors in the theoretical calculations were thought to account for the differences between the theoretical experimental results.

Theoretical calculations showed that approximately 5N is exerted on the pins from the lever arms alone. Some previous pin-on-plate wear tests have used a lever arm system in order to exert the required forces on the pins[73,74,83,84]. It is not clear, however, whether the lever arm has been taken into account in the calculation of the weights needed to exert the required pin force. If the weight of the lever arm was neglected then the force on the pins may have been underestimated, which would have been more significant with smaller forces.

75g placed at the fourth hole from the pivot and 575g placed at the fifth hole from the pivot of the lever arms were used in the pin on plate tests to exert 10N and 40N on the pins respectively.

APPENDIX FIVE

Pin-on-plate wear measurements, wear volume/sliding distance ratios and wear coefficients

Table A5.1 Pin and plate wear volumes (mm^3), XLPE-on-XLPE, Test 1, 10N

Dist (km)	Pin 1	Pin 2	Pin 3	Pin 4	Plate 1	Plate 2	Plate 3	Plate 4
0	0	0	0	0	0	0	0	0
2.98	0.211	0	0.211	0.105				
5.92	0.316	0	0.316	0.105				
12.52	0.316	0	0.316	0.421				
19.06	0.527	0.105	0.316	0.527				
29.14	0.632	0.105	0.421	0.738				
43.53	0.738	0.211	0.527	1.054	8.114	9.168	21.602	22.023
53.23	0.843	0.316	0.632	1.159	9.378	10.959	21.918	25.817
60.07	0.843	0.316	0.738	1.159	10.643	11.907	22.761	29.083
70.11	0.948	0.527	0.738	1.475	12.645	13.804	25.711	35.300
80.31	1.054	0.632	0.843	1.475	14.331	14.647	27.397	40.358
93.63	1.159	0.738	0.948	1.686	16.122	15.385	29.715	43.203
102.81	1.475	0.843	1.159	2.002	17.808	15.701	30.453	46.997
116.84	1.581	0.843	1.370	2.107	20.443	17.914	33.087	54.900
126.16	1.791	0.948	1.475	2.213	21.496	18.546	34.352	58.588
133.36	2.002	1.159	1.686	2.318	22.972	18.967	35.933	62.276
140.61	2.318	1.264	1.897	2.424	23.709	19.600	37.408	64.384
153.98	2.424	1.475	2.002	2.740	25.395	20.548	39.305	71.233
163.29	2.740	1.475	2.107	3.161	26.870	21.496	41.623	73.762
167.23	2.950	1.581	2.213		28.240	23.498	43.309	
201.72	3.477	1.686	2.634		32.771	26.870	52.582	
212.93	3.688	1.791	2.845		33.930	28.662	56.797	

Table A5.2 Pin and plate wear volumes (mm^3), XLPE-on-XLPE, Test 2, 10N

Dist. (km)	Pin 1	Pin 2	Pin 3	Plate 1	Plate 2	Plate 3
0	0	0	0	0	0	0
2.87	0	0	0	0.105	0	0.105
12.38	0	0	0	0.421	0	0.316
18.29	0	0	0	0.738	0	0.738
25.67	0	0	0	1.054	0	0.843
35.74	0	0	0	1.054	0	1.054
45.20	0	0	0	1.159	0	1.054
62.30	0.105	0.105	0	1.159	0	1.054
96.07	0.105	0.105	0	1.159	0	1.370
125.89	0.211	0.211	0.105	1.475	0	1.581
150.41	0.211	0.211	0.105	1.475	0	1.581
172.55	0.211	0.211	0.105	1.475	0	1.686

199.76	0.211	0.211	0.105	1.581	0	1.791
218.61	0.211	0.211	0.105	1.897	0	2.002
232.42	0.211	0.211	0.105	2.107	0	2.002
255.18	0.211	0.211	0.105	2.107	0	2.107
284.72	0.316	0.316	0.211	2.107	0	2.107
308.10	0.316	0.316	0.211	2.107	0	2.213
335.42	0.316	0.316	0.211	2.213	0	2.213
368.78	0.316	0.316	0.211	2.213	0	2.213
413.30	0.316	0.316	0.211	2.213	0	2.318
449.54	0.316	0.316	0.211	3.056	0	2.529
472.98	0.421	0.421	0.316	3.161	0	2.634
499.07	0.421	0.421	0.316	3.477	0	2.845
529.27	0.421	0.421	0.316	3.583	0.316	2.845
555.34	0.632	0.527	0.421	4.320	0.421	6.322
583.08	0.948	0.632	0.632	4.426	0.843	6.533
605.70	1.054	0.738	0.738	5.479	1.897	7.798

Table A5.3 Pin and plate wear volumes (mm^3), XLPE-on-XLPE, Test 3, 40 N

Distance (km)	Pin 1	Pin 3	Plate 1	Plate 2	Plate 3
0	0	0	0	0	0
8.82	0	0	0	0	0.105
18.50	0	0	0.632	0.421	0.421
41.25	0.105	0.105	1.370	1.054	0.948
63.76	0.105	0.105	1.897	1.370	1.264
92.26	0.211	0.211	2.213	1.581	1.581
115.04	0.316	0.211	2.213	1.686	1.686
141.37	0.316	0.316	2.213	1.791	1.791
161.21	0.421	0.316	2.318	1.897	2.318
202.89	0.421	0.316	6.428	3.793	9.378
238.46	0.421	0.421	9.800	7.271	12.856
274.95	0.632	0.527	10.643	7.587	13.593
297.37	0.632	0.632	11.064	8.008	14.015
319.65	0.738	0.843	11.697	8.535	14.858
349.22	0.738	0.948	12.329	9.062	15.595
374.60	0.843	0.948	13.382	9.905	16.544
398.06	0.843	1.159	13.488	9.905	16.544
420.23	0.948	1.264	13.699	10.011	16.754
444.18	1.054	1.475	13.909	10.221	16.965
466.95	1.159	1.581	14.225	10.432	17.597
476.55	1.159	1.581	14.647	10.854	17.808
499.38	1.159	1.581	14.752	10.854	17.914

Table A5.4 Pin and plate wear volumes (mm^3), XLPE-on-XLPE, Test 4, 10 N

Distance (km)	Pin 1	Pin 2	Pin 3	Plate 1	Plate 2	Plate 3
0	0	0	0	0	0	0
13.31	0	0	0	0	0	0
26.64	0	0	0	0.211	0.211	0.211
42.12	0	0.105	0	0.527	0.632	0.421
64.82	0.105	0.105	0.105	0.632	0.843	0.527
87.43	0.105	0.105	0.105	0.738	0.948	0.632
107.21	0.105	0.211	0.105	1.159	1.475	0.948
123.04	0.105	0.211	0.211	1.159	1.581	1.264
144.66	0.105	0.316	0.316	1.581	1.686	1.370
175.41	0.105	0.421	0.316	2.318	2.529	3.688
236.23	0.211	0.527	0.527	3.899	4.215	5.901
293.97	0.211	0.527	0.527	4.320	4.320	6.006
415.63	0.316	0.738	0.738	4.636	5.058	6.849
468.74	0.421	0.843	0.843	5.058	5.479	7.798
478.45	0.421	0.843	0.948	5.163	5.585	7.903
511.12	0.527	1.054	1.054	5.269	5.690	7.903
557.26	0.527	1.054	1.054	5.479	6.006	8.430

Table A5.5 Pin and plate wear volumes (mm^3), XLPE-on-XLPE, Test 5, 40 N

Distance (km)	Pin 1	Pin 2	Pin 3	Plate 1	Plate 2	Plate 3
0	0	0	0	0	0	0
13.33	0	0	0	0.105	0.105	0.211
26.24	0	0	0	0.316	0.105	1.054
49.56	0	0	0	0.316	0.421	1.581
73.53	0.105	0	0	1.054	0.948	2.002
96.25	0.105	0	0	1.054	0.948	2.002
119.01	0.105	0	0	1.054	1.054	2.107
141.60	0.105	0	0	1.054	1.159	2.213
164.43	0.105	0	0	1.054	1.159	2.213
183.08	0.211	0.105	0.105	1.686	1.475	2.845
204.95	0.211	0.105	0.105	1.897	1.897	3.056
232.18	0.316	0.105	0.105	2.845	2.213	3.477
262.12	0.316	0.105	0.105	2.950	2.634	3.583
289.75	0.421	0.211	0.211	3.161	2.950	3.688
314.25	0.421	0.316	0.211	3.161	2.950	3.793
348.08	0.632	0.316	0.316	3.267	3.161	4.004
390.24	0.632	0.316	0.316	3.688	3.899	4.320
461.77	0.632	0.421	0.421	4.426	4.953	5.479
519.52	0.738	0.421	0.421	5.058	6.533	6.639
587.79	0.738	0.421	0.421	5.479	6.744	6.639
683.63	0.738	0.527	0.527	8.219	8.535	8.114

Table A5.6 Pin and plate wear volumes (mm^3), UHMWPE-on-UHMWPE, Test 6, 10/40 N

	10 N	40 N	40 N	10 N	40 N	40 N
Distance (km)	**Pin 1**	**Pin 1**	**Pin 2**	**Plate 1**	**Plate 1**	**Plate 2**
0	0	0	0	0	0	0
2.54	0.210	0.839	0.630	2.938	7.765	8.709
5.73	0.839	4.617	2.623	5.352	16.684	19.412
9.51	1.889	10.913	6.401	9.969	26.758	30.011
14.80	3.778	18.573	10.808	13.956	36.831	43.022
20.46	5.771	26.653	15.215	15.740	49.318	55.299
25.91	8.080	30.955	17.838	19.937	61.490	64.533
28.93	9.549	34.208	20.252	22.770	72.823	74.502
32.25	11.962	37.776	22.980	25.813	83.421	84.155
35.52	13.641	40.819	24.974	27.492	92.235	89.507
41.84	15.110			30.535	108.919	100.420
45.35	17.314	46.800	30.850	31.794	116.055	106.191
50.67	19.622	51.102	33.998	34.628	134.313	118.888
54.20	21.406	52.886	35.782	36.097	139.455	122.141
63.23	25.918			39.454		
69.13	28.856			41.028		
72.46	30.325			42.078		
81.18	33.998			45.016		
88.98	36.936			47.639		
104.43	40.084			53.725		
123.12	41.868			62.644		
149.26	42.812			69.255		
178.77	44.386			75.341		
224.23	44.596			109.549		

Table A5.7 Pin and plate wear volumes (mm^3), UHMWPE-on-UHMWPE, Test 7, 10 N

Distance (km)	Pin 1	Pin 2	Pin 3	Plate 1	Plate 2	Plate 3
0	0	0	0	0	0	0
31.36	4.617	2.938	5.352	5.561	6.296	5.981
80.12	26.128	17.524	25.289	27.702	27.177	25.394
106.89	38.405	27.912	35.782	44.386	44.281	43.547
134.38	54.879	43.127	57.188	80.378	65.792	64.009
161.87	58.132	47.324	60.546	85.939	71.669	74.292

Table A5.8 Pin and plate wear volumes (mm^3), UHMWPE-on-UHMWPE, Test 8 10/40 N

	40 N	10 N	10 N	40 N	10 N	10 N
Distance (km)	**Pin 1**	**Pin 1**	**Pin 2**	**Plate 1**	**Plate 1**	**Plate 2**
0	0	0	0	0	0	0
9.03	9.444	3.148	2.864	32.109	11.123	5.264
14.93	16.369	5.666	4.302	50.892	16.684	13.221
18.27	19.517	6.821	4.769	58.657	18.468	15.328
26.98	26.548	11.438	5.845	87.828	24.974	18.401
34.78	33.159	14.376	6.716	108.710	28.017	21.721
50.21		19.098	7.554		35.572	26.245
68.91		20.567	8.814		44.071	31.794
95.05		21.511	13.956		50.053	44.386
124.51		24.554	27.387		62.015	70.168
170.52		38.405	38.510		90.242	92.345

Table A5.9 Pin and plate wear volumes (mm^3), UHMWPE-on-stainless steel, Test 9, 10 N

Distance (km)	**Pin 1**	**Pin 2**	**Pin 3**
0	0	0	0
25.05	0	0.210	0.105
41.27	0.105	0.210	0.210
70.37	0.210	0.420	0.315
93.32	0.210	0.420	0.345
116.12	1.154	0.525	0.653
137.93	1.259	0.839	0.932
160.35	1.259	0.944	1.002
183.16	1.259	1.049	1.101
202.65	1.259	1.049	1.101
222.71	1.259	1.154	1.134

Table A5.10 Pin and plate wear volumes (mm^3), UHMWPE-on-stainless steel, Test 10, 40 N

Distance (km)	Pin 1	Pin 2	Pin 3
0	0	0	0
26.27	0.735	0.315	0.595
42.36	1.469	0.735	1.051
71.93	2.623	1.679	1.945
95.21	3.043	2.308	2.489
117.65	3.253	3.778	3.148
138.02	3.778	4.827	3.801
161.51	4.407	5.981	4.621
184.13	4.512	6.191	4.854
203.63	4.722	6.506	5.102
224.56	5.037	6.716	5.548

Table A5.11 Pin and plate wear volumes (mm^3), XLPE-on-stainless steel, Test 11, 10 N

Distance (km)	Pin 1	Pin 2	Pin 3
0	0	0	0
23.03	0.000	0.316	0.293
45.37	0.105	0.632	0.486
71.80	0.316	0.738	0.632
108.59	0.527	0.948	0.845
148.39	0.632	3.056	1.045
167.13	0.843	3.583	1.421

Table A5.12 Pin and plate wear volumes (mm^3), XLPE-on-stainless steel, Test 12, 40 N

Distance (km)	Pin 1	Pin 2	Pin 3
0	0	0	0
23.42	5.374	1.581	3.246
46.07	7.376	7.903	7.456
72.23	8.219	17.914	8.419
110.59	9.378	27.503	10.015
149.43	10.011	39.937	14.549
168.28	10.221	42.150	18.078

Table A5.13 Equations to the trend-lines fitted to the wear curves, XLPE-on-XLPE, Test 1, 10N

	Distance (km)	Equation of graph	R-squared value
Plate 1	43.53 - 212.93	V = 0.1554D + 1.6598	0.9973
Plate 2	43.53 - 212.93	V = 0.1051D + 5.3633	0.9853
Plate 3	43.53 - 212.93	V = 0.1983D + 10.832	0.9766
Plate 4	43.53 - 163.29	V = 0.4366D + 3.3662	0.9969
Pin 1	19.06 - 93.63	V = 0.0083D + 0.3765	0.9931
	93.63 - 212.93	V = 0.0215D - 0.8290	0.9867
Pin 2	19.06 - 93.63	V = 0.0092D - 0.1487	0.9507
	93.63 - 212.93	V = 0.0095D - 0.1318	0.9312
Pin 3	19.06 - 93.63	V = 0.0084D + 0.1738	0.9847
	93.63 - 212.93	V = 0.0155D - 0.4261	0.9884
Pin 4	19.06 - 93.63	V = 0.0152D + 0.3060	0.9690
	93.63 - 163.29	V = 0.0183D - 0.0305	0.9358

Table A5.14 Equations to the trend-lines fitted to the wear curves, XLPE-on-XLPE, Test 2, 10N

	Distance (km)	Equation of graph	R-squared value
Plate 1	25.67 - 413.30	V = 0.0036D + 0.9724	0.9116
	413.30 - 529.27	V = 0.0114D - 2.3070	0.8905
	529.27 - 605.70	V = 0.0223D - 8.2037	0.8968
Plate 2	25.67 - 413.30	Negligible wear	
	413.30 - 529.27	Negligible wear	
	529.27 - 605.70	V = 0.0198D - 10.371	0.8280
Plate 3	25.67 - 413.30	V = 0.0039D + 0.9581	0.9252
	413.30 - 529.27	V = 0.0049D + 0.3358	0.9412
	529.27 - 605.70	V = 0.0587D - 27.468	0.8428
Pin 1	0 - 529.27	V = 0.0009D	0.9134
	529.27 - 605.70	V = 0.0087D - 4.1554	0.9812
Pin 2	0 - 529.27	V = 0.0009D	0.9134
	529.27 - 605.70	V = 0.0041D - 1.7468	0.9984
Pin 3	0 - 529.27	V = 0.0006D	0.9330
	529.27 - 605.70	V = 0.0058D - 2.7423	0.9858

Table A5.15 Equations to the trend-lines fitted to the wear curves, XLPE-on-XLPE, Test 3, 40N

	Distance (km)	Equation of graph	R-squared value
Plate 1	41.25 - 161.21	V = 0.0067D + 1.3517	0.7360
	161.21 - 238.46	V = 0.0969D - 13.2800	0.9999
	238.46 - 499.38	V = 0.0192D + 5.5206	0.9691
Plate 2	41.25 - 161.21	V = 0.0099D + 0.5825	0.9374
	161.21 - 238.46	V = 0.0689D - 9.5153	0.9550
	238.46 - 499.38	V = 0.0145D + 3.8737	0.9610

Plate 3	41.25 - 161.21	V = 0.0065D + 0.8926	0.9423
	161.21 - 238.46	V = 0.1373D - 19.4020	0.9782
	238.46 - 499.38	V = 0.0199D + 8.3680	0.9663
Pin 1	0 - 499.38	V = 0.0023D	0.9843
Pin 3	0 - 499.38	V = 0.0029D	0.9252

Table A5.16 Equations to the trend-lines fitted to the wear curves, XLPE-on-XLPE, Test 4, 10N

	Distance (km)	Equation of graph	R-squared value
Plate 1	26.64 - 144.66	V = 0.0105D - 0.0376	0.9533
	144.66 - 236.23	V = 0.0254D - 2.1108	0.9996
	236.23 - 557.26	V = 0.0048D + 2.8035	0.9778
Plate 2	26.64 - 144.66	V = 0.124D - 0.0014	0.9542
	144.66 - 236.23	V = 0.0276D - 2.3119	1
	236.23 - 557.26	V = 0.0059D + 2.7125	0.9856
Plate 3	26.64 - 144.66	V = 0.0099D - 0.0763	0.9565
	144.66 - 236.23	V = 0.0476D - 5.1790	0.9604
	236.23 - 557.26	V = 0.0084D + 3.7063	0.9571
Pin 1	0 - 557.26	V = 0.0009D	0.9629
Pin 2	0 - 557.26	V = 0.0019D	0.9811
Pin 3	0 - 557.26	V = 0.0019D	0.9811

Table A5.17 Equations to the trend-lines fitted to the wear curves, XLPE-on-XLPE, Test 5, 40N

	Distance (km)	Equation of graph	R-squared value
Plate 1	0 - 683.63	V = 0.0102D	0.9632
Plate 2	0 - 683.63	V = 0.0110D	0.9646
Plate 3	0 - 683.63	V = 0.0123D	0.9314
Pin 1	0 - 683.63	V = 0.0013D	0.9268
Pin 2	0 - 683.63	V = 0.0007D	0.8811
Pin 3	0 - 683.63	V = 0.0007D	0.8877

Table A5.18 Equations to the trend-lines fitted to the wear curves, UHMWPE-on-UHMWPE, Test 6, 10/40N

	Force (N)	Distance (km)	Equation of graph	R-squared value
Plate 1	40	0 - 54.20	V = 2.5756D	0.9975
Plate 2	40	0 - 54.20	V = 2.4168D	0.9835
Plate 3	10	0 - 224.23	V = 0.5087D	0.9251
Pin 1	40	0 - 54.20	V = 1.0701D	0.9730
Pin 2	40	0 - 54.20	V = 0.6826D	0.9954
Pin 3	10	0 - 224.23	V = 0.2927D	0.7921

Table A5.19 Equations to the trend-lines fitted to the wear curves, UHMWPE-on-UHMWPE, Test 7, 10N

	Distance (km)	Equation of graph	R-squared value
Plate 1	0 - 161.87	V = 0.5049D	0.9201
Plate 2	0 - 161.87	V = 0.4367D	0.9614
Plate 3	0 - 161.87	V = 0.4360D	0.9561
Pin 1	0 - 161.87	V = 0.3666D	0.9699
Pin 2	0 - 161.87	V = 0.2843D	0.9519
Pin 3	0 - 161.87	V = 0.3726D	0.9604

Table A5.20 Equations to the trend-lines fitted to the wear curves, UHMWPE-on-UHMWPE, Test 8, 10/40N

	Force (N)	Distance (km)	Equation of graph	R-squared value
Plate 1	40	0 - 170.52	V = 3.2114D	0.9962
Plate 1	10	0 - 170.52	V = 0.5520D	0.9213
Plate 2	10	0 - 170.52	V = 0.5357D	0.9791
Pin 1	40	0 - 170.52	V = 0.9922D	0.9908
Pin 1	10	0 - 170.52	V = 0.2376D	0.8620
Pin 2	10	0 - 170.52	V = 0.2027D	0.9372

Table A5.21 Equations to the trend-lines fitted to the wear curves, UHMWPE-on-stainless steel, Test 9, 10N

	Distance (km)	Equation of graph	R-squared value
Pin 1	0 - 222.71	V = 0.0066D	0.8182
Pin 2	0 - 222.71	V = 0.0054D	0.9703
Pin 3	0 - 222.71	V = 0.0056D	0.9513

Table A5.22 Equations to the trend-lines fitted to the wear curves, UHMWPE-on-stainless steel, Test 10, 40 N

	Distance (km)	Equation of graph	R-squared value
Pin 1	0 - 224.56	V = 0.0255D	0.9232
Pin 2	0 - 224.56	V = 0.0322D	0.9634
Pin 3	0 - 224.56	V = 0.0263D	0.9903

Table A5.23 Equations to the trend-lines fitted to the wear curves, XLPE-on-stainless steel, Test 11, 10 N

	Distance (km)	Equation of graph	R-squared value
Pin 1	0 - 167.13	V = 0.0046D	0.8444
Pin 2	0 - 167.13	V = 0.0179D	0.9532
Pin 3	0 - 167.13	V = 0.0080D	0.9574

Table A5.24 Equations to the trend-lines fitted to the wear curves, XLPE-on-stainless steel, Test 12, 40 N

	Distance (km)	Equation of graph	R-squared value
Pin 1	0 - 168.28	V = 0.0757D	0.4204
Pin 2	0 - 168.28	V = 0.2538D	0.9801
Pin 3	0 - 168.28	V = 0.1048D	0.9481

Table A5.25 Wear volume/sliding distance ratios and wear coefficients, XLPE-on-XLPE, Test 1, 10 N

	Distance (km)	V/D (mm^3/km)	Wear coefficient (x 10^{-6} mm^3/Nm)
Plate 1	43.53 - 212.93	0.1554	15.54
Plate 2		0.1051	10.51
Plate 3		0.1983	19.83
Plate 4		0.4366	43.66
Pin 1	19.06 - 93.63	0.0083	0.83
Pin 2		0.0092	0.92
Pin 3		0.0084	0.84
Pin 4		0.0152	1.52
Pin 1	93.63 - 212.93	0.0215	2.15
Pin 2		0.0095	0.95
Pin 3		0.0155	1.55
Pin 4		0.0183	1.83

Table A5.26 Wear volume/sliding distance ratios and wear coefficients, XLPE-on-XLPE, Test 2, 10 N

	Distance (km)	V/D (mm^3/km)	Wear coefficient (x 10^{-6} mm^3/Nm)
Plate 1	25.67 - 413.30	0.0036	0.36
Plate 2		N/A	N/A
Plate 3		0.0039	0.39
Plate 1	413.30 - 529.27	0.0114	1.14
Plate 2		N/A	N/A
Plate 3		0.0049	0.49
Plate 1	529.27 - 605.70	0.0223	2.23

Plate 2		0.0198	1.98
Plate 3		0.0587	5.87
Pin 1	0 - 529.27	0.0011	0.11
Pin 2		0.0010	0.10
Pin 3		0.0007	0.07
Pin 1	529.27 - 605.70	0.0087	0.87
Pin 2		0.0041	0.41
Pin 3		0.0058	0.58

Table A5.27 Wear volume/sliding distance ratios and wear coefficients, XLPE-on-XLPE, Test 3, 40 N

	Distance (km)	V/D (mm^3/km)	Wear coefficient (x 10^{-6} mm^3/Nm)
Plate 1	41.25 - 161.21	0.0067	0.1675
Plate 2		0.0099	0.2475
Plate 3		0.0065	0.1625
Plate 1	161.21 - 238.46	0.0969	2.4225
Plate 2		0.0689	1.7225
Plate 3		0.1373	3.4325
Plate 1	238.46 - 499.38	0.0192	0.4800
Plate 2		0.0145	0.3625
Plate 3		0.0199	0.4975
Pin 1	0 - 499.38	0.0023	0.0575
Pin 3		0.0029	0.0725

Table A5.28 Wear volume/sliding distance ratios and wear coefficients, XLPE-on-XLPE, Test 4, 10 N

	Distance (km)	V/D (mm^3/km)	Wear coefficient (x 10^{-6} mm^3/Nm)
Plate 1	26.64 - 144.66	0.0105	1.05
Plate 2		0.0124	1.24
Plate 3		0.0099	0.99
Plate 1	144.66 - 236.23	0.0254	2.54
Plate 2		0.0276	2.76
Plate 3		0.0476	4.76
Plate 1	236.23 - 557.26	0.0048	0.48
Plate 2		0.0059	0.59
Plate 3		0.0084	0.84
Pin 1	0 - 557.26	0.0009	0.09
Pin 2		0.0019	0.19
Pin 3		0.0019	0.19

Table A5.29 Wear volume/sliding distance ratios and wear coefficients, XLPE-on-XLPE, Test 5, 40 N

	Distance (km)	V/D (mm^3/km)	Wear coefficient (x 10^{-6} mm^3/Nm)
Plate 1	0 - 683.63	0.0102	0.2550
Plate 2		0.0110	0.2750
Plate 3		0.0123	0.3075
Pin 1	0 - 683.63	0.0013	0.0325
Pin 2		0.0007	0.0175
Pin 3		0.0007	0.0175

Table A5.30 Wear volume/sliding distance ratios and wear coefficients UHMWPE-on-UHMWPE, Test 6, 10/40 N

	Force (N)	Distance (km)	V/D (mm^3/km)	Wear coefficient (x 10^{-6} mm^3/Nm)
Plate 1	40	0 - 54.20	2.5756	64.39
Plate 2	40	0 - 54.20	2.4168	60.42
Plate 1	10	0 - 224.23	0.5087	50.87
Pin 1	40	0 - 54.20	1.0701	26.75
Pin 2	40	0 - 54.20	0.6826	17.07
Pin 1	10	0 - 224.23	0.2927	29.27

Table A5.31 Wear volume/sliding distance ratios and wear coefficients, UHMWPE-on-UHMWPE, Test 7, 10 N

	Distance (km)	V/D (mm^3/km)	Wear coefficient (x 10^{-6} mm^3/Nm
Plate 1	0 - 161.87	0.5049	50.49
Plate 2	0 - 161.87	0.4367	43.67
Plate 3	0 - 161.87	0.4360	43.60
Pin 1	0 - 161.87	0.3666	36.66
Pin 2	0 - 161.87	0.2843	28.43
Pin 3	0 - 161.87	0.3726	37.26

Table A5.32 Wear volume/sliding distance ratios and wear coefficients, UHMWPE-on-UHMWPE, Test 8, 10/40 N

	Force (N)	Distance (km)	V/D (mm^3/km)	Wear coefficient (x 10^{-6} mm^3/Nm)
Plate 1	40	0 - 170.52	3.2114	80.29
Plate 1	10	0 - 170.52	0.5520	55.20
Plate 2	10	0 - 170.52	0.5357	53.57
Pin 1	40	0 - 170.52	0.9922	24.81
Pin 1	10	0 - 170.52	0.2376	23.76
Pin 2	10	0 - 170.52	0.2027	20.27

Table A5.33 Wear volume/sliding distance ratios and wear coefficients, UHMWPE-on-~~UHMWPE,~~ SS Test 9, 10 N

	Distance (km)	V/D (mm^3/km)	Wear coefficient (x 10^{-6} mm^3/Nm
Pin 1	0 - 222.71	0.0066	0.66
Pin 2	0 - 222.71	0.0054	0.54
Pin 3	0 - 222.71	0.0056	0.56

Table A5.34 Wear volume/sliding distance ratios and wear coefficients, UHMWPE-on-stainless steel, Test 10, 40 N

	Distance (km)	V/D (mm^3/km)	Wear coefficient (x 10^{-6} mm^3/Nm)
Pin 1	0 - 224.56	0.0255	0.638
Pin 2	0 - 224.56	0.0322	0.805
Pin 3	0 - 224.56	0.0263	0.658

Table A5.35 Wear volume/sliding distance ratios and wear coefficients, XLPE-on-stainless steel, Test 11, 10 N

	Distance (km)	V/D (mm^3/km)	Wear coefficient (x 10^{-6} mm^3/Nm
Pin 1	0 - 167.13	0.0046	0.46
Pin 2	0 - 167.13	0.0179	1.79
Pin 3	0 - 167.13	0.0080	0.80

Table A5.36 Wear volume/sliding distance ratios and wear coefficients, XLPE-on-stainless steel, Test 12, 40N

	Distance (km)	V/D (mm^3/km)	Wear coefficient (x 10^{-6} mm^3/Nm
Pin 1	0 - 168.28	0.0757	1.8925
Pin 2	0 - 168.28	0.2538	6.345
Pin 3	0 - 168.28	0.1048	2.62

Table A5.37 Average pin wear coefficients (0 - ≈200 km)

Test	Material	Force (N)	Distance (km	Pin 1	Pin 2	Pin 3	Average of test
2	XLPE	10	199.76	0.12	0.12	0.05	0.123
4	XLPE	10	175.41	0.08	0.20	0.17	
3	XLPE	40	202.89	0.0575		0.0475	0.285
5	XLPE	40	204.95	0.0225	0.0075	0.0075	
6	UHMWPE	10	224.23	29.27			29.275
7	UHMWPE	10	161.87	36.66	28.43	37.26	

8	UHMWPE	10	170.52	23.76	20.27		
6	UHMWPE	40	54.20	26.750	17.070		22.876
8	UHMWPE	40	34.78	24.810			
9	UHMWPE/SS	10	222.71	0.660	0.540	0.560	0.587
10	UHMWPE/SS	40	224.56	0.638	0.805	0.658	0.700
11	XLPE/SS	10	167.13	0.460	1.790	0.800	1.017
12	XLPE/SS	40	168.28	1.893	6.345	2.620	3.619

Table A5.38 Average pin wear coefficients (0 - ≈600 km)

Test	Material	Force (N)	Distance (km)	Pin 1	Pin 2	Pin 3	Average of tests
2	XLPE	10	605.75	0.11	0.10	0.07	0.125
4	XLPE	10	557.26	0.09	0.19	0.19	
3	XLPE	40	499.38	0.0575		0.0725	0.395
5	XLPE	40	683.63	0.0325	0.0175	0.0175	

Table A5.39 Average plate wear coefficients (0 - ≈200 km)

Test	Material	Force (N)	Distance (km)	Pin 1	Pin 2	Pin 3	Average of tests
2	XLPE	10	199.76	1.03		1.12	1.176
4	XLPE	10	175.41	1.12	1.30	1.31	
3	XLPE	40	202.89	0.5725	0.3925	0.6525	0.410
5	XLPE	40	204.95	0.2175	0.2150	0.4075	
6	UHMWPE	10	224.23	50.87			49.567
7	UHMWPE	10	161.87	50.49	43.67	43.60	
8	UHMWPE	10	170.52	55.20	53.57		
6	UHMWPE	40	54.20	64.39	60.42		58.816
8	UHMWPE	40	34.78	80.29			

Table A5.40 Average plate wear coefficients (0 - ≈600 km)

Test	Material	Force (N)	Distance (km)	Plate 1	Plate 2	Plate 3	Average of tests
2	XLPE	10	605.75	0.740	0.840	0.840	1.060
4	XLPE	10	557.26	1.100	1.200	1.640	
3	XLPE	40	499.38	0.8125	0.5925	1.000	0.540
5	XLPE	40	683.63	0.2550	0.2750	0.3075	

Table A5.41 UHMWPE-on-stainless steel wear coefficients k (x 10^{-6} mm^3/Nm)

Reference	Force (N)	Lubricant	Distance (km)	k
Bellow[98]	88.96	DW		0.348-8.39
Brown[87]	25-145	DW	480	0.08-0.36
Cooper[81]	80	DW/Serum	506-1156	0.004-0.010
Cooper[93]	80	DW	200-1500	0.0035-1.3
	20	DW	900	0.007
Kumar[89]	38,220	Serum	40,65	2.77, 0.181
		Saline		9.05, 0.389
		DW		3.71, 0.112
Weightman[101]	223	Serum	200	0.006-0.011

Table A5.42 XLPE-on-XLPE plates wear coefficients k (x 10^{-6} mm^3/Nm)

Reference	Force (N)	Lubricant	Distance (km)	k
Short[83]	10	DW	27-50	2.05
	40	DW	27-50	1.66
Sibly[73]	10	DW	100	1.1
	40	DW	100	2.5
Walker[84]	10	DW	30	13.15, 1.5
	40	DW	30	5.77, 3.15

Table A5.43 UHMWPE-on-UHMWPE plates wear coefficients k (x 10^{-6} mm^3/Nm)

Reference	Force (N)	Lubricant	Distance (km)	k
Atkinson[97]	6	Synovial fluid	8	8.3
	12	Synovial fluid		9.4
	32	Synovial fluid		28.2
Short[83]	10	DW	27-50	101.34
	40	DW	27-50	65.11
Stokoe[74]	5	DW		5.6
	8.5	DW		12.4
	14	DW		14.2
	19	DW		18.8

Table A5.44 Other biomaterial combination wear coefficients k (x 10^{-6} mm^3/Nm)

Reference	Pin	Flat	Force (N)	Lubricant	Dist. (km)	k
Kumar[89]	UH	Al2O3	38,220	Serum		1.82, 0.101
				Saline		3.27, 0.057
				DW		1.18, 0.068
		ZrO2	38,220	Serum		1.07, 0.056
				Saline		0.75, 0.045
				DW		0.861, 0.038
Saikko[82]	UH	Co-Cr-Mo	225	DW	250	0.1
		Al2O3	225	DW	250	0.0033
		ZrO2	225	DW	350	0.0026
		Si3N4	225	DW	250	0.025

Table A5.45 Joint simulator wear coefficients k (x 10^{-6} mm^3/Nm)

Reference	Material	Lubricant	Cycles (million	Distance (km)	MC k	PP k
Stokoe[74] F				300	11.43	13.00
Walker[84] F	XLPE	Ringers	2	50	5.5	3.1
Sibly[73] F	XLPE	Ringers	10	267	2.4	1.3
Short[83] F	XLPE	Ringers		15	7.1	6.53
Range F					**2.4-11.43**	**1.3-13.00**
Cooper[93] H	UH/SS	DW	4.4		UH 4.3	

APPENDIX SIX

DAQCard-1200 and NI-DAQ driver software and the Apple-basic arthrograph data acquisition program[85]

A6.1 DAQCard-1200 and NI-DAQ driver software

The NI-DAQ driver software interfaces with the DAQCard-1200, the computer and the LabVIEW programming language. Figure A6.1 shows the assignment of connector pins for the DAQCard-1200 and Figure A6.2 shows the pin connections of the DAQCard-1200 in single ended-input mode (RSE). The specification for the arthrograph connection to the DAQCard-1200 was as follows:

* Referenced single-ended (RSE) analog input mode
* All input signals were referenced to one common ground which was connected to the analog ground input of the DAQCard-1200.
* Arthrograph ground connected to pin 9 (AIGND)
* Strain gauge output connected to channel 1 (pin 2)
* Potentiometer output connected to channel 0 (pin 1)
* Input signal range -5V to +5V
* Maximum input voltage rating -30V to +30V

Exceeding the input signal range distorts the input signals. Exceeding the maximum input voltage rating may damage the DAQCard-1200 board and the computer.

The DAQCard-1200 was a 12 bit card. Hence for a 10V range the resolution of the card was 2.441 mV. This was equivalent to (3.93×10^{-4}) Nm and $(1 \times 10^{-4})°$. Three hundred and twenty points were taken per cycle[85]. Hence for an average peak-to-peak torque of 0.0797 Nm and an angular displacement range of 38° the average step size between consecutive points was (4.98×10^{-4}) Nm and 0.238°.

A6.1 DAQCard-1200 I/O connector pin assignments

ACH0	1	2	ACH1
ACH2	3	4	ACH3
ACH4	5	6	ACH5
ACH6	7	8	ACH7
AISENSE/AIGND	9	10	DAC0OUT
AGND	11	12	DAC1OUT
DGND	13	14	PA0
PA1	15	16	PA2
PA3	17	18	PA4
PA5	19	20	PA6
PA7	21	22	PB0
PB1	23	24	PB2
PB3	25	26	PB4
PB5	27	28	PB6
PB7	29	30	PC0
PC1	31	32	PC2
PC3	33	34	PC4
PC5	35	36	PC6
PC7	37	38	EXTTRIG
EXTUPDATE*	39	40	EXTCONV*
OUTB0	41	42	GATB0
OUTB1	43	44	GATB1
CLKB1	45	46	OUTB2
GATB2	47	48	CLKB2
+5 V	49	50	DGND

A6.2 Single-ended input connections for the DAQCard-1200

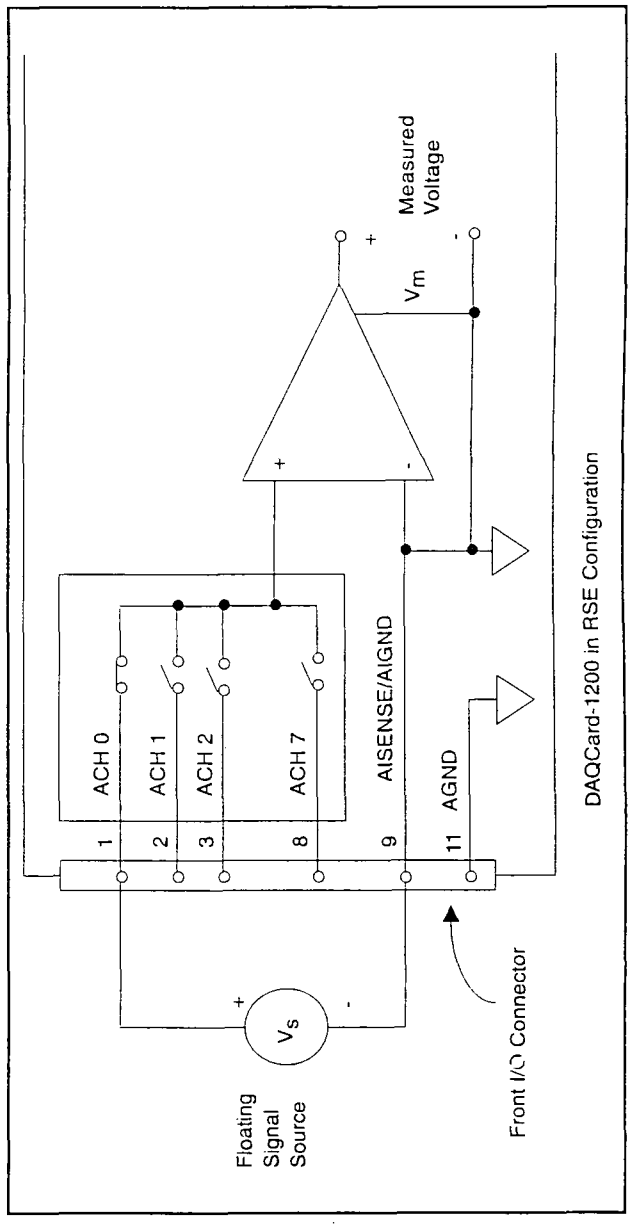

Configuration of DAQCard-1200 using NI-DAQ was achieved as follows:

Select the *NI-DAQ configuration utility* icon from the NI-DAQ4.9.0 menu in windows program manager. From the NI-DAQ configuration utility panel menu select the required device number *(1)*. From the device number panel select *device, DAQCards, DAQCard-1200.* From the Assign PCMCIA socket panel select the socket that the card is in *(1)* and then *OK.* Select *hardware*. From the polarity/range panel select *-5V to +5V.* From the mode panel seclect *RSE.* Select *configuration, save, configuration, return.* From the device number panel menu select *configuration, save, configuration, return* which returns you to the NI-DAQ configuration utility panel. Select *configuration, exit* which returns you to windows program manager.

It should be noted that after extensive testing it was found that the DAQCard-700 was not compatible with this system. This was confirmed by National Instruments who replaced the original DAQCard-700 with a DAQCard 1200.

A6.2 Apple-basic arthrograph data acquisition program[85]

A6.2.1 Apple-basic arthrograph data acquisition program notation

A	Patient's name
AA(I)	Angle at index I
AB	Scrolling angle
B	Date
C	Dominant hand
C1	Angle calibration value (59)
C2	Angle calibration value [0.36 (0.44)]
C3	Torque calibration value (0.0018)
EQ(1)	Angle at zero torque (whilst flexing MCPJ)
EQ(2)	Angle at zero torque (whilst extending MCPJ)
F	Date of birth
H	Maximum angle
L	Minimum angle
N	Number of readings taken (320)
SA(I)	Strain at index I
W	Assessment week number
X2	Index of maximum angle

Y2	Index of minimum angle
ZS	Zero torque (strain)

A6.2.2 Calculated parameters

Flexion, mid-position and extension slopes

The slopes of the best fit lines of three sections of the hysteresis loop were calculated using the least squares method. The slopes are flexion (slope of the best fit line to the last 10° of MCPJ flexion), mid-position (slope of the best fit line to the middle 20° of MCPJ motion) and extension (slope of the best fit line to the last 10° of MCPJ extension.

Flexion slope	EF	$AA(I) \geq B1$
Mid-Position Slope	MP	$B3 < AA(I) < B1$
Extension Slope	EE	$AA(I) \leq B3$

Slope = [(AC*XYSUM) - XSUM*YSUM] / [(AC*SQXSUM) - A]

Where A	XSUM * XSUM
B1	3(H-L)/4 + L
B3	(H-L)/4 + L
XYSUM	Sum of SA(I)*AA(I) (from I = 1 to N)
XSUM	Sum of AA(I) (from I = 1 to N)
YSUM	Sum of SA(I) (from I = 1 to N)
SQXSUM	Sum of AA(I)*AA(I) (from I = 1 to N)

Energy dissipation

The units of energy dissipation are Joules/cycle and is equivalent to the area of the Torque/angular displacement hysteresis loop (with the units of angular displacement as radians). The area of the hysteresis loop was found by dividing the loop into trapeziums and calculating the sum of the areas of the individual trapeziums (effectively integration).

Additional calculated parameters

Centre position of cycle	CP	[(H-L)/2 + L]
Mean equilibrium position	ME	[{EQ(1) + EQ(2)}/2]
	MT	(AB-CP) + ME

A6.2.3 Apple-basic arthrograph data acquisition program (Arthro2)

Bold typing has been added to indicate the different sections of the program

```
(CALIBRATION FACTORS AND DIMENSIONING)
2       HIMEM: 36863
3       LOMEM: 24576
5       C1 = 59:C2 = 0.36:C3 = 0.0018: REM CALIBRATION VALUES
6       DIM SA(750): DIM AA(750): DIM EQ(750)
7       C2  = 0.44
8       REM  ARTHROGRAPH CONTROL
9       REM  ADC/MUX IN SLOT 4
10      CALL  - 936: VTAB (1)

(TITLE)
11      INVERSE : PRINT "DURHAM UNIVERSITY ENGINEERING DEPT."
13      NORMAL : PRINT
14      INVERSE : PRINT "ARTHROGRAPH CONTROL PROGRAM (JB/1986)
15      NORMAL : PRINT : PRINT "DETERMINE ZERO STRAIN REFERENCE
        VALUE."

(PATIENT INFORMATION)
17      PRINT "PATIENT'S NAME"
18      INPUT A$
21      PRINT "DOMINANT HAND "
22      INPUT C$(5)
23      PRINT "D-OF-B"
24      INPUT F$(8)
25      PRINT "DATE"
26      INPUT B$(8)
27      PRINT "WEEK Nos"
28      INPUT W
31      PRINT "PRESS SPACE BAR WHEN READY"
32      GET Y$: IF  ASC (Y$)  < > 32 THEN 31
33      CALL  - 936

(PROCEDURE FOR ZERO STRAIN REFERENCE READING)
59      PRINT : PRINT "OBSERVE THE FOLLOWING :-"
61      VTAB (5): PRINT "ENSURE THAT THE FINGER HOLDER IS EMPTY."
70      PRINT : PRINT "SWITCH OFF MOTOR WHEN THE CARRIAGE": PRINT
        "IS AT FULL FLEXION"
```

```
90    VTAB (20): PRINT "PRESS SPACE BAR WHEN READY"
100   GET Y$: IF  ASC (Y$) < > 32 THEN 100
110   REM  READ ZERO STRAIN REFERENCE
120   ZS =  PEEK (49344): REM  CHANNEL 1
```

(JOINT STIFFNESS DATA ACQUISITION PROCEDURE)

```
130   CALL  - 936: VTAB (2): INVERSE: PRINT "CAREFULLY FOLLOW THE
      PROCEDURE BELOW"
140   NORMAL : VTAB (4): PRINT "(1) CORRECTLY LOCATE INDEX
      FINGER IN ": PRINT "   THE HOLDER"
150   VTAB (7): PRINT "(2) ENSURE THAT FOREARM AND WRIST ARE":
      PRINT "   POSITIONED CORRECTLY."
160   VTAB (10): PRINT "(3) ROTATE FINGER TO 40 DEG."
170   VTAB (12): PRINT "(4) SWITCH ON MOTOR"
180   VTAB (15): PRINT "THE PRESENT POSITION IS     DEG."
190   VTAB (21): PRINT "PRESS START KEY 'S' TO COMMENCE READINGS"
```

(DISPLAY ON SCREEN OF CARRIAGE ANGLE)

```
21200 REM  SCROLLING ANGLE DISPLAY
0     AB =  PEEK (49345): REM  CHANNEL 2
220   AB =  INT ((AB - C1) * C2)
230   VTAB (15): HTAB (25): CALL  -868: PRINT AB;" DEG."
240   IF  PEEK ( - 16384) = 211 THEN 260: REM  KEY "S"
250   GOTO 210
260   POKE  - 16368,0: POKE  - 16384,149: REM  REMOVE CHARACTER S BY
      BACK SPACE
```

(TORQUE/ANGLE DATA ACQUISITION)

```
270   CALL  - 936: PRINT "READINGS COMMENCED"
275   N = 320
280   FOR I = 1 TO N
290   AA(I) =  PEEK (49345):SA(I) = PEEK (49344)
295   FOR I1 = 1 TO 7
296   NEXT I1
300   NEXT I
310   VTAB (3): PRINT "READINGS COMPLETED"

320   VTAB (10): INVERSE : FLASH : PRINT "SWITCH OFF THE MOTOR"
325   NORMAL : NORMAL
330   VTAB (20): PRINT "PRESS SPACE BAR WHEN READY"
340   GET Y$: IF  ASC (Y$) < > 32 THEN 330
```

(CALCULATION OF NUMBER OF POINTS TAKEN, MEAN EQULIBRIUM POSITION AND CENTRE POSITION OF CYCLE)

```
350   CALL  - 936: PRINT "PRELIMINARY RESULTS BEING PROCESSED.":
      PRINT "PLEASE WAIT"
360   REM CALC. POSITIONS OF ZERO TORQUE AND HI LO ANGLE
365   GOSUB 2060: REM  XS DATA
370   NN = 1:H = AA(1):L = AA(1)
380   FOR I = 1 TO N
```

```
390   IF AA(I) > H THEN H = AA(I): X2 = I
400   IF AA(I) < L THEN L = AA(I): Y2 = I
410   IF SA(I) < > ZS THEN 430
420   EQ(NN) = AA(I): GOTO 490
430   IF I = 1 THEN 500
440   IF SA(I) > ZS THEN 470
450   IF SA(I + 1) > ZS THEN 480
460   GOTO 500
470   IF ZS < = SA(I + 1) THEN 500
480   EQ(NN) = (AA(I)+ AA(I + 1)) /2
490   NN = NN + 1
500   NEXT

510   REM CALC. MEAN EQULIBRIUM POSITION
520   FOR I = 2 TO N
530   IF EQ(I) > EQ(1) + 5 OR EQ(I) < EQ(1) - 5 THEN 550
540   NEXT
550   ME = (EQ(1) + EQ(I)) / 2
560   REM  READ PRESENT POS. OF JOINT
570   AB =  PEEK (49345): REM  READ CHANNEL 2
580   AB = (AB - C1) * C2: REM  INC SCALE FACTORS
590   ME = ((ME - C1) * C2)
600   MT = (AB - CP) + ME
610   CP = (((H - L) / 2) + L - C1)* C2

620   REM  CONVERT TO STRINGS FOR MANIP.
630   AB$ = STR$ (AB):CP$ = STR$ (CP):ME$ = STR$ (ME):MT$ = STR$ (MT)
```

(RESULTS DISPLAYED ON SCREEN)

```
640   VTAB (10): HTAB (17): INVERSE: PRINT "RESULTS"
645   NORMAL
650   VTAB (12): HTAB (1): PRINT "NUMBER OF POINTS TAKEN = ";N
660   VTAB (14): HTAB (1): PRINT "CENTRE POSITION OF CYCLE = ";
      LEFT$ (CP$,4)
670   VTAB (16): HTAB (1): PRINT "MEAN EQUILIBRIUM POSITION =";
      LEFT$ (ME$,4)
```

(PLOT OF HYSTERESIS LOOP ON SCREEN)

```
680   VTAB (22): HTAB (1): PRINT "TO SEE LOOP PRESS SPACE BAR": GET
      Y$  IF  ASC (Y$) < > 32 THEN 680
690   REM  CALC SCALE FACTORS
700   CT = (H - L) / 2 + L:CA = 279
705   CA = CA / 2:REM  CORRECTION
710   CO = 0.87
720   REM  PLOT AXES
730   HGR : HCOLOR= 3
740   HPLOT 0,0 TO 279,0 TO 279,159 TO 0,159 TO 0,0
750   HPLOT 139,0 TO 139,159
760   HPLOT 0,79 TO 279,79
```

```
770   FOR X = 139 TO 0 STEP  - 35
780   HPLOT X,76 TO X,81
790   NEXT X
800   FOR X = 139 TO 279 STEP 35
810   HPLOT X,76 TO X,81
820   NEXT X
830   FOR Y = 79 TO 0 STEP  - 20
840   HPLOT 136,Y TO 142,Y
850   NEXT Y
860   FOR Y = 79 TO 159 STEP 20
870   HPLOT 136,Y TO 142,Y
880   NEXT Y
890   HPLOT 130,3 TO 136,3: HPLOT 133,3 TO 133,10
900   HPLOT 272,82: HPLOT 271,83: HPLOT 270,84: HPLOT 273,83: HPLOT
      274,84
910   HPLOT 269,85: HPLOT 275,85
920   HPLOT 269,88 TO 269,85 TO 275,85 TO 275,88
930   REM  PLOT VALUES ON THE SCREEN
940   FOR I = 1 TO N
950   X = INT ((AA(I) - CT) * CA + 139)
960   Y = INT ((SA(I) - ZS) * CO + 79)
970   IF X < 0 OR X > 279 THEN 1000
980   IF Y < 0 OR Y > 159 THEN 1000
990   HPLOT X,Y
1000  NEXT
1010  GET Y$
1020  TEXT
```

(PROMPT TO TAKE ANOTHER SET OF DATA OR TO DO FINAL ANALYSIS ON THE PRESENT DATA)

```
1030  VTAB (24): HTAB (1): CALL  - 868: PRINT "IS THIS SATISFACTORY ?
      (Y/N)": GET Y$
1040  IF  ASC (Y$) = 78 THEN 130
1050  IF  ASC (Y$) = 89 THEN 1080
1060  GOTO 1030
```

(CALCULATION OF)

```
1080  CALL  - 936: PRINT "FINAL RESULTS BEING PROCESSED"

1090  REM CALCULATE SLOPES
1100  XYSUM = 0:XSUM = 0:YSUM = 0: SQXSUM = 0:AC = 0
1110  B1 = (3 / 4) * (H - L) + L:B3 = (1 / 4) * (H - L) + L
1120  FOR I = 1 TO N
1130  IF AA(I) > = B1 THEN AC = AC + 1: GOSUB 2000
1140  NEXT
1150  A = XSUM * XSUM
1160  EF = ((AC * XYSUM) - XSUM * YSUM) / ((AC * SQXSUM) - A)
1170  XYSUM = 0:XSUM = 0:YSUM = 0: SQXSUM = 0:AC = 0
1180  FOR I = 1 TO N
```

```
1190  IF AA(I) < B1 AND AA(I) > B3 THEN AC = AC + 1: GOSUB 2000
1200  NEXT
1210  A = XSUM * XSUM
1220  MP = ((AC * XYSUM) - XSUM *YSUM) / ((AC * SQXSUM) - A)
1230  XYSUM = 0:XSUM = 0:YSUM = 0: SQXSUM = 0:AC = 0
1240  FOR I = 1 TO N
1250  IF AA(I) < = B3 THEN AC = AC + 1: GOSUB 2000
1260  NEXT
1270  A = XSUM * XSUM
1280  EE = ((AC * XYSUM) - XSUM * YSUM) / ((AC * SQXSUM) - A)

1290  REM  CALCULATE HI LO STRAIN
1300  HG = SA(1):LG = SA(1)
1310  FOR I = 1 TO N
1320  IF SA(I) > HG THEN HG = SA(I):X1 = I
1330  IF SA(I) < LG THEN LG = SA(I):Y1 = I
1340  NEXT

1350  REM  CALCULATE AREA OF LOOP
1360  E1 = 0
1370  FOR I = X2 TO Y2 -1
1380  H = (AA(I) - AA(I + 1)) / 2
1390  S = SA(I) + SA(I + 1)
1400  E1 = H * S + E1
1410  NEXT
1420  E2 = 0
1430  FOR I = Y2 TO N - 1
1440  H = (AA(I + 1) - AA(I)) / 2
1450  S = SA(I) + SA(I + 1)
1460  E2 = H * S + E2
1470  NEXT
1480  E3 = 0
1490  FOR I = 1 TO X2 - 1
1500  H = (AA(I + 1) - AA(I)) / 2
1510  S = SA(I) + SA(I + 1)
1520  E3 = H * S + E3
1530  NEXT
1540  ES = (SA(N) + SA(1)) * (AA(1) - AA(N)) / 2
1550  E4 = E1 - E2 - E3 - E5

1560  REM  CONVERT TO REAL AND STRINGS
1570  HG$ = STR$ ((ZS - LG) * C3):LG$ =  STR$ ((ZS - HG) * C3)
1580  EF$ =  STR$ (EF * ( - C3 / C2)):MP$ =  STR$ (MP * ( - C3 / C2))
1590  EE$ =  STR$ (EE * ( - C3 / C2)):E4$ =  STR$ (E4 * C2 * (3.142 / 180) * C3)
1600  TR = VAL (HG$) -  VAL (LG$):TR$ =  STR$ (TR)

1610  REM  DUMP TO PRINTER
1611  D$ =  CHR$ (4):ESC$ =  CHR$(27)
```

```
1612  PRINT D$;"PR#1": PRINT ESC$; CHR$ (89): PRINT ESC$; CHR$(34):
      PRINT ESC$; CHR$ (78)
1620  D$ =  CHR$ (4):ESC$ =  CHR$(27)
1621  PRINT "NAME: ",A$
1623  PRINT "DATE OF BIRTH: ",F$(8)
1624  PRINT "DOMINANT HAND: ",C$(5)
1625  PRINT " "
1626  PRINT "DATE: ",B$(8)
1627  PRINT "WEEK ",W
1630  REM  TURN ON BOLDFACE AND UNDERLINE
1640  PRINT D$;"PR#1": PRINT ESC$; CHR$ (110): PRINT ESC$; CHR$(33):
      PRINT ESC$; CHR$ (88)
1650  PRINT "   RESULTS   "
1660  PRINT ESC$; CHR$ (89): PRINT ESC$; CHR$ (34): PRINT ESC$; CHR$
      (78): REM  RESET TABS
1670  PRINT "NUMBER OF POINTS TAKEN = ";N;" MEAN EQ. POSITION = ";
      LEFT$ (ME$,4);" DEG. "
1680  PRINT : PRINT "CENTRE OF CYCLE = "; LEFT$ (CP$,4);" DEG."
1690  PRINT  : PRINT "TORQUE RANGE (PEAK TO PEAK) = "; LEFT$
      (TR$,5);" NM."
1695  PRINT : PRINT "ENERGY DISSIPATION = "; LEFT$ (E4$,5); RIGHT$
      (E4$,4);" JOULES"
1700  PRINT : PRINT ESC$; CHR$ (88): PRINT " SLOPES-UNITS NM./DEG.":
      PRINT ESC$; CHR$ (89)
1710  PRINT : PRINT "FLEXION = "; LEFT$ (EF$,5); RIGHT$ (EF$,4)
1720  PRINT : PRINT "EXTENSION = "; LEFT$ (EE$,5); RIGHT$ (EE$,4)
1730  PRINT : PRINT "MID. POSITION = "; LEFT$ (MP$,5); RIGHT$ (MP$,4)
1740  PRINT ESC$; CHR$ (88): PRINT "HYSTERESIS LOOP"
1750  PRINT ESC$; CHR$ (89)
1760  PRINT "HORIZONTAL SCALE:- 1 DIVISION= 10 DEG."
1770  PRINT "VERTICAL SCALE  :-1 DIVISION=0.05 NM."
1780  PRINT : PRINT D$;"PR#0"
1790  CALL  - 936: PRINT "NOW LOADING GRAPHICS PROGRAM"
1800  PRINT D$;"RUN GRAPH3"
1810  END

2000  REM SUMMATION ROUTINE
2010  XYSUM = SA(I) * AA(I) + XYSUM
2020  XSUM = AA(I) + XSUM
2030  YSUM = SA(I) + YSUM
2040  SQXSUM = (AA(I) * AA(I)) + SQXSUM
2050  RETURN
2060  REM  XS DATA ROUTINE
2070  FOR I = 2 TO 320
2080  IF AA(I) < AA(1) THEN 2100
2090  NEXT
2100  FOR I = I TO 320
2110  IF AA(I) > AA(1) THEN N = I - 2: RETURN
2120  NEXT
```

APPENDIX SEVEN

LabVIEW Durham arthrograph calibration program

A7.1 Program structure (Cal.VI)

Run Cal.VI

↓

Call Sub VI Kgh.VI - Potentiometer calibration

0° reading at full extension
Full flexion reading
Calculation of calibration factors

↓

Return to Cal.VI

↓

Call Sub VI Untitled.VI - Strain gauge calibration

Enter weights to be applied to strain gauges
Weights applied and voltage readings taken
Enter number of readings taken
Enter moment arm
Calculation of calibration factors

↓

Return to Cal.VI

↓

Display of calibration factors

↓

Save calibration factors to file
C:\LabVIEW\hayley\test.doc

↓

END

A7.2 Arthrograph calibration program components

The program consists of a front panel which is seen when the program is run, and a sequence of four block diagrams (0-3) which are initiated in turn. Two SubVIs or sub-routines are called throughout the program. *Pot* is the potentiometer calibration SubVI and contains a front panel and three sequence block diagrams (0-2). *Sgc* is the strain gauge calibration SubVI and contains a front panel and a sequence of two block diagrams (0-1). The calibration values are then displayed on the front panel and the user is prompted to save then to file *C:\LabVIEW\hayley\test.doc*. These values are then read from this file by the arthrograph data acquisition program. This section details the components of the front panel and block diagrams of the calibration program followed by those for the SubVIs.

A7.2.1 Calibration program

Front Panel

Dialog box	The calibration factors are:
Numerical indicators	Cal1, Cal2, Cal3
Dialog box	Press 'File' to save calibration factors to file C:\LabVIEW\hayley\test.doc
Dialog button	File

Block Diagram

Sequence 0

POT SubVI	Reads in voltage values from the potentiometer and then calculates the calibration factors Cal1 (C1) and Cal2 (C2). SubVI is saved in file Kgh.VI
Numerical indicators	C1, C2

Sequence 1

SGC SubVI	Reads in voltage values from the strain gauge system and then calculates the calibration factor Cal3 (C3). SubVI is saved in file Untitled.VI
Numerical indicator	C3

Sequence 2

While loop	
Local variables	C1, C2, C3
Numerical indicators	Cal1, Cal2, Cal3
Dialog box TF	Press 'File' to save calibration factors to file

Sequence 3

Open/create/replace file.vi	Function (2: creates a new file or replaces a file and permission is given)
	Default name (C:\LabVIEW\hayley\test.doc)
Local variables	Cal1, Cal2, Cal3
To fractional	Number (Cal1, Cal2, Cal3)
F-format string	Cal1, Cal2, Cal3 in string format
String subset	String (Cal1, Cal2, Cal3)
	Length (8)
	Substring (Cal1, Cal2, Cal3)
Concatenate strings	Strings (Cal1, Cal2, Cal3)
	Concatenation of strings(Cal1Cal2Cal3)
Write file+ (string).vi	Refnum (reference number of file C:\LabVIEW\hayley\ test.doc)
	Error in (no error)
	String (Cal1Cal2Cal3)
	Dup refnum
	Error out
Close file+.vi	Refnum (reference number of file C:\LabVIEW\hayley\ test.doc)
	Error in (no error)
	Error out
Simple error handler.vi	Error in (no error)

A7.2.2 SubVIs

POT (Saved as file Kgh.VI)

Front Panel

Dialog box	Arthrograph calibration program (HA 1995)
	Centre for Biomedical Engineering
	University of Durham

	This program calculates the calibration factors for the Durham arthrograph
Dialog box	Potentiometer calibration
Dialog box	1) With the carriage at full extension, move it to 0 deg. 2) Press 'OK' to take the 0 Deg. potentiometer reading
Dialog button	OK
Numerical indicator	0 deg.
Dialog button	Continue
Dialog box	3) Switch on the motor until the carriage is at full flexion 4) Press 'OK' to take the full flexion potentiometer reading
Dialog button	OK
Numerical indicator	Full Flex
Dialog button	Continue
Dialog box	The calibration factors for the potentiometer are:
Numerical indicators	Cal1, Cal2
Dialog button	Press to continue

Block Diagram

Sequence 0

While loop	
Dialog button TF	0 deg.
Case structure	
AI sample channel.vi	Device (1: DAQ-card 1200) Channel (0: potentiometer) Sample (0 deg. voltage reading)
Numerical indicator	0 deg. voltage reading
Dialog button TF	Continue

Sequence 1

While loop	
Dialog button TF	Full Flex
Case Structure	
AI sample channel.vi	Device (1: DAQ-1200 card) Channel (0: potentiometer) Sample (Full Flex voltage reading)
Numerical indicator	Full Flex voltage reading
Dialog button TF	Continue

Sequence 2

While loop	
Local variables	Full Flex, 0 deg.
Numerical Indicators	Cal1, Cal2
Dialog button TF	Press to continue

SGC (Saved as file Untitled.VI)

Front Panel

Dialog box	Strain gauge calibration
Dialog box	1) Enter the weights applied to the strain gauges in the left hand column by clicking on the boxes 2) Apply the weights to the strain gauges and press the appropriate 'OK' to take a voltage reading 3) Enter the number of sets of readings taken and the moment arm of the weights applied to the strain gauges (m)
Array (numerical control)	Weight (Kg)
Dialog buttons	OK
Numerical indicators	Strain gauges voltage readings
Numerical controls	Number of sets of readings required, Moment arm
Dialog button	Press to continue
Numerical indicator	The calibration factor Cal3 is :
Dialog button	Press to continue

Block Diagram

Sequence 0

Dialog button TF	OK (1-10)
Case structures	
AI sample channel.vi	Device (1: DAQ-1200 card) Channel (1: strain gauge system)
Numerical indicators	1a-10a
Dialog button TF	Press to continue

Sequence 1

Array	Weight (Kg)
Numerical indicator	Moment arm (m)
Array subset	Array (weight Kg)

	Length (number of readings required)
Numerical indicator	Number of readings required
Numerical indicators	Strain gauge voltage readings
Build array	Strain gauge voltage readings
Array subset	Array (strain gauge voltage readings)
	Length (number of readings required)
Linear fit coefficients.vi	Y values (weight Kg)
	X values (strain gauge voltage readings)
	Slope (slope of best fit straight line through data Cal3)
Numerical indicator	Cal3
Dialog button TF	Press to continue

A7.3 Operating instructions

The following section shows the front panels which the user will see when the arthrograph calibration program is run and describes the interaction required from the user to run the whole program.

To run the calibration program select the *LabVIEW* icon in the LabVIEW windows menu. Select *File. Open. C:\LabVIEW\hayley\CAL.VI.* Press → from the CAL.VI front panel shown (making sure that the arthrograph is turned on and connected correctly to the computer and that the DAQCard-1200 is configured in NI-DAQ).

Front Panel I
Title page and potentiometer calibration

Arthrograph calibration program (HA 1995)
Centre for Biomedical Engineering, University of Durham
This program calculates the calibration factors for the Durham arthrograph

Potentiometer calibration
1) With the carriage at full extension, move it to 0 degrees
2) Press OK to take the 0 degree potentiometer reading

OK
0 degree reading
Continue

3) Switch on the motor until the carriage is at full flexion

4) Press OK to take the full flexion potentiometer reading

OK

Full flexion reading

Continue

The calibration factors for the potentiometer are

Cal 1

Cal 2

Press to continue

Turn on the motor until the carriage is at full extension. Move the carriage to 0 degrees. Press *OK* to take a reading and then *Continue*. Turn on the motor until the carriage is at full flexion, without manually moving the carriage. Press *OK* to take a reading and then *continue*. The calibration factors are displayed in the boxes. *Press to continue.*

Front Panel II

Strain gauge calibration

Strain gauge calibration

1) Enter the weights applied to the strain gauges in the left hand column by clicking on the boxes

2) Apply the weights to the strain gauges and press the appropriate OK button to take a voltage reading

3) Enter the number of sets of readings taken and the moment arm of the weights applied to the strain gauges in meters

Weight Kg

Number of readings (Maximum of 10)

Moment arm (m)

Press to continue

The calibration factor is

Cal 3

Press to continue

Enter the weights that are to be applied to the strain gauges via the pulley system in the left hand column. Apply a weight and in the box opposite that weight click on *OK* to take the strain gauge voltage reading for the weight applied. When all of the readings have been taken enter the number of readings taken and the moment arm. *Press to continue*. The calibration factor will be displayed in the box. *Press to continue.*

Front Panel III (Front Panel of Arthrograph Calibration Program)
Display of calibration factors and saving to file C:\LabVIEW\hayley\test.doc

The calibration factors are
Cal 1
Cal 2
Cal 3

Press File to save calibration factors to file C:\LabVIEW\haylay\test.doc

File

The calibration factors are displayed in the boxes. Press *File* to obtain the select file to save information under prompt. Press ***OK*** to select filename *C:LabVIEW\hayley\test.doc*

A7.4 Calibration program

Connector Pane

Front Panel

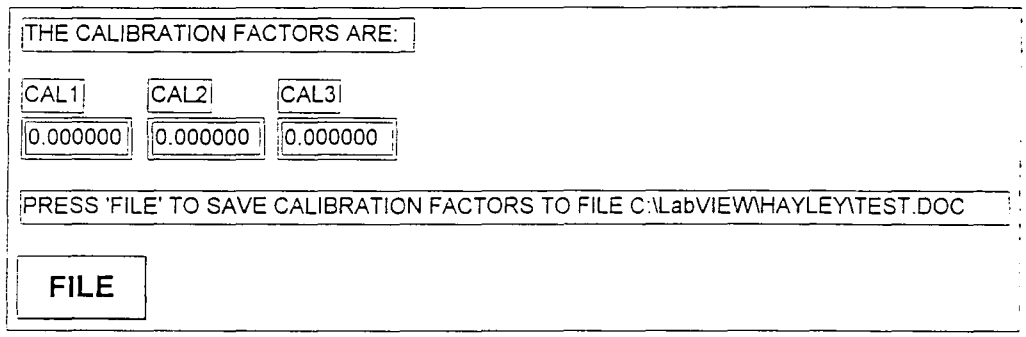

Block Diagram

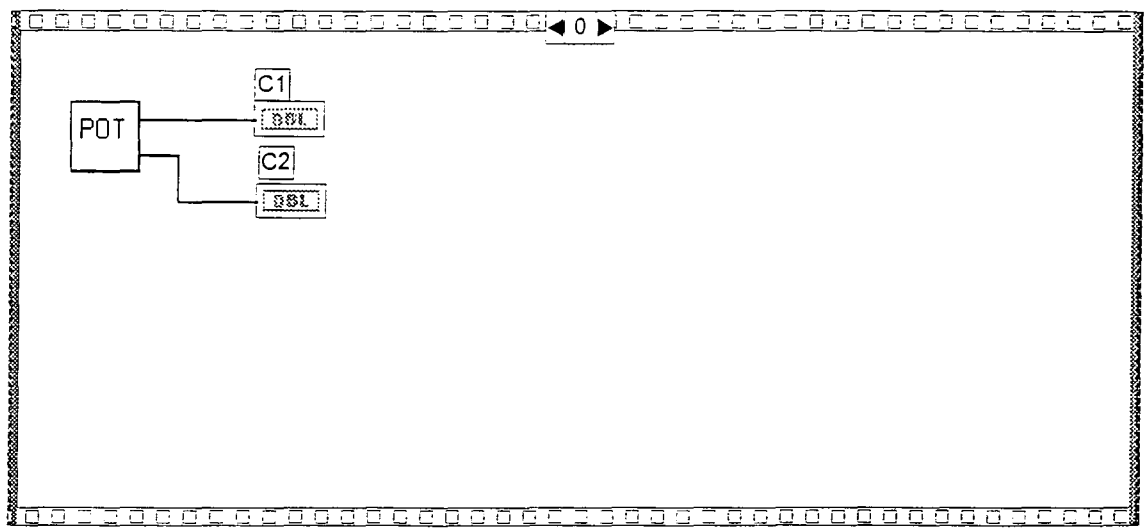

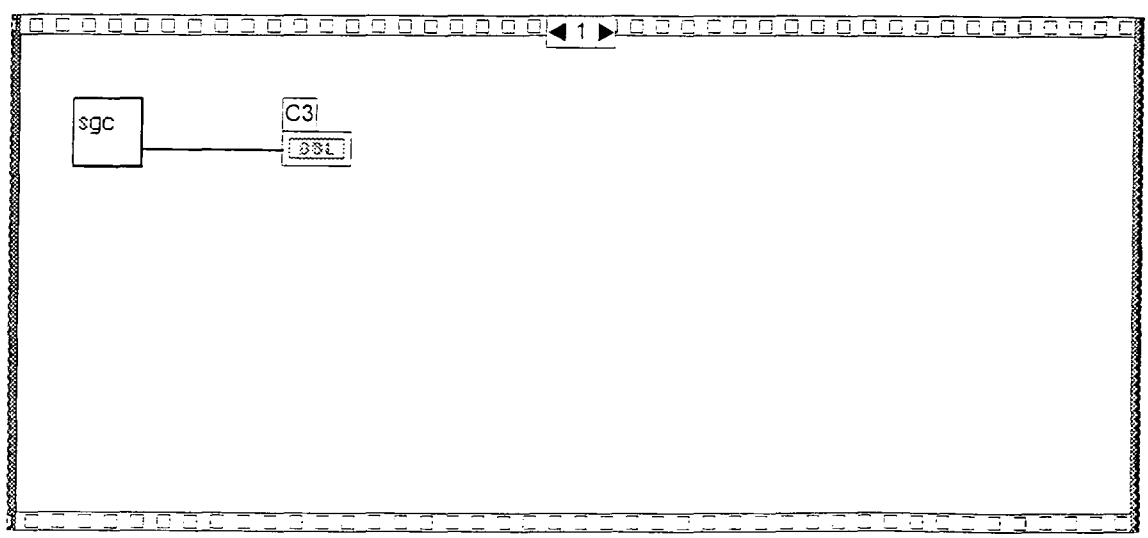

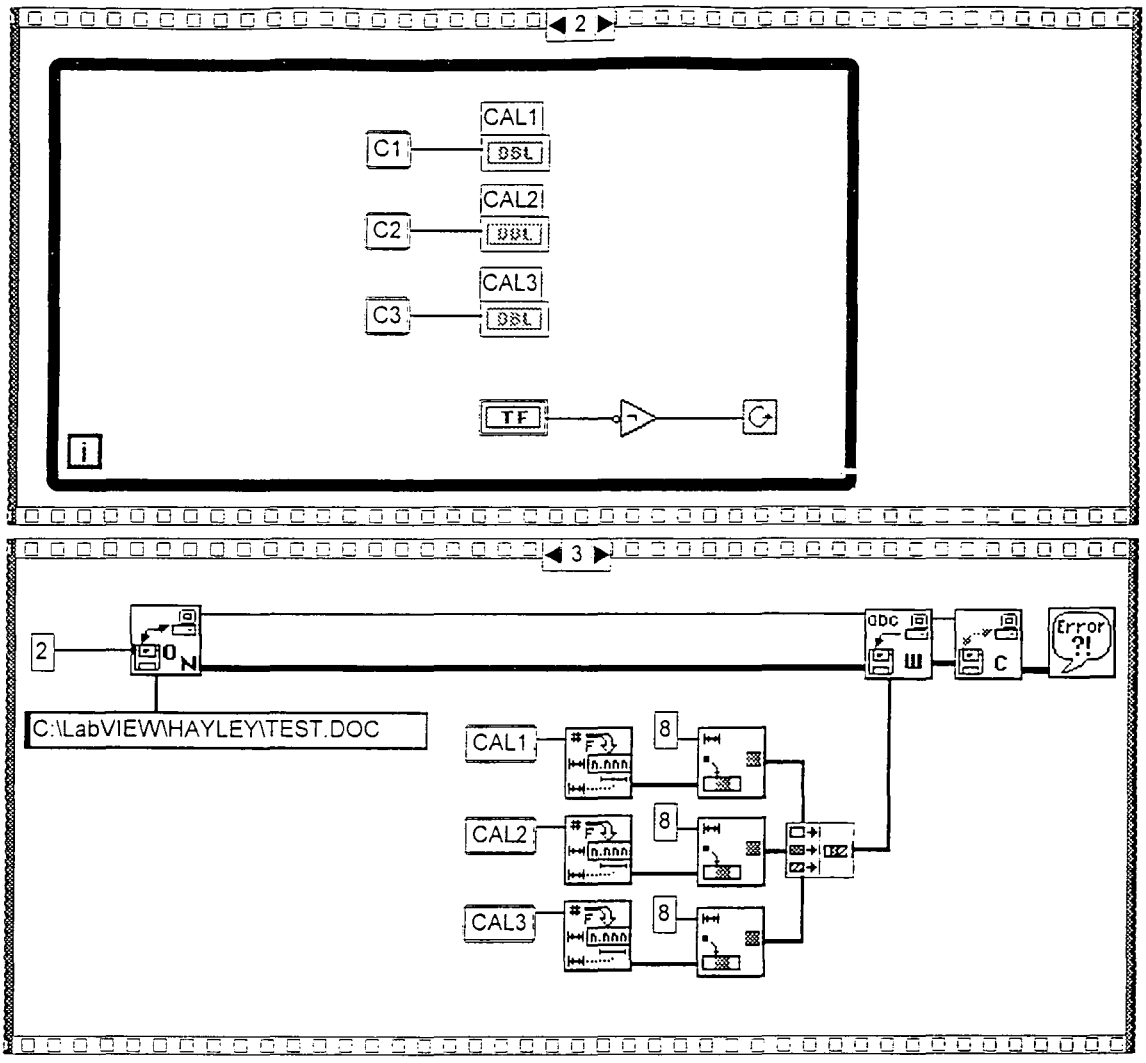

A7.5 SubVIs

Untitled.VI	Strain gauge calibration
KGH.VI	Potentiometer calibration

Connector Pane

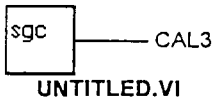

Front Panel

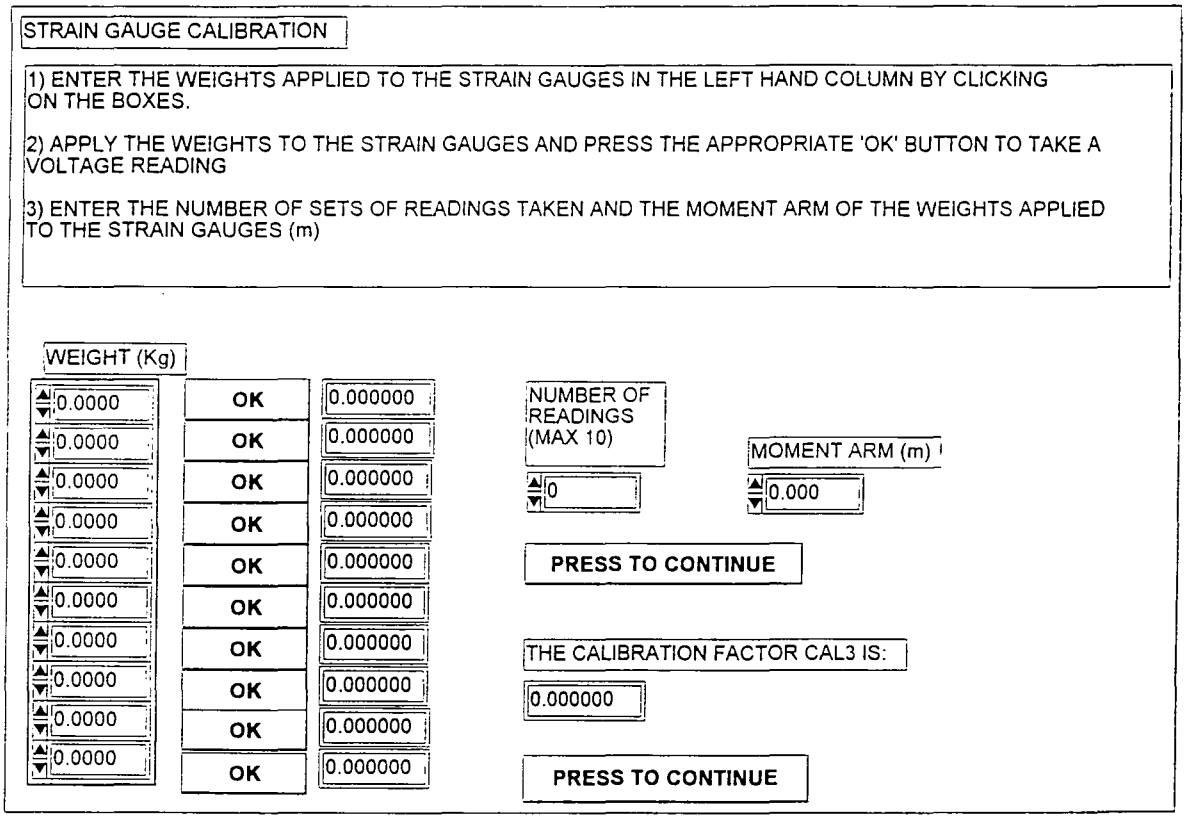

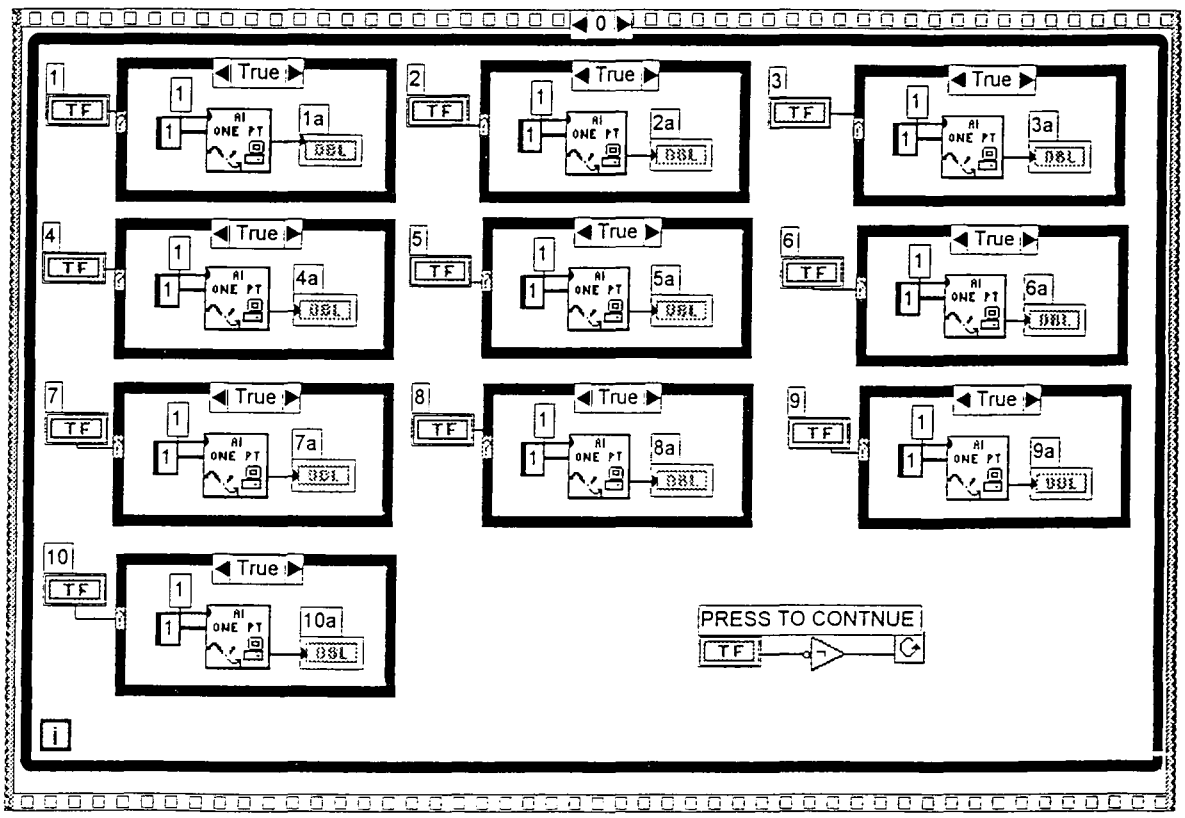

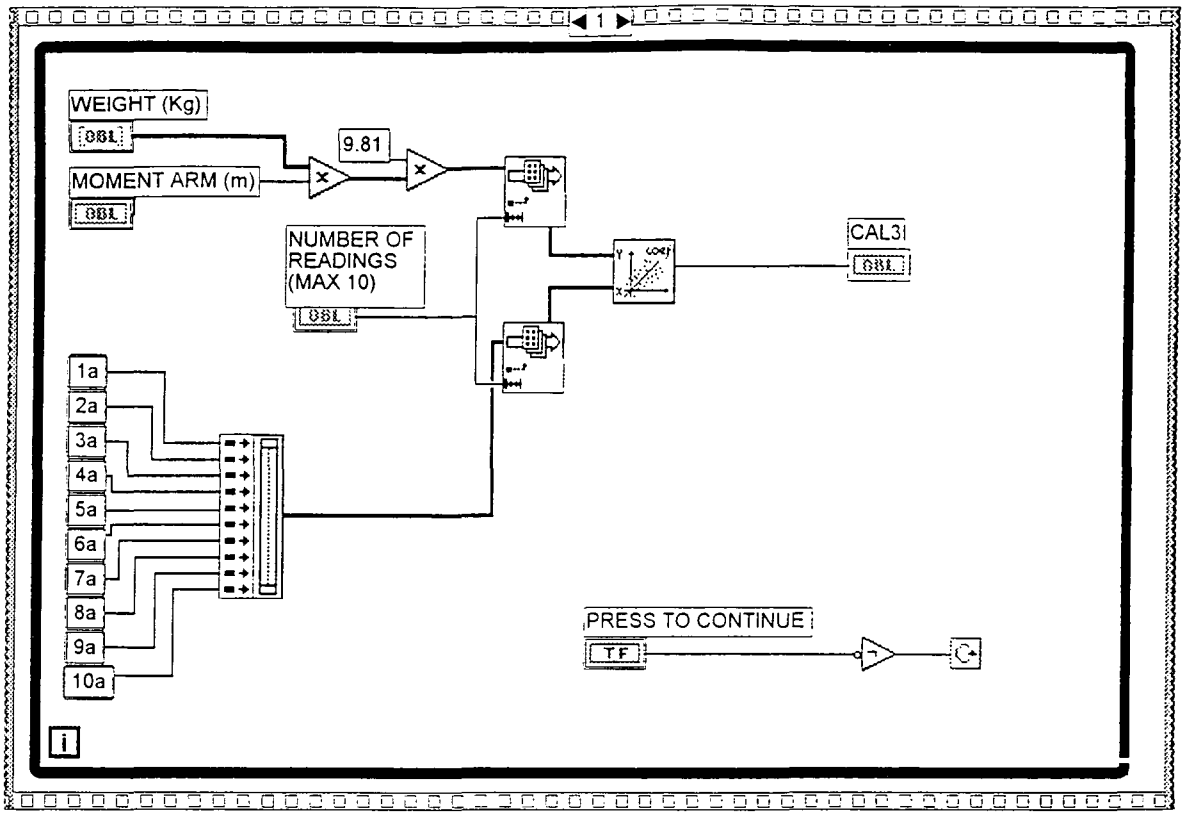

Connector Pane

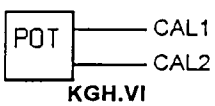

Front Panel

ARTHROGRAPH CALIBRATION PROGRAM (HA 1995)
CENTRE FOR BIOMEDICAL ENGINEERING, UNIVERSITY OF DURHAM
THIS PROGRAM CALCULATES THE CALIBRATION FACTORS FOR THE DURHAM ARTHROGRAPH

POTENTIOMETER CALIBRATION

1) WITH THE CARRIAGE AT FULL EXTENSION, MOVE IT TO 0 DEG.
2) PRESS 'OK' TO TAKE THE 0 DEG. POTENTIOMETER READING

OK | 0 DEG. 0.000000 | CONTINUE

3) Switch on the motor until the carriage is at full flexion.
4) Press OK to take the full flexion potentiometer reading.

OK | FULL FLEX 0.000000 | CONTINUE

THE CALIBRATION FACTORS FOR THE POTENTIOMETER ARE:

CAL1 0.000000 | CAL2 0.000000

PRESS TO CONTINUE

Block Diagram

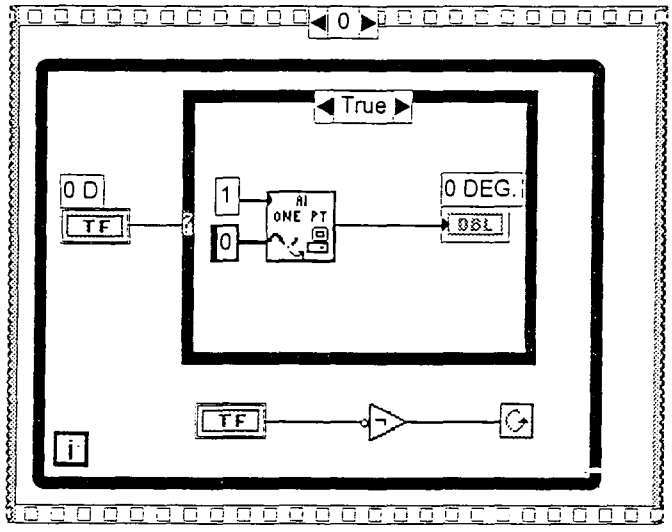

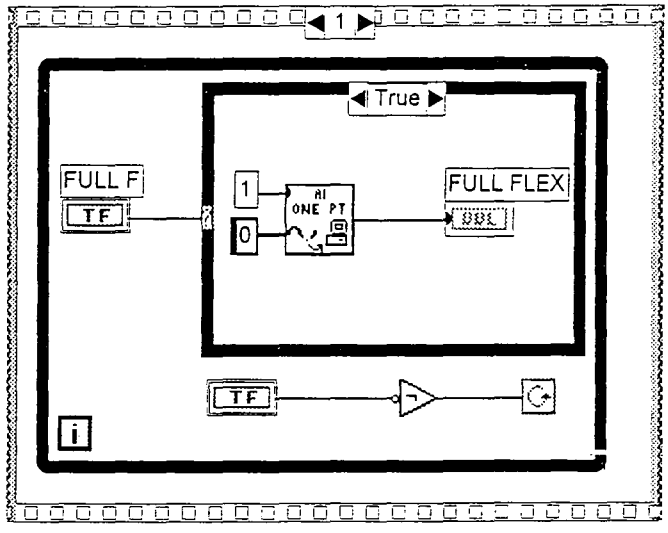

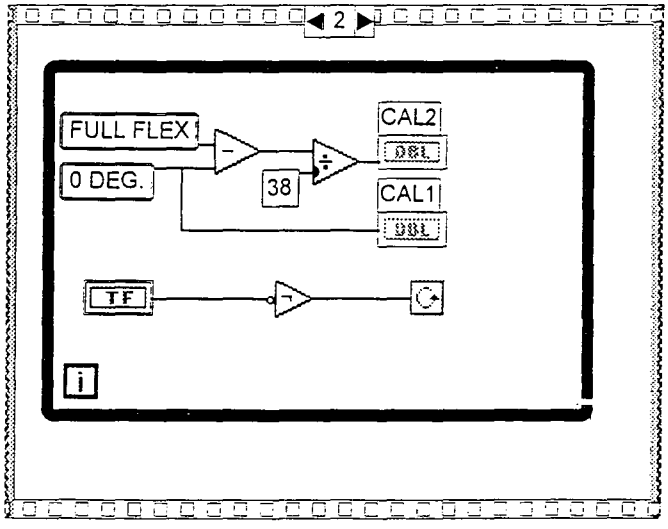

APPENDIX EIGHT

LabVIEW joint stiffness data acquisition program

A8.1 Program structure (Try3.VI)

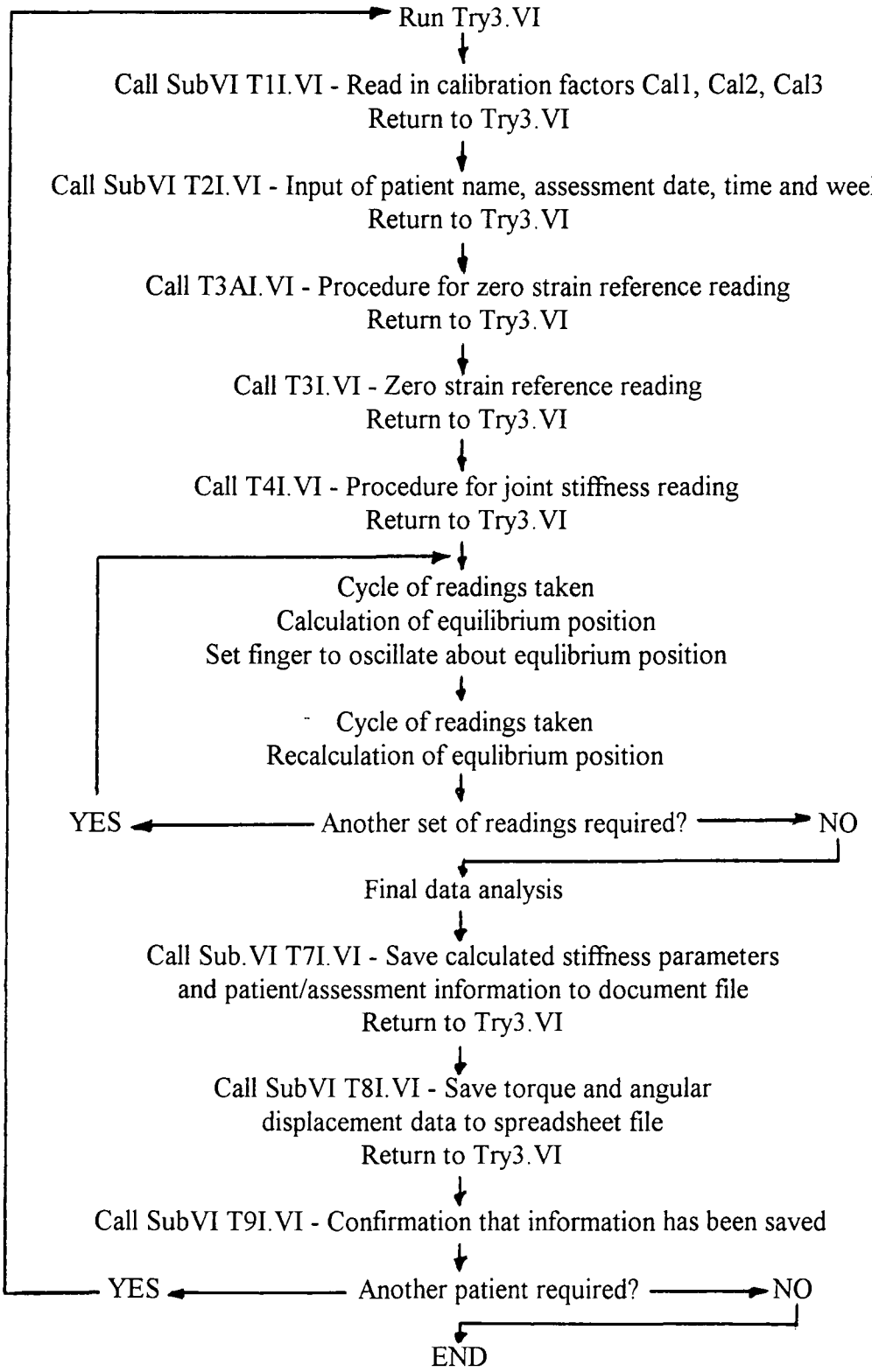

A8.2 Joint stiffness data acquisition program components

The program consists of a front panel which is seen when the program is run, and a sequence of fourteen block diagrams (0-13) which are initiated in turn. The SubVIs called throught the program (via the respective iicons) are:

CAL	Title page and summary of program sections
Pat Info	Input of assessment information Patient's name, assessment date, time and week
PZS	Prompt to ensure holder is at full flexion and empty for zero strain reference reading
ZS	Zero strain reading (ZS)
PJS	Prompt to locate finger correctly in the finger holder and to manually rotate the holder to the correct position (with a scrolling angle display)
OK	Prompt to enter file name under which patient information and stiffness parameters are to be stored
OK2	Prompt to enter file name under which torque and displacement data is to be stored in a spreadsheet
OK3	Prompt that stiffness test is completed and data has been stored to files

Calibration factors are read in from file C:\Labview\hayley\test.doc. Torque and displacement data is collected and the resultant hysteresis loop is shown on the screen. Initial analysis is conducted on the data to calculate the equilibrium position and the centre position of the cycle. Final analysis is they conducted and the parameters maximum torque, minimum torque, peak to peak torque, maximum angle, minimum angle, flexion slope, mid-position slope, extension slope and energy dissipation are calculated. The stiffness parameters and assessment information are then stored to a document file and the torque/displacement data is stored to a spreadsheet file. This section details the components of the front panel and block diagrams of the joint stiffness data acquisition program, followed by those for the individual SubVIs.

A8.2.1 Joint stiffness data acquisition program

Front Panel

Dialog box	1) Switch on the motor and after one cycle press 'Readings' Button to take a set of readings

	2) Switch off the motor when the carriage is at full extension 3) Manually move the carriage to (equilibrium position - 19°) and repeat (1 and 2) 4) If satisfied with the data continue for final analysis, otherwise repeat form (3)
Dialog button	Readings
Numerical indicator	Current angular position
XY graph	Torque against angular displacement
Numerical indicators	Flexion equilibrium position (EP1), extension equilibrium position (EP2), mean equilibrium position (EQPOS) and centre position of cycle
Dialog button	Press for final analysis
Numerical indicators	Maximum torque, minimum torque, peak to peak torque, maximum angle, minimum angle, flexion slope, mid-position slope, extension slope and energy dissipation
Dialog button	Press to save data

Block Diagram

Sequence 0

Dialog box	Title page and summary of program sections
CAL	Sub VI saved in file T1I.VI

Sequence 1

Open file+.vi	File path (C:\Labview\hayley\test.doc)
Read file+(string).vi	TF (selects to read from file in line mode) Refnum (reference number of file C:\LabVIEW\hayley\test.doc) Error in (no error) Count (0) String (Cal1Cal2Cal3) Error out
Split string	String (Cal1Cal2Cal3, Cal2Cal3) Offset (8) Substring before char (Cal1, Cal2) Char substing (Cal2Cal3, Cal3)
From exponential/fract/eng	String (Cal1, Cal2, Cal3) Number (Cal1, Cal2, Cal3)

Numerical indicator	Cal1, Cal2, Cal3
Close file+.vi	Refnum (reference number of file C:\LabVIEW\hayley\ test.doc)
	Error in (no error)
	Error out
Simple error handler	Error in

Sequence 2

Dialog box	Input of assessment information (patient's name, assesment date, time and week)
Get date/time	Date string
	Time string
Pat info	SubVI saved in file T2I.VI
String indicators	Patient's name, assessment date, time and week

Sequence 3

Dialog box	Prompt to ensure holder is at full flexion and empty for zero strain reference reading
PZS	Sub VI saved in file T3I.VI

Sequence 4

Dialog box	Zero strain reading (ZS)
ZS	Sub VI saved in file T3AI.VI
Numerical indicator	ZS

Sequence 5

Dialog box	Prompt to locate finger correctly in the finger holder and to manually rotate the holder to the correct position (with a scrolling angle display)
PJS	Sub VI saved in file T4I.VI

Sequence 6

While loop	
Dialog button	Press for final analysis
Dialog button TF	Readings
Case structure	

AI acquire waveforms.vi	Device (1: DAQ-Card 1200)
	Channels (0: potentiometer, 1: strain gauge system)
	Number of samples/channel (320)
	Scan rate, ccans/second (32)
	Waveform (torque/angular displacement data)
Index arrays	N-Dimension array (torque/angular displacement)
	Index (1: angle, 0: torque - *this is correct!!!*)
	Sub-array (torque, angular displacement data)
Local variables	Cal1, Cal2, ZS, Cal3
Numerical indicators	a2 (angular displacement data), t2 (torque data)
Negate	(torque positive when resisting flexion)
Bundle	Component 0 (angular displacement data)
	Component 1 (torque data)
	Cluster (torque/angular displacement data)
XY graph	Torque against angular displacement
Array size	Size of angular displacement data array
Array max and min	Array (angular displacement data)
	Max value
	Max index
	Min value
	Min index
Numerical indicator	Centre position fo cycle
Array size	Finds the number of elements in the angular displacement array
Rotate 1D array	(Rotates torque and angular displacement arrays to create arrays with the maximum and minimum values first)
Array max and min	Array (rotated displacement data arrays)
	Max index
	Min index
Array subset	Array (torque, angular displacement data)
	Sub-array (torque, angular displacement arrays from max to min values and min to max values)
Index and bundle cluster	Pairs torque with angular displacement data
Threshold 1D array	Array (indexed torque/angular displacement data)

	Threshold Y (0: zero torque)
	X output (angle at zero torque)
Numerical indicators	EP1, EP2, EQPOS
AI sample channel.vi	Device (1: DAQ-card 1200)
	Channel (0: angular displacement)
Local variables	Cal1, Cal2
Numerical indicator	Current angular position
Wait until next ms multiple	Millisecond multiple (250)

Sequence 7

Local variable	t2 (torque data)
Array max and min	Array (torque)
	Max value
	Max index
	Min value
	Min index
Numerical indicators	Maximum torque, minimum torque, peak-to-peak torque
Local variable	a2 (angular displacement data)
Array size	Size of angular displacement data array
Rotate 1D arrays	Rotates torque and angular displacement data by one element
Add array elements	Adds the multiplied torque and angular displacement data together
Numerical indicator	Energy dissipation (Joules/cycle)
Array max and min	Array (angular displacement data)
	Max value
	Min value
Numerical indicators	Maximum angle and minimum angle
Array size	Size of angular displacment data array
Rotate 1D arrays	Rotates torque and angular aisplacment arrays to maximum angular position first
Split 1D array	Divides the torque and displacement data into four arrays
Threshold 1D array	Finds the indexes of the position of one and three quarters of the cycle (by angular displacement)

Split 1D array	Splits the data into the flexion quarter, the extension quarter and the middle half of the cycle
Build array	Combines the data from the two halves of the cycle (as the flexion quarter, the extension quarter and the middle half of the cycle)
Linear fit coefficients.vi	Y values (torque data) X values (angular displacement data) Slope
Numerical indicators	Flexion slope, extension slope, mid-position slope

Sequence 8

While loop	
Dialog button TF	Press to save data

Sequence 9

Dialog box	Prompt to enter file name under which patient information and stiffness parameters are to be stored
OK	Sub VI stored in file T7I.VI

Sequence 10

Local variables	Patient's name, date of assessment, time of assessment, assessment week, EP1, EP2, EQPOS, energy dissipation, maximum torque, minimum torque, peak to peak torque, flexion slope. mid position slope, extension slope, maximum angle, minimum angle, centre position of cycle)
To fractional	Number (e.g. maximum torque) Precision (4: decimal places) F-Format String
String	Dialog (e.g. Equilibrium position (Deg. =)
Concatenate strings	
Write characters to file.vi	Character string (patient and assessment information and calculated stiffness parameters)

Sequence 11

Dialog box	Prompt to enter file name under which torque and displcement data is to be stored in a spreadsheet
OK2	Sub VI stored in file T8I.VI

Sequence 12

Local variables	a2 (angular displacement data), t2 (torque data)
Decimate 1D arrays	Divides input array into four sub-arrays like dealing cards
Interleave 1D arrays	Interleaves sub-array (Re: this has been done because for the precision of 0.0001 Nm in the calculation of the stiffness parameters 320 readings per cycle are required however the spreadsheet has a limit of 250 sets of data hence every fourth data point has been discarded)
Build array	Concatenates torque and displacement arrays
Write to spreadsheet file.vi	2D Data (torque and angular displacement data) Transpose T (to column saved format)

Sequence 13

Dialog box	Prompt stiffness test completed and data stored to files
OK3	Sub VI saved in file T9I.VI

A8.2.2 Sub VIs

CAL (Saved in file T1I.VI)

Front Panel

Dialog box	Joint Stiffness Assessment, Arthrograph Control Program (HA 1995), Centre for Biomedical Engineering, University of Durham
Dialog box	The joint stiffness assessment procedure consists of five stages. Stage 1: Enter patient and assessment details Stage 2: Zero strain reading Stage 3: Joint stiffness data collection Stage 4: Analysis of stiffness data Stage 5 : Save data and results
Dialog button	Press to continue

Block Diagram

While loop	
Dialog button TF	Press to continue

Pat Info (Saved in file T2I.VI)

Front Panel

Dialog box	Stage 1: Enter patient and assessment details
Dialog box	Complete the following patient and assessment information, using the mouse to select the appropriate boxes
String contols	Patient's name, assessment week, date and time
Dialog button	Press to continue

Block Diagram

While loop	
String controls	Patient's name, assessment date, time and week
Dialog button TF	Press to continue
String indicators	Patient's name, assessment date, time and week

PZS (Saved in file T3AI.VI)

Front Panel

Dialog box	Stage 2: Zero strain reference reading
Dialog box	1) Ensure that the finger holder is empty 2) Switch off the motor when carriage is at full extension 3) Press start to take reading
Dialog button	Start

Block Diagram

While loop	
Dialog button TF	Press start to take reading

ZS (Saved in file T3I.VI)

Front Panel

Numerical indicator	Zero strain reference reading
Dialog button	Press to continue

Block Diagram

While loop	
AI sample	Device (1: DAQ-card 1200)
Channel.vi	Channel (1: strain gauge system) Sample (zero strain reference reading)
Numerical indicator	Zero strain reference reading

Dialog button TF	Press to continue

PJS (Saved in file T4I.VI)

Front Panel

Dialog box	Stages 3 and 4: Joint stiffness data collection and analysis of stiffness data
Dialog box	Carefully follow the following procedure 1) Correctly locate the right hand index finger in the holder 2) Ensure that the forearm, wrist, thumb and remaining fingers are positioned correctly 3) Manually rotate the finger holder to 40 DEG. or to a position of maximum flexion comfortable for the patient
Numercal indicator	The present carriage angle is:
Dialog button	Press to continue

Block Diagram

Sequence 0

Open file+.vi	Path name (C:\LabVIEW\hayley\test.doc)
Read file+(string).vi	Line mode (TF) Count (0) Dup Refnum (reference number for C:\LabVIEW\hayley\test.doc) String (Cal1Cal2Cal3) Error out
Split string	String (Cal1Cal2Cal3, Cal2Cal3) Offset (8) Substring before char (Cal1, Cal2) Char substring (Cal2Cal3, Cal3)
From exponential/fract/eng	String (Cal1, Cal2) Number (Cal1, Cal2)
Numerical indicator	Cal1, Cal2
Close file+.vi	Refnum (reference number for file C:\LabVIEW\hayley\test.doc) Error in (no error) Error out
Simple error handler.vi	Error in (no error)

Sequence 1

While loop	
AI sample channel.vi	Device (1: DAQ-card 1200) Channel (0: potentiometer) Sample (potentiometer output voltage)
Local variables	Cal1, Cal2
Numerical indicator	The present carriage angle is:
Dialog button TF	Press to continue

OK (Saved in file T7I.VI)

Front Panel

Dialog box	Stage 5: Save data and results
Dialog box	The information from this stiffness test will be stored in two files. The first stores the calculated stiffness parameters and patient information and the second stores the torque displacement data into a spreadsheet file
Dialog box	Press 'OK' to continue and enter the file name under which you wish to store the stiffness parameters and patient information in the format a:\filename.doc
Dialog button	OK

Block Diagram

While loop	
Dialog button TF	Press OK to continue

OK2 (Saved in file T8I.VI)

Front Panel

Dialog box	Press 'OK' to continue and enter the file name under which you wish to save the torque and angular displacement data into a spreadsheet in the format a:\filename.xls
Dialog button	OK

Block Diagram

While loop	
Dialog button TF	Press OK to continue

OK3 (Saved in file T9I.VI)

Front Panel

Dialog box	Results and data have been saved on disc
Dialog button	OK

Block Diagram

While loop

Dialog box TF	Press OK to continue

A8.3 Operating instructions

The following section shows the front panels which the user will see when the data acquisition program is run and describes the interaction required from the user to run the whole program. To run the joint stiffness data acquisition program select the *LabVIEW* icon in the LabVIEW windows menu. Select *File. Open. C:\LabVIEW\hayley\TRY3.VI.* Press → from the TRY3.VI front panel shown making sure that the arthrograph is turned on and connected correctly to the computer and that the DAQCard-1200 is configured in NI-DAQ.

Front panel I

Title page, summary of the program sections and stage 1: read in of calibration factors

Joint stiffness assessment
Arthrograph joint stiffness data acquisition program - (HA 1995)
Centre for biomedical engineering, University of Durham
This program collects and analyses MCPJ stiffness data

The joint stiffness assessment procedure consists of five stages

Stage 1	*Enter patient and assessment details*
Stage 2	*Zero strain reading*
Stage 3	*Joint stiffness data collection*
Stage 4	*Analysis of stiffness data*
Stage 5	*Save data and results*

Press to Continue

Front panel II
Input of patient and assessment information

Stage 1 *Enter patient and assessment details*
Complete the following patient and assessment information, using the mouse to select the appropriate boxes

Patient Name
Assessment week
Assessment date
Assessment time

Press to continue

Stage 1
Enter patient's name (initials) and the assessment week, and alter the assessment date and time if necessary by clicking on the boxes. *Press to continue* when details have been completed.

Front panel III
Zero strain reading procedure

Stage 2 *Zero strain reference reading*

1) Ensure that the finger holder is empty
2) Switch off the motor when the carriage is at full extension
3) Press start to take readings

Start

Stage 2
To take the zero strain reference reading make sure the carriage is empty and at full flexion and press *Start.*

Front panel IV
Zero strain reference reading displayed on screen

Zero strain reference reading

Press to continue

Front Panel V
Joint stiffness data acquisition set up description

Stages 3 and 4: Joint stiffness data acquisition and analysis of stiffness data

Carefully follow the following procedure
1) Correctly locate the right hand index finger in the holder
2) Ensure that the forearm, wrist, thumb and remaining fingers are positioned correctly
3) Manually rotate the finger holder to 40 deg. or to a position of maximum flexion comfortable for the patient

The present carriage angle is:

Press to continue

Stages 3 and 4
Before patients are tested using the arthrograph the MCP joints should be tested for the amount of flexion and extension comfortably allowed. The initial setting of the arhrograph consists of rotation of the joint between 0 and 40 degrees.. However if this range of motion is not comfortably possible by a patient then a different range should be used or the patient should not be tested at all.

The MCP finger joint should be correctly located in the arthrograph with the centre of rotation of the joint in alignment with the centre of rotation of the arthrograph. The rest of the fingers should be curled around the cylindrical support, the wrist in the neutral position and the thumb located in the thumb support sling. The carriage should be manually rotated to a full flexion position of 40 degrees or a position comfortable for the patient.

When this has been done *Press to continue*

Front panel VI (Front panel of arthrograph data acquisition program)
Data collection and analysis

1) *Switch on the motor and after one cycle press the readings button to take a set of readings*
2) *Switch off the motor when the finger is at full extension*
3) *Manually move the carriage to (Equilibrium position - 19 degrees) and repeat (1 and 2)*
4) *If satisfied with the data continue for final analysis, otherwise repeat from (3)*

Readings *Current angular position*
XY-Graph of Torque v Angular displacement
Equilibrium position 1
Equilibrium position 2
Mean equilibrium position
Centre position of cycle

Press for final analysis *Maximum angle*
Minimum angle
Maximum torque
Minimum torque
Peak to peak torque
Flexion slope
Mid-position slope
Extension slope
Energy dissipation

Press to save data

Stage 4 and 5

Start the motor and after one cycle press *Readings* to take a set of readings (starting when the joint is in full flexion). Switch off the motor when the readings have been taken. The equilibrium position of the joint is calculated and this should be within 0.5 degree of the centre position of the cycle. If it is not, manually reposition the carriage to a position of full flexion of equilibrium position + 19 degrees. Start the motor and after one cycle press *Readings* to take a second set of data. Repeat until the equilibrium position and centre of the cycle coincide.

Press for final analysis

Press to save data

Front panel VII
Prompt to save stiffness parameters

Stage 5 *Save data and stiffness parameters*

The information from this stiffness test will be stored in two files
The first stores the calculated stiffness parameters and patient information
The second stores the torque and angular displacement data into a spreadsheet file

Press OK to continue and enter the file name under which you wish to store the stiffness parameters and patient information in the format a:\filename.doc

OK

Stage 5
Press *OK* to obtain the file selection panel. Make sure the required disc is in the a:\ drive. Enter the file which you wish the calculated stiffness parameters and patient/assessment information to be saved under in the format *a:\filename.doc* and press *OK* to continue.

Front panel VIII
Prompt to save torque/angular displacement data

Press OK to continue and enter the spreadsheet file name under which you wish to save the torque and angular displacement data in the format

a:\filename.xls

OK

Press *OK* to obtain the file selection panel. Enter the file which you wish the joint stiffness data to be saved under in the format *a:\filename.xls* and press *OK* to continue.

Front panel IX

Confirmation of saving to files

Results and data have been saved on disc

Press OK to continue

OK

A8.4 Joint stiffness data acquisition program

Connector Pane

Front Panel

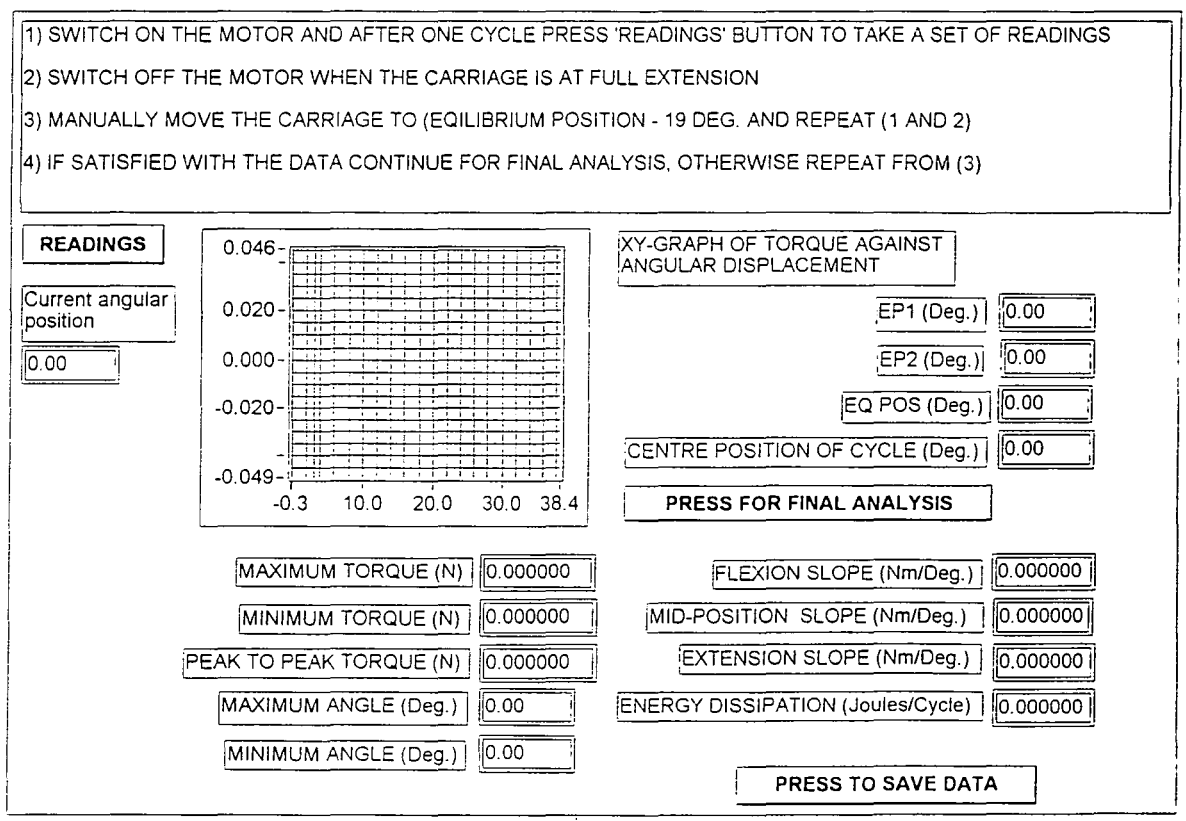

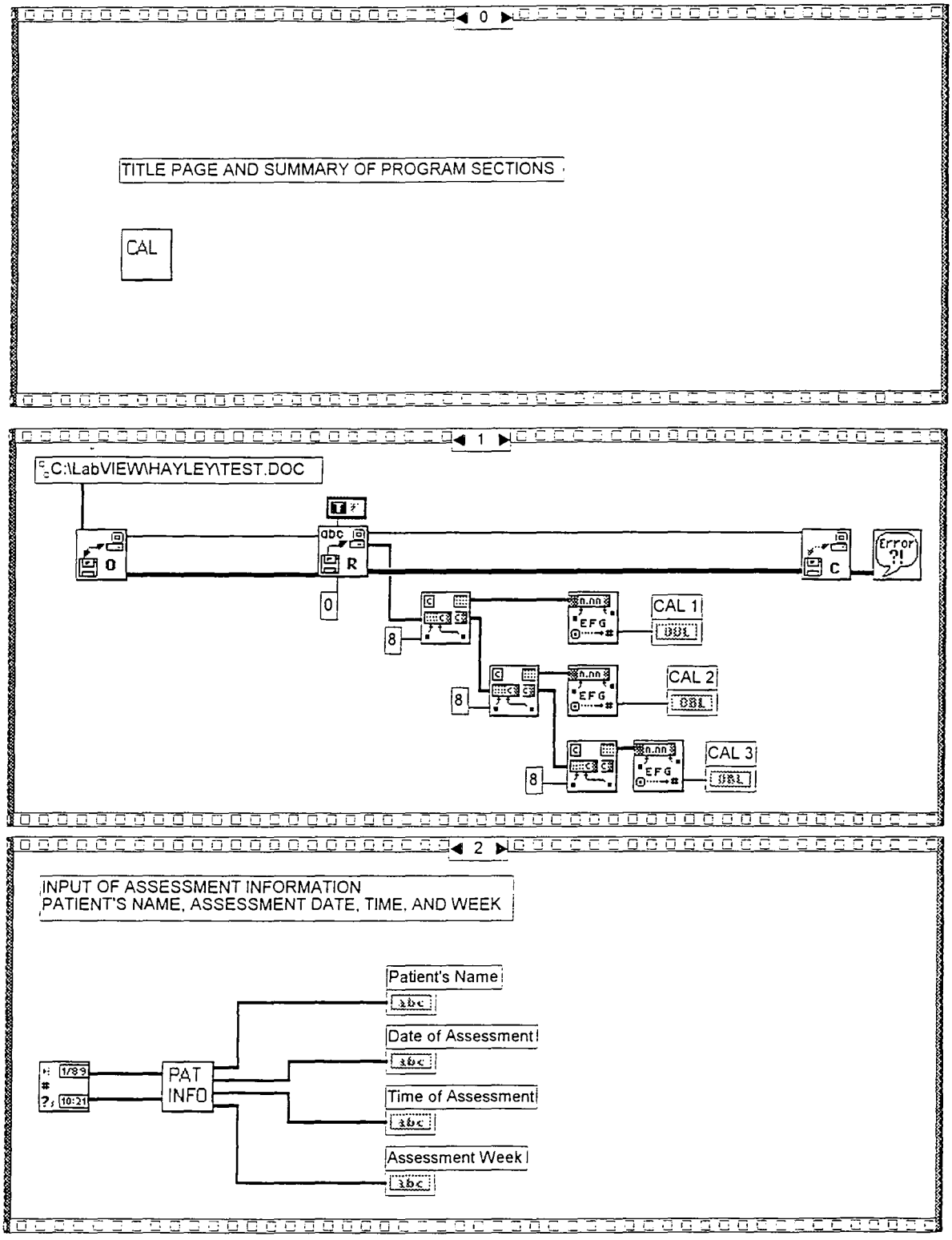
0
TITLE PAGE AND SUMMARY OF PROGRAM SECTIONS
CAL
1
C:\LabVIEW\HAYLEY\TEST.DOC
R
C
Error
CAL 1
CAL 2
CAL 3
2
INPUT OF ASSESSMENT INFORMATION
PATIENT'S NAME, ASSESSMENT DATE, TIME, AND WEEK
Patient's Name
Date of Assessment
Time of Assessment
Assessment Week
PAT
INFO

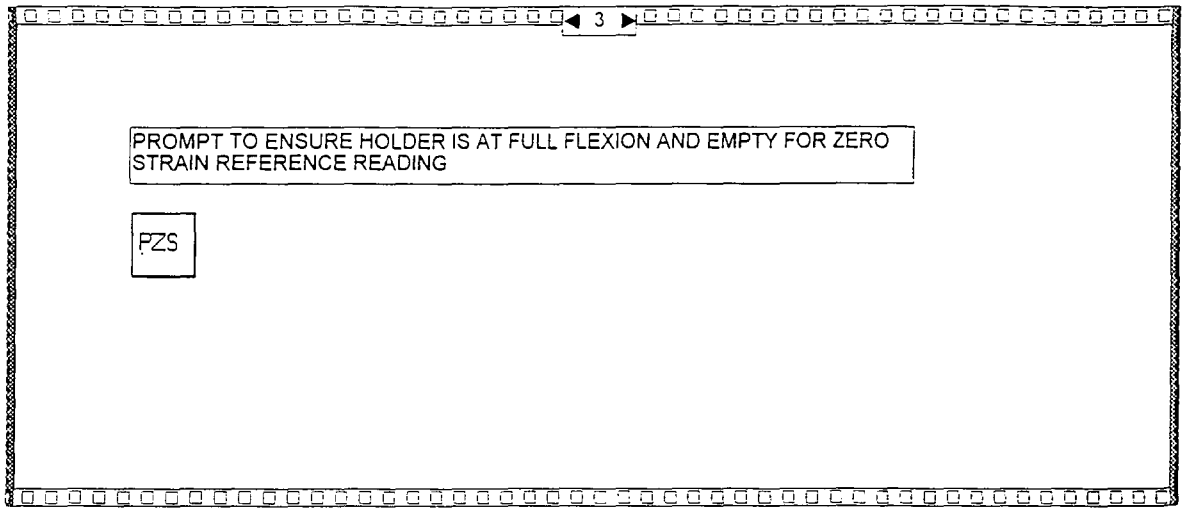
3
PROMPT TO ENSURE HOLDER IS AT FULL FLEXION AND EMPTY FOR ZERO STRAIN REFERENCE READING
PZS

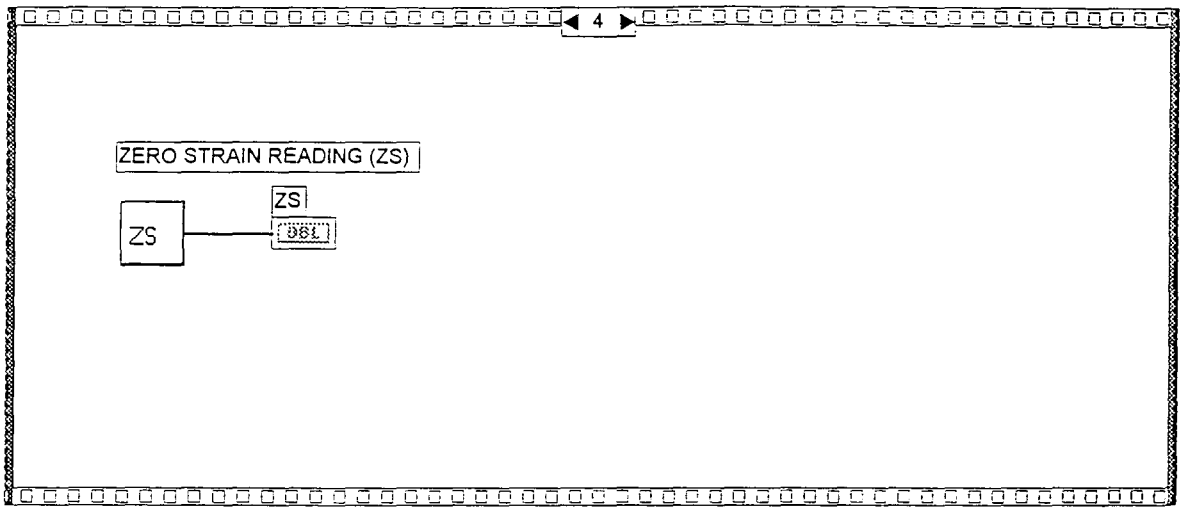
4
ZERO STRAIN READING (ZS)
ZS
ZS

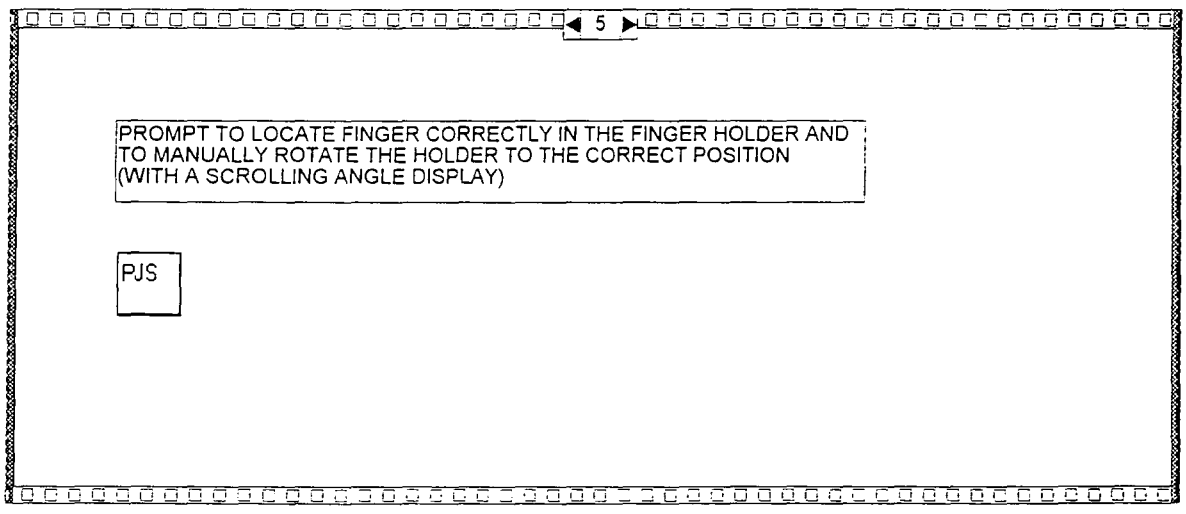
5
PROMPT TO LOCATE FINGER CORRECTLY IN THE FINGER HOLDER AND TO MANUALLY ROTATE THE HOLDER TO THE CORRECT POSITION (WITH A SCROLLING ANGLE DISPLAY)
PJS

Block Diagram

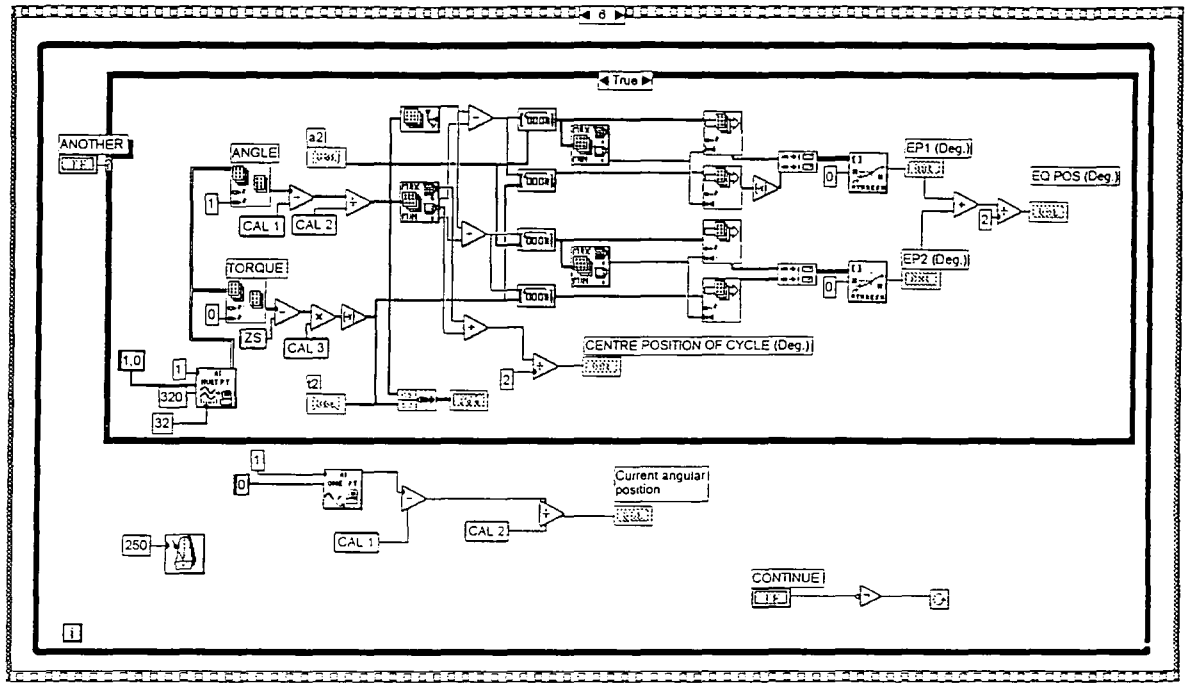

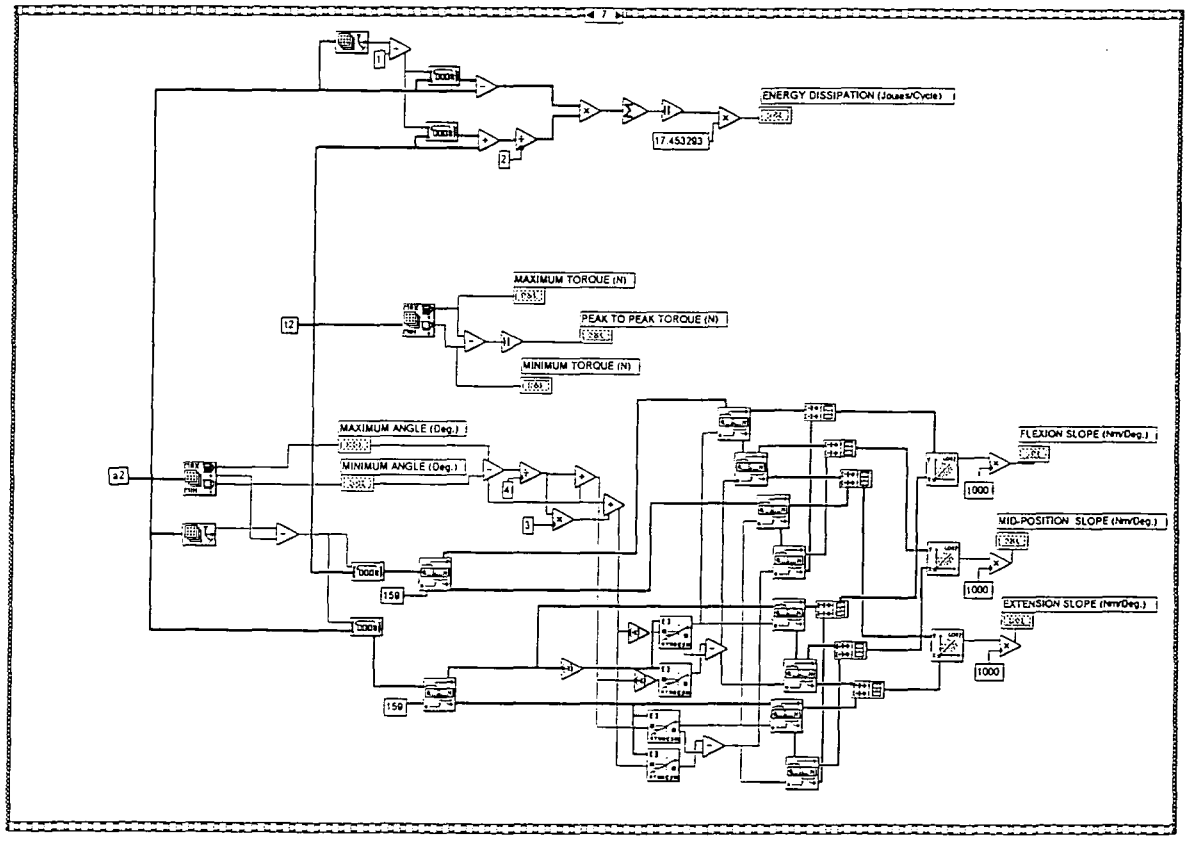

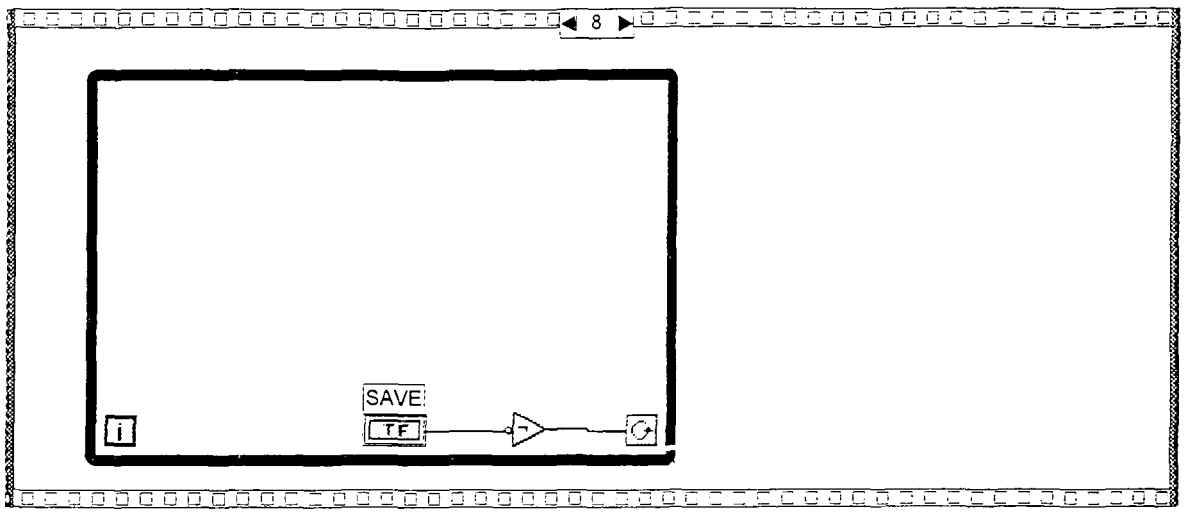
8
SAVE
TF

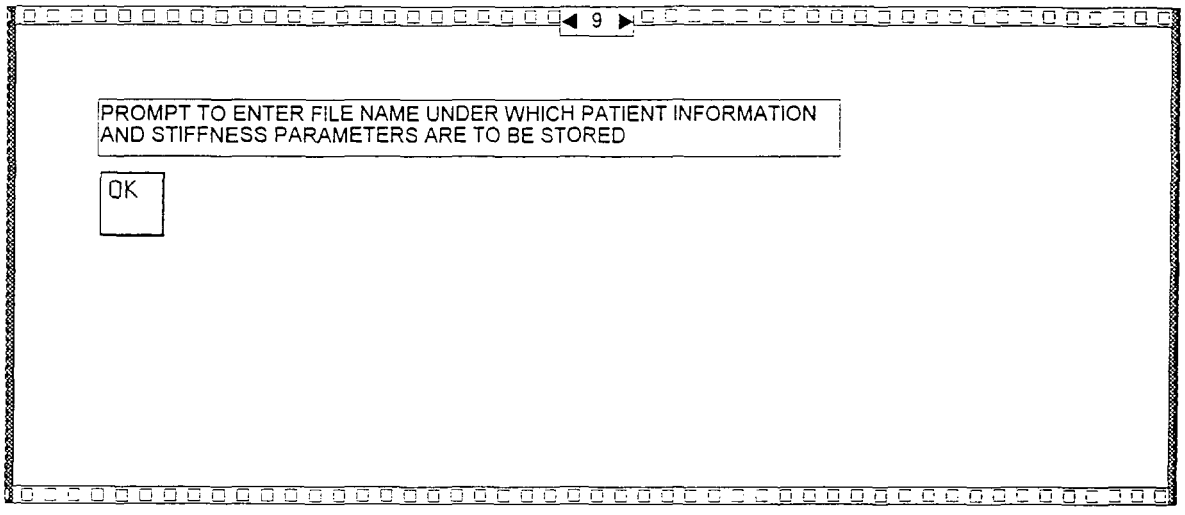
9
PROMPT TO ENTER FILE NAME UNDER WHICH PATIENT INFORMATION AND STIFFNESS PARAMETERS ARE TO BE STORED
OK

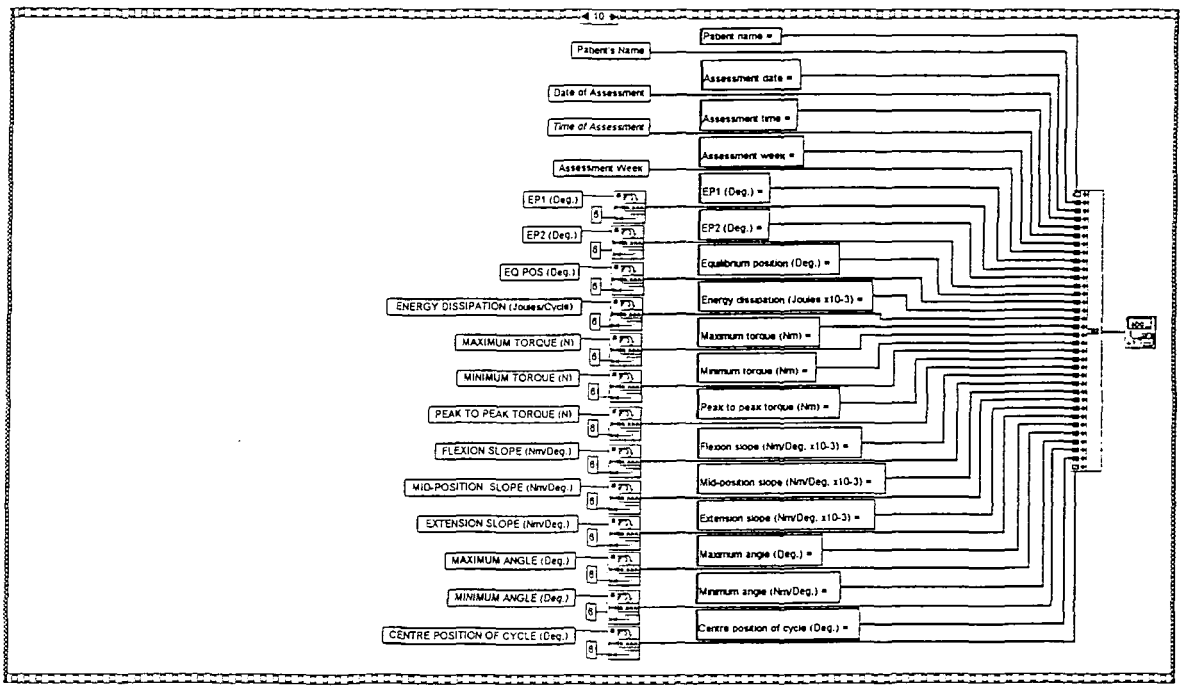
10
Patient's Name
Date of Assessment
Time of Assessment
Assessment Week
EP1 (Deg.)
EP2 (Deg.)
EQ POS (Deg.)
ENERGY DISSIPATION (Joules/Cycle)
MAXIMUM TORQUE (N)
MINIMUM TORQUE (N)
PEAK TO PEAK TORQUE (N)
FLEXION SLOPE (Nm/Deg.)
MID-POSITION SLOPE (Nm/Deg.)
EXTENSION SLOPE (Nm/Deg.)
MAXIMUM ANGLE (Deg.)
MINIMUM ANGLE (Deg.)
CENTRE POSITION OF CYCLE (Deg.)
Patient name =
Assessment date =
Assessment time =
Assessment week =
EP1 (Deg.) =
EP2 (Deg.) =
Equilibrium position (Deg.) =
Energy dissipation (Joules x10-3) =
Maximum torque (Nm) =
Minimum torque (Nm) =
Peak to peak torque (Nm) =
Flexion slope (Nm/Deg. x10-3) =
Mid-position slope (Nm/Deg. x10-3) =
Extension slope (Nm/Deg. x10-3) =
Maximum angle (Deg.) =
Minimum angle (Nm/Deg.) =
Centre position of cycle (Deg.) =

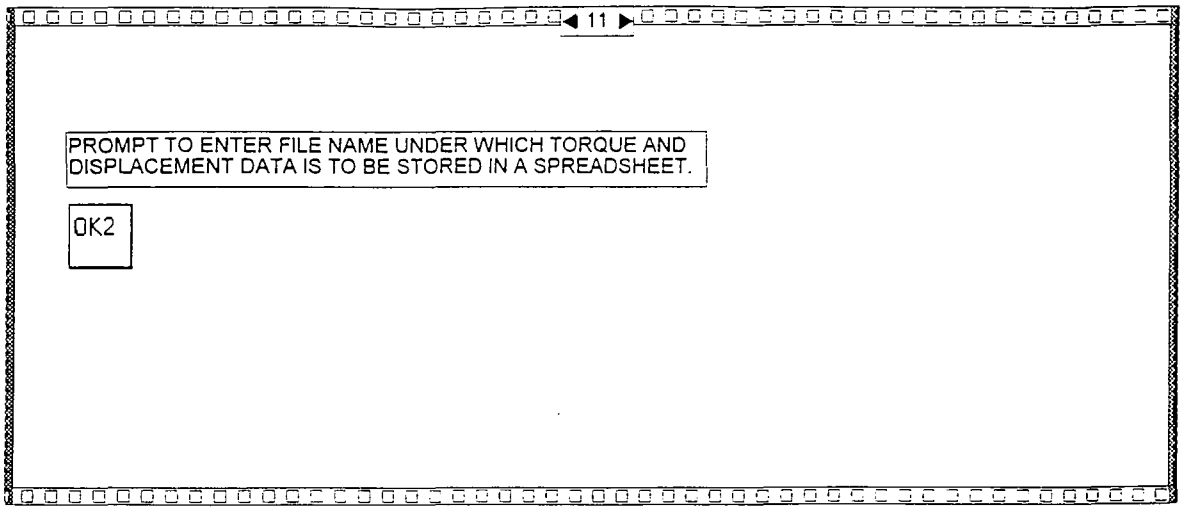
11
PROMPT TO ENTER FILE NAME UNDER WHICH TORQUE AND DISPLACEMENT DATA IS TO BE STORED IN A SPREADSHEET.
OK2

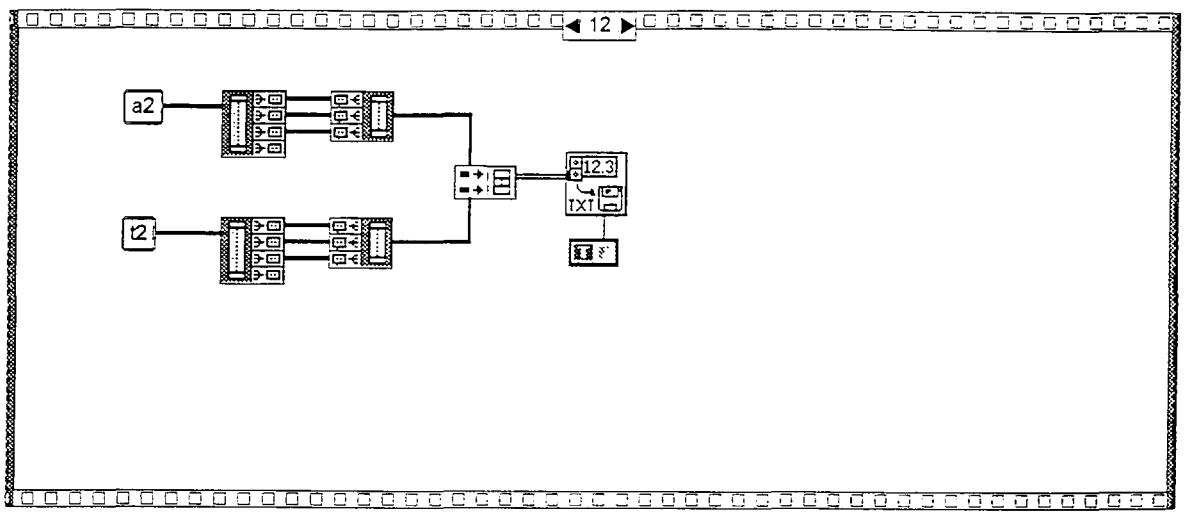
12
a2
t2
12.3
TXT

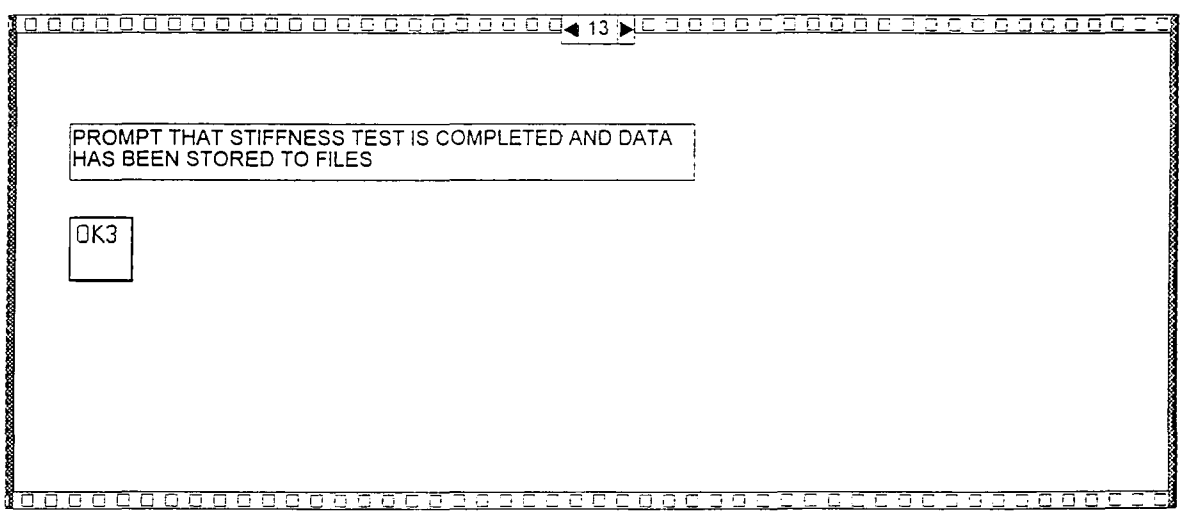
13
PROMPT THAT STIFFNESS TEST IS COMPLETED AND DATA HAS BEEN STORED TO FILES
OK3

A8.5 SubVIs

Connector Pane

Front Panel

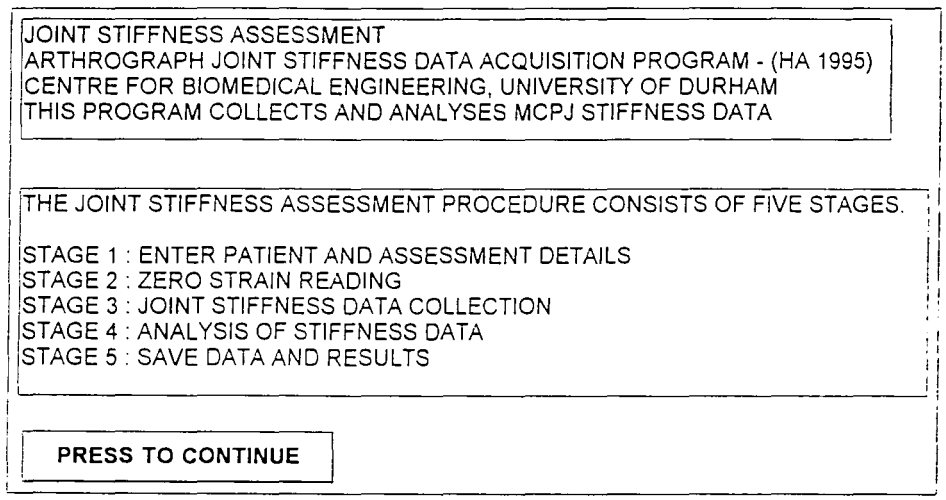

Block Diagram

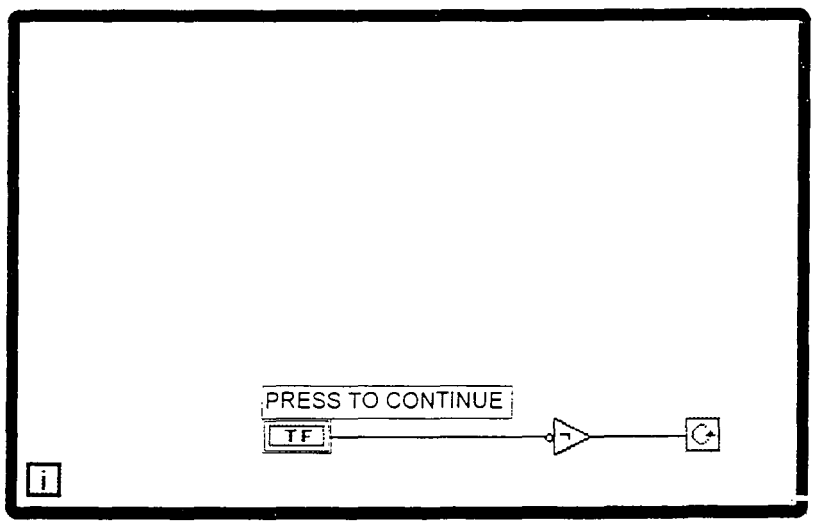

Connector Pane

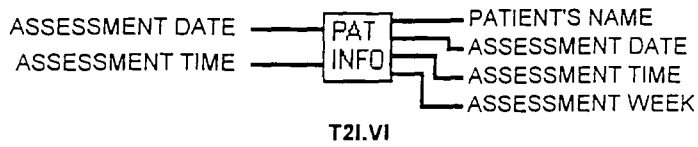

T2I.VI

Front Panel

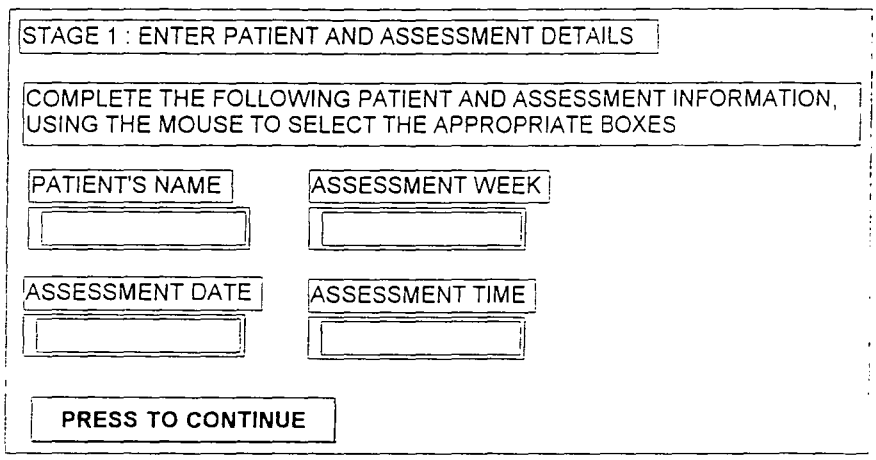

Block Diagram

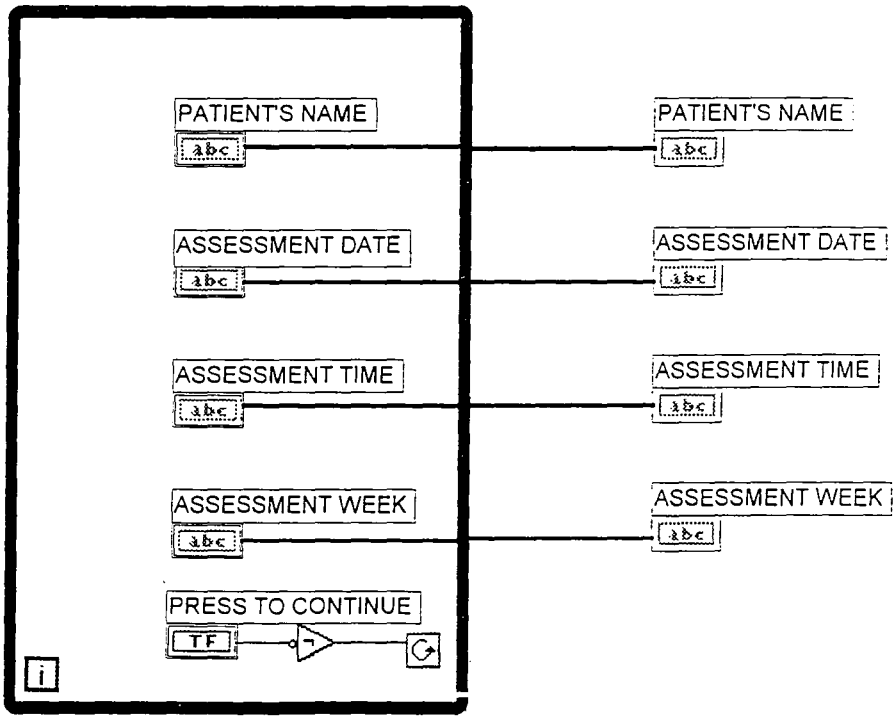

Connector Pane

T3AI.VI

Front Panel

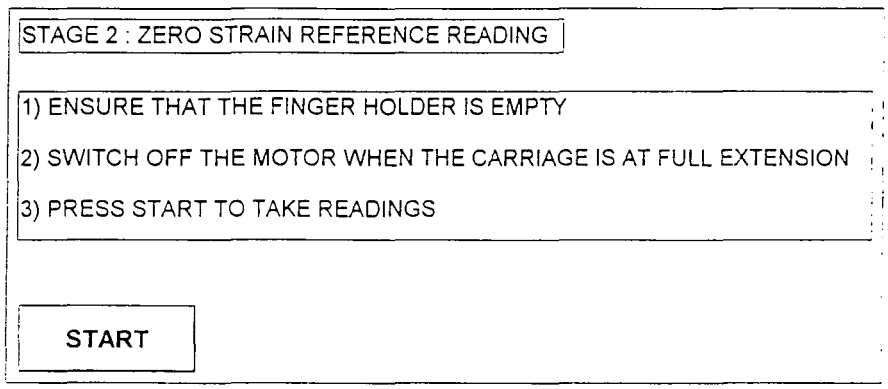

Block Diagram

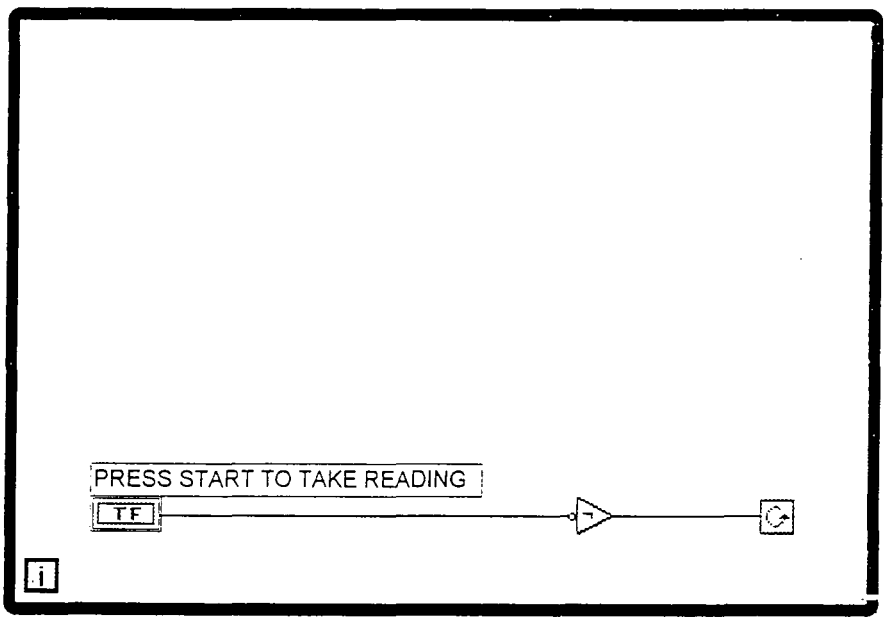

Connector Pane

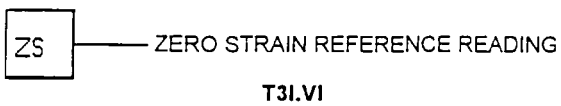

T3I.VI

Front Panel

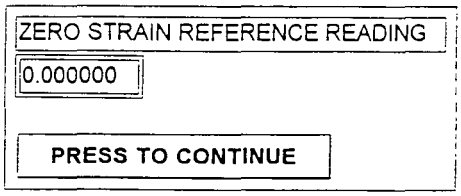

Block Diagram

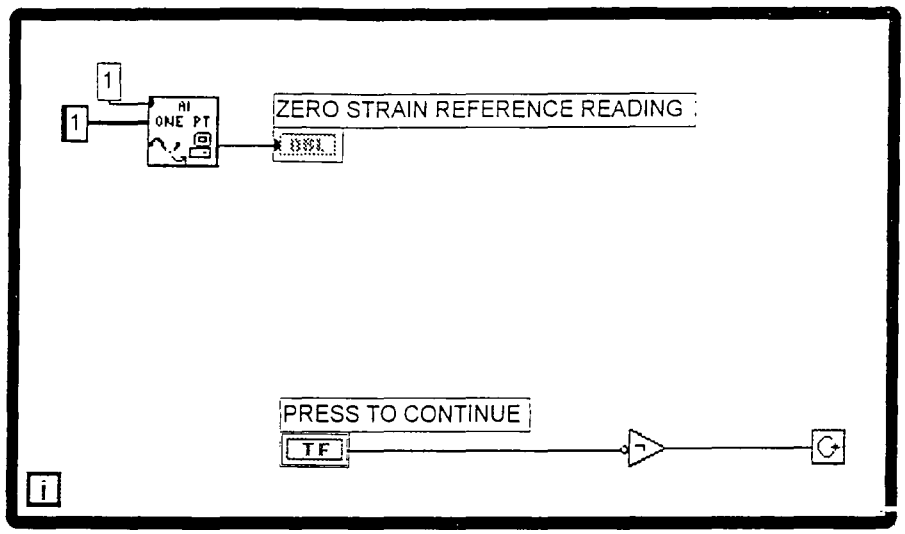

Connector Pane

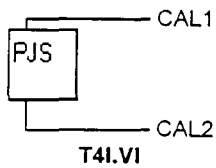

Front Panel

STAGES 3 AND 4 : JOINT STIFFNESS DATA COLLECTION AND ANALYSIS OF STIFFNESS DATA

CAREFULLY FOLLOW THE FOLLOWING PROCEDURE

1) CORRECTLY LOCATE THE RIGHT HAND INDEX FINGER IN THE HOLDER

2) ENSURE THAT THE FOREARM, WRIST, THUMB AND REMAINING FINGERS ARE POSITIONED CORRECTLY

3) MANUALLY ROTATE THE FINGER HOLDER TO 0 DEG. OR TO A POSITION COMFORTABLE FOR THE PATIENT

THE PRESENT CARRIAGE ANGLE IS:

0.0

PRESS TO CONTINUE

Block Diagram

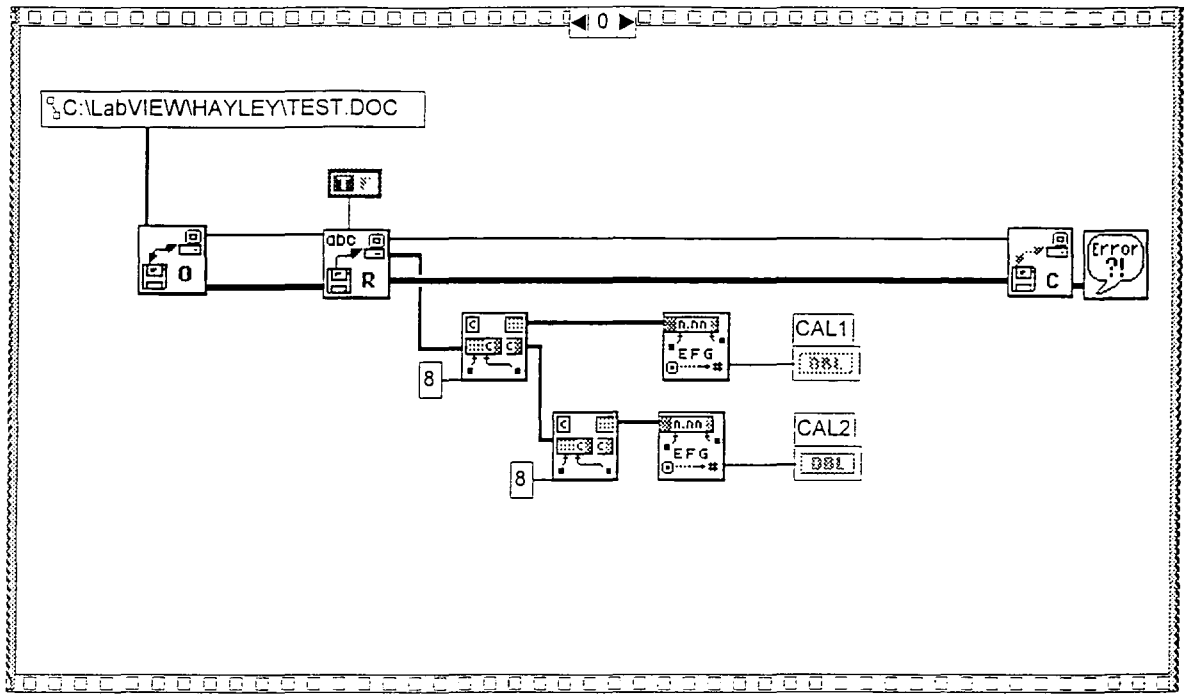

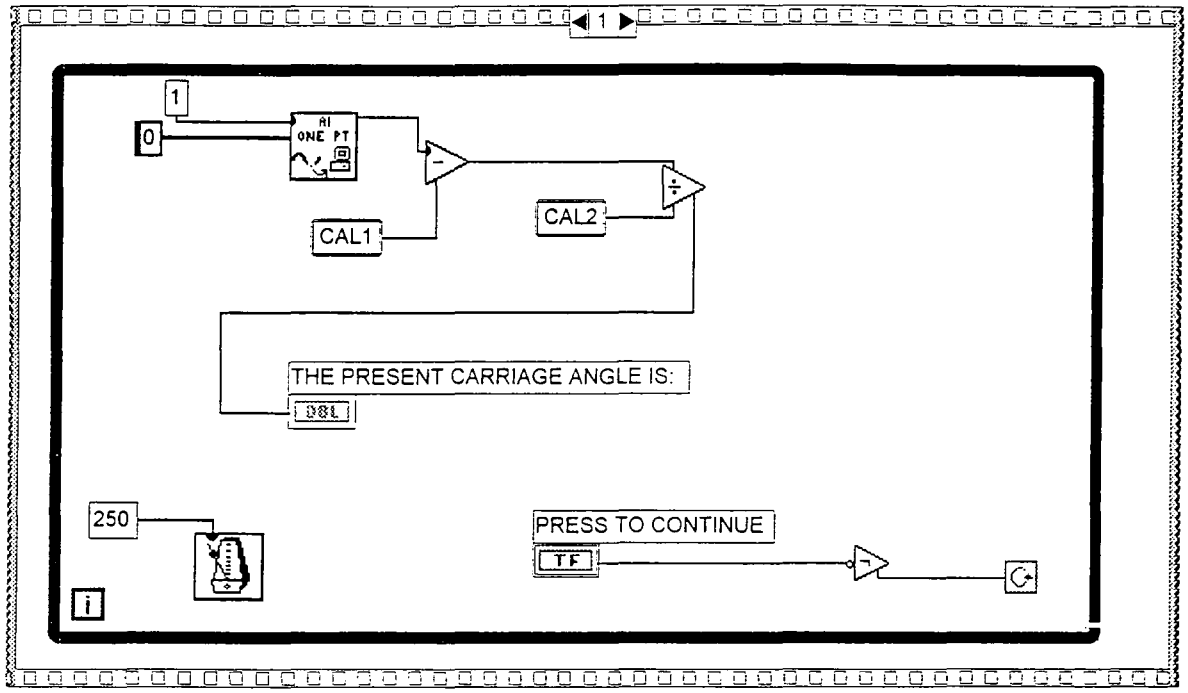

Connector Pane

T7I.VI

Front Panel

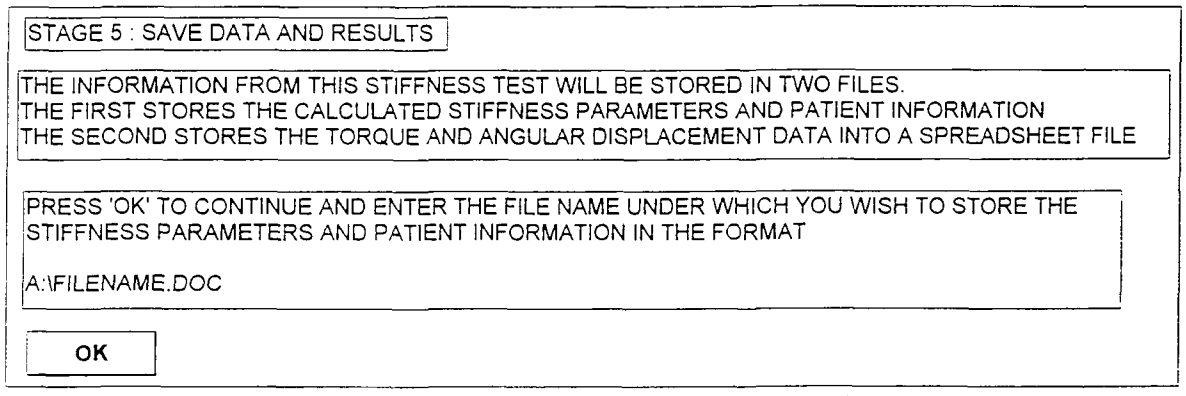

Block Diagram

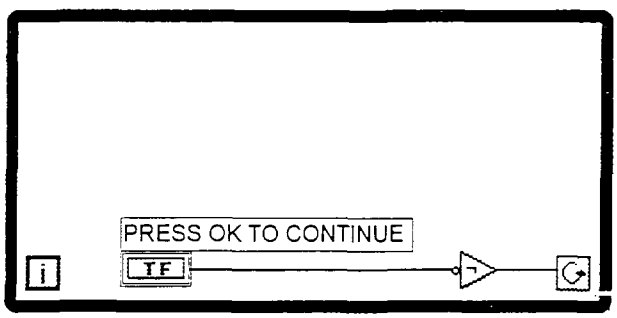

Connector Pane

T8I.VI

Front Panel

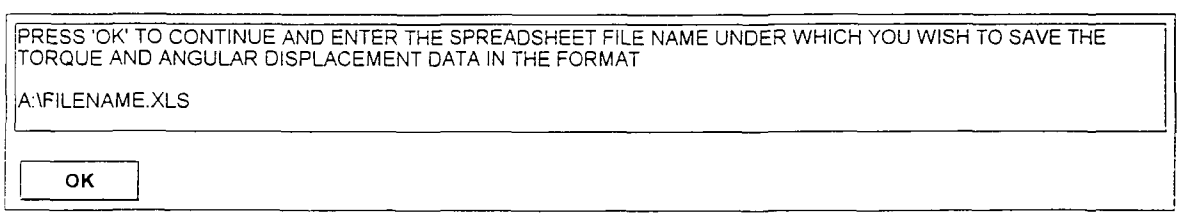

Block Diagram

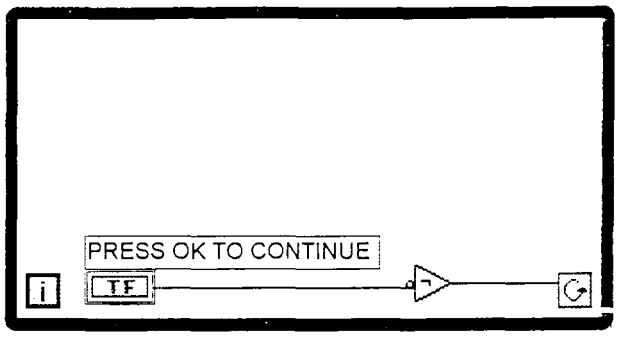

Connector Pane

Front Panel

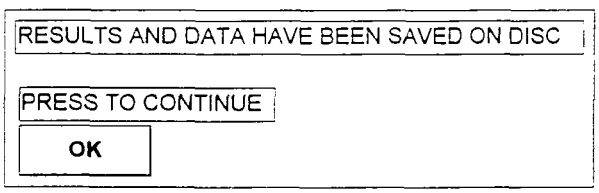

Block Diagram

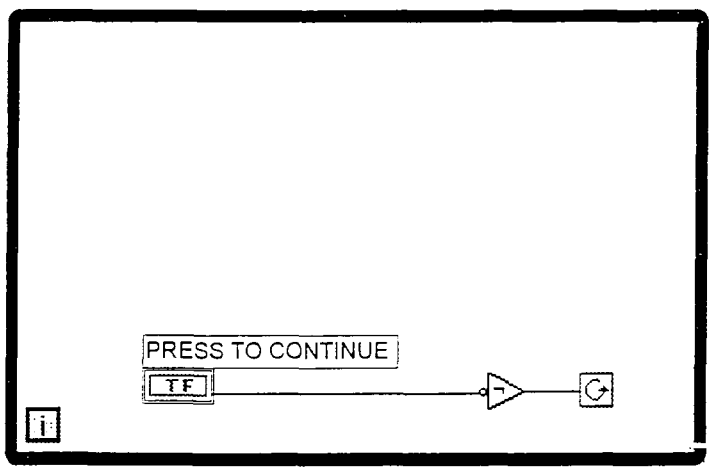

APPENDIX NINE

Pre-operative and post-operative questionnaires for the subjective assessment of the Durham metacarpo-phalangeal joint surface replacement prosthesis

A9.1 Pre-operative patient assessment questionnaire

Introduction

A new artificial joint is being designed at the University of Durham to replace finger joints badly affected by arthritis. We are interested in looking at arthritis from the patient's point of view, hence the following questionnaire will ask you about your arthritis and how it affects you and your daily activities. For those people who are going to have their finger joints replaced you will be asked to fill in a second questionnaire about a month after your operation to find out how your new joints are doing. We would like to thank you for your help with this project which is very much appreciated.

If you do not know the answer to a question, do not understand what a question is asking, do not wish to answer a question, or think that a question is not applicable then please leave the answer blank.

Section 1) Patient details

Surname
Initials
Hospital Number

Date and Time of Assessment
Dominant Hand Right / Left
Occupation/Hobbies

Section 2) About your arthritis

1) How long have you had arthritis in your hands or wrists? _____ Years

2) Please mark with crosses on Figure 1 which of your joints are affected by arthritis, and circle the joints that are affected the worst.

3) Do any of the following describe your hand/wrist joints? Please tick.

Unstable		Swollen		Weak	
Tender to touch		Stiff		Painful	
Reduced range of movement					

4) Do you experience morning stiffness in your hands/wrists? Yes / No
If yes, on average for how long after you get up in the morning? _____minutes

5) Please rate your finger joints over the past week for the following categories by marking the scales with a vertical line e.g.

Pain with resisted motion

Pain with non-resisted motion

Figure 1

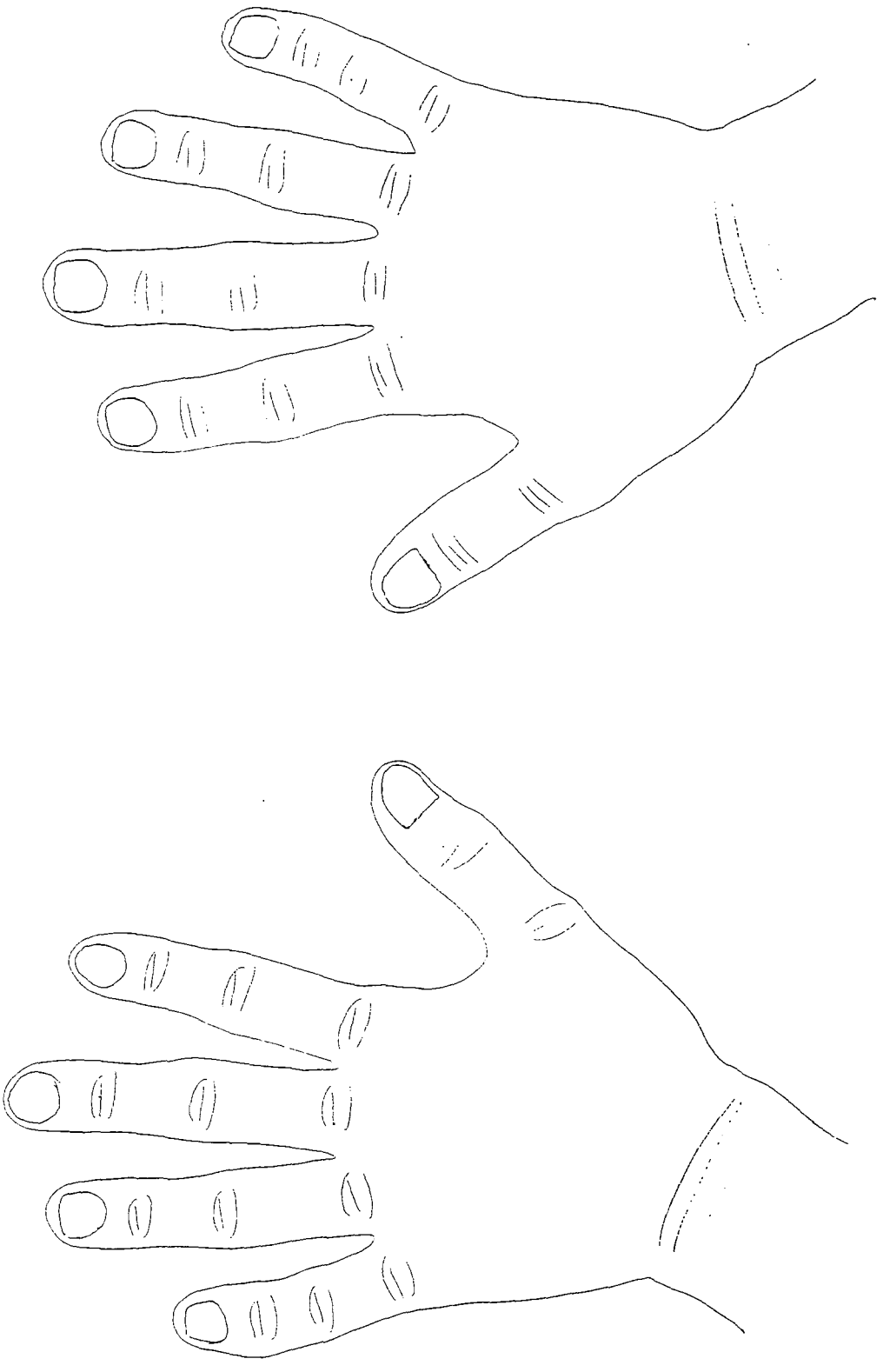

Joint stiffness

Section 3) Daily activities

On the following page there is a list of possible daily activities. Please rate how difficult the following have been for you to do over the past week without help from another person, and also indicate any specific reasons for the difficulty because of the condition of your hands. Please tick as many reasons as are applicable from the following lists. If you do not usually perform any of the activities then please state this but putting NA (not applicable) by the activity.

Difficulty	**Reasons for difficulty**
No difficulty in performing this activity	1 = weakness
Slight difficulty in performing this activity	2 = pain
Moderate difficulty in performing this activity	3 = lack of range of movement
Severe difficulty in performing this activity	4 = sensory problems
Impossible to do this activity	5 = other reasons

	Difficulty					Reasons				
	None	Slight	Mod.	Severe	Impos.	1	2	3	4	5
Dressing Activities										
Buttons										
Zips										
Shoelaces										
Socks/stockings/tights										
Shaving/make up										
Hygiene Activities										
Taps										
Washing/brushing hair										
Cleaning teeth										
Wash and dry body										
Eating and Cooking										
Using knife and fork										
Drinking from cup										
Opening cartons										
Lifting jug, teapot, kettle										
Pouring jug, teapot, kettle										
Unscrewing lids										
Using a tin-opener										
Preparing vegetable										
Housework										
Vacuuming										
Using a broom										
Hand washing										
Ironing										
Others										
Carrying bags/boxes										
Handling money										
Writing										
Sewing or knitting										
Using door key										
Driving										

THANK YOU FOR SPENDING THE TIME TO FILL IN THIS QUESTIONNAIRE

A9.2 Post-operative patient assessment questionnaire

Introduction

Before you had some of your finger joints replaced you may have been asked to complete a questionnaire on the severity and extent of your arthritis and how it affected daily activities. In order to assess the performance of your new finger joints we are asking you to complete this follow up questionnaire. Once again we thank you for your help with this project.

If you do not know the answer to a question, do not understand what a question is asking, do not wish to answer a question, or think that a question is not applicable then please the answer blank.

Section 1) Assessment of your joint condition

Surname
Initials
Hospital Number
Date and Time of Assessment

Please rate your finger joints from over the past week for the following categories by marking the scales with a vertical line e.g.

Pain with resisted motion

Pain with non-resisted motion

Joint stiffness

Section 2) Comparison of pre-operative and post-operative condition

Please rate the following categories comparing your replaced finger joints with your joints before they were replaced, by marking the scales with a vertical line e.g.

Joint pain

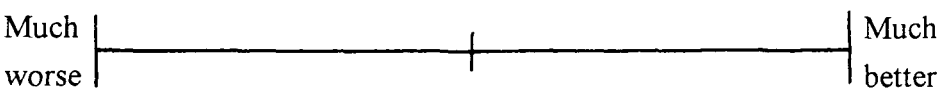

Joint stiffness

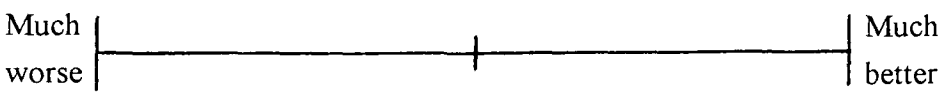

Range of movement

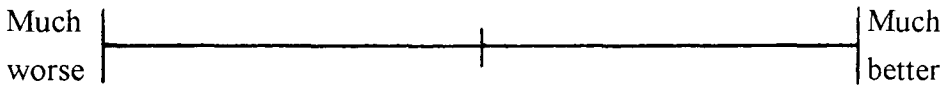

Overall hand function

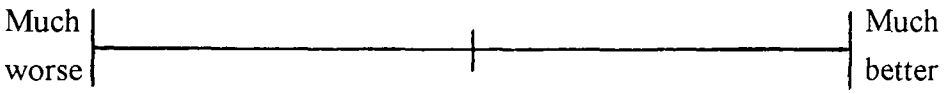

Appearance

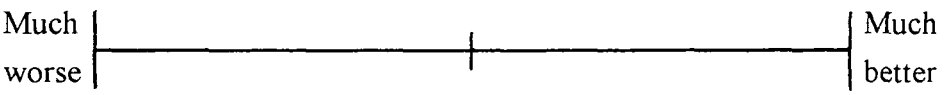

Overall hand strength

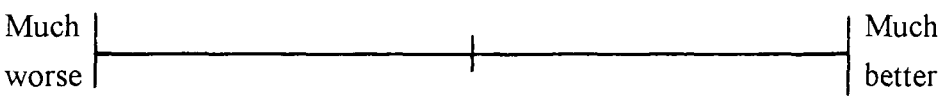

Section 3) Daily activities

On the following page there is a list of possible daily activities. Please rate how difficult the following are for you to do without help from another person, and also indicate any specific reason for the difficulty because of the condition of your hands from the following lists. Please tick as many reasons as are applicable. If you do not usually perform any of the activities then please state this but putting NA (not applicable) by the activity.

Difficulty	Reasons for difficulty
No difficulty in performing this activity	1 = weakness
Slight difficulty in performing this activity	2 = pain
Moderate difficulty in performing this activity	3 = lack of range of movement
Severe difficulty in performing this activity	4 = sensory problems
Impossible to do this activity	5 = other reasons

	Difficulty					Reasons				
	None	Slight	Mod.	Severe	Impos.	1	2	3	4	5
Dressing Activities										
Buttons										
Zips										
Shoelaces										
Socks/stockings/tights										
Shaving/make up										
Hygiene Activities										
Taps										
Washing/brushing hair										
Cleaning teeth										
Wash and dry body										
Eating and Cooking										
Using knife and fork										
Drinking from cup										
Opening cartons										
Lifting jug, teapot, kettle										
Pouring jug, teapot, kettle										
Unscrewing lids										
Using a tin-opener										
Preparing vegetable										
Housework										
Vacuuming										
Using a broom										
Hand washing										
Ironing										
Others										
Carrying bags/boxes										
Handling money										
Writing										
Sewing or knitting										
Using door key										
Driving										

THANK YOU FOR SPENDING THE TIME TO FILL IN THIS QUESTIONNAIRE

The wear of cross-linked polyethylene against itself

T J Joyce, BEng, MSc, **H E Ash,** BSc, MSc and **A Unsworth,** MSc, PhD, DEng, FIMechE
Centre for Biomedical Engineering, School of Engineering, University of Durham

Cross-linked polyethylene (XLPE) may have an application as a material for an all-plastic surface replacement finger joint. It is inexpensive, biocompatible and can be injection-moulded into the complex shapes that are found on the ends of the finger bones. Further, the cross-linking of polyethylene has significantly improved its mechanical properties. Therefore, the opportunity exists for an all-XLPE joint, and so the wear characteristics of XLPE sliding against itself have been investigated. Wear tests were carried out on both reciprocating pin-on-plate machines and a finger function simulator.

The reciprocating pin-on-plate machines had pins loaded at 10 N and 40 N. All pin-on-plate tests show wear factors from the plates very much greater than those of the pins. After 349 km of sliding, a mean wear factor of 0.46 × 10^{-6} mm^3/N m was found for the plates compared with 0.021 × 10^{-6} mm^3/N m for the pins. A fatigue mechanism may be causing this phenomenon of greater plate wear. Tests using the finger function simulator give an average wear rate of 0.22 × 10^{-6} mm^3/N m after 368 km. This sliding distance is equivalent to 12.5 years of use in vivo. *The wear factors found were comparable with those of ultra-high molecular weight polyethylene (UHMWPE) against a metallic counterface and, therefore, as the loads across the finger joint are much less than those across the knee or the hip, it is probable that an all-XLPE finger joint will be viable from a wear point of view.*

Key words: finger prosthesis, cross-linked polyethylene, wear

1 INTRODUCTION

Currently, the most popular finger prosthesis in use in the United Kingdom is the Swanson prosthesis. This prosthesis is a single piece of silicone rubber which acts as both a flexible hinge and a spacer, around which encapsulation occurs. Surgery is straightforward, pain relief is achieved and deformity corrected (**1**). Despite this success, the prosthesis has several disadvantages. Clinical deformity gradually returns after surgery (**1**), there are concerns over synovitis due to the silicone material (**2**), and the prostheses often snap (**1**, **3**). Such breakage is thought to be due to the prosthesis flexing at the stem rather than the hinge, in combination with lacerations on the surface of the prosthesis (**4**). These lacerations, which may be produced by bony spurs, become surface cracks which then propagate through the prosthesis under the cyclic loading of finger flexion–extension. Therefore, an improved design of finger prosthesis has been sought.

By moving from the principles of the flexing hinge encompassed by the Swanson prosthesis, to the concept of a surface replacement joint in which the two separate surfaces slide over one another, several benefits can be achieved. The original joint dynamics can be restored, the ligaments which stabilize the joint can be maintained and, being two pieces, the prosthesis cannot snap. Instead wear between the articulating surfaces becomes of concern.

The metal/polymer combination widely used in knee and hip prostheses has also been applied to finger prostheses, but with varying degrees of success (**5**). As an alternative arrangement, as the loads across the finger joint are relatively low, a two-piece, all-polymer prosthesis has been considered. A polymeric prosthesis has the additional advantage of having material properties closer to those of rheumatoid bones than either metal or ceramic would have. Also, should it be necessary, such a prosthesis could be modified in theatre to suit the individual patient by simply trimming away small amounts of material from the edge (being careful not to damage the articular surface).

Polyethylene, in the form of UHMWPE, is the most widely used polymeric prosthetic material in a sliding joint. Ultra-high molecular weight polyethylene has been tested against itself on pin-on-plate rigs, but a combination of adhesive, abrasive and fatigue wear was found to occur leading to a large amount of polyethylene debris production, together with wear factors of the order of 2 × 10^{-5} mm^3/N m for the pins (**6**, **7**). Indeed, the wear factors were found to increase with the applied load. Polyethylene wear debris is to be avoided in the body as it can become deposited in surrounding tissues (**8**), leading to inflammation and bone resorption (**9**), and causing eventual loosening of the prosthesis, possibly with associated pain for the patient (**10**). Such high wear rates make an all-UHMWPE finger prosthesis unacceptable.

However, the cross-linking of polyethylene has improved the material's mechanical properties. Cross-linking has the additional advantage of permitting a lower molecular weight base material to be used, so that components can be injection-moulded rather than machined. Injection-moulding offers the opportunity of mass-producing complex three-dimensional shapes, such as those found on the end of the finger bones, to repeatable, close tolerances. Cross-linked polyethylene has been used in experimental hip implants for several years and has shown no adverse biological reaction (M. Wroblewski, 1995, personal communication). Therefore, in view of this blend of biocompatibility, low cost, ease of manufacture and appropriate mechanical properties, XLPE has been considered as a potential material for use as a surface replacement prosthesis for the finger joints, and its wear properties have been investigated and are reported here.

Cross-linked polyethylene pins and plates together with a prototype XLPE surface replacement metacarpophalangeal (MCP) prosthesis were tested. A prototype

This paper was presented at the Leeds Annual Day Conference on 'Biomechanics of upper limb joints and their replacements' held in Leeds on 6 January 1995. The MS was received on 6 February 1995 and was accepted for publication on 12 October 1995.

H00595 © IMechE 1996

Fig. 1 Swanson prosthesis and Durham prosthesis

Durham prosthesis, with a Swanson for comparison, is shown in Fig. 1. The XLPE test samples were manufactured from powdered polyethylene which was mixed with liquid silane. This mixture was then extrusion injection-moulded. The cross-linking process between the polyethylene molecules occurred by placing the samples in a steam autoclave. Finally, the samples were sterilized by irradiation. The degree of cross-linking was measured from a number of sacrificial samples by boiling away in xylene the non-cross-linked material. Therefore, the weight of the material remaining after this process, divided by the original weight, gave the percentage of cross-linking. The percentage of cross-linking measured in all sacrificial samples was identical in each case to within measurement error of 2 per cent.

2 APPARATUS AND METHOD

2.1 Finger function simulator

The finger function simulator has been described elsewhere and shown to be a device which effectively simulates the loads and motions encountered by a finger prosthesis *in vivo* (**11**). The simulator flexed a test XLPE prosthesis cyclically over a 90° range of motion to represent the light loading found during normal flexion–extension. It then applied a heavy static load to imitate pinch grip. Motion was uni-planar as flexion–extension is the predominant action of the finger. The light loading simulated those situations where loads were small (10–15 N) (**12**) but the finger was moving quickly. In contrast, situations such as turning a key or holding a handle show minimal motion but large joint forces. These situations are therefore mimicked by the pinch grip action of the simulator, which occurred once every 30 min. During this part of the cycle, the compressive force across the test prosthesis was increased to 100 N, and held at this level for 45 s. During light loading, the simulator ran at 112 r/min, equivalent to a sliding speed of 0.055 m/s, at an excursion of 14.7 mm. The test prosthesis was immersed in a bath containing distilled water at a temperature of 37 °C. A control XLPE prosthesis was also included to take account of any lubricant absorption. At regular intervals, the simulator was stopped and the XLPE prosthetic components, both test and control, were cleaned and weighed. Two tests were undertaken. The first test used prostheses which had a low percentage of cross-linking, the metacarpal component being 36 per cent cross-linked and the phalangeal component 66 per cent cross-linked. The second test used prostheses made with a high percentage of cross-linking, 87 per cent. The new XLPE finger prosthesis is designed to have conforming spherical surfaces, and all test prostheses had articulating surfaces of radius 9.5 mm, giving a nominal stress value of 0.08 MPa during flexion–extension.

2.2 Pin-on-plate test rig

Pin-on-plate machines are widely used as screening devices in wear studies (**13**, **14**). The pin-on-plate machine employed a reciprocating motion which mimicked the natural flexion–extension of the finger. Load, speed and stroke could all be varied as appropriate. The rig consisted of a sledge reciprocating along two fixed parallel bars. On this sledge was positioned a heated bed and a stainless steel bath. The sledge was driven by a 125 W d.c. shunt motor. Motor speed was controlled using a variable voltage supply and the stroke could be altered by adjusting the crank radius of the drive shaft. Heating of the distilled water, which acted as a lubricant, was provided by resistors positioned within the heated bed. These resistors, together with a thermocouple, were connected to a controller which maintained the lubricant at a constant, pre-set temperature of 37 °C. Four XLPE test plates were located in the stainless steel bath using a plastic frame into which suitable location slots had been milled. Each XLPE test pin was held within a holder and in turn each holder fitted within a machined arm. Each pin was notched at its upper end to provide good location and hence to prevent rotation. It also ensured that the pin was replaced in its original position after removal for weighing. On the top of each holder rested a cantilevered bar to which weights were added to provide an applied load. An automatic lubricant level controller was fitted, such that the fluid was maintained between pre-set maximum and minimum levels which prevented the rig from operating without any lubricant. Finally, an electronic counter was connected to the sledge and a glass cover fitted to minimize any contamination from the atmosphere.

Prior to the commencement of a test, the XLPE test plates and XLPE pins were carefully weighed, and the roughness of the plates measured using a Taylor Hobson Talysurf 4. In each test, an XLPE control pin was included to take account of any lubricant absorption. This pin was unloaded and kept with its unnotched end in the same distilled water as the test pins at 37 °C. At regular intervals, the test was stopped, all of

© IMechE 1996

the pins and plates were removed, cleaned with acetone, weighed, visually inspected and the roughness of the wear track on each of the test plates was measured. Pins and plates were weighed to the nearest 0.1 mg using a Mettler AE200 balance. Wear of the test pin was defined as the weight loss with respect to the initial weight, to which was added any weight gain of the control pin. Therefore, the weight gain of the control and test pins was assumed to be equal. The wear factors (k, units mm^3/N m) were calculated from the equation

$$k = \frac{V}{LD}$$

where

V = volume lost (mm^3)
L = load (N)
D = sliding distance (m)

but volume = mass/density, therefore

$$k = m/\rho LD \qquad \rho \text{ (XLPE)} = 949 \text{ kg/m}^3$$

Three pin-on-plate tests, each exceeding 300 km, were undertaken. All used XLPE with 86 per cent cross-linking after irradiation as material for pins and plates. Loads of 10 N and 40 N were employed. The 10 N load provided a 'normal' load for the MCP joint during motion, while the 40 N supplied a greater load to give a factor of safety and to provide the opportunity of discovering whether wear factors changed with load. The pins were turned to form flat-ended, circular cylinders, 20 mm long and of diameter 4 and 5 mm. The pin-on-plate machine employed a stroke of 20 mm and velocities of 0.037 m/s and 0.035 m/s. Test 3 employed a longer stroke to give a greater velocity (see Table 1).

3 RESULTS

3.1 Finger function simulator

Two tests were conducted, using prostheses with different percentages of cross-linking, and the results are shown in Fig. 2. As can be seen, the degree of cross-linking has a significant effect on the wear of XLPE. After 190 km, the prostheses with a low percentage of cross-linking had wear factors of 6.0×10^{-6} mm^3/N m for the metacarpal and 2.2×10^{-6} mm^3/N m for the phalangeal component. In contrast, after 368 km the prostheses with a high (87) percentage of cross-linking had wear factors of 0.25×10^{-6} mm^3/N m for the metacarpal and 0.16×10^{-6} mm^3/N m for the phalangeal component.

3.2 Pin-on-plate machine

Each of the XLPE tests summarized in Table 1 revealed similar characteristics, therefore test 1 has been reported

Table 1 Summary of XLPE pin-on-plate wear factors

Test number	1		2		3
Load (N)	10	40	10	40	40
Stress (MPa)	0.51	2.04	0.80	3.18	2.04
Pin diameter (mm)	5	5	4	4	5
Number of pins	2	2	2	2	2
Distance (km)	349	349	359	359	332
Cycles ($\times 10^6$)	8.73	8.73	8.98	8.98	4.88
Average velocity (mm/s)	35.3	35.3	37.3	37.3	47.6
Mean k plate ($\times 10^{-6}$ mm^3/N m)	0.50	0.42	0.68	0.48	0.58
Mean k pin ($\times 10^{-6}$ mm^3/N m)	0.030	0.012	0.014	0.014	0.065

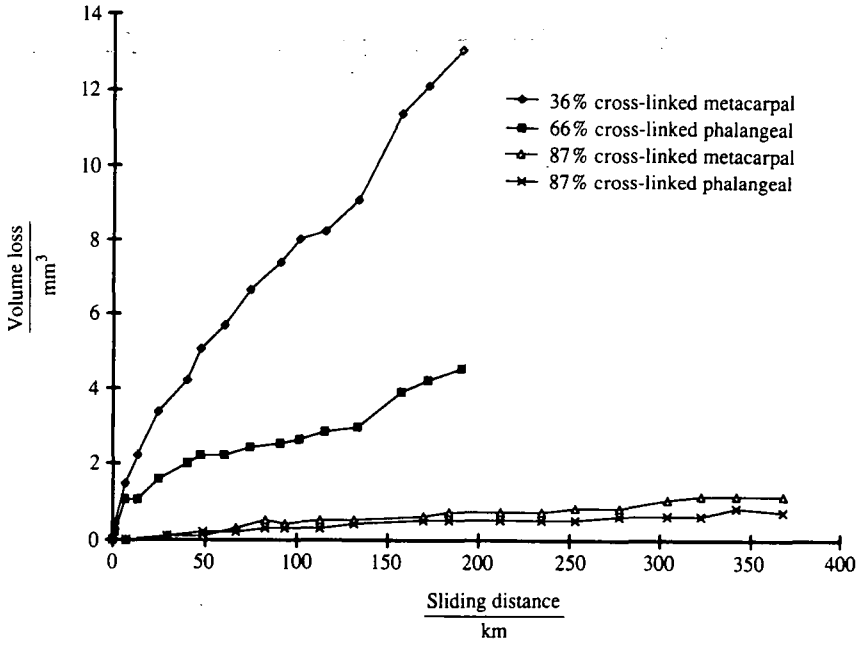

Fig. 2 Wear of metacarpal and phalangeal components in the finger function simulator

© IMechE 1996

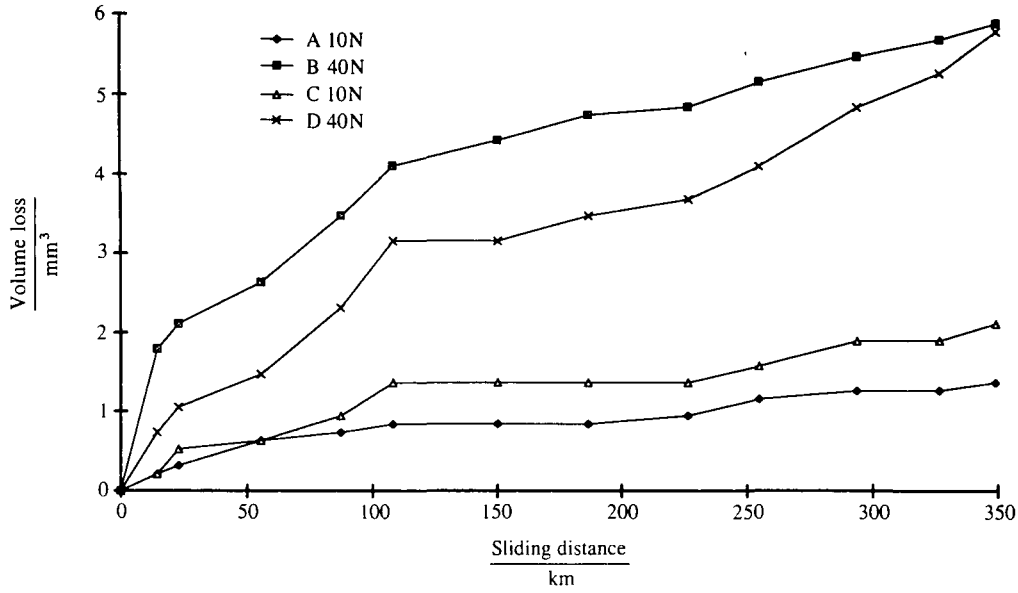

Fig. 3 Wear of XLPE plates loaded at 10 N and 40 N in the reciprocating pin-on-plate machine

in detail as this was illustrative of all three tests. Figure 3 shows XLPE plate wear at 10 N and 40 N from test 1. From this figure it can be seen that XLPE plate wear is related to load, as expected. There is an initial bedding-in period, after which the slope of the wear curve becomes relatively constant with increased sliding distance. Figure 4 shows a graph of the wear of corresponding XLPE pins and plates under 40 N loads. The XLPE test pins show virtually no wear. For reference, the XLPE control pin of test 1 showed no fluid absorption after 349 km. The roughness values of the wear tracks on the XLPE plates were measured throughout the test, and are shown in Fig. 5. The longitudinal values, in the direction of sliding, fell rapidly from a mean of 1.5 μm *Ra* to 0.05 μm *Ra* in the 40 N case. Transverse roughness values also fell from a similar start value to around 0.6 μm *Ra*.

4 DISCUSSION

Figure 2 clearly indicates the decrease in wear found with an increase in the percentage of cross-linking. That the metacarpal components showed higher wear factors than those of their respective phalangeal components can be explained by their geometrical differences, as it is known that convex surfaces tend to wear more than concave surfaces. Additionally, the XLPE prostheses have a wear curve which has a constant gradient, indicating that a period of fatigue wear seems not to have occurred. This conclusion is supported by visual inspection which revealed neither pitting nor delamination.

If a normal MCP joint is considered to perform one million cycles per year, then the 368 km (or 12.5 million cycles) achieved from the second test in the finger function simulator is equivalent to 12.5 years. At this point, the XLPE prostheses with a high percentage of cross-linking showed no cuts, no fractures and low wear. Further, the wear factors were calculated to be 0.25×10^{-6} mm³/N m for the metacarpal and 0.16×10^{-6} mm³/N m for the phalangeal component. These values correspond to wear volumes of 1.16 mm³ and 0.74 mm³ respectively. In turn, this total wear volume of 1.9 mm³ can be interpreted as a wear rate of 0.15 mm³ per million cycles, or per annum. Dowson (**14**) states that, for an artificial hip joint, a wear rate of 38 mm³ per annum is considered acceptable. However, a hip joint of radius 20 mm will have a capsule volume 23 times greater than that of a finger joint of radius

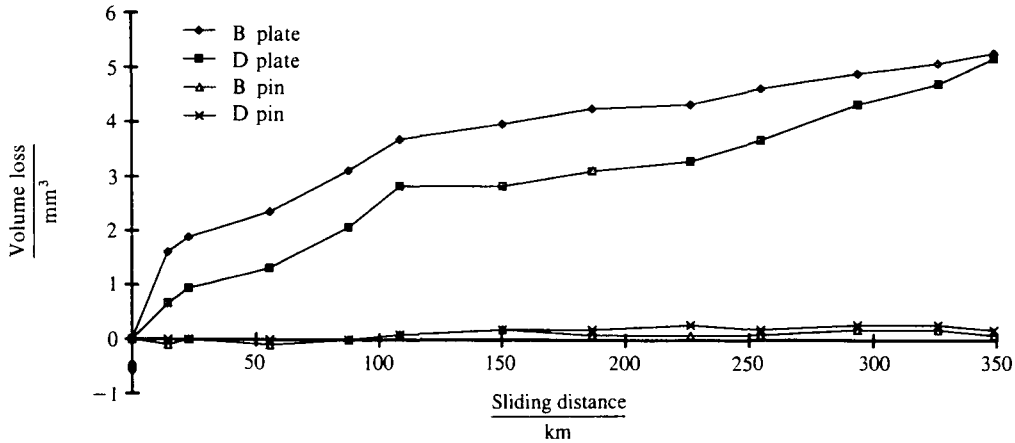

Fig. 4 Wear of XLPE pins and corresponding XLPE plates loaded at 40 N in the reciprocating pin-on-plate machine

© IMechE 1996

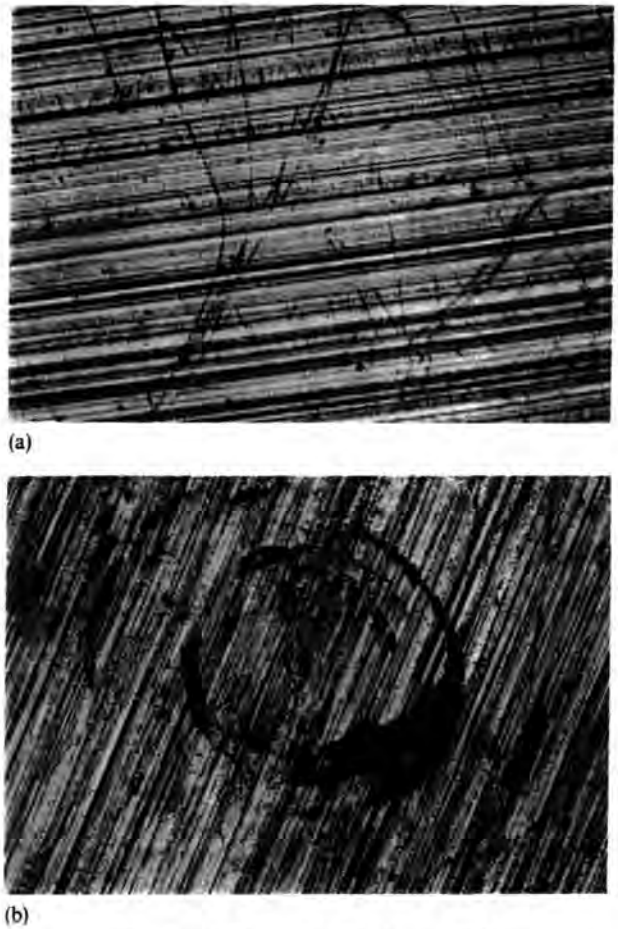

Fig. 5 (a) Plate after 350 km at 40 N
(b) Pin after 350 km at 40 N

7 mm. Therefore, for a finger joint, a wear rate of 1.65 mm^3 per annum should be acceptable. Consequently, the 0.15 mm^3 wear rate per million cycles reported here suggests that an all-XLPE finger prosthesis will be acceptable from a wear point of view.

Regarding the XLPE pin-on-plate tests, it should be asked why so little pin wear occurred compared with plate wear. The XLPE material used in each test was identical, originating from the same moulding. The pins were constantly loaded whereas the individual parts of the wear track on the plates undergo a cyclic load. Therefore, it is possible that there may be a fatigue element—but not in a gross sense of delamination or pitting (as is sometimes seen in the tibial components of knee prostheses for example) which is associated with a sudden increase in the amount of wear. It should also be noted that this is the first time that plate wear from an all-XLPE pin-on-plate test has been measured (**15**). Additionally, the plate wear of UHMWPE in a UHMWPE against UHMWPE pin-on-plate test has not been measured in previous studies (**6**, **7**). Atkinson (**7**) assumed that during such a UHMWPE test, plate wear equalled pin wear. The results reported here show this assumption to be incorrect for XLPE pins and plates. Indeed, a mean wear factor of 12×10^{-9} mm^3/N m for the XLPE pins under 40 N load was found from test 1. This value approaches that of UHMWPE pins against ceramic plates (**13**). Although significant differences in wear factors between XLPE pins and XLPE plates were measured, the XLPE plate wear factors were still of the order of those of the high percentage cross-linked prostheses. Further, pin-on-plate results allow comparison with other material combinations (**13**, **14**, **16**).

With both XLPE pins and XLPE plates, the dominant feature of the wearing surfaces was parallel grooves in the direction of sliding (Fig. 5) giving the appearance of abrasive wear. Once this surface finish was achieved, there was very little change (Fig. 6). The constant values of roughness which were measured imply no evidence of a transfer film. It has been suggested that serum would be a more appropriate medium in which to run pin-on-plate tests involving potential biomaterials (**17**). The reason being that, unlike distilled water, serum prevents the formation of a transfer film between UHMWPE and stainless steel and a transfer film is not found *in vivo*. Cooper *et al.* (**17**) indicated the presence of a transfer film by increased plate roughness at the cessation of a test. However, the XLPE pin-on-plate results reported here show no increase in the surface roughness of the plates and therefore indicate no evidence of a transfer film. Further, tests employing distilled water permit a fuller comparison with other

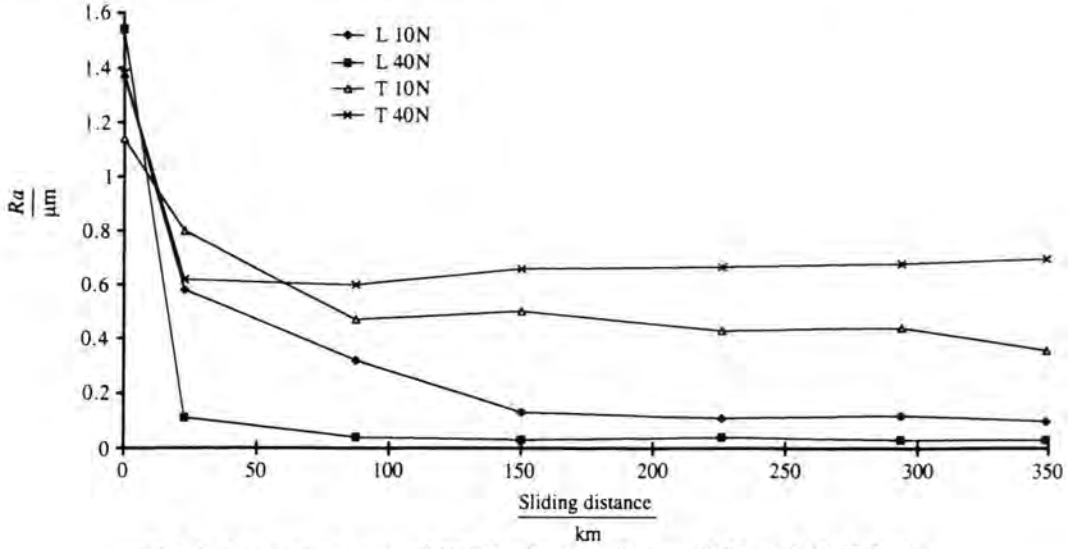

Fig. 6 Mean roughness of XLPE plates loaded at 10 N and 40 N in the transverse (T) and longitudinal (L) directions

© IMechE 1996

researchers (**13**, **14**, **16**). Visual inspection of XLPE pins and plates revealed little evidence of adhesive or fatigue wear. In the case of the XLPE pin shown in Fig. 5, the original concentric machining marks are still visible, indicating that the pins have experienced little wear, even after 349 km. There appears to be little correlation between roughness and wear, except perhaps in the initial stages.

If a comparison of wear factors is made between XLPE against itself, and UHMWPE against a metallic counterface, then a similarity is seen. Cooper *et al.* (**16**), also employing reciprocating rigs, de-ionized water and a test distance of 350 km (as was the case in this study), obtained wear factors from 0.18 to 1.3×10^{-6} mm^3/N m for UHMWPE pins rubbing against a metallic counterface. However, Saikko (**13**) obtained a wear factor of 0.1×10^{-6} mm^3/N m for UHMWPE pins rubbing against Co–Cr–Mo plates. These values compare with 0.42 to 0.68×10^{-6} mm^3/N m for XLPE plates from the reciprocating tests found in this study. Further, if coefficients of friction are considered, similarity is again seen. Tests using reciprocating pin-on-plate rigs gave a coefficient of friction of 0.14 for XLPE against itself (**15**). This value compares with a figure of 0.10 for UHMWPE against Co–Cr–Mo (**13**).

5 CONCLUSIONS

Wear factors of XLPE rubbing against itself have been found to be comparable with those of UHMWPE rubbing against a metallic counterface. Additionally, the coefficient of friction of XLPE against itself has been measured to be similar to that of UHMWPE against Co–Cr–Mo. Therefore, as the loads across the finger joints are so much smaller than those across the knee or the hip, and the total wear volume is directly proportional to load, it is felt that an all-XLPE finger prosthesis will be viable from a wear point of view.

ACKNOWLEDGEMENTS

The authors would like to thank Action Research (grant reference A/F/0475) for providing financial support. DePuy International Limited supplied the XLPE material and moulded the XLPE prostheses.

REFERENCES

1 **Blair, W. F., Shurr, D. G.** and **Backwalter, J. A.** Metacarpophalangeal joint implant arthroplasty with a silastic spacer. *J. Bone Jt Surg.*, 1984, **66A**, 365–370.
2 **Khoo, C. T. K.** Silicone synovitis. *J. Hand Surg.*, 1993, **18B**, 679–686.
3 **Beckenbaugh, R. D., Dobyns, J. H., Linscheid, R. L.** and **Bryan, R. S.** Review and analysis of silicone rubber metacarpophalangeal implants. *J. Bone Jt Surg.*, 1976, **58A**, 483–487.
4 **Swanson, A. B.** and **de Groot Swanson, G.** Flexible implant arthroplasty in the rheumatoid metacarpophalangeal joint. *Clin. Rheum. Dis.*, 1984, **10**(3), 609–629.
5 **Beevers, D. J.** and **Seedhom, B. B.** Metacarpophalangeal joint prostheses. a review of past and current designs. *Proc. Instn Mech. Engrs, Part H*, 1993, **207**(H4), 195–206.
6 **Stokoe, S. M.** A finger function simulator and surface replacement prosthesis for the metacarpophalangeal joint. PhD thesis, University of Durham, 1990.
7 **Atkinson, J. R.** An investigation into the wear of ultra-high molecular weight polyethylene when a polyethylene wear pin is loaded against a reciprocating polyethylene counterface lubricated by bovine synovial fluid at ambient temperature. Report, Department of Metallurgy, Leeds University, 1976, pp. 1–12.
8 **Malcolm, A. J.** Pathology of longstanding cemented total hip replacements in Charnley's cases. *J. Bone Jt Surg.*, 1988, **70B**, 153.
9 **Howie, D. W., Vernon-Roberts, B., Oakeshott, R.** and **Manthey, B.** A rat model of resorption of bone at the cement–bone interface in the presence of polyethylene wear particles. *J. Bone Jt Surg.*, 1988, **70A**, 257–263.
10 **Mirra, J. M., Marder, R. A.** and **Amstutz, H. C.** The pathology of failed total joint arthroplasty. *Clin. Orthop. Rel. Res.*, 1982, **170**, 175–183.
11 **Stokoe, S. M., Unsworth, A., Viva, C.** and **Haslock, I.** A finger function simulator and the laboratory testing of joint replacements. *Proc. Instn Mech. Engrs, Part H*, 1990, **204**(H4), 233–240.
12 **Tamai, K., Ryu, J., An, K. N., Linscheid, R. L., Cooney, W. P.** and **Chao, Y. S.** Three-dimensional geometric analysis of the metacarpophalangeal joint. *J. Hand Surg.*, 1988, **13A**, 521–529.
13 **Saikko, V.** Wear and friction properties of joint materials evaluated on a reciprocating pin-on-plate apparatus. *Wear*, 1993, **166**, 169–178.
14 **Dowson, D.** A comparative study of the performance of metallic and ceramic femoral head components in total replacement hip joints. Proceedings of *Austrib '94*, pp. 59–73.
15 **Sibly, T. F.** and **Unsworth, A.** Wear of cross-linked polyethylene against itself: a material suitable for surface replacement of the finger joint. *J. Biomed. Engng*, 1991, **13**, 217–220.
16 **Cooper, J. R., Dowson, D.** and **Fisher, J.** Macroscopic and microscopic wear mechanisms in ultra-high molecular weight polyethylene. *Wear*, 1993, **162–164**, 378–384.
17 **Cooper, J. R., Dowson, D,** and **Fisher, J.** The effect of transfer film and surface roughness on the wear of lubricated ultra-high molecular weight polyethylene. *Clin. Mater.*, 1993, **14**, 295–302.

© IMechE 1996

Proximal interphalangeal joint dimensions for the design of a surface replacement prosthesis

H E Ash, BSc, MSc and **A Unsworth**, BSc, MSc, PhD, DEng, CEng, FIMechE
School of Engineering, University of Durham

The bones from 83 proximal interphalangeal joints (PIPJs) were dissected in order to determine the shape and size of the articular surfaces. The bones were modelled in acrylic dental bone cement and the original bones and replicas were then sectioned and shadowgraphed. Dimensions were taken from these shadowgraphs to be used in the design of a surface replacement prosthesis for the PIPJ.

It was found that the bi-condylar heads of the proximal and middle phalanges were circular in the sagittal plane as was the base of the middle phalanx. However, the radius of curvature of the middle phalangeal base was greater than that of the proximal phalangeal head indicating that the PIPJ is not a conforming joint. The alignment of the radial and ulnar condyles of the proximal phalangeal bones was investigated and it was found that the index and middle finger bones tended to have a more prominent ulnar condyle while the ring and little finger bones tended to have a more prominent radial condyle. This was due to a slight difference in diameters of the two condyles.

The proximal phalangeal bone lengths L ranged from 29–52 mm, maximum head widths W from 8.5–15.5 mm and maximum diameters D of the best-fit circles to the sagittal profile of the bone head from 6–11 mm. The middle phalangeal bone lengths ranged from 16–35 mm, maximum head widths from 8.5–12 mm and maximum diameters from 5–7.5 mm. The relationships and ratios between these dimensions for the proximal and middle phalanges have been calculated.

Key words: dimensions, proximal interphalangeal joint, surface replacement prosthesis

NOTATION

DIPJ	distal interphalangeal joint
DP	distal phalanx
EDC	extensor digitorum communis
FDP	flexor digitorum profundus
FDS	flexor digitorum sublimis
I	index finger
IPJ	interphalangeal joint
L	left hand, lumbricals
M	middle finger
MC	metacarpal
MCPJ	metacarpophalangeal joint
MP	middle phalanx
PIPJ	proximal interphalangeal joint
PP	proximal phalanx
R	right hand, ring finger

1 INTRODUCTION

The most commonly used proximal interphalangeal joint (PIPJ) prosthesis is the Swanson joint although it produces no significant increase in hand strength post-operatively. Prosthetic fracture has occurred as has the recurrence of deformity (**1–3**). The total resection of the joint also requires the removal or repositioning of the collateral ligaments which can result in joint instability. However, there is no suitable alternative at the moment other than arthrodesis. As with the Swanson prosthesis, many of the previous designs of PIPJ prostheses tend to be smaller versions of those designed for the metacarpophalangeal joint (MCPJ) despite the differences in joint architecture and planes of motion. Hence there is a need to relook at the PIPJ and that is why a surface replacement prosthesis is being designed at the University of Durham.

The MS was received on 17 November 1995 and was accepted for publication on 6 March 1996.

There is inadequate information in the literature on the dimensions of the articular cartilage surfaces and the bones of the PIPJ to create a surface replacement prosthesis to match the shape of the original joints. Hence work was carried out to determine dimensions of the PIPJs. This paper reports the dimensions taken from shadowgraphs of the sectioned PIPJ bones and the relationships between the major bone dimensions. It also gives a brief introduction to the Durham PIPJ surface replacement prosthesis designed directly using these dimensions.

2 ANATOMY AND BIOMECHANICS OF THE PIPJ

The PIPJ is a bi-condylar hinge joint with one degree of freedom allowing active movement in flexion and extension only. However, a small amount of passive rotation, abduction–adduction and gliding is allowed during flexion–extension. The PIPJ consists of the convex head of the proximal phalanx and the concave base of the middle phalanx. The ends of the proximal and middle phalanges are covered in articular cartilage forming the bearing surfaces, which are broader anteriorly than posteriorly (Fig. 1).

The soft tissues surrounding the joint consist of a fibrous joint capsule, two collateral ligaments, a palmar ligament, a volar plate and flexor and extensor tendons. The joint has no muscular support in abduction–adduction and hence relies on the fibrous capsule and collateral ligaments for lateral stability. When a Swanson prosthesis is implanted, the bone ends are resected and the collateral ligaments are frequently lost or reattached in a different position. Whichever technique is used, this can result in a lack of lateral joint stability.

Proximal interphalangeal joint flexion is achieved by the flexor digitorum profundus (FDP) and the flexor digitorum superficialis (FDS). Extension is produced by the extensor digitorum communis (EDC). These are

H05795 © IMechE 1996

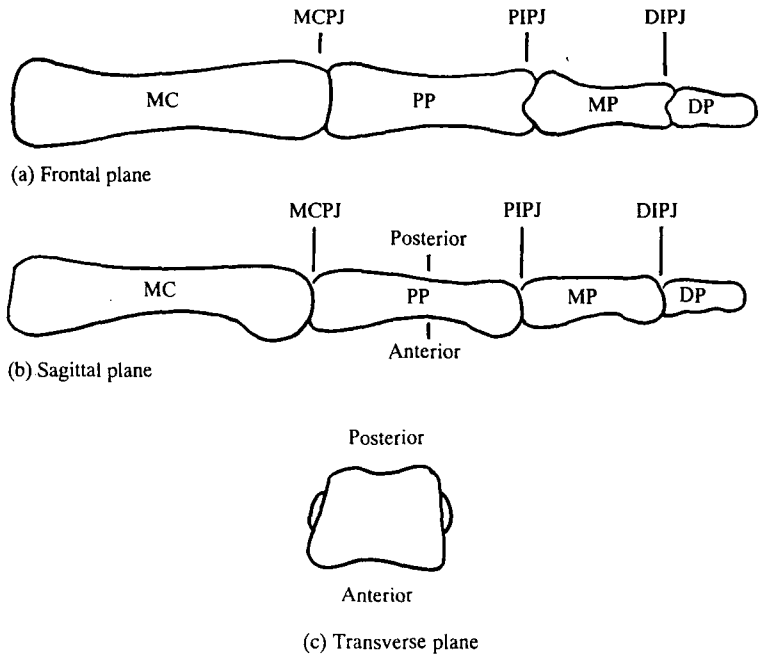

Fig. 1 Anatomy of the PIPJ bones

extrinsic muscles. The intrinsic interossei and lumbrical muscles also produce extension due to their attachments to the EDC (Fig. 2). The range of flexion has been reported as 115°, and hyperextension is limited by the tension of the digital flexors and palmar ligament. This is reported as 5° (**4**).

3 METHOD

Eighty-three PIPJs were dissected leaving the articular cartilage intact. The 83 joints came from 21 hands of 11 cadavers (7 males and 4 females) whose average age was 68.27 years (range of 55–81 years). The joints were preserved in formalin but it was thought that the dimensions of the cartilage and bones would not have been altered significantly by preservation. The individual details are shown in Table 1.

Silcoset rubber moulds were made of the bones and replica bones were then made from these moulds using acrylic dental bone cement. The replica bones were sectioned in the sagittal plane after being set in clear

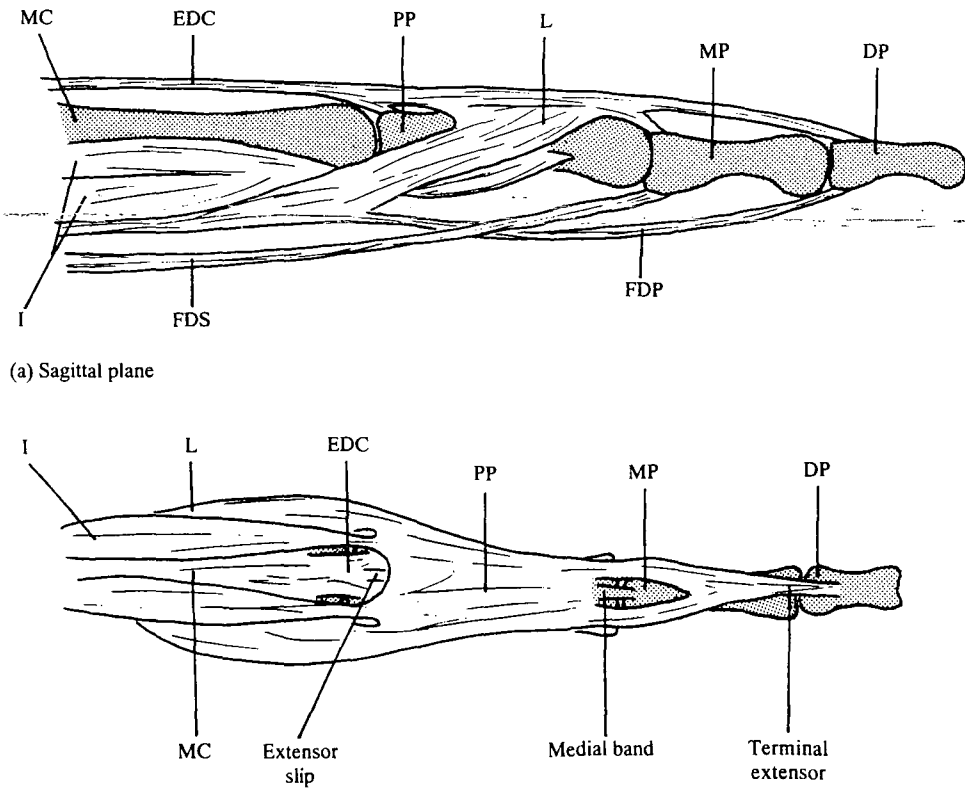

Fig. 2 Muscles and tendons of the fingers

© IMechE 1996

Table 1 Proximal interphalangeal joint specimen details

Cadaver	1	3	4	5	6	7	8	9	10	11	12
Sex	M	M	M	M	M	F	F	M	M	F	F
Age (years)	55	59	59	65	78	65	80	81	55	79	75

plastic so that the sections could be re-aligned correctly. The original bones were shadowgraphed in the frontal and sagittal planes along with the sagittal sections of the replica bones. The original bones were also rotated in the frontal plane to shadowgraph the profile of the articular cartilage around the bearing surface (Fig. 3).

The dimensions measured from the shadowgraphs are shown in Figs 4 and 5. The bone length L, the maximum bone head width in the frontal plane W and the maximum best-fit diameter of the sagittal profile of the bone head D were measured for the proximal and middle phalanges. The maximum base width in the frontal plane W_b was measured for the middle phalanx. The maximum and minimum condyle diameters of the articular cartilage from the sagittal sections were also measured for the middle phalangeal base, and the minimum best-fit diameter to the sagittal sections of the proximal and middle phalangeal heads.

The minimum thicknesses and widths (T_p, W_p, T_m and W_m) were measured for an indication of the size of stem required for fixation of a prosthesis within the medullary canal, although sectioning of the bones was required to measure the actual dimensions of the canal. The distance L_6 to a thickness of 6 mm T_6 and the depth of recess L_r were also measured on the middle phalangeal bones to be used in the design of the surface replacement joint.

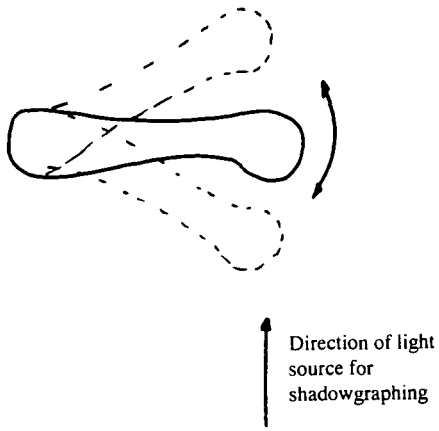

Fig. 3 Rotation of bones about the frontal plane for shadowgraphing of the articular surfaces of the proximal phalangeal head

4 RESULTS

4.1 Proximal phalangeal head shape

The shadowgraphs of the intact bones and replica sections showed that the proximal phalangeal head has a circular profile in the sagittal plane varying across its width. Best fit circles could be superimposed on the outlines of the shadowgraphs to find the diameters of the circular profiles. Shadowgraphs of the articular surfaces were taken by rotating the bone about the frontal planes to 45°, 22.5°, 0°, −22.5°, and −45° (Fig. 6).

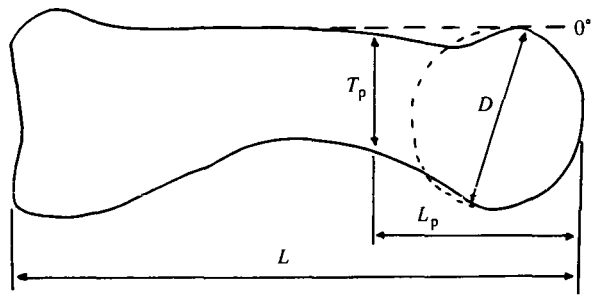

(a) Sagittal plane

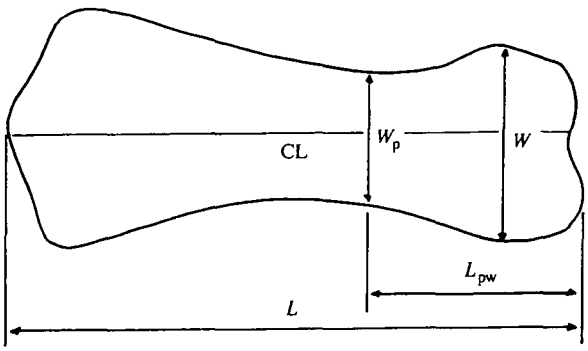

(b) Frontal plane

Fig. 4 Proximal phalangeal dimensions

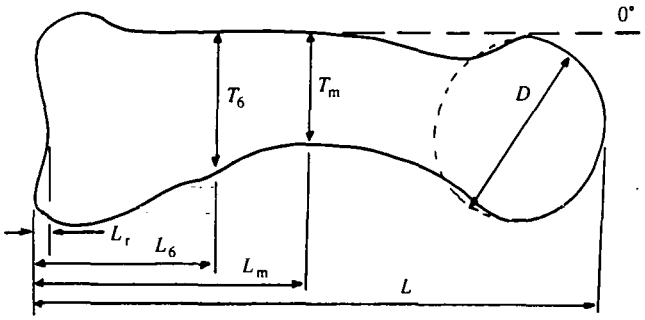

(a) Sagittal plane

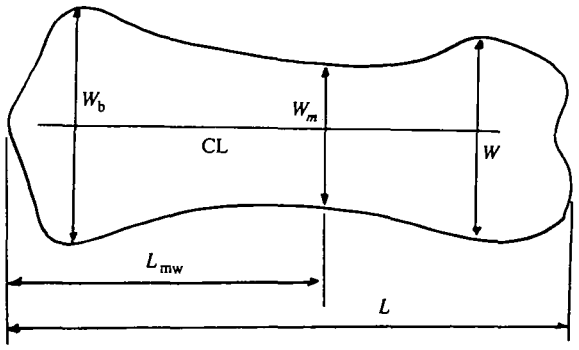

(b) Frontal plane

Fig. 5 Middle phalangeal dimensions

© IMechE 1996

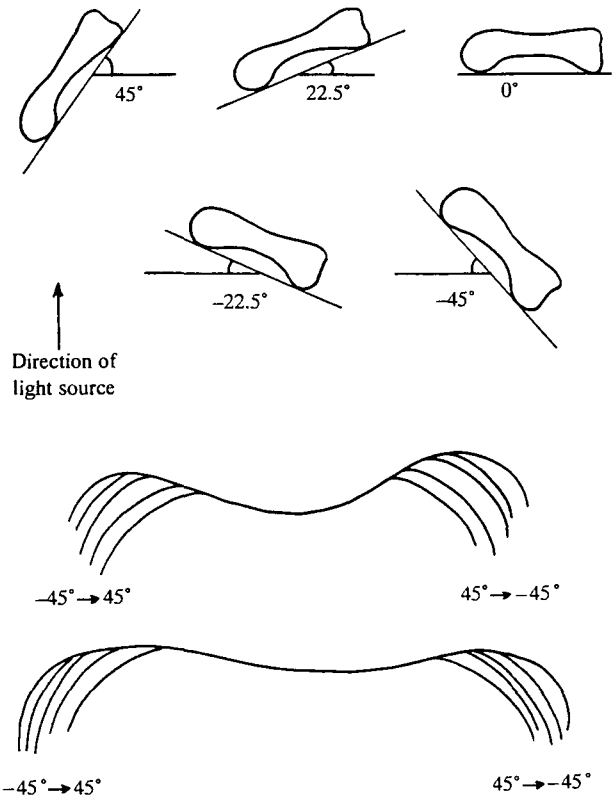

Fig. 6 Angles of rotation of bones for shadowgraphing in the frontal plane, with examples of the resultant superimposed shadowgraphs

These shadowgraphs were then superimposed on one another showing that the profile of the articular surface was constant around the bearing surface although broader at −45° than at 45°. Hence it can be concluded that the proximal phalangeal head consists of two sagittally circular condyles merged together forming a bicondylar articular surface, broader anteriorly than posteriorly (Fig. 7). The two condyles are not identical although they are of similar size.

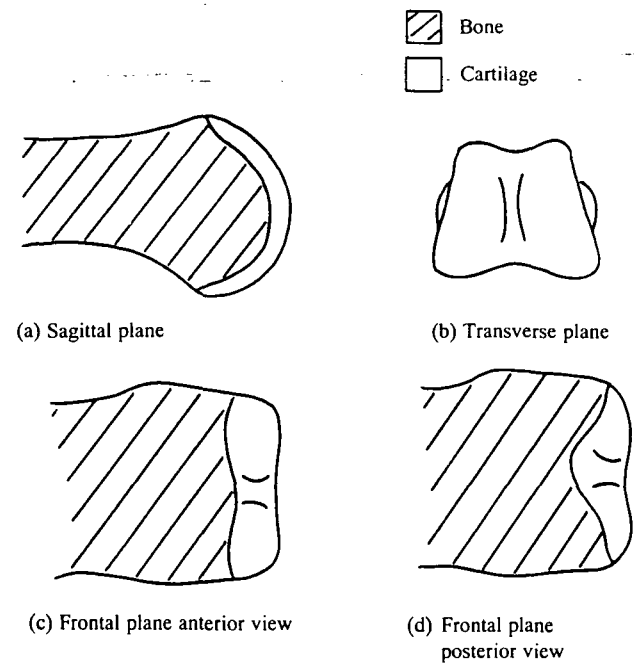

Fig. 7 Proximal phalangeal head shape in the sagittal, transverse and frontal planes

4.2 Middle phalangeal base shape

The cartilaginous surface of the middle phalangeal base is concave and bi-condylar to articulate against the proximal phalangeal head. However, shadowgraphs of the replica bones sectioned in the sagittal plane showed that the middle phalangeal base has a larger radius of curvature than the proximal phalangeal head, indicating that the joint is not conforming.

4.3 Bone length

The individual finger means, standard deviations (S.D.) and difference between male and female sizes as a percentage of the female mean are given in Tables 2 and 3. The bone length distribution graphs are shown in Figs 8, 9 and 10. The proximal phalangeal lengths ranged from 29–52 mm (mean 43.20 mm) and the middle phalangeal lengths from 16–35 mm (mean 27.12 mm). The middle finger proximal and middle phalangeal bones tended to be the longest followed by the ring, index and then little finger bones. The right hand bones tended to be slightly longer than the left hand bones and males tended to have longer bones than females.

4.4 Maximum bone head width in the frontal plane

The individual finger means, S.D. and difference between male and female sizes as a percentage of the female mean are given in Tables 4 and 5. The bone head width distribution graphs are shown in Figs 11, 12 and 13. The maximum bone head widths ranged from

Table 2 Proximal phalangeal bone length means (mm), S.D. and male–female differences

		Index	Middle	Ring	Little
Right	Mean	43.95	47.67	45.30	36.77
	S.D.	2.43	3.36	3.15	1.56
Left	Mean	43.50	47.54	44.82	35.98
	S.D.	3.00	3.33	3.33	3.47
Overall	Mean	43.88	47.61	45.09	36.38
	S.D.	2.73	3.35	3.24	2.72
Male	Mean	44.26	48.56	45.65	36.59
	S.D.	2.21	2.62	2.43	1.92
Female	Mean	42.88	46.06	44.04	35.97
	S.D.	3.23	3.79	4.17	3.74
Difference	(%)	3.22	5.43	3.66	1.72

Table 3 Middle phalangeal bone length means (mm), S.D. and male–female differences

		Index	Middle	Ring	Little
Right	Mean	26.35	31.46	29.63	21.70
	S.D.	2.22	2.72	2.69	1.44
Left	Mean	26.26	31.44	30.20	21.81
	S.D.	2.13	2.84	2.83	2.66
Overall	Mean	26.30	31.45	29.89	21.76
	S.D.	2.18	2.78	2.77	2.17
Male	Mean	26.44	32.28	30.82	21.90
	S.D.	1.89	2.19	1.92	1.48
Female	Mean	26.09	30.13	28.16	21.51
	S.D.	2.57	3.08	3.24	2.98
Difference	(%)	1.34	7.14	1.09	1.81

© IMechE 1996

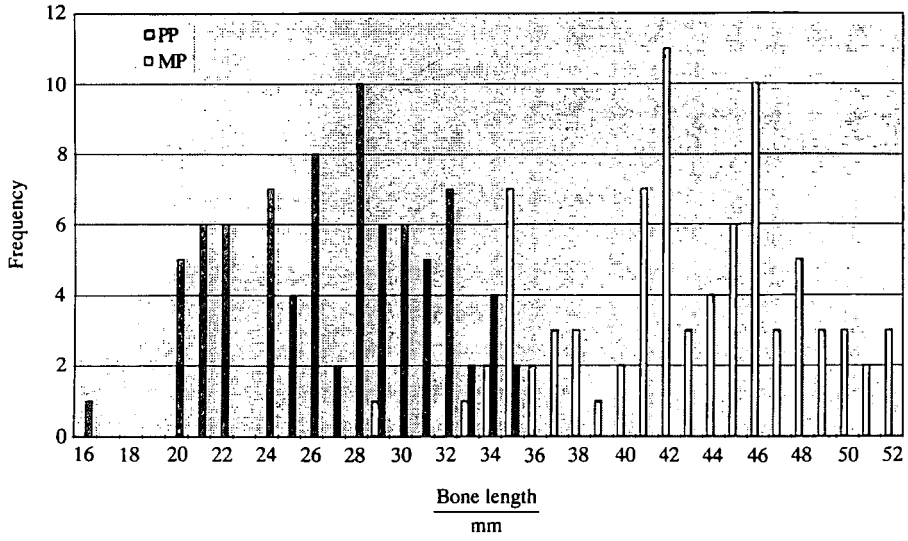

Fig. 8 Distribution of phalangeal bone lengths

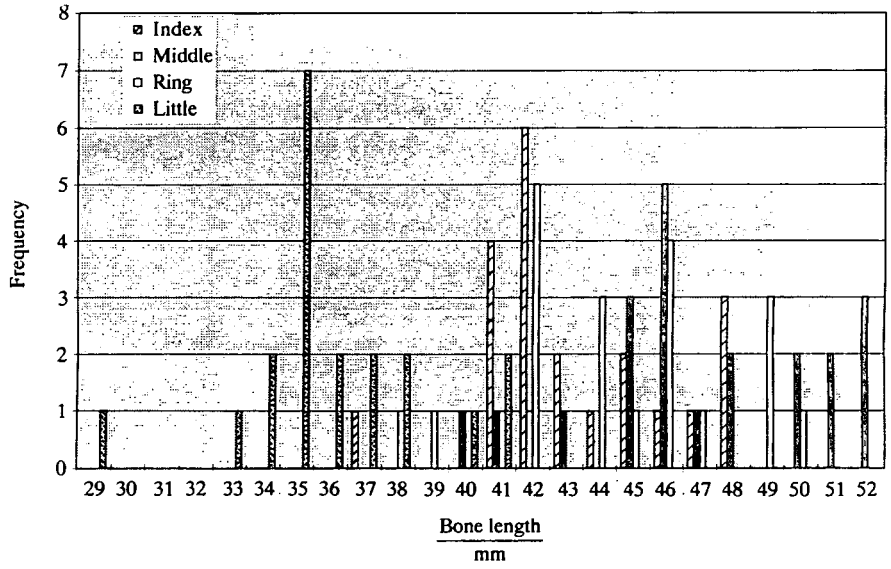

Fig. 9 Distribution of PP bone lengths for individual fingers

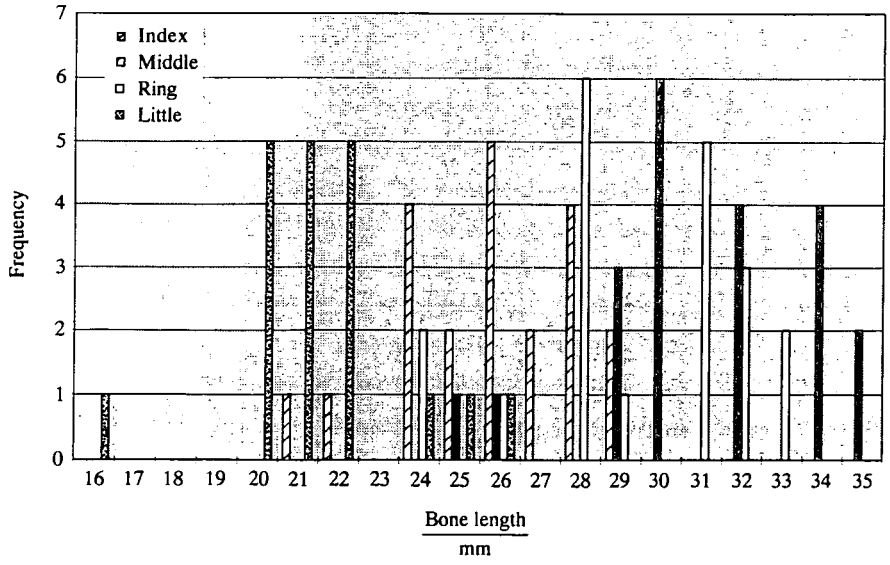

Fig. 10 Distribution of MP bone lengths for individual fingers

© IMechE 1996

Table 4 Proximal phalangeal maximum bone head width means (mm), S.D. and male–female differences

		Index	Middle	Ring	Little
Right	Mean	12.55	13.45	12.33	10.51
	S.D.	0.93	1.30	0.99	0.62
Left	Mean	12.59	13.09	12.20	10.31
	S.D.	0.84	1.09	0.93	0.85
Overall	Mean	12.57	13.28	12.27	10.41
	S.D.	0.89	1.22	0.97	0.75
Male	Mean	13.02	13.95	12.61	10.75
	S.D.	0.76	0.97	0.84	0.61
Female	Mean	11.84	12.19	10.76	9.77
	S.D.	0.51	0.65	1.46	0.54
Difference	(%)	9.97	14.44	17.19	10.03

8.5–15.5 mm (mean 12.14 mm) for the proximal phalanx and 8.5–12 mm (mean 10.43 mm) for the middle phalanx. The middle finger bones tended to be the widest followed jointly by the ring and index fingers and lastly the little finger bones. The right hand bones tended to have slightly larger maximum widths than the left hand bones and males tended to have larger bone head widths than females.

Table 5 Middle phalangeal maximum bone head width means (mm), S.D. and male–female differences

		Index	Middle	Ring	Little
Right	Mean	10.75	11.03	10.62	9.24
	S.D.	0.72	0.72	0.66	0.62
Left	Mean	10.39	11.21	10.64	9.34
	S.D.	0.78	0.69	0.66	0.65
Overall	Mean	10.58	11.11	10.63	9.29
	S.D.	0.77	0.71	0.66	0.64
Male	Mean	10.78	11.54	10.95	9.58
	S.D.	0.68	0.55	0.57	0.61
Female	Mean	10.24	10.43	10.03	8.81
	S.D.	0.79	0.26	0.29	0.32
Difference	(%)	5.27	10.64	9.17	8.74

4.5 Maximum and minimum bone head best-fit diameters

The individual finger means, S.D. and difference between male and female sizes as a percentage of the female mean are given in Tables 6 and 7. The distribution graphs of the maximum best-fit diameters are shown in Figs 14, 15 and 16. The maximum best-fit diameters to the sagittal profiles of the bones ranged from 6–11 mm (mean 8.67 mm) for the proximal phalangeal head and 5–7.5 mm (mean 6.23 mm) for the middle phalangeal head. The actual maximum condyle diameters measured from the sagittal plane sections were on average 0.45 mm less than those of the sagittal profiles due to a slight overlap of the condyles, and the minimum condyle diameters were on average 0.88 mm smaller than the maximum condyle diameters. The middle finger tended to have the largest best-fit diameters followed by the index, ring and then little finger bones. Overall the right hand bones tended to have slightly larger head diameters than the left hand bones and males tended to have larger head diameters than females.

4.6 Middle phalangeal maximum and minimum base best-fit diameters

The individual finger means, S.D. and difference between male and female sizes as a percentage of the female mean are given in Table 8. It can be seen that the radius of curvature of the middle phalangeal base is greater than that of the proximal phalangeal head (Table 6) showing that the proximal interphalangeal joint is not a conforming joint. The middle phalangeal base maximum condyle diameters are on average 3.36 mm greater than those of the proximal phalangeal head

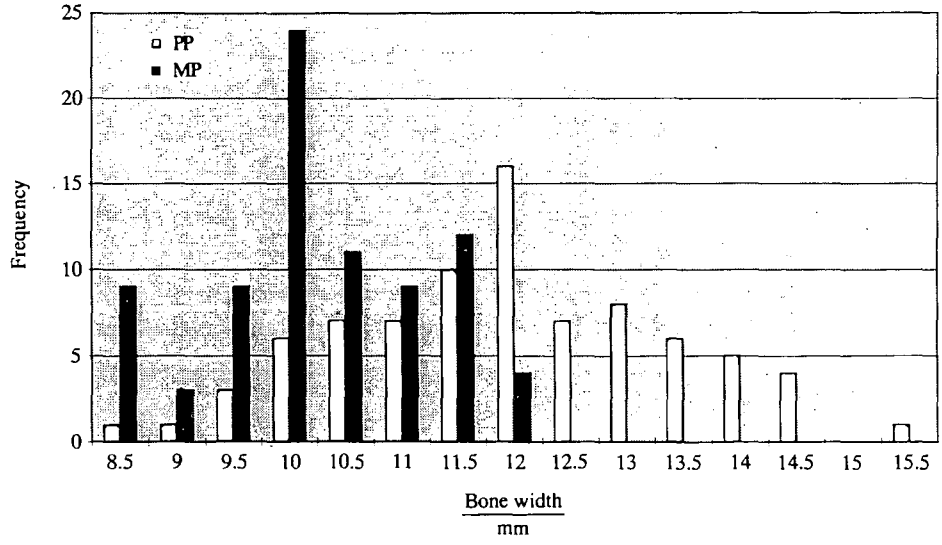

Fig. 11 Distribution of phalangeal maximum bone head widths

© IMechE 1996

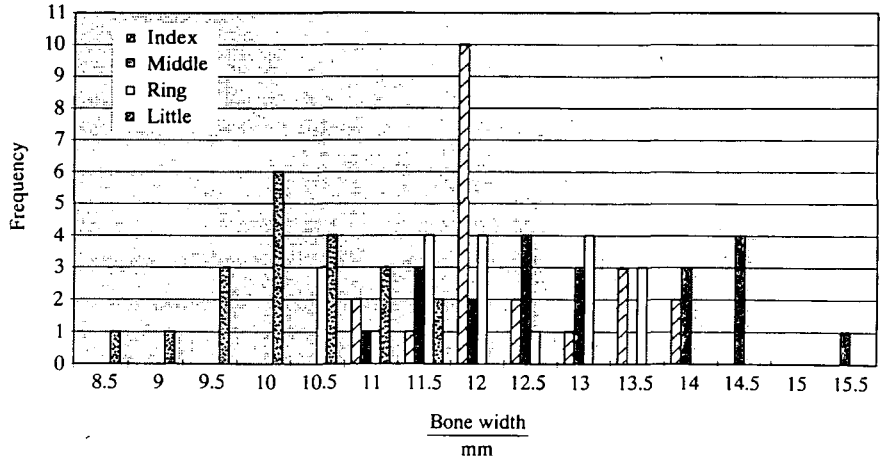

Fig. 12 Distribution of PP maximum bone head widths for individual fingers

and 1.06 mm greater for the minimum condyle diameters. However, it is proposed that the surface replacement prosthesis design will have a conforming middle phalangeal base and proximal phalangeal head in order to increase joint stability. The right hand bones tended to have slightly larger condyle diameters than the left hand bones and males tended to have larger condyle diameters than females.

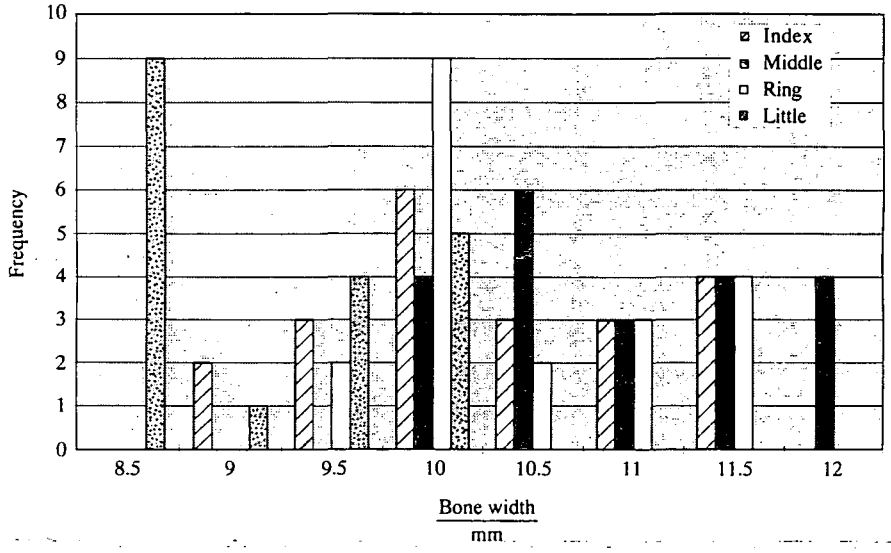

Fig. 13 Distribution of MP maximum bone head widths for individual fingers

Table 6 Proximal phalangeal head maximum and minimum best-fit diameter means (mm), S.D. and male–female differences (I = index, M = middle, R = ring, L = little)

		Maximum				Minimum			
		I	M	R	L	I	M	R	L
Right	Mean	9.14	9.36	8.86	7.60	7.68	8.00	7.59	6.45
	S.D.	0.80	0.96	0.64	0.44	0.49	0.74	0.47	0.35
Left	Mean	9.20	9.30	8.56	7.20	7.35	7.85	7.33	6.35
	S.D.	0.60	0.64	0.64	0.60	0.63	0.55	0.67	0.50
Overall	Mean	9.17	9.33	8.73	7.40	7.52	7.93	7.48	6.40
	S.D.	0.71	0.82	0.66	0.56	0.59	0.66	0.58	0.44
Male	Mean	9.42	9.73	9.04	7.58	7.73	8.15	7.77	6.58
	S.D.	0.65	0.67	0.46	0.43	0.50	0.56	0.32	0.38
Female	Mean	8.75	8.69	8.14	7.07	7.19	7.56	6.93	6.07
	S.D.	0.61	0.61	0.58	0.62	0.56	0.63	0.56	0.32
Difference	(%)	1.08	11.97	11.06	7.21	7.51	7.80	12.12	8.40

© IMechE 1996

Table 7 Middle phalangeal head maximum best-fit diameter means (mm), S.D. and male–female differences

		Index	Middle	Ring	Little
Right	Mean	6.68	6.68	6.36	5.33
	S.D.	0.49	0.57	0.53	0.33
Left	Mean	6.35	6.75	6.06	5.45
	S.D.	0.45	0.60	0.64	0.42
Overall	Mean	6.52	6.71	6.23	5.39
	S.D.	0.50	0.59	0.60	0.38
Male	Mean	6.58	6.96	6.46	5.42
	S.D.	0.43	0.57	0.46	0.40
Female	Mean	6.44	6.31	5.79	5.36
	S.D.	0.58	0.35	0.59	0.35
Difference	(%)	2.17	10.30	11.57	1.12

4.7 Middle phalangeal maximum base width

The individual finger means, S.D. and difference between male and female sizes as a percentage of the female mean are given in Table 9. It was found that the maximum middle phalangeal base width was on average 1.47 mm greater than the proximal phalangeal head. The right hand bones tended to have slightly larger maximum base widths than the left hand bones and males tended to have larger maximum base widths than females.

4.8 Dimension relationships

Figures 17 to 22 show the relationships between bone lengths, maximum best-fit bone head diameters and maximum bone head widths. The mean ratios are shown in Table 10. It can be seen that the ratios vary according to bone size so the best-fit line was plotted as well as the average ratio line. The mean proximal phalangeal ratios are $L/W = 3.57$ ($W/L = 0.28$), $L/D = 5.00$ ($D/L = 0.20$) and $W/D = 1.41$ ($D/W = 0.71$). The mean middle phalangeal ratios are $L/W = 2.62$ ($W/L = 0.38$), $L/D = 4.35$ ($D/L = 0.23$) and $W/D = 1.66$ ($D/W = 0.60$).

The equations of the best-fit lines are shown in Table 11 along with the R-squared values calculated for each

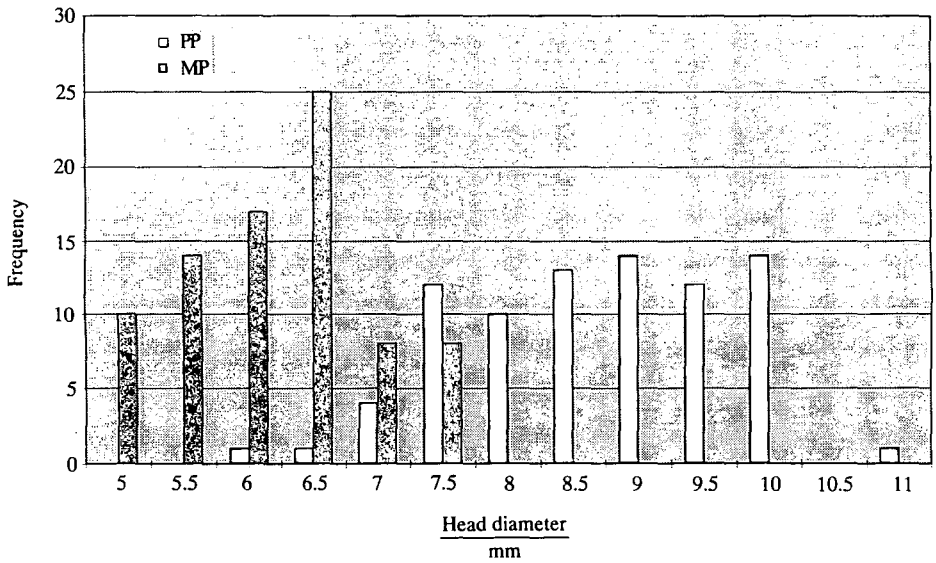

Fig. 14 Distribution of PP maximum and MP maximum best-fit bone head diameters

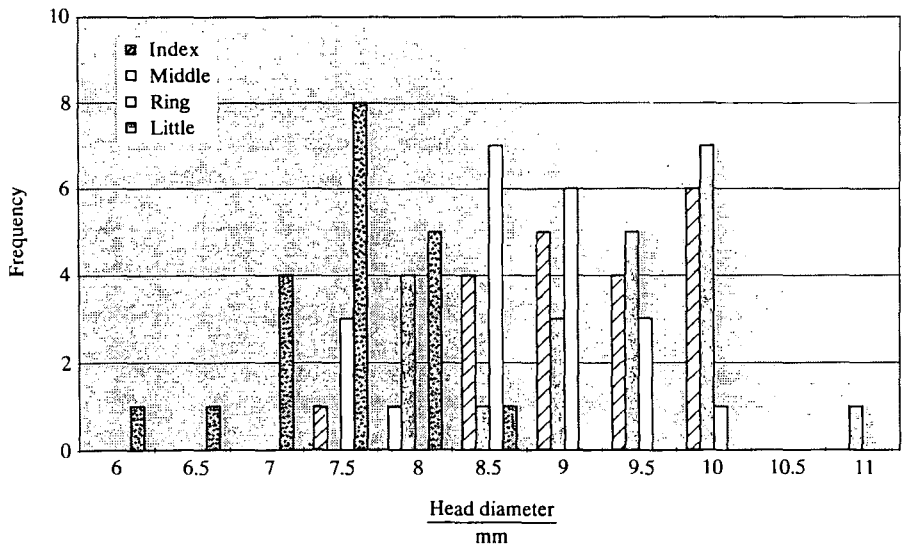

Fig. 15 Distribution of PP maximum best-fit bone head diameters

© IMechE 1996

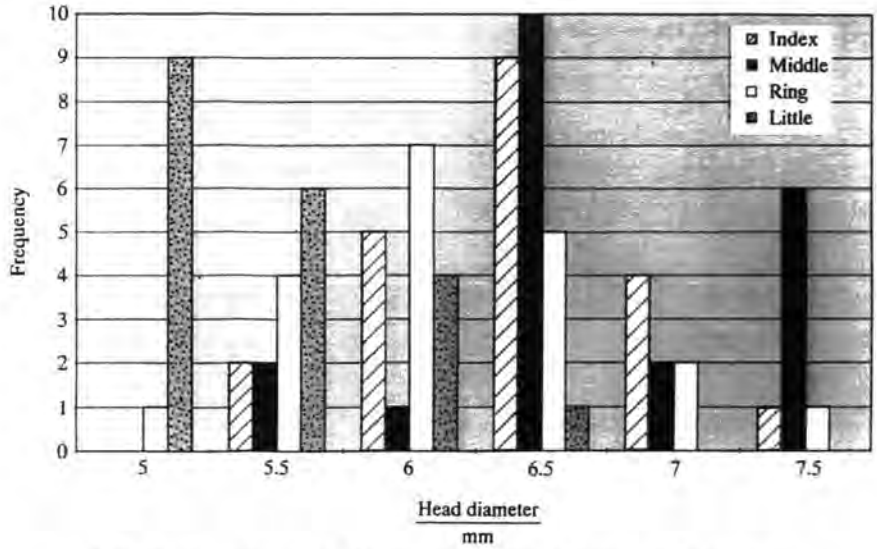

Fig. 16 Distribution of MP maximum best-fit bone head diameters

Table 8 Middle phalangeal base maximum and minimum best-fit diameter means (mm), S.D. and male–female differences (I = index, M = middle, R = ring, L = little)

		Maximum				Minimum			
		I	M	R	L	I	M	R	L
Right	Mean	12.09	12.20	11.82	10.38	9.09	9.10	8.91	7.75
	S.D.	1.08	1.08	1.19	1.58	0.90	1.14	0.79	0.66
Left	Mean	11.20	11.70	11.67	10.00	7.90	8.60	8.44	7.30
	S.D.	1.17	1.19	1.15	1.10	1.04	1.11	1.26	0.78
Overall	Mean	11.67	11.95	11.75	10.17	8.52	8.85	8.70	7.50
	S.D.	1.21	1.16	1.18	1.34	1.14	1.15	1.05	0.76
Male	Mean	12.15	12.38	11.77	10.17	8.84	8.92	9.08	7.67
	S.D.	0.77	0.74	0.89	1.34	0.77	1.00	0.83	0.75
Female	Mean	10.88	11.14	11.71	10.17	8.00	8.75	8.00	7.17
	S.D.	1.36	1.36	1.58	1.34	1.41	1.60	1.07	0.69
Difference	(%)	11.70	11.16	0.51	0.00	10.50	1.94	13.50	6.97

best-fit line. These equations can be used to predict the sizes of prosthesis required before surgery from X-rays. For example if a patient's maximum bone head widths were ascertained then the maximum best-fit head diameters could be calculated and hence the sizes of prostheses required.

Table 9 Middle phalangeal maximum base width means (mm), S.D. and male–female differences

		Index	Middle	Ring	Little
Right	Mean	14.00	14.79	13.57	12.24
	S.D.	0.84	0.97	1.05	1.14
Left	Mean	13.92	14.68	13.77	11.90
	S.D.	0.86	1.03	0.95	1.00
Overall	Mean	13.93	14.74	13.66	12.06
	S.D.	0.85	1.00	1.01	1.08
Male	Mean	10.78	11.54	10.95	9.58
	S.D.	0.68	0.55	0.57	0.61
Female	Mean	10.24	10.43	10.03	8.81
	S.D.	0.79	0.26	0.29	0.32
Difference	(%)	5.27	10.64	9.17	8.74

R-squared values range between 0 and 1 for a best-fit line. An *R*-squared value near 0 indicates a poor fit, whereas a value near 1 indicates a good fit. It can be seen that the *R*-squared values for the proximal phalanx are nearer 1 than those for the middle phalanx. Hence the relationships between bone length, head diameter and width relationships for the proximal phalanx are more meaningful than those for the middle phalanx. The low *R*-squared values indicate the natural biological variations in the bone dimensions.

4.9 Alignment of the proximal phalanx head condyles

From the shadowgraphs in the frontal plane it was obvious that in many cases the condyles of the proximal phalangeal heads were not in alignment. Hence, the angle of alignment of the radial and ulnar condyles was measured and positive and negative angles of alignment defined as shown in Fig. 23. It was found that the little finger PIPJs showed the greatest average misalignment

© IMechE 1996

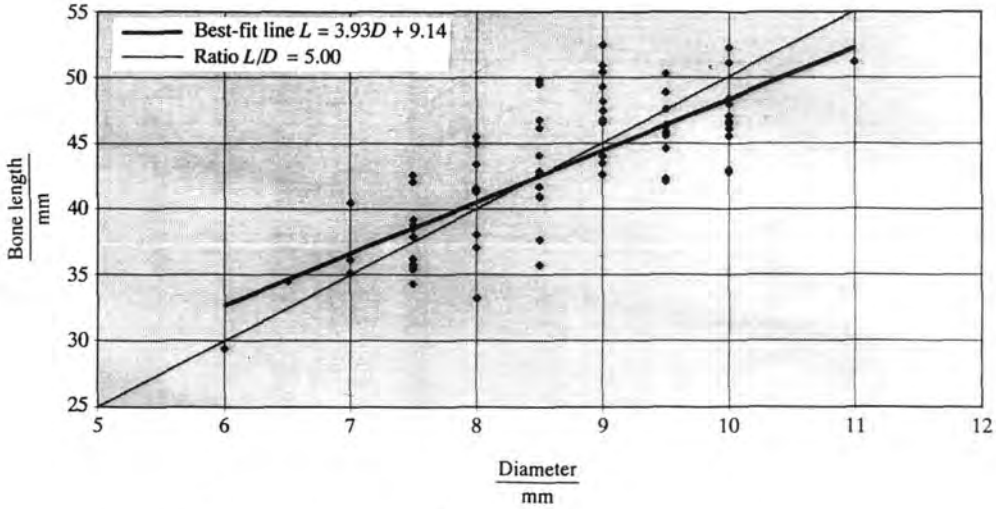

Fig. 17 Relationship between PP maximum head diameter and bone length

of condyles followed by the ring, index and then the middle finger (Table 12).

The direction of misalignment was dependent on the individual fingers. The right hand was approximately a mirror image of the left. The little and ring PIPJs tended to have a more prominent radial condyle while the index and middle finger PIPJs had a more prominent ulnar condyle (Fig. 24). However, it was proposed

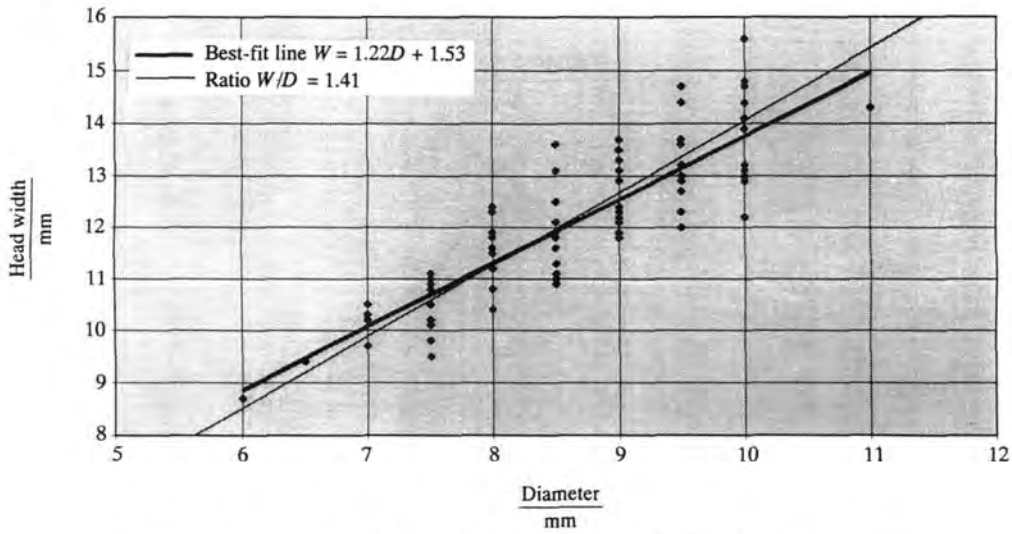

Fig. 18 Relationship between PP maximum head diameter and maximum bone head width

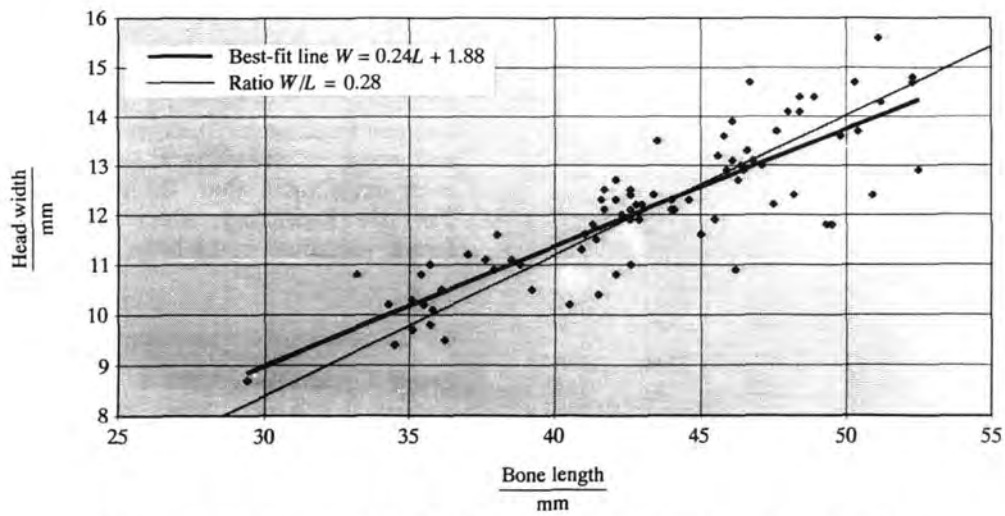

Fig. 19 Relationship between PP bone length and maximum bone head width

© IMechE 1996

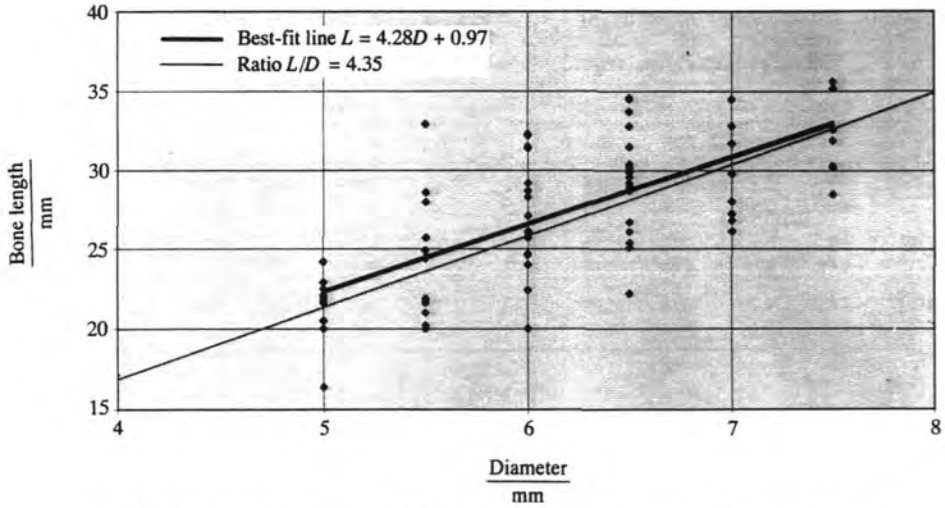

Fig. 20 Relationship between MP maximum head diameter and bone length

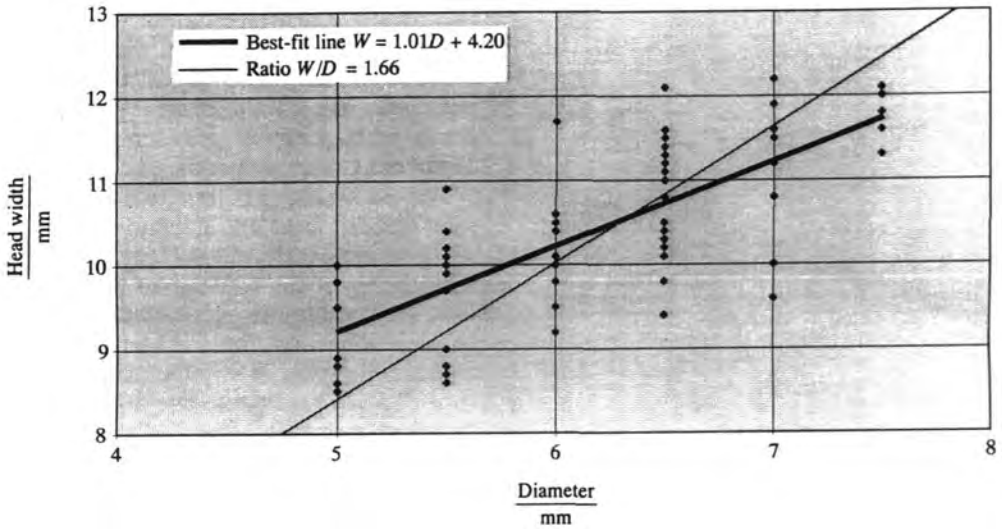

Fig. 21 Relationship between MP maximum head diameter and maximum bone head width

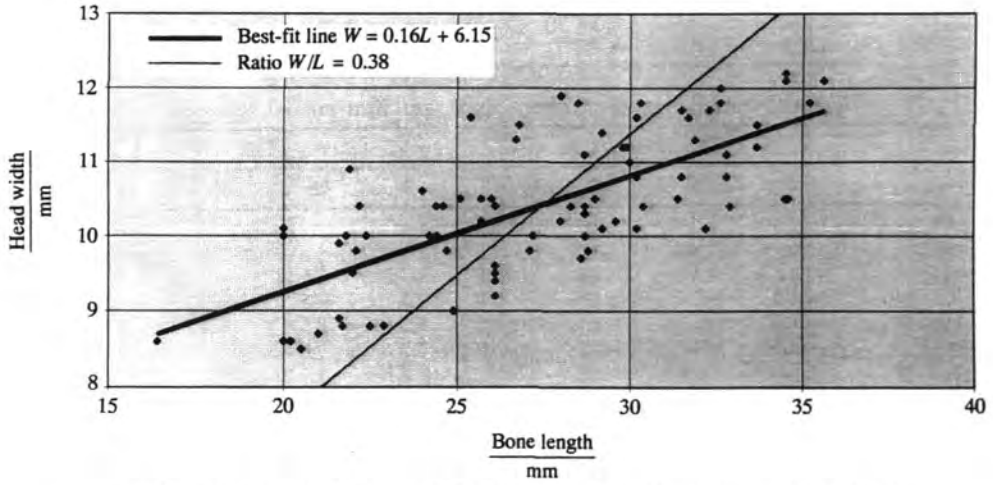

Fig. 22 Relationship between MP bone length and maximum bone head width

© IMechE 1996

Table 10 Mean ratios between bone lengths, maximum best-fit bone head diameters and maximum bone head widths (I = index, M = middle, R = ring, L = little, PP = proximal phalangeal, MP = middle phalangeal)

		Right				Left					
		I	M	R	L	I	M	R	L	Mean	S.D.
L/W	PP	3.51	3.56	3.69	3.51	3.46	3.64	3.68	3.49	3.57	0.23
	MP	2.46	2.86	2.79	2.35	2.54	2.81	2.84	2.34	2.62	0.31
L/D	PP	4.84	5.12	5.12	4.86	4.74	5.02	5.25	5.01	5.00	0.41
	MP	4.01	4.60	4.68	4.03	4.14	4.68	5.02	3.61	4.35	0.62
W/D	PP	1.38	1.44	1.39	1.39	1.37	1.40	1.43	1.44	1.41	0.09
	MP	1.63	1.64	1.68	1.74	1.64	1.67	1.59	1.72	1.66	0.13

that for the design of the surface replacement prosthesis the angle of misalignment would be neglected and compensated for in the middle phalangeal base and soft tissue reconstruction. This would simplify the design and decrease the number of different sized and shaped prostheses required.

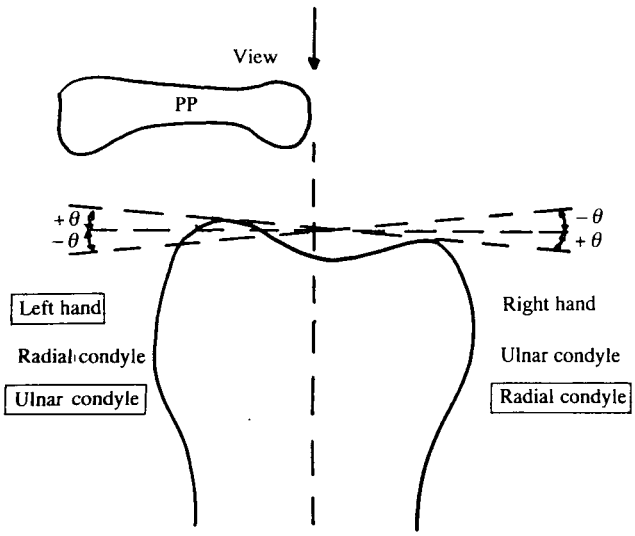

Fig. 23 Definition of condyle angle of misalignment

5 THE DURHAM PIPJ SURFACE REPLACEMENT PROSTHESIS DESIGN

The same principles applied to the design of the Durham metacarpophalangeal surface replacement prosthesis are being employed to develop a PIPJ prosthetic design (**5–7**). The MCPJ prosthesis consists of a two-part unconstrained joint with a spherical-shaped hollow convex metacarpal head and a conforming concave proximal phalangeal base. Similarly it is proposed that the PIPJ surface replacement will consist of a convex bi-condylar proximal phalangeal head and a conforming concave middle phalangeal base.

The unconstrained joint will provide a little lateral joint stability from the bi-condylar surfaces, however, it will predominantly rely on any necessary relocation or rebalancing of the soft tissues and tendons around the joint for stability. In particular, the lateral stability will be dependent on the collateral ligaments and joint capsule. However, it is hoped that a PIPJ design which is as close as possible to the original joint anatomy will be more successful than its predecessors as this will produce similar joint mechanics and alignment to those

Table 11 Relationships between bone lengths, maximum best-fit bone head diameters and maximum bone head widths (best-fit line equations to Figs 17 to 22) and the *R*-squared values for the relationships

Proximal phalanx		Middle phalanx	
Relationship	*R*-squared value	Relationship	*R*-squared value
$L = 3.93D + 9.14$	0.60	$L = 4.28D + 0.97$	0.48
$W = 0.24L + 1.88$	0.73	$W = 0.16L + 6.15$	0.52
$W = 1.22D + 1.53$	0.75	$W = 1.01D + 4.20$	0.57

Table 12 Alignment of proximal phalangeal head condyles (degrees)

	Right				Left			
	I	M	R	L	I	M	R	L
1	−1.0	1.5	1.5	6.5				
3	0	4.0	1.5	6.5	0	−1.5	−3.0	−8.5
4	1.0	−1.0	3.0	5.5	0	2.0	−3.5	−7.0
5	−1.0	−2.0	3.5	5.0	1.5	0.5	−4.0	−7.5
6	−6.0	−2.5	6.5	7.0	6.0	4.0	−6.0	−8.0
7	−2.5	0	−1.0	5.0	2.5	2.0		−4.0
8	6.0	−1.0	1.0		1.5	−1.5	−2.5	−3.0
9	−2.5	−0.5	0	−3.5	0.5	1.0	−1.0	−5.0
10	−1.5	1.5	6.0	5.0	1.5	1.5	−1.0	−5.0
11	5.0	0	−4.5	8.0	0.5	0.5	−5.5	−7.0
12	−2.0	−2.0	1.5	3.0	1.5	3.0	−2.0	−5.0
Mean	−0.41	−0.18	1.70	4.80	1.55	1.15	−3.17	−6.00
S.D.	3.26	1.82	2.95	3.06	1.59	1.67	1.68	1.67

© IMechE 1996

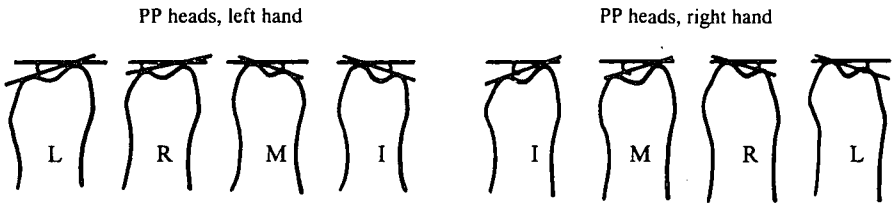

	$+\theta$	$-\theta$
Left hand:	Radial condyle	
		Ulnar condyle
Right hand:		Radial condyle
	Ulnar condyle	

Fig. 24 PP head condyle misalignment

of the natural joints. This design will also require less bone removal than existing prostheses do.

It should be possible to design a prosthesis which would not require the complete removal of the proximal phalangeal head, and hence the removal or repositioning of the collateral ligaments. However, a design would require the removal of some of the proximal phalangeal head and not just the cartilaginous surface due to the small sizes of the PIPJ (low bone stock), combined with the need for adequate fixation of the prosthesis to prevent movement between it and the bone. Hence a surface replacement design is now being developed.

5.1 Surface prosthesis sizes

The PIPJ maximum bone head diameters ranged from 6–11 mm and the proposed surface replacement prostheses sizes will be based on these dimensions. Ideally the range of prostheses should cover the total anatomical range and it is proposed that this will be done in sizes of 1 mm difference. Figure 25 shows the distribution of PIPJ sizes by maximum best-fit head diameter when sorted into sizes increasing by a step of 1 mm (either integer sizes or half sizes). From this data it can be seen that prosthetic sizes of 7, 8, 9 and 10 mm would cover 97.6 per cent of the population, and sizes 7.5, 8.5 and 9.5 mm would cover 91.5 per cent of the population (although the latter range cuts off the 6.5 and 6 sizes which tend to be those of the little finger). In fact 20 per cent of the little finger joints are not included in the latter range. Hence the four integer sizes would be preferable.

6 SUMMARY

The proximal interphalangeal joint is made up from the convex head of the proximal phalanx and the concave base of the middle phalanx, although the two surfaces are not conforming. The proximal phalangeal head and middle phalangeal base are circular in the sagittal plane across the width of the bone but with a varying diameter producing the bi-condylar shape. The middle phalangeal base maximum condyle diameters are on average 3.36 mm greater than those of the proximal phalangeal head, and 1.06 mm greater for the minimum condyle diameters. The articulating surface is broader anteriorly than posteriorly.

The bone lengths ranged from 29–52 mm (mean 43.20 mm) for the proximal phalanx and 16–35 mm (mean 27.12 mm) for the middle phalanx, with the middle finger tending to have the longest bones followed by the

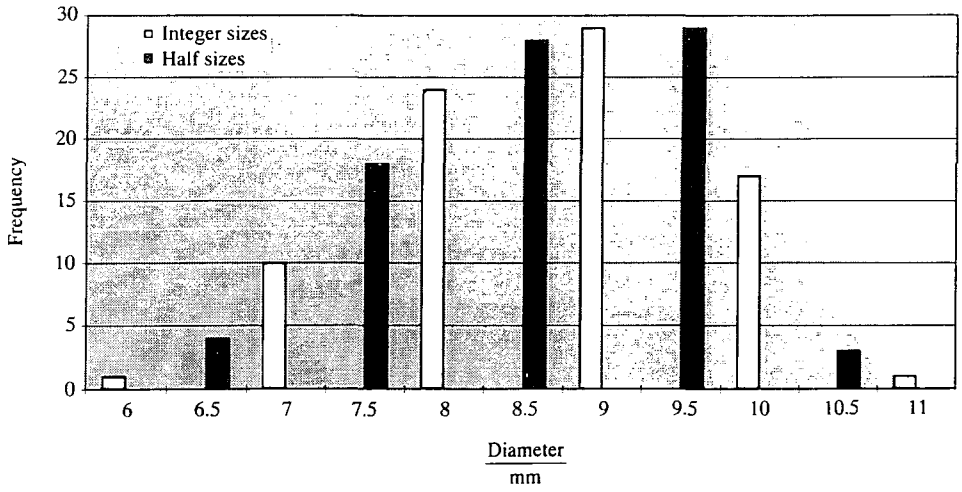

Fig. 25 Distribution of PIPJ sizes (by PP head diameter) when restricted to 1 mm step sizes for integer and half sizes

© IMechE 1996

ring, index and then the little fingers. The maximum bone head widths ranged from 8.5–15.5 mm (mean 12.14 mm) for the proximal phalanx and 8.5–12 mm (mean 1.43 mm) for the middle phalanx, with the middle finger tending to have the widest bones followed jointly by the index and ring finger bones and then the little finger. The maximum best-fit diameters to the circular profile of the bones in the sagittal plane ranged from 6–11 mm (mean 8.67 mm) for the proximal phalanx and 5–7.5 mm (mean 6.23 mm) for the middle phalanx, with the middle finger tending to have the largest diameters followed by the index, ring and then little finger.

Relationships and ratios between the maximum best-fit bone head diameter, the bone length and the maximum bone head width were calculated which can be used to predict the sizes of prostheses needed from information gained from X-rays. These were $L = 3.93D + 9.14$, $W = 1.22D + 1.50$ and $W = 0.24L + 1.88$ for the proximal phalanx, and $L = 4.28D + 0.97$, $W = 1.01D + 4.20$ and $W = 0.16L + 6.15$ for the middle phalanx. The ratios were $L/W = 3.57$, $L/D = 5.00$ and $W/D = 1.41$ for the proximal phalangeal bones and $L/W = 2.62$, $L/D = 4.35$ and $W/D = 1.66$ for the middle phalangeal bones.

The little and ring fingers tended to have a more prominent radial condyle while the index and middle fingers tended to have a more prominent ulnar condyle. This was due to a slight difference in diameters of the two condyles rather than the axis of rotation not being perpendicular to the shaft of the bone. A range of sizes of 7, 8, 9 and 10 mm or 7.5, 8.5 and 9.5 mm maximum proximal phalangeal head diameters for the surface replacement prosthesis would cover 97.6 per cent and 91.5 per cent of the population respectively, however, the latter range would neglect 20 per cent of the little finger PIPJ population.

REFERENCES

1 **Beckenbaugh, R. D.** and **Linscheid, R. L.** Arthroplasty in the hand and wrist. *Operative Hand Surg.*, 1982, **6**, 141–156.

2 **Mannerfelt, L.** and **Andersson, K.** Silastic arthroplasty of the rheumatoid hand. *Irish Med. J.*, 1975, **80**(2), 58–60.

3 **Hagert, C. J., Oddvar, E., Ohlsson, N., Aschan, W.** and **Mvin, A.** Metacarpophalangeal joint implants. *Scand. J. Plast. Reconstr. Surg.*, 1975, **9**, 147–157.

4 **Linscheid, R. L., Dobyns, J. H., Beckenbaugh, R. D.** and **Cooney, W. P.** Proximal interphalangeal joint arthroplasty with a total joint design. *Mayo Clinic Proc.*, 1979, **54**, 227–240.

5 **Unsworth, A.** and **Alexander, W. J.** Dimensions of the metacarpophalangeal joint with particular reference to joint prostheses. *Engng in Medicine*, 1979, **8**(2), 75–80.

6 **Stokoe, S. M.** A finger function simulator and surface replacement prosthesis for the metacarpophalangeal joint. PhD thesis, 1990, University of Durham.

7 **Joyce, T. J.** and **Unsworth, A.** The design of a surface replacement metacarpophalangeal prosthesis. (To be published).

© IMechE 1996

Biomechanics of the distal upper limb

H. E. Ash, T. J. Joyce, A. Unsworth

INTRODUCTION

The hand is not only a crucial tool for everyday life and work, but a means of conveying and receiving information. It is a mechanism of great complexity and intricacy. This paper will discuss the forces acting on, and movement of, the joints of the distal upper limb, the metacarpo-phalangeal, proximal interphalangeal and the distal interphalangeal joints together with the joints of the thumb and the wrist.

FORCES IN THE JOINTS OF THE DISTAL UPPER LIMB

In-vivo joint, tendon and muscle forces are difficult to measure directly, and the large number of muscles and ligaments involved make the task of modelling, and then calculating these forces equally as difficult. The positions of the joint and its surrounding joints must be specified as these will directly affect the forces acting on it. Due to this complexity, models have to be simplified.

Experimental measurements of forces

Value of measurements

The clinical measurement of hand strength allows pathological conditions and their response to treatment to be assessed, feasible treatment goals to be set, and the effectiveness of different surgical procedures to be compared. Measurement must be reliable and valid, necessitating the use of standardized equipment, procedures and positioning of the hand.

Definitions of hand and finger strength

Tip, pulp, lateral and three-point pinch, grip strength, long finger flexion force and thumb force have all been extensively measured.[1-24] However, the definitions of the type of forces being measured have often been contradictory and vague. The following pinches and grips are defined in order to compare experimental results and to apply this information to the various theoretical models reviewed, (Fig. 1).

Grip strength-power grip. The fingers and thumb gripping an object, producing maximum hand grip strength.

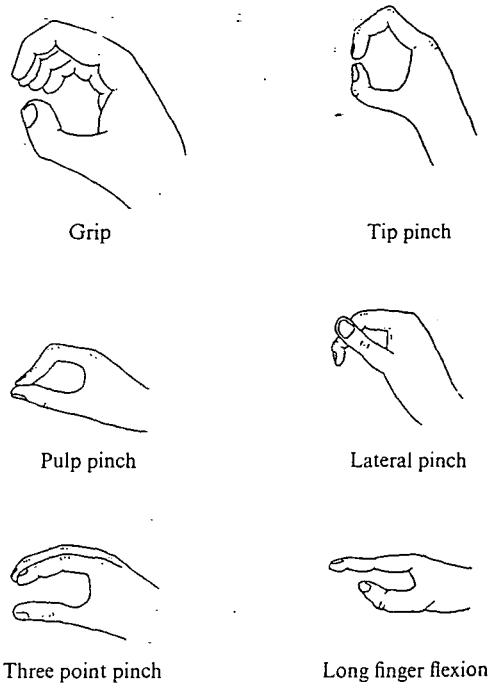

Fig. 1—Definitions of hand and finger strength.

H. A. Ash BSc MSc, T. J. Joyce BEng MSc, A. Unsworth MSc PhD DEng FIMechE, School of Engineering, University of Durham, Science Laboratories, South Road, Durham DH1 3LE, UK.

Current Orthopaedics (1996) 10, 25–36
© 1996 Pearson Professional Ltd

UNIVERSITY OF DURHAM 25

Tip pinch. The tip of the index, middle, ring or little finger against the tip of the thumb, with the interphalangeal joint (IPJ) flexed.

Pulp pinch. The distal phalangeal pad of the index, middle, ring or little finger against the distal phalangeal pad of the thumb, (the IPJs are more extended than in tip pinch).

Lateral radial pinch. The distal phalangeal pad of the thumb against the lateral or radial side of the middle phalanx of the index finger, the other fingers being clenched in support.

Three point palmar pinch. The index and middle fingers reacting against the thumb. Pinching with the pads or tips is not always defined. However, Kellor[1] defined palmar pinch using the pads of the fingers and thumb and three-point pinch using the tips.

Long finger flexion. The pad of the distal phalanx of the finger exerting a force in a neutral, cantilever position.

Thumb force. The pad of the distal phalanx of the thumb exerting force, with the angles of joints defined.

Equipment used

A popular method of measuring grip strength is to squeeze an inflated bag connected to a manometer and to note the increase in pressure. However, different techniques of squeezing give different results, as indeed will different original bag volumes or pressures.[25] Additionally, the contribution of individual fingers cannot be determined.[2] Strain-gauged devices, however, offer the ability to measure the force of a grip, rather than the pressure indicated by an inflated bag. With certain strain-gauged devices, the magnitude and contribution of the individual fingers, and finger segments, to the grip strength can also be determined.

Influential factors

It has been found that the forces acting on and around the joints of the hand depend on environmental, mechanical and human factors, the latter including the patient's cooperation. From past investigations, comparison between different authors' results show that these factors include age,[1,3–7] sex,[1,3–10] pathological condition,[11–16,26] bilateral hand function,[1,4,6,8,9,14,15,17,18] occupation and exercise,[6,17,18] measuring device or size of object being grasped,[2,19,25] technique of grasp,[25] difference in hand function,[1,6–9,17] temperature,[18,27] diurnal or circadian effects,[11,13,18] and drugs.[4,13] In addition, the orientation of other joints in the upper limb may influence joint forces.

Grip strength

The grip strength of subjects and patients has been measured and shows total grip strength ranging from a minimum of 80N in normal women to a maximum of 520N in normal men (Table 1). Arthritic patients were only one-third as strong. The range of grip-strength data shows that either the equipment itself influences the values recorded[19] or that there is a large subject to subject variation which is also influenced by the variation of the position of the finger joints.

The distal phalangeal force component of the total grip strength was found to be the largest, followed by the proximal then the middle phalanx (Table 2).[7,19] The mean contributions of the fingers to grip strength were found to be 30% index, 30% middle, 22% ring and 18% little.[19]

Table 1 Hand grip strength (N)

Reference	Sex	Hand	No.	Mean force or range of means	Maximum or range of force
Mathiowetz et al[8]	M	R	310		142–783
	M	L	310		138–712
	F	R	328		111–610
	F	L	328		102–512
Reikeras[9]	M	D	30	186	
	M	ND	30	182	
	F	D	30	105	
	F	ND	30	106	
Swanson et al[6]	M	D	50	467	
	M	ND	50	441	
	F	D	50	241	
	F	ND	50	220	

Table 2 Individual finger grip strength (N)

Reference	Finger	No.	Total finger	Distal phalanx	Middle phalanx	Proximal phalanx
Amis[19]	I	17	150	80	30	45
	M	17	160	70	40	50
	R	17	125	55	30	35
	L	17	105	50	25	30

Table 3 Additional factors affecting grip strength (N)

Factor	Reference	Normal/RA	No.	Hand	Force	Force
Diurnal	Pearson et al[18]	Normal	10	D	am 65	pm 68
		Normal	10	ND	am 65	pm 67
Temp.	Pearson et al[18]	Normal	13	D	10°C 48	40°C 49
		Normal	13	ND	10°C 50	40°C 49
		RA	11	D	10°C 18	40°C 18
		RA	11	ND	10°C 18	40°C 17
Exercise	Pearson et al[18]	Normal	13	D	pre 50	post 50
		Normal	13	ND	pre 51	post 50
		RA	11	D	pre 17	post 18
		RA	11	ND	pre 17	post 17
Sports	Cutts and Bollen[17]	Climbers	13	R	507	
		Climbers	13	L	532	
		Normal	12	R	445	
		Normal	12	L	412	

Males were found to be stronger than females in grip strength, female grip strength being approximately 50–80% that of males.[1,3,4,6–9] Pathological conditions such as rheumatoid arthritis and osteoarthritis also severely reduce grip strength. Grip-strength values are greater than tip and pulp pinch. The influence of additional factors is shown in Table 3.

Pinch forces

Pinch strength depends on the type of pinch and the finger–thumb combination, i.e. tip, pulp, three point or lateral. The experimental data show that males have greater pinch strengths than females. Tip, pulp and long finger flexion all seem to produce similar force ranges. Lateral and three-point pinch in general have a greater upper value of force than tip and pulp pinch possibly because more than one finger is involved either in pinch or in support. For tip and pulp pinch, the index finger is approximately equal in strength to the middle finger, with the ring finger next and then the little finger (Tables 2, 4–6).

Table 4 Tip pinch force (N)

Reference	Finger	Sex	No.	Maximum force	Range of force
An et al[7]	I	M	18	63	
		F	22	47	
	M	M	18	63	
		F	22	46	
Cantrell[16]	I				34–49
	M				34–49
	R				22–49
	L				20–39

Table 6 Lateral pinch force (N)

Reference	Finger	Sex	No.	Mean force
An et al[7]	I	M	18	75
		F	20	59
	M	M	18	68
		F	20	51

BIOMECHANICS OF THE FINGERS

Joint anatomy

The metacarpo-phalangeal joint (MCPJ) is a complex joint, with local soft tissue structures making important contributions to both joint function and stability. It consists of the convex metacarpal head and the concave base of the proximal phalanx, forming a condylar joint stabilized by the metacarpo-phalangeal and metacarpo-glenoidal ligaments, volar plate and joint capsule.

The metacarpo-phalangeal (or collateral) ligaments arise from each side of the metacarpal head and are the primary link between the metacarpal and proximal phalanx. These ligaments run obliquely, so the tension in the ligaments increases as the joint moves from 0° to 90°. Quantitative results exist to show that the collateral ligaments are the primary means of stabilizing the MCPJ. In addition the flexor tendon sheath is supported by the metacarpo-glenoidal ligaments.[29]

The IPJ which consist of the proximal interphalangeal joint (PIPJ) and the distal interphalangeal joint (DIPJ), are bicondylar with 1° of freedom. They have no muscular support in abduction and adduction

Table 5 Pulp pinch force (N)

Reference	Finger	Sex	No.	Maximum force	Sex	No.	Maximum force
An et al[7]	I	M	18	66	F	22	45
	M	M	18	62	F	22	45
Swanson et al[6]	I	M	50	52D 47ND	F		35D 32ND
	M	M	50	55D 56ND	F		35D 33ND
	R	M	50	37D 35ND	F		25D 24ND
	L	M	50	23D 22ND	F		17D 16ND

hence the fibrous capsule, volar plate, and palmar and collateral ligaments provide joint stability.

Range of motion

The MCPJ has 2° of freedom, allowing active motion in flexion, extension, abduction and adduction, and a small amount of passive motion in axial rotation. The range of motion in flexion is typically 0–100°, in extension 0–45°, and in abduction–adduction, 0–60°. Passive movement is greater than active in both the flexion–extension plane and the radio-ulnar plane.[21,29] There is little difference in motion between men and women and between different age groups; although there is a decline in manipulative ability with age.[21] The IPJ have 1° of freedom, allowing active motion in flexion and extension, and a small amount of passive axial rotation and lateral movement to accommodate externally applied forces. The range of movement in flexion is typically 0–90° and 0–100° for the DIPJ and PIPJ respectively,

Centre of rotation

The centre of rotation of the MCPJ lies within the head of the metacarpal, although its exact location is open to debate. Flatt and Fischer[30] found that in the sagittal plane, the MCPJ has a fixed centre of rotation. Their work was done with living hands rather than cadavers and joint motion was studied rather than simply the geometry of the joint itself. This is important because the centre of rotation depends not only on the geometry of the joint surfaces, but on the ligaments too, which have an offset attachment relative to any centre of the metacarpal head. Other work examining only the dimensions of the MCPJ has of necessity involved the removal of the ligaments surrounding these joints but has agreed with their findings.[31]

Youm et al[29] using an X-ray technique, also found the centre of rotation of the MCPJ to be constant in both the sagittal and transverse planes. Additionally, using an analytical method, and taking into account possible errors, they concluded that the centre of rotation was fixed within a 1.5 mm sphere. This result was also found by Unsworth & Alexander[31] who showed that the MCPJ has a single centre of rotation in both sagittal and transverse planes.

However, other researchers disagree with the concept of a fixed centre of rotation. Pagowski & Piekarski[32] using measurements from cadavers, calculated the centre of rotation to travel on an arc of radius 1.5 mm. One aspect of their argument against a fixed centre of rotation was that a point load would result, leading to localized wear. Obviously, this localized wear does not occur. However, the lack of wear is due to the cartilage forming a compliant surface, and has little to do with the position of the centre of rotation. An additional assumption was that the collateral ligaments are always taut. However, the tension in the ligaments varies with flexion, so that at maximum flexion, tension in the ligaments is such that abduction–adduction is eliminated.

Walker & Erkman[33] again using cadavers, fixed the phalanx and moved the metacarpal bones, then graphically determined the position of the centre of rotation. Results gave its position as within 3 mm of the centre of the metacarpal head; much greater than that found by any other researchers. Tamai et al[34] attached springs to the tendons and muscles of cadavers to simulate normal loading, then analysed the MCPJ. They concluded that a fixed centre of rotation did not exist but did not give the dimensional variance.

If a fixed centre of rotation is assumed, then a pin jointed model can be employed. Most theoretical models are based on a pin-jointed structure, assuming a constant centre of rotation.[22,23,35–41]

Inter-relationships between the finger joints

The PIPJ and DIPJ are tightly restrained, moving synchronously in flexion and extension.[42] The DIPJ angle is also dependent on the PIPJ angle.[30] Retinacular ligaments encourage synchronous motion between the PIPJ and the DIPJ, with the amount of flexion supposedly in a ratio of 2:1 respectively.[43] The retinacular ligaments run from the flexor tendon sheaths on the proximal phalanx to the terminal tendon on the distal phalanx linking movement of the DIPJ and the PIPJ.

Reciprocal and synchronous angular movement between IPJ and MCPJ is possible.[43] The range of movement of the MCPJ and PIPJ are interrelated. With a more flexed MCPJ the PIPJ range of movement increases. This inter-relationship is influenced by the centres of rotation of the joints and the anatomy of the tendon systems that couple the two joints.[30]

Finger tendons and muscles

There are two main groups of muscles and associated tendons that act on the fingers, the extrinsics and the intrinsics.

Extrinsics

The extensor digitorum communis (EDC) inserts on the distal phalanx via the terminal extensor, on the middle phalanx via the central slip, and on the proximal phalanx via the extensor slip, extending the MCPJ and the IPJ. The flexor digitorum profundus (FDP) inserts on base of the distal phalanx flexing the MCPJ and the IPJ. The flexor digitorum superficialis (FDS) inserts on the middle phalanx flexing the MCPJ and PIPJ.

Intrinsics

The lumbricals (L) originate from the FDP tendon and insert on the EDC tendon extending the IPJ. The

interossei originate from the sides of the metacarpals and insert on the proximal phalanges abducting and adducting the MCPJ and extending the IPJ. The lumbricals and interossei muscles extend the IPJ due to their partial attachment to the EDC.

Finger tendon and muscles roles in hand function

Effective hand function requires stability and strength from the balanced action of the extrinsic tendons, intrinsic muscles, constraining forces and joint contact forces.[35] Extrinsic tendons transmit the force for 'power' grip and exert compressive and subluxing forces on the IPJ. Intrinsic muscles allow fine positioning of the fingers and thumb and contribute to the strength of the hand. Interossei muscles position the pulps of the fingers and the lumbricals modify the relative tensions between flexors and extensors about the IPJ acting as a feedback system.[43]

Antagonists and synergists stiffen the joint for control purposes increasing joint stability and also increasing the joint contact force.[44] Antagonists produce counterbalancing moments, reduce subluxation forces and increase axial compressive forces. The extensor mechanism probably acts passively as an antagonist and stabilizer to increase joint stability, other tendon forces and the joint contact forces.

Tendons have primary and secondary functions. Secondary contributions vary greatly throughout the population. Variation of joint orientation varies the contributions of the tendons, giving the fingers different functional capacities in different positions with optimum configurations.[36] The maximum grip strength also changes with joint angle.[37]

THEORETICAL MODELS

Smith et al[38] developed a two-dimensional index finger pulp-pinch model for analysis of tendon and joint forces from simplified planar analysis. Since then many three-dimensional models have been developed[35,36,37,39] to analyse static isometric functions using forces and moments to determine the resultant forces on the load bearing structures of the finger joints.

Weightman & Amis[22] after reviewing previous models, suggested that one of the most important factors influencing discrepancies between previous finger joint models was the differences in postures adopted in the different models. They found that the joint contact forces increased as the pinching position moved from tip to pulp.

Berme et al[23] and Purves et al[44] developed three-dimensional models of an isometric moment on a water tap and the cap of a jar. The externally applied forces, when applying a maximum clockwise moment, were measured on a six component strain gauged load transducer. Variance in measurements was thought to be due to habitual and anatomical differences. They found that joint contact forces during twist were greater than those during pinch grip.

Storace & Wolf[40,41] applied the principle of virtual work and kinematic analysis to a simple pin-jointed model producing indeterminate equilibrium equations without constraining forces, for the MCPJ and the PIPJ. Relationships of displacement of working tendons with respect to joint angles were calculated and thought to be more accurate than the determination of moment arms. Actual tendon forces could not be calculated but the model was used to predict conditions of instability of joints for abnormal anatomy such as volar subluxation of the extensor tendon.

Tamai et al[34] have also offered some figures for MCPJ forces. Though not providing a model, they calculated forces from contact area and contact pressure. Such a method gave a force of 14N for a static MCPJ in the 'neutral' position due to the balance of muscle forces alone.

Model assumptions

Due to the complexity of hand functions, the involvement of many tendons, and the additional involvement of the soft tissue structures of the joints, theoretical models produced to analyse the roles of the load-bearing structures of the finger and thumb joints were statically indeterminate. This meant that assumptions had to be made in order to obtain solutions which were thought most closely to match the forces encountered in normal hand function.

In most models frictional, inertial and viscoelastic effects of the soft tissues were neglected, and the tendons and tendon sheaths were modelled as frictionless cables and pulleys. The joint contact forces were constrained to act through the bearing surface for joint stability, and models where this was not the case were modified with additional antagonistic stabilisers to increase the joint stability. Joint forces were required to be compressive, and tendon forces tensile. Centres of rotation of the joints were commonly assumed to be constant producing pin-jointed models, and intrinsic forces were assumed to have a single line of action even though they have a broad base of insertion.

Relationships between tendons

Assumptions have been made about the relationships between the interossei, the lumbricals, and the bands of the EDC in order to reduce the numbers of unknowns in the analysis of different hand functions.[22,35,37,39] The relationships were derived from information of the anatomy of the hand and the insertion and orientation of the tendons. Weightman & Amis[22] believed these to be dependent on the angle of flexion of the joints, although all of the authors used set relationships regardless of joint flexion.

Extensor action

In their analysis of the different hand functions An et al[35] and Chao & An[37] assumed the extensor tendon to play an active role. However, Chao et al[39] assumed the extensors had an antagonistic stabilizing role and solutions and results where extensor forces were large enough to imply active and not passive involvement were eliminated. Purves et al[44] introduced extensor or collateral ligament activity only in unstable joints to modify the line of action of joint contact forces to bring them within the bearing surface, stabilizing the joint.

Several models[22,38] have neglected to include the extensor tendon involvement during pinch or grip analysis because EMG results have shown them to be inactive. However, Linscheid & Chao[43] assumed the extensor to assume a passive role during pinch activities providing another joint constraint acting as an antagonist and stabilizer. Passive muscle activity is not always detected by EMG because the thresholds for certain muscles under various levels of activities are too low to detect.[36] Hence, in some models EMG results may have caused the passive stabilizing role of the extensors to be overlooked.

Physiological cross-sectional area

The strength of a muscle was thought to be proportional to the number of sarcomeres firing simultaneously, which in turn was thought to be proportional to the physiological cross-sectional area (PCSA) of the muscle. Estimations of the PCSA of each muscle have been used to predict the maximum strength of individual muscles. Hence, upper strength limits can be imposed on individual muscles in the analysis of hand function. An et al,[35] Chao & An[37] and Chao & An[36] utilized this method estimating the PCSA for muscles of the hand. Results where muscles exerted a force greater than the upper strength limit of the muscle were modified or eliminated. Weightman & Amis[22] also used this theory to develop inter-relationships between the lumbrical and interossei muscles in the ratios of radial interrosei (RI): ulnar interrosei (UI): L = 4.3:1.45:0.52.

Two- and three-dimensional models

The majority of authors have modelled pinch and grip activities in three dimensions,[35,36,39,43] apart from Smith et al[38] and Weightman & Amis[22] who assumed pinching to be simply two-dimensional. However, from three-dimensional models it can be seen that pinch and grip activities have lumbrical and interossei active involvement as well as the flexor and extensor systems. Hence the two-dimensional analyses without lumbrical and interossei involvement produce oversimplified models of the true pinch and grip activities. Joint contact forces are the resultant of the axial compressive force and the volar and lateral shear forces. However, neglecting the lumbrical and interossei involvement in two-dimensional models eliminates the lateral shear force component.[22,38]

Moment arms

Flatt & Fischer[30] suggest that extensor moment arms decrease slightly and flexor moment arms increase with increasing flexion of the finger joints. However, Linscheid et al[42] believed that the flexor sheaths kept the flexor moment arms virtually constant during flexion with respect to the centre of rotation of the joints. Youm et al[29] found that the extensor moment arm was almost constant during flexion, although the flexor moment arms increased by 50% at full flexion. The palmar aspect of the phalangeal base also increased the flexor moment arm during flexion, increasing its mechanical advantage. However, although the flexor moment arm appears to change significantly during flexion of the finger joints, it has been neglected in most models.

Joint surface load sharing

Most models appear to assume that the bearing surfaces of the joints share the joint contact force. However, Purves et al[44] investigated the possibility that either both PIPJ condyles support the joint contact force with both the collateral ligaments and the extensors slack, or only one condyle supports the joint contact force with the opposite collateral ligament in tension. They surprisingly found that the PIPJ radial ligament was load bearing and joint loading was exclusively in the ulnar compartment.

The effects of these assumptions have in some cases been analysed to investigate their effects on the resulting force distribution between the load bearing structures of the hand during upper limb functions. In some cases they have made little difference, although they must account for some of the discrepancies between the models. However, such assumptions are needed in some cases to simplify the force analysis of a joint and produce a determinate model.

Theoretical forces

The forces from the theoretical models were calculated in terms of unit force applied to the distal phalanx in tip and pulp pinch and unit force applied to the radial side of the middle phalanx in lateral pinch. Three forces were applied normal to the long shaft of the proximal, middle and distal phalanges for grip hand functions. Chao & An[36] and Chao et al[39] applied three unit forces; however, An et al[35] determined the ratios experimentally and applied forces in the ratios of DP:MP:PP = 1:0.34:0.66, compared with 1:0.52:0.77[7] and 1:0.375:0.56.[19]

Conclusions

Difficulties occur in the comparison of the different theoretical models and in combining experimentally measured forces with the theoretical models in order to calculate joint contact forces. Confusion in the definition of the different hand functions has occurred, and forces have been applied to the models in different positions, directions and distributions. Differences occur within the joint angles used during specific hand functions and with those encountered when experimentally measuring the forces during the different activities.

Joint angle

Differences in joint angles during pinch and grip hand functions are responsible for some discepancy between the calculated forces. For example, for a constant pinch force with increased joint flexion the FDP force decreased, FDS force and shear components increased, and the intrinsic tension remained constant. The joint force decreased due to the reduction of moment arm of the external force from pulp to tip, and its direction of action changed.[22]

Joint contact forces

The maximum forces being applied to the fingers during grip hand functions are greater than in pinch functions (Tables 1, 4–6). This would possibly imply that joint contact forces during gripping would be larger than those during pinching. However, in some models this is not so.[36,39] This is possibly due to assumptions in the distribution of forces. Chao & An[36] and Chao et al[39] applied unit forces at each of the phalanges and found the joint contact forces in tip pinch to be greater than in grip. However, An et al[35] experimentally measured the distribution of forces between the three phalanges in grip and used a unit ratio of these forces in their model and found the joint contact forces of grip to be greater than tip pinch which would be expected.

To make a fair comparison between the joint contact forces between pinch-and-grip hand functions realistic forces must be used. For instance, the maximum measured forces in grip, (Table 2), are far greater than those of pinch, (Table 4), hence comparing models using unit forces for both is totally unjustifiable. If unit forces are applied to both pinch and grip functions, tip pinch joint contact forces may well come out larger than those of grip due to the increased distance of the force from the joints.

By matching experimental hand function positions with the theoretical models as far as possible it was found that grip joint contact forces are greater than pinch joint contact forces. For grip function, inserting 80N DP component[19] into An's model[35] gives maximum joint contact forces of 279N, 437N, 387N for the DIPJ, PIPJ, and MCPJ respectively. For tip pinch function inserting 66N[7] gives maximum joint contact forces of 180N, 331N, 299N. (Results from Amis[19] were used and not An et al[7] as the distribution of forces is closer to that of the theoretical model). In all hand activities it has also been shown that in general, joint contact forces increase with more proximal joints, possibly due to the increase in the moment arm of the externally applied force.

Comparison between pinch and grip hand functions

There is some discrepancy in the comparison of muscle forces between grip and pinch activities. Chao & An[36] found that flexor forces were slightly greater in gripping but intrinsic forces (lumbricals and interossei) were less because they are more important for stability in pinch which is a more unstable position. In pinching flexor forces were still greater than intrinsic forces.

However, Chao et al[39] found that the FDP force was greater in pinch than grip, but the FDS force and the intrinsic forces were less. In grip the intrinsic muscles provided greater forces than flexor tendons, but in pinch the flexor tendons produced greater forces than the intrinsic muscles. An et al[35] found that flexor forces were in general greater in grip than in tip or pulp pinch, but intrinsic forces were about the same. Flexor forces were greater than intrinsic forces.

In general it seems that the flexors contribute greatly to hand strength in all hand functions. The intrinsic muscle forces seem to be smaller than the flexor forces in the majority of cases but still contribute appreciably to hand strength and stability of the joints. Muscle contributions vary with position of grip.

Stability

The finger joints rely on soft tissues and tendons around the joints for joint stability. Muscles are recruited to increase joint stability and can act as antagonists to other muscles such as the flexors, whose forces increase to overcome the effects of the antagonists. This increase in muscle forces in turn increases the joint contact forces. The majority of models ignore the involvement of the fibrous joint capsule, joint ligaments, and volar plate in force analyses of the finger joints due to their complexity. However, it is generally recognized that these structures play an important role in resisting the shear forces of the joints and towards increasing joint stability. The collateral ligaments decreased the volar shear component of the joint force and increased the axial compressive component, resulting in a slight increase in the joint contact force.[22,38]

The EDC has also been ignored in the majority of models, even though it probably exerts a passive tension across the joints, and consequently increases joint stability.[41] Muscle forces in tip and pulp pinch cover

similar ranges, however, lateral pinch has increased EDC and radial interossei forces to resist the greater shear forces which then stabilises the joint. Storace & Wolf[40,41] showed that intrinsic interossei muscles were required in addition to extrinsic FDP and EDC tendons for stability in hand function.

Pathological condition

Rheumatoid arthritic joints show gross deformity due to a loss of the balance of tendon forces, constraining ligaments and joint architecture. The radial interossei tend to have a larger force than the ulnar interossei showing that the proximal phalanx has a tendency to try to move in an ulnar direction. Volar and ulnar forces are usually resisted by the collateral ligaments and joint capsule; however, a loss of integrity in the supporting structures allows ulnar drift and subluxation to occur.

The paths of the tendons and muscles also affect the balance of joints.[42] A small disturbance in their position will upset the balance of forces around a joint resulting in deformation of the fingers. Storace & Wolf[40,41] found that volar relocation of the long extensor produced an unstable finger, that is one where the line of action of the joint contact force acted outside the articular surface of the joint. Rheumatoid arthritic patients often have better 'power' grip function than precision handling due to the increased stability of their hand function.[36]

BIOMECHANICS OF THE THUMB

The thumb provides strength, stability, and increased manipulation of the hand in its various activities. In precision pinch it acts as a pillar for the fingers to act against, and in 'power' grip it reacts directly against the object being held. Strength in hand functions relies heavily on the stability of the thumb which in turn depends on the configuration of the articulating surfaces and the surrounding soft tissues. Antagonist muscles also help to stabilise the joint. If the ligaments or tendons of the thumb are damaged, such as in rheumatoid arthritis, then the strength of the hand is significantly reduced.

Joint anatomy and range of movement

The IPJ is bicondylar with 1° of freedom allowing active movement in flexion and extension and a small amount of passive axial rotation and lateral movement. The range of movement is typically 0–90° of flexion and 0–20° of extension. The collateral ligaments, volar plate, joint capsule, and supporting soft tissues provide joint stability.

The MCPJ is condylar with 2° of freedom allowing active movement in flexion, extension, abduction and adduction, and a small amount of passive axial rotation. The range of movement is typically 0–60° of flexion and 0–10° of extension. The collateral ligaments and volar plate-sesamoid bones complex limit abduction, adduction and axial rotation. The fibrous capsule, collateral ligaments, and volar plate with sesamoid bones provide joint stability.

The carpo metacarpal joint CMCJ or trapezium-metacarpal joint, is a biconcave saddle joint with 2° of freedom allowing active movement in flexion, extension, abduction and adduction, and a small amount of passive axial rotation depending on the congruity of the articulating surfaces maintained by the ligaments. The range of movement is typically 0–15° of flexion, 0–20° of extension, and 0–70° abduction/adduction. The CMCJ of the fingers allow little movement and contribute little to the manipulation of the hand. However, the thumb CMCJ has a wide range of movement, allowing the hand to manipulate a wide range of objects.

Tendons and muscles

The main load-bearing structures of the thumb are the flexor, extensor, adductor and abductor muscles and associated ligaments, the joint constraining ligaments and the articular surfaces. The main load-bearing muscles are the flexors and adductors. The abductors, extensors and constraining ligaments act mainly as antagonists or stabilizers, increasing the stability of the joints. There are two main groups of muscles acting on the thumb, the extrinsics and the intrinsics (Fig. 2)

Extrinsics

The extensor pollicis brevis (EPB), the extensor pollicis longus (EPL), the abductor pollicis longus (APL), the flexor pollicis brevis (FPB), and the flexor pollicis longus (FPL).

Intrinsics

The abductor pollicis brevis (APB), the adductor pollicis (ADD), and the opponens pollicis (OPP).

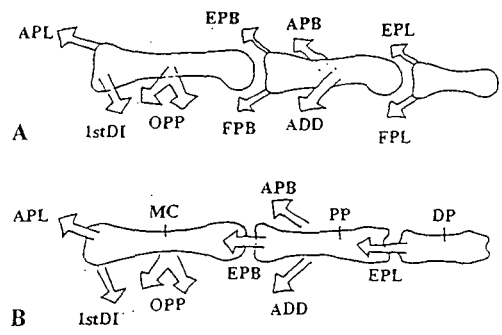

Fig. 2—Muscles and tendons of the thumb; (A) sagittal plane, (B) posterior frontal plane.

Theoretical models

Three theoretical models of the thumb have been considered for this paper. The first was developed by Hirsch[45] who modelled the thumb MCPJ producing two-dimensional lateral and pulp pinch models with point forces applied perpendicular to the long axis of the bones. The location and orientation of the load-bearing structures were estimated from cadaveric samples, although it was found that varying the angles of the tendons did not affect the results significantly. The forces exerted on the thumb in lateral and pulp pinch were measured in 70 males and seven females. These were found to be 89N for pinch force and 42N for lateral force and were used to estimate joint contact forces.

The second model considered was developed by Cooney & Chao[46] who produced three-dimensional finger force models for pinch and grip actions. A two-dimensional model was developed but this proved inadequate in calculating the joint and tendon forces. Joint and tendon locations and orientations were obtained from biplanar roentgenograms of cadaveric specimens. Forces in the relevant tendons and joint contact forces were calculated from equilibrium equations using assumed loads applied to the tip of the thumb in tip, lateral and pulp pinch. The orientations of each segment were defined by Eulerian angles. No attempt to calculate the forces in the individual joint ligaments was made.

The final model to be considered was developed by Toft & Berme[47] who produced a three-dimensional model of the CMCJ, the MCPJ and the IPJ of the thumb. Position and orientation of load-bearing structures were observed from cadavers, and spatial configuration of the hand functions from cine cameras and skin markers. Force readings were taken from four female subjects applying isometric twist and squeeze grips to a 45 mm diameter strain gauged cylindrical force transducer. The grip positions varied between lateral, pulp and grip.

Assumptions

Assumptions were required in all cases to solve the statically indeterminate models. Simplification of the hand functions is required in order to produce statically determinate models due to the complexity of the thumb and the number of muscles involved for different hand functions and stability.

Tendons and tendon sheaths were modelled as inextensible cables running on frictionless pulley systems. Tendon moment arms were assumed to be constant about the centres of rotation of the joints, due to the tendons being constrained within their sheaths.[46] Deformation of the bones, and frictional, viscoelastic and mass effects were also neglected.[46]

Joint motion

The IPJ was modelled as a hinge joint allowing movement in flexion and extension only, with axial rotation and lateral bending neglected. The MCPJ and the CMCJ were modelled in three dimensions as universal joints allowing movement in flexion, extension, abduction and adduction only, with no axial movement. Two-dimensional models neglect abduction and adduction movement as well, allowing only flexion and extension movement.

Cooney & Chao[46] assumed that all the joint articular surfaces shared the loads. However, the possibility of either both condyles of the IPJ sharing the load with lax collateral ligaments, or one condyle taking the load and the opposite collateral ligament being active was investigated by Toft & Berme[47]. Joint forces were assumed to act through the joint surface contact area for stability, with antagonists and/or ligament forces incorporated to modify the line of the joint force if necessary.

Tendon involvement

Cooney & Chao[46] assumed that the extensor tendons, had a passive role only to enhance the stability of the joints. Their contribution to the joint contact forces and other tendon forces was investigated. The FPB and OPP were assumed to act as one combined force at the CMCJ. The shear forces were assumed to be resisted by the collateral ligaments, capsule, volar plate and bone architecture although this was not investigated further.

Hirsch[45] neglected all antagonists and stabilizing ligaments when determining the joint forces, assuming their contribution to the joint force to be small. All muscles were assumed to have a single line of action even though anatomically they have broad insertions. The transverse and oblique heads of the ADD were assumed to act as one. Toft and Berme[47] neglected the extensors and the constraining ligaments although their roles as stabilisers were investigated. The contributions of the antagonists and the adductors were included. Tendon and ligament forces had to be tensile and joint reaction forces compressive.

Calculated forces

The different models assumed different loads or forces to be acting on the thumb in the different positions assumed. Cooney & Chao[46] applied pinch forces of 9.8N (normal 9.8–98N), and grip forces of 98N (normal 49–196N) to the thumb. Hirsch[45] applied a pinch force of 89N and a lateral force of 42N to the thumb. Toft & Berme[47] applied an average force of 74N, with no significant difference between the squeeze and twist, due to the difference in grip positions and direction of applied force.

Joint contact force

No significant difference between the joint contact forces in different types of pinch was found; however, there was a significant increase with grip. In grip the thumb exerts much greater forces than in pinch in

order to resist the forces of all four of the fingers, rather than just one as in pinch functions. The joint contact force increases from the IPJ to the CMCJ showing that the more proximal the joint, the higher the joint contact force, as with the finger joints.

Flexor and adductor forces

No significant difference between the forces of the FPL, FPB or ADD in different types of pinch was found. However, there was a significant increase with grip. The separate adductor forces contribute to the joint contact force but do not alter its line of action significantly.[47]

Antagonists and stabilisers

EPL and EPB contributions to the joint contact forces and other tendon forces are insignificant, increasing them only slightly, but enhancing joint stability.[46] The extensors and collateral ligaments also increase joint stability by modifying the line of action of the joint contact force to within the bearing surface, increasing the flexor tension and the joint force slightly.[47] Stability was possible without the APB, which acted as an antagonist to the adductors and a synergist to the flexors, minimally increasing the joint contact force.[47]

Finally, it was found that axial rotation moments at all joints and lateral bending moment at the IPJ occurred during pinch functions showing that three-dimensional analysis of pinch functions is necessary for valid hand function analysis.[46]

Summary

The intrinsic muscles are important joint stabilisers and transmit active forces across the MCPJ and the CMCJ. Large intrinsic forces occur due to need of the thumb for stability and strength in pinch and grip.[46] A combination of antagonists and collateral ligaments are necessary to stabilise the joints,[47] especially in pinch which adopts a more unstable configuration than grip. Flexor, adductor and joint contact forces are much greater in grip than pinch due to the thumbs resisting the forces of all four fingers in grip which increases the required counterbalancing forces in muscles and hence increases the joint contact force. Lateral shear force and bending moment are restrained by the collateral ligaments, volar plate, fibrous capsule, and bone architecture, providing the necessary stability for the joints.[45–47]

BIOMECHANICS OF THE WRIST

The wrist joint is a complex linkage of bones and ligaments between the forearm and the hand which, while offering an impressive arc of motion, retains a remarkable degree of stability.

Anatomy of the wrist

The wrist consists of the radio-carpal, ulnar-carpal, inter-carpal and the carpo-metacarpal joints. The inter-carpal joint is complex, consisting of two transverse rows of four carpal bones each, together with ligaments.

These bones are interconnected by a network of ligaments, which are divided into two general classes, intrinsic and extrinsic. The intrinsic ligaments interconnect the carpal bones, while the extrinsic ligaments connect the carpal bones to either the metacarpals, radius or ulna. Of particular interest is the triangular fibrocartilage complex, the ligamentous and cartilaginous structure that suspends the distal radius and ulnar carpus from the distal ulna.[48]

Range of motion

Normal subjects have an average of 133° of maximum flexion–extension and 40–50° of maximum radio-ulnar deviation.[49,50] In full extension or flexion, abduction–adduction is eliminated.

Normal use

The normal functional range of wrist motion has been found to consist of 5–10° of flexion, 30–35° of extension, 10° of radial deviation and 15° of ulnar deviation, i.e. the majority of tasks require little wrist motion, but it is necessary to be three-dimensional.[49]

Palmer et al[49] undertook a number of of standardized tasks on volunteers and found that, of 24 tasks, 21 were performed with the wrist in extension and 15 with the wrist in ulnar deviation. These 24 tasks were divided into three groups: personal hygiene tasks such as 'comb hair' and 'tie shoe'; culinary tasks such as 'eat with fork' and 'drink from cup'; and other activities of daily living such as 'put phone to ear' and 'turn key'.

A similar experiment was carried out in which the loss of wrist motion was simulated by volunteers wearing splints, the volunteers then performing 10 standardized activities of daily living.[50] The splints provided for four different positions of wrist immobilization; 15° of palmar flexion, neutral, 15° of palmar extension and 20° of ulnar deviation. Results disclosed that the least compromised hand function was with wrists immobilized in 15° of extension, while wrists placed in 20° of ulnar deviation exhibited the greatest degree of disability.

Rotation and bone movement

The wrist joint has 3° of freedom, these being flexion–extension, radioulnar deviation and rotation.[50] However, rotation of the hand results from motion arising at the proximal and distal radial ulnar joints; it does not occur through the carpal complex.

The radius and hand move in relation to, and function about, the distal ulna.[48] Forearm rotation of up

to 150° occurs at the distal radioulnar joint, with the distal radius and its fixed distal member (the hand) rotating about the ulnar head. However, the ulnar head itself is not immobile during rotation of the forearm, but moves slightly dorsally in pronation and slightly toward the palm in supination.[48] The centre of rotation of the wrist is located in the head of the Capitate.

Forces in the wrist

The loads transmitted by the wrist joint during normal activities are not precisely known but are thought to be great. Observations of the articular surfaces of the bones of the wrist suggest that significant compressive loads are dealt with in a static fashion.[50] For example, the opposing joint surfaces of the mid-carpal articulation have a close conformity, and depressions exist for the scaphoid and lunate on the articulating surface of the distal radius.

By applying compressive loads across the proximal carpal articulation with the wrist in a neutral position, it was found that these loads have a resultant line of action which passes through the head of the capitate to the scapho-lunate junction, and then to the distal radial and ulnar surfaces.[50] When the forearm of cadavers, including the elbow, were loaded in a neutral position it was found that the radius, through its articulation with the lateral carpus, carried approximately 80% of the axial load of the forearm, and the ulna, through its articulation with the medial carpus via the triangular fibrocartilage complex, 20%.[48] The same experiment revealed peak pressure across the articulations of the wrist to have a maximum value in the order of 4MPa.

Effect of wrist position on grip strength

No significant difference in grip strength with the wrist positioned at 0° and 15° ulnar deviation and 0° and 15° extension, or any combination of these, has been found[51,52] However, both studies did find grip strength to be significantly less at 15° of palmar flexion.

REFERENCES

1 Kellor M, Frost J, Silberberg N, Iverson I, Cummings R. Hand strength and dexterity. Am J Occup Ther 1971; 25: 77–83
2 Jones AR, Unsworth A, Haslock I. A microcomputer controlled hand assessment system used for clinical measurement. Engng Med 1985; 14: 191–198
3 Agnew J, Maas F. Hand function related to age and sex. Arch Phys Med Rehabil 1982; 63: 269–271
4 Smith HB. Smith hand function evaluation. Am J Occup Ther 1983; 27: 244–251
5 Sperling L. Evaluation of upper extremity function in 70-year-old men and women. Scand J Rehabil Med 1980; 12: 139–144
6 Swanson AB, Matev IB, De Groot G. The strength of the hand. NY University Medical School Interclinical Information Bulletin 1974; 13, 1: 1–8
7 An KN, Cooney III WP, Chao EYS, Linscheid RL. Functional strength measurement of normal fingers. Orthopaedic Biomechanics Laboratory, Mayo Clinic 1978
8 Mathiowetz V, Kashman N, Volland G, Weber K, Dowe M, Rogers D. Grip and pinch strength: normative data for adults. Arch Phys Med Rehabil 1985; 66: 69–74
9 Reikeras O. Bilateral differences of normal hand strength. Arch Orthop Trauma Surg 1983; 101: 223–224
10 Ellison MR, Kelly JK, Flatt AE. The results of surgical synovectomy of the digital joints in rheumatoid disease. J Bone Joint Surg 1971; 53-A: 1041–1060
11 Harkness JAL, Richter MB, Panayi GS, Van de Pette K, Unger A, Pownall R. Circadian variation in disease activity in rheumatoid arthritis. BMJ 1982; 284: 551–554
12 Clawson DK, Souter WA, Carthum CJ, Hymen ML. Functional assessment of the rheumatoid hand. Clinical Orthopaedics and Related Research 1971; 77: 203–210
13 Kowanko IC, Pownall R, Knapp MS, Swannell AJ, Mahoney PGC. Circadian variations in the signs and symptoms of rheumatoid arthritis and in the therapeutic effectiveness of flurobiprofen at different times of day. J Clin Phar 1981; 11: 477–484
14 Myers DB, Grennan DM, Palmer DG. Hand grip function in patients with rheumatoid arthritis. Arch Phys Med Rehabil 1980; 61: 369–373
15 Labi MLC, Gresham GE. Hand function in osteoarthritis. Arch Phys Med Rehabil 1982; 63: 438–440
16 Cantrel T. Measurement of weakness and dysfunction in the rheumatoid hand. Rheumatol Rehabil 1976; 15: 182–184
17 Cutts A, Bollen SR. Grip strength and endurance in rock climbers. Proc Instn Mech Engrs 1993; 207: 87–92
18 Pearson R, MacKinnon MJ, Meek AP. Diurnal and sequential grip function in normal subjects and effects of temperature change and exercise of the forearm on grip function in patients with rheumatoid arthritis and in normal controls. Scand J Rheumatol 1982; 11: 113–118
19 Amis AA. Variation of finger forces in maximal isometric grasp tests on a range of cylinder diameters. J Biomed Eng 1987; 9: 313–320
20 Kroemer KHE, Gienapp EM. Hand-held device to measure finger (thumb) strength. J Appl Physiol 1970; 29, 4: 526–527
21 Walker PS, Davidson W, Erkman MJ. An apparatus to assess function of the hand. J Hand Surg 1978, 3, 2
22 Weightman B, Amis AA. Finger joint force predictions related to design of joint replacements. J Biomed Eng 1982; 4: 197–205
23 Berme N, Paul JP, Purves WK. A biomechanical analysis of the metacarpo-phalangeal joint. J Biomech 1977; 10: 409–412
24 Dickson RA, Petrie A, Nicolle FV, Calnan JS. A device for measuring the force of the digits of the hand. Biomed Eng 1972: 270–273
25 Unsworth A, Haslock I, Vasandakumar V, Stamp J. A laboratory and clinical study of pneumatic 'grip strength' devices. Br J Rheumatol 1990; 29: 440–444
26 Baron M, Dutil E, Berkson L, Lander P, Becker R. Hand function in the elderly: relation to osteoarthritis. J Rheumatol 1987; 14: 815–819
27 Laws CA, Myers BD, Palmer DG. The effect of temperature on work and power output during hand grip assessment of rheumatoid patients and controls. Wellcome Medical Research Institute Department of Medicine 1979: 45–46
28 Ohtsuki T. Inhibition of individual fingers during grip strength exertion. ERGOA 1981; 24: 21–36
29 Youm Y, Gillespie TE, Flatt AE, Sprague BL. Kinematic investigation of normal MCP joint. J Biomech 1978; 11: 109–118
30 Flatt AE, Fischer GW. Biomechanical factors in the replacement of rheumatoid finger joints. Ann Rheum Dis 1969; 28: Supp 36–41
31 Unsworth A, Alexander WJ. Dimensions of the metacarpo-phalangeal joint with particular reference to joint prostheses. Engng Med 1979; 8: 75–80
32 Pagowski S, Piekarski K. Biomechanics of the metacarpo-phalangeal joint. J Biomech 1977; 10: 205–209
33 Walker PS, Erkman MJ. Laboratory evaluation of a metal plastic type of metacarpo-phalangeal joint prosthesis. Clin Orthop 1975; 112: 349–356
34 Tamai K, Ryu J, An KN, Linscheid RL, Cooney WP, Chao EYS. Three dimensional geometric analysis of the metacarpo-phalangeal joint. J Hand Surg 1988; 13-A, 4

35 An KN, Chao EYS, Cooney WP, Linscheid RL. Forces in the normal and abnormal hand. J Orthop Res 1985; 3, 2: 202–211
36 Chao EY, An KN. Determination of the internal forces in human hand. J Engng Mech Div Proc ASCE 1978: 255–272
37 Chao EY, An KN. Graphical interpretation of the solution to the redundant problem in biomechanics. J Biomechan Eng 1978; 100: 159–167
38 Smith EM, Juvinall RC, Bender LF, Pearson JR. Role of the finger flexors in rheumatoid deformities of the metacarpo-phalangeal joints. Arth Rheum 1964; 7, 5: 467–480
39 Chao EY, Opgrande JD, Axmear FE. Three dimensional force analysis of finger joints in selected isometric hand functions. J Biomech 1976; 9: 387–396
40 Storace A, Wolf B. Functional analysis of the role of the finger Tendons. J Biomech 1979; 12: 575–578
41 Storace A, Wolf B. Kinematic analysis of the role of the finger tendons. J Biomech 1982; 15, 5: 391–393
42 Lincheid RL, Dobyns JH. Total joint arthroplasty, the hand. Mayo Clin Proc 1979; 54: 516–526
43 Linscheid RL, Chao EYS. Biomechanical assessment of finger function in prosthetic joint design. Orthop Clin North Am 1973; 4, 2: 317–330
44 Purves WK, Berme N, Paul JP. Finger joint biomechanics. Disability – Proc Seminar Rehab (RM Kenedi, JP Paul, J Hughes eds), Macmillan; London 1979: 318–332
45 Hirsch D, Page D, Miller D, Dumbleton JH, Miller EH. A biomechanical analysis of the metacarpo-phalangeal joint of the thumb. J Biomech 1974; 7: 343–348
46 Cooney WP, Chao EYS. Biomechanical analysis of static forces in the thumb during hand function. J Bone Joint Surg 1977; 59-A: 27–36
47 Toft R Berme N. A biomechanical analysis of the joints of the thumb. J Biomech 1980; 13: 353–360
48 Palmer AK, Werner FW. Biomechanics of the distal radioulnar joint. Clin Orthop Relat Res 1984; 187: 26–35
49 Palmer AK, Werner FW, Murphy BS, Glisson R. Functional wrist motion: a Biomechanical study. J Hand Surg 1985; 10-A: 39–46
50 Volz RG, Leib M, Benjamin J. Biomechanics of the wrist. Clin Orthop Relat Res 1980; 149: 112–117
51 Kraft GH, Detels PE. Position of function of the wrist. Arch Phys Med Rehabil 1972; 53: 272–275
52 Pryce JC. The wrist position between neutral and ulnar deviation that facilitates the maximum power grip strength. J Biomech 1980; 13: 505–511